FAILURE CHARACTERISTICS OF CONCRETE

by

O.T. Sigvaldason, B.Sc., D.I.C.

A thesis submitted for the Degree of Doctor of Philosophy in the Faculty of Engineering of the University of London

Imperial College of Science
and Technology, London.

June, 1965.

ABSTRACT

The first half of the thesis is an investigation of testing machines and their calibration. A study of biaxial tension and tension-compression strength properties of concrete and mortar is presented in the second part, including the development of suitable testing techniques to achieve such states of stress. The thesis is subdivided into three parts.

PART I: A study of calibration devices is made , followed by the results of the calibrations of testing machines in the Concrete Department at Imperial College. The non-axial loading of calibration devices and testing machines showed that relatively large errors arise, and that the calibrations obtained, based on ideal loading conditions, are not as free from error as had been previously supposed.

PART II: After examining the influence of different testing machine characteristics and the effect of the three basic methods of uniaxial loading on the strength properties of concrete, a theoretical and experimental investigation was conducted to assess which of these characteristics was most influencial in observed variations of strength. Then, the behaviour of spherical seatings was examined by experimenting with four seatings, using different lubricants. It was shown that seatings could be pinned or fixed or attain some condition between these extremes. A further investigation into the influence of testing machine characteristics on concrete strengths showed that the behaviour of the spherical seating, method of loading, machine restraint, misalign-

ment, and lateral stiffness all had a significant influence on the cube and cylinder strengths, as well as on the ratio of these strengths. Recommendations and specifications are proposed for testing machines used for control testing of concrete.

PART III: After examining the results of previous investigations on biaxial tension and tension-compression, it was apparent that the shortcomings of such investigations lay in the unsatisfactory testing techniques employed and in the fact that the experiments were limited usually to obtaining only the short term ultimate strengths. To develop a satisfactory technique for achieving the desired biaxial states of stress, pilot investigations were conducted on an aluminum plate. These included the concentric loading of circular plates, thereby inducing pure moments of equal magnitude and the same sign, the corner loading of square plates to obtain pure moments of equal magnitude and opposite sign, and the corner loading of rhombus plates resulting in pure moments of different magnitude and opposite sign. The theory for the rhombus test was developed by the author. By using the same testing technique, mortar and concrete specimens were tested for stresses and strains at the discontinuity level, the applicability of the laws of elasticity, and the values of modulus of rupture in biaxial states of stress. In order to examine biaxial tension-compression strength characteristics where the compression to tension ratio is greater than unity, rhombus plates suitably reinforced woro also investigated. From the analysis, it was shown that the failure values for mortar could be expressed in terms of Coulomb's internal friction expression, whereas, for the concrete, it was more reasonable to show the strength as being a function of the bond strength at the cement paste-aggregate interface.

ACKNOWLEDGEMENTS

The author is grateful to Professor A.L.L. Baker, D.Sc., M.I.C.E., M.I.Struct.E., under whose general supervision the research was conducted.

Special gratitude is extended to Mr. K. Newman who suggested the research programme, and provided guidance and encouragement throughout. Mr. Newman's help in the preparation of the thesis manuscript and technical papers is also very much appreciated.

Thanks are extended to fellow research students and laboratory personnel at Imperial College. In particular, the author would like to thank Dr. M.A. Ward, with whom some of the research was conducted. Thanks are given also to Messrs. G.W.D. Vile, and G.S. Robinson. In addition, a debt of gratitude is owing to Messrs. J.R. Turner and H. Wilson whose ready assistance during the casting of concrete specimens and the manufacture of moulds was of great benefit.

To Messrs. B. Swindells and R.C. Dobnam at the National Physical Laboratory is extended sincere thanks for their ready co-operation in connection with all calibrations performed by the author.

To personnel at the Road Research Laboratory, the author is extremely grateful for all the assistance provided. In particular, he thanks Mr. P.J.F. Wright and Dr. R.H.H. Kirkham, for permitting research to be conducted at their laboratory.

The author is especially grateful to Mr. W. Amer for the many hours provided by him.

While conducting this research, the author was sponsored by the Athlone Fellowships and the National Research Council of Canada, to whom he is most grateful. Thanks are also extended to the Department of Scientific and Industrial Research who financed all materials and labour for the research conducted at the Road Research Laboratory.

TABLE OF CONTENTS

CHAPTER I

INTRODUCTION TO THESIS

1.1 INTRODUCTION

The work described in this thesis, which was suggested by Mr. K. Newman, follows a pattern of research in the Concrete Technology Department at Imperial College directed towards assessing the properties of concrete under all possible combinations of stress. It is hoped that the entire research programme, of which this thesis forms one part, will not only produce a better understanding of the strength and deformational characteristics of concrete and its mechanism of fracture and failure, but will also be of benefit to the practising engineer by providing useful information for the rational design of various structures.

1.1.1 Previous Research at Imperial College

Previous researchers, Lachance[1] and Ward[2] designed testing machines and developed suitable specimens to ensure that a uniform state of uniaxial compressive or tensile stress could be induced throughout a finite volume of material. By obtaining deformation and ultimate strength values on their specimens, a considerable amount of information was obtained concerning the behaviour of concrete on the phenomenalogical level under uniaxial states of stress.

So that a better understanding of the inter-particle behaviour of concrete could be obtained, Anson[3,4] performed a programme of research aimed at developing Baker's[5] lattice theory - an idealized model of the internal structure of concrete.

1.1.2 Objective of Thesis

Although much remained to be investigated concerning the behaviour of concrete when subjected to uniaxial states of stress, particularly with reference to creep, shrinkage and drying properties, it was considered that information on the behaviour of concrete in biaxial states of stress would be more useful, for the following reasons:

(1) An investigation of the strength and deformational behaviour of concrete under biaxial stress would provide a better understanding of the probable mechanism of failure for concrete under different states of stress.

(2) Numerous structures are subjected to biaxial loading systems. Arch dams, shell structures, and the floor slabs, wall panels, roof slabs, footings and column-beam connections of buildings, to name only a few, are all subjected to biaxial stress. Therefore, the importance of obtaining a better understanding of concrete under such loading systems is readily apparent.

An investigation at Imperial College of the behaviour of concrete under biaxial compression was begun by Robinson[6] and is currently being continued by Vile[7]. This thesis, meanwhile, considers the behaviour of concrete and mortar in biaxial tension and tension-compression states of stress.

In addition to the investigation on the biaxial strength and deformational properties of concrete, this thesis also describes work concerned with establishing reliable testing techniques for achieving the desired state of stress in specimens under any combination of load. That such an investigation was necessary was apparent when, in an initial examination at Imperial College, on the strength of concrete under complex states of stress, suspicious inconsistencies occurred in the principal stress plot. It was thus considered that the calibrations for the different testing machines were in error or that the machines were not applying the load in accordance with theoretical assumptions or that the specimen shape was not inducing the correct states of stress. Furthermore, it was even possible that all of these factors could be having a significant influence. That a problem existed even with the simple cube crushing machines became apparent when vastly different results in strength of virtually identical cube specimens were obtained from different machines. The other major portion of this thesis is directed, therefore, towards examining both theoretically and experimentally , the errors which are likely to arise as a result of variations in the different characteristics of testing machines as well as calibration procedures.

From the investigations of calibration procedures and testing machine characteristics, several shortcomings of British Standards 1610 (8) and 1881 (9) are revealed. In the author's papers, (10-13) the importance of improved British Standard specifications for testing machines is discussed in detail. It is hoped that the portion of the thesis which is concerned with testing machines, together with relevant papers will lead to improvements in materials test methods. In particular, this could lead to quality control tests on concrete specimens being accepted with a greater degree of reliability.

1.2 OUTLINE OF THESIS

The theis has been subdivided into three parts.

PART I: An examination of calibration instruments and techniques is presented followed by a discussion of the calibration results of the various testing machines in the Concrete Technology Department at Imperial College. An investigation into the effects of the off-centre loading of both calibration devices and testing machines on the indicated load leads to a discussion of possible improvements in calibration instruments and calibration methods.

PART II: A theoretical investigation into the influence of different testing machine characteristics on the uniaxial strength of concrete, together with initial experiments on testing machines at Imperial College revealed that the main problems concerning variations in results from compression testing machines, were due to the behaviour of the spherical seating, platen restraint and misalignment. From this, an initial programme of research was conducted on different spherical seatings lubricated with different lubricants to show the factors which have a significant influence on the behaviour of the spherical seating under load. A subsequent programme of research was conducted which shows the influence of variations in spherical seating behaviour, platen restraint effect, and misalignment, as well as other testing machine characteristics on the cube and cylinder strength.

From this investigation, it is shown that for any test, the method of loading(effectively pinned end conditions, or effectively fixed end conditions) must be specified as not **only** the ultimate strengths are affected, but similarly, certain deformational properties, and even the mode of failure, can be influenced. Finally, definite recommendations and suggestions for specifications for the requirements of compression testing machines for inclusion in British Standard 1881 are given.

PART III: The importance of using the correct testing technique in any investigation of concrete under complex states of stress becomes apparent when reviewing the results of previous researchers. Not only are there large and inconsistent discrepancies between their results, but a preliminary investigation into establishing that the experimental results are in close agreement with the theoretical analysis has never been conducted.

Since the adopted method of test was under flexural states of stress, the first specimen shape was a rectangular plate with the load being applied on two diagonally opposite corners while being supported at the other two corners. Thus biaxial tension-compression stresses are produced where the tension and compression stresses are equal. In order to obtain different combinations of biaxial tension -compression stresses, parallelogram shaped specimens were loaded and supported at the corners. For achieving biaxial tension stresses, a circular plate was uniformly loaded concentrically, while being supported uniformly along the periphery.

For all these specimens, the initial invetigation to establish both the precision of the test method and the validity of the theory was performed on an aluminum specimen which was cut into the various required shapes. It was thus shown, after considerable development of the testing technique that the method of test on similarly shaped specimens by previous investigators had been highly erroneous. Furthermore, by having established a satisfactory testing technique, it was then possible to test concrete and mortar specimens with the same test method, having confidence that the results obtained were more accurate.

Although the parallelogram shaped specimens induce biaxial tension-compression states of stress where the tension and compression stresses are different, failure of such specimens will always propagate from that face which has a compression to tension ratio less than or equal to unity. In order to examine the behaviour of concretes and mortars where the compression to tension ratio is greater than unity, while simultaneously ensuring flexural states of stress, parallelogram shaped specimens suitably reinforced to resist the larger induced tensile force were tested.

Following the series of tests on concrete and mortar specimens having the different shapes discussed above, the results are examined in terms of the elasticity values obtained, the stresses and strains at the discontinuity level[14] and the ultimate strengths. For concrete, special consideration is given to interpreting failure in terms of the bond strength at the cement paste aggregate interface and the mechanism by which the bond begins to fail.

PART I

TESTING MACHINE CALIBRATIONS

CHAPTER 2

CALIBRATION TECHNIQUES

2.1 INTRODUCTION

Although British Standard 1610 [8] specifies that testing machines should be calibrated every 24 months, this rule often is not followed. Consequently, when suspect results are obtained, the calibration of the testing machine is called into question. At Imperial College, during 1961-2, a large series of tests was performed on the strength of concrete subjected to various combinations of stress. Unrealistic discontinuities appeared in the failure envelopes. It was thus apparent that either the testing technique was at fault, or the machines' scale readings, or a combination of the two.

The logical first course of action was to investigate the accuracy of the testing machines' scales. This involved an examination of the more common calibration devices and an investigation of the basic standard to which they all refer.

2.2 THE BASIC LOAD CALIBRATION

Measurements of load or force are usually measured in units based on the earth's gravitational pull under defined standard conditions, on a given mass. The international standard acceleration is 980.665cm./sec.^{2};the equivalent in the foot-pound-second system of units may be taken as 32.1740ft./sec^2. Hence, the British technical unit of force is that force which, acting alone, will give to a one pound mass, an acceleration of 32.1740ft./sec.^{2} [15].

The National Physical Laboratory at Teddington houses standard 5 ton-force and 50 ton-force deadweight machines. These weights have been adjusted to allow both for the difference between the acceleration due to gravity at Teddington and the standard acceleration and for air bouyancy. Standardizations thus produced at Teddington are in terms of technical units of force. Plate 2.1 shows a model of the 50 ton force deadweight standard machine which has an accuracy of 1 part in 25,000 throughout its range.

For the measurement of compression loads exceeding 50 tonf. (abbreviation for tons-force), the National Physical Laboratory employs secondary load standards built up from units calibrated in the 50 tonf. deadweight standard machine. The first technique employs the calibration of a 150 tonf. load cell composed of 5 struts each dimensioned for a maximum load of 30 tonf. (see Plate 2.2). In the second technique, three separate load measuring devices are set up so as to share the load applied to a fourth. Plate 2.3 shows a typical set-up where proving rings are employed. N.P.L. uses this method for standardizing its secondary standard load measuring devices up to 1000 tonf. in compression from standards of 50 tonf. capacity. For tension calibrations exceeding 50 tonf., similar methods are employed.

2.3 LOAD CLIBRATION DEVICES

Load calibration devices are used for the verification of the load indication mechanism of materials testing machines with the calibration device being inserted in the testing machine in place of the material specimen. They must consequently be light,

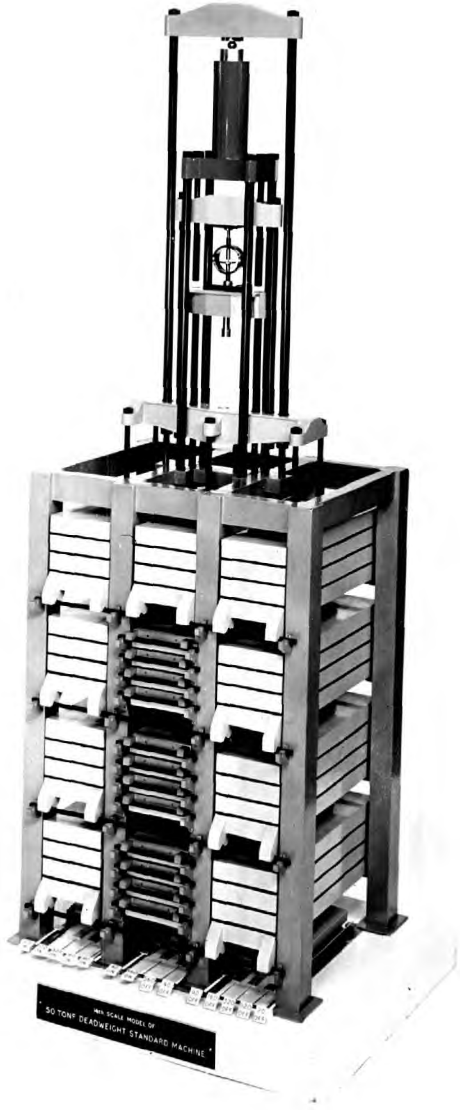

PLATE 2.1 Model of 50 tonf. deadweight machine at the National Physical Laboratory

PLATE 2.2 150 tonf. electrical resistance strain gauge load cell used as a secondary load standard at the National Physical Laboratory

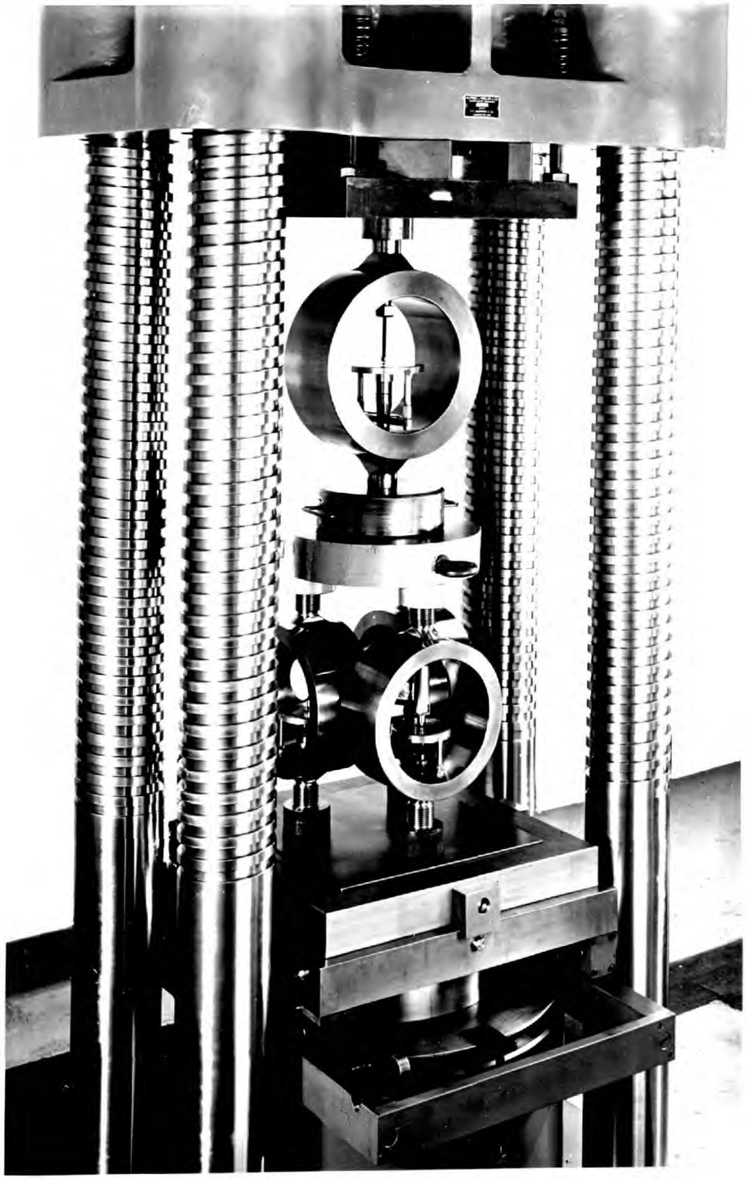

PLATE 2.3 Calibration of a proving ring for use as a secondary load standard

compact, sturdy and accurate. Although the most commonly used devices have been described in detail elsewhere,[15,16,17] a brief review will be presented here.

2.3.1 Proving Rings

The better proving rings are machined from high quality steel to give diametrically opposite loading bosses integral with the ring. The load, either tension or compression, is applied through these loading bosses, thus producing an increase or decrease in length, respectively, between the bosses. These deflexions are usually measured by a micrometer screw or dial gauge mounted within the ring (see Plate 2.4). The less expensive rings have compression loading pads clamped to a plain ring by bolting of the pads to bridge pieces contacting the inner cylindrical surface of the ring. These rings are more susceptible to changes of calibration owing to yielding of the pad or transformation of the line of contact.

The load carrying capacity of proving rings extends from a maximum load of a few hundreds pound-force to about 200 tonf. However, rings having a maximum capacity in excess of 100 tonf. tend to be very bulky and less accurate than other proving devices.

2.3.2 Standardizing Boxes

Basically, the standardizing box is a hollow steel cylinder which is loaded in an axial direction, the load being measured by the change of volume it produces. When loaded, the cylinder changes in length, but the rigid ends severely restrict change in diameter. In order to measure the resulting changes in volume,

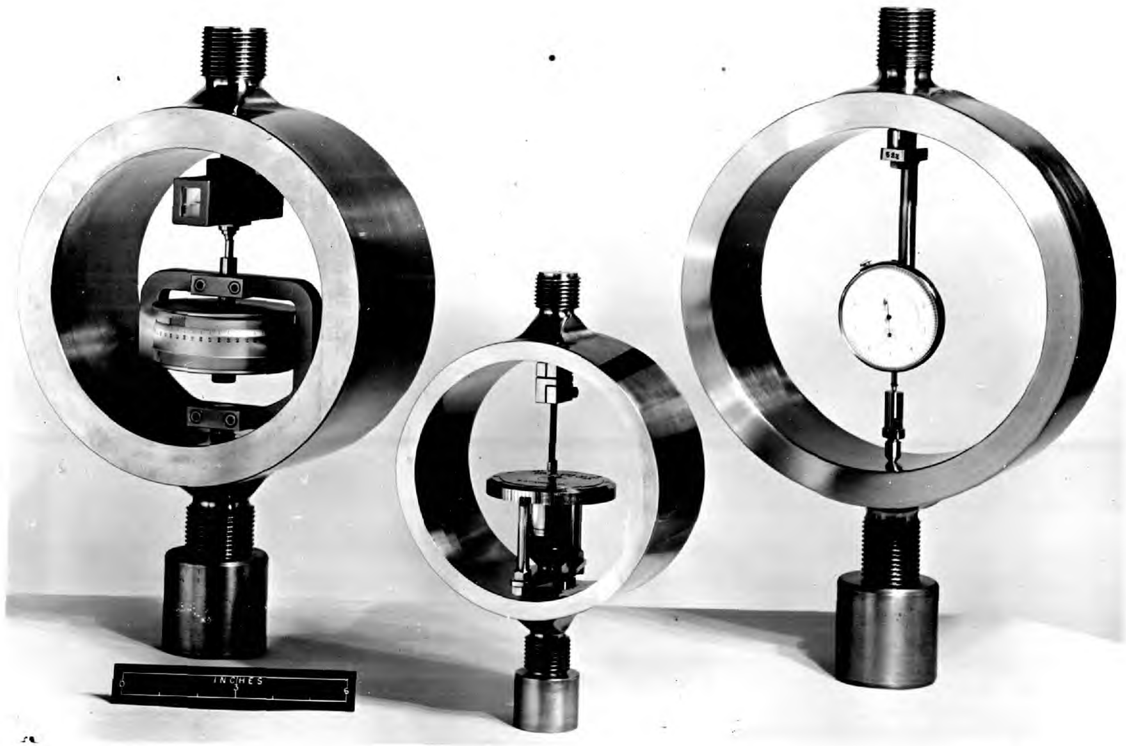

PLATE 2.4 Proving rings

the hollow cylinder is filled with mercury. The fine bore sighting tube seen on the left of Plate 2.5 carries a datum mark and communicates with the cylinder, whilst a small diameter cylindrical plunger attached to a micrometer spindle enters the mercury space from the opposite side of the box. The application of load with its change of volume requires a movement of the micrometer screw in order to maintain the mercury on the datum mark in the sighting tube. These deflexions are calibrated in terms of standard units of force.

Standardizing boxes are made to cover a range of loads from 15 tonf. to 300 tonf. in tension and up to 1000 tonf. in compression.

2.3.3 Electrical Resistance Strain Gauge Load Cells

In its simplest form, the load cell comprises a single strut or tension member to which at least four strain gauges are attached, two laterally and two longitudinally. The strain gauges, which are connected in the form of a Wheatstone bridge circuit, produce resistance changes with loading of the cell. The resulting electrical potential change is measured with a precision potentiometer. Plate 2.2 shows a secondary load cell composed of five individual electrical resistance strain gauge load cells.

These load cells may be designed to have a maximum capacity ranging from a few tonf. to 1000 tonf. or more in compression, and up to 500 tonf. in tension.

2.3.4 Hydrostatic Load Capsules

In this principle, the load is converted into a pressure

PLATE 2.5 Standardizing load cell

acting over the cross-sectional area of a ram. The pressure, which is measured by means of a Bourdon tube gauge, thus, indicates the load.

Hydrostatic load capsules are used mainly for the measurement of compressive loads ranging from a few hundred pounds force to a thousand tonf.

2.3.5 The Four Strut Mechanical Load Cell

The most recent calibration device, which was developed at the National Physical Laboratory, consists essentially of a steel cylinder machined from the solid, to incorporate four load carrying struts.[16,17] The load on the instrument is determined by the average shortening produced in the struts. This load is measured by a dial gauge, operated by a lever mechanism giving a 4:1 magnification(see Plate 2.6).

At present, the N.P.L. has developed 50 tonf., 150 tonf., 250 tonf., and 500 tonf. maximum capacity load cells for calibration in compression only.

2.4 CALIBRATION PROCEDURE

In general, the calibration of one instrument by another requires the basic instrument to be approximately five times as accurate as the secondary one, that is, the one being calibrated. For example, when calibrating a proving device in the N.P.L. deadweight machine, the former can be checked for accuracy to a limit of about 1 in 5,000, as the latter has an accuracy of 1 in 25,000.

PLATE 2.6

Four strut mechanical load cell

Internal components of four strut mechanical load cell

2.4.1 Calibration Instruments

At any load stage, the quality or accuracy of a proving device is determined by its sensitivity and repeatability, on the basis of the maximum difference in load indication from three loadings. In a Grade 1 calibration instrument, this above difference expressed as a percentage of the applied load, does not exceed 0.2% at loads below 50 tonf. and 0.4% at loads between 50 tonf. and 500 tonf. For a Grade 2 device, these values are 0.4% and 0.6%, respectively. There is also a requirement for change in no-load readings as shown in B.S. 1610.(8)

It is usually more convenient to have a calibration instrument which can be used for verification at random loads, particularly when verifying machines with standard pressure gauges instead of load gauges(see Chapter 3). Proving devices for such calibrations must conform to a linearity grading. After loading the device three times to at least eight points uniformly distributed over the calibration range, and drawing the best smooth curve through the calibration graph(see Figures 3.1 and 3.3), the linearity grading is then determined as follows. At any load up to 50 tonf., the departure from linearity shall not be greater than ±0.1% for a Grade 1 instrument, and ±0.2% for a Grade 2 device. For loads in excess of 50 tonf., the above limits are ±0.3% and ±0.4%, respectively.

2.4.2 Testing Machines

As with proving devices, testing machines are graded according to their repeatability. However, as most testing machines have a load indicating scale, the grading of a testing machine is based on both accuracy and repeatability. Again, the basic instrument, which, in this case, is the calibration device, must be at least five times as accurate as the secondary instrument, which, in this instance, is the testing machine.

The calibration is performed by setting the calibration instrument in the testing machine with the load applied along the loading axis of the machine. The calibration is performed three times with at least five test loads uniformly distributed over the range of the testing machine scale.

For all scale ranges, two Grades, A and B, are recognized. However, where additional precision is required, a third grading, A_1 is also used for loads not exceeding 50 tonf.

For Grade A machines, verified with Grade 1 proving devices only, the maximum permissible difference between the highest and lowest readings in relation to the verification load shall be 1.0% in the upper 80% of the machine scale range whereas the accuracy of the machine's indicated load, in this same range, shall be within ±1.0%. In the lower 20% of the scale range, the repeatability and accuracy requirements, expressed in terms of the machine scale full load reading shall be 0.2% and ±0.2%, respectively. For Grade A_1 and B machines, all the above limits shall be halved and doubled, respectively. For example, in the upper 80% of the scale range, the requirements for repeatability of a Grade A_1 machine is 0.5% while that for accuracy is ±0.5%. A Grade B machine may be calibrated with either a Grade 1 or 2 calibration instrement.

2.5 CALIBRATION DEVICES FOR DEPARTMENT OF CONCRETE TECHNOLOGY, IMPERIAL COLLEGE

TABLE 2.1 TESTING MACHINES IN CONCRETE DEPARTMENT, IMPERIAL COLLEGE

Testing Machine	Function	Maximum Capacity	Usual Working Range
Denison Compression	Compression tests on cubes, cylinders and prisms	200 tonf.	20 tonf. to 150 tonf.
Denison Compression	Splitting tensile test	40 tonf.	10 tonf. to 40 tonf.
Amsler Compression	Compression tests on cubes, cylinders and prisms	300 tonf.	5 tonf. to 250 tonf.
Uniaxial Compression	Strength and deformation tests on prisms	50 tonf.	5 tonf. to 50 tonf.
Robinson Compression	Biaxial compression	200 tonf.	10 tonf. to 200 tonf.
Ward Tension	Direct tension	4 tonf.	0.5 tonf. to 4 tonf.
Flexural	Flexural tests on beams 4" x 4" x 20"	2 tonf.	0.5 tonf. to 2 tonf.
Biaxial Flexural	Slab tests	3.5 tonf.	0.5 tonf. to 3.5 tonf.
Biaxial Flexural	Disc tests	14 tonf.	1 tonf. to 10 tonf.

It will be observed, from Table 2.1, that the working range of all the testing machines extends continuously from 0.5 tonf. to 250 tonf. A calibration device generally contains the necessary repeatability to be in accordance with British Standard 1610, only in the upper 80 to 90% of its working range. Consequently, for verification devices to be used to cover the full range above, a minimum of three was required. It was, furthermore, considered necessary that these devices should be capable of producing Grade 1 repeatability over the full range of loads mentioned above, as it is important that all testing machines used in a laboratory for research purposes be of at least Grade A quality.

Two alternatives presented themselves to the department;
(1) to own the calibration devices and to have these calibrated every two years at the N.P.L., or
(2) to have a qualified body come to verify the testing machines every two years.
After considering such factors as convenience, economy, availability of equipment and probable repeatability of existing equipment, it was considered most suitable to have the necessary calibration devices which would be calibrated by the N.P.L. every two years. The devices recommended were:
(1) 5 tonf. tension-compression proving ring No. 383(see calibration curve, Figure3.1)
(2) 50 tonf. compression proving ring No. 343(see calibration curve, Figure 3.3)
(3) 250 tonf. four strut mechanical load cell.

The above mentioned 5 tonf. and 50 tonf. proving rings owned by the Civil Engineering Department, Imperial College, were manufactured integral with the loading bosses from high quality steel. The 5 tonf. ring also contains the necessary assembly units for tension calibration. It was considered that these rings would be Grade 1 calibration devices over the upper 80% and probably, the upper 90% of their working ranges.

As the 250 tonf. four strut mechanical load cell can be manufactured with Grade 1 repeatability over the upper 90% of its working range, and is also inexpensive to manufacture, it was selected as the third calibration instrument.

CHAPTER 3

CALIBRATION OF TESTING MACHINES IN CONCRETE TECHNOLOGY DEPARTMENT.

3.1 CALIBRATION OF THE PROVING DEVICES

3.1.1 Five Tonf. Calibration Ring No. 383

The 5 tonf. tension-compression ring was sent to the National Physical Laboratory for calibration. The ring had Grade 1 repeatability over the upper 90% of its working range in both tension and compression. The calibration values corrected for a standard temperature of 20°C are presented in Table 3.1 and the calibration graphs are shown in Figure 3.1.

In order to satisfy the linearity requirement in British Standard 1610, the maximum allowable deviation between the best smooth curve and any plotted point shall not exceed ±0.1% for loads up to 50 tonf. From Figure 3.1, it is observed that, for both tension and compression calibration, this requirement is satisfied. Consequently, this ring can be used for calibration at all load values between 1000 and 10000 lbsf. and not only at the calibrated loads (as would have been the case if the requirement of linearity had not been satisfied). This is of particular importance for the calibrations conducted on the testing machines at Imperial College Concrete Technology Department as almost all have pressure gauges instead of load gauges. The load corresponding to a specified number of increments on the gauge therefore is generally random.

TABLE 3.1 CALIBRATION VALUES IN TENSION AND COMPRESSION FOR CALIBRATION RING NO. 383

APPLIED LOAD (LBSF)	COMPRESSION CALIBRATION RING DEFLECTION (DIVS.) TEST 1	TEST 2	TEST 3	AVERAGE	LOAD DEPL.	TENSION CALIBRATION RING DEFLECTION TEST 1	TEST 2	TEST 3	AVE.	LOAD DEPL.
1,000	101.4	101.3	101.3	101.3	9.872	99.7	99.8	99.7	99.7	10.030
2,000	202.8	202.7	202.8	202.8	9.862	199.9	199.9	199.8	199.9	10.005
3,000	304.3	304.2	304.2	304.2	9.862	300.1	300.1	300.2	300.1	9.997
4,000	407.1	407.0	407.1	407.1	9.825	400.2	400.2	400.2	400.2	9.995
5,000	509.5	509.5	509.5	509.5	9.814	500.8	500.8	501.0	500.9	9.982
6,000	612.9	612.8	612.8	612.8	9.796	599.8	599.8	599.9	599.8	10.003
7,000	716.8	716.5	716.6	716.6	9.768	698.4	698.2	698.5	698.4	10.023
8,000	820.1	820.0	820.1	820.1	9.755	796.7	796.6	796.7	796.7	10.041
9,000	924.2	924.1	924.1	924.1	9.739	894.1	894.0	894.3	894.1	10.066
10,000	1029.5	1029.3	1029.2	1029.3	9.715	991.9	991.8	992.0	991.9	10.082

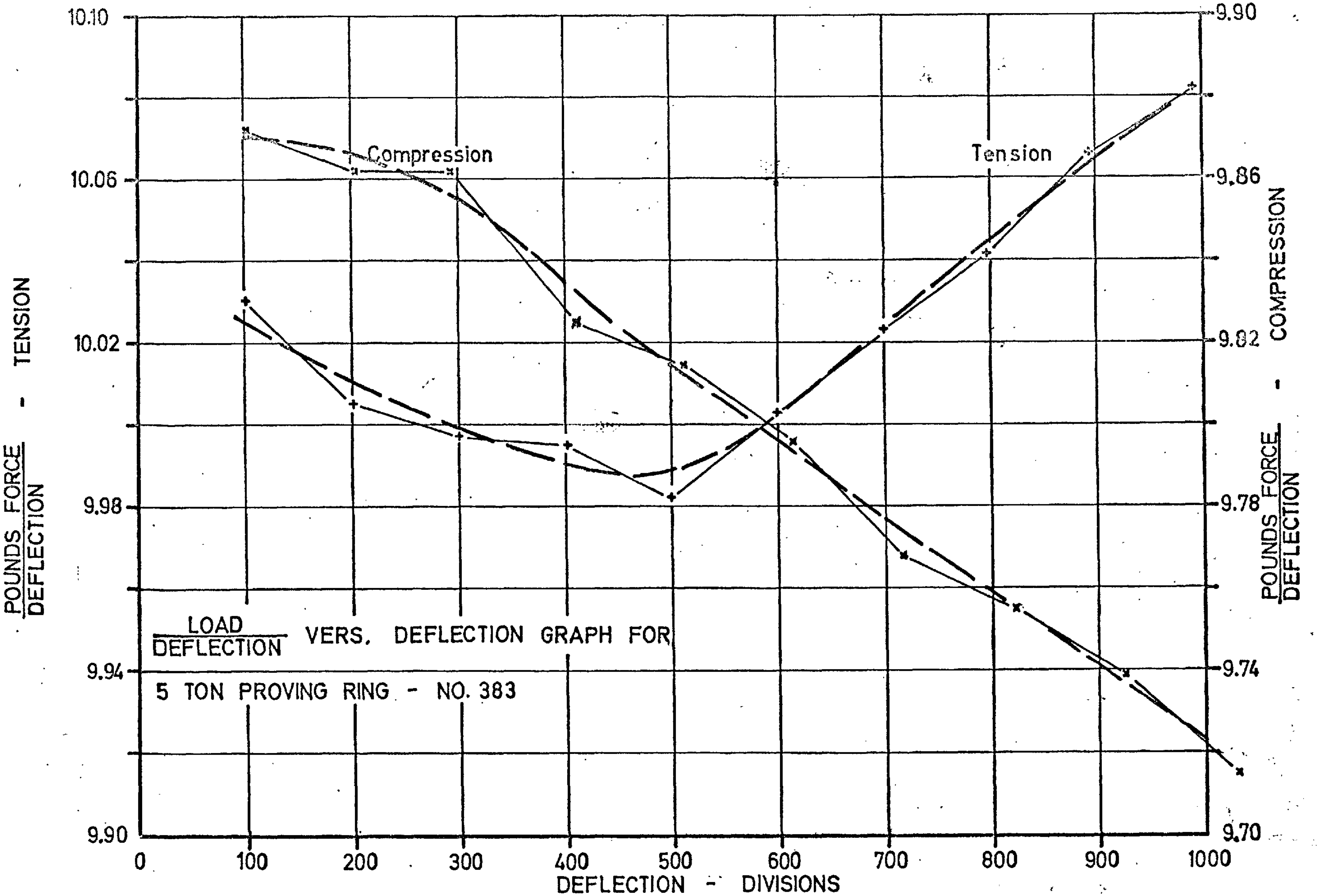
Compression
Tension
LOAD / DEFLECTION VERS. DEFLECTION GRAPH FOR
5 TON PROVING RING - NO. 383
POUNDS FORCE / DEFLECTION - TENSION
POUNDS FORCE / DEFLECTION - COMPRESSION
DEFLECTION - DIVISIONS
10.10
10.06
10.02
9.98
9.94
9.90
9.70
9.74
9.78
9.82
9.86
0
100
200
300
400
500
600
700
800
900
1000

FIG. 3.1

3.1.2 Fifty Tonf. Calibration Ring NO. 343

The calibration of the 50 tonf. compression ring was performed against a 50 tonf. electrical resistance strain gauge load cell owned by the National Physical Laboratory, who had kindly lent the device to Imperial College. The cell had been calibrated to 50 tonf. in 5 tonf. increments in the 50 tonf. deadweight calibration machine. It was a Grade 1 calibration device throughout its entire range with a repeatability of 1 part in 2000 at 5 tonf. and 1 part in 5000 at 50 tonf. In calibrating one device against another, the National Physical Laboratory considers that the basic calibration device should be 5 times as repeatable as the instrument receiving calibration. As proving rings with dial gauges are generally repeatable to 1 part in 1000 in the upper range and 1 part in 500 over the lower range, this procedure was considered satisfactory.

3.1.2.1 Method of calibration

The calibration by H. Ward and the author was performed by placing the load cell on top of the proving ring in a 200 tonf. Class A Avery testing machine (see Plate 3.1). The 50 tonf. range on the machine was selected. After carefully centering the instruments in the machine, they were loaded to 55 tonf. 5 times over a period of approximately 15 minutes. After allowing 2 minutes for adiabatic cooling of the proving ring, the temperature was noted and the calibration commenced.

The instruments were loaded in 5 tonf. increments to 50 tonf. At each load stage, the load was held constant while the

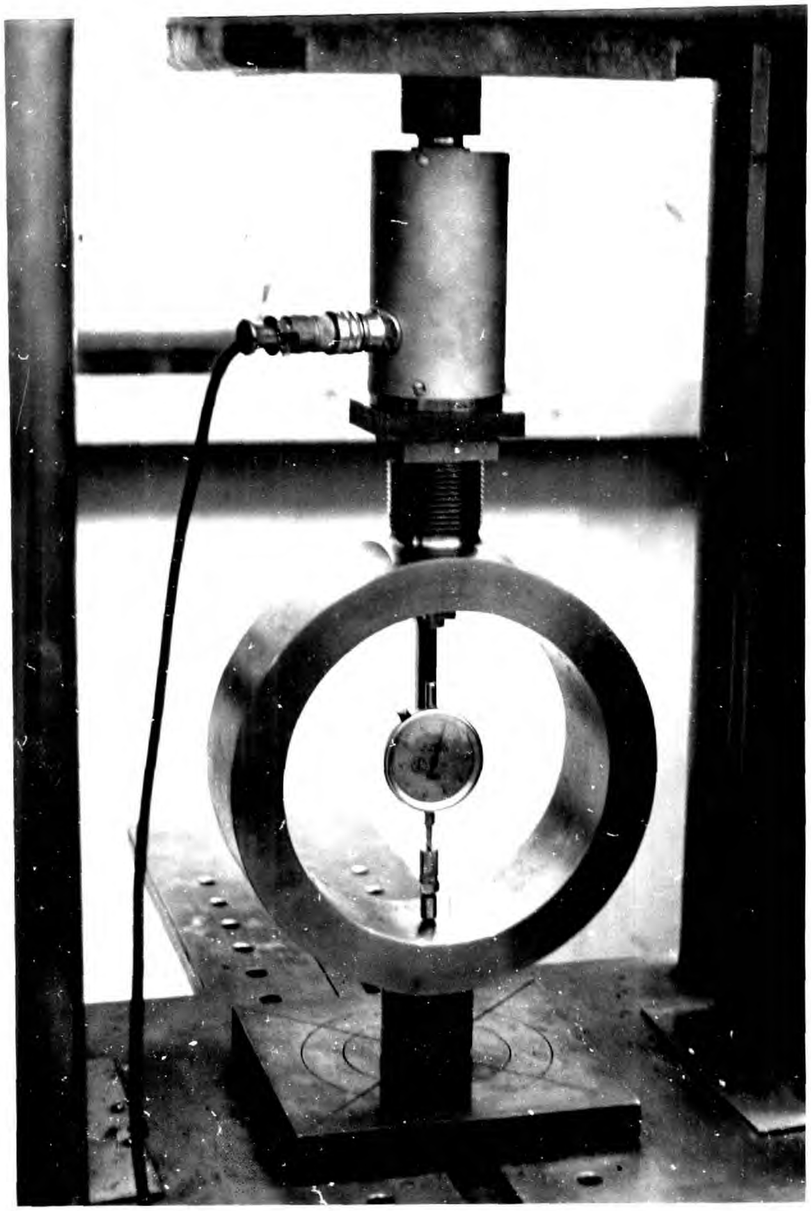

PLATE 3.1 Calibration of proving ring against the N.P.L. 50 tonf. electrical resistance strain gauge load cell

reading on the two devices were recorded. This procedure was repeated 3 times, allowing 2 minutes between each series of readings for temperature stabilization of the proving ring. The temperature was also recorded between each series of readings.

Although every effort was made to keep the load constant, there tended to be a small drift in the load at each load stage. As it was impossible to read both devices accurately simultaneously, the procedure of reading the load cell potentiometer before and after the proving ring dial gauge was adopted. The proving ring force corresponding to its dial gauge reading was then assumed to be equal to the load cell force correspondint to the average of the two potentiometer readings.

The dial gauge was tapped lightly before each reading to overcome any sticking of the pointer.

3.1.2.2 Results of calibration

The calibration graph of the 50 tonf. load cell is shown in Figure 3.2 while that of the 50 tonf. proving ring No. 343 is shown in Figure 3.3. The data for these calibrations is presented in Table 3.2

In accordance with British Standard 1610, the proving ring has Grade 1 repeatability from 20 tonf. to 50 tonf. and Grade 2 repeatability from 10 tonf. to 15 tonf. It satisfies linearity requirements over the range 25 tonf. to 50 tonf.

TABLE 3.2 CALIBRATION VALUES FOR N.P.L. 50 TONF. ELECTRICAL RESISTANCE STRAIN GAUGE LOAD CELL AND 50 TONF. CALIBRATION RING NO. 343

Calibration for N.P.L. 50 tonf. Load Cell			Calibration for 50 Tonf. Proving Ring No. 343			
Applied Load (lbsf.)	Defl. (divs)	Load(lbsf.) / Defl. (divs.)	N.P.L. Load Cell Read.	Load (lbsf.)	Defl. (divs.) (20°C.)	Load(lbsf.) / Defl.(divs.)
			Test No. 1			
11,200	5,401	2.07369	5,417	11,233	72.5	154.94
22,400	10,798	2.07446	10,734	22,267	144.9	153.67
33,600	16,216	2.07203	16,257	33,685	218.4	154.24
44,800	21,644	2.06986	21,729	44,976	290.4	154.88
56,000	27,051	2.07016	27,000	55,894	362.2	154.32
67,200	32,397	2.07427	32,488	67,389	436.3	154.46
78,400	37,792	2.07451	37,738	78,288	506.5	154.57
89,600	43,204	2.07388	43,196	89,583	580.1	154.43
100,800	48,603	2.07395	48,629	100,854	654.7	154.05
112,000	54,024	2.07315	54,086	112,128	278.0	154.02
			Test No. 2			
			5,311	11,013	71.4	154.24
			10,752	22,305	145.2	153.62
			16,156	33,476	217.3	154.05
			21,609	44,728	289.0	154.77
			27,042	55,981	362.6	154.39
			32,461	67,353	436.0	154.43
			37,771	78,356	507.0	154.55
			43,176	89,542	580.1	154.36
			48,636	100,869	654.5	154.12
			54,063	112,081	728.0	154.96
			Test No. 3			
			5,402	11,202	72.5	154.51
			10,804	22,412	145.8	153.72
			16,166	33,496	217.4	154.08
			21,631	44,773	289.3	154.76
			27,089	56,079	363.3	154.36
			32,443	67,296	436.0	154.35
			37,821	78,460	508.0	154.45
			43,283	89,764	581.6	154.34
			48,661	100,920	655.2	154.03
			54,002	111,954	727.2	153.95

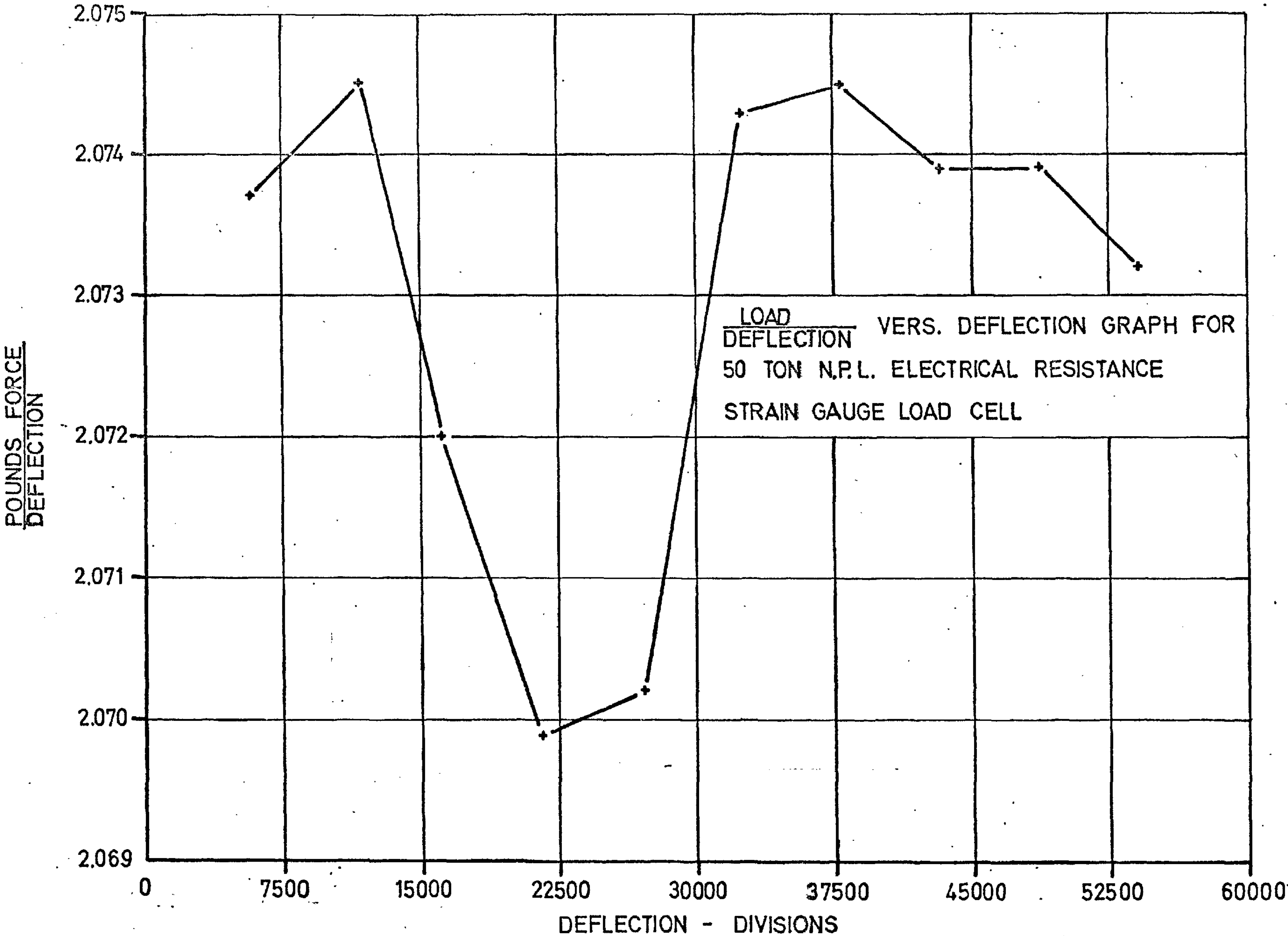
LOAD / DEFLECTION VERS. DEFLECTION GRAPH FOR
50 TON N.P.L. ELECTRICAL RESISTANCE
STRAIN GAUGE LOAD CELL
POUNDS FORCE / DEFLECTION
2.075
2.074
2.073
2.072
2.071
2.070
2.069
0
7500
15000
22500
30000
37500
45000
52500
60000
DEFLECTION - DIVISIONS

FIG. 3.2

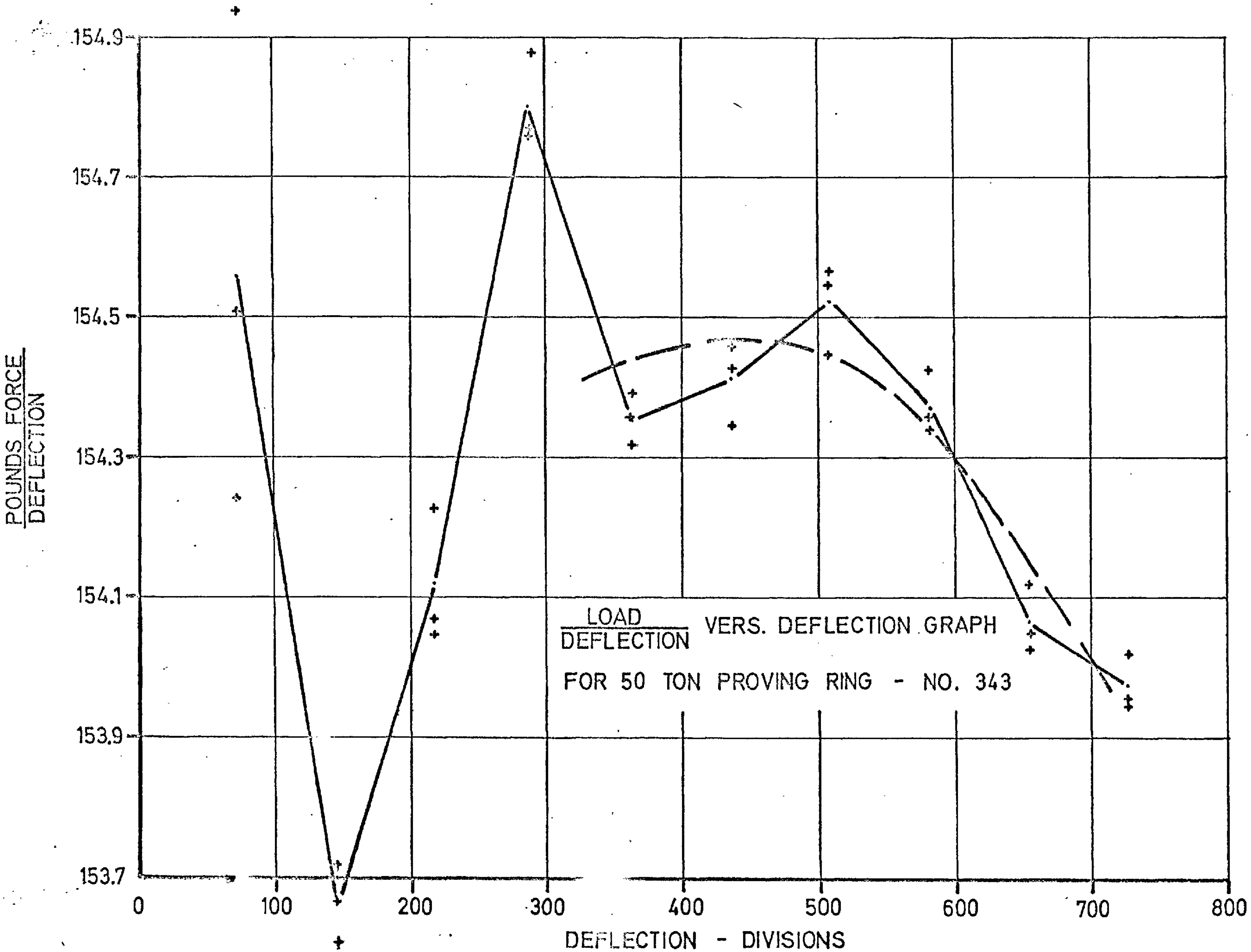

POUNDS FORCE / DEFLECTION
154.9
154.7
154.5
154.3
154.1
153.9
153.7
0
100
200
300
400
500
600
700
800
DEFLECTION - DIVISIONS
LOAD / DEFLECTION VERS. DEFLECTION GRAPH
FOR 50 TON PROVING RING - NO. 343

FIG. 3.3

3.1.3 150 Tonf. Four Strut Mechanical Load Cell

Although a 250 tonf. four strut mechanical load cell was selected as the third calibration device, it was not manufactured at the time of these calibrations. In its place, the National Physical Laboratory had very kindly lent its 150 tonf. four strut mechanical load cell which proved suitable for the Denison compression machine. It is seldom used in excess of 150 tonf. The other machines to be used above 150 tonf. (see Table 2.1) were not a part of the laboratory equipment at the time of these calibrations.

The load cell calibration values are given in Table 3.3 and its graph is shown in Figure 3.4. It had Grade 1 repeatability from 20 tonf. to 150 tonf. and Grade 2 repeatability at 10 tonf. As the Denison is to be calibrated at the same load stages as the load cell, the requirement for linearity was not necessary.

TABLE 3.3 CALIBRATION VALUES FOR 150 TONF. FOUR STRUT MECHANICAL LOAD CELL

Load (tonf.)	Load (lbsf.)	Deflection (divs)	Load (lbsf.) / Defl. (divs)
10	22,400	60.0	373.33
20	44,800	122.0	367.21
30	67,200	181.2	370.86
40	89,600	242.3	369.79
50	112,000	302.6	370.13
60	134,400	363.0	370.25
70	156,800	424.6	369.29
80	179,200	483.7	370.48
90	201,600	545.5	369.57
100	224,000	605.0	370.25
110	246,400	665.4	370.30
120	268,800	727.6	369.43
130	291,200	788.1	369.50
140	313,600	849.8	369.03
150	336,000	910.5	369.03

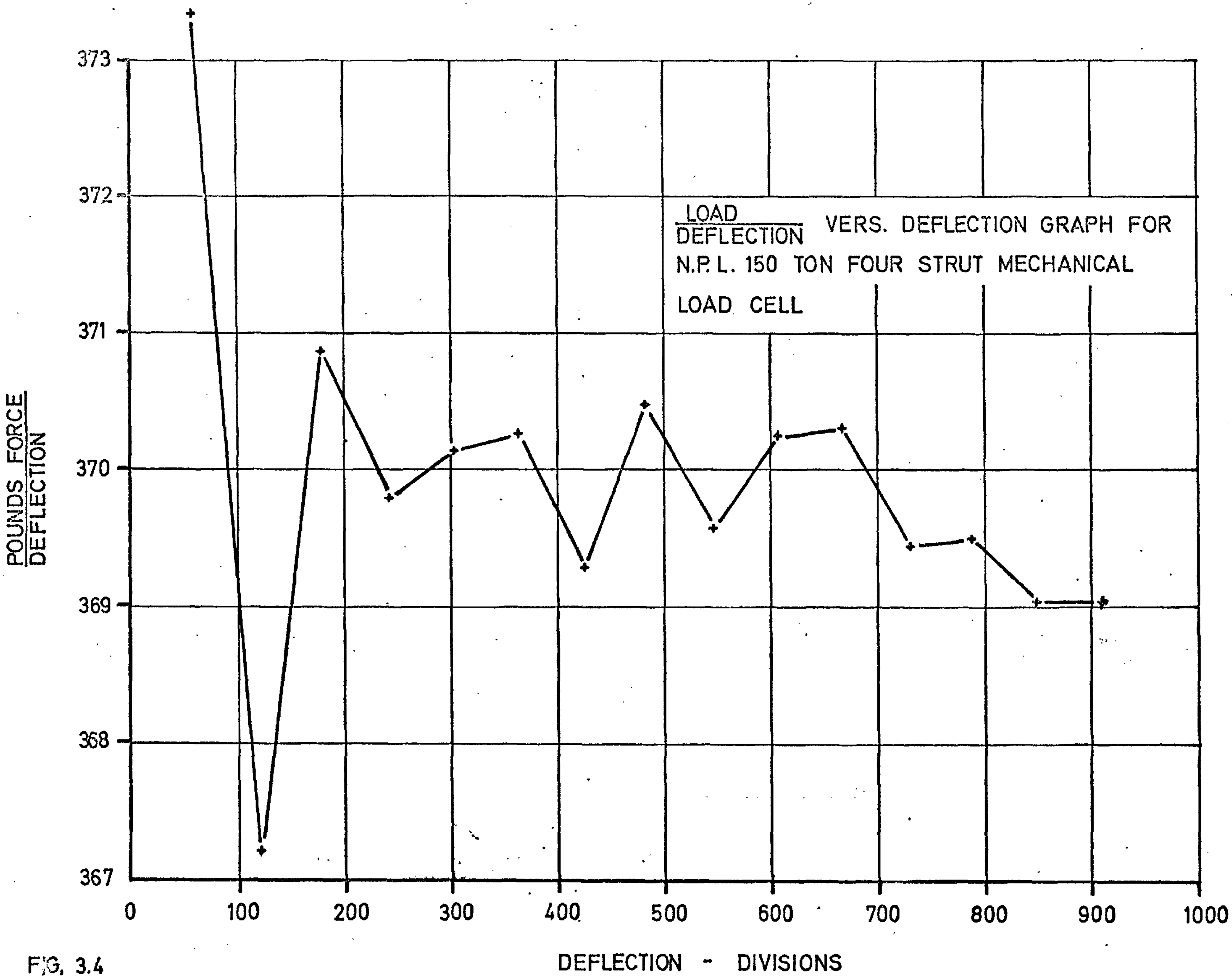

LOAD / DEFLECTION VERS. DEFLECTION GRAPH FOR
N.P.L. 150 TON FOUR STRUT MECHANICAL
LOAD CELL
POUNDS FORCE / DEFLECTION
373
372
371
370
369
368
367
0
100
200
300
400
500
600
700
800
900
1000
DEFLECTION - DIVISIONS

FIG. 3.4

3.2 PROCEDURE FOR CALIBRATING THE TESTING MACHINES

The calibration device was inserted in the testing machine in place of the material specimen with particular care given to centring the instrument. It was then loaded to the maximum calibration load five times and the room temperature recorded after the last loading. A two minute interval was allowed for adiabatic cooling of the device before commencing the calibration. An exception was made in this procedure when using the 50 tonf. electrical resistance strain gauge load cell. As this device was temperature compensated, no time interval was necessary.

While one person loaded the calibration device to each of the prearranged testing machine scale divisions, a second person read the proving device. At least ten points, linearly distributed, were selected over the normal working range of the testing machine scale except in the case of the biaxial flexural machine 4,000 p.s.i. gauge where only seven points were selected. The calibration method conformed strictly to British Standard 1610 specifications.

The requirement for accuracy as stated in British Standard 1610 does not strictly apply to machines which have a pressure gauge. The load corresponding to any random pressure will be calculated from the calibration value obtained from the best smooth curve through the calibration points (see Figures 3.6 to 3.9). The maximum deviation from this smooth curve is then analogous to the maximum error, as defined in B.S. 1610. The accuracy of the machine is thereby obtained by examining this deviation in terms of the accuracy requirements for different gradings.

As the proving device calibrations are for a standard temperature of 20°C., all deflection values as given in Tables 3.4 to 3.9 are corrected to this temperature.

3.3 TESTING MACHINE CALIBRATIONS

3.3.1. Denison Compression Machine 200 Tonf. Scale (March, 1963)

This machine contains 3 load gauges, all of which are connected to the hydraulic system. The central and top gauges are of 200 tonf. capacity while the bottom one is of 40 tonf. capacity (see Section 3.3.2). Of the upper two gauges, only the lower, with its accompanying maximum load indicator, was calibrated. This was considered adequate as the top gauge is seldom used, and the lower one is never used without the load indicator.

The 150 tonf. four strut mechanical load cell was loaded in 10 tonf. increments to 150 tonf. The calibration graph, Figure 3.5 and Table 3.4 shows that the machine has Grade B repeatability over its full range, and Grade B accuracy over the range 40 tonf. to 150 tonf. Below 40 tonf., its accuracy falls outside the limits considered in British Standard 1610.

3.3.2 Denison Compression Machine 40 Tonf. Scale (March, 1963)

The 50 tonf. electrical resistance strain gauge load cell belonging to the National Physical Laboratory was used for this calibration (see Figure 3.2 for the calibration graph of this).

TABLE 3.4 CALIBRATION VALUES FOR DENISON COMPRESSION MACHINE 200 TONF. SCALE

Indicated Load (tonf.)	Load Cell Read. (divs.)	Load(lbsf.) Defl. (divs)	Load Tonf.	Load(tonf.) Indicated Load(tonf.)	Average
10	53.2	373.33	8.87	0.887	0.880
20	116.1	367.21	19.03	0.952	0.946
30	174.7	370.86	28.92	0.964	0.973
40	240.5	369.79	39.70	0.993	0.991
50	301.3	370.13	49.78	0.996	0.998
60	365.3	370.25	60.38	1.006	1.008
70	422.8	369.29	69.70	0.998	0.999
80	489.8	370.48	81.00	1.013	1.011
90	547.5	369.57	90.33	1.004	1.006
100	609.3	370.25	100.71	1.007	1.007
110	670.1	370.30	110.77	1.007	1.008
120	731.1	369.43	120.57	1.005	1.006
130	799.7	369.50	131.91	1.015	1.015
140	859.9	369.03	141.66	1.012	1.013
150	927.9	369.03	152.86	1.019	1.019
10	51.4	373.33	8.57	0.857	
20	114.2	367.21	18.72	0.936	
30	177.1	370.86	29.32	0.972	
40	239.6	369.79	39.55	0.989	
50	301.1	370.13	49.75	0.995	
60	365.7	370.25	60.44	1.007	
70	422.5	369.29	69.65	0.995	
80	489.7	370.48	80.99	1.012	
90	549.1	369.57	90.59	1.007	
100	609.8	370.25	100.79	1.008	
110	671.8	370.30	111.05	1.010	
120	733.7	369.43	121.00	1.008	
130	800.3	369.50	132.00	1.015	
140	860.1	369.03	141.69	1.012	
150	927.8	369.03	152.84	1.019	
10	53.8	373.33	8.97	0.897	
20	115.9	367.21	19.00	0.950	
30	177.1	370.86	29.32	0.972	
40	240.4	369.79	39.68	0.992	
50	303.9	370.13	50.21	1.004	
60	366.5	370.25	60.58	1.010	
70	425.8	369.29	70.19	1.003	
80	487.8	370.48	80.67	1.008	
90	549.5	369.57	90.65	1.007	
100	609.2	370.25	100.69	1.007	
110	670.2	370.30	110.79	1.007	
120	730.7	369.43	120.50	1.004	
130	799.6	369.50	131.89	1.015	
140	859.6	369.03	141.61	1.012	
150	927.6	369.03	152.81	1.019	

TABLE 3.5 CALIBRATION VALUES FOR DENISON COMPRESSION MACHINE 40 TON SCALE

Indicated Load (tonf.)	Load Cell Read. (divs.)	Load(lbsf.) / Defl. (divs.)	Load (tonf.)	Load(tonf.) / Indicated Load(tonf.)	Average
6	4,601	2.0740	4.260	0.700	0.704
9	7,193	2.0739	6.659	0.740	0.742
12	9,764	2.0743	9.041	0.753	0.756
15	12,359	2.0738	11.445	0.763	0.761
18	14,885	2.0726	13.772	0.765	0.763
21	17,565	2.0715	16.243	0.774	0.769
24	20,099	2.0705	18.577	0.774	0.773
27	23,005	2.0700	21.304	0.789	0.783
30	25,453	2.0701	23.521	0.784	0.783
33	27,950	2.0709	25.839	0.783	0.783
36	30,376	2.0727	28.105	0.781	0.783
39	33,436	2.0743	30.961	0.794	0.792
6	4,531	2.0740	4.195	0.699	
9	7,191	2.0739	6.657	0.740	
12	9.808	2.0743	9.082	0.757	
15	12,302	2.0738	11.389	0.759	
18	14,941	2.0726	13.824	0.768	
21	17,452	2.0715	16.138	0.768	
24	20,052	2.0705	18.534	0.772	
27	22,938	2.0700	21.196	0.785	
30	25,416	2.0701	23.487	0.783	
33	27,892	2.0709	25.785	0.781	
36	30,620	2.0727	28.331	0.787	
39	33,143	2.0743	30.690	0.787	
6	4,622	2.0740	4.279	0.713	
9	7,243	2.0739	6.705	0.745	
12	9,828	2.0743	9.100	0.758	
15	12,320	2.0738	11.405	0.760	
18	14,728	2.0726	13.626	0.757	
21	17,352	2.0715	16.046	0.764	
24	20,070	2.0705	18.550	0.773	
27	22,660	2.0700	20.939	0.775	
30	25,432	2.0701	23.502	0.783	
33	27,984	2.0709	25.870	0.784	
36	30,445	2.0727	28.169	0.783	
39	33,475	2.0743	30.997	0.795	

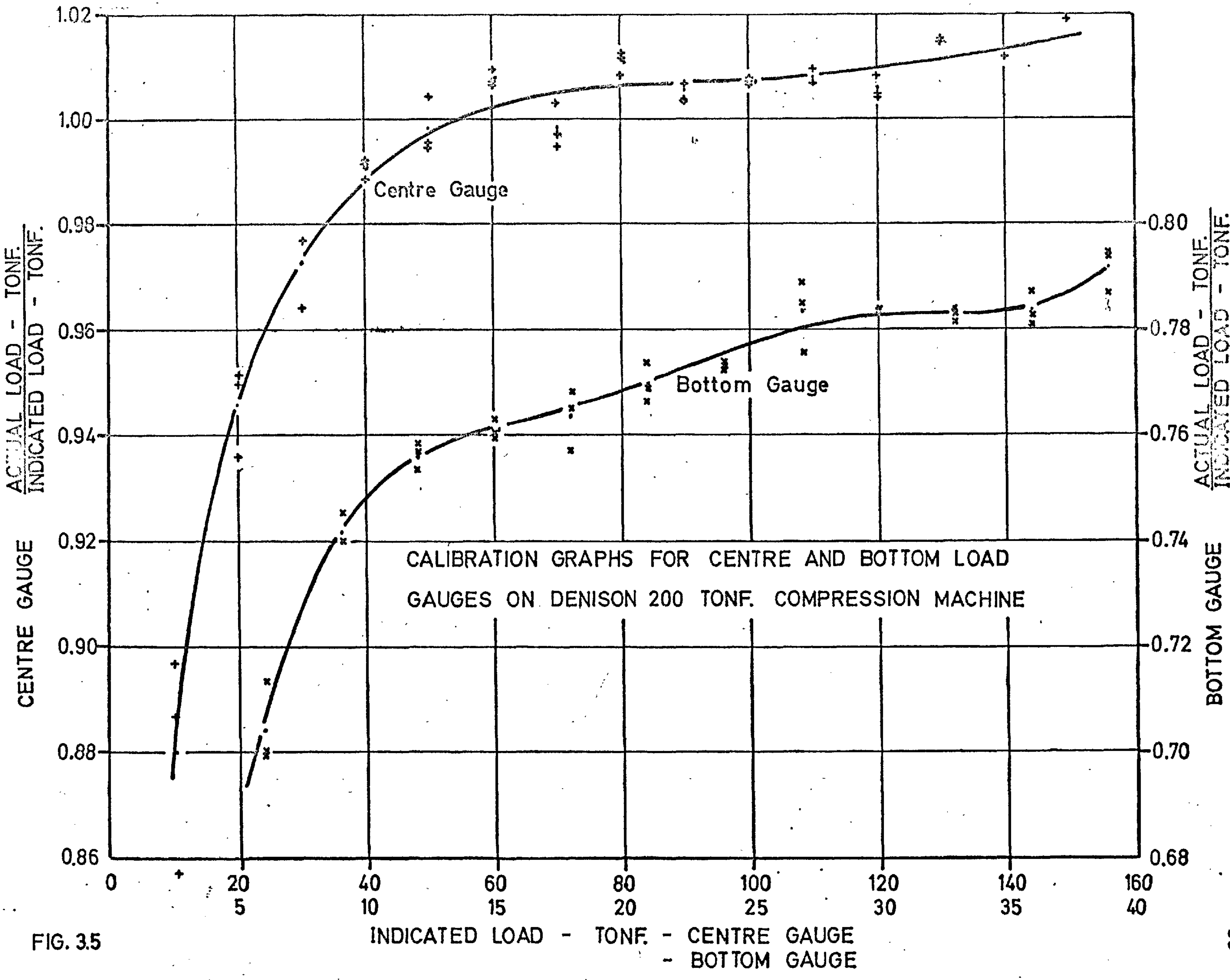
1.02
1.00
0.98
0.96
0.94
0.92
0.90
0.88
0.86
0.80
0.78
0.76
0.74
0.72
0.70
0.68
Centre Gauge
Bottom Gauge
CALIBRATION GRAPHS FOR CENTRE AND BOTTOM LOAD GAUGES ON DENISON 200 TONF. COMPRESSION MACHINE
CENTRE GAUGE ACTUAL LOAD - TONF. / INDICATED LOAD - TONF.
BOTTOM GAUGE ACTUAL LOAD - TONF. / INDICATED LOAD - TONF.
0
20
40
60
80
100
120
140
160
5
10
15
20
25
30
35
40
INDICATED LOAD - TONF. - CENTRE GAUGE
- BOTTOM GAUGE

FIG. 3.5

Twelve calibration points at 3 tonf. increments were selected from 6 tonf. to 39 tonf. inclusive.

The calibration values from Table 3.5 and the accompanying graph, Figure 3.5 shows the inaccuracy to be about 22%. This is outside the bounds of accuracy as expressed in British Standard 1610. Although the repeatability is Grade B, the dial gauge is completely unacceptable for accuracy requirements.

3.3.3 50 Tonf. Uniaxial Compression Machine (March, 1963)

The calibration at 500 p.s.i. increments to 5,000 p.s.i. was performed with the N.P.L. 50 tonf. electrical resistance strain gauge load cell. The calibration graph, Figure 3.6 and Table 3.6 shows that the machine has both Grade A repeatability and accuracy.

3.3.4 Ward Tension Machine (November, 1963)

The 5 tonf. proving ring No. 383 was positioned in the testing machine with assembly units for transmitting tension to the ring being cast into 4 inch cubes which fitted accurately into the grips of the testing machine.(2) The load indication was performed with 2 Budenberg pressure gauges, a 400 p.s.i. one, No. 8736305 and a 1500 p.s.i. one, No. 8742425. These were calibrated over their normal working ranges; the 400 p.s.i. gauge in 100 p.s.i. increments to 300 p.s.i. and the 1500 p.s.i. gauge in 100 p.s.i. increments from 300 p.s.i. to 1200 p.s.i. inclusive.

On observing Figure 3.7 and Table 3.7, it can be seen

TABLE 3.6 CALIBRATION VALUES FOR 50 TONF. UNIAXIAL COMPRESSION MACHINE

Gauge Pressure (p.s.i.)	Load Cell Read. (divs.)	Load(lbsf.) / Defl. (divs.)	Load (lbsf.)	Load(lbsf.) / Gauge Pressure - 35	Average
500	4875	2.074	10111	21.744	21.696
1000	10126	2.0744	21005	21.767	21.735
1500	15403	2.0724	31921	21.789	21.751
2000	20671	2.0703	42795	21.779	21.796
2500	25984	2.0701	53789	21.821	21.770
3000	31231	2.0734	64754	21.839	21.797
3500	36395	2.0744	75498	21.789	21.797
4000	41654	2.0741	86395	21.789	21.774
4500	46976	2.0739	97424	21.819	21.805
5000	52058	2.0734	107937	21.740	21.740
500	4837	2.074	10032	21.574	
1000	10106	2.0744	20964	21.724	
1500	15359	2.0724	31830	21.727	
2000	20716	2.0703	42888	21.826	
2500	25902	2.0701	53620	21.753	
3000	31178	2.0734	64644	21.802	
3500	36584	2.0744	75890	21.902	
4000	41617	2.0741	86318	21.770	
4500	46977	2.0739	97426	21.820	
5000	52051	2.0734	107923	21.737	
500	4881	2.074	10123	21.770	
1000	10101	2.0744	20954	21.714	
1500	15373	2.0724	31859	21.747	
2000	20675	2.0703	42803	21.783	
2500	25882	2.0701	53578	21.735	
3000	31101	2.0734	64485	21.749	
3500	36413	2.0744	75535	21.799	
4000	41604	2.0741	86291	21.763	
4500	46882	2.0739	97229	21.776	
5000	52064	2.0734	107949	21.742	

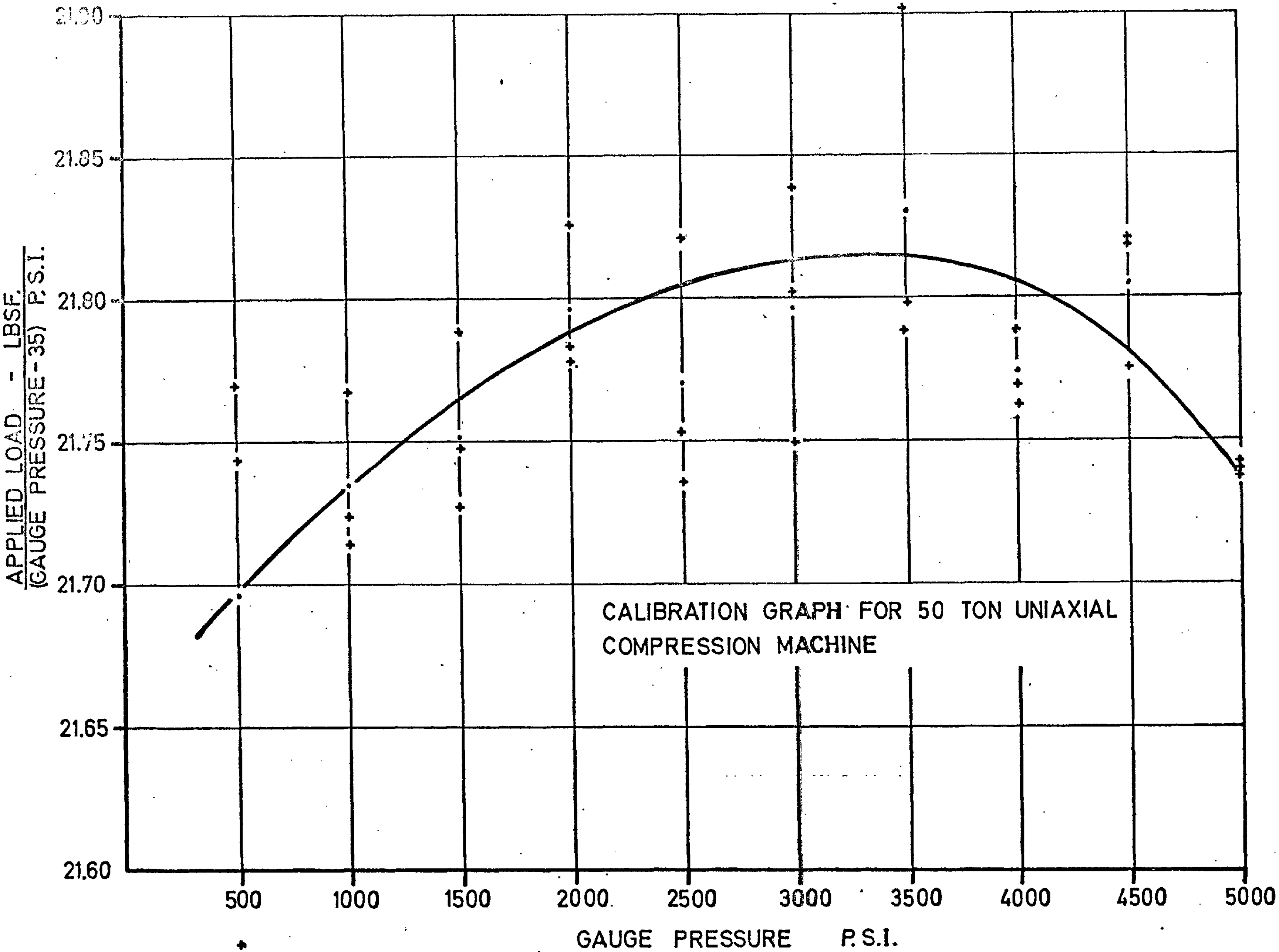

21.90
21.85
21.80
21.75
21.70
21.65
21.60
APPLIED LOAD - LBSF.
(GAUGE PRESSURE - 35) P.S.I.
500
1000
1500
2000
2500
3000
3500
4000
4500
5000
GAUGE PRESSURE P.S.I.
CALIBRATION GRAPH FOR 50 TON UNIAXIAL COMPRESSION MACHINE

FIG. 3.6

TABLE 3.7 CALIBRATION VALUES FOR WARD TENSION MACHINE

Gauge Pressure (p.s.i.)		Proving Ring No. 383 Reading (divs.)	Load(lbsf.) / Defl. (divs)	Load (lbsf.)	Load(lbsf.) / (Gauge Pressure -28)	Average
400 p.s.i. Gauge 8736305	1500 p.s.i. Gauge 8742425					
100		52	10.05	522.6	7.258	7.212
200		123	10.024	1230.0	7.151	7.137
300		196	10.006	1961.2	7.210	7.149
	300	197	10.006	1971.2	7.247	7.223
	400	269	10.000	2690.0	7.231	7.204
	500	342	9.996	3418.6	7.243	7.222
	600	412	9.993	4117.1	7.198	7.169
	700	482	9.984	4812.3	7.161	7.154
	800	553	9.993	5530.0	7.163	7.153
	900	623	10.008	6235.0	7.150	7.143
	1000	695	10.022	6965.3	7.166	7.159
	1100	763	10.035	7656.7	7.142	7.139
	1200	834	10.050	8381.7	7.152	7.146
100		51	10.05	512.6	7.119	
200		123	10.024	1230.0	7.151	
300		193	10.006	1931.2	7.100	
	300	196	10.006	1961.2	7.210	
	400	268	10.000	2680.0	7.204	
	500	340	9.996	3398.6	7.200	
	600	410	9.993	4097.1	7.163	
	700	481.5	9.984	4807.3	7.154	
	800	551	9.993	5506.1	7.132	
	900	621	10.008	6215.0	7.127	
	1000	694	10.022	6955.3	7.156	
	1100	763	10.035	7656.7	7.142	
	1200	833	10.050	8371.6	7.143	
100		52	10.05	522.6	7.258	
200		122	10.024	1222.9	7.110	
300		194	10.006	1941.2	7.137	
	300	196	10.006	1961.2	7.210	
	400	267	10.000	2670.0	7.177	
	500	341	9.996	3408.6	7.222	
	600	409	9.993	4087.1	7.145	
	700	481	9.984	4802.3	7.146	
	800	553	9.993	5530.0	7.163	
	900	623	10.008	6235.0	7.150	
	1000	694	10.022	6955.3	7.156	
	1100	762	10.035	7646.7	7.133	
	1200	833	10.050	8371.6	7.143	

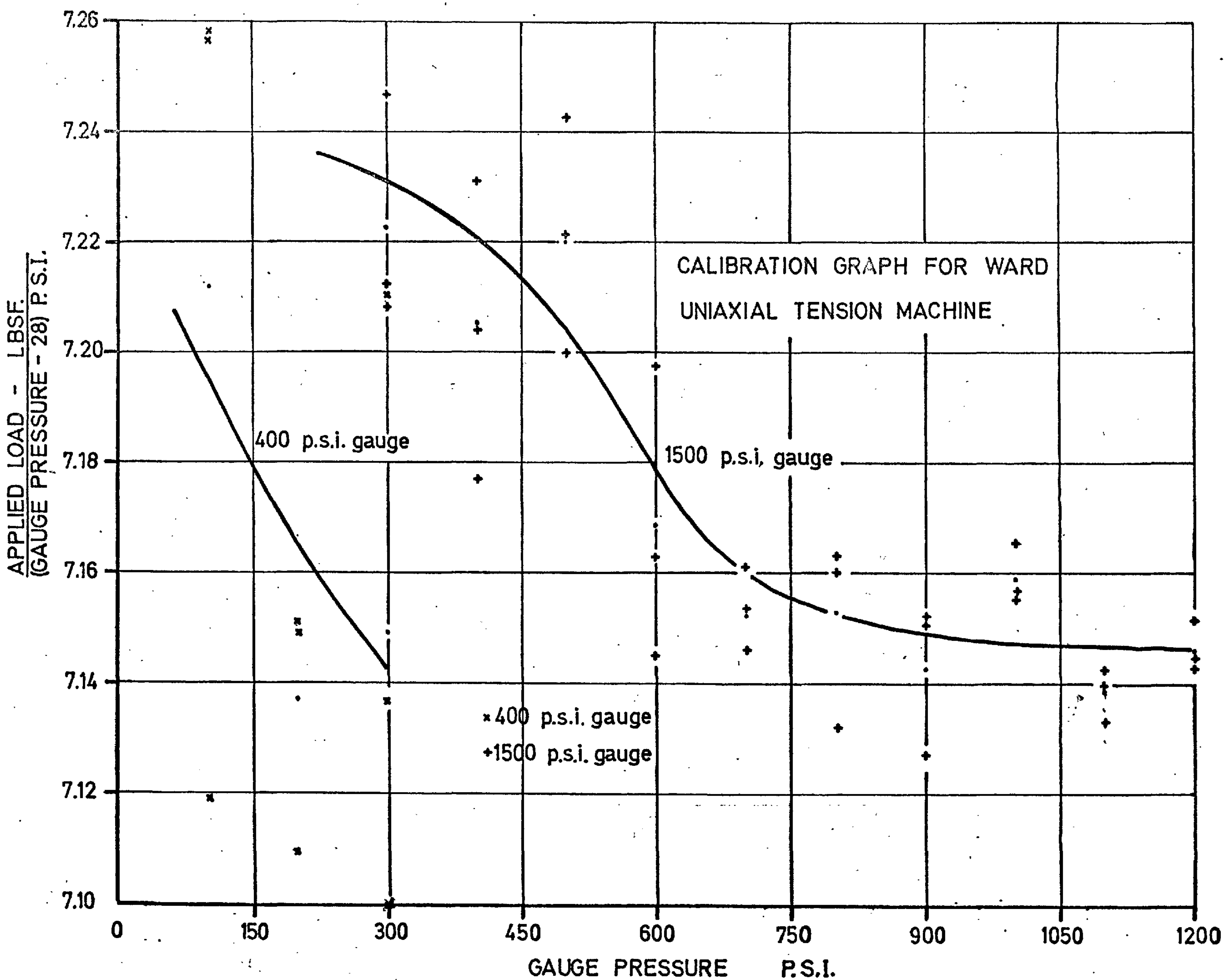
CALIBRATION GRAPH FOR WARD UNIAXIAL TENSION MACHINE
APPLIED LOAD - LBSF.
(GAUGE PRESSURE - 28) P.S.I.
400 p.s.i. gauge
1500 p.s.i, gauge
×400 p.s.i. gauge
+1500 p.s.i. gauge
GAUGE PRESSURE P.S.I.
7.26
7.24
7.22
7.20
7.18
7.16
7.14
7.12
7.10
0
150
300
450
600
750
900
1050
1200

FIG. 3.7

that the 400 p.s.i. gauge has Grade B repeatability whereas the 1500 p.s.i. gauge has Grade A repeatability. Both gauges satisfy Grade A_1 requirements for accuracy.

3.3.5 Flexural Machine (November, 1963)

The 5 tonf. proving ring, No. 383, used for the calibration of this machine was loaded in increments of 200 p.s.i. on the 2,000 p.s.i. Budenberg pressure gauge, No. 8742423, to 2,000 p.s.i. From Table 3.8 and Figure 3.8 the machine is observed to have Grade A repeatability over the range 800 p.s.i. to 2,000 p.s.i., and Grade B. repeatability over its lower working range. Its accuracy is Grade A throughout.

3.3.6 Biaxial Flexural Machine- 3.5 Tonf. Load Cell (November, 1963)

The proving ring, No. 383 was positioned in the biaxial flexural machine as shown in Plate 3.2 (for detailed description of machine, see Chapter 12). The electrical resistance strain gauge load cell which was connected to a Peekel potentiometer was loaded in 600 Peekel division increments from 1,200 divisions to 6,600 divisions. As this machine is used exclusively with the 1,000 division range on the Peekel potentiometer, this was the only calibration conducted.

The calibration graph, Figure 3.9 and its corresponding Table 3.9 indicate repeatability well within Grade A_1 requirements. The Peekel potentiometer was more sensitive than the proving ring by a factor of 5 owing to this ratio of scale divisions. Therefore, this machine owing to its highly sensitive and repeatable nature, can be assessed as a very accurate

TABLE 3.8 CALIBRATION VALUES FOR FLEXURAL MACHINE

Gauge Pressure (p.s.i.)	Proving Ring No. 383 defl. (divs)	Load(lbsf.) / Defl. (divs)	Load (lbsf.)	Load(lbsf.) / Gauge Pressure-10	Average
200	43.1	9.88	425.8	2.2416	2.217
400	88.7	9.873	875.7	2.2454	2.237
600	133.7	9.869	1319.5	2.2364	2.224
800	178.6	9.864	1761.7	2.2300	2.228
1000	223.9	9.862	2208.1	2.2304	2.224
1200	269.1	9.862	2653.9	2.2302	2.224
1400	313.8	9.858	3093.4	2.2255	2.225
1600	361.1	9.842	3553.9	2.2352	2.230
1800	406.1	9.826	3990.3	2.2292	2.228
2000	451.8	9.820	4436.7	2.2295	2.229
200	42.4	9.88	418.9	2.2047	
400	88.4	9.873	872.8	2.2379	
600	132.8	9.869	1310.6	2.2214	
800	178.4	9.864	1759.7	2.2275	
1000	223.1	9.862	2200.2	2.2224	
1200	267.9	9.862	2642.0	2.2202	
1400	313.4	9.858	3089.5	2,2227	
1600	359.6	9.842	3539.2	2.2259	
1800	405.9	9.826	3988.4	2.2282	
2000	452.0	9.820	4438.6	2.2305	
200	42.4	9.88	418.9	2.2047	
400	88.0	9.873	868.8	2.2277	
600	132.3	9.869	1305.7	2.2131	
800	178.2	9.864	1757.8	2.2251	
1000	222.9	9.862	2198.2	2.2204	
1200	268.2	9.862	2645.0	2.2227	
1400	313.8	9.858	3093.4	2.2255	
1600	360.0	9.842	3543.1	2.2284	
1800	405.7	9.826	3986.4	2.2270	
2000	451.5	9.820	4433.7	2.2280	

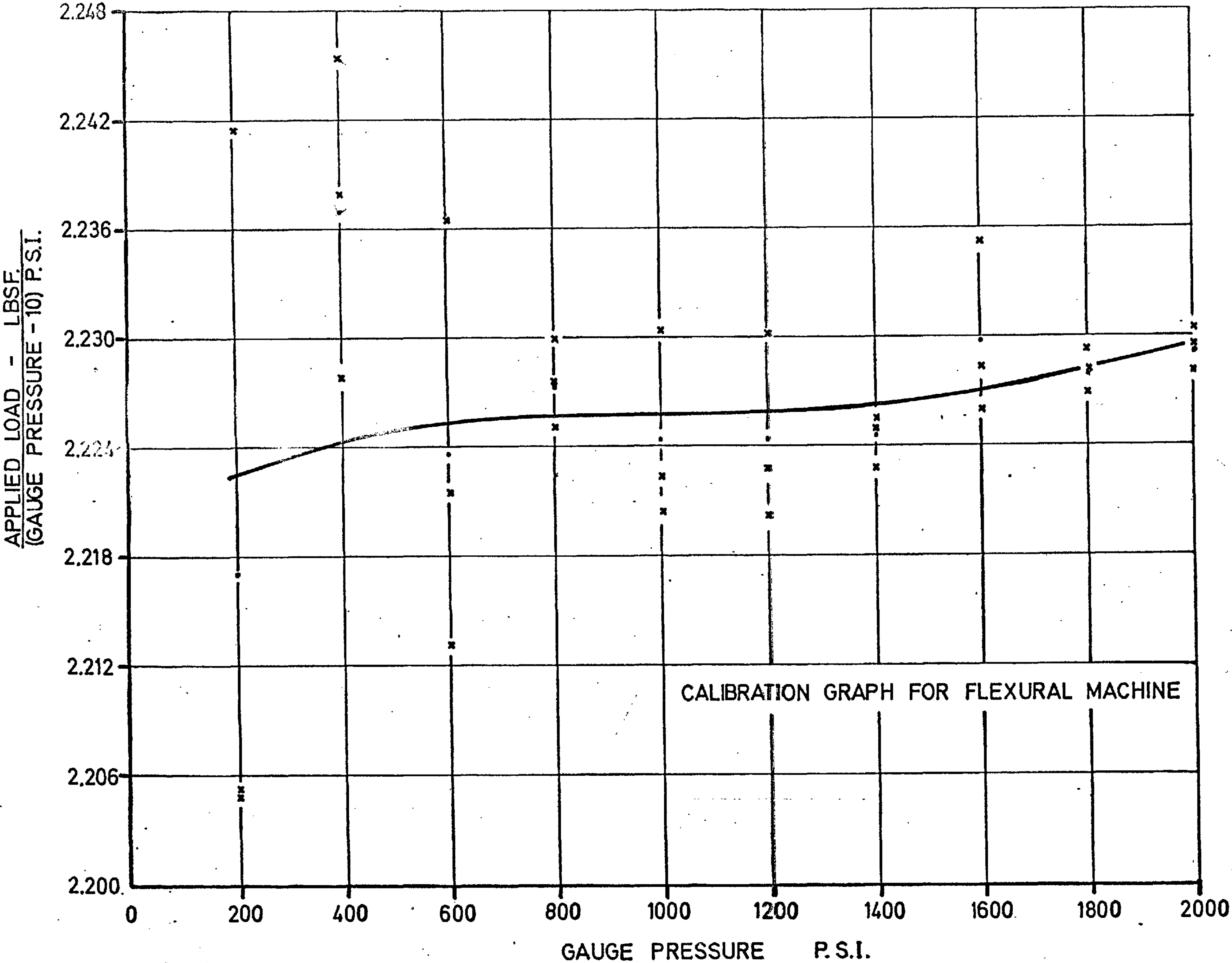

APPLIED LOAD - LBSF. / (GAUGE PRESSURE -10) P.S.I.
2.248
2.242
2.236
2.230
2.224
2.218
2.212
2.206
2.200
0
200
400
600
800
1000
1200
1400
1600
1800
2000
GAUGE PRESSURE P.S.I.
CALIBRATION GRAPH FOR FLEXURAL MACHINE

FIG. 3.8

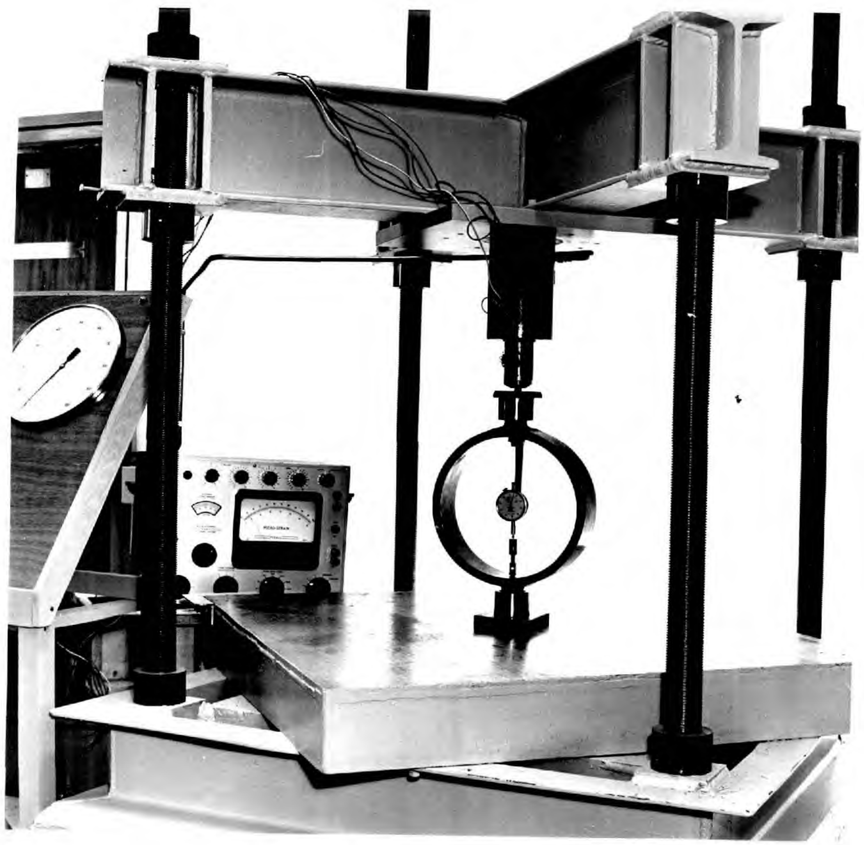

PLATE 3.2 Calibration of biaxial flexural machine
with 5 tonf. proving ring, no. 383

TABLE 3.9 CALIBRATION VALUES FOR BIAXIAL FLEXURAL MACHINE WITH 3.5 TONF. LOAD CELL

Peekel Potentio-meter (divs.)	Proving Ring No. 383 Defl. (divs.)	Load(lbsf.) / Defl.(divs.)	Load (lbsf.)	Load(lbsf.) / Peekel (defl.)	Average
1200	109.0	9.871	1075.9	0.8966	0.8969
1800	163.0	9.866	1608.2	0.8934	0.8931
2400	216.3	9.862	2133.2	0.8888	0.8895
3000	270.8	9.862	2670.6	0.8902	0.8903
3600	324.7	9.855	3199.9	0.8889	0.8886
4200	379.2	9.834	3729.1	0.8879	0.8879
4800	432.5	9.822	4248.0	0.8850	0.8850
5400	487.2	9.816	4782.4	0.8856	0.8851
6000	542.0	9.809	5316.5	0.8861	0.8854
6600	596.7	9.798	5846.5	0.8858	0.8852
1200	109.1	9.871	1076.9	0.8974	
1800	162.9	9.866	1607.2	0.8929	
2400	216.3	9.862	2133.2	0.8888	
3000	270.9	9.862	2671.6	0.8905	
3600	324.7	9.855	3199.9	0.8889	
4200	379.4	9.834	3731.0	0.8883	
4800	432.8	9.822	4251.0	0.8856	
5400	486.9	9.816	4779.4	0.8851	
6000	541.4	9.809	5310.6	0.8851	
6600	596.0	9.798	5839.6	0.8848	
1200	109.0	9.871	1075.9	0.8966	
1800	162.9	9.866	1607.2	0.8929	
2400	216.8	9.862	2138.1	0.8909	
3000	270.8	9.862	2670.6	0.8902	
3600	324.4	9.855	3197.0	0.8881	
4200	379.1	9.834	3728.1	0.8876	
4800	432.2	9.822	4245.1	0.8844	
5400	486.6	9.816	4776.5	0.8845	
6000	541.4	9.809	5310.6	0.8851	
6600	596.1	9.798	5840.6	0.8849	

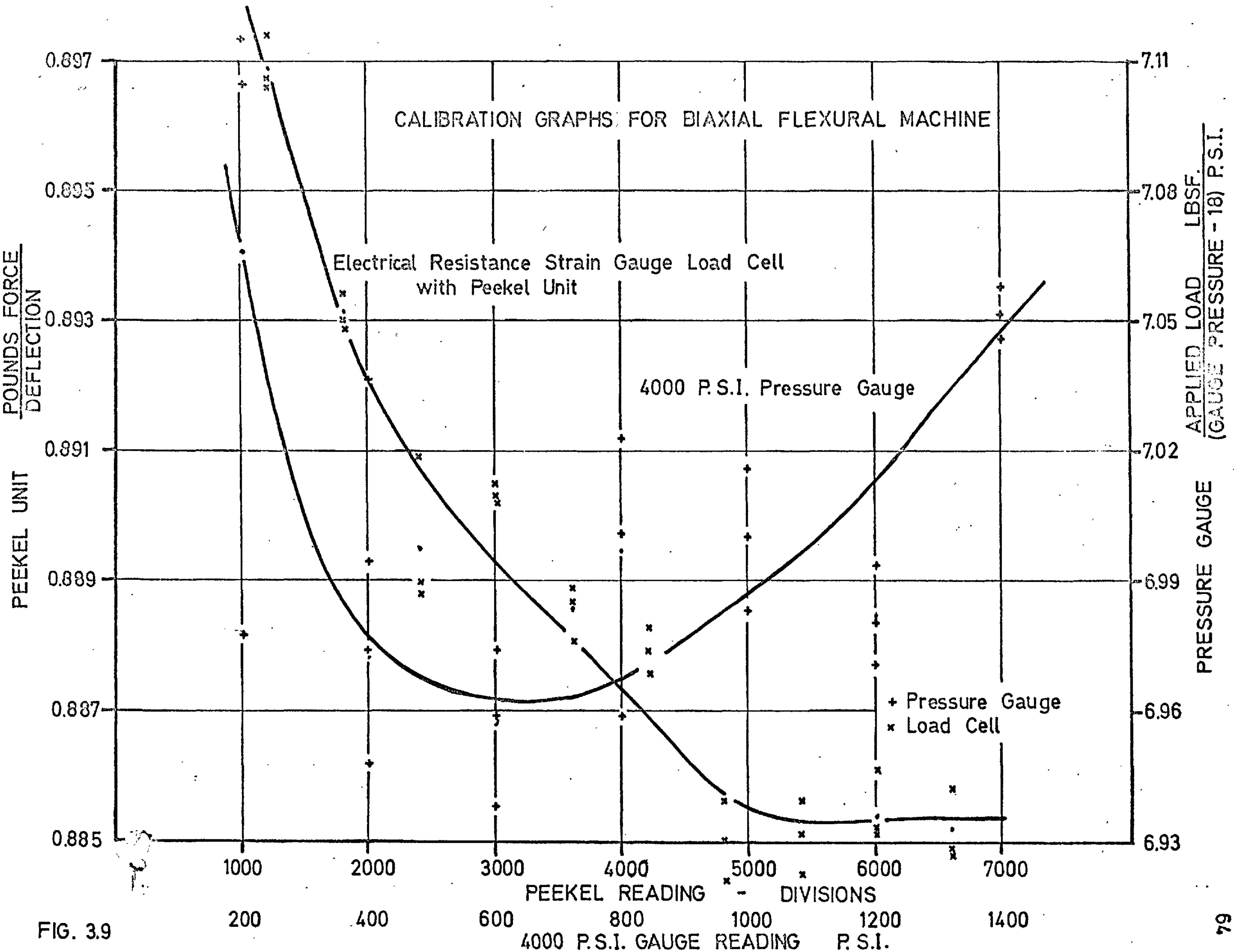
CALIBRATION GRAPHS FOR BIAXIAL FLEXURAL MACHINE
Electrical Resistance Strain Gauge Load Cell with Peekel Unit
4000 P.S.I. Pressure Gauge
+ Pressure Gauge
× Load Cell
POUNDS FORCE / DEFLECTION
PEEKEL UNIT
APPLIED LOAD LBSF. / (GAUGE PRESSURE - 18) P.S.I.
PRESSURE GAUGE
0.897
0.895
0.893
0.891
0.889
0.887
0.885
7.11
7.08
7.05
7.02
6.99
6.96
6.93
1000
2000
3000
4000
5000
6000
7000
PEEKEL READING - DIVISIONS
200
400
600
800
1000
1200
1400
4000 P.S.I. GAUGE READING P.S.I.

FIG. 3.9

Grade A_1 machine.

3.3.7 Biaxial Flexural Machine - Budenberg 4,000 P.S.I. Gauge (December, 1964)

TABLE 3.10 CALIBRATION VALUES FOR BIAXIAL FLEXURAL MACHINE WITH BUDENBERG 4,000 P.S.I. GAUGE No. 8742420

Gauge Pressure (p.s.i.)	Proving Ring No. 383 Defl. (divs)	Load(lbsf.) / Defl(divs.)	Load (lbsf.)	Load(lbsf.) / Gauge Press 18	Average
200	128.7	9.869	1270	6.9780	7.066
400	269.1	9.862	2654	6.9476	6.972
600	411.0	9.825	4038	6.9381	6.957
800	555.0	9.805	5442	6.9591	6.997
1000	701.8	9.772	6858	6.9837	7.001
1200	846.3	9.749	8251	6.9805	6.982
1400	1003.3	9.721	9753	7.0572	7.052
200	131.2	9.869	1295	7.1154	
400	272.6	9.862	2688	7.0366	
600	413.1	9.825	4059	6.9742	
800	560.1	9.805	5492	7.0230	
1000	703.8	9.772	6878	7.0041	
1200	848.0	9.749	8267	6.9941	
1400	1002.5	9.721	9745	7.0514	
200	131.0	9.869	1293	7.1044	
400	270.9	9.862	2672	6.9948	
600	412.2	9.825	4050	6.9588	
800	559.0	9.805	5481	7.0090	
1000	705.1	9.772	6890	7.0163	
1200	845.1	9.749	8239	6.9704	
1400	1001.8	9.721	9738	7.0463	

For loading in excess of 3.5 tonf., the load cell is removed and the load is determined from pressure indication on the Budenberg 4,000 p.s.i. gauge No. 8742420. The load was applied to the proving ring, No. 383 in 200 p.s.i. increments to 1400 p.s.i. on the pressure gauge. From the calibration graph, Figure 3.9 and the Table 3.10, it is apparent that the repeatability conforms to Grade A requirements, while the accuracy is Grade A_1.

3.4 COMMENTS ON RESULTS

Although a thorough discussion of some of the testing machines will be presented in Chapter 7 considering both the machine calibration and the mode of deforming and failing the specimen, comments on the calibration results are presented at this stage.

The Denison compression machine with the 200 tonf. gauge may be regarded as having low accuracy, but satisfactory for cube testing in the range 40 tonf. to 140 tonf. (see British Standard 1881 [9]). However, this is quite inadequate as the majority of 4 inch cubes have a crushing strength less than 40 tons. Consequently, corrections to failing loads must be applied to all such readings in accordance with Figure 3.5. It is, however, more suitable to avoid these corrections, and therefore, the replacement of this gauge by a larger, more sensitive and accurate gauge is recommended.

The 40 ton scale of the above machine is highly inaccurate and should definitely be replaced. It has probably been overstrained at some time in its past, and consequently, its long term repeatability is questionable.

The Ward tension, 50 tonf. uniaxial compression and flexural machines each contain industrial jacks with a piston-type pump for applying the load. The hydraulic system contains two valves for controlling the loading rate. As the cross-sectional area of the ram decreases, the volume of oil passing through the valves decreases, thereby resulting in reduced control of a uniform loading rate. This is reflected in poorer calibration repeatability. For example, the 50 tonf. unixial compression machine containing approximately 22 square inches of cross-sectional area resulted in Grade A_1 repeatability over the entire range while the flexural machine with only 2.2 square inches had Grade A and B repeatability. From the difficulties experienced in maintaining a uniform loading rate, it is obvious that the load application systems on the flexural and tension machines require an improved construction before better gradings can be achieved.

Although smooth curves which best fit the values obtained have been drawn in Figures 3.6 to 3.9, a simple mathematical formula for load in terms of pressure is often more convenient. However, such a simplification will often reduce the accuracy of the results. For example, the relation between pressure and load for the Ward tension machine may be represented as

$$\text{Load(lbsf.)} = 7.17\ (\text{Gauge pressure} - 28) \qquad \ldots 3.1$$

The accuracy obtained by using this formula is Grade A as opposed to Grade A_1 with the smooth curves drawn in Figure 3.7.

Alternatively, with the 50 ton uniaxial compression machine, and the flexural machine, simple mathematical formulae can be used with no loss of accuracy. For these machines, the formulae would be, respectively,

$$\text{Load (lbsf.)} = 21.76\ (\text{Gauge pressure} - 35) \qquad \ldots 3.2$$

and,

$$\text{Load(lbsf.)} = 2.227 \text{ (Gauge pressure } -10) \qquad \ldots 3.3$$

The results of the biaxial flexural machine calibrations reveal the errors possible arising from the use of industrial jacks. The calibration of a pressure gauge in the hydraulic system showed Grade A repeatability while that of the electrical resistance strain gauge load cell placed on the specimen side of the hydraulic ram showed a highly sensitive and repeatable Grade A_1 machine. This is due to the load cell being immune from variable frictional properties of the ram.

The method of load application in this machine was more uniform and easier to control than with either the tension or flexural machine. This is attributed to the use of a centrifugal pump instead of a piston type pump(see Chapter 5), as well as precision control valves.

It is imperative that the calibration be performed every two years in accordance with British Standard 1610. Table 3.11 has therefore been prepared to show the dates of the next calibrations.

TABLE 3.11 CALIBRATION DATES FOR TESTING MACHINES

Testing Machine	Calibration Date	Next Calibration
Denison Compression	March, 1963	March, 1965
Ward Tension	November, 1963	November, 1965
Flexural Machine	November, 1963	November, 1965
Biaxial Flexural-3.5 tonf. Load Cell	November, 1963	November, 1965
Biaxial Flexural - Budenberg 4000 p.s.i. pressure gauge	December, 1964	December, 1966

CHAPTER 4

THE INFLUENCE OF NON-AXIAL LOADING ON CALIBRATION DEVICES AND TESTING MACHINES

4.1 INTRODUCTION

The verification of a testing machine with the subsequent issuing of a certificate implying its accuracy and repeatability generally assures the owner that the maximum error possible in testing is that which is contained within the bounds of this grading. Yet, Cole[(18)] showed that large errors occur with calibration instruments for compression when the platens are not plane, the maximum error measured being 9.1%.

As Cole's investigation was restricted to carefully centred calibrations, the influence of small misalignments would be expected to cause additional errors. For example, as explained in Chapter 7, a 50 tonf. compression machine with Grade A load indication proved to be completely unacceptable for cube testing and research work because of the misalignment in the assembly of its components. It has also been mentioned in private conversation with National Physical Laboratory personnel that calibration discrepancies have occured when the instrument was not accurately centred. In addition, as discussed in Section 6.5, the centroid of specimen resistance may be displaced in excess of 1/4" in routine testing. Although the 50 tonf. uniaxial compression machine, discussed in Section 7.2.2, was probably an exceptional case, it is apparent that this magnitude of misalignment can exist solely from manufacture of components. Yet, British Standard 1610 specifies that it is essential that the verifying load shall be applied along the loading axis of the machine.

An off-centre loading on the ram in hydraulic machines creates a mechanical couple between the ram and ram cylinder. Due to the resulting increase in normal forces and frictional resistance, the load indication, when connected to the hydraulic system would be greater than that actually passing through the specimen. This would be reflected in high apparent strength results.

Although the magnitude of this discrepancy might at first be thought easily investigated by simply placing the load calibration instrument off-centre in the machine, the results would be unsatisfactory when analyzing the manner in which the device is loaded. As shown in Chapter 6, off-centre loading can produce lateral movement in the machine which would create non-axial loadings in the proving device. No information is available on the behaviour of calibration instruments under these systems of loading. The importance of a technique capable of divorcing machine errors from possible calibration instrument errors is therefore appreciated.

An investigation of off-centre or skew loading on the device becomes even more important when considering routine calibration with the device located axially. The initial application of load usually involves lifting the top cross-head or a portion of it a small distance limited by the tolerances in the manufacture of these components. During this stage, an unstable loading sustem is in operation which may result in these components displacing laterally. Subsequent loading will cause binding, thereby inducing lateral deflections and forces into the proving instrument. The resultant loading is a skew loading. Similarly, a misaligned machine may produce non-axial loading even with apparently perfect centring. The above non-axial loadings will subject the calibration instrument to a different force system from that occuring in any of the basic N.P.L. machines. Special considerations in the design of the N.P.L. machines have provided a completely stable loading system at all load stages and very accurate alignment of components, thereby always ensuring that the resultant will be axial.

This chapter is therefore, initially, an investigation into results of calibration instruments and, subsequently, establishing whether non-axial calibrations of hydraulic testing machines indicate significant discrepancies in results.

4.2 OFF-CENTRE AND SKEW LOADING OF CALIBRATION DEVICES

4.2.1. Testing Procedure

The most suitable testing procedure would require placing the calibration instrument to be investigated(hereafter referred to as the secondary calibration instrument) between two effective pins and placing a second calibration instrument(the basic calibration instrument) axially coincident with the line of the pins. The line of action would therefore pass in a straight line between the two pins and through the axis of the basic calibration instrument. By placing the secondary calibration instrument axially coincident also, a basic calibration can be established for the secondary instrument in terms of the basic instrument. Subsequently, off-centre and skew loadings can be performed by simply moving the secondary instrument laterally or in a skew manner while maintaining the basic calibration and two pins fixed in space. The calibration values obtained as a result can then be compared directly to the axial calibration.

As shown in Chapter 8, an effectively pinned condition can be obtained with spherical seatings and the proper lubricant. The 3" radius seating with Rocol A.S.P. and the 7" radius with Rocol M.G. lubricants with coefficient of friction values of 0.10% were used to 100 tonf.

The first test was performed by placing the N.P.L. 150 tonf. four strut mechanical load cell (see Plate 2.6) in a 500 tonf. Avery machine at the Road Research Laboratory, Harmondsworth, (see Plate 8.4) with all testing being performed on the 200 tonf. scale range. The 7" radius spherical seating was then positioned on top of the load cell with the female section supporting the male section for stability. The secondary device, a 50 tonf. proving ring, No. 343 owned by Imperial College Civil Engineering department, was accurately centred on the dowelled platen and maintained vertical by ensuring that the male face of the 7" spherical seating was completely level. Subsequently, the 3" radius seating with the accompanying platen were accurately positioned centrally on top of the proving ring. Before applying load, a check was again made to ensure that the male face of the 7" seating was perfectly level.

This test proved to be unacceptable, however, as approximately 3.5 feet of headroom was required for performing the test. The excessive lateral movement of the top cross-head due to the inherent instability characteristic (see Section 5.4.2.) resulting in a skew loading of the basic calibration device was, therefore, unsatisfactory. The test was consequently altered by removing the four strut mechanical load cell and resetting the equipment as shown in Plate 4.1 thereby reducing the headroom to about 2.5 feet. The resulting increased stability produced negligible lateral movements. The machine of Grade A accuracy and repeatability (see Section 8.3.4 for detailed description) with a very fine control valve consequently became the basic calibration instrument. To offset the reduction in accuracy with this test method, it was decided to repeat each test five times, and to use a statistical approach to determine the significance in differences measured.

To avoid all extraneous errors, the following precautions were taken:

1. The entire series of tests on each proving device was performed in succession during a morning or afternoon to avoid long term machine effects.

2. The temperature for the complete test series on each cal-

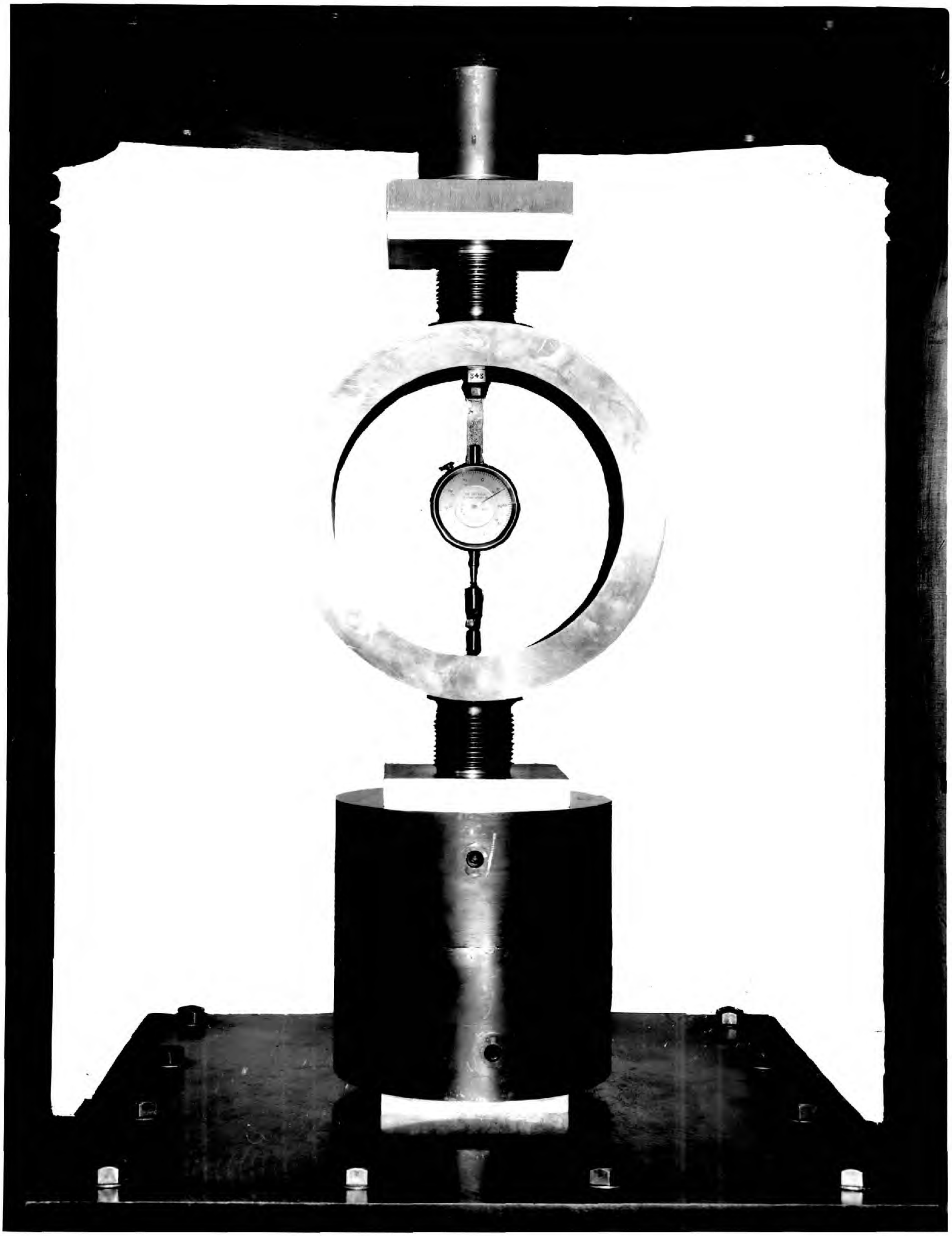

PLATE 4.1 Test assembly for pin-end loading of proving ring

ibration instrument was at all times controlled to ± 0.5° Centigrade.

3. The instrument was preloaded 5 times to the maximum load used in the test series over a period of about 15 minutes. After altering the location of the instrument between the seatings prior to each successive series of runs, one preloading was performed.

4. One minute was allowed after each run for adiabatic cooling of the instrument.

5. To ensure that the machine was applying the load identically in every case, two checks were used. First, the face of the male portion of the 7" radius spherical seating was checked for level in both directions. Then, the repeatability of contact between the female portion of the 3" radius seating and the top cross-head was ensured with the aid of check-markings on the top cross-head. Both these checks were conducted in every run except for the skew tests when only the latter could be carried out.

6. To avoid discrepancies in ram behaviour over its normal travel, the position of testing was maintained constant by fixing the location of the top cross-head for the entire test series.

4.2.2. Tests on N.P.L. 150 tonf. Four Strut Mechanical Load Cell

For the off-centre calibrations, the instrument was moved 1/2" laterally. Two test series were performed with the axis of the instrument positioned north of the axis of the effective pins and testing machine, and subsequently east of the pins with the dial gauge at all times facing west. For the skew calibrations, the spherical seatings were tilted in their seatings and the instrument placed 0.25" off-centre at each end in opposite directions, (west at the bottom and east at the top) thereby providing 0.50" of skew loading in its 9.25" length. The resultant force as indicated on the machine scale therefore consisted of an axial component and a shearing force. Consequently,

$$\text{axial load in load cell} = \text{resultant load} \times \cos\theta \qquad \ldots 4.1$$

where

$$\theta = \tan^{-1}\frac{0.50}{9.25} \qquad \ldots 4.2$$

As only the axial force is assumed to produce deflection in the instrument, the results of instrument readings of the other test series, in order to be directly compared, must be multiplied by $\cos\theta$ where θ is as in equation 4.2. Alternatively, a direct comparison can be obtained by multiplying the instrument readings of this test series by $\dfrac{1}{\cos\theta}$.

Table 4.1 and the graph, Figure 4.1, give the results of the calibration series along with percentage differences between axial and non-axial loadings. The results of a statistical analysis, as presented in Table 4.2 (19,20) indicate that differences between axial and non-axial calibrations can be highly significant.

In order to eliminate doubt about a drift in machine behaviour, the initial test with the calibration device located

TABLE 4.1 AXIAL AND NON-AXIAL CALIBRATIONS OF N.P.L. 150 Tonf. FOUR STRUT MECHANICAL LOAD CELL

Indicated Load on Machine (Tonf.),	Series 1 Load Cell Centred (Tonf.)	Series 2 Load Cell 1/2" North (Tonf.)	Series 3 Load Cell 1/2" East (Tonf.)	Series 4 Load Cell Askew (Tonf.)	Series 5 Load Cell Centred (Tonf.)
Run 40	40.71	40.58	40.77	41.03	40.76
1 70	71.32	71.11	71.26	71.76	71.47
100	101.38	101.09	101.25	102.07	101.52
Run 40	40.77	40.52	40.97	41.03	40.69
2 70	71.35	70.98	71.51	71.97	71.35
100	101.53	100.97	101.52	102.16	101.48
Run 40	40.58	40.63	40.87	40.98	40.63
3 70	71.35	71.21	71.35	71.76	71.22
100	101.50	101.39	101.27	102.12	101.32
Run 40	40.80	40.49	40.80	40.95	
4 70	71.36	71.01	71.30	71.75	
100	101.57	100.82	101.22	102.17	
Run 40	40.73	40.63	40.73	40.97	
5 70	71.35	71.17	71.21	71.79	
100	101.47	101.28	101.18	101.98	
Average					
40	40.72	40.57	40.83	40.99	40.69
70	71.35	71.09	71.33	71.81	71.35
100	101.49	101.11	101.29	102.10	101.44
Numerical and Percentage Increase from Average of Readings of Series 1 and 5.					
40		-0.14 -0.34%	0.12 0.30%	0.28 0.69%	
70		-0.26 -0.36%	-0.02 -0.03%	0.46 0.65%	
100		-0.36 -0.35%	-0.18 -0.18%	0.63 0.62%	

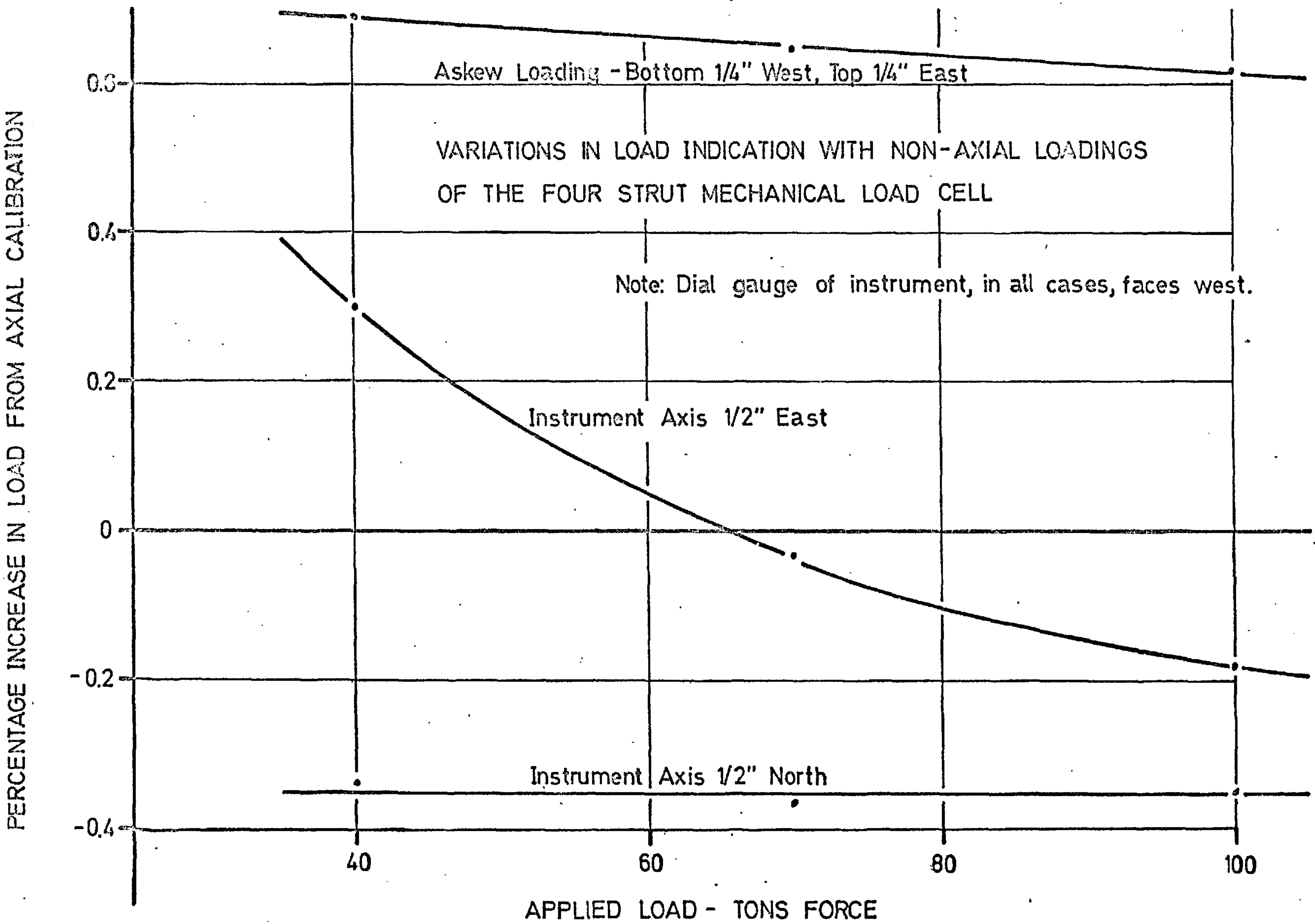
VARIATIONS IN LOAD INDICATION WITH NON-AXIAL LOADINGS
OF THE FOUR STRUT MECHANICAL LOAD CELL
Note: Dial gauge of instrument, in all cases, faces west.
Askew Loading - Bottom 1/4" West, Top 1/4" East
Instrument Axis 1/2" East
Instrument Axis 1/2" North
PERCENTAGE INCREASE IN LOAD FROM AXIAL CALIBRATION
0.6
0.4
0.2
0
-0.2
-0.4
40
60
80
100
APPLIED LOAD - TONS FORCE

FIG. 4.1

TABLE 4.2 SIGNIFICANCE OF DIFFERENCES BETWEEN AXIAL AND NON-AXIAL CALIBRATIONS OF N.P.L. 150 TONF. FOUR STRUT MECHICAL LOAD CELL

	Instrument Centred and Instrument 1/2" North	Instrument Centred and Instrument 1/2" East	Instrument Centred and Instrument Askew
40 Tonf.			
$s(x_1-x_2)$	0.0473	0.0512	0.0368
x_1-x_2	0.14	0.12	0.28
$\frac{x_1-x_2}{s(x_1-x_2)}$	2.96	2.34	7.62
Significance Level	5%	8%	1%
70 Tonf.			
$s(x_1-x_2)$	0.0496	0.0518	0.0421
x_1-x_2	0.26	0.02	0.46
$\frac{x_1-x_2}{s(x_1-x_2)}$	5.25	0.39	10.9
Significance Level	<1%		<1%
100 Tonf.			
$s(x_1-x_2)$	0.1070	0.0663	0.0449
x_1-x_2	0.36	0.18	0.63
$\frac{x_1-x_2}{s(x_1-x_2)}$	3.37	2.72	14.0
Significance Level	3%	5%	<1%

Notation:

$s(x_1-x_2)$ standard deviation of differences

x_1-x_2 actual mean differences in results

Significance Level probability that both sets of data are from the same universe axially was repeated after performing the off-centre and skew calibrations. The minute differences between these two tests are insignificant as shown from comparison of the results of series 5 and series 1 in Table 4.1.

The load cell was assessed as Grade 1 over the range 10 tonf. thereby guaranteeing a repeatability of ±0.1% to 50 tonf. and ±0.2% to 150 tonf. However, the results obtained indicate variations of 1.0% Furthermore, it appears reasonable to suppose that this variation can be even greater with the results of greater non-axiality.

4.2.3 Tests on 50 Tonf. Proving Ring NO.343

One off-centre calibration was performed with the proving ring displaced 0.50" north. In the skew calibration, the ring was displaced south at the bottom and north at the top a distance of 0.375" in each direction making a 0.75" skew in its 17.25" length. In both cases, the dial gauge faced west.

The test series was intended to be performed at 25 tonf. and 45 tonf. However, due to excessive indentation of the platens at 45 tonf. with off-centre calibration, this load stage was abandoned.

The results of this test series are presented in Table 4.3. Although the differences obtained are not considered significant, it would seem that the proving ring might be somewhat influenced by non-axial loadings. However, these differences are small and certainly less than those obtained with the four strut mechanical load cell.

TABLE 4.3 AXIAL AND NON-AXIAL CALIBRATIONS OF PROVING RING NO. 343

Run No.	Series 1 Proving Ring Centred (Tonf.)	Series 2 Proving Ring 1/2" North (Tonf.)	Series 3 Proving Ring Askew (Tonf.)
1	25.627	25.634	25.534
2	25.627	25.579	25.568
3	25.627	25.558	25.554
4	25.641	25.496	25.562
5	25.613	25.462	25.582
Average	25.627	25.546	25.560

4.3 OFF-CENTRE LOADING ON TESTING MACHINES

4.3.1 Testing Procedure

The importance of being able to divorce testing machine errors from calibration instrument errors was emphasized in Section 4.1. As observed in Section 4.2, the errors in calibration devices can be large and highly significant. Consequently, for this test series, the N.P.L. 150 tonf. four strut mechanical load cell was accurately centered between the two spherical seatings as explained in Section 4.2.1 Special care was taken to insure that the face of the male portion of the 7" spherical seating was at all times level. The machine was then calibrated against the load cell 5 times at 40, 70, and 100 tonf. axially.

For the off-centre calibrations, the entire assembly including the 2 spherical seatings was moved laterally a predetermined distance. Care was taken to ensure that the seatings and load cell were unaltered in relation to each other and that the entire assembly was vertical at the beginning of each run. The machine was then again calibrated at 40, 70, and 100 tonf. 5 times.

To avoid extraneous errors, the following precautions were taken.

1. A series of tests for comparing the results of 2 1/4" off-centre, 4 1/2" off-centre and axial calibration were performed in succession in the course of an afternoon. As it was later deemed necessary to include a calibration at 1 1/8" off-centre, this calibration was performed immediatly after doing another axial calibration.
2. The temperature during each complete series on either day was controlled to $\pm 0.5^{\circ}C$.
3. Before the test series on either day, the instrument was preloaded to 100 tonf. 5 times over a period of about 15 minutes. The subsequent calibrations were preceded by one preloading.
4. One minute was allowed for adiabatic cooling after each run.
5. To eliminate discrepancies in ram behaviour over its normal travel, the vertical location of all calibrations was maintained constant by fixing the top cross-head.

4.3.2. Results of Off-centre Calibrations

The results of this series of tests are presented in Table 4.4 and plotted in Figure 4.2. It is apparent that, as the magnitude of off-centre calibration increases, the reduction of load through the calibration device likewise increases.

TABLE 4.4 AXIAL AND NON-AXIAL CALIBRATIONS OF AVERY COMPRESSION TESTING MACHINE

Indicated Load on Machine (Tonf.)	First Day Tests: Instrument Centred (Tonf.)	First Day Tests: Instrument 2 1/4" North (Tonf.)	First Day Tests: Instrument 4 1/2" North (Tonf.)	Second Day Tests: Instrument Centred (Tonf.)	Second Day Tests: Instrument 1 1/8" North (Tonf.)
40	40.42	39.57	37.72	41.13	40.87
70	70.81	69.31	66.00	71.60	71.26
100	100.66	98.45	93.52	101.63	101.63
40	40.47	39.57	37.72	40.91	40.80
70	70.79	69.30	65.98	71.42	71.20
100	100.54	98.62	93.48	101.38	101.53
40	40.41	39.52	37.74	40.90	40.85
70	70.72	69.24	65.98	71.38	71.27
100	100.54	98.57	93.59	101.30	101.65
40	40.36	39.50	37.64	40.87	40.90
70	70.75	69.23	65.93	71.31	71.27
100	100.49	98.48	93.57	101.30	101.63
40	40.44	39.42	37.65	40.90	40.77
70	70.93	69.24	66.03	71.28	71.22
100	100.82	98.44	93.62	101.31	101.47
Average					
40	40.42	39.52	37.69	40.94	40.84
70	70.80	69.26	65.98	71.40	71.24
100	100.61	98.51	93.57	101.38	101.59

Numerical and Percentage Reduction from Axial Calibration

Indicated Load on Machine (Tonf.)	Instrument Centred	Instrument 2 1/4" North	Instrument 4 1/2" North	Instrument Centred	Instrument 1 1/8" North
40		0.90 2.23%	2.73 6.76%		0.10 0.25%
70		1.54 1.98%	4.82 6.82%		0.16 0.22%
100		2.10 2.09%	7.04 7.00%		-0.21 -0.21%
Average		2.10%	6.86%		0.09%

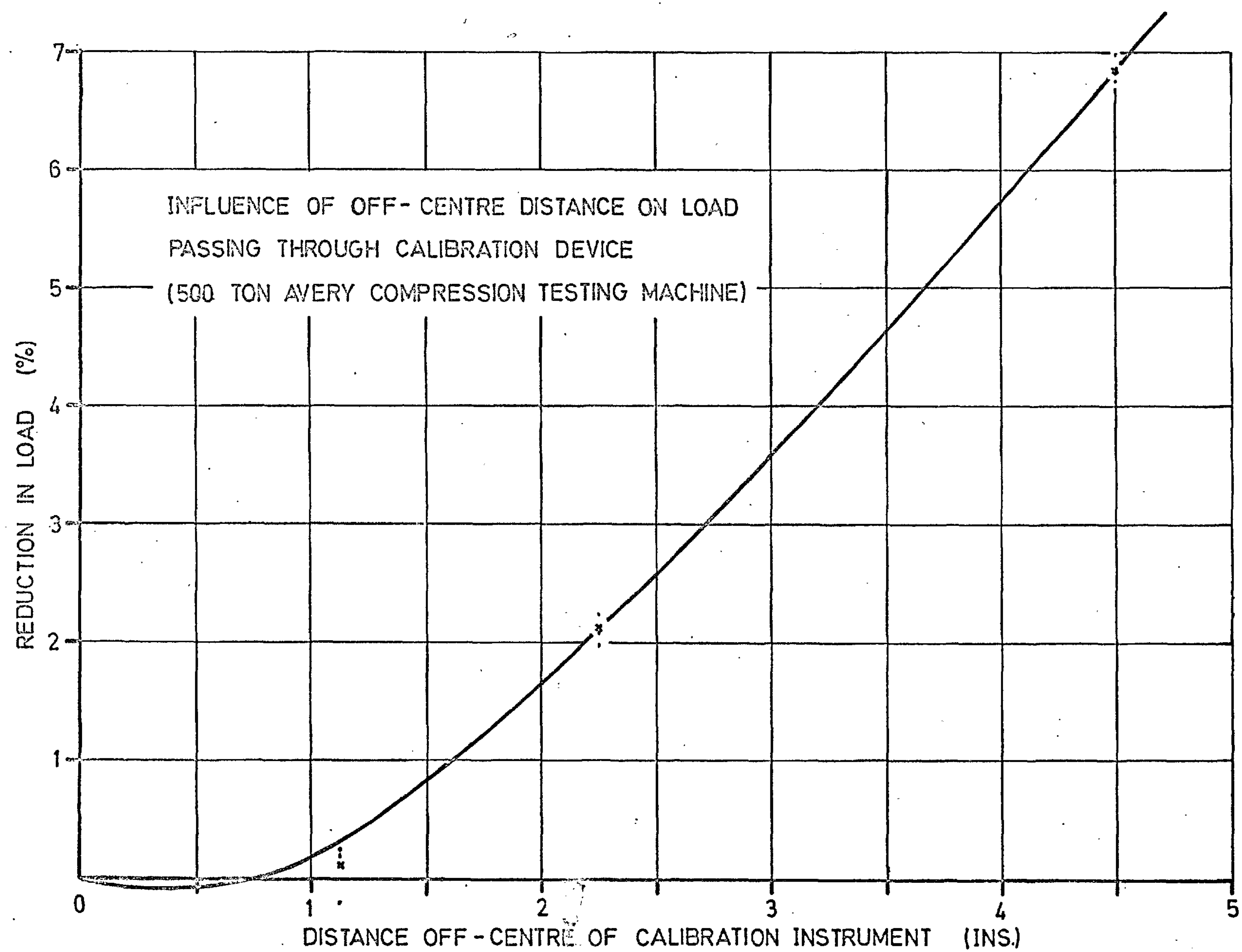
INFLUENCE OF OFF-CENTRE DISTANCE ON LOAD
PASSING THROUGH CALIBRATION DEVICE
(500 TON AVERY COMPRESSION TESTING MACHINE)
REDUCTION IN LOAD (%)
DISTANCE OFF-CENTRE OF CALIBRATION INSTRUMENT (INS.)
0
1
2
3
4
5
6
7
FIG. 4.2

This is as expected due to increased frictional forces at the ram-cylinder interface.

It will be observed, however, that this relationship is not necessarily linear. In this particular case, the rate of change of load increases with increasing misalignment of the calibration device. This may be explained by a binding action at the ram-cylinder interface which becomes more severe with increasing misalignment.

The ram has about 18" of contact with the ram cylinder. In addition, a sliding contact at the columns as shown in the bottom corners of Plate 4.1 is 2" in length and about 4" above the top of the cylinder. It is therefore appreciated that the effective length of contact is very much greater than usually encountered with concrete compression machines. As normal forces and resulting frictional forces are generally inversely proportional to the length of the ram, it will be appreciated that discrepancies encountered in machines with short rams will be very much greater than those shown in Figure 4.2. Poor machining producing a binding action in the ram would amplify these discrepancies. Furthermore, a small diameter ram would tend to localize the normal forces on the ram-cylinder interface. The resulting lubrication breakdown would result in increased frictional forces due to steel sliding on steel as shown in Chapter 8.

4.4 CONCLUSIONS AND RECOMMENDATIONS

It is apparent from Section 4.2 that, unless calibration devices are loaded axially as in their initial calibrations at the National Physical Laboratories, discrepancies in results very much in excess of their specified accuracy, are entirely possible. Furthermore, such errors can be of the same magnitude or even greater than the accuracy necessary for assessing the grading of the testing machine. A Grade A machine has no error greater than ±0.5% to 50 tonf. and ±0.75% to 150 tonf. As a calibration device should be 5 times as accurate as the machine being verified, calibration instruments showing inaccuracies of the order of ±0.5% would be unsuitable for such calibrations. Because a guarantee that the machine is loading the device axially can seldom be provided, it is appreciated that the calibration results are not as free from error as was previously supposed. Although a more sensitive and accurate basic calibration device as well as a thorough examination of all calibration devices (See Chapter 2) would have been more satisfactory, the results of this analysis indicate conclusively that discrepancies as large as 0.7% and probably more are possible in a Grade 1 proving instrument. According to British Standard 1610, Grade 1 implies a repeatability of 0.2% to 50 tonf. and 0.4% to 150 tonf. The proving ring is less susceptible to non-axial calibration than the four strut mechanical load cell.

The realization that the centroid of resistance of the specimen may be displaced 1/4" off-centre and often more in routine testing (see Chapter 6) stresses the importance of determining the behaviour of the testing machine under such non-axial loadings. This problem, as discussed in Section 4.3 is particularly severe in testing machines containing short, small diameter rams with poor machining and large tolerances on the cylinder-ram interface.

Eventually, a complete verification of a testing machine should include calibrating off-centre a fixed distance, say 1/2" in two mutually opposite directions, as well as the axial calibration. This distance is safe when considering effectively fixed seatings of 5" minimum radius (as specified in Chapter 10). From the results of Chapter 8, these seatings will remain fixed to an off-centre loading of 0.75", (assuming a coefficient of friction of 0.15). A second spherical seating, effectively pinned, could be positioned beneath the calibration device to assure that the load is passing into the ram the necessary distance off-centre. The axial calibration should require the same degree of repeatability and accuracy as exists in the current British Standard 1610 while the non-axial calibration, taken as an average of two runs at each location, should have an accuracy within 1.5 x the accuracy at central loading.

The most reliable technique for off-centre calibration is one which incorporates an effective pin at both ends of the calibration device. However, this requires a large amount of head room which usually is not available in concrete control testing machines. Alternatively, the simple movement of the calibration device laterally is also not suitable as the centroid of action will not pass through the axis of the calibration device, but will rather be displaced towards the centreline of the machine. The method suggested above, where an effectively pinned spherical seating is positioned between the calibration instrument and the ram of the machine will allow the load to be displaced a known distance off-centre, while increasing the required head-room by only about 6". It is appreciated, however, that for this verification technique, the calibration instrument must be relatively immune from lateral force effects.

It is obvious that a better understanding based on further experimental investigation into the behaviour of proving devices and testing machines under non-axial loading is necessary. This chapter has simply shown conclusively that this problem is a serious one.

PART II

TESTING MACHINES USED FOR THE DEFORMATION AND STRENGTH PROPERTIES OF CONCRETE

CHAPTER 5

THE INFLUENCE OF TESTING MACHINES ON THE STRENGTH OF CONCRETE

5.1 THE MEANING OF TESTING TECHNIQUE

The term "testing technique" is used to imply the confidence of all experimental work. For the author's purposes, the term is defined as the extent to which the experimental behaviour is identical with the assumed behaviour. The testing technique is therefore a measure of the reliability of the results obtained. Generally, a good testing technique involves a certain amount of preliminary research directed towards proving that the experiment is truly conforming to the theoretical predictions. It is unfortunate that this most vital portion of research is often eliminated, the assumption being made that undesirable influences are negligible.

In the testing of material specimens for deformation and strength properties, the problem of a correct testing technique is subdivided as follows:

(1) the effect of the testing machine with its undesirable forces inherent due to manufacture and/or inter-relation between the force system of the testing machine and the specimen.

(11) the stresses in the specimen influenced by the specimen shape and size.

In the past, much effort has been directed at the selection of a suitably shaped specimen. For example, Lachance and Newman,[1,21] in developing a uniaxial compression specimen, showed that a height to diameter ratio of at least 2 1/2, and preferably 3, effectively eliminated the influence of platen or end restraint in the central section, thereby resulting in a state of true uniaxial stress.

The influence of the testing machine, however, has been too often overlooked or disregarded in the past, with the result that large variations in strength have occurred. This section of the thesis, Chapters 5 to 10, analyzes the testing machine and examines its influence on strength and deformational properties of concrete. Definite recommendations are given in order to achieve more consistent and meaningful results in the future.

5.2 DIFFERENCES IN RESULTS OF COMPRESSION TESTING MACHINES

Several investigations have indicated that large differences[18,22-25] in the average strength of concrete cubes can be obtained when supposedly identical specimens are tested in different testing machines which conform to the relevant clauses of B.S. 1881[9] and A.S.T.M. C39-64[27]. In addition, it has been found that the coefficient of variation of concrete cube results is undoubtedly influenced by the type of compression machine used[18,22,23,]. By varying certain characteristics of any one testing machine within the limits allowed by current specifications, considerable variations in the failure values of similar concretes are obtained. In particular, Tarrant[28,29] has shown that differences in the behaviour of the spherical seating will cause differences in the ultimate strength results of concrete cubes while Dwyer[30] indicated that variations in platen planeness will create differences in the failure strengths of mortar cubes.

Figure 5.1 shows the results of sets of twelve 6" cubes tested at eight separate laboratories after the cubes had been cast and cured in a standard condition at a central unit for 7 days.[(23)] The average strength varies by 19%, from 6130 p.s.i. to 7290 p.s.i. The limit below which 1% of the results would be expected to fall on the basis of a statistical analysis ranged from 4210 p.s.i. to 6810 p.s.i., a difference of 62%.

It is no exaggeration to say that nearly all branches of the building industry are dependent on concrete compression tests in one way or another, yet there is sufficient evidence to show that the testing technique is not producing the precise, reproducible, accurate results expected[(31)]. It must be emphasized that, although certain aspects of testing machines and their calibration are covered by the relevant clauses in B.S. 1881 and 1610 and the A.S.T.M. specifications C39 and E4, these specifications are inadequate.

In order to assess the possible causes of the inconsistencies in failure results, the three methods of loading specimens uniaxially are presented. Subsequently, an examination of the various characteristics of testing machines are defined and explained. The possible influence which these might have on ultimate strength results and the method of loading, are also discussed.

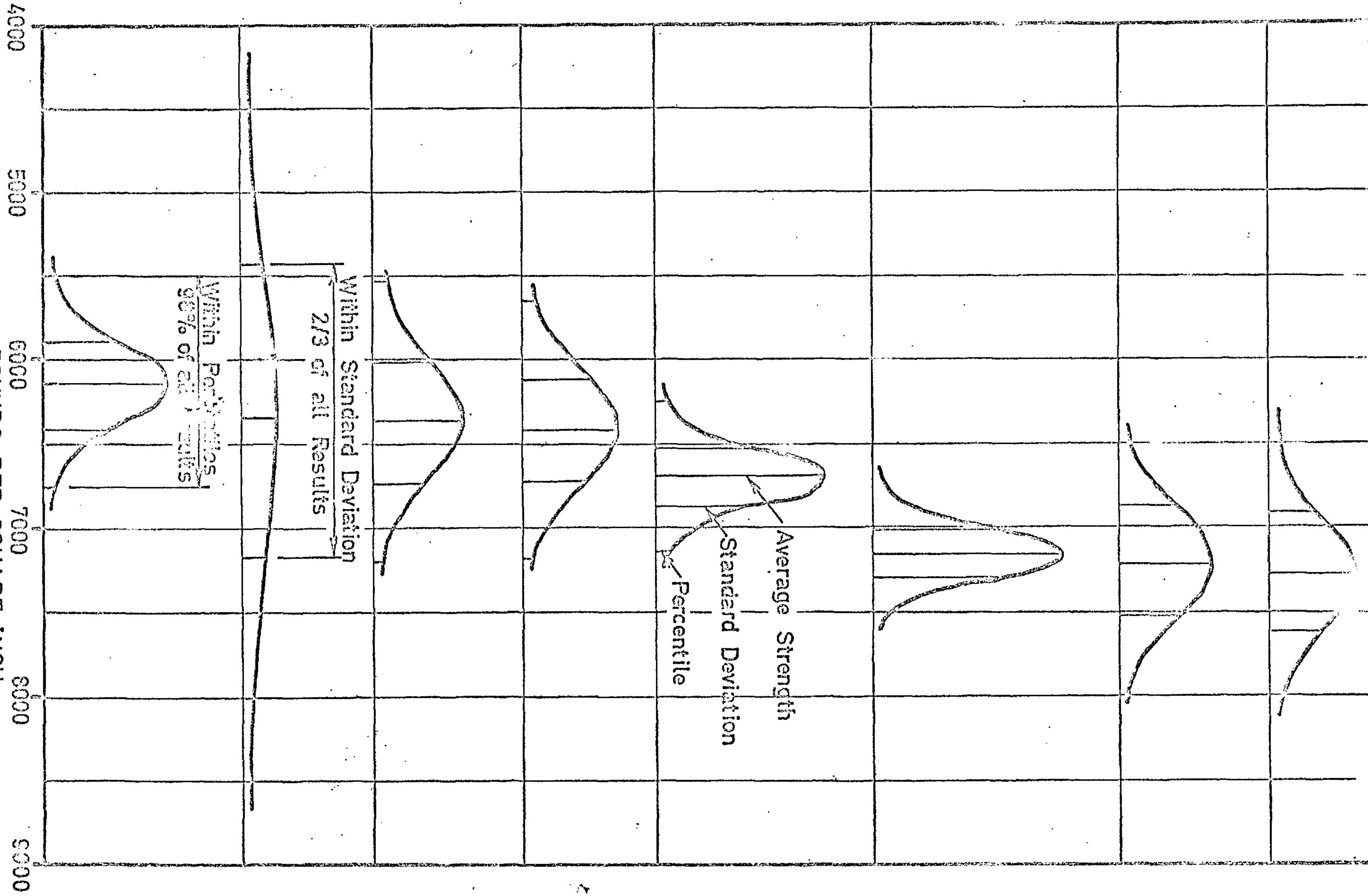

FIG. 5.1 CUBE STRENGTH RESULTS ON IDENTICAL CONCRETE AS REPORTED BY 8 LABORATORIES
(Compliments of M. Barclay, Ove Arup & Partners)

5.3 THE PHILOSOPHIES OF UNIAXIAL TESTING

The uniaxial testing of material specimens involves loading the specimens at their ends. The resulting mode of deformation and failure of the specimen is much affected by the manner in which these loads are applied. In principle three basic methods or philosophies of loading must be recognised in the uniaxial testing of materials(see Figure 5.2).

1. Both ends of the specimen are effectively pinned.
2. Both ends of the specimen are effectively fixed.
3. One end of the specimen is effectively pinned whilst the other is effectively fixed.

The first philosophy requires that, at all stages of loading the action of the testing machine will be applied in a straight line between the pins. Concrete specimens are rarely uniform or homogeneous, and due to segregation during casting, the modulus of elasticity will vary through the cross-section. Consequently, on loading, elements within the specimen will strain at different rates as it tries to maintain its centroid of resistance co-linear with the line of action. When the weakest element fails, the load it was carrying will be transferred to adjacent elements which in turn fail, and eventually, complete failure of the specimen on the weakest side occurs. Plate 5.1 shows a concrete cube which has been tested with both ends effectively pinned. The method of achieving this condition will be described in Chapter 9. Excessive failure can be seen on the weaker half of the specimen and not only is there no visible

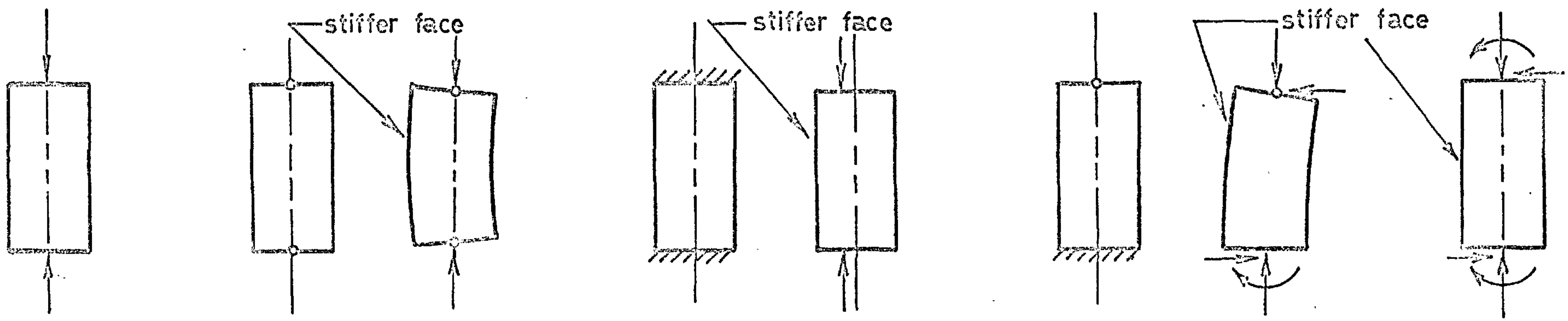

(a) Assumed Force System

(b) Both Ends Effectively Pinned

(c) Both Ends Effectively Fixed

(d) One End Pinned; One End Fixed

(e) Actual General Force System

FIG. 5.2 PHILOSOPHIES OF UNIAXIAL TESTING

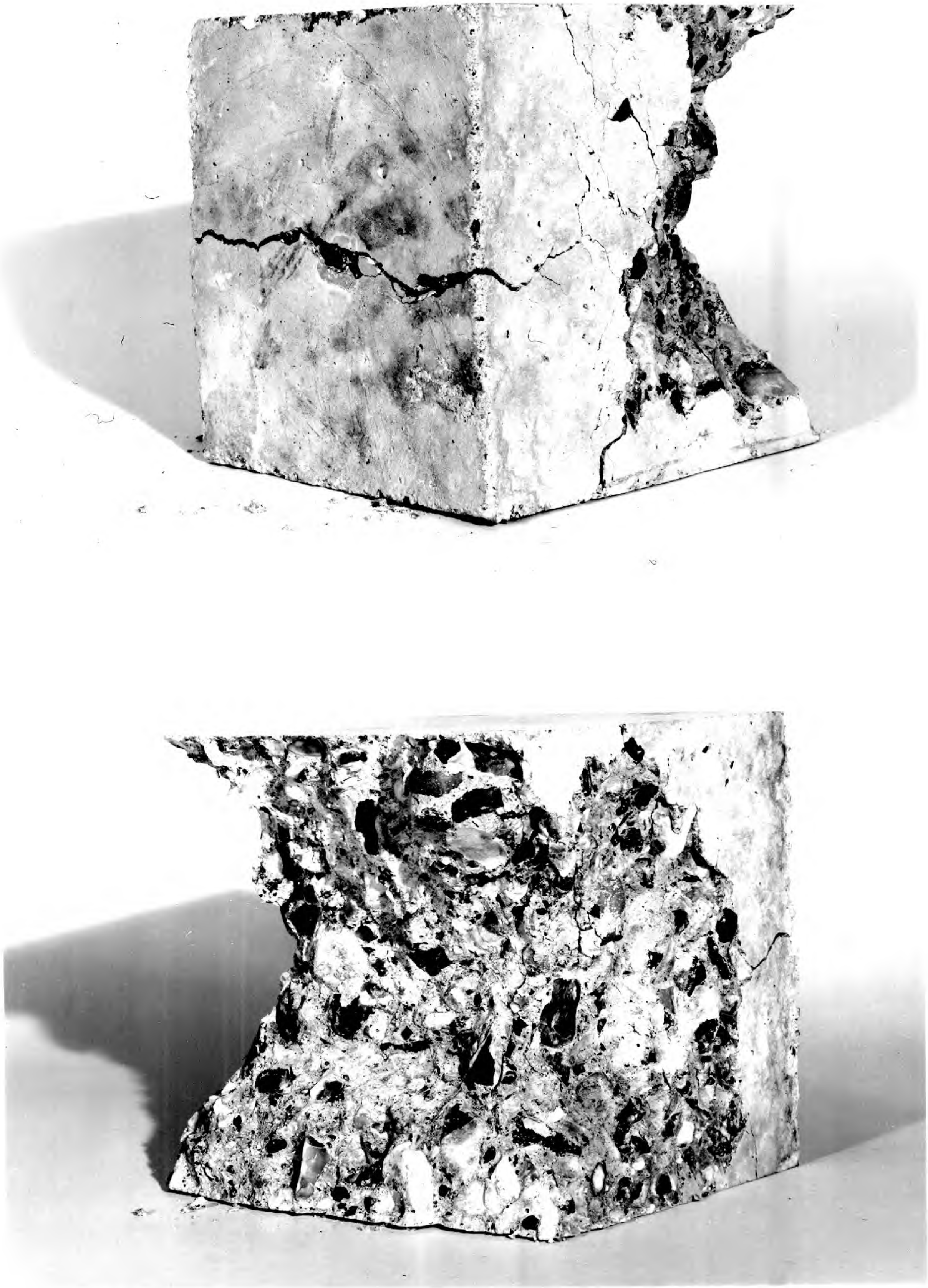

PLATE 5.1 The four faces of a 6" concrete cube failed with both ends effectively pinned

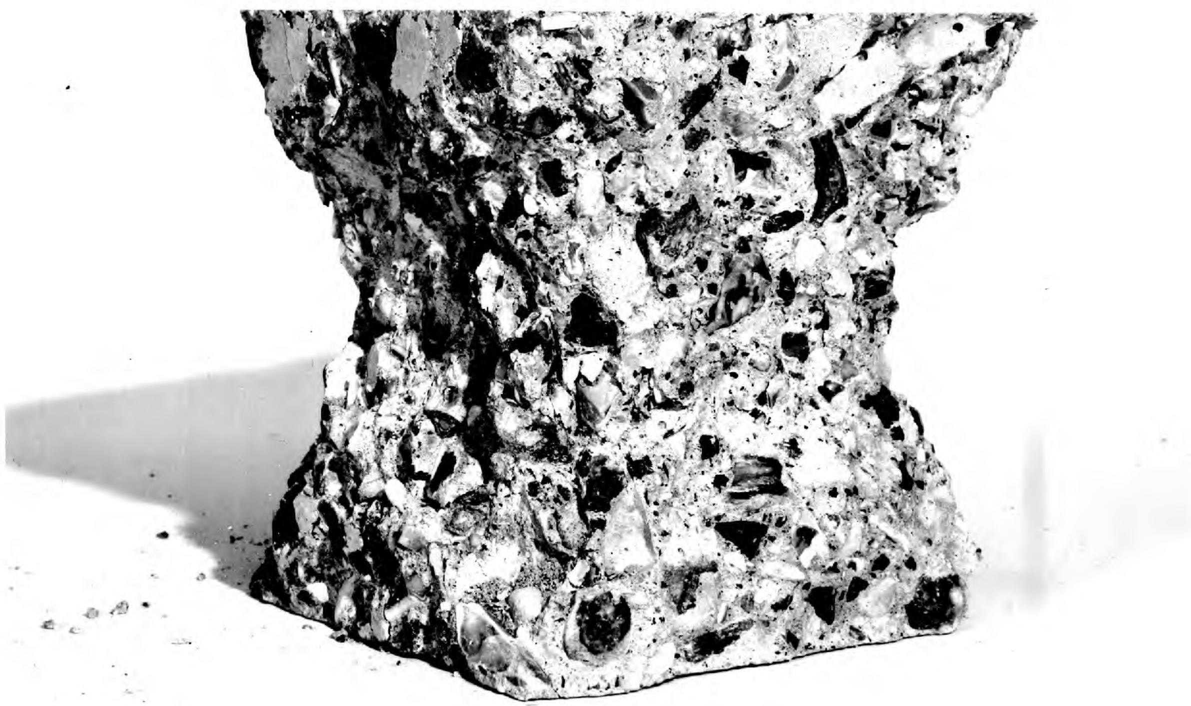

PLATE 5.2 The four faces of a 6" concrete cube failed with both ends effectively fixed

compression failure on the opposite face but in this case, a horizontal tension crack has occurred. Near failure, the failing face deformed so excessively that an internal hinge developed. The resulting rotation caused the compression stresses on the strong face to reduce, eventually becoming tension.

The second philosophy requires that, at any load stage, the total deformation of the specimen is the same throughout. In a segregated concrete specimen, the modulus of elasticity decreases from the bottom of the specimen as cast to the top. When it is tested on its side, the centroid of resistance of the specimen will be located towards the stiffer face. If the specimen is to be deformed uniformly, the testing machine must be able to transfer its centroid of action until it is co-linear with the centroid of resistance of the specimen. Furthermore, adjustments must take place as certain elements in the specimen fail. Complete failure of the specimen occurs when all the elements on the weakest cross-section have exceeded their load carrying capacity. In concrete testing, this philosophy is indicated by an equal amount of failure on all faces of the specimen as seen in Plate 5.2(see Chapter 9).

At first sight, the third philosophy might be considered as a combination of the other two. However, the actual system of forces induced is dependent on the degree of homogeneity and mode of failure of the specimen. If the specimen is perfectly homogeneous and failure occurs simultaneously and uniformly throughout, the behaviour is identical to that indicated in the first philosophy. Owing to the non-uniformity of concrete specimens the differential straining rate causes the weakest face of the specimen to deform more rapidly than the others, particularly as failure approaches. Any lateral displacement of the pinned end with reference to the fixed end of the specimen due to this differential straining rate will be accentuated at failure. This creates a lateral reaction whose magnitude is a compatability function of the lateral stiffnesses of the machine and specimen and the degree of non-homogeneity of the specimen. On analysing the force system (see Figure 5.2d) it can be seen that the maximum stress variation will occur at the fixed end and the maximum stress on the stiffer face. Failure may propagate from this point of maximum stress at a loading stage which is dependent upon the lateral stiffness of the machine and the characteristics of the specimen.

5.3.1 Uniaxial Testing

It is usually assumed in the uniaxial test that the testing machine applies the load through the centre of the specimen(see Figure 5.2a). It is apparent that this philosophy can be satisfied only in the case of effectively pinned ends. As a frictionless spherical seating is a pinned device, it may be thought that the tests on uniaxial machines which have spherical seatings satisfy the third philosophy. However no spherical seating is friction-free, and a resistance moment is created upon tilting. Therefore, it must be recognised that the system of loading is more complex than any of the three philosophies described above (see Figure 5.2e).

The frictional resistance in the spherical seating may vary between large limits (28). It can be so great that the spherical seating is incapable of tilting during the course of the test, so exhibiting a condition of complete fixity. In this case, the loading system becomes identical with the second philosophy shown in Figure 5.2c. On the other hand, if the moment resistance is very small, the system of loading is similar to that explained in the third philosophy. With testing machines of low lateral stiffness, the lateral reaction of the testing machine on the specimen and resulting moment at the fixed end both approach zero. Under these conditions, the specimen may be analysed as being effectively pinned at both ends.

5.4 TESTING MACHINE CHARACTERISTICS AND THEIR EFFECT ON THE UNIAXIAL TEST

The testing machine characteristics which are likely to have an effect on the strength of uniaxial specimens include the longitudinal and lateral stiffness, stability, type of platens and spherical seating used, alignment of components, the method of testing the specimen, load application rate, ram effect and operator technique. These characteristics must be considered in relation to the philosophies of testing as well as the effect on the strength of the compression specimen.

5.4.1 Longitudinal Stiffness

Any testing machine can be considered as a combination of springs, represented by the specimen and various testing machine parts. Figure 5.3 shows diagrammatically the relation between the deformation of specimen and testing machine during loading. As a certain volume of hydraulic fluid is pumped into the ram cylinder, the ram would be displaced a distance Δ_T if no resistance were provided by the specimen. However, the specimen does produce a resistance which is simultaneously accompanied by a change in its length, Δ_S. The remainder of the total displacement Δ_T is absorbed by the elasticity of the testing machine components, Δ_M, which include elongation of the columns, deflection of the crossheads, compression of the end blocks, compression of the hydraulic fluid, expansion of the hydraulic lines and movements in the load indicator.

As the load produced by the machine is directly proportional to the combined deformation of its components, each machine

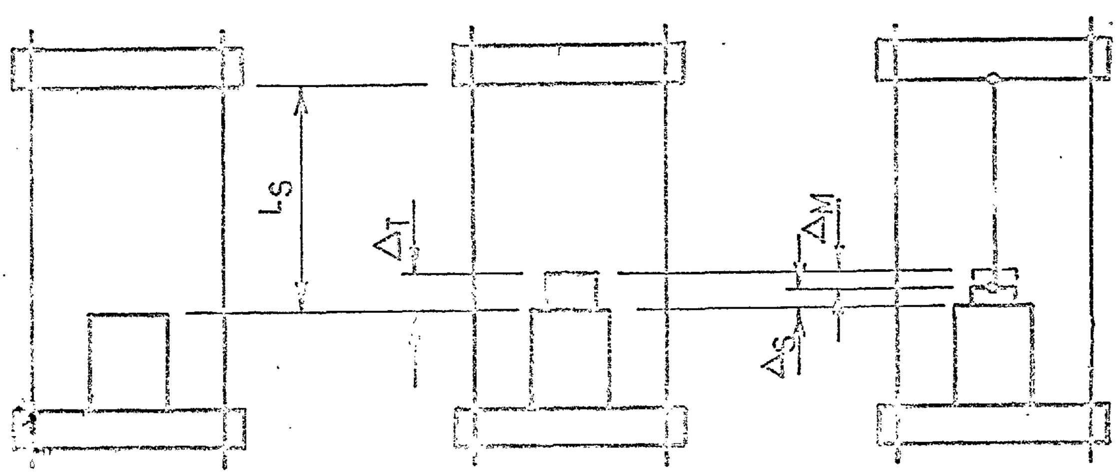

FIG. 5.3 DIAGRAMMATIC RELATIONSHIP BETWEEN DEFORMATIONS OF SPECIMEN AND TESTING MACHINE

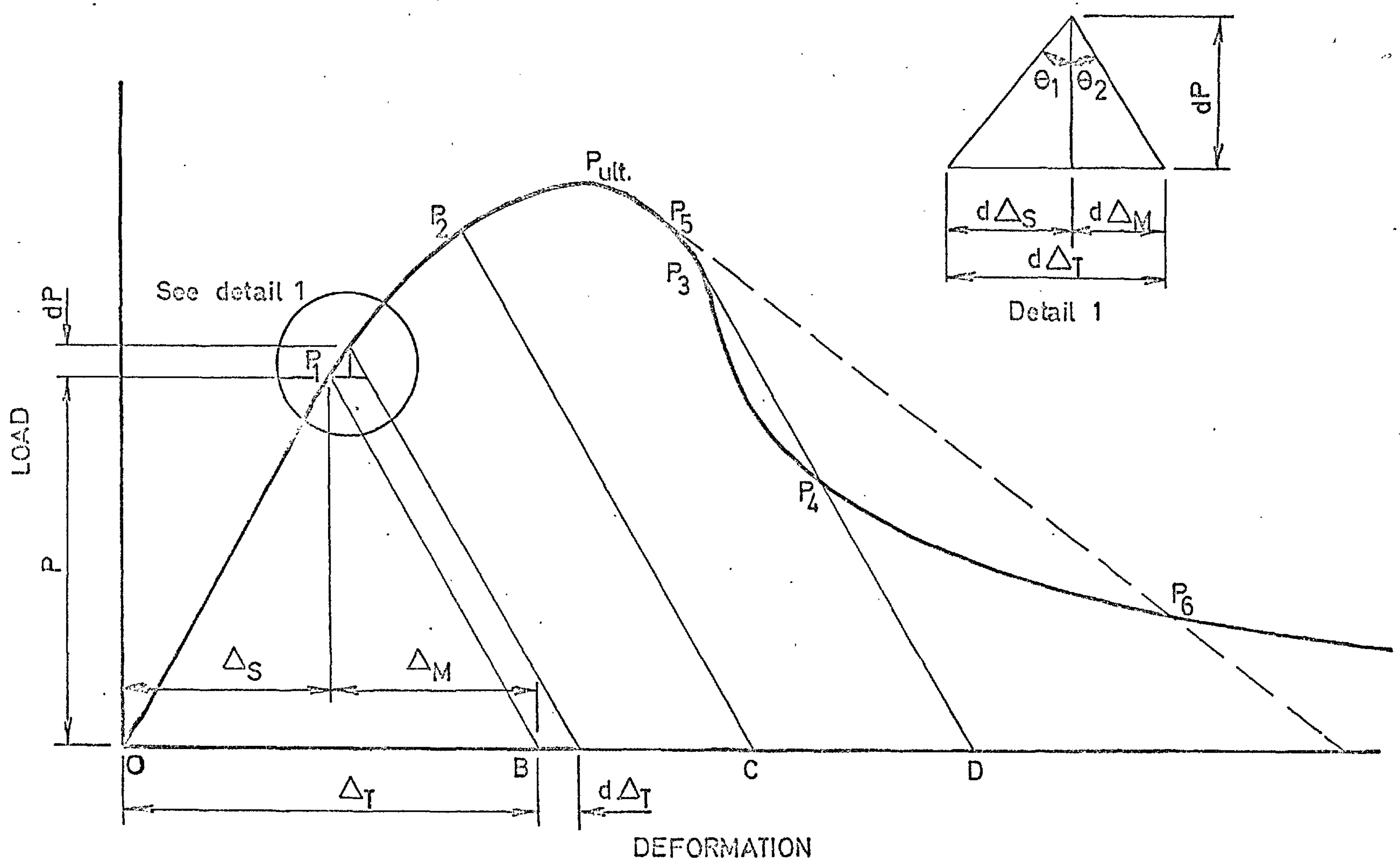

FIG. 5.4 GRAPHICAL RELATIONSHIP BETWEEN DEFORMATIONS OF SPECIMEN AND TESTING MACHINE

has a particular load deformation characteristic or longitudinal stiffness, indicated by the lines BP_1CP_2etc. in Figure 5.4. Similarly, the complete load deformation characteristic of the specimen is shown by the line AP_3P_6. The series of intersections of the load-deformation curves of the specimen and machine at increasing loads P_1, P_2, etc. indicate a state of equilibrium of the composite system. However, after the maximum load is passed, a point P_3 may be reached where the load-deformation characteristic of the machine is less steep than that of the specimen. The composite system then becomes unstable as the load drops suddenly to point P_4.

Testing machines can be defined as soft when the elastic deformation of the machine is much larger than the deformation of the specimen or as hard when the elastic deformation of the machine is of the same order of magnitude or smaller than that of the specimen (93). The load deformation characteristic of a soft machine can be represented by the comparatively flat line P_5P_6 in Figure 5.4. After the maximum load of the specimen has been reached, the period of non-equilibrium is greater than in a hard machine. The greater period of instability will produce a more violent or explosive failure of concrete specimens. With soft testing machines, such failures can have a psychological effect on the operator causing him to reduce the loading rate near failure in order to avoid the period of instability. This will reflect itself in relatively low results.

Hoff (32) has shown, from tests on column buckling, that the longitudinal stiffness of the machine has a pronounced influence on the shape of the load-deformation curve obtained during actual buckling. Similarly, with the testing of steel, Bernhard (33) showed that the stress-strain curve is very dependent on the testing machine's longitudinal stiffness. To obtain the complete stress-strain curve for any material, it is necessary to have a very stiff machine. With such a method, investigations have been recently conducted on concrete specimens at both the Universities of Cambridge and Birmingham, (34, 35, 36).

A recent development in overcoming the lack of stiffness in soft testing machines is the load compensator designed by Avery Ltd. (37). With this device introduced into the hydraulic system, it is possible to increase the stiffness to virtually infinity.

5.4.2 Stability

During loading, the main members of compression testing machines are in tension. The possibility of buckling of such machines might at first appear to be illogical. Chilver (38) has shown, however, that the stability of a compression machine may be more difficult to ensure than that of a tension machine. Figure 5.5 shows diagrammatically the test machine and test specimen. It is assumed that the ends of the connecting columns, length L_T are built into the cross members and that the test specimen, length L_S, is effectively pinned at both ends. If at some load stage, the top cross-head moves laterally a small distance δ, then the change in length of L_S, although very small,

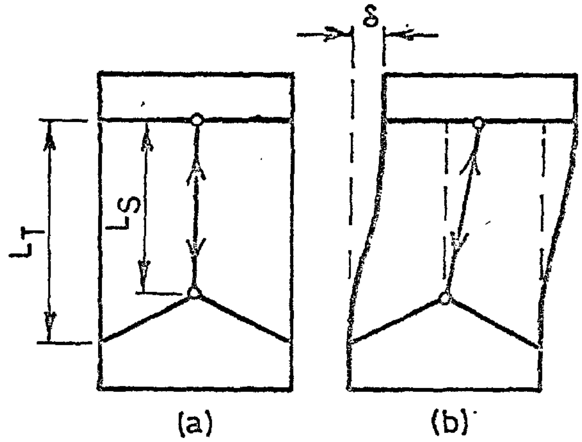

FIG. 5.5 DIAGRAMMATIC RELATIONSHIP BETWEEN TESTING MACHINE AND SPECIMEN WITH EFFECTIVELY PINNED ENDS. (a) Assumed Condition (b) Actual Condition

will be greater than that for L_T as long as $L_T > L_S$. In a compression test, this will result in a reduction of the deformation and load on the specimen. As it is natural for a system to assume a condition of least energy, the composite system will acquire this state at every load stage.

Equilibrium of the composite system is ensured if the lateral resistance of the machine balances the lateral component of the force P in the specimen. If it is assumed that the lateral component of the force P is resisted equally by n columns of the machine of uniform flexural stiffness EI, it can be shown that the value of P, at which the testing machine buckles about the specimen is given by the root of the equation:

$$\frac{L_S}{L_T} = 1 - \frac{\tanh \phi_t}{\phi_t} \qquad \text{........5.1}$$

in which

$$\phi_t^2 = P L_T^{\,2} / 4nEI \qquad \text{........5.2}$$

For relevant values of ϕ_t, the right hand side of equation 5.1 is always less than unity. Consequently, instability is only possible with $L_S < L_T$; that is, with a specimen shorter than the connecting columns. As L_S approaches zero, instability of the machine will occur at a lower load and this is confirmed by the difficulties encountered in the testing of short struts [38]. As 4" and 6" cubes are relatively short specimens, the problem of buckling becomes significant, especially in testing machines with long columns of small cross-sectional area.

Flint [39] indicated that in a compression machine with only two columns, buckling of the machine would not be as indicated in Figure 5.5. In that instance of a plane frame, the least buckling load would probably correspond to bowing of the columns out of their original plane which would then be given by equation 5.1 where

$$\phi_t^2 = PL_T^2/nEI \qquad \text{.......... } 5.3$$

This is created by the absence of fixity between the columns and the cross-head in the direction of buckling.

In tension machines with the connecting columns encastré with the cross-heads, Chilver has indicated two modes of buckling as defined by the solution of the equations:

$$\sin\ \phi_S = 0 \qquad \text{...........} 5.4$$

or

$$\frac{L_T}{L_S} = 1 - \frac{\tan\ \phi_S}{\phi_S} \qquad \text{.......... } 5.5$$

where $\phi_S = PL_S^2 / 4nEI$ 5.6

Equation 5.4 defines a condition of instability arising at the critical load, $\phi_S = \pi$. In this case, the columns of the testing machine buckle by a typical column buckling arising from too large a "slenderness ratio".

The second buckling mode, possible only with $L_T < L_S$, arises from a tendency for the top cross-head to move laterally with respect to the bottom cross-head, thus creating a reduction in the deformation and load on the specimen. Equation 5.5 thus defines the stage at which the testing machine buckles about the specimen in a manner analagous to the buckling of compression machines as represented by equation 5.1.

It has been shown (39) that for two column tension machines, buckling out of the plane of the frame would occur at a load defined by

$$\cot \phi_S = 1/2 \frac{P}{4nEI} (L_T - L_S) \qquad \text{...5.7}$$

for both positive and negative values of the right hand expression. When $L_T = L_S$, $\phi_S = \pi/2$ in contrast to a value of $\phi_S = \pi$ for collapse in the mode defined by equation 5.4 and the columns would require a stiffness out of their plane double that in their plane if the two modes of collapse were to coincide.

A buckled mode could also occur in which the tops of the columns were displaced by an amount δ in a direction normal to the diagonal across the head. The consequent twist of the top cross-head with respect to the bottom would result in a reduction of load on the specimen.

The foregoing assumes that both ends of the specimen are effectively pinned. Under the conditions of loading whereby either one or both ends are effectively fixed, rotation of both ends of the specimen simultaneously is impossible. Under these conditions, therefore, the problem of instability does not arise.

5.4.3 Lateral Stiffness

According to the third philosophy of testing, the laterally induced force is dependent on the machine lateral stiffness, that is, the relative force necessary to displace one end of the testing machine relative to the other. In existing concrete compression machines, the lateral stiffness can vary from about 6×10^2 lbs/inch to 2×10^5 lbs/inch while the lateral stiffness of 4" and 6" cubes is of the order of 1×10^6 to 5×10^6 lbs/inch. Cube specimens are therefore very stiff laterally in relation to the testing machine and so, in general, are not likely to be influenced by induced lateral forces. However, with very stiff machines, the larger lateral forces will have some effect which will be more pronounced on longer specimens such as the American cylinder and the 4" x 4" x 12" prism (21). This will be explained in detail in Chapter 6.

Under effectively fixed conditions, rotation of the ends of the specimen is impossible. Consequently, there can be no lateral movement of one end of the specimen relative to the other and induced lateral forces therefore do not occur.

5.4.4 Spherical Seating Effect

Information concerning spherical seatings is given in both B.S. 1881[9] and A.S.T.M. -C39-64[27]. British Standard 1881 states,"One of the platens (preferably the one that normally will bear on the upper surface of the cube) shall be fitted with a ball seating in the form of a portion of a sphere, the centre of which coincides with the central point of the face of the platen. The movable portion of the spherically seated compression platen shall be held on the spherical seat, but the design shall be such that the bearing face can be rotated freely and tilted through small angles in any direction.

The first function of a spherical seating is to allow the machine platen to bear evenly on the specimen before loading even though opposite faces of the specimen are not geometrically parallel. It is important that the two parts of the spherical seating are maintained in close contact during the initial clamping down on to the specimen; otherwise, a non-uniform contact may result in tilting and sliding of the sphere during loading so inducing shear forces and moments into the specimen.

The spherical seating performs a second function during the course of loading when it can either tilt freely, thereby being effectively pinned, or lock, thus becoming fixed, or a condition between these extremes. Yet, the specifications make no reference to the action of the spherical seating during testing.

The behaviour of any spherical seating will depend on its moment resistance, that is, the product of its radius and the normal force and coefficient of friction at the interface. The coefficient of friction is dependent on the area and type of contact, surface finish and type of lubricant used. Tarrant (29) has shown that the lubricant used in the spherical seating can break down under load so that seatings can behave differently for concretes of different strength.

5.4.5 Platen Effect

The action of applying the compressive load to the specimen through machine platens introduces a complex state of stress in the ends of the specimen which depends on various factors. (40) In order that the platen restraint be identical in different testing machines, it is necessary to;

1. ensure that all machines have platens of the same rigidity and degree of finish and / or
2. use sufficiently long compression specimens that failure occurs on the central zone where platen effects have been eliminated as shown by Newman and Lachance (1,21,40).

Cube strength results are dependent on the size of the platens of the machine. Ideally, it would be preferable to have platens of infinite rigidity, but in practice even large end blocks undergo small lateral expansions. Moreover, the machine platens become scratched and deformed through continuous testing and the use of removable intermediary platens which can easily be reground is to be recommended.

Newman and Lachance[21] showed that, when intermediary steel platens of the same cross-sectional dimension and having a thickness equal to half the specimen width are used, the restraint effect would become constant. Platens of this size, however, become massive and difficult to handle; a 6" platen would weigh 30 lbs. It seems reasonable, therefore, that 1/2" thick intermediary platens of the same dimensions as the specimen be interposed between the ends of the specimen and the machine platens. The lower intermediary platen would be located by dowels to the machine platen to facilitate accurate setting up of the test specimen. Such platens should provide the same degree of restraint in all testing machines which have large machine platens.

Non-uniform contact between the specimen ends and the machine platens can be the cause of inconsistent strength results. Investigators[30,41] have shown that concavity or excessive convexity of the platens produce reduced strengths while a small convexity results in a slight increase in strength. L'Hermite[42] has also shown that surface irregularities arising from wear of the moulds, and platen faces of the machine, can account for as much as a 15% difference in average strengths. Consequently, the importance of maintaining the mould ends and platens plane in accordance with the standard specifications cannot be over-emphasized.

5.4.6 Specimen Alignment

Although it is accepted that specimens should be properly centred in the machine, the necessity for extreme care in aligning the specimen with the vertical axis of the testing machine is not always realised. For example, a misalignment of 1/32" will introduce a stress variation of 9% on a 4" square section under effectively pinned conditions. Specimens loaded in this manner will show both a lower strength and a larger variation of results.

Under effectively fixed conditions, the specimen is deformed uniformly and results would be expected to be less susceptible to misalignment. However, when a spherical seating is used, misalignment can be sufficient to overcome its moment of resistance thereby producing a varying degree of end fixity.

5.4.7 Load Application Considerations

5.4.7.1 Hydraulic machines

British Standard 1881 requires the applied load P to be increased at a constant rate, that is, $\frac{dP}{dt} = k$ (constant), where t is time. As the specimen approaches failure, the tangent value of the modulus of elasticity decreases, resulting in a corresponding increase in the deformation rate, From Figure 5.4,

$$\cot \theta_1 = \frac{dP}{d\Delta_S} = X_S \qquad \text{.... 5.8}$$

is the tangent load deformation value of the specimen at any load stage, P. Similarly,

$$\cot \theta_2 = \frac{dP}{d\Delta_M} = X_M \qquad \text{.... 5.9}$$

is the corresponding load deformation characteristic of the machine. From Equation 5.8

$$d\Delta_S = \frac{1}{X_S}\,dP \qquad \ldots 5.8a$$

from which, by differentiating both sides with respect to time.

$$\frac{d\Delta_S}{dt} = \frac{1}{X_S}\frac{dP}{dt} \qquad \ldots 5.10$$

Similarly, from Equation 5.9

$$d\Delta_M = \frac{1}{X_M}\,dP \qquad \ldots 5.9a$$

from which,

$$\frac{d\Delta_M}{dt} = \frac{1}{X_M}\frac{dP}{dt} \qquad \ldots 5.11$$

Adding 5.10 and 5.11 gives

$$\frac{d\Delta_T}{dt} = \frac{dP}{dt}\left(\frac{1}{X_M} + \frac{1}{X_S}\right) \qquad \ldots 5.12$$

As the specimen approaches its ultimate strength, X_S will decrease eventually becoming zero at the peak point, $P_{ult.}$ and $1/X_S$ simultaneously becomes infinite. Near failure, the continued application of stress therefore depends on the pumping rate capacity of the pump, $d\Delta_T/dt$. As the tangent modulus of elasticity at 99% of the ultimate strength of concrete is about 5% of the modulus at zero stress, it is suggested that compression testing machines should be designed to apply a minimum deformation rate of 0.5 ins/min. to the specimen($=\frac{d\Delta_S}{dt}$) at ultimate strength.

Soft testing machines require a greater pumping capacity than hard testing machines, and therefore a constant rate of stress increase up to ultimate can be more readily achieved on machines which are longitudinally stiff.

As it is important that the load be applied smoothly, piston type pumps should, in general, be avoided.

5.4.7.2 Screw type machines

A.S.T.M. specifications C39-64[27] states that, for screw type machines, the moving head shall travel at a rate of about 0.05 in. per minute when the machine is running idle. That is, $\frac{d\Delta_T}{dt} = 0.05$ in/min. Under this condition, it will be seen that the load application rate on the specimen will vary proportionally to $\frac{X_M X_S}{X_M + X_S}$ (from equation 5.12) That is,

$$\frac{dP}{dt} = k \frac{X_M X_S}{X_M + X_S} \qquad \ldots 5.13$$

where k is a constant. It is, therefore, obvious that the stress rate is not only a function of the stiffness of the specimen, but also of the machine.

In order to examine if any variation is observed in the load application rate by two testing machines of different longitudinal stiffness at any load stage when the initial stress rates are identical, the following analysis is conducted.

From Equation 5.12 and Figure 5.4, for testing machine No. 1 at the initiation of loading, that is, at the origin, o, the relation between the loading rate and the total deformation rate is

$$\left(\frac{d\Delta_T}{dt}\right)_{01} = \left(\frac{dP}{dt}\right)_{01} \left[\frac{1}{X_{S0}} + \frac{1}{X_{M1}}\right] \qquad \ldots 5.14$$

and for testing machine No. 2, it is

$$\left(\frac{d\Delta_T}{dt}\right)_{02} = \left(\frac{dP}{dt}\right)_{02}\left[\frac{1}{X_{SO}} + \frac{1}{X_{M2}}\right] \qquad \ldots 5.15$$

Dividing Equation 5.14 by Equation 5.15, and noting that

$\left(\frac{dP}{dt}\right)_{01} = \left(\frac{dP}{dt}\right)_{02}$, we obtain

$$\frac{\left(\frac{d\Delta_T}{dt}\right)_{01}}{\left(\frac{d\Delta_T}{dt}\right)_{02}} = \frac{\left(X_{M1} + X_{SO}\right) X_{M2}}{\left(X_{M2} + X_{SO}\right) X_{M1}} \qquad \ldots 5.16$$

At a certain load stage, P, for testing machine No. 1

$$\left(\frac{d\Delta_T}{dt}\right)_{P1} = \left(\frac{dP}{dt}\right)_{P1}\left[\frac{1}{X_{SP}} + \frac{1}{X_{M1}}\right] \qquad \ldots 5.17$$

and for testing machine No. 2

$$\left(\frac{d\Delta_T}{dt}\right)_{P2} = \left(\frac{dP}{dt}\right)_{P2}\left[\frac{1}{X_{SP}} + \frac{1}{X_{M2}}\right] \qquad \ldots 5.18$$

Dividing Equation 5.17 by Equation 5.18, we obtain

$$\frac{\left(\frac{d\Delta_T}{dt}\right)_{P1}}{\left(\frac{d\Delta_T}{dt}\right)_{P2}} = \frac{\left(\frac{dP}{dt}\right)_{P1}}{\left(\frac{dP}{dt}\right)_{P2}} \frac{\left(X_{M1} + X_{SP}\right)}{\left(X_{M2} + X_{SP}\right)} \frac{X_{M2}}{X_{M1}} \qquad \ldots 5.19$$

For a screw-type machine, the total deformation rate is constant at all load stages. Therefore, for testing machine No. 1

$$\left(\frac{d\Delta_T}{dt}\right)_{01} = \left(\frac{d\Delta_T}{dt}\right)_{P1} \qquad \ldots 5.20$$

and similarly

$$\left(\frac{d\Delta_T}{dt}\right)_{O2} = \left(\frac{d\Delta_T}{dt}\right)_{P2} \qquad \ldots 5.21$$

Substituting Equation 5.16 into Equation 5.19 and using the relationships of Equations 5.20, and 5.21, we obtain the ratio of loading rates at any load stage P for the two testing machines, as

$$\frac{\left(\frac{dP}{dt}\right)_{P1}}{\left(\frac{dP}{dt}\right)_{P2}} = \frac{(X_{M1} + X_{SO})(X_{M2} + X_{SP})}{(X_{M2} + X_{SO})(X_{M1} + X_{SP})} \qquad \ldots 5.22$$

From Equation 5.22, it is seen that the loading rate will be equal for the two machines only when:

(1) $X_{SO} = X_{SP}$, that is, the stiffness of the specimen at point P is identical to that at the origin. After the proportional limit has been exceeded, this relationship will not apply.

(2) $X_{M1} = X_{M2}$, that is, the stiffnesses of the two machines are identical.

Ultimate strength results are dependant on the loading rate, particalarly near failure (40,43,44). From Equations 5.13 and 5.22, it is seen that this loading rate will vary between wide limits as testing machines used for concrete have longitudinal stiffnesses ranging approximately from 10×10^5 to 10×10^7 lbs/in. For example, when testing a 6" x 12" concrete cylinder with $E = 4.2 \times 10^6$ p.s.i. ($X_S = 10 \times 10^6$ lbs./in. reducing to 5×10^5 lbs / in. at 99% of ultimate load) in a testing machine of $X_M = 10 \times 10^5$ lbs / in. at a total deformation rate of 0.05 in/min., the stress rate on the specimen will reduce from 20 tons/min. at the beginning of loading to 7 tons /min. at 99% of ultimate strength. On the other hand, a machine with $X_M = 10 \times 10^7$, the loading rate at the same total deformation rate will reduce from 200 ton/min. to 11 ton/ min. at 99% of ultimate load. For the alternative analysis, where the loading rate at initiation of loading is constant for different machines, say 20 ton/min. on the concrete cylinder described above, the stressing rates at 99% of ultimate load will be 7 and 1.1 ton/min. respectively, for machines with $X_M = 10 \times 10^5$ lbs/in. and 10×10^7 lbs/in. Such large variations in the stress rate will produce variations in concrete strengths of the order of 5 %.

5.4.8 Ram Effect

Hydraulic testing machines are calibrated with the calibration device aligned co-axially with the centre-line of the ram. The assumption that the centroid of resistance of the specimen will also always pass symmetrically through the ram is misleading, Particularly, with control testing, the accuracy of placing the specimen is not always as good as with placing the calibration device. In addition, concrete specimens may have their centroid of resistance located away from their centre-line towards the stiffest face. Consequently, it is reasonable to suggest that the centroid of specimen resistance may be located up to 1/2" off centre. The normal forces and resulting frictional forces created between the ram and ram cylinder will thereby increase with an increase in the misalignment of the specimen (as shown in Section 4.3.2). This will be reflected in high ultimate strength results. Inconsistency in this misalignment will create an increased scatter in results.

The frictional forces created on the ram cylinder-ram interface are a function of the contact length, specimen misalignment, degree of surface finish, type of lubrication, rate of sliding, machining tolerances and differential temperature through the ram and ram-cylinder. Errors due to ram effect may be deduced by :

1. Having a ram of large diameter
2. Having a long length of contact between the ram and ram-cylinder.
3. High machining standards, close tolerances and a high quality of surface finish

4. Causing the ram to rotate during loading, thus reducing the friction from a static to a sliding value.
5. Using clean hydraulic fluid capable of good lubrication
6. Performing the tests in a temperature controlled laboratory.

The lateral deformation of a concrete specimen under load can cause a lateral expansion in the end of the ram. This may be significant in rams of small cross-sectional area even causing partial binding of the ram in the ram-cylinder. To prevent this, the top of a ram of small diameter should be at least 2" above the cylinder at the beginning of its travel.

5.4.9 Operator Technique

A uniaxial strength test involves the following operations:
1. placing the specimen in the testing machine,
2. loading the specimen by some prescribed method,
3. recording the load.

The manner in which these are carried out can be termed operator technique. Variation in results on supposedly identical specimens tested in the same machine by different operators is due to operator technique.

Uniform contact between the ends of the specimen and machine platens and the correct alignment of the specimen in the machine are both essential if consistent results are to be achieved. It is important that small pieces of grit on the specimen ends or platens which can cause zones of stress concentration are wiped off before testing. For compression testing, accurate and consistent alignment of specimens could be more readily achieved if intermediary platens of the same cross-section as the specimens are used, the lower one of which is accurately dowelled into the testing machine.

On the more modern testing machines, pacing devices are provided which help the operator to control the loading rate. Such facilities will reduce considerably the variations attributed to operator technique. However, the opening of the control valve in hydraulic machines is still performed manually and the degree of control can be improved if testing machines are provided with,

1. A very fine control valve which allows the fluid flow to be more easily regulated,

2. A large ram area which ensures low working pressures in the fluid and a large flow through the control valve.

The precision with which a load may be read is described in British Standard 1610[8]. A large load indicating device well marked out will result in greater precision of load reading and less error due to operator technique.

5.4.10 Other Factors

As regards accuracy of the testing machine, British Standard 1881 states that the machine shall comply with Grades A or B of British Standard 1610. This specification refers only to the accuracy with which a load may be determined and the repeatability of the testing machine in load indication. However, there are certain machine characteristics which have no effect during load verification, yet can produce complex force systems and variable results when concrete specimens are tested. Tests carried out by the author show that especially on machines which are long and laterally flexible, it is difficult to reproduce deformational behaviour in the same specimen from one set-up to the next(see Chapter 7). It is found that, in general, machines with loose fitting components are most likely to produce undesirable stress effects. Consequently, the necessity of the design and manufacture of all the components of a machine to close tolerances cannot be overemphasised. The alignment of components is particularly important as the susceptibility of strength results to the misalignment of the specimen in the machine can be similarly reflected in misalignment of components of the machine.

In hydraulic machines, there will be a pressure lag between the pump and ram owing to friction losses in the fluid in the connecting lines. Improvement in the accuracy of readings can be achieved by placing the load measuring unit near the specimen and designing the connecting lines to reduce frictional losses to a minimum.

5.5 SUMMARY

In the past, there has been a tendency to assume that testing machines which are designed for a specific purpose, such as cube testing, do produce repeatable and accurate results. The lack of knowledge concerning the behaviour of testing machines in practise has simply added weight to this supposition. However, discrepancies of the magnitude shown in Figure 5.1 are too large to attribute to the scatter of concrete strengths. In addition, Cole[18] has shown that the errors found in the compressive testing of cubes and those errors found in the calibration of testing machines are not of the same form.

For all strength testing, it is important that testing machines load the specimen in an explicitly definable manner conforming to one of the basic philosophies of loading. Tests performed for determining fundamental properties of a material require further investigation into specimen shape and size to assure that a fundamental state of stress or strain is being achieved. For routine control testing, the importance of loading specimens in a single machine from one set-up to another or between testing machines, in a repeatable manner is obvious. In addition, the method of placing and testing the spcimens, for control purposes must be simple to perform and relatively immune from operator technique.

An historical example of the incongruity of control testing and operator technique was the 'briquet test'. Its replacement with the compressive test was necessitated by the susceptibility of its values by misalignment of the specimen. Evans[45], in conducting strain measurements on opposite sides of several different sizes of briquet specimens, showed conclusively that the strain distribution depended on the initial location of the specimen in the grips. These strain variations, he showed, could vary by up to 100% in routine testing.

From the discussion of this chapter, several shortcomings in current specifications on testing machines are apparent. They are:

(1) The explicitly definable method of loading specimens is not stated.

(2) A lower limit of longitudinal stiffness for preventing explosive failures is not given.

(3) Spherical seating properties such as size, degree of surface finish, type of lubrication as well as its behaviour during loading should be included.

(4) If the philosophy of one end pinned and the other end fixed is adopted as the method of loading specimens, then upper and lower limits of lateral stiffness should be included.

(5) The limit of machine restraint effect is not given for cube testing.

(6) A minimum deformation rate for straining the specimen at its ultimate load should be included.

(7) There are no specifications on the allowable error for off-centre loading on hydraulic rams.

(8) Specifications for improvement in operator technique such as control fineness, pacing devices, and dowelled platens for accurate setting up could be introduced.

From previous research, there is an obvious lack of knowledge to answer these questions. The author, in an attempt to produce a coherent picture of the actual behaviour of testing machines began by investigating testing machines at Imperial College. The results of this are presented in Chapter 7. Simultaneously, a theoretical investigation was conducted on the influence of the lateral stiffness and misalignment of the specimen and testing machine and the degree of non-homogeneity of the specimen on strength characteristics under each of the three basic methods of loading. These are presented in Chapter 6. From these two investigations, it was apparent that the main cause for inconsistency in strength results between different testing machines was due to differences in the behaviour of spherical seatings. The results of an experimental investigation on spherical seating behaviour and its influence on concrete strengths are given in Chapters 8 and 9.

CHAPTER 6

THE INFLUENCE OF LATERAL STIFFNESS, MISALIGNMENT, SPECIMEN NON-HOMOGENEITY AND METHOD OF LOADING ON CONCRETE PROPERTIES

6.1 INTRODUCTION

Testing machines, generally, contain a ram operating inside a ram-cylinder at one end of the specimen with a spherical seating at the other. As the ram is incapable of tilting during the course of a test, it may be considered effectively fixed. The spherical seating may likewise be unable to tilt in its seating due to too large a frictional resistance on its mating surfaces, thereby producing also, an effectively fixed condition. This system of loading will produce no horizontal movement and thereby, no lateral forces because of an equal amount of deformation on all sides of the specimen at every load stage.

The spherical seating may alternatively be considered as pinned, if the mating surfaces are virtually frictionless. Under this system of loading, as shown in Figure 5.2(d), differential straining of opposite sides of the specimen will result in a lateral displacement of one end of the specimen relative to the other. This movement induces a lateral force which is a compatability function of the lateral stiffnesses and misalignments of the specimen and machine, and the degree of non-homogeneity of the specimen.

In order to assess the influence of such characteristics on the resulting stress distribution in a specimen, the following analysis is conducted on the most general case of a misaligned specimen with a varying modulus of elasticity, loaded uniaxially with one end pinned and one end fixed. From this case, the stress distributions are also obtained for loading with both ends pinned and with both ends fixed. A subsequent theoretical investigation shows the expected differences in ultimate strengths, stresses and strains at the discontinuity level (14) and even modulus of elasticity as a function of the test method.

6.2 THEORETICAL ANALYSIS

6.2.1 One End Pinned, One End Fixed Load Method

The specimen considered is prismatic in shape with length L, breadth b and depth d, having a modulus of elasticity which varies linearly from E_1 on the soft face to E_2 on the stiff face. The specimen is   to be loaded uniaxially and, as the ends of the specimen are assumed to remain plane, there will be a linear variation in longitudinal deformation or strain δ from δ_1 on the soft face to δ_2 on the stiff face. This differential straining of the specimen causes it to bend, which produces a lateral movement of the pinned end of the specimen relative to the fixed end, thereby creating a lateral reaction in the machine as shown in Figure 6.1. The resulting force system can be considered as the summation of:

(1) the specimen loaded axially in a pinned end condition (see Figure 6.2a) and

(2) the specimen loaded laterally as a cantiliver (see Figure 6.2.b)

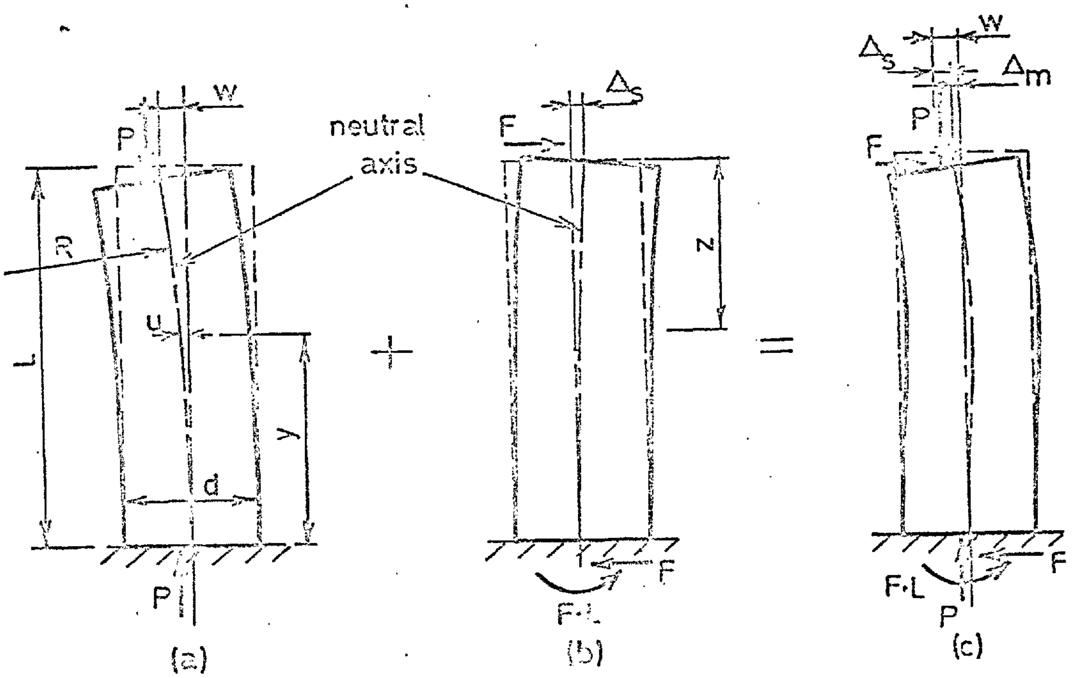

FIG. 6.1 DIAGRAMMATIC REPRESENTATION OF LATERAL MOVEMENT IN SPECIMEN AND TESTING MACHINE

(a) Natural Lateral Movement of Loaded Specimen

(b) Return Lateral Movement due to Induced Machine Force

(c) Actual Displacement Pattern

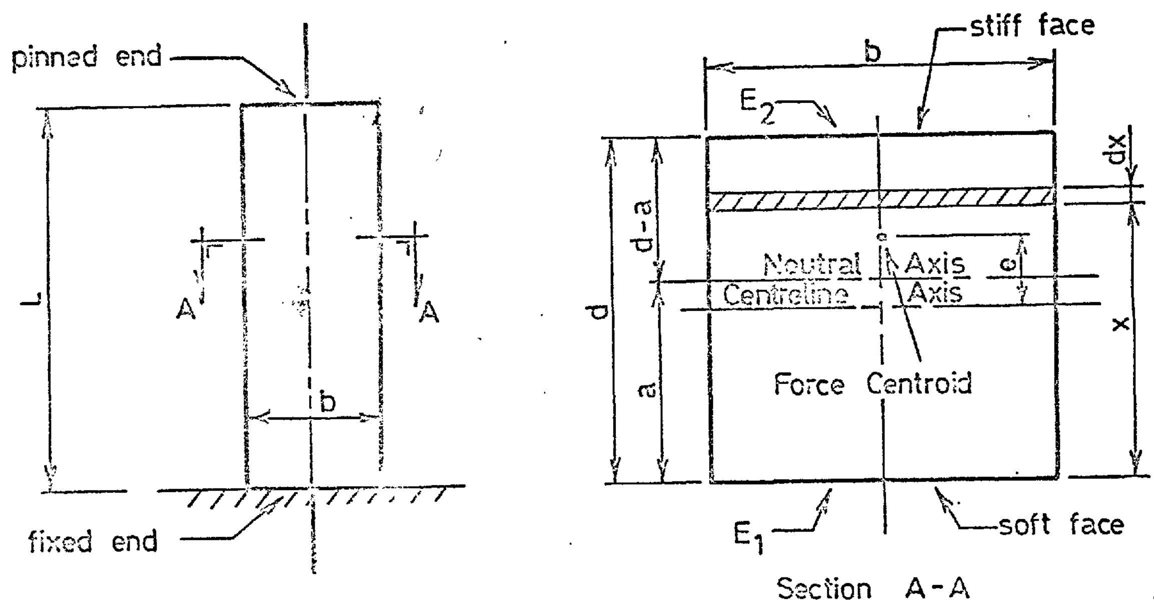

FIG. 6.2 ELEVATION VIEW AND CROSS-SECTION OF SPECIMEN

6.2.1.1 Axial loading

On the strip shown in Figure 6.2

$$E = E_1 + (E_2 - E_1)\frac{x}{d} \qquad \text{...6.1}$$

and

$$\delta = \delta_1 + (\delta_2 - \delta_1)\frac{x}{d} \qquad \text{...6.2}$$

where δ denotes strain and the subscripts 1 and 2 refer to the conditions on the soft and stiff faces respectively.

At any point, $\sigma = \delta E$ ...6.3

where σ denotes stress.

$$\text{Therefore, } \sigma = \left[E_1 + (E_2 - E_1)\frac{x}{d}\right]\left[\delta_1 + (\delta_2 - \delta_1)\frac{x}{d}\right] \qquad \text{...6.4}$$

Force on the strip

$$= \sigma \cdot bdx \qquad \text{...6.5}$$

$$= \left[E_1 + (E_2 - E_1)\frac{x}{d}\right]\left[\delta_1 + (\delta_2 - \delta_1)\frac{x}{d}\right] bdx \qquad \text{...6.6}$$

Integrating Equation 6.6 over the dimension d yields;

Total Force on Cross-section =

$$\frac{bd}{6}\left[2(E_1\delta_1 + E_2\delta_2) + E_1\delta_2 + E_2\delta_1\right] \qquad \text{...6.7}$$

Moment of force on strip about soft face, = Force on strip $\cdot$ x

$$= \sigma\, bxdx \qquad \text{(from Equation 6.5)}$$

$$= \left[E_1 + (E_2 - E_1)\frac{x}{d}\right]\left[\delta_1 + (\delta_2 - \delta_1)\frac{x}{d}\right] b\, xdx \qquad \text{...6.8}$$

Integrating Equation 6.8 over the dimension, d yeilds;

$$\text{Moment of Force} = \frac{bd^2}{12}\left[E_1\delta_1 + E_1\delta_2 + E_2\delta_1 + 3E_2\delta_2\right] \qquad \text{...6.9}$$

Equating the total force on the cross-section to P, then from Equation 6.7,

$$P = \frac{bd}{6}\left[2(E_1\delta_1 + E_2\delta_2) + E_1\delta_2 + E_2\delta_1\right] \qquad \text{...6.10}$$

From Equation 6.9, with an eccentric load application of e units

$$P\left(\frac{d}{2} + e\right) = \frac{bd^2}{12}\left[E_1\delta_1 + E_1\delta_2 + E_2\delta_1 + 3E_2\delta_2\right] \qquad \text{...6.11}$$

By solving Equations 6.10 and 6.11 simultaneously for δ_1 and δ_2, we obtain

$$\delta_1 = \frac{6P\left[E_2 d_2 - 2e(E_1 + 2E_2)\right]}{bd^2\left[E_1^2 + 4E_1E_2 + E_2^2\right]} \qquad \ldots 6.12$$

$$\delta_2 = \frac{6P\left[E_1 d_2 + 2e(2E_1 + E_2)\right]}{bd^2\left[E_1^2 + 4E_1E_2 + E_2^2\right]} \qquad \ldots 6.13$$

By substituting Equations 6.12 and 6.13 into Equation 6.4, we obtain the expression for the stress at any point due to axial loading as,

$$\sigma_a = \frac{6P}{bd^3(m^2 + 4m + 1)}\left[md^2 + x(d - x)(m - 1)^2 + \frac{e}{d}\left(6x^2(m^2 - 1) - 4xd(m^2 - 2m - 2) - 2d^2(2m + 1)\right)\right] \qquad \ldots 6.14$$

where $m = \frac{E_2}{E_1}$ ...6.15

It is observed that, even under axial loading ($e=o$), the stress will vary parabolically across the cross-section. For the particular case of a uniform specimen ($m = 1$), Equation 6.14 reduces to the well-known form for a misaligned specimen

$$\sigma_a = \frac{P}{bd} + \frac{Pe\left(x - \frac{d}{2}\right)}{\frac{bd^3}{12}} \qquad \ldots 6.16$$

6.2.1.2 Cantilever loading

In order to find the stress distribution across the specimen due to the induced lateral force, it is necessary to calculate the lateral movement of the pinned end of the specimen. Firstly, under the loading system considered above, that is, pinned end, axially loaded, the lateral movement, w, due to bending of the specimen is given by the double integration of the Equation[46] (see Figure 6.1a),

$$\frac{d^2u}{dy^2} = \frac{1}{R} \qquad \ldots 6.17$$

where y is the distance from the fixed end of the specimen, u is the lateral deformation at distance y and R is the radius of curvature which is given by[46].

$$R = \frac{d}{\delta_1 - \delta_2} \qquad \ldots 6.18$$

Integrating Equation 6.17 twice yields;

$$w = \frac{1}{R}\,\frac{L^2}{2} \qquad \ldots 6.19$$

from which, by substituting in Equation 6.18, we obtain

$$w = \frac{(\delta_1 - \delta_2)}{d}\,\frac{L^2}{2} \qquad \ldots 6.20$$

Substitution of Equations 6.12 and 6.13 into Equation 6.20 yields;

$$w = \frac{3\,L^2P\,\left[d(E_2 - E_1) - 6e(E_1 + E_2)\right]}{bd^3\left[E_1^2 + 4E_1E_2 + E_2^2\right]} \qquad \ldots 6.21$$

Although the displacement w would be the movement if no lateral resistance was induced, the actual movement m is somewhat less as shown in Figure 6.1c, that is,

$$\Delta_s + \Delta_m = w \qquad \ldots 6.22$$

In order to determine the lateral induced force, F, a knowledge is required of the lateral stiffnesses (that is, the lateral force required to cause a unit lateral displacement of one end relative to the other) of both the specimen and testing machine. The lateral stiffness, k, of the testing machine, is,

$$k = \frac{F_m}{\Delta_m} \qquad \ldots 6.23$$

For the specimen, the lateral stiffness is obtained from the conventional force-displacement relationship for a laterally loaded cantilever,[47] that is,

$$\frac{F_s}{\Delta_s} = \frac{3EI}{L^3} \qquad \ldots 6.24$$

However, the lateral force in the machine F_m must equal the lateral force in the specimen F_s, that is,

$$F_s = F_m = F \qquad \ldots 6.25$$

With a specimen having a varying modulus of elasticity E, the effective EI value in Equation 6.24 can be computed from the relation,[46]

$$EI = MR \qquad \ldots 6.26$$

where R is given in Equation 6.18. Due to pure bending on the cross-section, the strain will vary linearly from a zero value on the neutral axis to maximum values, δ_{1b} and δ_{2b} at the soft and stiff faces, respectively. On the strip shown in Figure 6.2 the strain due to pure bending, δ_b is

$$\delta_b = \frac{(x - a)\ (\delta_{1b} - \delta_{2b})}{d} \qquad \ldots 6.27$$

From Equations 6.3 and 6.27, the resulting stress is

$$\sigma_b = \frac{(x - a)(\delta_{1b} - \delta_{2b})E}{d} \qquad \ldots 6.28$$

By substituting Equation 6.1 into Equation 6.28, and multiplying by the area of the strip, then Force on strip

$$= \sigma_b \, b \, dx$$

$$= \frac{(x - a)(\delta_{1b} - \delta_{2b})}{d} \left[E_1 + (E_2 - E_1)\frac{x}{d}\right] bdx \qquad \ldots 6.29$$

Integration of Equation 6.29 between the limits a and d yields

Total Force above Neutral Axis

$$= \frac{b(\delta_{1b} - \delta_{2b})}{d} \frac{(d - a)^2}{6} \left[(E_1 + 2E_2) + \frac{a}{d}(E_2 - E_1)\right] \qquad \ldots 6.30$$

Similarly, by integrating Equation 6.29 between the limits 0 and a, then, Total Force below Neutral Axis

$$= - \frac{b(\delta_{1b} - \delta_{2b})}{d} \frac{a^2}{6} \left[3E_1 + \frac{a}{d}(E_2 - E_1)\right] \qquad \ldots 6.31$$

Multiplying Equation 6.31 by (-1) and equating to Equation 6.30, we obtain the location of the neutral axis as

$$a = \frac{d}{3} \frac{(E_1 + 2E_2)}{(E_1 + E_2)} \qquad \ldots 6.32$$

The moment of resistance of the section is then determined by integrating over the distance d, the product of the force on any strip and its distance from the neutral axis, from which,

$$M = \frac{bd^2(\delta_{1b} - \delta_{2b})}{36} \frac{(E_1^2 + 4E_1E_2 + E_2^2)}{(E_1 + E_2)} \qquad \ldots 6.33$$

From Equations 6.18, 6.26 and 6.33, we obtain the flexural stiffness of the specimen, that is,

$$EI = \frac{bd^3}{36} \frac{(E_1^2 + 4E_1E_2 + E_2^2)}{(E_1 + E_2)} \qquad \ldots 6.34$$

From Equations 6.22, 6.23, 6.24, and 6.25, we obtain for the laterally induced force, $F = \dfrac{W}{\left(\dfrac{1}{k} + \dfrac{L^3}{3EI}\right)}$ ...6.35

From Figure 6.1, it is observed that the moment at any section under consideration is

$$M = Fz \qquad \ldots 6.36$$

From Equations 6.18, 6.26, and 6.28, the strain on the strip due to the pure bending (Figure 6.2) is;

$$\delta_b = \frac{M}{\overline{EI}} (x - a) \qquad \ldots 6.37$$

By inter-relating Equations 6.3, 6.36, and 6.37, then

$$\sigma_b = \frac{Fz(x - a)}{\overline{EI}} \left[E_1 + \frac{x}{d}(E_2 - E_1)\right] \qquad \ldots 6.38$$

Then, by suitable substitution of F, (Equation 6.35) w, (Equation 6.21) and m, (Equation 6.15), we obtain;

$$\sigma_b = \frac{9zP(x - a)\left[d(m - 1) - 6e(m + 1)\right]\left[d + x(m - 1)\right]}{Lbd^4 (m^2 + 4m + 1)} \frac{k}{\left[k + \frac{3EI}{L^3}\right]} \qquad \ldots 6.39$$

where a and EI are obtained from Equations 6.32 and 6.34, respectively.

For a homogeneous specimen, that is, m is equal to unity and a is equal to d/2, Equation 6.39 reduces to;

$$\sigma_b = \frac{18zPe\left(\frac{d}{2} - x\right)}{Lbd^3} \left[\frac{k}{k + \frac{3EI}{L^3}}\right] \qquad \ldots 6.40$$

The actual stress at any point in the general non-homogeneous specimen is obtained by the sum of Equation 6.14 and 6.39. For a homogeneous specimen, the stress can be obtained directly from the summation of Equations 6.16 and 6.40.

6.2.2 Both Ends Pinned Load Method

With both ends pinned, no lateral forces arising from the bending of the specimen can be induced and therefore, $k = 0$. Thus, Equations 6.39 and 6.40 are zero in every case and the stresses are computed directly from Equations 6.14 and 6.16.

6.2.3 Both Ends Fixed Load Method

In this method, no differential straining is possible, that is, $\delta_1 = \delta_2$. By solving Equations 6.12 and 6.13, simultaneously we obtain;

$$e = \frac{d}{6}\left(\frac{m - 1}{m + 1}\right) \qquad \ldots 6.41$$

This means that the centroid of action is displaced by the above e - distance to be co-linear with the centroid of resistance of the uniformly deformed specimen. From Equations 6.15, 6.32 and 6.41, it is observed that with this loading method, the centroid of the applied force will coincide with the neutral axis. (see Figure 6.2)

By substituting Equation 6.41 into Equation 6.39, σ_b equals zero, that is, no lateral force is induced. The stress distribution is thus obtained by substitution of Equation 6.41 into Equation 6.14 to give;

$$\sigma = \frac{P}{\frac{bd}{2}(E_1 + E_2)}\left[E_1 + \frac{x}{d}(E_2 - E_1)\right] \qquad \ldots 6.42$$

Equation 6.42 shows that the stress varies linearly across any section, being directly proportional to the E value at the point in consideration.

6.3 THE INFLUENCE OF METHOD OF LOADING AND SPECIMEN AND MACHINE CHARACTERISTICS

From Equations 6.14 and 6.42, the variables which affect the stress at any point in the specimen at any load stage under every method of loading are the dimensions b, d and L, the location on the cross-section represented by the distance, x and the varying modulus of elasticity, E_1 to E_2. With at least one end pinned, the eccentricity of load application, e must also be considered. Under the method of loading where one end is pinned and the other fixed, the distance from the pinned end to the section in consideration, z and the machine lateral stiffness k must also be taken into account (see Equation 6.39).

In the following discussion, the influence of the different methods of loading on the stress distribution and mode of failure- are discussed. This is followed by a detailed examination of the influence of the relative lateral stiffness of specimen and testing machine, as well as the effect of misalignment on the stress distribution in typical concrete specimens, under the one end pinned, one end fixed load method. Finally, the influence of the method of loading on the discontinuity level stresses and strains and the modulus of elasticity for a typical concrete are discussed.

6.3.1 Effect of Method of Loading on Stress Distribution and Modes of Failure

Table 6.1 gives values of the stresses at the corners of a uniaxially loaded specimen, 4 x 4 in. cross-section, as calculated from Equations 6.14, 6.39 and 6.42, under the different

TABLE 6.1 THE VARIATION OF STRESS DISTRIBUTION, STRESSES AND STRAINS AT YIELD POINT AND MODULUS OF ELASTICITY WITH END LOADING CONDITION, MISALIGNMENT, MACHINE LATERAL STIFFNESS AND SPECIMEN NON-HOMOGENEITY.

A (Stiff Face E_2), B (Soft Face E_1), C, D	END LOADING CONDITIONS											
	Top End Pinned Bottom End Fixed				Both Ends Pinned				Both Ends Fixed			
Condition at Point	A	B	C	D	A	B	C	D	A	B	C	D
Case 1 $E_1 = E_2 = 5 \times 10^6$ lb./in.^{2} $m = 1.00$, $e = 0$												
Stress $(\times \frac{P}{bd})$	1.00	1.00	1.00	1.00	1.00	1.00	1.00	1.00	1.00	1.00	1.00	1.00
Stress Y.P. lb./in^2	3000		3000		3000		3000		3000		3000	
Strain Y.P. $(\times 10^{-6})$	600		600		600		600		600		600	
Measured $E(\times \frac{E_1 + E_2}{2})$	1.00		1.00		1.00		1.00		1.00		1.00	
Case 2 (a) $E_1 = E_2 = 5 \times 10^6$ lb/in^2, $m = 1.00$, $e = +2/15''$, $b = d = 4''$, $k = \frac{3EI}{L^3}$												
Stress $(\times \frac{P}{bd})$	1.20	0.80	1.05	0.95	1.20	0.80	1.20	0.80	1.00	1.00	1.00	1.00
Stress Y.P. lb/in^2	2500		2855		2500		2500		3000		3000	
Strain Y.P. $(\times 10^{-6})$	500		571		500		500		600		600	
Measured $E(\times \frac{E_1 + E_2}{2})$	1.00		1.00		1.00		1.00		1.00		1.00	
(b) $E_1 = E_2 = 5 \times 10^6$ lb/in^2. $m = 1.00$, $e = +2/15''$, $b = d = 4''$, $k \gg \frac{3EI}{L^3}$												
Stress $(\times \frac{P}{bd})$	1.20	0.80	0.90	1.10	1.20	0.80	1.20	0.80	1.00	1.00	1.00	1.00
Stress Y.P. lb./in^2	2500		2725		2500		2500		3000		3000	

Continued

	END LOADING CONDITIONS											
	Top End Pinned Bottom End Fixed				Both Ends Pinned				Both Ends Fixed			
Condition at Point	A	B	C	D	A	B	C	D	A	B	C	D
Strain Y.P. $(\times 10^{-6})$	500			545	500			500	600			600
Measured $E(\times \frac{E_1+E_2}{2})$	1.00			1.00	1.00			1.00	1.00			1.00
Case 3 (a) $E_1 = 4 \times 10^6$ lb/in^2, $E_2 = 6 \times 10^6$ lb/in^2, $m = 1.50$, $e = 0$, $b = d = 4''$, $k = \frac{3EI}{L^3}$												
Stress $(\times \frac{P}{bd})$	0.973	0.973	1.143	0.843	0.973	0.973	0.973	0.973	1.20	0.80	1.20	0.80
Stress Y.P. lb/in^2	2470			2850	2470			2470	3000			3000
Strain Y.P. $(\times 10^{-6})$	500			572	500			500	600			600
Measured $E(\times \frac{E_1+E_2}{2})$	0.987			0.997	0.987			0.987	1.00			1.00
(b) $E_1 = 4 \times 10^6$ lb/in^2, $E_2 = 6\times10^6$ lb/in^2, $m = 1.50$, $e = 0$ $b = d = 4''$, $k \gg \frac{3EI}{L^3}$												
Stress $(\times \frac{P}{bd})$	0.973	0.973	1.314	0.713	0.973	0.973	0.973	0.973	1.20	0.80	1.20	0.80
Stress Y.P. lb/in^2	2470			2740	2470			2470	3000			3000
Strain Y.P. $(\times 10^{-6})$	500			545	500			500	600			600
measured $E(\times \frac{E_1+E_2}{2})$	0.987			1.008	0.987			0.987	1.00			1.00
Case 4 (a) $E_1 = 4 \times 10^6$ lb/in^2, $E_2 = 6 \times 10^6$ lb/in^2, $m = 1.50$, $e = +2/15''$, $b = d = 4''$												
Stress $(\times \frac{P}{bd})$	1.20	0.80	1.20	0.80	1.20	0.80	1.20	0.80	1.20	0.80	1.20	0.80
Stress Y.P. lb/in^2	3000			3000	3000			3000	3000			3000
Strain Y.P. $(\times 10^{-6})$	600			600	600			600	600			600

Continued

	END LOADING CONDITIONS											
	Top End Pinned Bottom End Fixed				Both Ends Pinned				Both Ends Fixed			
Condition at Point	A	B	C	D	A	B	C	D	A	B	C	D
Measured $E(x\frac{E_1+E_2}{2})$	1.00		1.00		1.00		1.00		1.00		1.00	
(b) $E_1 = 4 \times 10^6$ lb/in^2, $E_2 = 6 \times 10^6$ lb/in^2, m = 1.50, e = -2/15", $k = \frac{3EI}{L^3}$												
Stress $(x\frac{P}{bd})$	0.746	1.147	1.086	0.888	0.746	1.147	0.746	1.147	1.20	0.80	1.20	0.80
Stress Y.P. lb/in^2	2090		2705		2090		2090		3000		3000	
Strain Y.P. $(x10^{-6})$	430		545		430		430		600		600	
Measured $E(x\frac{E_1+E_2}{2})$	0.974		0.994		0.974		0.974		1.00		1.00	
(c) $E_1 = 4 \times 10^6$ lb/in^2, $E_2 = 6 \times 10^6$ lb/in^2, m = 1.50, e = -2/15", $k \ggg \frac{3EI}{L^3}$												
Stress$(x\frac{P}{bd})$	0.746	1.147	1.427	0.628	0.746	1.147	0.746	1.147	1.20	0.80	1.20	0.80
Stress Y.P. lb/in^2	2090		2520		2090		2090		3000		3000	
Strain Y.P. $(x10^{-6})$	430		498		430		430		600		600	
Measured $E(x\frac{E_1+E_2}{2})$	0.974		1.015		0.974		0.974		1.00		1.00	

end conditions of loading. Four representative cases have been analyzed;

1. a perfectly homogeneous specimen accurately centred
2. a perfectly homogeneous specimen misaligned by 2/15 in. (about 3% of the specimen width)
3. a non-homogeneous specimen accurately centred
4. a non-homogeneous specimen misaligned by 2/15 in. both towards and away from the stiff face.

In case 2,3 and 4, the effect of the lateral stiffness of the testing machine is examined by considering both a medium stiffness machine (lateral stiffness k equal to that of the specimen) and an infinitely stiff machine (see Equation 6.39).

The non-homogeneous specimen is assumed to have a linearily varying modulus of elasticity from 4 to 6 x 10^6 lb./in.^{2}, that is, m = 1.5 Although this ratio may be considered initially as being somewhat high, it is shown in Figure 9.2 that the centroid of resistance of 4" cubes may be displaced up to 1/8 in. from the centre-line of the specimen when loaded perpendicularly to the direction of casting. As different concretes fail at similar strain values and have similar stress-strain curves, it is possible to equate Equations 6.12 and 6.13 to solve for a ratio of E_2/E_1, giving an e of 1/8 in. The calculated ratio of 1.46 was rounded off to 1.50 for ease of calculation.

The assumption that a uniaxial state of stress exists in the specimen is, of course, partially incorrect, particularly in the shorter specimens, because of the restraint effect of the platens.

However, the stress concentrations given in Table 6.1 are of the right order and do account for the differences in failure strengths and modes of failure that do arise, (see Section 9.8)

Case 1 represents the stress distribution that is generally assumed to exist in all uniaxial test specimens. Yet, case 2 shows that, even with a homogeneous specimen, a misalignment of only 3% of the specimen width, when one or both ends are pinned, can cause an increase in stress of 20%! With the one end pinned, one end fixed condition, the effect of misalignment of a homogeneous specimen depends also on the lateral stiffness of the machine. In this case, the resultant force at the fixed end will be transferred in the direction opposite to the misalignment, by an amount which depends on the relative lateral stiffness of the machine (see Figure 6.3). For a laterally flexible machine ($k = 0$) no displacement of the resultant force occurs and the stress system is identical to that with both ends pinned (see Figure 6.3.b). As the value of $k/(k + \frac{3EI}{L^3})$ in Equations 6.39 and 6.40 increases, so does the variation in stress (see Figures 6.3(c) and (d)). In the extreme case of a very stiff machine, the resultant force is displaced across the neutral axis, resulting in diagonally opposite corners A and D being highly stressed. With failure being initiated on these diagonally opposite corners, the failure on a phenomenological level will appear to be a shearing mode.

A similar apparent shearing mode of failure can occur when perfectly centred non-homogeneous specimens are loaded with one

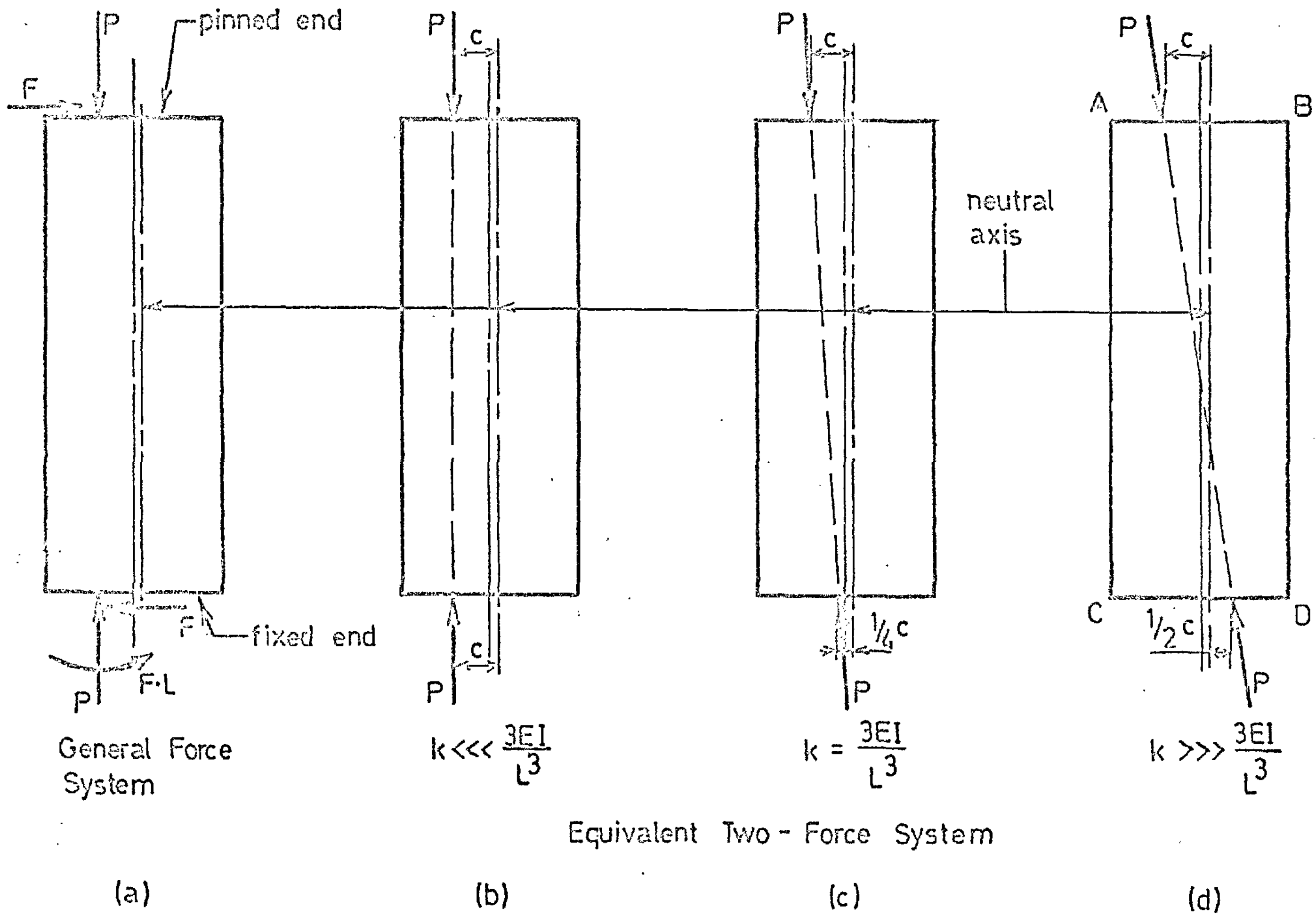

FIG. 6.3 INFLUENCE OF RELATIVE LATERAL STIFFNESS OF SPECIMEN AND MACHINE ON LOCATION OF RESULTANT

end pinned, one end fixed (see case 3, in Table 6.1). The neutral axis in such cases will not coincide with the centre-line, but will be displaced towards the stiff face by the distance (a - d/2). The resulting bending and the induced lateral force at the pinned end will produce a variable stress distribution at the fixed end which will depend on the relative stiffness of the specimen and machine. Cracking and failure will tend to be initiated at the soft face at the pinned end, point B, and the more highly stressed stiff face at the fixed end, point C. Since these points are diagonally opposite, the specimen will fail apparently in shear.

The effect of misalignment will depend on its direction with respect to the neutral axis of the specimen. In case 4a, a misalignment of 2/15 in. (i.e. about 3% of the width) towards the stiff face ensures that the specimen is loaded at the neutral axis(i.e. e conforms with the value given by Equation 6.41), and the stress patterns for the three end conditions of loading are identical. However, a similar misalignment in the opposite direction (cases 4b and 4c) causes large variations in the stress distribution. At the fixed end in the infinitely stiff machine, the stress will vary from 63 to 143% of the average, a difference of 80%.

6.3.2 Examination of Lateral Stiffness of Specimen and Testing Machine under One End Pinned, One End Fixed Load Method

In order to examine the influence of the lateral stiffness of the testing machine on the stress distribution of concrete specimens, several testing machines were selected to cover the full range of machines in practice. A description of these machines with the stiffness value, k, computed on the basis of the lateral load-deformation characteristics of the machine columns is given in Table 6.2. From Figure 6.4, the influence of the lateral stiffness of the machine on the stress distribution at the pinned and fixed ends of the specimen is seen for various lengths of a 4" square cross-section having an E gradient of 4×10^6 to 6×10^6 p.s.i. Individual coefficients have been computed from adding Equations 6.14 and 6.39. Figure 6.5 shows the effect on a specimen identical to the one above except for E values varying from 2×10^6 to 3×10^6 p.s.i. while Figure 6.6 demonstrates the influence of varying the dimensions b and d while maintaining all other properties constant. In all the above cases, the eccentricity of load application is zero.

Although the stress distribution at the fixed end only has been shown on the graphs (Figure 6.4, 6.5 and 6.6), it is possible to determine the stress at any point in the specimen. At the pinned end of the specimen, that is, at z = 0 in Equation 6.39, the stresses are calculated from Equation 6.14 and are equal to the asymptotic values for k = 0 as shown. From Equation 6.39, it will be observed that the stress is linearly proportional to the distance from the pinned end, z. Therefore, the stresses [illegible] and [illegible] at any value of z and k can be directly interpolated from the extreme values on the graph, i.e. between z = 0 and z = L.

TABLE 6.2 LATERAL STIFFNESS OF TESTING MACHINES

Machine No.	Description of Machine	Lateral Stiffness k(lbs. / in.)
1	Hydraulic platen	0.
2	4 columns - 2"φ x 48" long Columns encastré with bottom cross-head and pinned to top cross-head.	2.57×10^3
3	4 columns - 3"φ x 48" long columns encastré with bottom cross-head and pinned to top cross-head.	1.30×10^4
4	4 columns - 3"φ x 30" long columns encastré with bottom cross-head and pinned to top cross-head.	5.31×10^4
5	4 columns - 5"φ x 30" long columns encastré with bottom and top cross-heads	2.12×10^5
6	4 columns - 4"φ x 24" long columns encastré with bottom and top cross-heads	1.31×10^6
7	4 columns - 6"φ x 24" long columms encastré with bottom and top cross-heads	6.64×10^6
8	Theoretical machine	∞

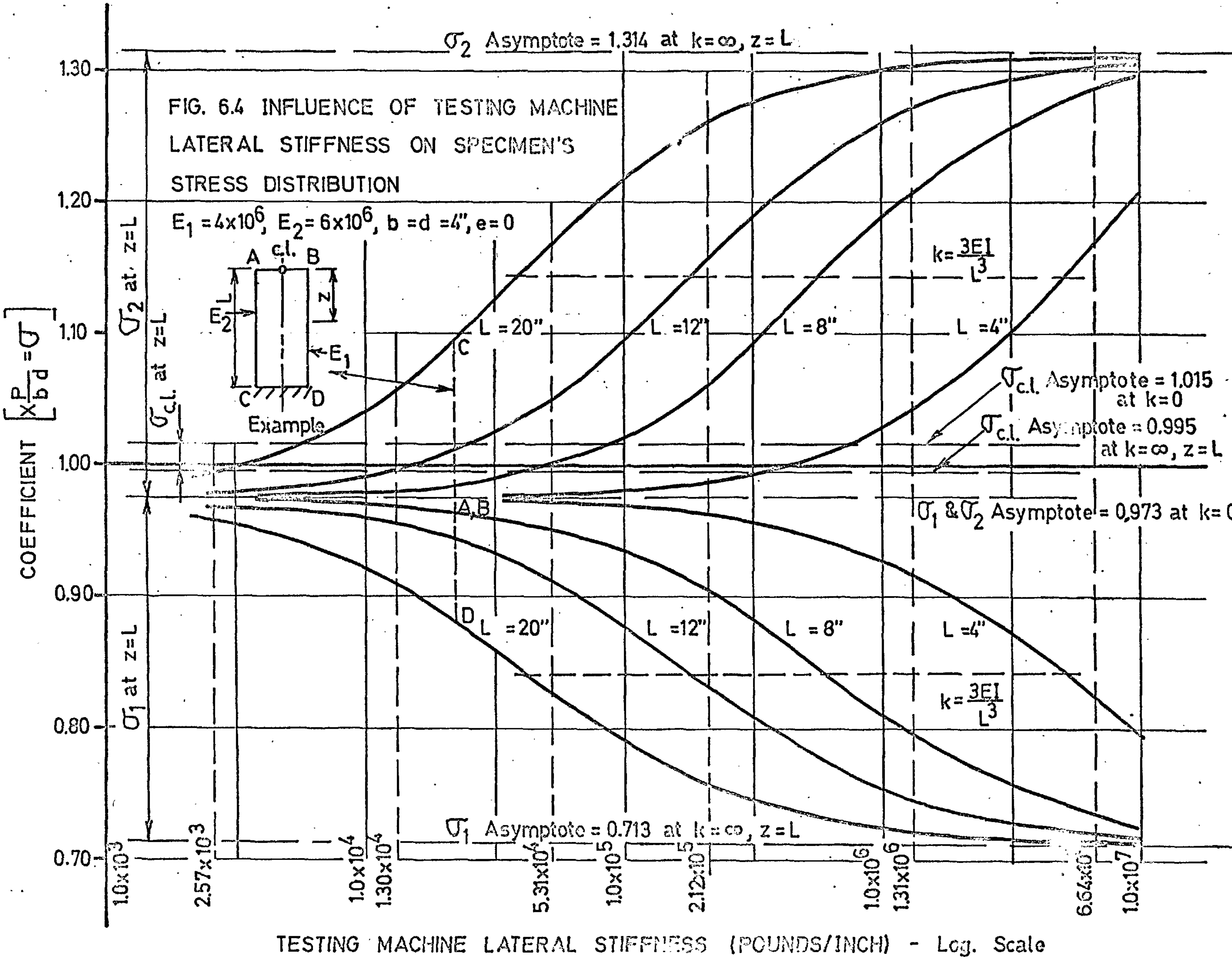

FIG. 6.4 INFLUENCE OF TESTING MACHINE LATERAL STIFFNESS ON SPECIMEN'S STRESS DISTRIBUTION

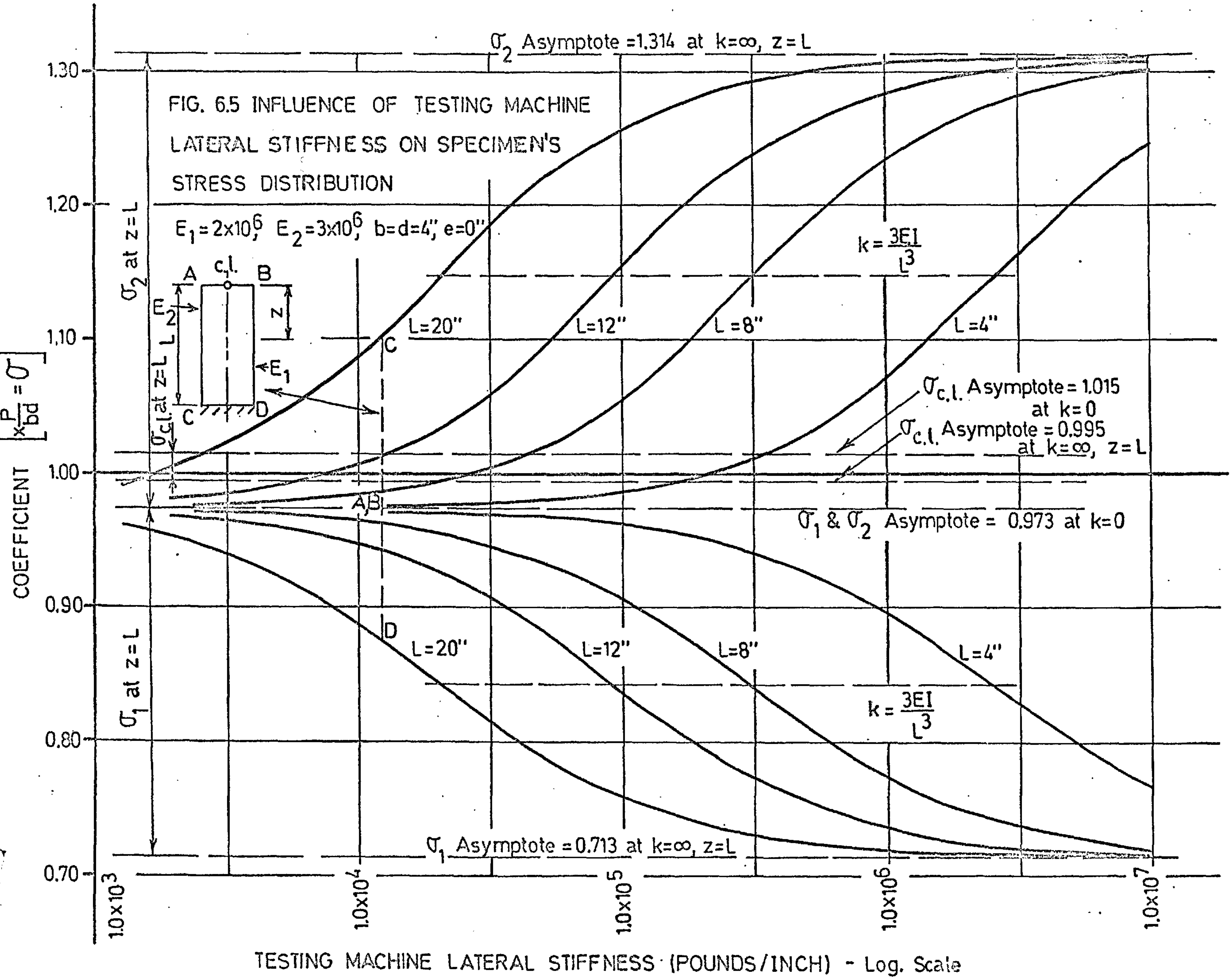

FIG. 6.5 INFLUENCE OF TESTING MACHINE LATERAL STIFFNESS ON SPECIMEN'S STRESS DISTRIBUTION

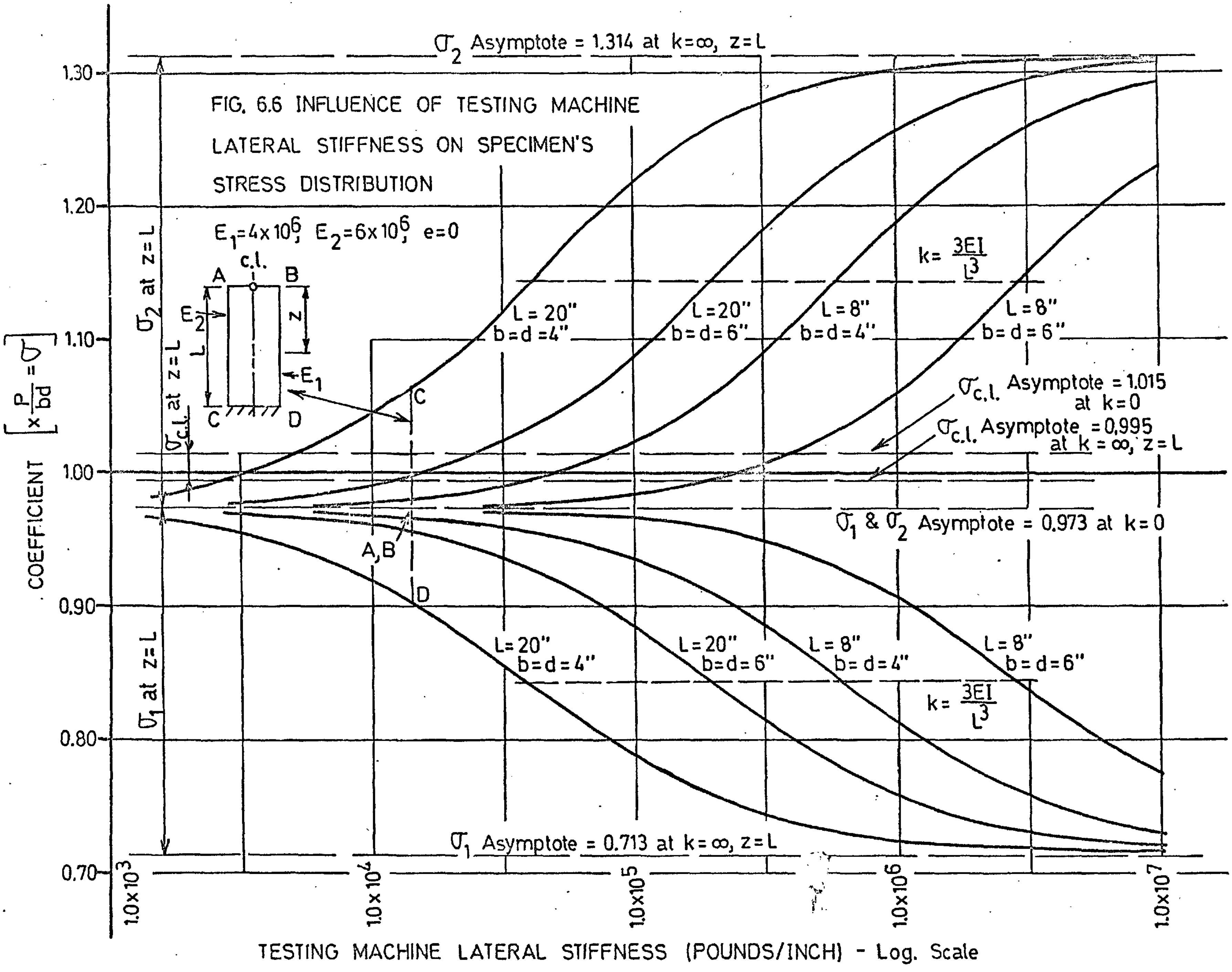

FIG. 6.6 INFLUENCE OF TESTING MACHINE LATERAL STIFFNESS ON SPECIMEN'S STRESS DISTRIBUTION

From the graphs (Figures 6.4, 6.5 and 6.6), the two following observations are made:

1. An increase in the lateral stiffness of the testing machine, k, will result in an increase of variation of stress distribution on any cross-section.

2. An increase in the lateral stiffness of the specimen, that is, a reduction in the length of the specimen or an increase in the flexural stiffness will reduce variations in stress distribution. Increasing the flexural stiffness is performed either by increasing the modulus of elasticity values, E_1 and E_2 while maintaining their ratio value constant or by increasing the cross-sectional dimensions, b and d.

Concrete control tests in Great Britain are conducted on 4" and 6" cubes. As these specimens are observed to be almost always very significantly stiffer, laterally, than the testing machine, the stress distribution is little affected by the induced lateral force. However, in the stiffer machines, i.e. lateral stiffness greater than about 2×10^5 lbs./ in., a significant influence on the stress variation may account for some differences in strength results. With the centroid of action of the specimen when tested, in these stiffer machines being displaced towards the stiff face, the reduction in stress on the softer, generally weaker face would be reflected in higher strength results.

4" x 4" x 12" prisms have acquired importance over the past few years as a control specimen as well as a suitable specimen for determining fundamental properties of concrete [21,40]. In America, 6" diameter by 12" long cylinders cast on their side are also being used. It is apparent, from Figures 6.4 and 6.5, that the stress distribution in these specimens is very much dependent on the lateral stiffness of the machines (6" diameter by 12" long cylinders, due to having similar dimensions as 4" x 4" x 12" prisms, will be affected similarly to the 12" long prisms). It seems reasonable to suggest that the stiffer machines, i.e. lateral stiffness > about 2×10^5 lbs. / in., will usually produce shear failures in these specimens while the more flexible machines will produce apparent compression failures. It also appears reasonable that specimens tested in machines of medium stiffness (2×10^4 lbs/in. to 2×10^5 lbs/in.) will produce the highest failure results. This can be explained as follows.

Flexible testing machines with lateral stiffness less than about 2×10^4 lb./in. will load the entire specimen nearly axially. This results in the entire soft face, which is the weakest face, being stressed at approximately the average stress. It is expected that failure would propagate across the weakest cross-section from this face soon after reaching its ultimate stress capacity (see Section 6.4). The medium stiffness machines will displace the centroid of action towards the stiff face in proportion to the distance from the pinned end. This will reduce the area of the soft face subjected to average stress. The weakest-link theory as explained by Wright [48] will then suggest higher ultimate strengths. With the stiffer machines, i.e. about 2×10^5 lb./in., the tendency will be for the stiff face at the fixed end to display the first signs of failure. Propagation of failure from this point will consequently occur more prematurely as the machine lateral stiffness continues to increase.

6.3.3 Examination of Misalignment under One End Pinned, One End Fixed Load Method

Figure 6.7 shows the influence of specimen misalignment and machine stiffness on the stress distribution in a concrete specimen having a varying modulus of elasticity of 4 to 6×10^6 p.s.i.

As concretes tend to fail at similar strains, it seems reasonable to suggest that the highest strengths will occur when the entire specimen is strained uniformly. This will be in accordance with the method of loading whereby both ends of the specimen are effectively fixed. Therefore, by equating Equation 6.12 and 6.13, it is theoretically possible to solve for a value of eccentricity of load application which will produce this system of loading under the system of one end pinned and the other end fixed. For the case in consideration, $e = \frac{2}{15}$ in. (see Case 3 and 4 in Table 6.1). The solution of Equation 6.14 thereby produces values of $\sigma_1 = 0.80 \frac{P}{bd}$ and $\sigma_2 = 1.20 \frac{P}{bd}$ with a linear stress distribution across the section (see Equations 6.41 and 6.42). As there is no differential straining, no induced lat-

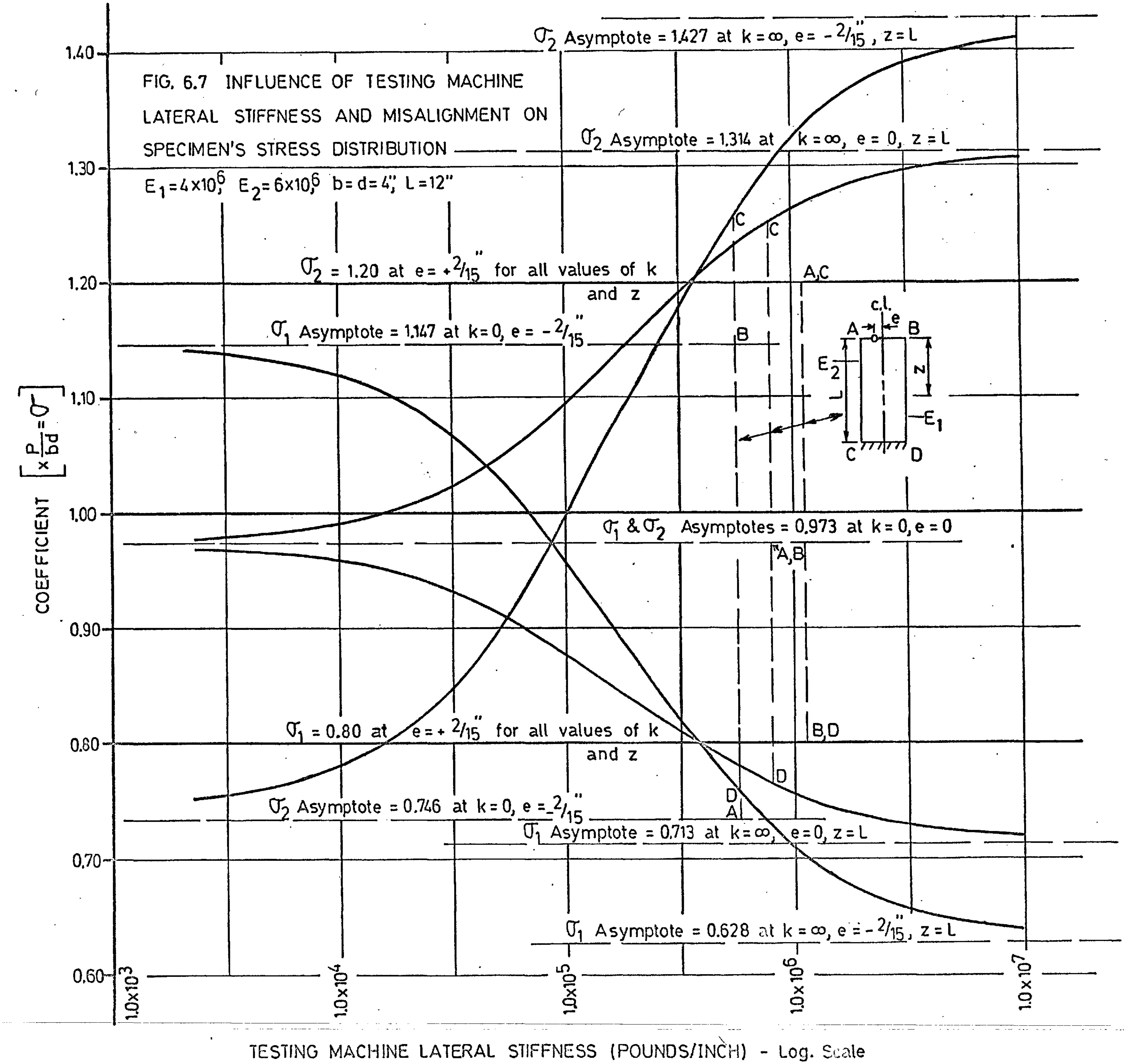

FIG. 6.7 INFLUENCE OF TESTING MACHINE LATERAL STIFFNESS AND MISALIGNMENT ON SPECIMEN'S STRESS DISTRIBUTION

eral force is created. Therefore, the stress at any point in the specimen is independent lf the machine stiffness. The results therefore, in Figure 6.7 appear as straight horizontal lines with the asymptotes for $k = 0$ and $k = \infty$ coincident. This has also been shown in Case 4a, Table 6.1 where the three methods of loading produce identical stress patterns.

It is apparent, from examination of Figure 6.7, that the stress system in a specimen is very sensitive to its location in the testing machine. For the case in consideration, assuming a very stiff machine, the stress on the soft face with a misalignment of only approximately 1/8" (about 1/4" from the effective neutral axis) can vary from 63% to 114% of the average stress in the specimen. Simultaneously, the stress on the stiff face will range from 143% to 75%. Such specimens will undoubtedly exhibit extremely low ultimate strength results with an apparent shearing type failure mode. The more flexible machines on the other hand would exhibit a crushing failure on the soft face at a low ultimate strngth as a result of the entire soft face being stressed 18% in excess of the average stress in the specimen. The maximum stress on the soft face increases from 80% to 118% of the average with e changing from $+\frac{2}{15}$" to $-\frac{2}{15}$". As this could be the face from which failure propagates in both cases, the difference in ultimate strength could be of the order of 45%. However, due to non-linearity of the stress-strain curve near failure there will be some shedding of the load to the unfailed portion of the section in the latter case. Consequently, this figure will be somewhat reduced.

It must be recognized that very large differences in strength results would be expected with apparently small misalignments in placing the specimen or by testing in machines of different lateral stiffness. It must also be appreciated that inconsistencies in aligning the specimen will produce large variations in ultimate strength which is not a property of the material, but due rather, to operator technique. It would appear that a method of test, whereby the results are independent of the lateral stiffness of the testing machine and immune from small misalignments, would be the most desirable, particularly for control testing. Loading in accordance with the philosophy of having both ends fixed conforms to this requirement and therefore appears to be most suitable.

6.3.4 Yield Point and Modulus of Elasticity

Most materials exhibit a definite yield point when the strains are no longer elastic. Concrete and other brittle materials exhibit an analogous discontinuity limit (14) when severe cracking begins. For a typical concrete, this discontinuity level occurs at a uniaxial compressive strain of about 600×10^{-6} lb./in. In a uniformly deformed concrete, the specimen will exhibit discontinuity at the above strain, whereas when one or both ends are pinned, the specimen is deformed non-uniformly and discontinuity will occur as soon as any one face reaches the above strain.

Strain measurements in uniaxial tests are made usually by averaging the surface strains δ_1 and δ_2 on two opposite faces of the specimen. Assuming that, for this material, the discontinuity or yield point is reached when any part of the specimen reaches a compressive strain of 600×10^{-6} in./in., Table 6.1 shows the effect of misalginment, lateral stiffness and specimen non-homogeneity on the average stresses and strains at the yield point at the top and bottom of the specimen. Whereas, for any specimen, the discontinuity level remains unchanged under effectively fixed end conditions, this level becomes very sensitive when either one or both ends are pinned. Furthermore, under the one end pinned, one end fixed condition, the discontinuity level will occur at different load stages at different sections.

The modulus of elasticity of a material is usually obtained by dividing the average stress $\frac{P}{bd}$ by the measured strain $(\delta_1 + \delta_2)/2$. Therefore, from Equations 6.12, 6.13 and 6.15, the measured modulus of elasticity for the both ends pinned condition is found to be

$$E = \frac{E_1 d(1 + 4m + m^2)}{3\left[d\ (m + 1) - 2e(m - 1)\right]} \qquad \ldots 6.43$$

For the both ends effectively fixed condition, the specimen is loaded along the neutral axis. By substituting Equation 6.41 into Equation 6.43, we obtain,

$$E = 1/2\ (E_1 + E_2) \qquad \ldots 6.44$$

i.e. the calculated E value is the arithmetic mean of the extreme values of E_1 and E_2.

The values of E also given in Table 6.1 show that, with non-homogeneous specimens even the modulus of elasticity is dependent on the end loading conditions. With the one end pinned, one end fixed condition, the measured E will depend on the location of the strain gauges since the specimen appears to become stiffer towards the fixed end.

6.4 THE INFLUENCE OF THE METHOD OF LOADING THE SPECIMEN ON ITS DEFORMATION AND ULTIMATE STRENGTH PROPERTIES

The theoretical presentation in Section 6.2 has been based on the assumption that the stress-strain curve is linear. Consequently, the discussion of Section 6.3 was concerned with examining the influence of the method of loading and machine and specimen properties on the stress state before non-linearity as well as providing an indication of the nodes of failure and ultimate strength results.

After non-linearity, the excessive deformation of the failing faces, particaularly near failure, will result in large differential strains on opposite faces of the specimen. The resulting increase in lateral displacement of the pinned end will be considerable reduced by a reduction in the flexural stiffness of the specimen. It will be appreciated, however, that there will be some increase in lateral movement of the specimen and consequently, a continual tendency to transfer more stress to the stiffer face. This transfer will, of course, continue to be affected by the stiffness of the machine.

From the discussion of the results of Table 6.1 and Figures 6.4, 6.5, 6.6 and 6.7, it can generally be assumed that a system of loading under the philosophy of effectively fixed conditions will produce the highest strengths while a system of loading under effectively pinned conditions will produce the lowest strengths. However, in cases where the lateral stiffness of the machine is very significantly greater than for the specimen, the induced shearing-type failures may produce still lower results.

In order to show the difference in concrete characteristics after the discontinuity level, two generally extreme cases have been considered. A 4" square cross-section with E varying linearly from 4×10^6 p.s.i. to 6×10^6 p.s.i. in the elastic range is loaded in accordance with the philosophies of both ends fixed and both ends pinned. The results of one end pinned and the other fixed would be expected generally to lie between these extremes.

A typical stress-strain curve for concrete was simplified into a series of straight lines as shown in Figure 6.8. From this, the stress strain curves for several locations on the cross-section for the non-homogeneous specimen with E varying from 4 to 6×10^6 p.s.i. in the elastic range have been determined (see Figure 6.9).

Under effectively pinned loading conditions, where the specimen is perfectly aligned, the resultant load must be coi-

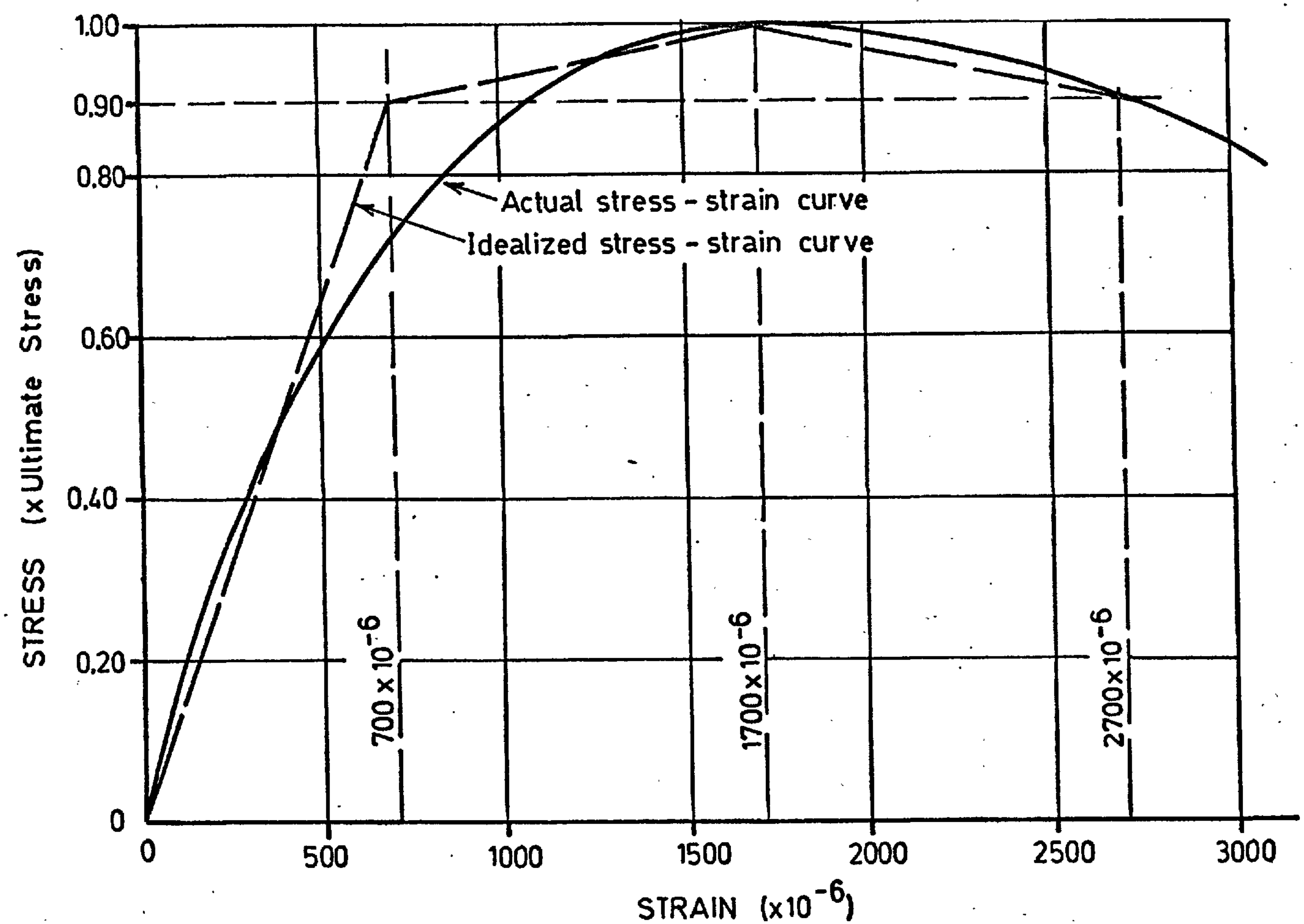

FIG. 6.8 ACTUAL AND IDEALIZED STRESS - STRAIN CURVE FOR CONCRETE

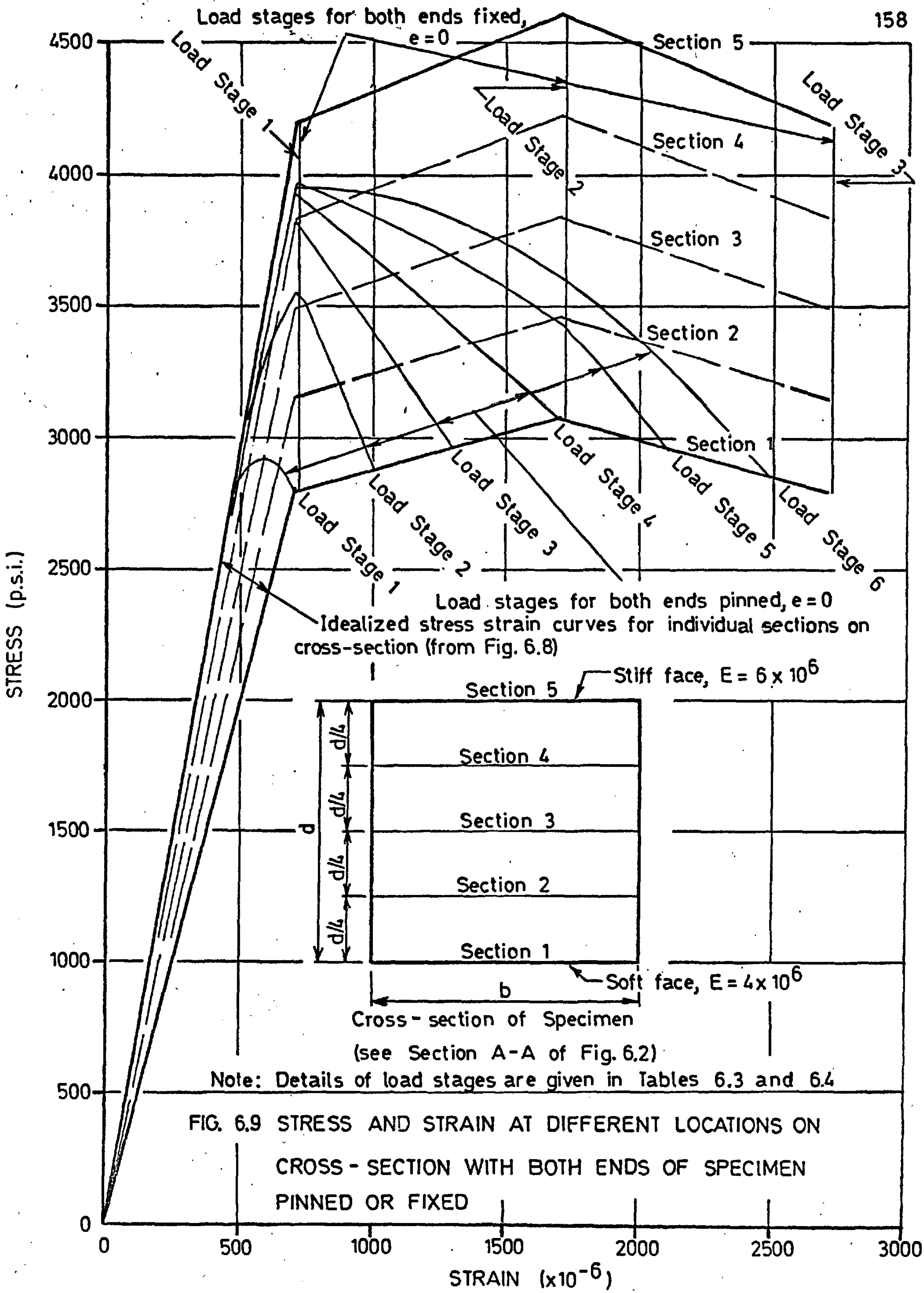

FIG. 6.9 STRESS AND STRAIN AT DIFFERENT LOCATIONS ON CROSS-SECTION WITH BOTH ENDS OF SPECIMEN PINNED OR FIXED

TABLE 6.3 STRESS AND STRAIN DISTRIBUTION ON SPECIMEN CROSS-SECTION UNDER EFFECTIVELY PINNED LOADING CONDITIONS

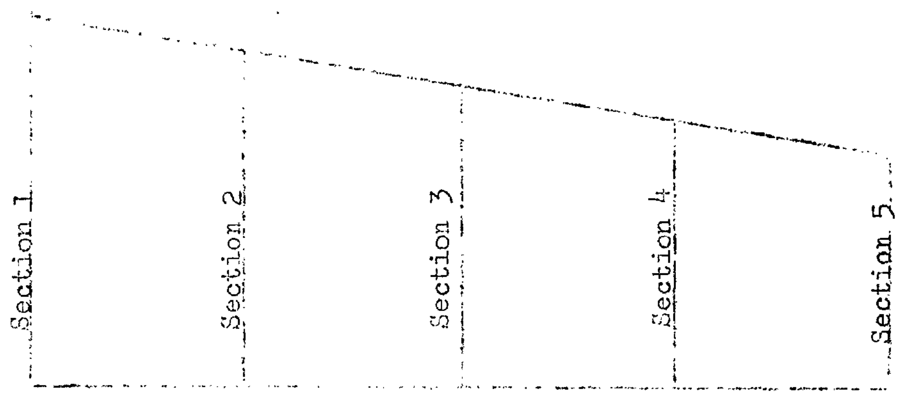

Load Stage No. 1

δ	7.00×10^{-4}	6.41×10^{-4}	5.83×10^{-4}	5.25×10^{-4}	4.67×10^{-4}
E(p.s.i.)	4.00×10^{6}	4.50×10^{6}	5.00×10^{6}	5.50×10^{6}	6.00×10^{6}
σ (p.s.i.)	2800	2890	2920	2890	2800

Average stress = 2875 p.s.i.
Average strain = 583×10^{-6}
E = 4.94×10^{6}

Load Stage No. 2

δ	10.00×10^{-4}	8.67×10^{-4}	7.35×10^{-4}	6.03×10^{-4}	4.70×10^{-4}
E(p.s.i.)	2.88×10^{6}	3.69×10^{6}	4.78×10^{6}	5.50×10^{6}	6.00×10^{6}
σ (p.s.i.)	2880	3200	3510	3320	2820

Average stress = 3220 p.s.i.
Average strain = 735×10^{-6}
E = 4.39×10^{6}

Load Stage No. 3

δ	13.00×10^{-4}	10.90×10^{-4}	8.80×10^{-4}	6.70×10^{-4}	4.60×10^{-4}
E(p.s.i.)	2.28×10^{6}	3.00×10^{6}	4.04×10^{6}	5.50×10^{6}	6.00×10^{6}
σ (p.s.i.)	2970	3270	3560	3680	2760

Average stress = 3340 p.s.i.
Average strain = 880×10^{-6}
E = 3.80×10^{6}

Load Stage No. 4

δ	17.00×10^{-4}	13.93×10^{-4}	10.86×10^{-4}	7.79×10^{-4}	4.72×10^{-4}
E(p.s.i.)	1.81×10^{6}	2.41×10^{6}	3.34×10^{6}	4.98×10^{6}	6.00×10^{6}
σ (p.s.i.)	3080	3360	3630	3870	2830

Average stress = 3460
Average strain = 1086×10^{-6}
E = 3.19×10^{6}

TABLE 6.3 STRESS AND STRAIN DISTRIBUTION ON SPECIMEN CROSS-SECTION UNDER EFFECTIVELY PINNED LOADING CONDITION (cont.)

Load Stage No. 5

δ	21.00×10^{-4}	16.90×10^{-4}	12.80×10^{-4}	8.70×10^{-4}	4.60×10^{-4}
E (p.s.i.)	1.41×10^{6}	2.04×10^{6}	2.89×10^{6}	4.50×10^{6}	6.60×10^{6}
σ (p.s.i.)	2960	3450	3700	3910	2730

Average stress = 3480
Average strain = 1280×10^{-6}
E = 2.72×10^{6}

Load Stage No. 6

δ	25.00×10^{-4}	19.80×10^{-4}	14.70×10^{-4}	9.50×10^{-4}	4.30×10^{-4}
E (p.s.i.)	1.14×10^{6}	1.71×10^{6}	2.56×10^{6}	4.15×10^{6}	6.00×10^{6}
σ (p.s.i.)	2850	3390	3760	3940	2580

Average stress = 3450
Average strain = 1470×10^{-6}
E = 2.35×10^{6}

TABLE 6.4 STRESS AND STRAIN DISTRIBUTION ON SPECIMEN CROSS-SECTION UNDER EFFECTIVELY FIXED LOADING CONDITIONS

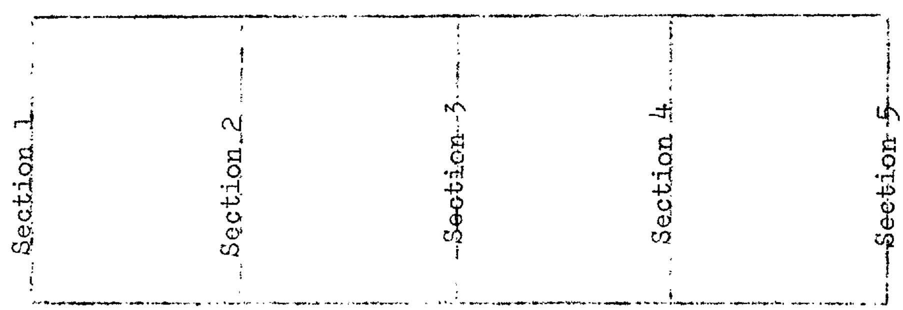

Load Stage No. 1

δ	7.00×10^{-4}	7.00×10^{-4}	7.00×10^{-4}	7.00×10^{-4}	7.00×10^{-4}
E (p.s.i.)	4.00×10^{6}	4.50×10^{6}	5.00×10^{6}	5.50×10^{6}	6.00×10^{6}
σ (p.s.i.)	2800	3150	3500	3850	4200

Average stress = 3500
Average strain = 700×10^{-6}
E = 5.00×10^{6}

Load Stage No. 2

δ	17.00×10^{-4}	17.00×10^{-4}	17.00×10^{-4}	17.00×10^{-4}	17.00×10^{-4}
E (p.s.i.)	1.81×10^{6}	2.03×10^{6}	2.26×10^{6}	2.50×10^{6}	2.72×10^{6}
σ (p.s.i.)	3080	3450	3850	4250	4630

Average stress = 3850
Average strain = 1700×10^{-6}
E = 2.16×10^{6}

Load Stage No. 3

δ	27.00×10^{-4}	27.00×10^{-4}	27.00×10^{-4}	27.00×10^{-4}	27.00×10^{-4}
E (p.s.i.)	1.04×10^{6}	1.17×10^{6}	1.30×10^{6}	1.42×10^{6}	1.56×10^{6}
σ (p.s.i.)	2810	3150	3500	3840	4200

Average stress = 3500
Average strain = 2700×10^{-6}
E = 1.30×10^{6}

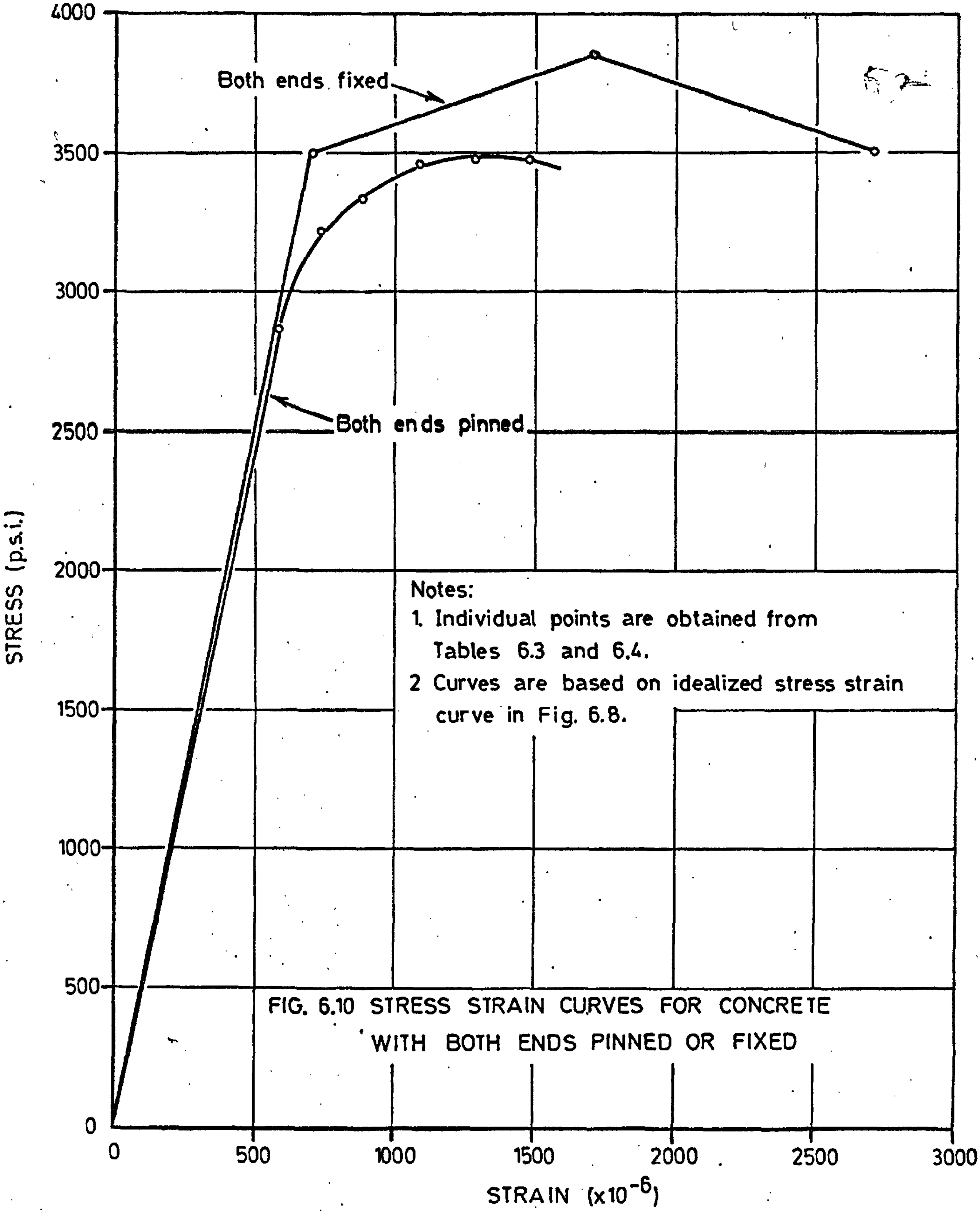

FIG. 6.10 STRESS STRAIN CURVES FOR CONCRETE WITH BOTH ENDS PINNED OR FIXED

ncident with the centre of the cross-section, at any load stage. Table 6.3 shows the distribution of stress and strain on the cross-section at progressing load stages. Under effectively fixed loading conditions, the strain distribution on any cross-section at every load stage will be constant. The resulting distribution of stress and strain is given in Table 6.4. These progressing load stages under both systems of loading are plotted in Figure 6.9. In Figure 6.10, the stress values are obtained from the relationship $\sigma = P/bd$ whilst the strains are the average from the opposite faces of the specimen, i.e. $(\delta_1 + \delta_2)/2$ (see Section 6.3.4). Thus, the stress strain curves in Figure 6.10 would agree closely with the experimental results obtained under the two methods of loading.

Observation of Figures 6.9 and 6.10 reveals that several differences in the indicated behaviour of concrete can arise solely as a function of the system of loading. They are:

1. The modulus of elasticity in the elastic range may be different. For this particaular case, the observed difference was 1.5% (This has been shown also in Section 6.3.4).

2. The onset of non-linearity will occur at a later stage under effectively fixed conditions. This will be the case in both average stress and average strain terms (see also Table 6.1).

3. The ultimate strength will be greater under effectively fixed loading conditions. The case analyzed displayed a 10% difference.

4. The strain at ultimate strength will be greater in spec-

imens loaded under effectively fixed conditions.

It is of interest to observe that, (see Figure 6.9), as the ultimate load is being reached under effectively pinned conditions, the strain and stress are reducing on the stiff face. In fact, the maximum stress on the stiff face reaches only a fraction of its load carrying capacity. (60% in this case.)

6.5 SUMMARY

The theoretical analysis of this chapter suggests that the method of loading the specimen and the lateral stiffness of the testing machine are critical in establishing such fundamental properties of materials as modulus of elasticity, ultimate stress and strain, proportional limit stress and strain and mode of failure. It would appear that concrete specimens loaded with both ends pinned will exhibit a lower modulus of elasticity, a lower proportional limit stress and strain and a lower ultimate stress and strain than when tested with both ends fixed. The former loading condition will exhibit excessive failure on the soft face while the stiffer face is stressed to only a fraction of its capacity. The increased load carrying capacity of specimens loaded with both ends fixed is accounted for by considering that the entire specimen is loaded to its ultimate stress.

In testing machines with one end pinned and the other fixed, all results will again generally be lower than with both ends fixed. In very stiff machines, these results may be expected to be even lower than the results from testing under effectively pinned conditions owing to the very high stressing of the stiff face at the fixed end. The failure mode, may, as a result, be altered to an apparent shearimg pattern.

Current specifications make no reference to the accuracy with which a specimen should be placed in a testing machine. It is reasonable to suppose that a careful machine operator will place specimens up to 1/8" off centre. This may be amplified by misalignment in the testing machine, inherent from its manufacture. The sensitivity of results to misalignment was revealed when it was shown that a misalignment of 1/8" on a 4" square cross-section could cause a change in stress of 20% when either one or both ends were pinned. Furthermore, inconsistency in placing the specimen accurately would contribute to a scatter of results which would not be a specimen property, but rather attributable to operator technique.

Cube specimens, due to being very much stiffer laterally than testing machines are usually affected negligibly by the lateral stiffness of the machine. However, with the stiffer machines, that is, greater than about 2 x 10^5 lb./in. differences would be expected in segregated specimens. However, the sensitivity to misalignment would again be reflected in failure results and the scatter of strengths. The longer specimens, such as the 4" x 4" x 12" prism, will be very significantly influenced by the lateral stiffness of all testing machines in practice. Therefore, if this test method is to be used, it is obviously of importance to correlate all results to those obtained on a standard machine with a standard lateral stiffness. Alternatively, the replacement of this method of test by loading with both ends pinned or fixed, thereby eliminating the influence of lateral stiffness has obvious merits.

Along with the theoretical examination of strength properties of concrete, as presented in this chapter, an experimental investigation was conducted on three testing machines to examine their behaviour under load(see Chapter 7). In Chapter 8, the results of an experimental investigation on spherical seatings are presented with special emphasis being placed on achieving pinned and fixed end conditions. In Chapter 9, the influence of the various testing machine characteristics on concrete strengths are examined on the basis of experiment observations. These include the influence of method of loading, misalignment and lateral stiffness.

CHAPTER 7

INVESTIGATION OF BEHAVIOUR OF UNIAXIAL TESTING MACHINES

7.1 INTRODUCTION

7.1.1 The Need For Investigating The True Behaviour Of Testing Machines

Following the calibrations as presented in Chapter 5, it was apparent that, although the verifications were far from being perfect, errors in load indication could not account for the large inconsistencies in results of concretes subjected to complex stresses, (see Section 3.1). Consequently, it was concluded that the testing technique must be at fault(see Section 5.1). Two queries presented themselves;

1) How do testing machines deform and fail concrete specimens?

2) How should testing machines deform and fail concrete specimens?

As explained in Section 5.3, testing machines apply load to specimens under effectively pinned conditions, effectively fixed conditions or a system between these extremes. Wright,[22] in a survey of several compression testing machines showed that some machines deform specimens uniformly while others exhibit peculiar differential deformation patterns. His investigation was, however, limited to examining the deformation on opposite sides of cubes as cast and did not include a study of the differential deformations expected to arise from variations in specimen properties such as would occur from the top, as cast, to the bottom.

It is very important that all components of testing machines be in good alignment. Wright[22] showed that a misaligned machine (of the order of 1/4") may produce large differential straining on opposite sides of specimens, consistent failure patterns in one direction, inconsistent ultimate strength values and relatively low average strengths.

Before embarking on an investigation into the manner in which testing machines should deform specimens, it was deemed necessary to examine the actual behaviour of some existing uniaxial machines. Two compression and one tension machine in the Concrete Department, Imperial College were examined for the manner in which specimens, and machine were deformed. Particular attention was given to misalignment of load application.

7.1.2 The Use Of Intermediary Platens

At a symposium on Testing Techniques at Wexham Springs, organized by the Cement and Concrete Association, the subject of intermediary platens received much attention. Testing machines with spherical seatings are usually manufactured with their centre of rotation at the centre of the face of the male bearing block. Strictly speaking, the use of an intermediary platen does not conform with the requirements of British Standard 1881. Displacement of the centre of the spherical seating from the centre of the face of the specimen will, under differential straining, produce a shearing force at the specimen-platen interface. However, loading specimens through the bearing block without the use of intermediary platens has several shortcomings. They are:

1. As removing the spherical seating and regrinding it is troublesome, time consuming and costly, and the machine is rendered useless during this operation, there is a tendency to delay this work until the planeness is considerably worse than that allowed by British Standard 1881.

2. The case hardened surface of the bearing block will be gradually removed by both the wearing action of the specimens and the repeated grinding.

3. When testing 4" and 6" cubes, non-uniform support will result from non-uniform wearing of the bearing face.

4. Strictly speaking, the removal and installation of the spherical seating constitutes a major adjustment. Therefore, to be in accordance with British Standard 1610, a re-calibration is necessary after every instalment of the spherical seating.

If the spherical seating were to behave in an effectively fixed condition, the danger of undesirable shearing forces would be eliminated, and the use of intermediary platens would be, therefore, recommended. Alternatively, when the spherical seating does tilt, shearing forces might be expected to influence the results. Whether or not this is significant, constitutes the second investigation of this Chapter.

7.2 ANALYSIS OF 200 TON DENISON COMPRESSION MACHINE

This machine, (see Plates 7.1 and 7.2) used continually for standard cube crushing, has also been used considerably as a research machine[1,2]. Its verification revealed Grade B accuracy and repeatability over most of its working range and, as such, is considered acceptable over this range. (see Sections 3.3.1 and 3.4)

Although reasonably consistent failing strengths were obtained with this machine, this could be misleading, as a procedure for always placing the cast face west (to the right in Plates 7.1 and 7.2) had been adopted. The following investigation was therefore conducted to investigate differences in strength and failure pattern associated with the orientation of the specimen as well as examining the pattern of movements in both the specimens and machine.

7.2.1 Tilting Platen Tests

7.2.1.1 Deformation measuring assembly

The assembly, shown in Plate 7.1 consisted of 2 rigid frameworks. The upper frame is firmly screwed into the upper machine bearing block which actually is the male portion of the spherical seating. This frame contains the 4 dial gauges, graduated in 0.0001" increments, which were positioned with their centre lines coinciding with the centre line axis of the cube in each of its 2 principal directions. The pointer of each gauge rides on a smooth, horizontal surface contained in the bottom framework which, in turn is rigidly attached to the lower machine bearing block.

7.2.1.2 Description of specimens

Two groups of 16 - 6" cubes were tested, the first being a mortar of W/C ratio, 0.50 and A/C ratio, 4.0 and the second

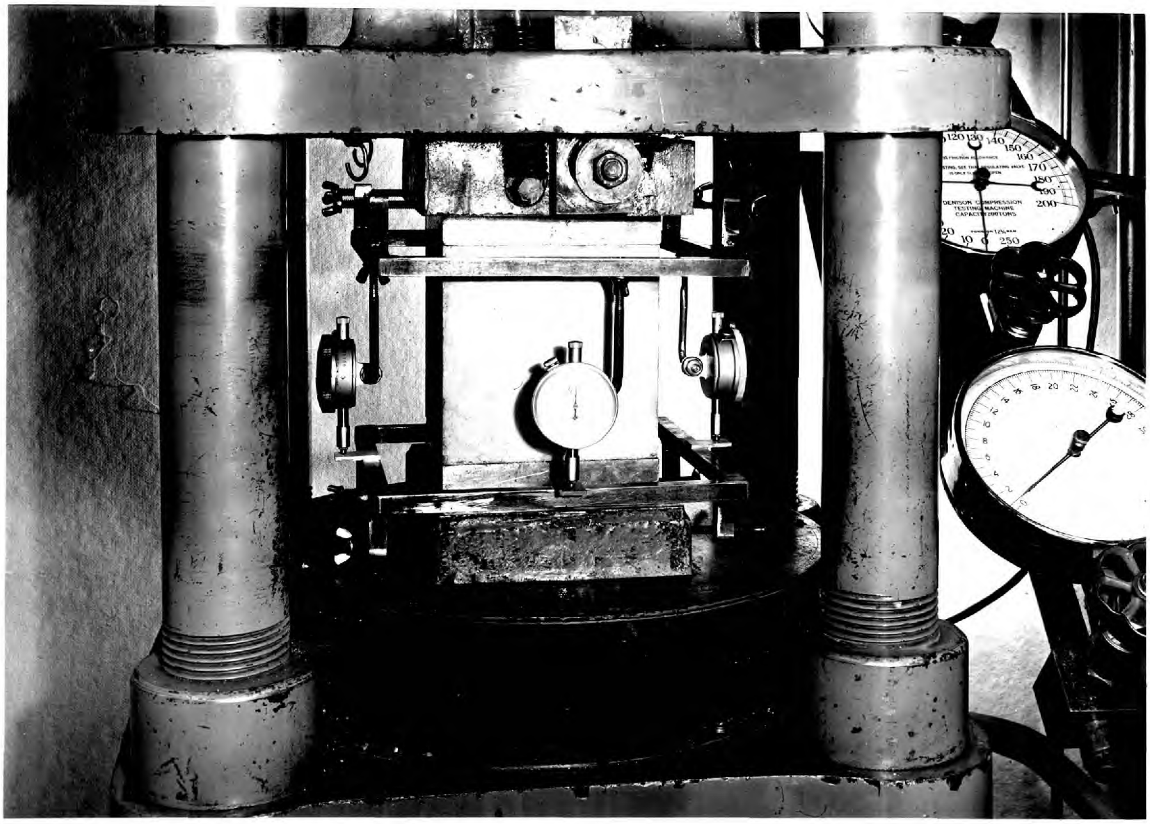

PLATE 7.1 Test apparatus for tilting platen tests on Denison compression machine

a concrete of W/C, 0.65, A/C ratio 8.0, and coarse aggregate/fine aggregate ratio of 65/35. The aggregate used was Thames Valley River Gravel, and the cement was Ordinary Portland. For a detailed description of the materials used, their preparation and casting, vibration, mould stripping and curing procedure, see Ward's thesis, Chapter 6 (2).

Of the mortar specimens, 8 were tested at 31 days and the other 8 at 39 days. The concrete specimens were tested at 54 and 56 day strength, 8 on each day.

7.2.1.3 Testing procedure

Each specimen, taken directly from the curing tank was removed of surplus water and grit with a clean hand towel and then placed directly into the testing machine. Intermediary platens 6" x 6" x 7/8" were used, the bottom one being located axially with the aid of dowelling pins. The specimen and upper platen were accurately positioned and finally, the upper bearing block was screwed down to come into full contact with the upper platen. The dial gauges were checked to ensure that they were truly vertical, in contact with their respective pads, and had sufficient freedom of movement to prevent being damaged.

Prior to commencing the test, the dial gauges were all tapped lightly with a pencil and their readings recorded. The specimens were loaded at the rate of 24 tons per minute by one operator while two other people read the dial gauges. All readings were initially recorded into a tape recorder and subsequently transferred to paper.

The upper machine bearing block, suspended by springs, tended to hang slightly askew when not in use. Consequently, for the first eight mortar cubes, the upper block was maintained parallel to the upper surface of the cube by one operator while a second operator screwed the block down. For the second 8 mortar cubes, this precaution was eliminated. For the concrete specimens, the upper block was screwed down twice in quick succession in order to achieve uniform contact.

As it was impossible to test 16 specimens, in any one day, care was taken to ensure that an equal number of those specimens tested on any one day was orientated in each of the four principal directions.

7.2.1.4 Test results

The dial gauge readings obtained have been processed to show the deformation at the specimen face. Tables 7.1 and 7.2 consequently give the deformation results at the centre lines of each of the 4 exposed faces of the cube for 12 of the 32 specimens tested. These results are expressed graphically in Figures 7.1,7.2 and 7.3 whilst a record of the failure patterns and strengths is given in Table 7.3. A check was provided continually by averaging the deformations on the north and south faces and comparing with the east-west average. At each load stage, these average deformations should be equal.

The relatively large deformations which occur over the first 15% of loading indicate a settling-in action. This may be

TABLE 7.1 TILTING PLATEN TESTS DEFORMATIONS ON 6" MORTAR CUBES IN 200 TON DENISON COMPRESSION MACHINE

Indicated Load (tons)	Deformation of Face Centre line (in. x 10^{-4})							
	Specimen No. 2				Specimen No. 3 (see Table 7.3)			
	North	South	West	East	North	South	West	East
Cast Face North								
10	64	46	72	38	63	62	25	100
20	85	64	96	57	85	79	42	123
40	117	91	128	88	122	106	68	153
60	150	119	157	121	156	130	97	188
80	191	148	188	159	195	155	130	224
90	216	164	212	192	219	169	149	243
95	252	176	236	213	241	179	166	252
100	300	187	272	240	266	187	185	276
105	369	211	320	279				
Cast Face South								
10	30	56	42	41	20	41	29	33
20	46	74	60	59	39	63	49	51
40	73	103	89	88	70	94	79	84
60	100	135	115	119	100	124	109	115
80	132	178	155	166	136	161	144	151
90	151	218	188	198	158	186	165	183
95	164	404	317	321	173	208	175	203
100					195	267	211	253
Cast Face West								
10	51	45	67	32	23	53	36	42
20	74	64	90	51	38	77	52	57
40	106	93	123	79	68	108	83	96
60	138	123	159	109	92	140	111	126
80	178	157	203	140	135	169	143	155
90	203	179	234	156	158	186	167	188
95	228	200	269	169	182	202	183	209
100	253	227	318	187	207	216	201	236
Cast Face East								
10	39	31	24	49	28	178	90	110
20	57	46	34	68	41	206	112	133
40	87	76	70	100	70	238	141	165
60	115	104	96	131	100	268	173	198
80	152	140	127	173	141	301	206	240
90	173	161	144	198	170	326	228	275
95	193	182	151	223	205	342	247	311
100	215	206	162	257	254	362	268	380

Note: Deformation patterns of specimens 2 and 3 are presented graphically in Figures 7.1 and 7.2, respectively.

TABLE 7.2 TILTING PLATEN TESTS DEFORMATIONS ON 6" CONCRETE CUBES IN 200 TON DENISON COMPRESSION MACHINE

Indicated Load (tons)	Deformation of Face Centre line (in x 10^{-4})							
	North	South	West	East	North	South	West	East
	Cast Face North				Cast Face South			
5	24	27	23	23	14	23	8	28
10	39	42	37	39	30	39	22	48
15	49	52	47	49	40	49	31	57
20	58	60	55	58	48	57	39	66
40	89	86	83	88	76	85	66	95
60	120	111	110	119	110	117	100	129
65	131	119	119	130	124	125	112	141
70	142	130	129	142	140	135	125	154
75	159	148	146	161	183	149	160	185
80	177	176	167	187	241	166	202	217
85	203	236	215	237	305	191	272	263
90	263	332	341	369				
	Cast Face West				Cast Face East			
5	17	24	20	21	20	34	41	16
10	33	40	36	37	35	54	60	32
15	46	50	50	49	45	65	70	42
20	52	56	56	52	53	73	78	50
40	83	83	87	79	80	101	104	81
60	115	109	120	106	113	131	131	116
65	127	119	129	117	126	141	144	130
70	141	127	140	133	140	153	156	144
75	171	146	157	164	175	178	186	176
80	201	163	178	195	220	207	227	220
85	254	197	223	252	304	263	318	311

Note: Deformations are presented graphically in Figure 7.3

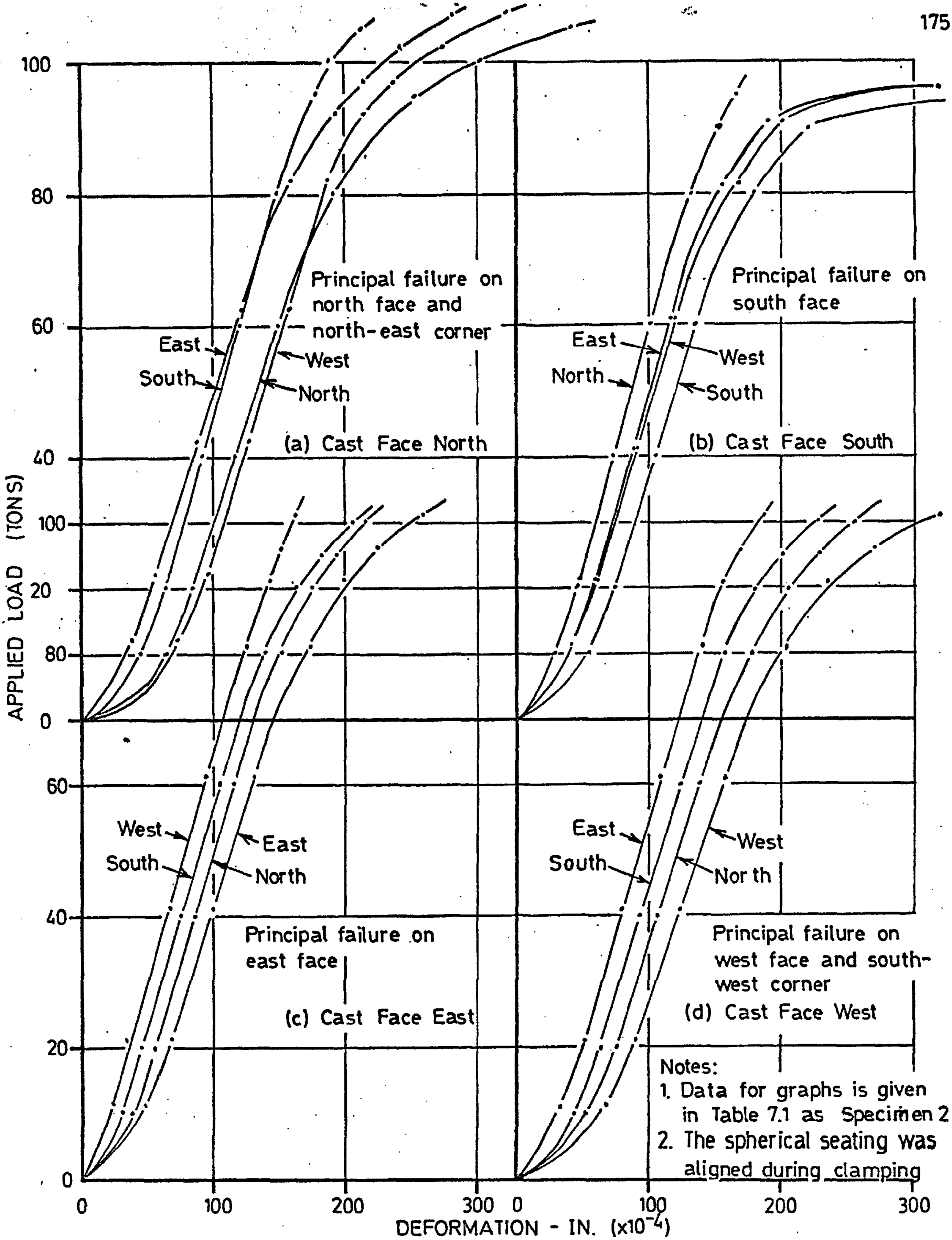

FIG. 7.1 LOAD DEFORMATION GRAPHS FOR 6" MORTAR CUBES IN TILTING PLATEN TESTS ON DENISON COMPRESSION MACHINE

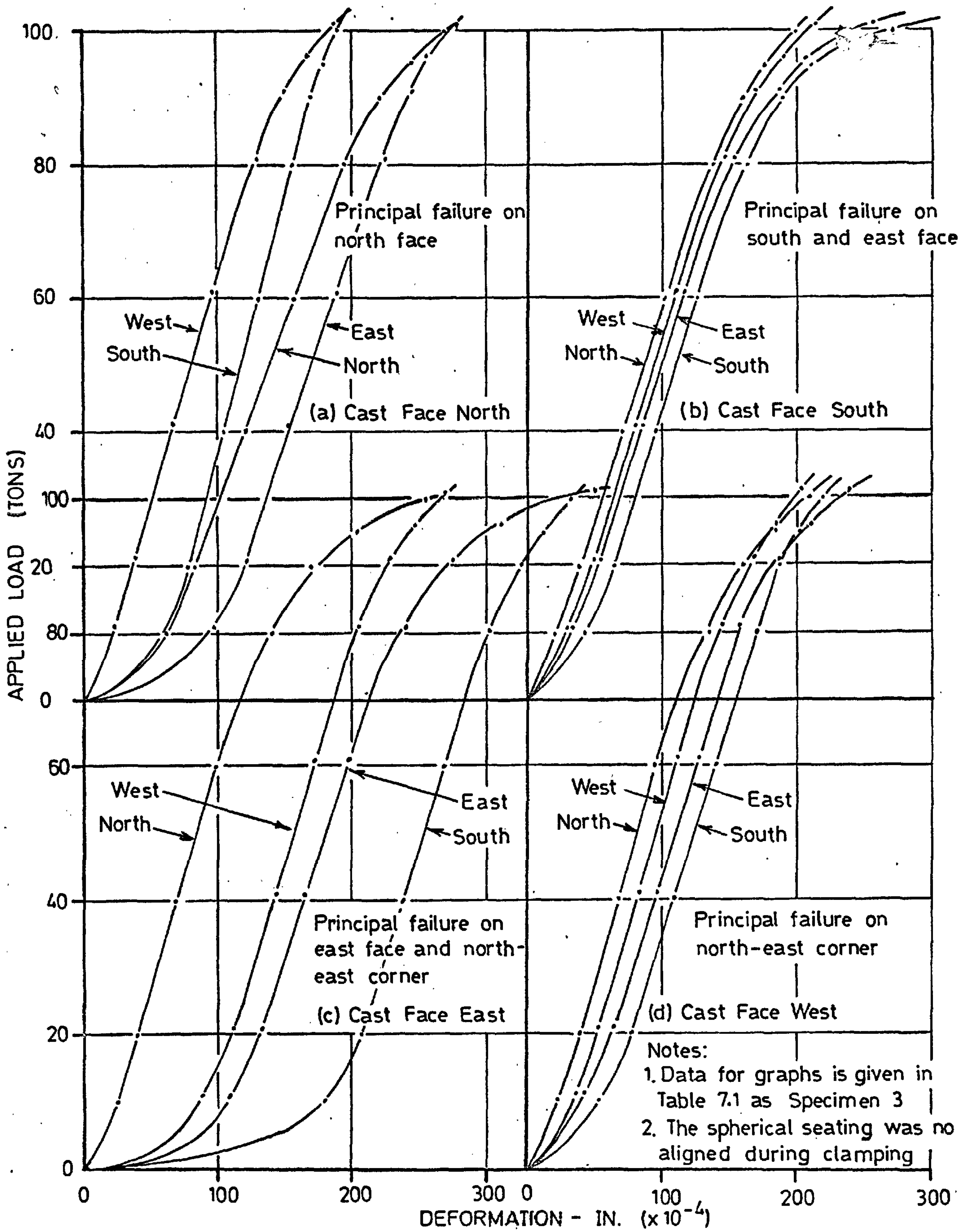

FIG. 7.2 LOAD DEFORMATION GRAPHS FOR 6" MORTAR CUBES IN TILTING PLATEN TESTS ON DENISON COMPRESSION MACHINE

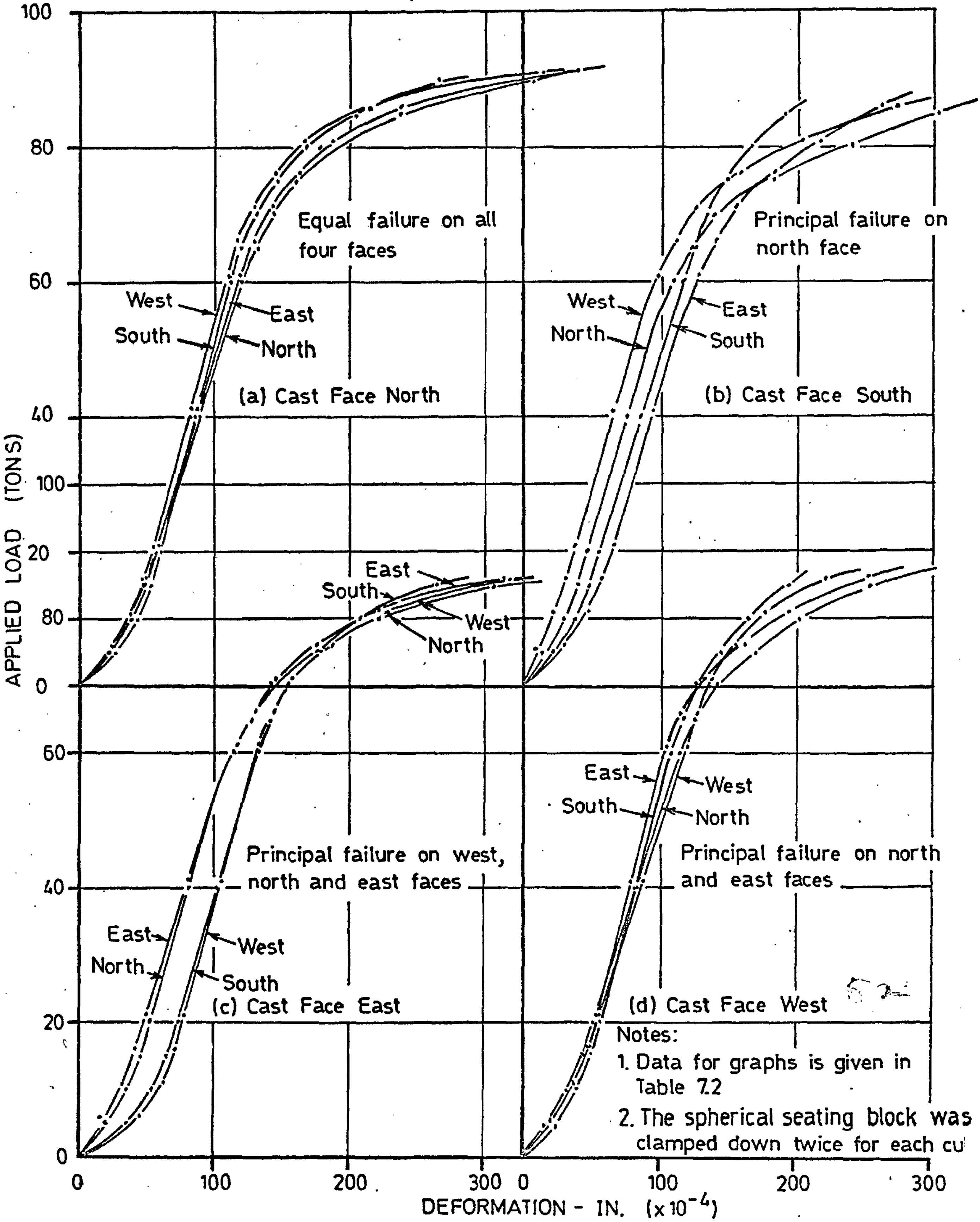

FIG. 7.3 LOAD DEFORMATION GRAPHS FOR 6" CONCRETE CUBES IN TILTING PLATEN TESTS ON DENISON COMPRESSION MACHINE

TABLE 7.3 FAILURE PATTERNS AND FAILING LOADS OF CUBES IN TILTING PLATEN TEST SERIES ON DENISON COMPRESSION MACHINE

Orientation of cast face	Specimen No.	Location of severe failure	Failing Load (tons)
Mortar cubes			
North	1	N.E. corner to N. face	
	2	N. face	
	3	N. face	
	4.	N. face	
South	1.	S. face	
	2.	S. face	
	3.	S., lesser failure on E. face	
	4.	S., lesser failure on W. face	
West	1.	S. W. corner to W. face	
	2.	N. W. corner	
	3.	N. E. corner	
	4.	N. E. corner	
East	1.	E. face	
	2.	E. face	
	3.	N. E. corner to E. face	
	4.	E. face	
Concrete cubes			
North	1.	Equal failure on all faces	90
	2.	Equal failure on all faces	90
	3.	S. E. corner to N.E. and S.W. corners	89
	4.	Equal failure on all faces	91
South	1.	N. face-lesser failure on E. and W.	80
	2.	Failure on all faces - most on N. face	89
	3.	Failure on all faces - most on N. face	87
	4.	S. face - most on S. E.	90
West	1.	E. face - most on N. E.	87
	2.	N. and E. face	90
	3.	E. face	90
	4.	S. and E. face	91.5
East	1.	Failure on all faces - most on N. W. corner	85
	2.	Failure on all faces - least on S. face	89
	3.	N. and W. face	89
	4.	E. face - lesser failure on N. face	89

Note: The deformation history of mortar specimens 2 and 3 is given in Table 7.1, and Figures 7.1 and 7.2; likewise, concrete specimen 2, in Table 7.2 and Figure 7.3. S.N.W. and E. denote south north, west, and east, respectively.

due to loading irregularities arising from minute pieces of grit at the two specimen-platen and two platen-machine block interfaces. However, as the specimens and platens were cleaned of all surface moisture and grit, it seems more likely that some binding action, possibly between the upper bearing block and platen would have prevented complete contact being achieved on all the interfaces. This would explain the excessive movements occurring when no precautions were taken in bringing the upper bearing block down into full contact with the upper platen (see Figure 7.2(a) and (c). In addition, part of these initial deformations are caused by the breakdown of the cement paste film which cover the two bearing surfaces of each specimen.

In most cases, there was a uniform deforming pattern to the onset of failure. Exceptions are Figures 7.1(a), 7.2(a) 7.3(a) and(d). It is particularly interesting to observe that the failing face began deforming more rapidly from 60-70% of the ultimate cube strength. This indicates that the spherical seating does tilt and is very sensitive to local weaknesses and minute misalignments of the specimen. This is amplified by the fact that both the mortar and concrete specimens were relatively homogeneous due to their immunity to segregation effects and that the specimens were aligned in the machine with great care.

Although slightly more failures occurred on the east face and north east corner, this is not significant. From Table 7.3, it is obvious that the direction of tilting of the spherical seating is very dependent on the orientation of the specimen in the machine. This fact, combined with the obvious sensitivity of the spherical seating, and the relative homogeneity of the specimen, confirms that the machine is in good alignment.

The excessive initial differential deformations which occur do not appear to determine the eventual failing face. It must be appreciated, however, that the initial application of load with its accompanying tilting and sliding may physically move the specimen laterally, thereby creating a non-axial loading system. Perhaps this is what happened to the specimen represented in Figure 7.2(a).

7.2.2 Lateral Movement Tests

7.2.2.1 Deformation measuring assembly

The assembly, shown in Plate 7.2, was a rigid framework, firmly attached to the bottom machine bearing block. Eight dial gauges, graduated in 0.0001" increments, rigidly connected to the assembly, were positioned to measure lateral movements of the machine in the two principal directions above and below the spherical seating. As two gauges were positioned to measure the movement in each direction at each location, the calculated average provided more signigicant data. In addition, comparing these two opposite gauge readings provided a continual check. The pointers of the four lower gauges rode on the edge of the ground platens, while the upper gauges had their pointers positioned on the surface of smooth pads, firmly glued to the upper framework of the machine.

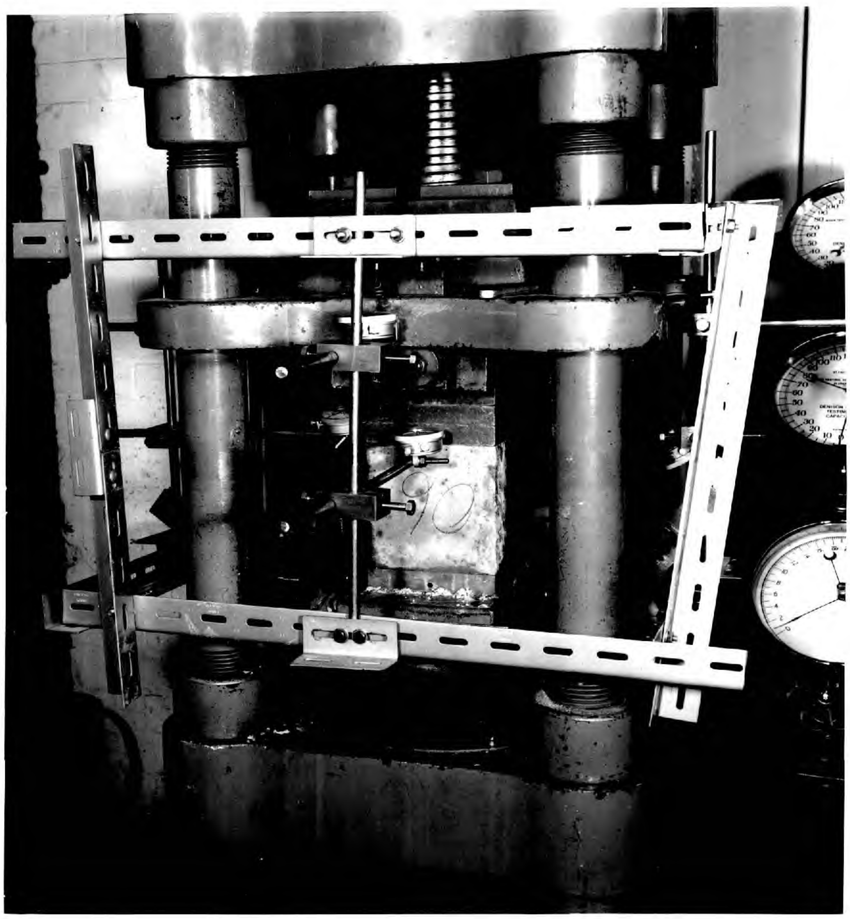

PLATE 7.2 Test apparatus for lateral movement tests on Denison compression machine

7.2.2.2 Description of specimens

The 6" cube specimens used in this test series were cast from the same mixes as those used to investigate intermediary platen effect (see Section 7.5). Detailed information is given in Table 7.4.

TABLE 7.4 CONCRETES AND MORTARS USED FOR LATERAL MOVEMENT TESTS ON DENISON COMPRESSION MACHINE AND INTERMEDIATE PLATEN THICKNESS TESTS

Series No.	W/C Ratio	A/C Ratio	Fine Aggregate / Coarse Aggregate	Age at Testing (days)	No. of Specimens
1	0.60	6.0	40/60	47	10
2	0.55	7.5	40/60	78	12
3	0.40	2.0	Mortar	26	12
4	0.60	6.0	40/60	85	20

For the tests considered in this series, two specimens of each of test series 1, 2 and 3, only, were tested.

7.2.2.3 Testing procedure

The test procedure was essentially identical with that described in the first two paragraphs of Section 7.2.1.3. However, two intermediary platens were used between the upper bearing block and cube specimen as one platen would not allow the two lower north-south gauges to be properly positioned. For achieving uniform contact with the upper platens, the bearing block was screwed down twice in quick succession.

7.2.2.4 Test Results

These results, presented in Table 7.5 and Figures 7.4, 7.5 and 7.6 show the lateral movements of specimen and machine arising in routine testing. It is noteworthy that the major

TABLE 7.5 LATERAL MOVEMENT OF DENISON 200 TON COMPRESSION MACHINE TESTING 6" CUBES

Indicated load (tons)	LATERAL MOVEMENTS							
	Specimen 1-cast face west				Specimen 2-cast face east			
	Movement below seating (in) (x 10^{-4})		Movement above seating (in) (x 10^{-4})		Movement below seating (in) (x 10^{-4})		Movement above seating (in) (x 10^{-4})	
	West	South	West	South	West	South	West	South
Series No. 1								
6			7	95.5			9.5	14.5
12	3.5	32.5			0.	13		
18			21.5	98			8.5	30
24	6.	33.5			-0.5	19		
30			34	101			6	35.5
36	14	35			-1	22.5		
42			43.5	101			5.5	38.5
48	19	35			-2	23.5		
54			54.5	101.5			2	39
60	23.5	34.5			-4			
66			59	102			1.5	34.5
72	26.5	36			-6.5	17.5		
78			27.5	97.5			38	6
84	-25.5	30			68	-9.5		
87.5			-94					
90							225	-15
Series No. 2								
6	0	5.5	4.5	12.5	0	-0.5	3	0
12			7.5	17.5			2.5	0
18	0	7.5			-0.5	-1.5		
24			9	19.5			4	0
30	-0.5	10			-0.5	-1.5		
36			13	23.5			4	-0.5
42	0.5	10.5			0.	3.5		
48			17.5	23.5			2.5	0.5
54	-1	11			0.5	2.5		
60			32	18			4.5	-5.5
66	15.5	1			0.5	-1.5		
72	49	-38	84.5	-23	0	-13.5	-2.5	-32.5
78	78.5	-188	170.5	-133.5	-2	-32.5	-2.5	-66.5
84					31.5	-114.5	10.5	-117.5

(cont.)

TABLE 7.5 LATERAL MOVEMENT OF DENISON 200 TON COMPRESSION MACHINE TESTING 6" CUBES (cont.)

Indicated load (tons)	LATERAL MOVEMENTS							
	Specimen 1-cast face west				Specimen 2-cast face east			
	Movement below Seating (in) (x 10^{-4})		Movement above Seating (in) (x 10^{-4})		Movement below Seating (in) (x 10^{-4})		Movement above Seating (in) (x 10^{-4})	
	West	South	West	South	West	South	West	South
Series No. 3								
6	80	10.5	117.5	55	13	0.5	14.5	9.5
12			134.5	60			15	18
18	109.5	12.5			25	4.5		
24			134	73.5			13.5	22
30	112	14.5			25	6		
36			135	81			13	28
42	112	15.5			29.5	6.5		
48			135.5	84			10.5	29
54	112	17.5			27.5	7		
60			139.5	87			10	30
66	112	18			27	7.5		
72			144	89.5			10	30
78	115	20			27	7.5		
84			152.5	92			10	30.5
90	119	20.5			25	7.5		
96			163.5	98.5			6	31
102	125.5	23			24	8		
108			181	103			0.5	32
114	134	24			20	8.5		
120			432	83.5	17	9.5	-5.5	32.5
126					14.5	10.5	-11.5	35
132					10.5	12	-19.5	35.5
138							-34	36.5

Note: Results of Series 1, 2 and 3, are presented graphically in Figures, 7.4, 7.5 and 7.6, respectively.

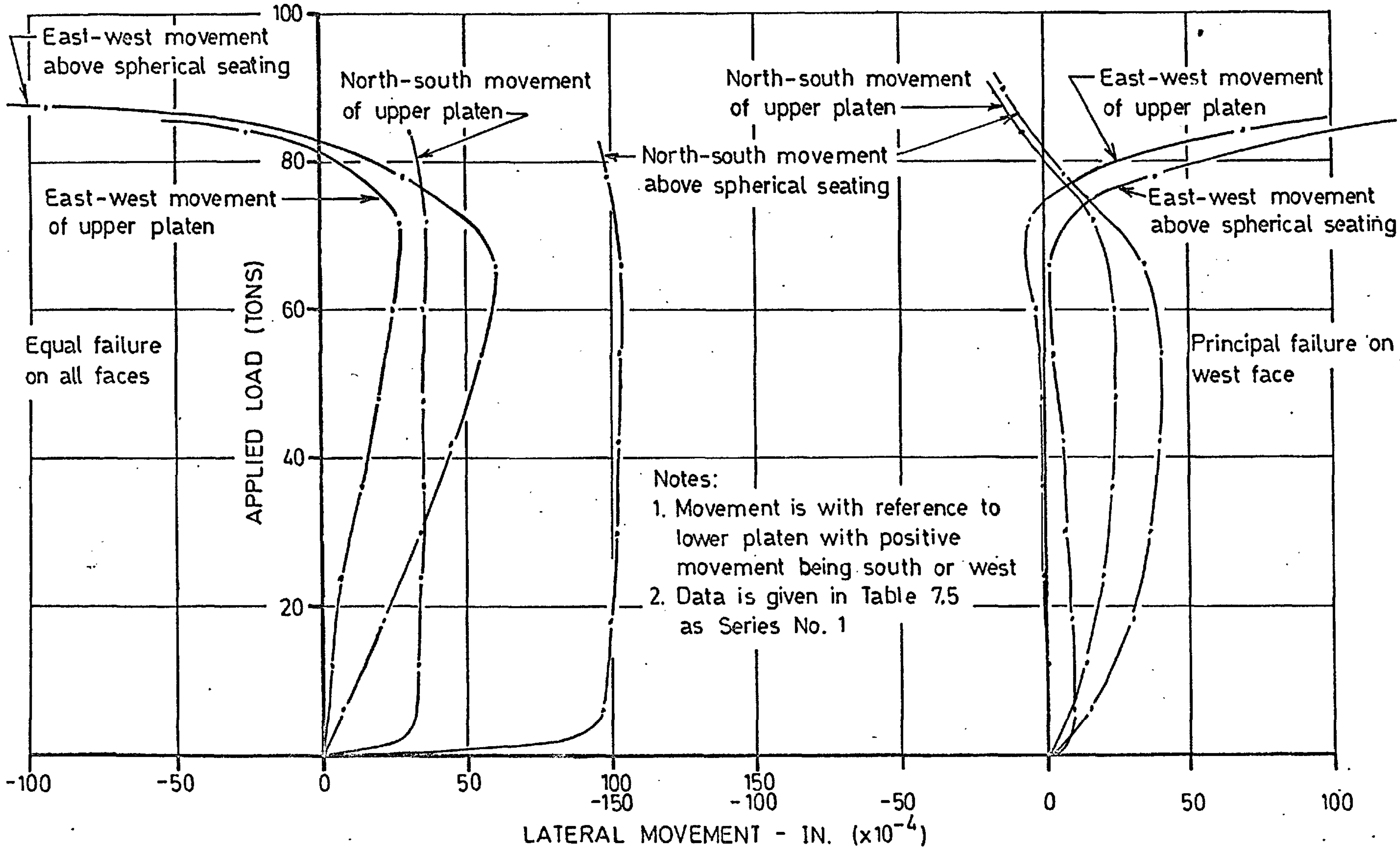

FIG. 7.4 LOAD DEFORMATION GRAPHS FOR 6" CONCRETE CUBES IN LATERAL MOVEMENT TESTS ON DENISON COMPRESSION MACHINE

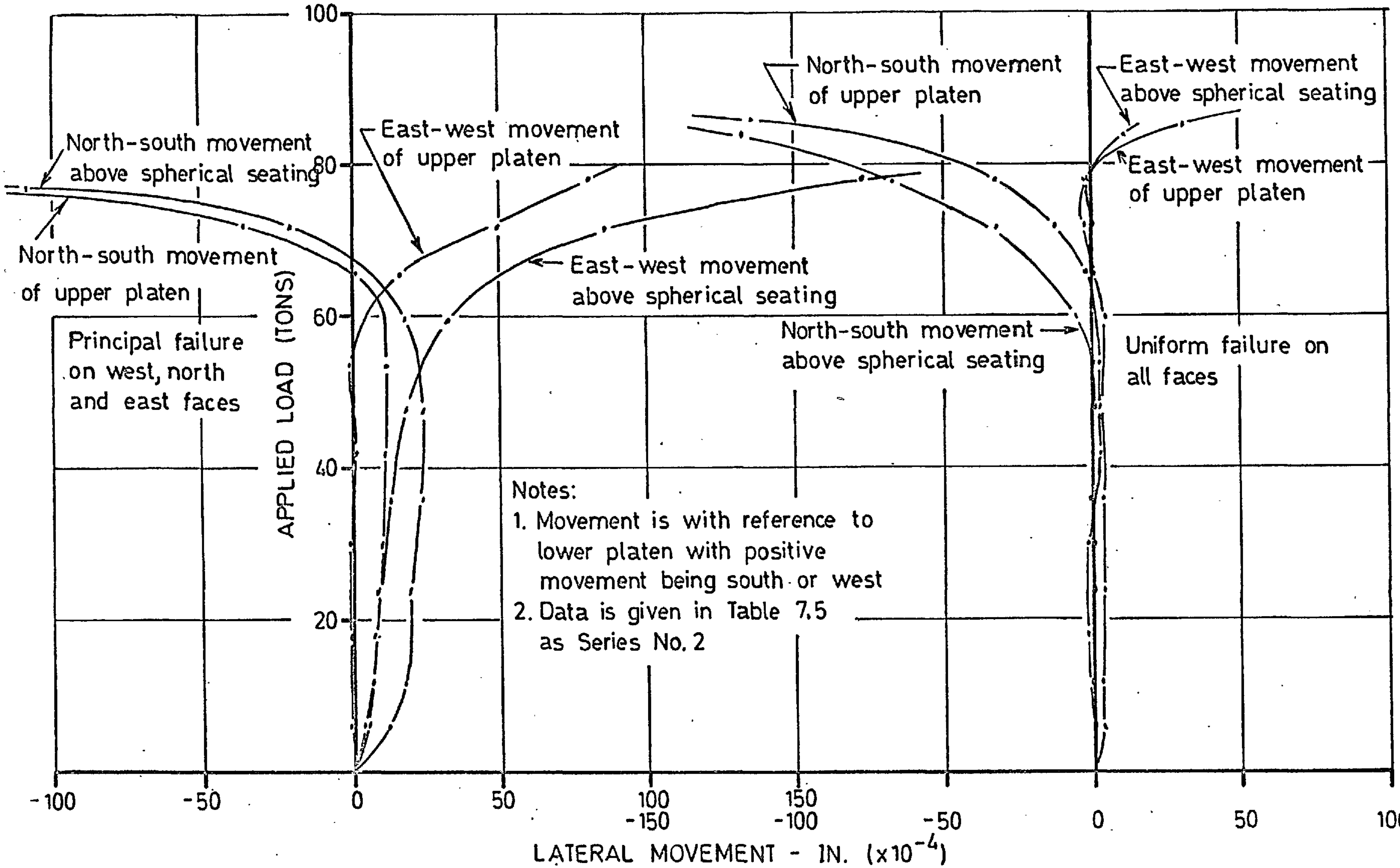

SPECIMEN NO. 1 - Cast Face West

SPECIMEN NO. 2 - Cast Face East

FIG. 7.5 LOAD DEFORMATION GRAPHS FOR 6" CONCRETE CUBES IN LATERAL MOVEMENT TESTS ON DENISON COMPRESSION MACHINE

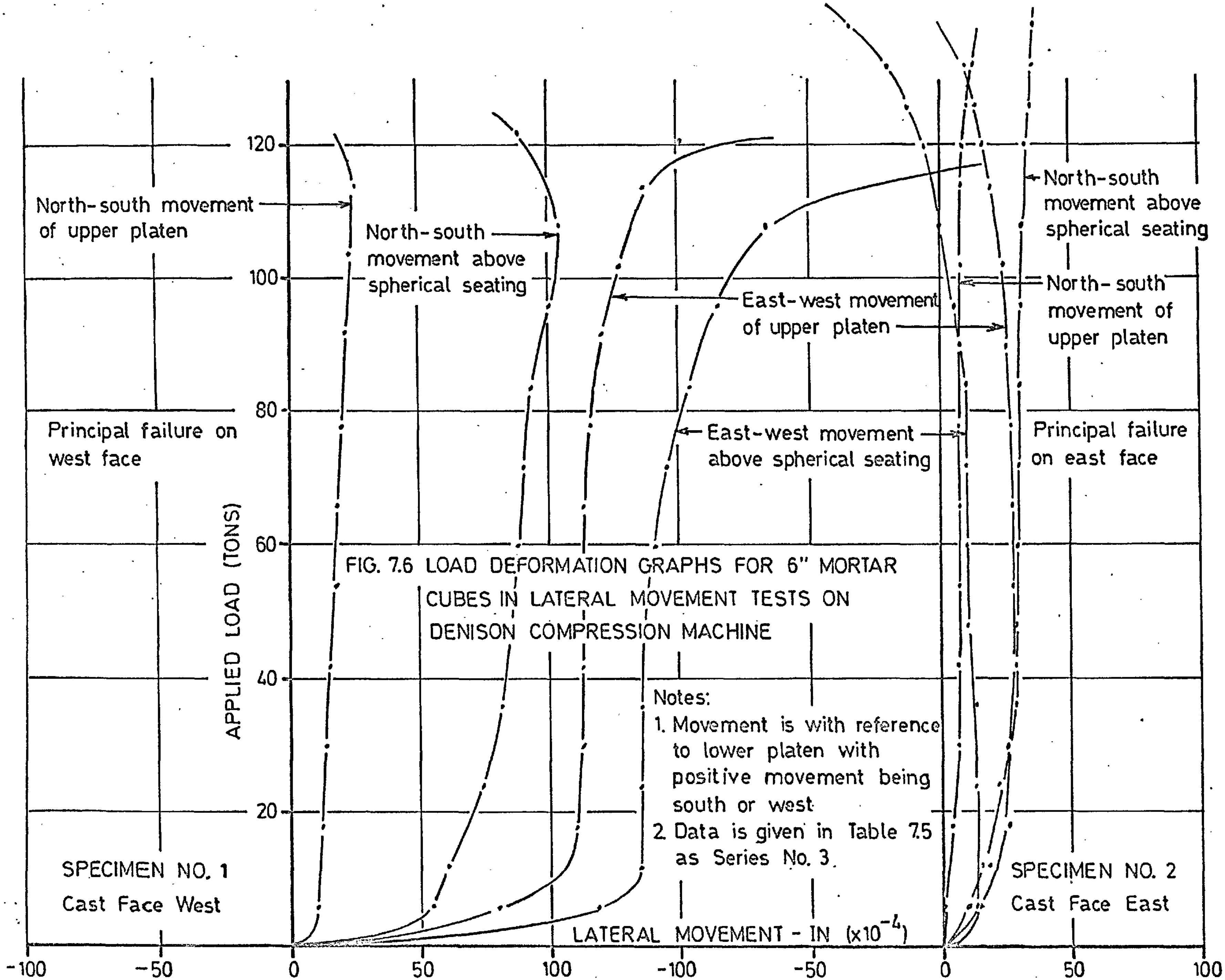

FIG. 7.6 LOAD DEFORMATION GRAPHS FOR 6" MORTAR CUBES IN LATERAL MOVEMENT TESTS ON DENISON COMPRESSION MACHINE

movement, occurring over the last 30% of loading, took place in the same oction as the orientation of the failing face. This agrees with the theoretical analysis of Chapter 6.

It was suggested from theoretical considerations, that machines having lateral stiffness less than 2×10^5 lbs./inch, would have an insignificant effect on the ultimate strength of concrete specimens. However, this machine with lateral stiffness, 1.75×10^5 would produce a lateral force of 2.5 tons for 300×10^{-4}in. lateral movement (see Figure 7.6 - Specimen 1). The resulting displacement of the resultant at the fixed end by approximatley 1/8" would have a very significant influence on the stress distribution and, probably, on the ultimate strength. Consequently, the suggested limit of 2×10^5 lbs/inch, is high, the correct limit being probably about 1×10^5 lbs./inch.

Despite the care taken in bringing the upper bearing block into uniform contact with the intermediary platen, there was an initial lateral movement which varied greatly in magnitude, but always occurred in a south and west direction. This movement, however, seemed to have no effect on determining the failing face.

The sensitivity of the spherical seating to tilt as discussed in Section 7.2.1.4 is again revealed here by the direction of movement of the machine near failure. The fact that the movement, beginning at about 70% of ultimate load, is more sensitive to local weaknesses in the specimen than any other machine property is further proof of its good alignment characteristic.

7.2.3 Appraisal of Machine

The machine is in good alignment , capable of producing consistent failures independent of the orientation of the specimen under test. The spherical seating is very sensitive to slight misalignments and non-uniform specimen properties, thereby behaving in a manner approaching an effectively pinned condition to applied loads of about 100 tons. The machine does contain inherent idiosyncracies which cause the upper machine platen to move initially south and west. However, this has no influence on the specimen strength and its failure patterns. The lateral stiffness of the machine, 1.75×10^5 lbs./inch, is sufficient to produce lateral forces, large enough to significantly influence the stress pattern and, probably, the failure strength.

Its calibration is, however, poor (see Section 3.3.1) and, therefore, its load indicating mechanism should be replaced or, at least, improved.

7.3 ANALYSIS OF 50 TON UNIAXIAL COMPRESSION MACHINE

This machine was developed and used as a research tool for investigating the uniaxial compression properties of concrete. However, owing to a very low longitudinal stiffness resulting in highly explosive failures, it proved unacceptable for cube testing and even unsuitable for determining the ultimate strengths of 4" x 4" x 12" prisms for which it was designed (see Section 5.4.1). It was used, however, by several researchers for determining such fundamental properties as modulus of elasticity and Poisson's ratio.(1-3)

The machine differed from most compression machines in that it had two loading jacks side by side. The investigation was therefore an examination of possible misalignment effects and inherent idiosyncrasies as well as possible undesirable influences from using two loading jacks.

7.3.1 Tilting Platen Tests

7.3.1.1 Test procedure

The assembly, shown in Plate 7.3, is essentially identical to that used on the Denison compression machine(see Plate 7.1 and Section 7.2.1.1).

The specimen, in every case a 4" cube, was placed in the machine, after removal of surface moisture and grit. Intermediary platens, 4" x 4" x 1/2" were used, with the bottom one being dowelled into the machine bearing block. A steel prism 4" x 4" x 12", acting as a spacing block was positioned between the lower platen and specimen. After accurately positioning the specimen, steel prism and platens, the upper machine block was brought down into contact with the upper platen and the four column nuts screwed down by hand until firmly in contact with the cross-head.

Prior to commencing the test, the dial gauges were all tapped lightly with a pencil and their readings recorded. The

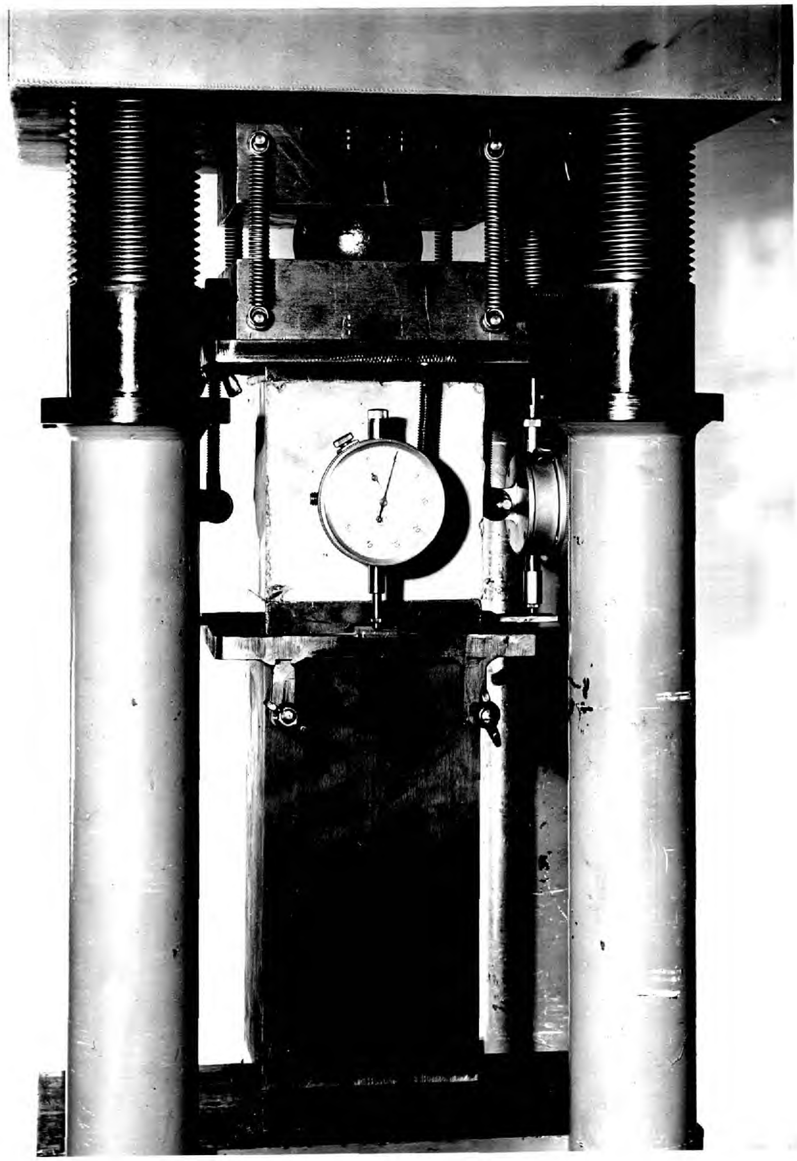

PLATE 7.3 Test apparatus for tilting platen tests on 50 ton uniaxial compression machine

specimens were loaded to failure in approximately 10 minutes. All readings were recorded by a tape recorder and were, subsequently, transferred to paper.

7.3.1.2 Test results

Of the 8 specimens tested, four concrete and four mortar, only the results of the mortar specimens are presented here, as they were representative of the rest (see Table 7.6 and Figure 7.7).

TABLE 7.6 TILTING PLATEN TESTS DEFORMATIONS ON 4" MORTAR CUBES IN 50 TON UNIAXIAL COMPRESSION MACHINE

Load (tons)	Deformation of Face Centre line (Ins.)($x 10^{-4}$)							
	North	South	West	East	North	South	West	East
	Cast Face North				Cast Face South			
5.5	45	30	42	30	44	71	64	55
9.4	58	41	54	41	56	86	77	68
14.2	71	52	67	53	69	99	90	82
19.1	83	62	77	64	81	111	101	94
24.0	95	72	88	74	92	121	111	105
28.8	108	83	98	85	105	134	122	118
32.7	118	92	107	96	115	143	130	129
36.6	131	101	118	107	127	154	141	142
40.5	147	111	129	122	142	168	153	158
44.4	173	122	142	142	165	185	166	182
46.3	206	128	152	161	184	194	174	202
48.3					233	212	182	240
	Cast Face West				Cast Face East			
5.5	101	41	89	48	40	128	60	110
9.4	114	53	100	62	53	143	72	127
14.2	127	64	112	74	67	156	85	142
19.1	138	74	121	86	79	168	95	156
24.0	149	83	130	97	90	180	105	169
28.8	162	94	142	109	103	193	116	183
32.7	172	102	150	120	114	202	125	195
36.6	185	110	161	131	127	214	133	208
40.5	203	121	173	147	143	226	144	229
44.4	240	136	193	174	185	251	154	279
46.3	280	143	209	193				

Note: These results are presented graphically in Figure 7.7.

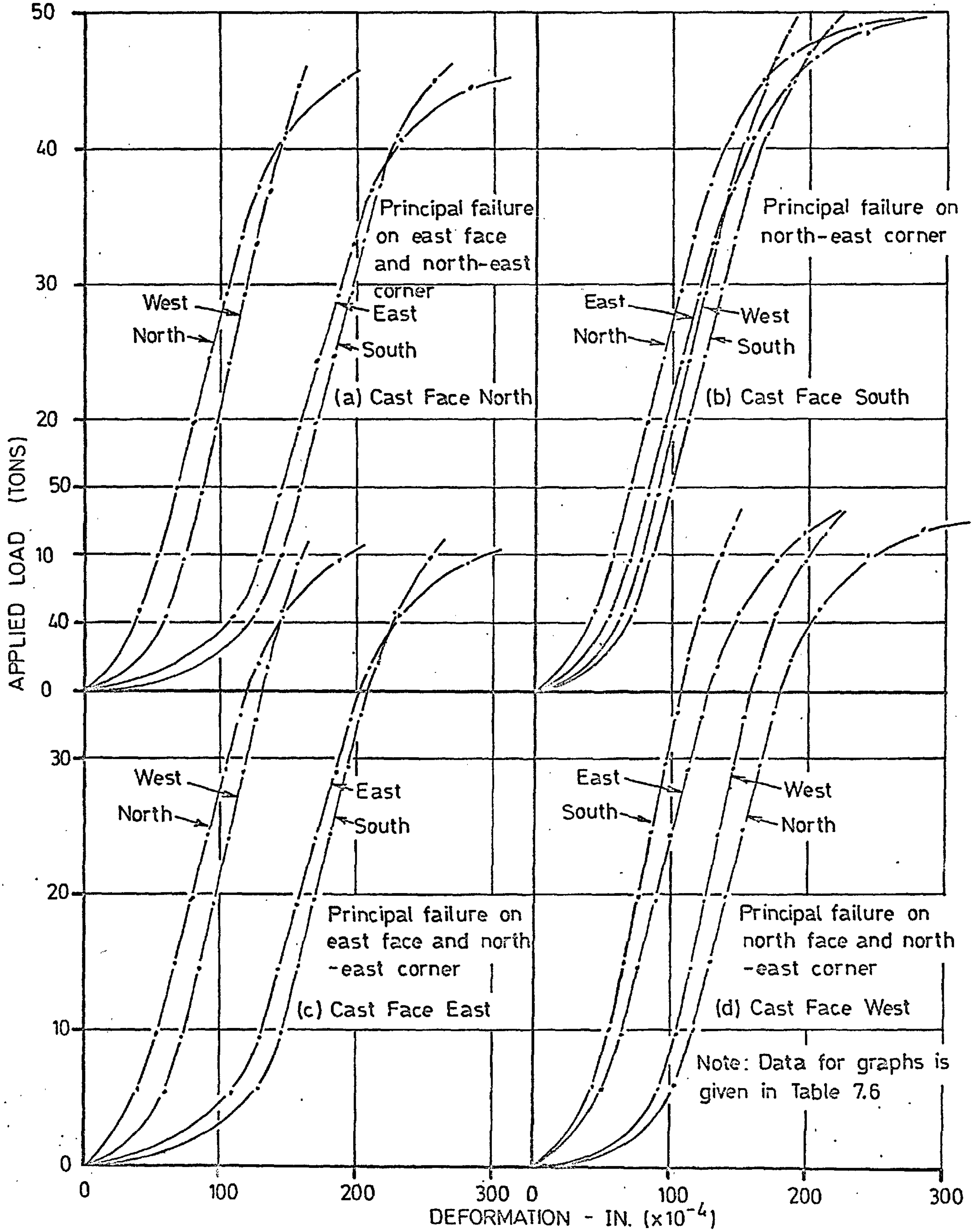

FIG. 7.7 LOAD DEFORMATION GRAPHS FOR 4" MORTAR CUBES IN TILTING PLATEN TESTS ON 50 TON UNIAXIAL COMPRESSION MACHINE

The mix proportions of the specimens were identical to those used in the Denison tilting platen tests. (see Section 7.2.1.2) The concretes and mortars were tested at 56 and 73 day strength, respectively.

In contrast to the tilting platen test results on the Denison, the deformation pattern on this machine indicates a definite off-centre load application towards the north and east sides. These two faces deform more rapidly than their opposite faces and show the first and most severe signs of failure, independent of specimen orientation or the deformation pattern in the first 15% of loading.

As the spherical seating is sensitive to local weaknesses in the specimen (it deforms the failing face at an increasing rate from about 70% of ultimate load) as well as being sensitive to machine misalignment, it approaches an effectively pinned behaviour.

7.3.2 Lateral Movement Tests

7.3.2.1 Deformation measuring assembly

The assembly, shown in Plate 7.4 comprised a rigid framework firmly attached to the bottom cross-head. Although the set-up shown in Plate 7.4 includes a 4" x 4" x 20" mortar prism, the test series was performed on 4" cubes, with the 4" x 4" x 12" steel prism positioned beneath it as shown in Plate 7.3. In addition to the gauges shown in Plate 7.4, four other ones, with their pointers horizontally positioned in contact with the steel prism were included, located 3/4" below the bottom of the cube

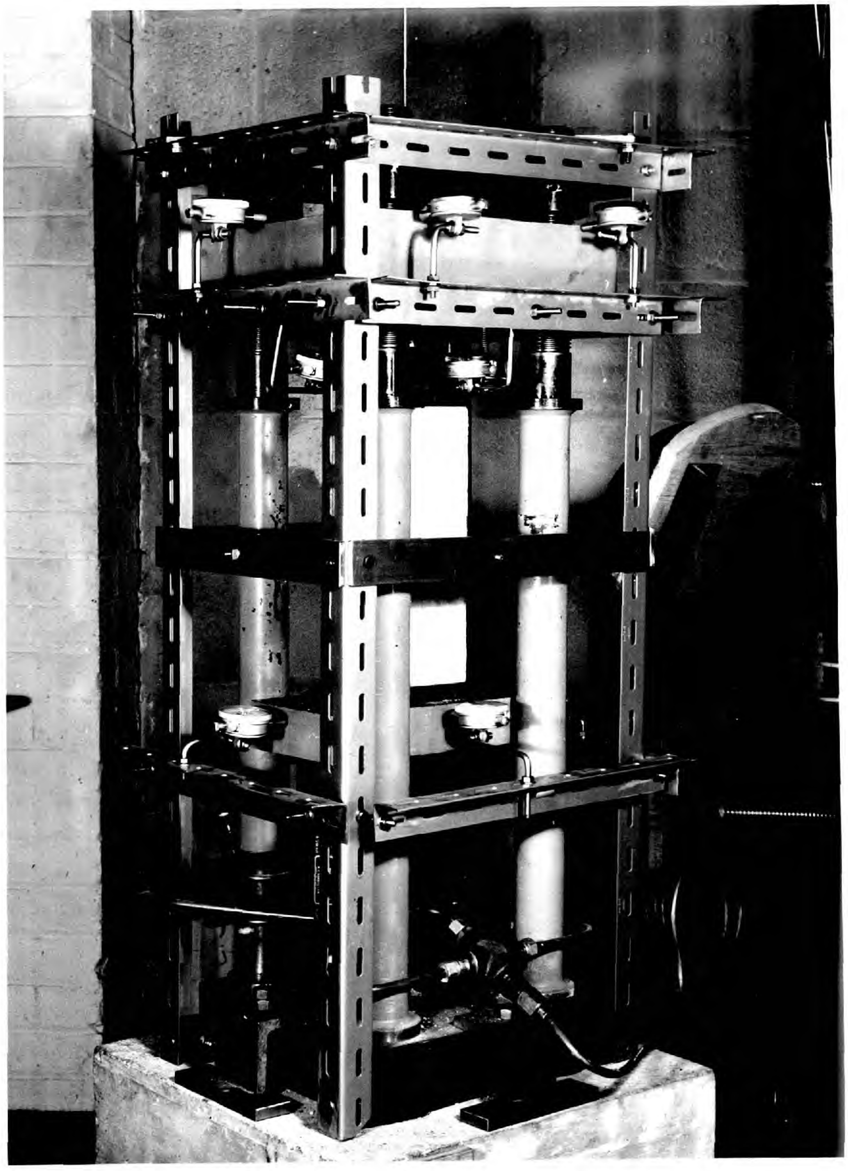

PLATE 7.4 Test apparatus for lateral movement tests on 50 ton uniaxial compression machine

specimen. Care was taken that the pointer of each gauge was located centrally on one of the principal axis of the machine except for two gauges on the east side at the top cross-head. These were positioned to measure rotation of the top cross-head about a vertical axis. With gauges on all four sides at each of the four levels, (17 gauges altogether) the movement in each principal direction at each level was calculated as the average of the movements of two diametrically opposed gauges. This provided a continuous check as well as more significant data.

7.3.2.2. Testing procedure

Four mortar specimens, W/C = 0.40, A/C = 2.0 and 70 day strength were tested with each specimen orientated differently from the other three.

The manner of positioning the specimen and preparing for test were essentially the same as used for the tilting platen tests (see Section 7.3.1.1). However, instead of loading continually to failure, the load was held constant at each load stage while the 17 dial gauges were read.

After loading to approximately 70% of ultimate load, the load was released, and the dial gauges immediately above and below the specimen removed. This was necessitated by the highly explosive failures which would damage these gauges. The specimens were then loaded to failure with readings taken on the nine remaining gauges at each of several load stages.

7.3.2.3 Test results

The data in Table 7.7 and accompanying Figure 7.8 represents

TABLE 7.7 LATERAL MOVEMENT OF 50 TON UNIAXIAL COMPRESSION MACHINE, TESTING 4" CUBES

Load Tons	LATERAL MOVEMENT (in)($\times 10^{-4}$) Level No. 1 West	South	Level No. 2 West	South	Level No. 3 West	South	Level No. 4 West	South
Specimen No. 1 -Cast Face West								
0.6	50.5	-19	20.5	-177.5	21.5	-102.5	5	-41.5
2.6	132	17	95	-133.5	77	-66.5	27	-34.5
4.5	157	22.5	116.5	-125	93	-60.5	33	-34
9.4	196	67.5	147.5	-86.5	118.5	-33.5	45.5	-25.5
14.2	198	78	153	-75.5	121.5	-26.5	46	-25.5
19.1	201	90.5	155	-60	122.5	-17	46.5	-22.5
24.0	203	104	158	-48	124.5	-7	47	-18.5
28.8	204	114.5	159.5	-37	126.5	0.5	47	-15
Specimen No. 2 -Cast Face East								
0.6	17	40	71	125	82	50	31	53
2.6	67	55.5	131	140.5	134	50	51	54.5
4.5	87	56.5	146.5	145.5	145	50	53	55.5
9.4	108	64.5	163.5	156	158.5	52	61	57
19.1	124	79	176	172.5	173.5	57	77	62.5
28.8	131	89.5	189.5	186.5	184.5	57	81.5	64
33.7	136	98	196.5	196	192.5	59	88.5	66.5
38.5	141.5	104.5	202	204	202.5	61	95.5	68.5

Note: Results are presented graphically in Figure 7.8.

TABLE 7.8 TWISTING MOVEMENT OF TOP CROSS-HEAD OF 50 TON UNIAXIAL COMPRESSION MACHINE TESTING 4" CUBES

Load (tons)	LATERAL MOVEMENT in 2 gauges bearing on east side of top cross-head (in)($\times 10^{-4}$) Specimen No. 1 South gauge	Specimen No. 1 North gauge	Specimen No. 2 South gauge	Specimen No. 2 North gauge
0.6	60	53	1	20
2.6	143	130	49	72
4.5	169	157	67	94
9.4	206	192	83	124
14.2	209	198		
19.1	210	199	97	130
24.0	211	202		
28.8	211	205	102	139
33.7			107	143
38.5			111	149

Note: All readings imply a west movement.

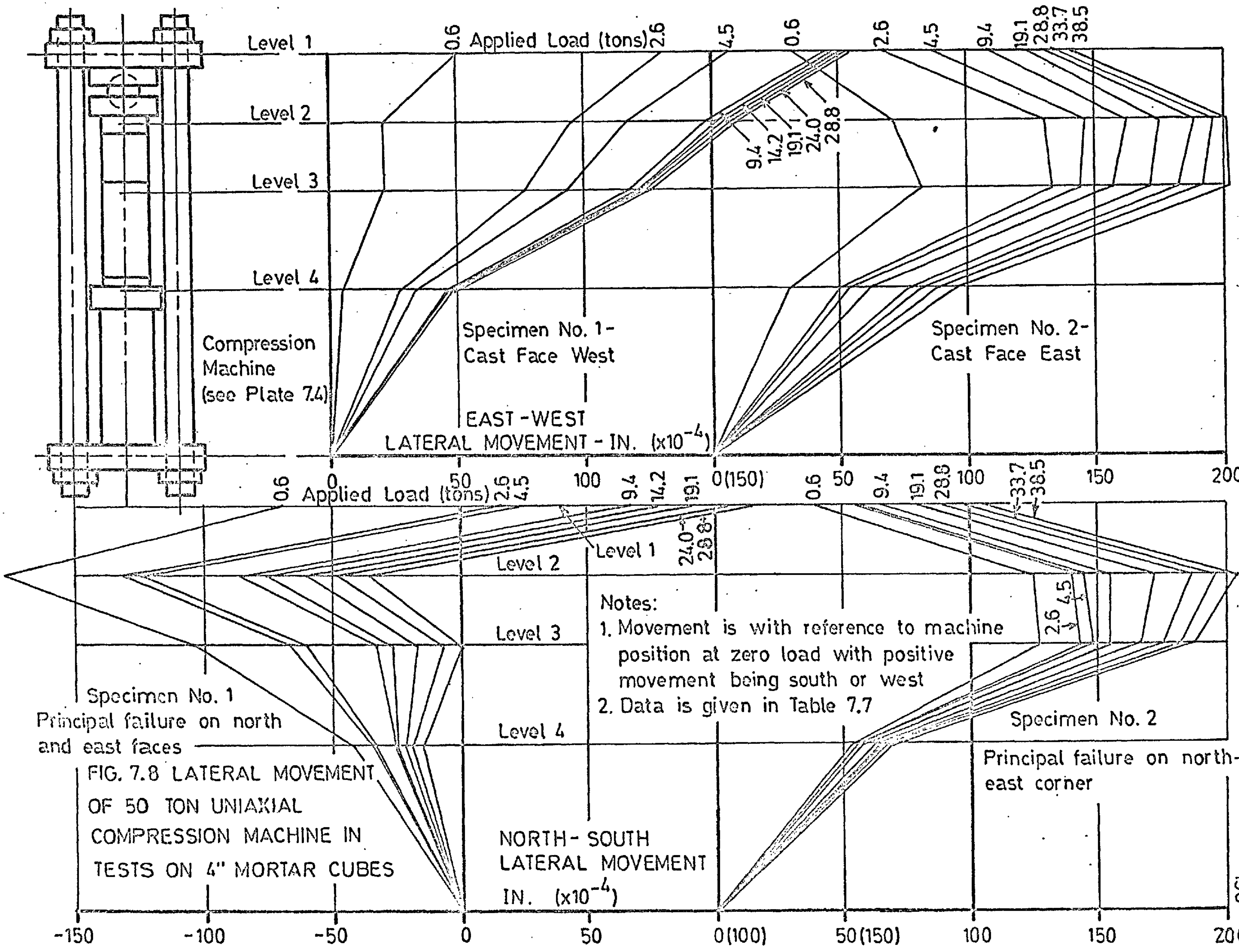

FIG. 7.8 LATERAL MOVEMENT OF 50 TON UNIAXIAL COMPRESSION MACHINE IN TESTS ON 4" MORTAR CUBES

the deformation pattern to 70% of the ultimate load of two of the four specimens tested. Table 7.8 represents the rotational motion of the upper cross-head.

Large initial lateral movements of the order of 1/64" associated with the settling-in action do occur which, as in the case of the tilting platen tests, are in a random direction. Such misalignment can have a very significant influence on both the stress pattern and failing strength (see Sections 5.4.6 and 6.3.5). Inconsistency in this misalignment, dependant on this settling-in action, will result in variable ultimate strengths and an increased coefficient of variation.

Following the settling-in action, the movement of all components of the machine are in a south and west direction. In addition, the movement of the top platen is relatively faster than either the lower platen or upper cross-head. Such movements are a natural consequence of the relatively faster deformations of the north and east faces of the specimen.

It was observed that the relatively slow movement from 10 to 30 tons increased very markedly at failure. This general pattern corresponds to that which occurred in the lateral movement tests on the Denison compression machine.

The twisting action (see Table 7.8) indicated a further idiosyncrasy in the testing machine. The possibility of torsional instability as presented by Flint (39) applies only to tension machines and could, therefore, not account for the motion here. This rotation, small in comparison to the other deformations is consequently a by-product of the machine's loose construction and inherent misalignment.

The columns of the testing machine approach a pinned condition in their cross-head connections due to loose fit and lack of fixity; nuts exist on one side only. Consequently, the lateral stiffness and induced shear forces are both insignificant, thereby producing effectively pinned conditions at both ends of the specimen (see Sections 5.3 and 7.3.1.2).

7.3.3 Further Investigations

As the two previous tests proved that the specimen was loaded repeatedly in a misaligned manner and that the machine was deformed laterally excessively in a consistent direction, it was obvious that improvements in machine behaviour were necessary before further testing could be conducted.

With a metal scale graduated in 1/64 " divisions, a check was made on the alignment of the assembled machine. The bottom platen was found to be displaced 1/64 " towards the west side and 3/64 " towards the south side. In addition, by using a clinometer, the slope of this platen was measured as 0.0065 in. per in. with the north side being high. This produced a further misalignment of 1/16 " at the centre height of the specimen. This misalignment of 7/64 " in the north-south direction is reduced to 3/32 " by the south jack moving first, thereby reducing the slope of the machine platen. As the spherical seating, which approaches a pinned condition, would load the specimen vertically coincident with its own centre, the misalignments above would explain the faster deformation rates which occur on the north and east faces.

The lack of effective fixity in the column cross-head connections with its resulting random behaviour of load application was further aggravated by loose ram-machine platen connections. The use of two supposedly identical jacks has severe disadvantages. When loaded, any differential force in the jacks results in a significant moment on the machine platen. Resulting tilting or bending can create misalignment as it did in this case. Furthermore, a rigid connection could produce binding at the ram-cylinder interfaces with differential force in the jacks. This would be a result of either differential jack properties or specimen misalignment.

7.3.4 Appraisal of Machine

The 50 ton uniaxial compression machine was condemned for the following reasons:

1. It was in poor alignment.
2. It had loose-fitting connections resulting in specimens deforming in a non-repeatable manner.
3. It was too soft longitudinally.
4. The spherical seating (see Plate 7.3) had its centre of rotation located above the centre of the bearing face of the upper machine platen. It thereby did not conform to the specifications of British Standard 1881.
5. Two loading jacks side by side proved unsuitable for a un-

iaxial test.

The investigation of this machine revealed conclusively the danger of applying blind faith to a calibration performed in accordance with British Standard 1610 (8); its calibration was Grade A_1. It is to be appreciated that the current calibration technique appraises only the load indication device and, in no way, whatsoever, gives a guarantee of the reliability of test results. The importance of a calibration technique capable of sensing the effects of misalignment of load are readily appreciated. Some experimental investigation towards this end has been conducted and is presented in Chapter 4. It is hoped that an improved calibration technique would appraise not only the load indicating device, but would also reflect on the reliability of machine behaviour during routine testing.

7.4 ANALYSIS OF WARD TENSION MACHINE

A machine for performing uniaxial tension tests on concrete specimens was successfully designed and manufactured by Ward (2), see Plate 7.5. In the design of this machine, special attention was given to alignment of components, stability and lateral and longitudinal stiffnesses. In contrast to the 50 ton uniaxial compression machine, encastre connections between the columns and cross-heads exist, achieved with locking nuts on both sides of the cross-heads. The specimen is loaded under a system approaching effectively pinned conditions, - obtained by using two lubricated pins at right angles to each other at each end of the specimen. Furthermore, this had the advantage over spherical seatings of preventing a tendency to torsional instability (see

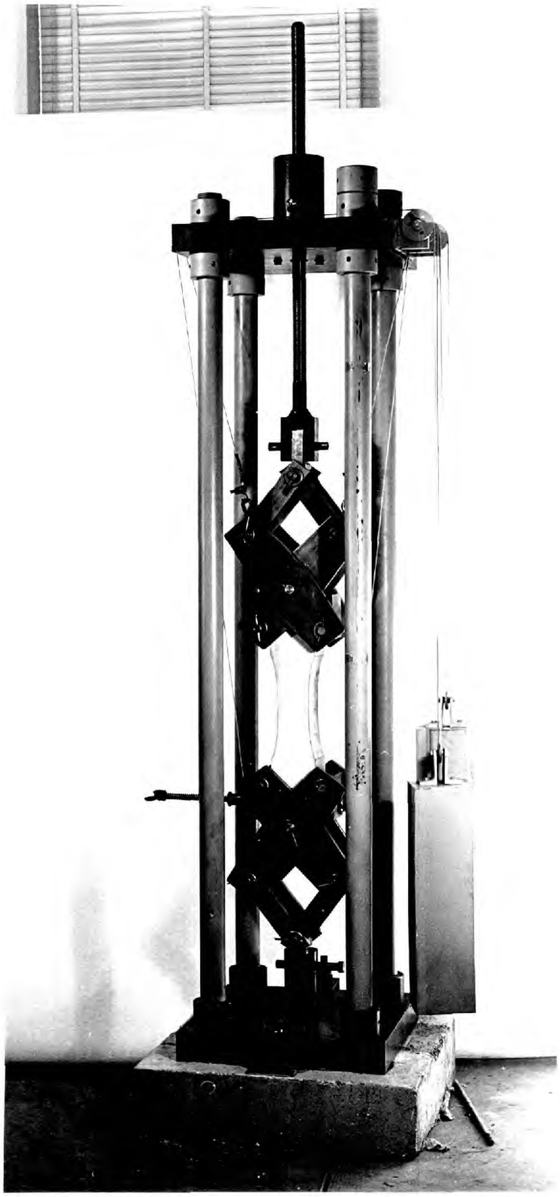

PLATE 7.5 Ward tension machine

Section 5.4.2). As the effective specimen length is less than the machine length, the combined assembly is, theoretically, inherently stable at all loads less than the combined buckling load of the columns. The grips and specimen were designed with great emphasis on achieving precise alignment- see Ward's thesis p. 62-87 (2) .

7.4.1 Experimental Investigation

The first of two investigations was conducted by Ward to check the specimen behaviour under load. By testing an aluminum specimen and, subsequently, a mortar specimen, both with strain gauges on all faces, a check for any inherent misalignment effects was conducted. Two further mortar specimens with strain gauges on two opposite faces were tested. All these tests revealed that the strain readings were uniform to within ±1 microstrain (the sensitivity of the strain measuring instrument used) to the onset of failure. Thereafter, with the mortar specimens, differential strains which occurred displayed the behaviour of specimens loaded under pinned conditions thereby giving evidence that the machine behaved in accordance with this method of loading.

The second investigation conducted by the author in conjunction with Ward was performed to corroborate the theoretical condition of adequate lateral stiffness and inherent stability. A rigid framework was firmly attached to the lower machine crosshead. Dial gauges, graduated in 0.0001" divisions, were positioned with the pointers riding horizontally on the edge of the upper machine cross-head. Three gauges were positioned on the centre lines of the west, north and east sides whilst the two remaining gauges on the south side were displaced laterally, similarly to the assembly on the 50 ton compression machine as seen in Plate 7.4. The first three gauges measured lateral movement while the latter two indicated rotational movement about the vertical axis of the machine (39). With the testing of two specimens, no movement was observed on any of the five gauges thereby confirming the theoretical considerations of adequate lateral stiffness and inherent lateral and torsional stability.

7.4.2 Appraisal of Machine

The theoretical considerations and subsequent experimental investigation confirmed that the machine is inherently stable and sufficiently stiff laterally to ensure a repeatable loading behaviour. The specimen, furthermore, has lateral machine properties eliminated by virtue of being loaded under a system approaching effectively pinned conditions. The great care taken in the manufacture of the grips and specimen has provided further evidence of the ability of the machine to produce a true uniaxial stress state.

The machine does, however, suffer from a relatively poor loading system. The valves, which are quite crude industrial types, produce an insensitive load control with insufficient movement between no-load and ultimate strength. The piston-type pump producing slight oscillations of load and the relatively small load indicating device all contribute to Grades A and B calibrations (see Section 3.3.4).

7.5 THE INFLUENCE OF THE THICKNESS OF THE INTERMEDIATE PLATEN ON THE COMPRESSIVE STRENGTH OF CONCRETE

7.5.1 Test Procedure

For determining the influence of the distance from the centre of rotation of the spherical seating to the upper bearing face of the cube, on the cube strength, four groups of cubes were tested with varying platen thickness. In the first three groups, that is, Test Series 1-3 in Table 7.4, two specimens were tested at each of several thicknesses of intermediate platen. These thicknesses were obtained by placing a varying number of 6" x 6" x 7/8" platens between the bearing face of the upper bearing block and the upper face of the specimen.

Prior to placing in the machine, surface moisture and grit were removed from the specimen with a clean towel and the cube was then accurately positioned on the lower dowelled platen. The upper platens were then accurately positioned on top of the specimen, care being taken to have the same face of the same platen always in contact with the specimen, except, of course, when no platens were used. The bearing block was screwed down twice in quick succession in order to achieve uniform contact

7.5.2 Test Results

The results of Test Series 1 and 2, presented in Table 7.9, indicated that some influence from the thickness of the interm-

TABLE 7.9 THE INFLUENCE OF INTERMEDIATE PLATEN THICKNESS ON THE ULTIMATE STRENGTH OF CONCRETE SPECIMENS

	Specimen Failure - tons					
	Platen Thickness (in.)					
	0	7/8"	1 3/4"	2 5/8"	3 1/2"	4 3/8"
Test Series No. 1						
Cube 1		90.0	87.5	84.2	85.0	82.0
Cube 2		83.5	90.5	89.5	84.5	84.5
Average		86.8	89.0	86.8	84.8	83.2
Test Series No. 2						
Cube 1	82.5	80.5	82.2	81.5	84.5	88.5
Cube 2	80.5	84.0	85.0	84.0	83.5	85.5
Average	81.5	82.2	83.6	82.8	84.0	87.0
Test Series No. 3						
Cube 1	142.5	142.0	122.5	138.0	136.5	134.5
Cube 2	133.5	144.0	139.0	131.0	141.0	140.0
Average	138.0	143.0	130.2	134.5	138.8	137.2
Test Series No. 4						
Cube 1		96.0		95.1		94.7
Cube 2		95.8		97.5		99.9
Cube 3		98.0		96.0		96.7
Cube 4		96.2		99.1		94.5
Cube 5		95.5		96.8		98.6
Cube 6		98.3		97.7		99.2
Cube 7		97.8				99.7
Average		96.8		97.0		97.6

ediate platen could exist - even though the trends were in opposite directions. Test series 3, alternatively showed no consistent trend. Test series 4, performed to corroborate or disprove the trend of series 1, was conducted on a larger number of specimens at fewer positions for significance determination. From these results (series 4), it is apparent that the influence of intermediate platen thickness up to 4.5 in. is insignificant.

In almost every case, it was visibly obvious that the spherical seating had tilted thereby resulting in lateral movement and induced lateral forces. As these were most pronounced on the concretes in series 1 and 4, it is obvious that the lateral forces, if influential, would be most significant in these test series. The fact that they are not, gives conclusion to the fact that the thickness of the intermediate platen (up to 4.5") has no effect on the ultimate strength of specimens tested in this particular machine. Although the lateral stiffness of this machine will only produce small influences (see Chapter 6), there is a significant effect on the stress pattern and probably, on the ultimate strength(see Section 7.2.2.4). Furthermore, the discussion on platen thickness effect at the C. and C.A. symposium (see Section 7.1.2) was with reference to platens of only about 1/2 " thickness. It is therefore reasonable to conclude that no significant effect on ultimate strength will occur with platens of 1/2" thickness in any testing machine.

7.6 SUMMARY

Three uniaxial testing machines, two compression and one tension, have been investigated for the manner in which they load specimens to failure. The tension machine and Denison compression machine displayed good alignment characteristics with random specimen failures while the 50 ton uniaxial compression machine was condemned due to several shortcomings including poor misalignment, inadequate lateral and longitudinal stiffness and improper spherical seating design. The tension machine and 50 ton uniaxial compression machine loads specimens in a manner which approaches effectively pinned end conditions while the Denison 200 ton compression machine loads in accordance with the philosophy of having one end pinned whilst having the other end fixed to at least 100 tons.

The investigation also revealed the fallacy of placing great confidence in calibration results. The tension and Denison compression machines produced Grade A or B calibrations over most of their working ranges, whereas the 50 ton uniaxial machine was Grade A_1. The importance of devising a verification sensitive to other machine properties than just the load indication device must be appreciated.

From the investigations conducted, some definite conclusions and recommendations for the design of uniaxial testing machines are put forth.

1. The use of 1/2" thick intermediary platens, plane in accordance with B.S. 1881, and positioned between the machine bearing blocks and specimen do not influence the ultimate strength of concrete cubes. Furthermore, the use of such platens should

be encouraged, possibly by incorporating into British Standard 1881.

2. Owing to the importance in achieving precise alignment, the bottom platen should be accurately dowelled to the centre of the machine bearing block.

3. The machine must be manufactured with close tolerances in mind. Loose fitting components are prone to misalignment effects and non-repeatable loading conditions.

4. The use of two loading jacks side by side is to be avoided.

5. The longitudinal stiffness must be sufficient to eliminate explosive failures (see section 5.4.1).

From this investigation, there was insufficient evidence to provide definite recommendations for the behaviour of spherical seatings during test. In particular, it was necessary to investigate the true behaviour of different seatings under load and the effect that variations in this behaviour would have on the cube and cylinder strength. The details of such an investigation are given in the next two chapters.

CHAPTER 8

THE BEHAVIOUR OF SPHERICAL SEATINGS

8.1 INTRODUCTION

8.1.1 PREVIOUS RESEARCH ON SPHERICAL SEATINGS

In 1913, Schuyler[49] stated that the A.S.T.M. specifications required that spherical seatings be used for the compression testing of concrete specimens. However, these specifications made no mention of the details of the design of such seatings. After an investigation of several seatings, Schuyler concluded that, in general, spherical seatings compensate for the lack of parallelism in the ends of the specimen during initial setting-up, but became effectively fixed during loading. In more recent investigations where pinned end conditions have been required for particular tests, special designs have been used. For example, Templin[50] used a hydraulically supported spherical seating with a continual flow of oil being maintained along the seating interface. In the testing of columns pinned in one direction and fixed in the other, Huber[51] used fixtures with cylindrical bearing surfaces. These, he claimed, were satisfactory to an applied load of about 2×10^6 lbs.

Examination of the behaviour of the spherical seatings in testing machines used for the control testing of concrete cubes and cylinders has also been a subject of investigation by both Tarrant[28] and Wright[22]. In his tests, Tarrant measured coefficient of friction values in one seating under four conditions of lubrication.

These values, ranging from 4% to 60%, were an example of the large possible variation of behaviour of different seatings with different lubricants in different testing machines. Lower cube results were generally obtained with the well lubricated seating, although this difference, which was not consistent, was also dependent on the composition and degree of segregation of the specimen (29).

Wright, when measuring the rate of deformation of opposite sides of concrete cubes, showed that some machines deform specimens uniformly, while others exhibit tilting characteristics in the spherical seating. However, as his gauges were not positioned to measure the direction of tilt that would normally be expected, that is, either towards or away from the cast face, none of his results necessarily represent fixed end conditions. (see Section 5.3)

From research as presented in Chapter 7, it is shown that the spherical seating in both the Denison compression and 50 ton uniaxial machines behaved in a manner approaching effectively pinned conditions.

8.1.2 Importance of a Complete Understanding of Spherical Seating Behaviour

Although more than fifty years have elapsed since Schuyler (49) stated the shortcomings in specifications concerning spherical seating behaviour in compression testing machines, current specifications still do not specify the function of the seating under load. As a result, there is confusion as to whether a seating should or should not tilt freely under load. Yet, from the limited past research, it is apparent that consistent results between machines cannot be obtained unless a closer control is placed on the manner in which specimens are deformed and failed.

The method of loading a specimen(see Section 5.3) is ultimately integrated with the spherical seating behaviour. Consequently, the question asked in Section 7.1, "How should testing machines deform and fail concrete specimens?", cannot be answered until a full understanding of spherical seatings and its effect on concrete strengths has been achieved.

In addition, questions concerning the possibility of obtaining effectively pinned or fixed loading conditions with a spherical seating needs to be answered. Not only is this of prime importance for closer control of testing machine behaviour, but also, numerous structures and commercial machines rely on pinned connections between components.

8.1.3 Factors Influencing the Behaviour of the Spherical Seating

The possible factors which influence the characteristic behaviour of the spherical seating are:

1. radius of seating
2. area of contact at seating interface
3. type of contact, that is, full contact or strip contact
4. machining finish of the interface
5. type of lubricant
6. applied force

8.2 ADOPTED METHOD OF TEST

Tarrant's method of obtaining coefficient of friction values for spherical seating, which is to be described is, in principle, an excellent method of investigating the seating's behaviour in routine testing.(28) For, not only does the seating tilt at a very similar rate as in the testing of concrete specimens, but, also, the set-up and test are simple and accurate and the calculations relatively free from extraneous influences. It was, therefore, used in the following test series with improved modifications.

Tarrant, although indicating that a serious problem existed, performed insufficient experimentation to provide definite suggestions as to the type of lubrication which should be used. In addition, as his experiments were confined to one seating, the results did not take into account variables associated with the manufacture of the spherical seating- see points 1 to 4 in Section 8.1.3. To fully analyze these variables, several spherical seatings, specially manufactured with suitable extremes in their properties, were tested to establish the influence of these properties.

8.3 DESCRIPTION OF EQUIPMENT USED

8.3.1 Spherical Seatings

As spherical seatings are very costly components when manufactured properly, the investigation was necessarily limited. The four seatings that were designed and manufactured as shown in Plate 8.1, have radii varying from 3" to 7". This

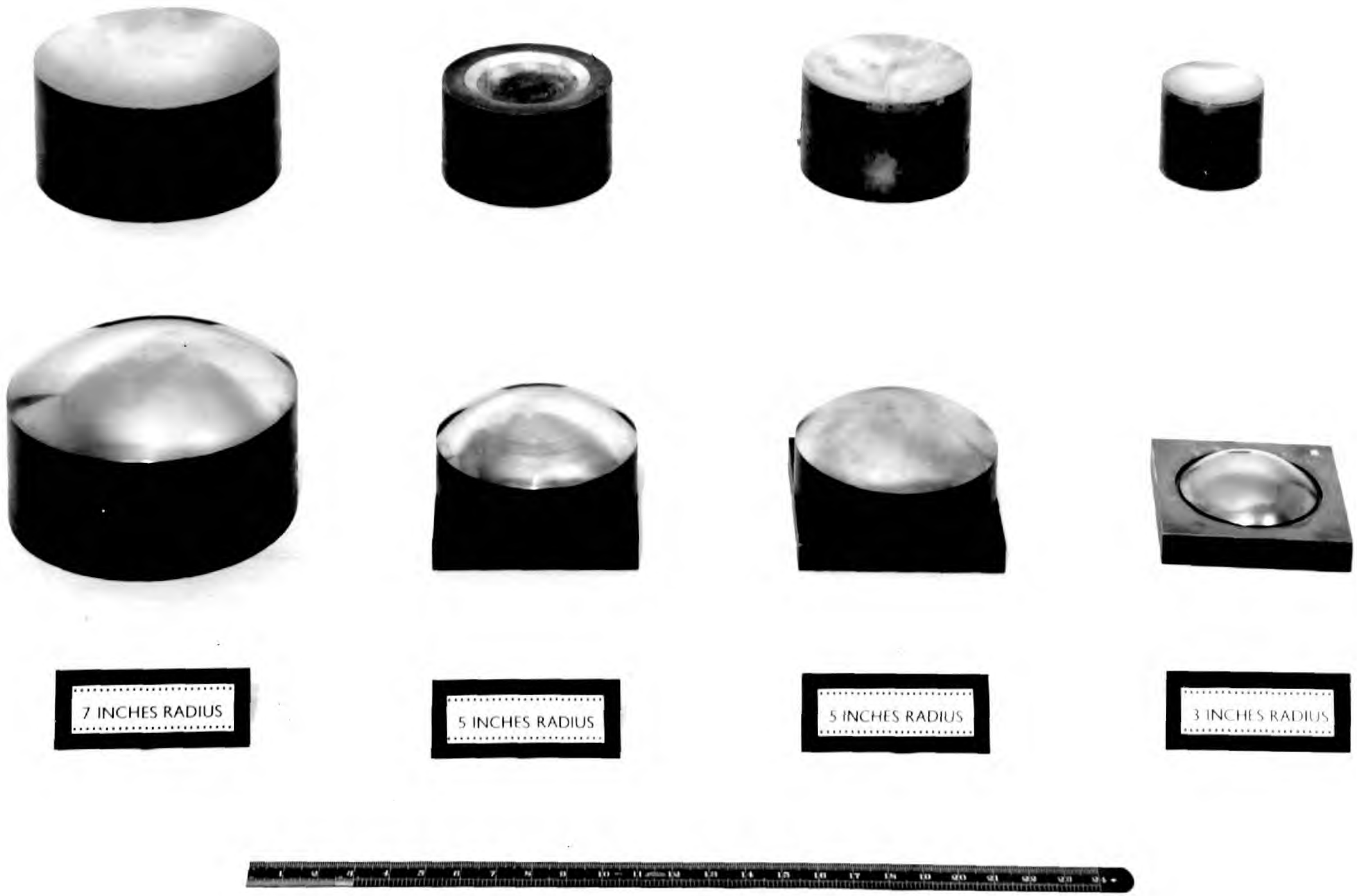

PLATE 8.1 Spherical seatings used in investigation of spherical seating behaviour

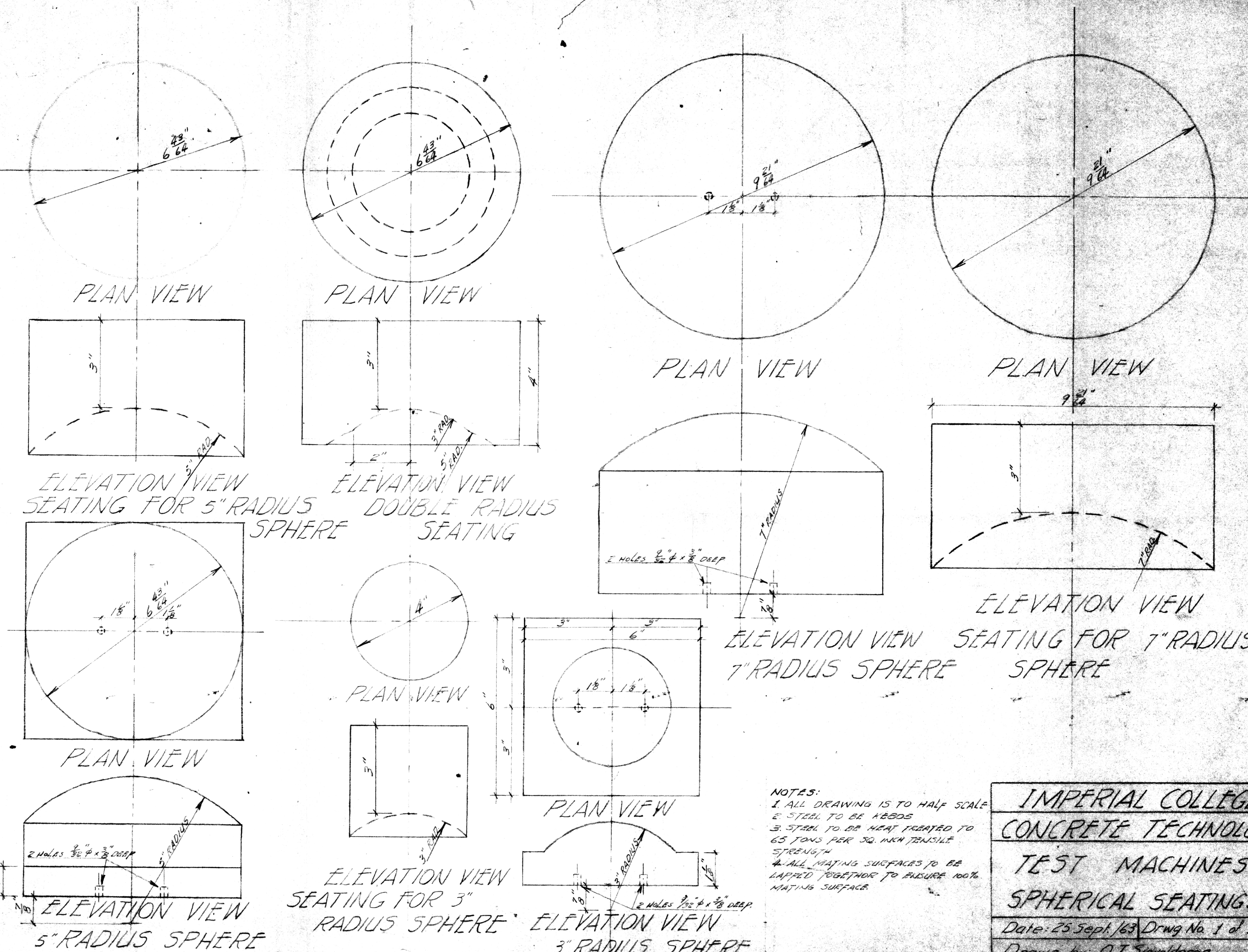

NOTES:
1. ALL DRAWING IS TO HALF SCALE
2. STEEL TO BE KE805
3. STEEL TO BE HEAT TREATED TO 65 TONS PER SQ. INCH TENSILE STRENGTH
4. ALL MATING SURFACES TO BE LAPPED TOGETHOR TO ENSURE 100% MATING SURFACE.

IMPERIAL COLLEGE
CONCRETE TECHNOLOGY
TEST MACHINES SPHERICAL SEATINGS
Date: 25 Sept./63 Drwg No. 1 of 1
Drawn by: O.T. Sigvaldason

covers the general range of radii existing in concrete compression testing machines . The three full contact seatings are constructed with the contact area dimensions geometrically similar. Consequently, the area of contact is proportional to the square of the radius, thus providing a ratio of 5.45 between the contact areas of the 7" and 3" radii seatings. By producing the machined surfaces of these two seatings with the same degree of finish and assuring full contact, an evaluation of the contact area influence was possible.

The machined finish of the 3" and 7" radii and the 5" radii with line contact were all classified as 4 to 8 microinch finish. This defines a maximum difference between low and high spots on any mean arc across the surface of 4 to 8 microinches. This degree of finish and assurance of full contact at the interface was only achieved by means of a very lengthy lapping process. Consequently, it must be appreciated that the quality of this finish is very high and considerably better than that existing in almost all commercial testing machines.

In order to investigate the influence of surface finish, a 5" radius seating having no lapping performed on it was also manufactured. The finish, defined as 150-200 microinch, is worse than that existing in most machines. However, from examination of the interface during the test series, this seating appeared to have uniform contact over the entire interface area.

A large number of spherical seatings in existing machines have, instead of a full contact, a strip contact following an irregular ring. To investigate the influence of such a contact, a 5" radius seating seating with the same surface finish as the 3" and 7" radii seatings was included in the investigation. With 0.5" width of contact and 7.0 sq. in. of contact area, it provided a good comparison with the 3" and 7" radii seatings containing 14.5 and 78.5 sq.in. of contact, respectively.

The steel, heat treated to 65 tons per sq.in. tensile strength was KE 805. These specifications were kindly supplied by W. and T. Avery Ltd. All the spherical seatings were manufactured by Morfax Ltd. Further details of the seatings are given in Figure 8.1.

8.3.2 Load Transfer Assembly

An assembly for transferring the force from the spherical seating into the two load measuring devices (in this case, proving rings) should be:

1. hinged or pinned at the connections with the proving rings
2. dimensioned so that no lateral movements are induced when rotation in the spherical seating occurs
3. capable of locating the seatings accurrately and simply
4. able to support each of the three different sizes of spherical seating
5. light enough to be positioned easily
6. strong enough to transfer loads of approximately 100 tons
7. infinitely stiff, thereby applying a uniform resistance to the male face of the seating.

The assembly, shown in Figure 8.2 and Plate 8.2, was designed with these 7 points in mind.

In order to obtain a hinged connection, two knife edges, 6" long, were manufactured which, so as to resist the very large applied forces, were designed relatively flat - see Figure 8.2. As the punching action of this knife edge was likewise very severe, its groove was machined out of 1" thick high strength steel with an additional 1" stiffener plate welded on top. The knife edges and assembly were dimensioned so that the centre of rotation of the spherical seatings and the knife edges were on one horizontal line. This prevented any component of lateral displacement arising at the knife edges with the small rotations of the sphere in its seating.

The transfer assembly contained two dowelling pins which allowed very accurate axial placement of the seating, estimated at $\pm \frac{1}{128}$". In order to achieve a very repeatable set-up, the pins were manufactured with a firm fit in both the seatings and the transfer assembly.

The transfer assembly was light enough to be lifted into place and located accurrately with ease. However, it was not infinitely stiff as this could only have been achieved with a very elaborate and expensive device. Consequently, the load on the male spherical seating face varies from a maximum at the edges to a minimum at the centre due to the flexural behaviour of the transfer assembly.

In an initial series of tests, loads to 100 tons were ap-

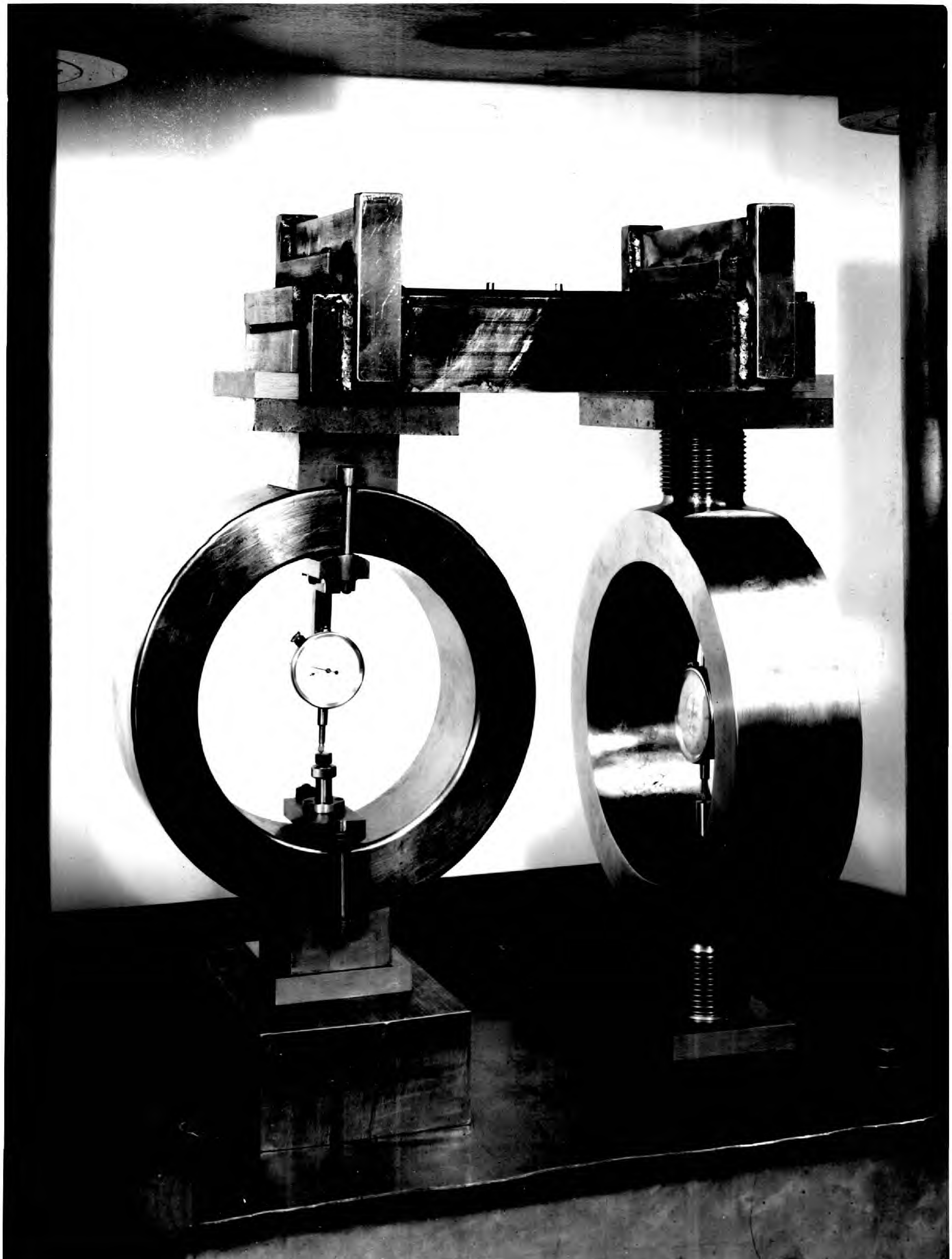

PLATE 8.2 Load transfer assembly positioned on top of proving rings

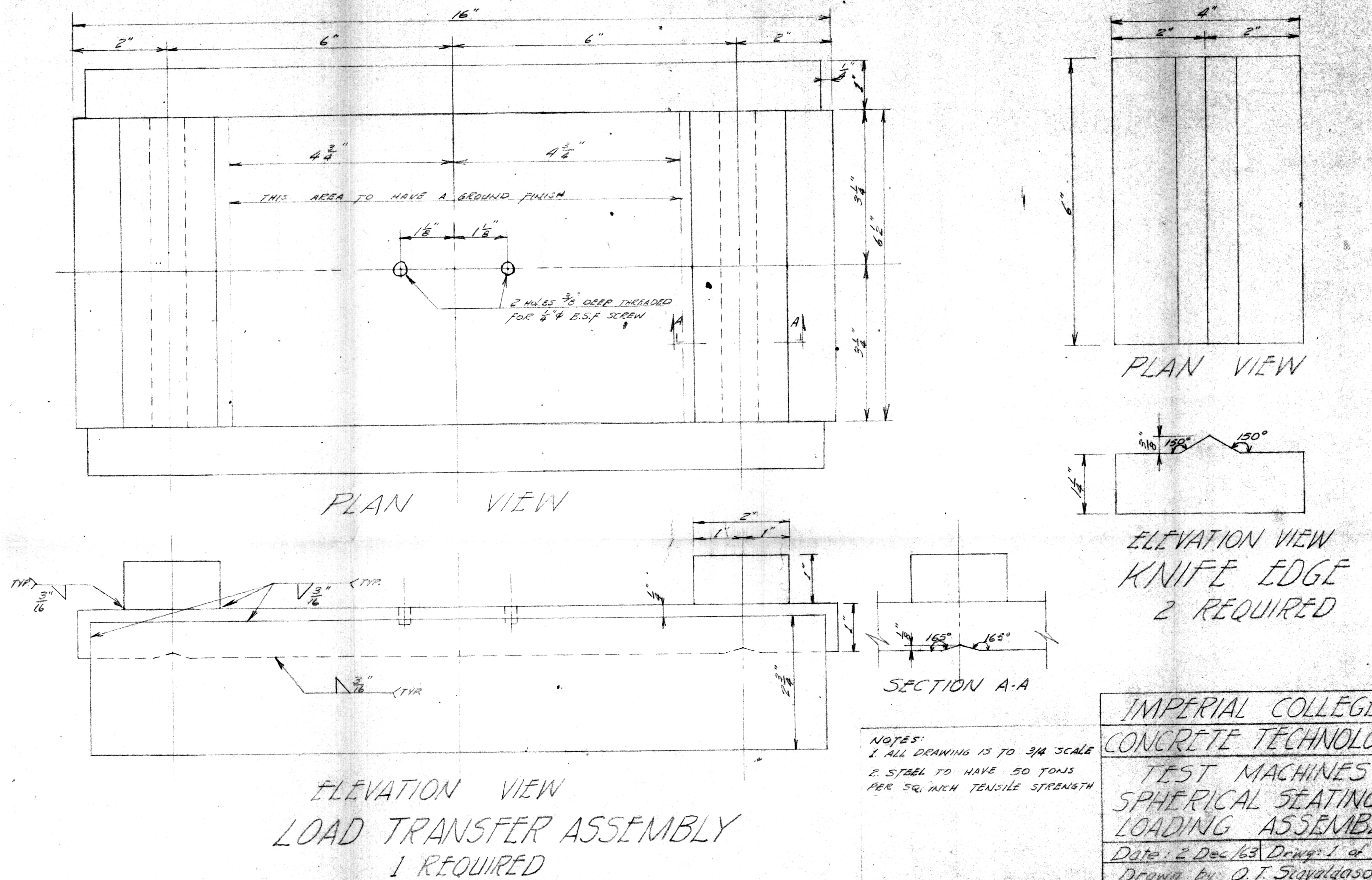

NOTES:
1. ALL DRAWING IS TO 3/4 SCALE
2. STEEL TO HAVE 50 TONS PER SQ. INCH TENSILE STRENGTH

IMPERIAL COLLEGE
CONCRETE TECHNOLOGY
TEST MACHINES
SPHERICAL SEATINGS
LOADING ASSEMBLY
Date: 2 Dec /63 Drwg: 1 of 1
Drawn by: O.T. Sigvaldason

plied, but it was found that the weld between the sideplates and top plate nearest the knife edges failed due to a severe over-stressing. The welds here were replaced and a stiffener frame over each knife edge was welded on (as shown in Plate 8.2) to relieve this concentration of load. So as to eliminate further failures, tests were performed thereafter to 80 tons only. As some distinct minute weld failures occurred at a later date, two more stiffener frames were welded on. This relieved the stresses sufficiently to allow the entire test series to be completed.

8.3.3 Load Indication Devices

It was necessary that the two load measuring devices should have:

1. sufficient difference in stiffness to measure the large coefficient of friction values of the non-lubricated seatings.
2. high sensitivity to load indication.
3. repeatability and accuracy so as to discern the repeatability in the behaviour of lubricants and provide accurate values of its coefficient of friction.

On the basis of these requirements, a 50 ton proving ring and a 100 ton proving ring were selected, the latter being approximately twice as stiff as the former. This selection proved adequate for conducting all the proposed friction tests. The 100 ton proving ring was Grade 1 from 10 tons to 100 tons while the 50 ton ring was Grade 1 from 10 tons to 50 tons[(8)]. Both instruments can , in addition, be considered highly sensitive to changes in load. As each division was sub-divided into tenths for every reading, the 50 ton ring would have 5,900 increments at 40 tons applied force while the 100 ton ring would indicate 3,200 increments.

8.3.4 Testing Machine

The loading assembly complete with a spherical seating, as shown in Plate 8.3 required loading to each of a series of predetermined loads. The requirements of a testing machine for performing this operation are:

1. sufficient head-room
2. excellent load control
3. high degree of accuracy and repeatability
4. ease of removing its existing spherical seating
5. horizontal flat contact area on the lower face of the upper cross-head
6. large lateral and longitudinal stiffness
7. immunity from inherent lateral movement

With these requirements in mind, an Avery testing machine belonging to the Road Research Laboratories, was selected as being the most suitable available (see Plate 8.4). Its headroom was sufficient to meet the 33" required for the test. A Grade A calabration over its entire load range and excellent load control were proof of the merits of this machine. In addition, it was a very stiff machine, both laterally and longitudinally by virtue of having 7.5" Ø columns and an 18 "Ø loading ram. Although it had two columns only, thereby reducing the lateral

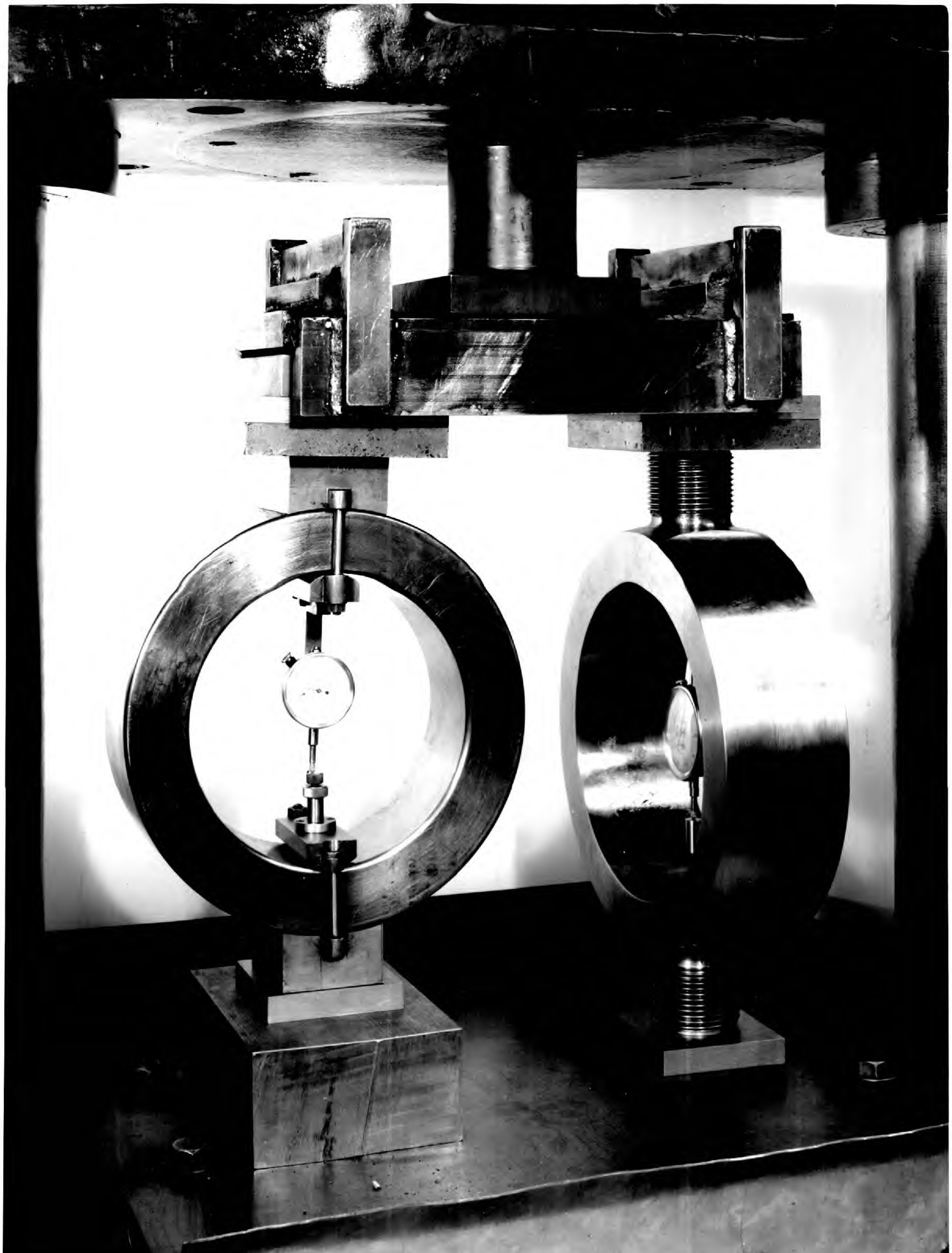

PLATE 8.3 Test assembly for coefficient of friction tests

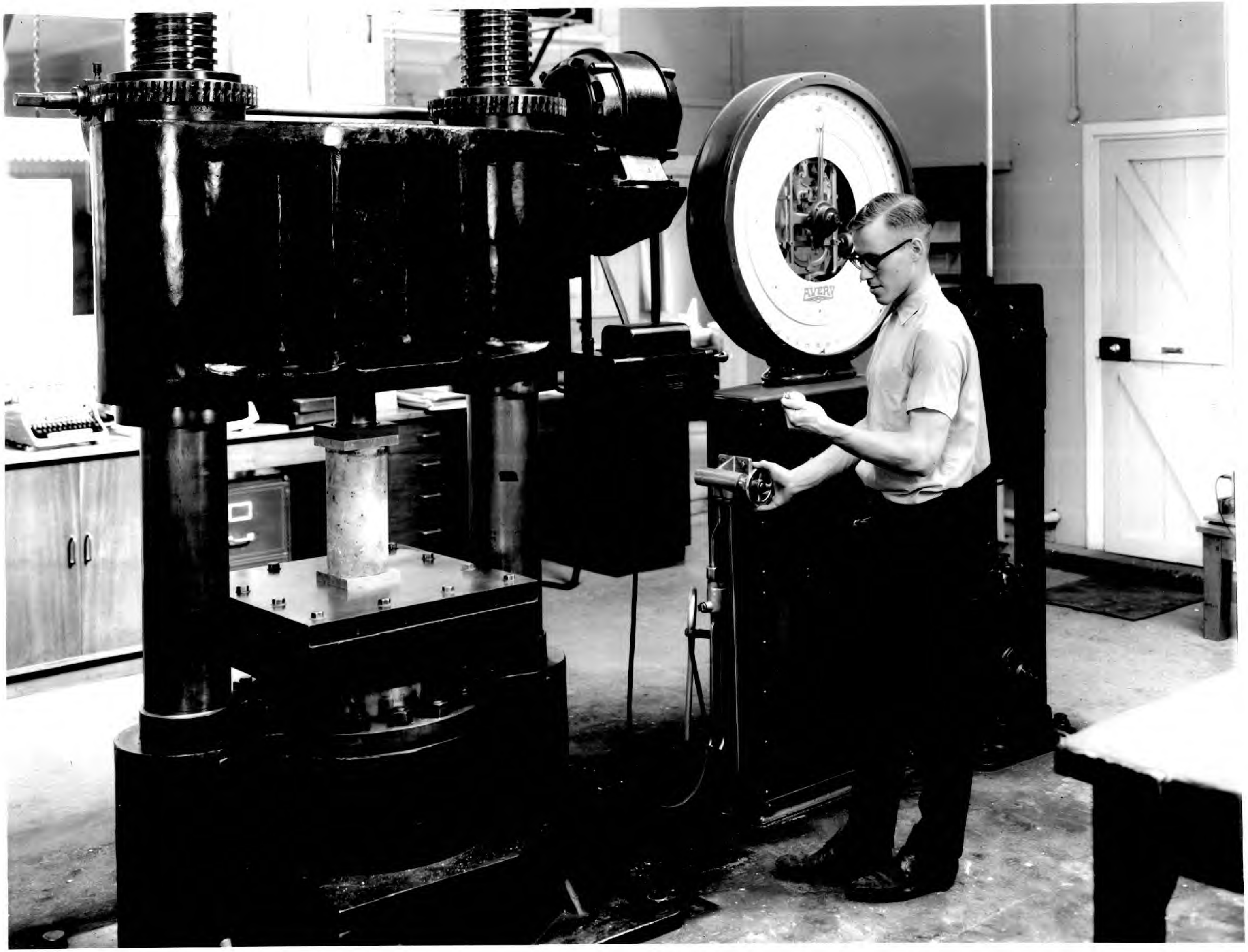

PLATE 8.4 Testing machine used for coefficient of friction tests on spherical seatings

stiffness out of the plane of the frame, this was not considered serious as all tests were being performed in the plane of the frame. Its spherical seating was easily disassembled thereby providing uniform contact for the bearing faces of the female portions of the different seatings.

It was discovered, however, after the tests were well underway, that the machine contained an idiosyncrasy. On applying the initial load, the top cross-head did not lift uniformly in the space provided by its tolerances. Instead, the left side as shown in Plate 8.4 lifted first until firmly in contact with the back side of the threads. The subsequent lifting induced a rotation about the left side of the upper cross-head which created a lateral component of movement through the test assembly (see Plate 8.3) thereby inducing a lateral force. To check for this, a magnetized base, with a vertical arm supporting a horizontal dial gauge, graduated in 0.0001" divisions, was secured to the machine base. The dial gauge, whose pointer was positioned on the edge of the transfer assembly, was able to measure the lateral movement occurring through the assembly. The movement occurred mostly in the first 2 tons of load application with only slight movement after 10 tons and no movement after 20 tons. After repeating the test several times, it was concluded that the entire movement was very repeatable as the upper cross-head returned to the same position and the magnitude of lateral movement was constant in every case.

To correct for this unfortunate idiosyncrasy, the entire assembly was reversed and 2 tests were performed with the set-up in this manner. With this information, it was possible to apply an accurate correction to the test results(see Section 8.5).

8.4 LUBRICANTS

After consultation with the major testing machine manufacturers, the lubricants shown in Table 8.1 were selected as being generally used on spherical seating interfaces.

TABLE 8.1 TYPES OF LUBRICANTS USED ON SPHERICAL SEATING INTERFACE

Lubricant	Penetration (cm) (A.S.T.M. D217-60)	Description
Molybdenum Disulphide Lubricants		
Rocol A.S.P	2.50	50% MoS_2 in refined petroleum residue
Rocol M.G.	3.60	10% MoS_2 in viscous based oil grease
Graphite Lubricants		
Amsler grease	≈2.00	50% graphite in Shell Rhodina 2
Graphite-tallow mixture	≈0.50	50% graphite in yellow tallow
Graphite -Shell Rhodina 2 mixture	≈2.00	50% graphite in Shell Rhodina 2
Shell Barbatia 4	1.80	graphite dispersion in lime-base grease
Other Lubricants		
Shell Rhodina 2	2.65	lime-base grease with pressure additives
Shell Livona 3	2.20	Lime-base grease with pressure additives
Stauffers grease	≈5.00	soft grease
Yellow tallow	≈1.00	hard grease
Sternol Grade 140 Motor oil		high viscosity oil
Fish oil		low viscosity oil
graphite		commercial black lead
no lubricant		

The Rocol greases consist of a semi-colloidal dispersion of molybdenum disalphide in grease. Molybdenum disulphide is a black crystalline solid, occurring in nature as molybdenite, which shears easily, has a low coefficient of friction (about 0.04) and has high pressure resistance [52]; measurements have been taken at pressures of 475,000 p.s.i. [53]. In addition, it has thermal stability over the range, -300 to 750° Fahrenheit. It adheres very strongly to metal surfaces, and is inert chemically, non-toxic and resistant to water and solvents. Rocol A.S.P. contains approximately 50% of Molybdenum disulphide by weight while the M. G. grease contains 10%.

Graphite suspension greases include Amsler and Shell Barbatia 4 greases, while two mixtures containing graphite were manufactured by the author. In both the graphite-tallow and graphite-Rhodina mixtures, the graphite was finely pulverized with a knife edge, before mixing with an equal weight of the second component. Amsler grease, also manufactured by mixing graphite and Shell Rhodina 2 was very similar in appearance to the author's mixture. Although being quite hard, particularly in relation to the Rocol greases, it was considerably softer than the graphite-tallow mixture, which had a consistency similar to a thick paste. The Shell Barbatia grease, the least viscous of the graphite greases was basically a lime-base grease with only a small percentage of graphite.

A comparison of the properties of graphite and molybdenum disulphide has been conducted by several investigators [52,54,55,].

Graphite, in addition to being a cheaper material, is simpler to suspend stably in oils and greases. Also, it is a very inert material and can withstand extreme temperatures. On the other hand, molybdenum disulphide has a slightly lower coefficient of friction and a greater resistance to extreme pressures as well as being a better material for the prevention of wear and delaying seizure between adjacent running machine components.

Tarrant's investigation in 1954, was conducted on Shell Rhodina 2 and Livona 3 greases. Both are lime-base greases with extra pressure additives. Essentially, they remain unchanged from the time of Tarrant's tests except for an alteration in the type of fatty oil in the Rhodina grease.

Tests conducted on the graphite and tallow individually were performed to see if the lubricating behaviour of the mixture resembled that of either of its components. The other lubricants tested, Stauffer's grease and the two oils would not be expected to provide good lubrication.

8.5 THEORETICAL PRESENTATION

In Figure 8.3, which shows the force system acting on the male portion of the spherical seating and load transfer assembly, it is shown that the entire stress system at the spherical seating interface can be vectorized into normal and tangential components. By suitably taking moments about the centre of rotation of the sphere, the moment of the entire normal force is equal to zero, while the total frictinal force, F, can be multiplied by the radius, R. That is, as $M_B = 0$ ...8.1

Notes:

1. The integration of the frictional force 'f' over the area of the seating interface yields the total resistance to sliding, F.
2. The summation of the normal forces, p, is approximately equal to $P_{st.} + P_{so.}$.

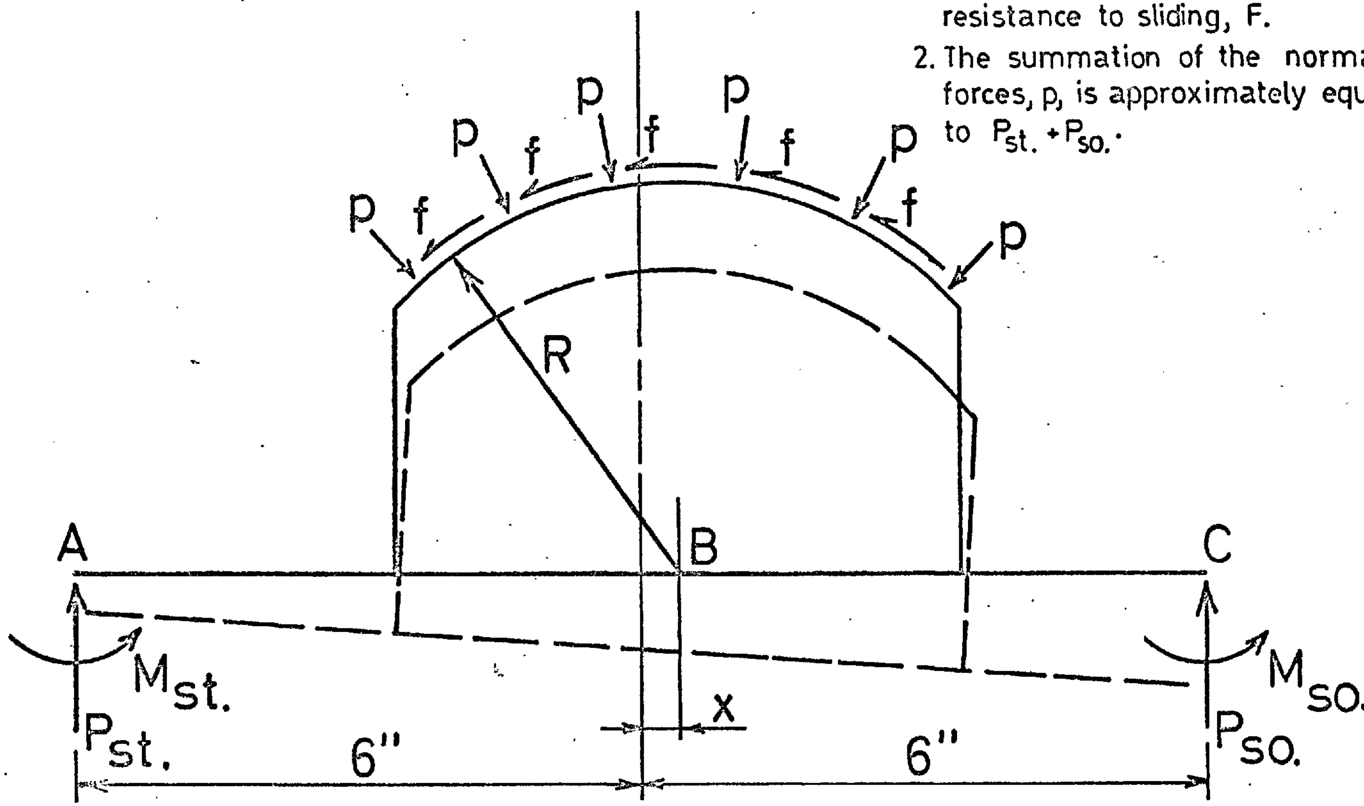

FIG. 8.3 FORCE SYSTEM ON MALE SECTION OF SPHERICAL SEATING AND LOAD TRANSFER ASSEMBLY

and, as the distance between the knife edges is 12", then

$$P_{st}(6 + x) - P_{so}(6 - x) - M_{st} - M_{so} - FR = 0 \qquad \ldots 8.2$$

where P_{st} and P_{so} represent the applied forces of the stiff and soft proving rings, respectively, x is the misalignment of the spherical seating towards the soft ring, and, M_{st} and M_{so} are the fixing moments at the connections between the rings and transfer assembly.

Although the fixing moments at the knife edges, M_{st} and M_{so}, are only very minute, it is necessary to take them into account in the calculations as precise values for coefficient of friction, µ, are required. The radius, r, of the knife edge contact was measured as $\frac{1}{16}$" while the coefficient of friction, µ, based on values for steel sliding on steel, as obtained from Figures 8.7, 8.8, 8.9 and 8.10, was assumed equal to 0.16.

But $\qquad M_{st} = \mu P_{st} r \qquad \ldots 8.3$

Therefore $\qquad M_{st} = 0.01 P_{st} \qquad \ldots 8.4$

Similarly $\qquad M_{so} = 0.01 P_{so} \qquad \ldots 8.5$

By substituting equations 8.4 and 8.5 into equation 8.2, then;

$$(P_{st} - P_{so})\, 6 + (x - 0.01)(P_{st} + P_{so}) = FR \qquad \ldots 8.6$$

From the definition of coefficient of friction,

$$F = \mu \text{ (applied force at the interface)} \qquad \ldots 8.7$$

But, (applied force at the interface) $\simeq (P_{st} + P_{so})$ $\quad \ldots 8.8$

The right hand side of equation 8.8 which is the applied vertical force through the seating is somewhat less than the total normally applied force at the interface, with this difference becoming greater as the suspended arc of contact area increases. Assuming the pressure, p, to be uniform over the entire contact area, then the ratio of the integration of the vertical components of the pressure to the integration of the total pressure over the contact area is simply calculated. For all the full contact settings in this investigation, this ratio is 0.873. However, the true value will be in excess of this, approaching 1.00, due to the pressure, assumed constant, above in practice, actually reducing from a maximum at the centre to a minimum at the edges. On this basis, the expression 8.8 is assumed to be a true equation.

Substituting Equations 8.7 and 8.8 into Equation 8.6, then,

$$\mu = \frac{6}{R} \left\{\frac{P_{st} - P_{so}}{P_{st} + P_{so}}\right\} + \frac{x}{R} - \frac{0.01}{R} \qquad \ldots\ 8.9$$

From Equation 8.9, it is observed that the influence of the fixing moments at the knife edges will cause variations in μ values of only about 0.002.

Following an initial series of tests, the calculations showed small negative values for the coefficient of friction. This was due to the small sideways movement of the testing machine (see Section 8.3.4) which induced an external moment into the test assembly. To determine the magnitude of this effect, the proving rings and load transfer assembly were reversed in the testing machine and tests repeated on the 3" and 7" radii seatings lubricated with Rocol M.G. grease. The results of these tests as well as those obtained in the routine tests are presented in Table 8.2 and Figure 8.4.

Examination of Figure 8.4 shows that the true difference in indicated loads on the two proving rings should be greater in the routine set-up and less in the reverse set-up with the corrections applied to either being equal to half the difference observed. That is, if no external effect existed, the values obtained for $(P_{st} - P_{so})$ would be independent of the orientation of the set-up. Consequently, Table 8.3 has been presented to show the magnitudes of these half differences of $(P_{st} - P_{so})$ values between the routine and reverse set-ups. These values, plotted in Figure 8.5, indicate that the required correction is linear and independent of the spherical seating size as the two lines are parallel. As the lines in Figure 8.5 would be horizontal if the machine had behaved perfectly, the corrections required for the measured $(P_{st} - P_{so})$ values in Equation 8.9 is that required to change the indicated slope in Figure 8.5 to a horizontal line. That is, the correction for $(P_{st} - P_{so})$ is equal to $5.22 \times 10^{-3}(P_{st} + P_{so})$ where -3.22×10^{-3} is the slope of the lines in Figure 8.5 Therefore, from Equation 8.9

$$\mu = \frac{6}{R(P_{st}+P_{so})}\left[(P_{st} - P_{so}) + 3.22 \times 10^{-3}(P_{st} + P_{so})\right] + \frac{x}{R} - \frac{0.01}{R} \qquad \ldots 8.10$$

which, on simplifying, becomes

$$\mu = \frac{6}{R}\,\frac{(P_{st} - P_{so})}{(P_{st} + P_{so})} + \frac{0.009}{R} + \frac{x}{R} \qquad \ldots 8.11$$

From Equation 8.10, it is observed that the magnitude of this testing machine correction is very small, resulting in alterations of μ by only about 0.003.

TABLE 8.2 DIFFERENCES IN LOAD IN 2 PROVING RINGS FOR ROUTINE AND REVERSE SET-UPS OF ASSEMBLY AND PROVING RINGS (see Figure 8.4)

Indicated Load (tons)	Routine Set-up Indicated Load (lbsf)			Reverse Set-up Indicated Load (lbsf)		
	P_{st}	P_{so}.	$(P_{st}-P_{so})$	P_{st}.	P_{so}.	$(P_{st}-P_{so})$
	3" Radius Seating with Rocol M.G. Lubricant					
Run 1						
10	11,300	11,370	-70	11,250	11,420	-170
20	22,540	22,580	-40	22,010	22,160	-150
30	34,050	34,100	-50	33,150	33,210	-60
40	45,370	45,380	-10	44,300	44,170	130
50	56,890	56,780	110	55,690	55,390	300
60	68,350	68,080	270	67,190	66,680	510
Run 2						
10	11,250	11,300	-50	11,160	11,330	-170
20	22,480	22,520	-40	21,950	22,110	-160
30	34,050	34,100	-50	33,120	33,120	0
40	45,310	45,300	10	44,270	44,080	150
50	56,890	56,730	160	55,720	55,260	460
60	68,400	67,970	430	67,160	66,530	630
Run 3						
10	11,250	11,310	-60	11,160	11,330	-170
20	22,510	22,540	-30	21,920	22,030	-110
30	33,990	34,110	-120	33,120	33,070	50
40	45,400	45,440	-40	44,270	44,000	270
50	57.030	56,950	80	55,740	55,200	540
60	68,430	68.160	270	67,160	66,400	740
Average						
10			-60			-170
20			-40			-140
30			-70			0
40			-10			180
50			130			470
60			320			630
7" Radius Seating with Rocol M.G. lubricant						
Run 1						
10	11,500	11,700	-200	11,360	11,540	-180
20	22,790	22,980	-190	22,200	22,420	-220
30	34,130	34,420	-290	33,430	33,580	-150
40	45,170	45,500	-330	44,630	44,680	-50
50	56,740	57,060	-320	56,240	56,210	30
60	68,030	68,500	-470	67,670	67,570	100
Run 2						
10	11,440	11,570	-130	11,330	11,530	-200
20	22,620	22,820	-200	22,170	22,380	-210
30	33,930	34,230	-300	33,400	33,540	-140

(cont.)

TABLE 8.2 DIFFERENCES IN LOAD IN 2 PROVING RINGS FOR ROUTINE AND REVERSE SET-UPS OF ASSEMBLY AND PROVING RINGS (see Figure 8.4) (Cont.)

Indicated Load (tons.)	Routine set-up Indicated Load (lbsf.)			Reverse set-up Indicated Load (lbsf.)		
	P_{st}	P_{so}	$(P_{st}-P_{so})$	P_{st}	P_{so}	$(P_{st}-P_{so})$
7" radius seating with Rocol M.G. Lubricant (cont.)						
Run 2 (cont.)						
40	45,120	45,440	-320	44,600	44,640	-40
50	56,540	56,920	-380	56,160	56,100	60
60	67,860	68,270	-410	67,530	67,420	110
Run 3						
10	11,470	11,620	-150	11,250	11,470	-220
20	22,540	22,750	-210	22,060	22,260	-200
30	33,900	34,190	-290	33,320	33,450	-130
40	45,010	45,330	-320	44,520	44,570	-50
50	56,540	56,890	-350	56,110	56,010	100
60	67,830	68,250	-420	67,420	67,290	130
Average						
10			-160			-200
20			-200			-210
30			-290			-140
40			-320			- 50
50			-410			60
60			-450			110

TABLE 8.3 CORRECTIONS FOR SPHERICAL SEATINGS DUE TO LATERAL MOVEMENT OF TESTING MACHINE (see Figure 8.5)

Applied Load (tons.)	$(P_{st}-P_{so})$ from Table 8 2							
	3" Radius w/Rocol M.G.				7" radius w/Rocol M.G.			
	Routine Set-up	Reverse Set-up	Diff.	Diff. x1/2	Routine Set-up	Reverse Set-up	Diff.	Diff. x1/2
10	-60	-170	110	55	-160	-200	40	20
20	-40	-140	100	50	-200	-210	10	5
30	-70	0	-70	-35	-290	-140	-150	-75
40	-10	180	-190	-95	-320	-50	-270	-135
50	130	470	-340	-170	-410	60	-470	-235
60	320	630	-310	-155	-450	110	-560	-280

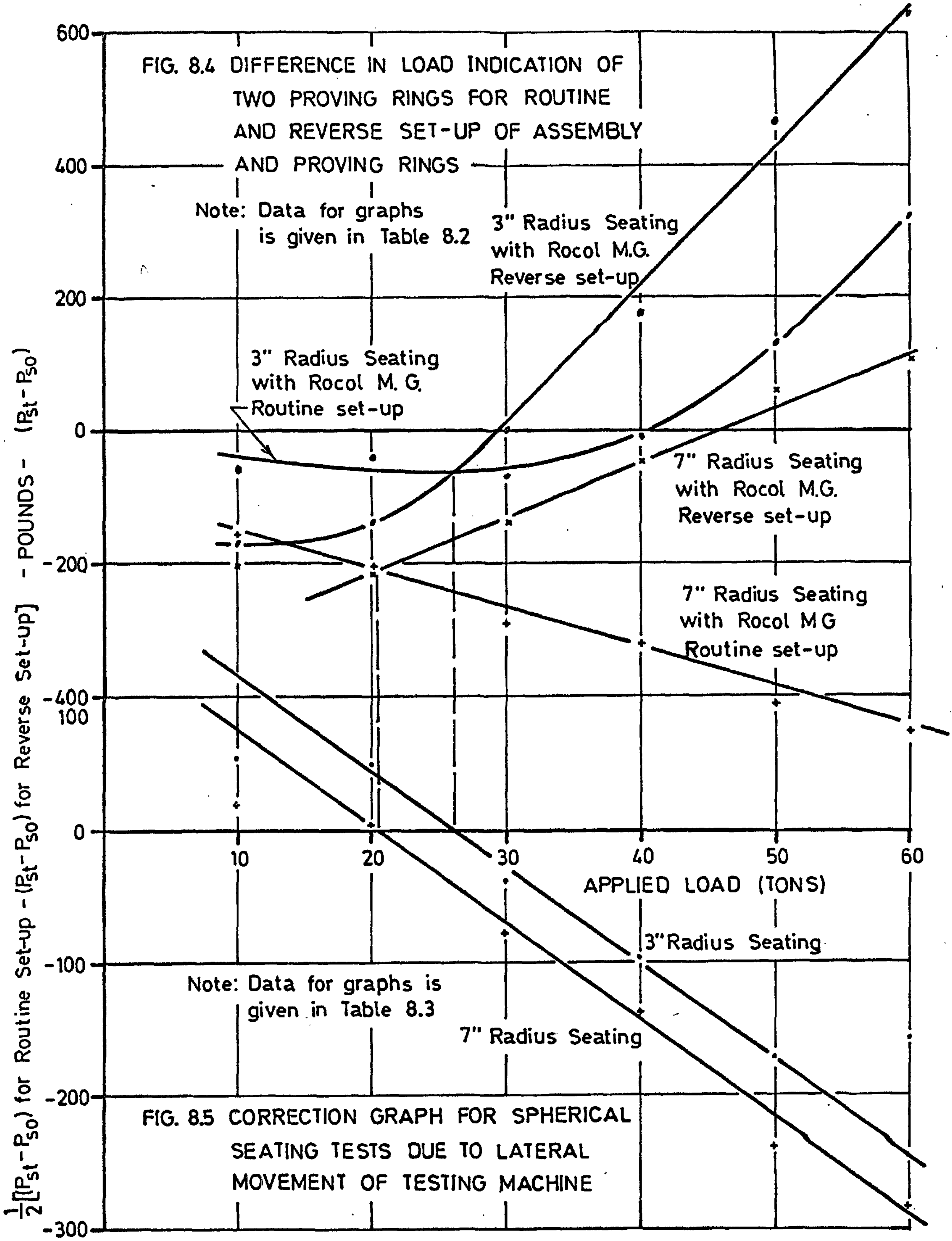

FIG. 8.4 DIFFERENCE IN LOAD INDICATION OF TWO PROVING RINGS FOR ROUTINE AND REVERSE SET-UP OF ASSEMBLY AND PROVING RINGS

FIG. 8.5 CORRECTION GRAPH FOR SPHERICAL SEATING TESTS DUE TO LATERAL MOVEMENT OF TESTING MACHINE

It is also observed in Figures 8.4 and 8.5, that the lines do not always pass through the origin. This was probably due to the pointer on the 100 ton proving ring moving slightly sideways on its contact face as a result of the lateral movement in the machine. A small zero correction, amounting to a fraction of one division, was therefore made to the readings in the tests where μ values less then 0.5% were obtained. This was justified as the values plotted on a graph behaved in a very linear manner, but usually had a y-ordinate value. Above μ values of 0.5%, such a correction was deemed to have a negligible influence.

The 3" radius and 5" radius line contact seatings were manufactured with their dowelling holes perfectly centred while the 7" radius and 5" radius full contact seatings had misalignments of 0.01" and 0.008", respectively. Although these would result in only a very small difference in the value of μ (of the order of 0.0015) these corrections were necessary in view of some of the extremely low coefficient of friction values being obtained. With these misalignment values substituted into Equation 8.11, the equations for calculating the μ values for the different seatings are therefore as follows;

3" radius seating;

$$\mu = 2\,\frac{(P_{st} - P_{so})}{(P_{st} + P_{so})} + 0.0030 \qquad \ldots 8.12$$

5" radius seating, line contact;

$$\mu = \frac{6}{5}\,\frac{(P_{st} - P_{so})}{(P_{st} + P_{so})} + 0.0015 \qquad \ldots 8.13$$

5" radius seating, full contact - misaligned towards stiff ring;

$$\mu = \frac{6}{5} \frac{(P_{st} - P_{so})}{(P_{st} + P_{so})} \qquad \ldots 8.14$$

7" radius seating, - misaligned towards stiff ring

$$\mu = \frac{\frac{6}{7}(P_{st} - P_{so}) - 0.0005}{(P_{st} + P_{so})} \qquad \ldots 8.15$$

7" radius seating- misaligned towards soft ring,

$$\mu = \frac{6\ (P_{st} - P_{so})}{7\ (P_{st} + P_{so})} + 0.0025 \qquad \ldots 8.16$$

8.6 TESTING PROCEDURE

8.6.1 Calibration of Proving Rings

Both proving rings had been calibrated previously; the soft ring at Imperial College (see Section 3.1.2) and the stiff ring in the deadweight machine at the National Physical Laboratory. However, as possible differential errors in their calibrations, arising from the difference in the manner in which the two calibrations were performed, would result in significant changes in μ, it was necessary to re-calibrate both rings in the same machine with the same operators. In addition, the 100 ton proving ring had only been calibrated at 10 ton increments whereas in the coefficient of friction tests, the loading stages occurred at 5 ton increments on each ring. Interpolation was not considered good enough. Also, due to lateral movements occurring, the importance of calibrating the rings in the Avery testing machine, thereby simulating the loading pattern under test, was recognized.

The 50 ton proving ring, No. 343, was calibrated against the N.P.L. electrical resistance strain gauge load cell by locating the latter on top of the former accurately and axially in the Avery testing machine. After 5 preloadings, the calibration was conducted 10 times to 40 tonf. and 3 times to 50 tonf. at 5 tonf. increments (see Section 3.1.2.1 for test procedure). The calibration of the 100 ton proving ring, No. 100, was then conducted by placing it on top of the 50 ton ring and calibrating as described above. In the latter case, the well lubricated 3" radius spherical seating with Rocol A.S.P. lubricant was placed axially on top of the 100 ton ring to ensure that the resultant force passed through its centre of rotation.

The data from these calibration tests are given in Table 8.4 while the calibration graphs are presented in Figure 8.6.

As the load on the Avery testing machine could be maintained very constant due to its excellent load control, accurate indications of load could be obtained on both proving rings with negligible drift occurring between the readings. This was particularly important when investigating the well lubricated seatings as the difference between these relatively large loads was very small(see Equation 8.11). Possible errors arising from temperature corrections have also been eliminated as the proving rings are obviously at the same temperature during the calibration. Errors arising from operator technique are, likewise,

TABLE 8.4 CALIBRATION OF PROVING RINGS No.343 AND No. 100
(see Figure 8.6)

Indicated Load (tons)	P.R. 343 Calibration: Load on N.P.L. Load Cell (lbsf)	P.R. 343 (divs)	Load (lbsf) / Rdg. (divs)	Aver.	P.R. 100 Calibration: Load on P.R. 343	P.R. 100 (divs)	Load / Rdg.	Aver.
Run 1								
5	11,630	75.5	154.15	153.69	11,405	40.9	278.85	279.07
10	23,191	151.0	153.58	153.28	22,872	82.0	278.93	278.89
15	34,824	224.3	155.26	154.33	34,435	123.1	279.73	279.54
20	45,593	294.5	154.81	154.73	45,192	162.3	278.45	278.54
25	56,724	367.4	154.39	154.23	56,533	203.2	278.21	278.32
30	68,146	441.1	154.49	154.46	67,572	241.8	279.45	279.51
35	79,185	513.0	154.36	154.39	78,590	279.9	280.78	280.79
40	90,409	586.3	154.20	154.22	90,007	319.7	281.54	281.01
45	101,779	660.5	154.09	154.08	101,213	356.9	283.59	283.70
50	113,375	735.8	154.08	154.09				
Run 2								
5	11,532	75.2	153.35		11,405	40.9	278.85	
10	23,014	150.3	153.12		22,942	82.3	278.85	
15	34,452	223.4	154.22		34,142	122.2	279.39	
20	45,352	293.1	154.73		45,172	162.3	278.35	
25	56,406	365.6	154.28		56,486	202.9	278.39	
30	67,901	439.4	154.53		67,587	241.9	279.40	
35	78,817	510.3	154.45		78,451	279.6	280.58	
40	90,174	584.7	154.22		89,837	318.6	281.97	
45	101,439	658.4	154.07		101,444	357.6	283.68	
50	112,960	733.1	154.09					
Run 3								
5	11,416	74.2	153.85		11,389	40.8	279.14	
10	22,827	148.9	153.30		22,811	81.8	278.86	
15	34,262	222.0	154.33		34,343	122.7	279.89	
20	45,327	292.8	154.81		45,439	163.0	278.77	
25	56,415	365.5	154.35		56,656	203.5	278.41	
30	67,891	439.4	154.51		67,695	242.1	279.62	
35	78,998	517.4	154.47		78,991	281.2	280.91	
40	90,218	584.9	154.25		90,145	319.5	282.14	
45	101,544	659.0	154.08		101,567	357.9	283.79	
50	113,085	733.8	154.11					
Run 4								
5	11,355	73.9	153.65		11,404	40.9	278.85	
10	22,822	148.7	153.48		22,796	81.8	278.68	
15	34,253	222.0	154.29		34,466	123.2	279.76	
20	45,261	292.4	154.79		45,439	163.1	278.60	
25	56,402	365.5	154.31		56,471	202.9	278.32	
30	67,764	438.8	154.43		67,773	242.4	279.59	

(cont.)

TABLE 8.4 CALIBRATION OF PROVING RINGS No. 343 AND No. 100 (see Figure 8.6) (cont.)

	P.R. 343 Calibration			P.R. 100 Calibration		
Indicated Load (tons)	Load on N. P.L. Load Cell (lbsf)	P.R. 343 divs)	Load(lbsf) Rdg. (divs)	Load on P.R. 343	P.R. 100 (divs)	Load Rdg.
Run 4 (cont.)						
35	78,851	510.6	154.43	78,991	281.2	280.91
40	90,185	584.6	154.27	90,192	319.6	282.20
45				101,614	358.2	283.60
Run 5						
5	11,468	74.7	153.52	11,416	41.0	279.66
10	22,936	150.0	152.21	22,888	82.0	279.12
15	34,388	223.0	154.21	34,405	122.9	279.94
20	45,402	293.0	154.96	45,347	162.8	278.54
25	56,539	366.5	154.35	56,440	202.8	278.30
30	67,982	440.0	154.50	67,804	242.6	279.50
35	79,054	512.0	154.40	79,037	281.5	280.77
40	90,299	585.5	154.23	90,300	320.0	282.19
45				101,536	357.8	283.78
Run 6						
5	11,451	74.4	153.91			
10	22,898	149.5	153.16			
15	34,354	222.7	154.26			
20	45,334	293.0	154.72			
25	56,448	366.0	154.23			
30	67,852	439.5	154.38			
35	78,927	511.3	154.37			
40	90,295	585.5	154.22			
Run 7						
5	11,389	74.2	153.49			
10	22,936	149.4	153.52			
15	34,404	223.2	154.14			
20	45,334	293.1	154.67			
25	56,480	366.2	154.23			
30	67,894	439.8	154.37			
35	78,915	511.2	154.37			
40	90,264	585.5	154.17			
Run 8						
5	11,258	73.4	153.38			
10	22,840	149.1	153.19			
15	34,202	221.8	154.20			
20	45,210	292.9	154.32			
25	56,299	365.9	153.86			
30	67,771	439.0	154.38			
35	78,910	511.2	154.36			
40	90.050	583.9	154.22			
(cont.)						

	P.R. 343 Calibration		
Indicated Load (tons)	Load on N. P.L. Load Cell (lbsf)	P.R. 343 (divs)	Load(lbsf) Rdg. (divs)
Run 9			
5	11,368	74.0	153.62
10	22,838	149.0	153.28
15	34,219	222.0	154.14
20	45,240	292.5	154.67
25	56,288	365.1	154.17
30	67,678	438.5	154.34
35	78,923	511.2	154.39
40	90,112	584.3	154.22
Run 10			
5	11,270	73.2	153.96
10	22,815	148.9	153.22
15	34,208	221.8	154.23
20	45,286	292.6	154.77
25	56,384	365.8	154.14
30	67,748	438.0	154.68
35	78,867	511.0	154.34
40	90,216	585.0	154.22

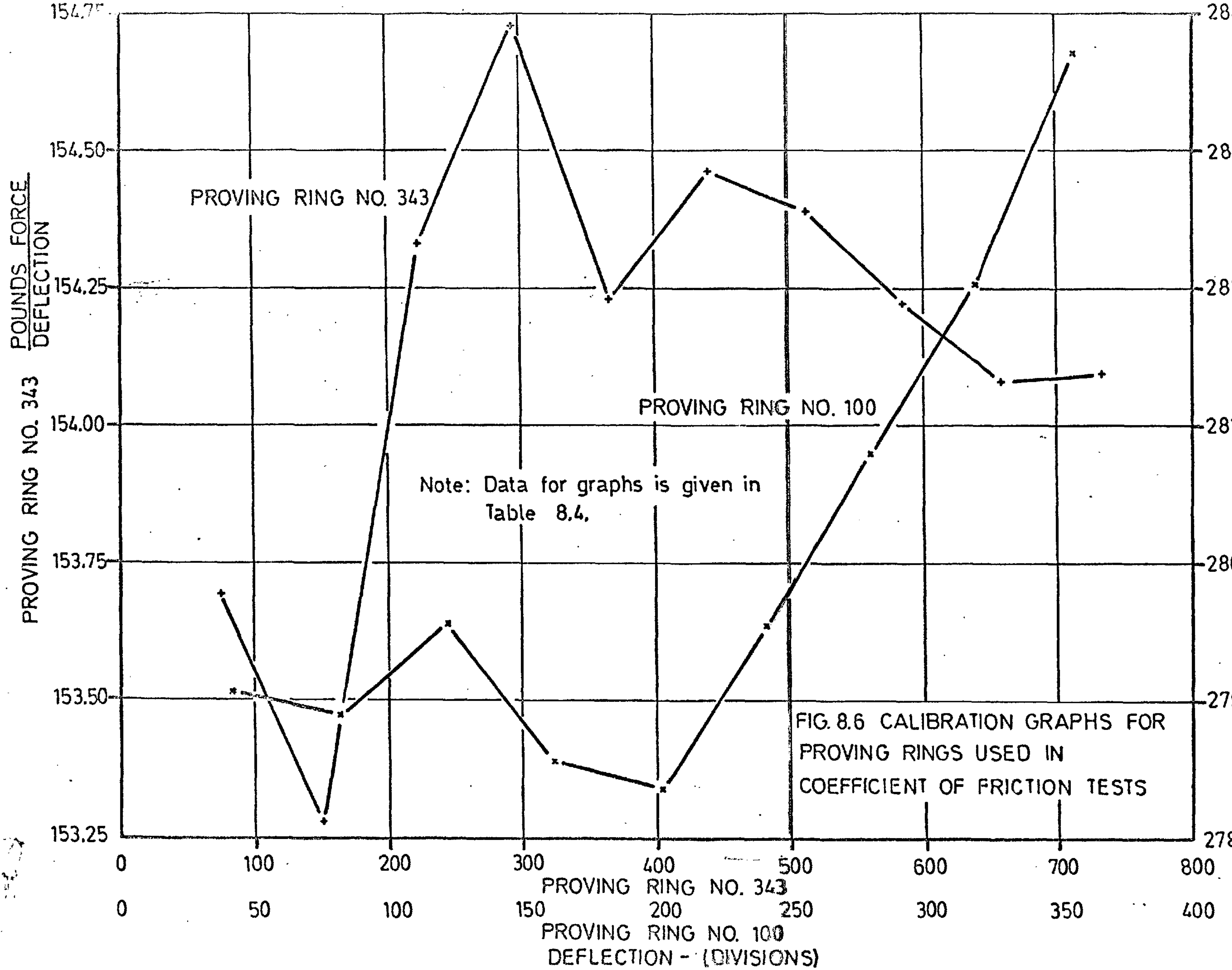

FIG. 8.6 CALIBRATION GRAPHS FOR PROVING RINGS USED IN COEFFICIENT OF FRICTION TESTS

eliminated as the same person, in this case, the author, read and recorded all proving ring readings in both the calibration and coefficient of friction tests.

8.6.2 Preparation For Testing

The load transfer assembly proving rings, platens and spacers were positioned as shown in Plate 8.2 with particular emphasis on proper centring, achieved with a steel rule graduated in 1/64" divisions. This involved care in placing the entire assembly axially coincident with the machine, locating the proving ring centre line axial with the knife edges and ensuring that the major axis of the entire test assembly was coincident with the testing machine's major axis.

The spherical seating interfaces, prior to application of grease, were thoroughly cleaned with ether, using a clean cloth, until all grease and dirt had been completely removed. Both faces were then coated with a surplus of the grease being tested and brought into contact. After placing in a 200 ton compression machine, 100 tons force was applied slowly and maintained for two minutes. The surplus grease, which had squeezed out, was wiped off. After removing the load completely, the loading cycle was repeated twice(making three loadings altogether). The seating was then transferred and positioned on the load transfer assembly as shown in Plate 8.3. After taking care in ensuring that the female bearing face was in uniform contact with the upper cross-head, 80 tons was applied slowly and held constant for 1/2 minute. Following complete removal of the load, this loading cycle was repeated twice.

After the first loading cycle in the 200 ton compression machine, very little lubricant squeezed out. Although a small amount was obvious in the high viscosity lubricants, such as commercial tallow and graphite-Rhodina mixture, this had visibly ceased before taking readings commenced. Consequently, this stable condition, where the lubricant had acquired its inherent thickness, was evidence that these tests were a representative indication of the behaviour of seating and lubricant under long term conditions.

8.6.3 Testing Procedure

After the six preloadings, testing was commenced. While one operator loaded the testing machine in 10 ton increments to 80 tons, a second operator, the author, simultaneously read and recorded the readings of the dial gauges on the two proving rings. Great care was taken to ensure that the load was held stationary or was increasing slightly, at each load stage, but never was allowed to decrease. Also, the readings were taken immediately after the loading at each stage had been attained to avoid any load equalization which could occur from creep effects in the lubricant. This test procedure was repeated twice making 3 test runs for each combination of spherical seating and lubricant. Fifty combinations were tested.

8.7 TEST RESULTS

The coefficient of friction values given in Table 8.5 and plotted in Figures 8.7, 8.8, 8.9 and 8.10 show very low values

TABLE 8.5 COEFFICIENT OF FRICTION VALUES FOR SPHERICAL SEATINGS WITH DIFFERENT LUBRICANTS

Applied Load (tons)	Coefficient of Friction (°/o)							
	Run 1	Run 2	Run 3	Aver.	Run 1	Run 2	Run 3	Aver.
7" Radius Seating								
	w/Rocol A.S.P.				w/Rocol M.G.			
10	0.10	0.10	0.20	0.15	-0.10	0.20	0.10	0.05
20	0.05	0.15	0.15	0.10	0.10	0.10	0.05	0.10
30	-0.05	0.05	0.	0.	0.	0.	0.	0.
40	0.05	0.05	0.05	0.05	0.05	0.05	0.05	0.05
50	0.05	0.10	0.10	0.10	0.10	0.05	0.05	0.05
60	0.05	0.10	0.10	0.10	0.	0.05	0.05	0.05
70	0.05	0.05	0.10	0.05	0.05	0.05	0.05	0.05
80	0.05	0.10	0.10	0.10	0.05	0.05	0.05	0.05
	w/Shell Rhodina 2				w/Shell Livona 3			
10	-0.15	-0.10	0.05	-0.05	-0.25	-0.15	-0.10	-0.15
20	0.	0.10	0.15	0.10	0.15	0.20	0.20	0.20
30	0.	0.05	0.05	0.05	0.10	0.20	0.20	0.15
40	0.	0.	0.	0.	0.20	0.25	0.20	0.20
50	0.05	0.05	0.05	0.05	0.25	0.25	0.25	0.25
60	0.05	0.05	0.05	0.05	0.25	0.25	0.25	0.25
70	0.05	0.05	0.05	0.05	0.25	0.25	0.25	0.25
80	0.05	0.05	0.05	0.05	0.25	0.30	0.30	0.30
	w/Shell Barbatia 4				w/Amsler Grease			
10	-0.10	0.20	0.10	0.05	1.85	2.10	2.10	2.00
20	0.10	0.25	0.25	0.20	1.70	1.80	1.80	1.75
30	0.15	0.20	0.20	0.20	1.25	1.35	1.40	1.35
40	0.15	0.20	0.20	0.20	1.15	1.25	1.30	1.25
50	0.15	0.20	0.25	0.20	1.25	1.25	1.30	1.25
60	0.15	0.15	0.20	0.15	1.15	1.15	1.15	1.15
70	0.15	0.20	0.20	0.20	1.10	1.10	1.10	1.10
80	0.20	0.25	0.20	0.20	1.05	1.05	1.00	1.05
	w/Stauffer's Grease				w/Rhodina-graphite Mixture			
10	-0.10	0.10	0.	0.	0.50	0.80	1.15	0.80
20	0.20	0.15	0.20	0.20	0.50	0.70	0.85	0.70
30	0.10	0.10	0.05	0.10	0.45	0.45	0.60	0.50
40	0.10	0.10	0.10	0.10	0.40	0.35	0.55	0.45
50	0.10	0.10	0.05	0.10	0.50	0.55	0.55	0.55
60	0.10	0.10	0.10	0.10	0.55	0.55	0.55	0.55
70	0.15	0.10	0.15	0.15	0.60	0.65	0.65	0.65
80	0.15	0.15	0.15	0.15	0.65	0.65	0.70	0.65

(cont.)

TABLE 8.5 COEFFICIENT OF FRICTION VALUES FOR SPHERICAL SEATINGS WITH DIFFERENT LUBRICANTS (cont.)

Applied Load (tons)	Coefficient of Friction (%) Run 1	Run 2	Run 3	Aver.	Run 1	Run 2	Run 3	Aver.
7" Radius Seating (cont.)								
	w/Sternol Grade 140 Motor Oil				w/Fish Oil			
10	-0.10	0.15	0.20	0.10	1.45	0.90	1.75	1.35
20	0.	-0.10	0.05	0.	1.00	0.60	1.25	0.95
30	-0.05	-0.05	-0.05	-0.05	0.90	0.55	0.95	0.80
40	-0.10	-0.10	-0.05	-0.10	1.05	0.75	1.05	0.95
50	0.	-0.05	0.	0.	1.35	1.00	1.30	1.20
60	0.	0.	0.	0.	1.50	1.20	1.40	1.35
70	0.05	0.05	0.05	0.05	1.75	1.35	1.65	1.60
80	0.05	0.05	0.10	0.05	1.95	1.60	1.95	1.85
	w/No Lubricant							
10	20.60	21.10	21.60	21.10				
20	20.00	20.45	20.80	20.40				
30	18.95	19.30	19.65	19.30				
40	17.80	18.10	18.35	18.10				
50	16.95	17.25	17.50	17.25				
60	16.30	16.60	16.75	16.55				
70	15.95	16.15	16.30	16.15				
80								
5" Radius Seating - Line Contact								
	w/Rocol A.S.P.				w/Rocol M.G.			
10	0.05	0.05	-0.25	-0.05	0.10	0.20	0.20	0.15
20	0.05	0.05	0.15	0.10	0.65	0.60	0.60	0.60
30	-0.10	-0.15	-0.05	-0.10	1.00	1.05	0.90	1.00
40	-0.05	-0.05	0.	-0.05	1.40	1.35	1.30	1.35
50	0.	0.	-0.10	-0.05	1.70	1.65	1.60	1.65
60	0.05	0.	0.	0.	1.85	1.85	1.75	1.80
70	0.10	0.15	0.05	0.10	2.00	2.00	1.90	1.95
80	0.20	0.15	0.10	0.15	2.05	2.10	2.00	2.05
	w/Shell Rhodina 2				w/Shell Livona 3			
10	1.00	1.35	1.20	1.20	1.45	1.55	1.60	1.55
20	1.80	1.80	1.95	1.85	2.50	2.35	2.25	2.35
30	2.30	2.40	2.35	2.35	2.85	2.80	2.70	2.80
40	2.95	2.90	2.90	2.90	3.40	3.25	3.15	3.25
50	3.40	3.30	3.30	3.35	3.70	3.60	3.40	3.55
60	3.60	3.55	3.45	3.55	3.85	3.70	3.55	3.70
70	3.80	3.70	3.60	3.70	3.95	3.85	3.65	3.80
80	3.95	3.85	3.70	3.85	3.95	3.90	3.70	3.85

(cont.)

TABLE 8.5 COEFFICIENT OF FRICTION VALUES FOR SPHERICAL SEATINGS WITH DIFFERENT LUBRICANTS (cont.)

	Coefficient of Friction ($^o/_o$)							
Applied Load (tons)	Run 1	Run 2	Run 3	Aver.	Run 1	Run 2	Run 3	Aver.
5" Radius Seating -- Line Contact (cont.)								
	w/Shell Barbatia 4				w/Amsler Grease			
10	0.30	0.35	0.25	0.30	0.55	0.30	0.25	0.35
20	0.55	0.50	0.45	0.50	0.30	0.30	0.15	0.25
30	0.50	0.45	0.45	0.45	0.15	0.15	0.05	0.10
40	0.65	0.55	0.60	0.60	0.10	0.05	0.05	0.05
50	0.75	0.75	0.75	0.75	0.15	0.05	0.10	0.10
60	0.85	0.85	0.80	0.85	0.10	0.05	0.05	0.05
70	1.05	1.00	1.00	1.00	0.10	0.10	0.10	0.10
80	1.15	1.15	1.10	1.15	0.15	0.15	0.20	0.15
	w/Stauffer's Grease				w/Rhodina-Graphite Mixture			
10	5.40	5.45	5.15	5.35	0.75	0.60	0.75	0.70
20	6.40	6.65	6.65	6.55	0.50	0.30	0.35	0.40
30	6.35	6.75	6.60	6.60	0.30	0.20	0.30	0.25
40	6.95	7.15	7.10	7.05	0.25	0.10	0.05	0.15
50	7.20	7.40	7.25	7.30	0.25	0.15	0.15	0.20
60	7.30	7.40	7.25	7.30	0.20	0.15	0.10	0.15
70	7.45	7.55	7.40	7.45	0.30	0.30	0.25	0.30
80	7.50	7.55	7.45	7.50	0.45	0.50	0.40	0.45
	w/Yellow Tallow				w/Graphite-Tallow Mixture			
10	0.30	0.30	0.30	0.30	0.	-0.15	0.05	-0.05
20	-0.15	-0.05	-0.10	-0.10	-0.05	-0.05	-0.10	-0.05
30	-0.15	-0.15	-0.15	-0.15	-0.10	-0.10	-0.05	-0.10
40	-0.05	-0.10	-0.05	-0.05	0.	0.	0.	0.
50	0.	0.15	0.05	0.05	0.10	0.05	0.05	0.05
60	0.15	0.15	0.10	0.15	0.05	0.10	0.10	0.10
70	0.30	0.30	0.25	0.30	0.20	0.20	0.15	0.20
80	0.35	0.35	0.35	0.35	0.35	0.35	0.40	0.35
	w/Sternol Grade 140 Motoroil				w/Fish oil			
10	1.85	2.30	2.45	2.20	7.55	7.40	7.35	7.45
20	3.55	3.80	3.90	3.75	8.75	8.45	8.40	8.55
30	4.20	4.55	4.50	4.40	8.80	8.60	8.45	8.60
40	5.00	5.05	5.10	5.05	9.40	9.15	9.05	9.20
50	5.30	5.65	5.20	5.40	9.55	9.40	9.25	9.40
60	5.45	5.85	5.30	5.45	9.45	9.30	9.15	9.30
70	5.60	5.85	5.45	5.65	9.55	9.40	9.35	9.45
80	5.75	5.85	5.60	5.75	9.60	9.50	9.40	9.50

(cont.)

TABLE 8.5 COEFFICIENT OF FRICTION VALUES FOR SPHERICAL SEATINGS WITH DIFFERENT LUBRICANTS (cont.)

Applied Load (tons)	Coefficient of Friction (%) Run 1	Run 2	Run 3	Aver.	Run 1	Run 2	Run 3	Aver.
5" Radius Seating - Line Contact (cont.)								
	w/No Lubricant							
10	21.05	19.75	19.00	19.95				
20	19.90	19.95	19.75	19.85				
30	18.05	18.10	17.75	17.95				
40	17.20	17.25	16.85	17.10				
50	16.35	16.35	16.10	16.25				
60	15.60	15.65	15.35	15.55				
70	15.15	15.20	15.00	15.10				
80	14.75	14.85	14.65	14.75				
5" Radius Seating - Full Contact;								
	w/Rocol A.S.P.				w/Rocol M.G.			
10	10.45	8.55	9.15	9.40	8.55	8.55	8.40	8.50
20	9.85	8.35	9.65	9.30	7.70	7.80	7.90	7.80
30	9.15	8.10	9.60	8.95	7.45	7.50	7.70	7.55
40	9.55	8.70	10.00	9.40	8.04	8.10	8.20	8.10
50	9.85	9.15	10.20	9.75	8.45	8.45	8.60	8.50
60	9.85	9.30	10.15	9.75	8.70	8.70	8.75	8.70
70	10.05	9.65	10.30	10.00	9.05	9.00	9.10	9.05
80	10.55	10.15	10.65	10.45	9.35	9.30	9.45	9.35
	w/Shell Rhodina 2				w/Shell Livona 3			
10	15.00	15.55	16.25	15.60	8.80	9.30	9.20	9.10
20	13.95	14.40	14.95	14.45	8.20	8.50	8.45	8.40
30	13.30	13.45	13.95	13.55	7.98	8.15	8.15	8.10
40	13.15	13.30	13.75	13.40	8.50	8.55	8.60	8.55
50	13.05	13.15	13.70	13.30	8.90	8.90	8.95	8.90
60	12.85	12.90	13.30	13.00	9.05	9.10	9.15	9.10
70	12.70	12.75	13.20	12.90	9.40	9.40	9.40	9.40
80	12.90	12.95	13.35	13.05	9.70	9.70	9.75	9.70
	w/Shell Barbatia 4				w/Amsler grease			
10	6.65	6.70	7.05	6.80	2.70	3.05	3.15	2.95
20	4.45	4.30	4.75	4.50	2.65	2.75	2.80	2.75
30	3.05	3.10	3.30	3.15	2.00	2.10	2.10	2.05
40	2.40	2.35	2.55	2.45	1.75	1.80	1.85	1.80
50	1.85	1.85	1.90	1.85	1.50	1.55	1.50	1.50
60	1.40	1.50	1.55	1.50	1.30	1.30	1.30	1.30
70	1.15	1.25	1.20	1.20	1.05	1.15	1.10	1.10
80	0.90	1.00	0.95	0.95	1.00	1.00	1.05	1.00

(cont.)

TABLE 8.5 COEFFICIENT OF FRICTION VALUES FOR SPHERICAL SEATINGS WITH DIFFERENT LUBRICANTS (cont.)

Applied Load (tons)	Coefficient of Friction (%) Run 1	Run 2	Run 3	Aver.	Run 1	Run 2	Run 3	Aver.
5" Radius Seating - Full Contact (Cont.)								
	w/Stauffer's Grease				w/Rhodina-graphite Mixture			
10	7.80	7.20	8.05	7.70	2.85	2.65	2.80	2.75
20	6.15	5.75	6.65	6.20	1.15	1.20	1.25	1.20
30	6.15	5.90	6.50	6.20	0.60	0.60	0.65	0.60
40	7.90	6.80	7.25	7.30	0.40	0.40	0.45	0.40
50	7.75	7.45	7.77	7.65	0.30	0.30	0.35	0.30
60	8.10	7.90	8.04	8.00	0.10	0.10	0.20	0.15
70	8.60	8.35	8.35	8.45	0.05	0.10	0.15	0.10
80	8.75	8.55	8.60	8.65	0.	0.05	0.10	0.05
	w/Yellow Tallow				w/Graphite-tallow Mixture			
10	7.30	7.40	8.10	7.60	0.84	1.15	1.05	1.00
20	6.90	6.95	7.10	7.00	0.65	0.70	0.70	0.70
30	6.15	6.35	6.60	6.35	0.50	0.55	0.50	0.50
40	5.75	6.00	6.25	6.00	0.55	0.55	0.55	0.55
50	5.30	5.50	5.84	5.55	0.60	0.55	0.55	0.55
60	4.70	4.90	5.20	4.95	0.55	0.55	0.55	0.55
70	4.30	4.55	4.90	4.60	0.55	0.55	0.55	0.55
80	3.85	4.15	4.35	4.10	0.55	0.50	0.55	0.55
	w/Sternol Grade 140 Motoroil				w/No Lubricant			
10	14.80	14.65	14.55	14.65	18.10	17.85	17.90	17.95
20	13.00	13.00	13.05	13.00	14.40	14.50	14.65	14.50
30	11.75	11.85	11.75	11.80	12.60	12.75	13.15	12.85
40	11.75	11.75	11.75	11,75	12.35	12.60	13.00	12.65
50	11.85	11.80	11.90	11.85	12.35	12.65	12.95	12.65
60	11.70	11.65	11.75	11.70	12.10	12.35	12.55	12.35
70	11.80	11.75	11.80	11.80	12.10	12.40	12.70	12.40
80	11.80	11.85	11.90	11.85	12.05	12.30	12.60	12.30
3" Radius Seating:								
	w/Rocol A.S.P.				w/Rocol M.G.			
10	1.65	1.30	1.20	1.40	0.30	0.50	0.40	0.40
20	1.15	1.00	1.25	1.15	0.45	0.45	0.50	0.45
30	0.85	0.80	0.85	0.85	0.35	0.35	0.15	0.30
40	0.95	0.95	0.95	0.95	0.50	0.50	0.35	0.45
50	0.90	1.00	1.00	0.95	0.60	0.70	0.55	0.60
60	0.85	0.95	1.00	0.95	0.80	1.05	0.80	0.90
70	0.95	1.00	0.95	0.95	1.20	1.35	1.05	1.20
80	0.90	0.95	0.85	0.90	1.60	1.70	1.50	1.60

(cont.)

TABLE 8.5 COEFFICIENT OF FRICTION VALUES FOR SPHERICAL SEATINGS WITH DIFFERENT LUBRICANTS (cont.)

Applied Load (tons)	Run 1	Run 2	Run 3	Aver.	Run 1	Run 2	Run 3	Aver.
	Coefficient of Friction (°/o)							
3" Radius Seating: (Cont.)								
	w/Shell Rhodina 2				w/Shell Livona 3			
10	-0.25	0.20	0.40	0.10	-0.30	0.05	0.20	0.
20	-0.10	0.10	0.35	0.10	0.10	0.60	1.05	0.60
30	0.	0.20	0.75	0.30	0.50	0.	1.55	0.80
40	0.40	0.70	1.25	0.80	1.20	1.75	2.35	1.75
50	0.85	1.40	1.85	1.35	1.80	2.65	3.05	2.50
60	1.30	1.90	2.55	1.95	2.20	3.00	3 40	2.85
70	1.85	2.30	3.00	2.40	2.60	3.30	3.75	3.10
80	2.25	2.60	3.30	2.70	2.90	3.50	3.90	3.25
	w/Shell Barbatia 4				w/Amsler Grease			
10	1.70	1.55	1.15	1.45	2.10	2.40	2.65	2.40
20	1.20	1.20	1.05	1.15	1.65	1.70	1.95	1.75
30	1.25	0.95	0.85	1.00	1.40	1.45	1.50	1.45
40	1.20	1.05	1.10	1.10	1.50	1.50	1.55	1.50
50	1.15	1.15	1.10	1.15	1.60	1.50	1.50	1.55
60	1.25	1.20	1.15	1.20	1.60	1.55	1.50	1.55
70	1.30	1.25	1.25	1.25	1.45	1.45	1.45	1.45
80	1.40	1.35	1.35	1.35	1.40	1.45	1.35	1.40
	w/Stauffer's Grease				w/Rhodina-graphite Mixture			
10	0.70	1.75	2.75	1.75	0.75	0.75	0.75	0.75
20	2.30	3.75	4.20	3.40	0.55	0.70	0.60	0.60
30	3.70	4.35	4.65	4.25	0.60	0.40	0.50	0.50
40	4.95	5.40	5.70	5.35	0.65	0.60	0.55	0.60
50	5.10	5.45	5.60	5.40	0.60	0.65	0.65	0.65
60	5.50	5.65	5.70	5.60	0.55	0.60	0.60	0.60
70	5.70	5.90	5.80	5.80	0.55	0.60	0.60	0.60
80	5.90	5.95	5.75	5.85	0.55	0.60	0.60	0.60

(cont.)

TABLE 8.5 COEFFICIENT OF FRICTION VALUES FOR SPHERICAL SEATINGS WITH DIFFERENT LUBRICANTS (cont.)

Applied Load (tons)	Coefficient of Friction (°/o) Run 1	Run 2	Run 3	Aver.	Run 1	Run 2	Run 3	Aver.
3" Radius Seating (cont.)								
	w/Yellow Tallow				w/Graphite-tallow Mixture			
10	0.90	0.90	1.25	1.00	0.20	0.05	0.05	0.10
20	0.20	0.20	0.35	0.25	0.15	0.	0.05	0.05
30	0.20	0.25	0.30	0.25	0.10	0.05	0.15	0.10
40	0.30	0.25	0.25	0.25	0.20	0.30	0.10	0.20
50	0.20	0.30	0.35	0.30	0.30	0.20	0.30	0.25
60	0.25	0.30	0.35	0.30	0.15	0.25	0.25	0.20
70	0.30	0.30	0.30	0.30	0.35	0.35	0.40	0.35
80	0.30	0.30	0.30	0.30	0.25	0.35	0.35	0.30
	w/Sternol Grade 140 Motoroil				w/Fish oil			
10	0.75	2.30	4.75	2.60	11.30	12.55	13.40	12.40
20	2.05	4.30	6.20	4.20	11.95	13.05	13.60	12.85
30	3.00	4.70	6.80	4.85	11.50	12.30	12.70	12.15
40	4.05	5.60	7.25	5.65	11.65	12.45	12.90	12.35
50	4.85	6.40	7.60	6.30	11.50	12.30	12.65	12.15
60	5.35	6.70	7.60	6.55	11.10	11.75	12.15	11.65
70	5.80	7.00	7.85	6.90	11.00	11.55	11.95	11.50
80	6.15	7.20	8.00	7.10	10.65	11.20	11.55	11.15
	w/Graphite (Black Lead)				w/No Lubricant			
10	4.2	3.0	1.8	3.0	13.9	12.5	11.1	12.5
20	6.6	5.5	5.0	5.7	14.1	13.3	12.2	13.3
30	8.6	7.8	7.1	8.3	13.4	12.9	12.0	12.8
40	9.9	9.2	8.7	9.3	13.9	13.4	12.7	13.3
50	10.3	9.8	9.6	9.9	13.8	13.4	12.8	13.3
60	10.5	10.2	10.0	10.2	13.4	13.2	12.6	13.1
70	10.4	10.3	10.1	10.3	13.3	13.1	12.7	13.0
80	10.5	10.4	10.6	10.5	13.1	12.9	12.6	12.9

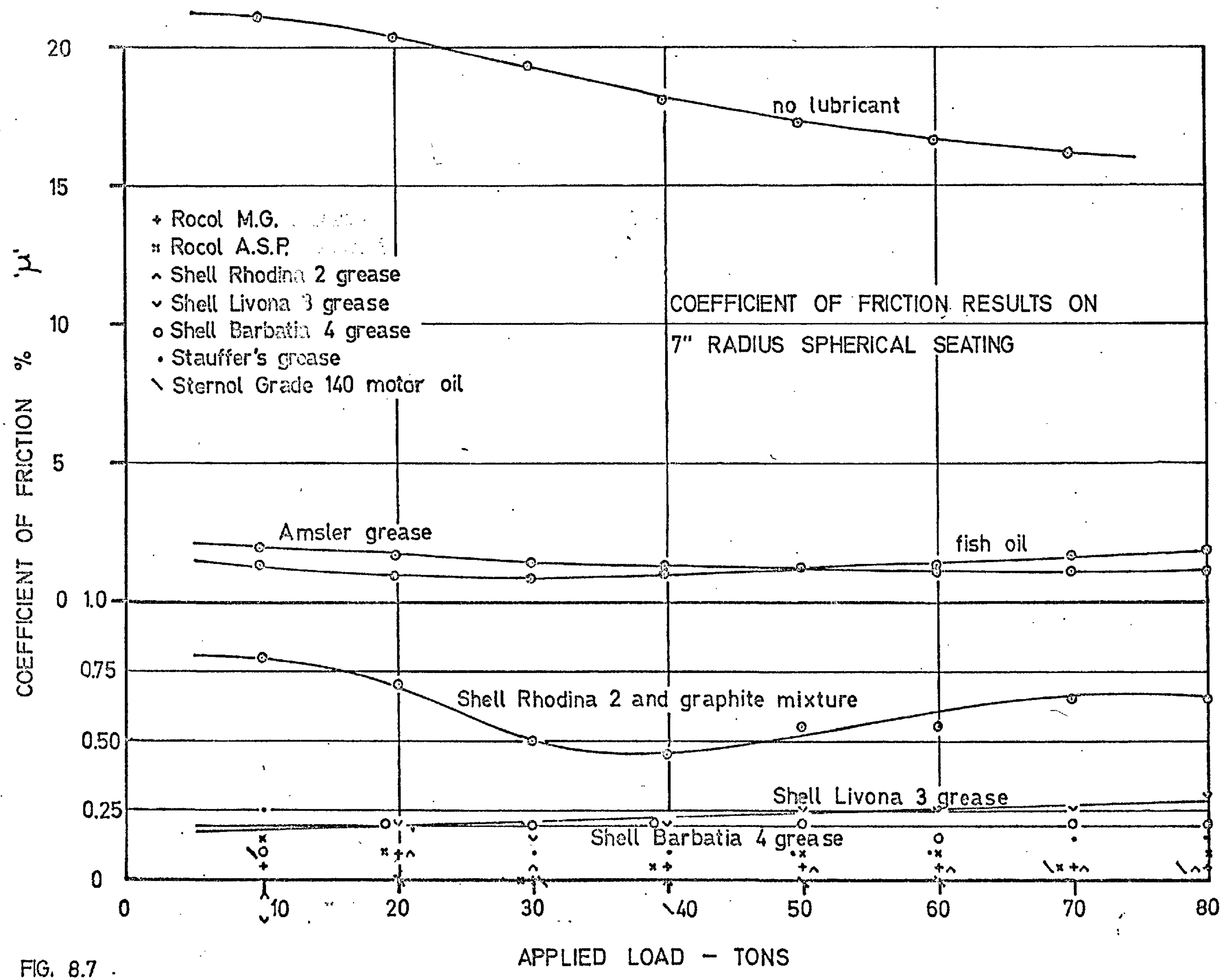
20
15
10
5
0 1.0
0.75
0.50
0.25
0
'μ'
COEFFICIENT OF FRICTION %
0
10
20
30
40
50
60
70
80
APPLIED LOAD - TONS
+ Rocol M.G.
× Rocol A.S.P.
^ Shell Rhodina 2 grease
v Shell Livona 3 grease
o Shell Barbatia 4 grease
• Stauffer's grease
\ Sternol Grade 140 motor oil
COEFFICIENT OF FRICTION RESULTS ON
7" RADIUS SPHERICAL SEATING
no lubricant
Amsler grease
fish oil
Shell Rhodina 2 and graphite mixture
Shell Livona 3 grease
Shell Barbatia 4 grease

FIG. 8.7

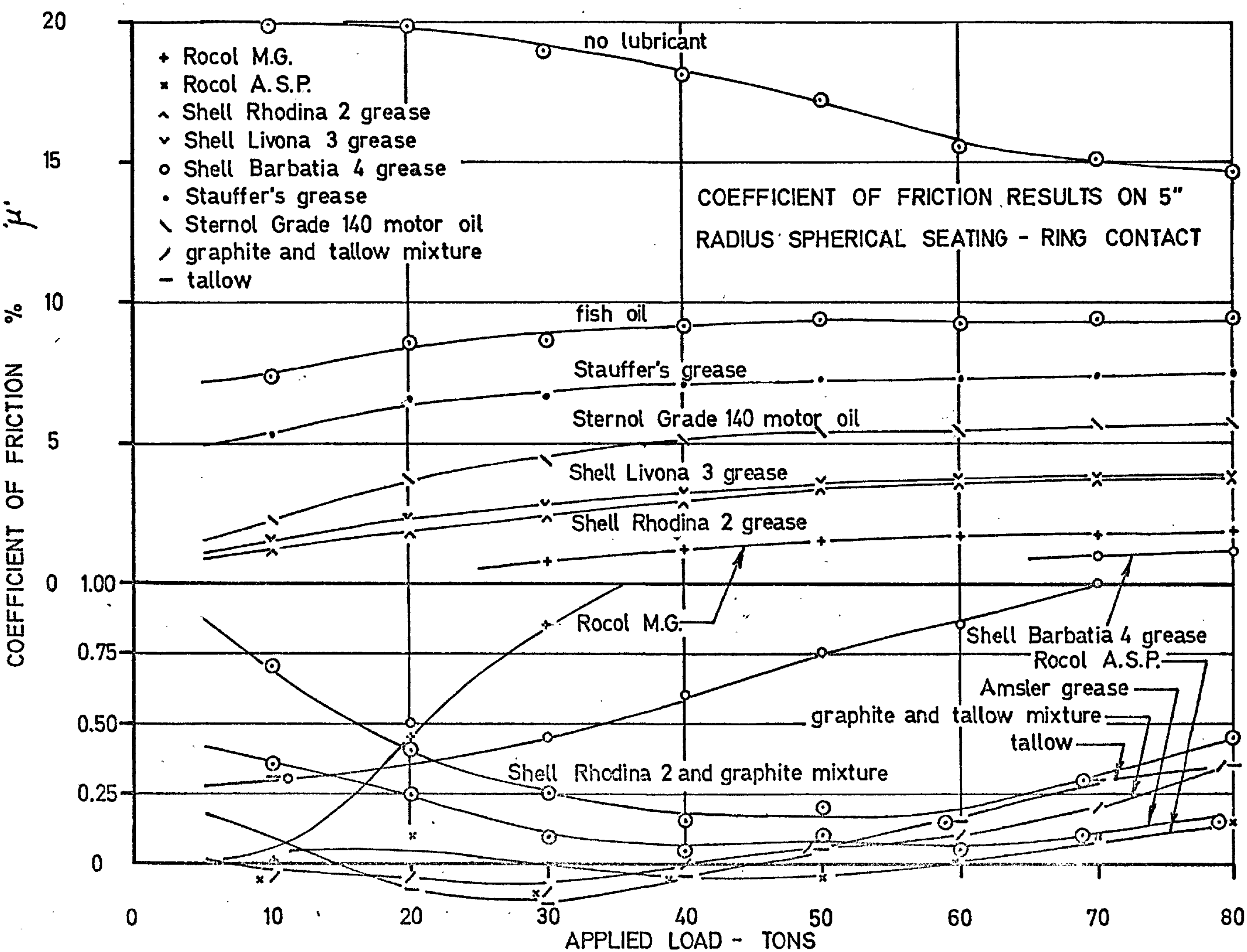
+ Rocol M.G.
× Rocol A.S.P.
^ Shell Rhodina 2 grease
v Shell Livona 3 grease
o Shell Barbatia 4 grease
• Stauffer's grease
\ Sternol Grade 140 motor oil
/ graphite and tallow mixture
– tallow
COEFFICIENT OF FRICTION RESULTS ON 5" RADIUS SPHERICAL SEATING - RING CONTACT
no lubricant
fish oil
Stauffer's grease
Sternol Grade 140 motor oil
Shell Livona 3 grease
Shell Rhodina 2 grease
Rocol M.G.
Shell Barbatia 4 grease
Rocol A.S.P.
Amsler grease
graphite and tallow mixture
tallow
Shell Rhodina 2 and graphite mixture
COEFFICIENT OF FRICTION % 'μ'
APPLIED LOAD - TONS
20
15
10
5
0
1.00
0.75
0.50
0.25
0
0
10
20
30
40
50
60
70
80

FIG. 8.8

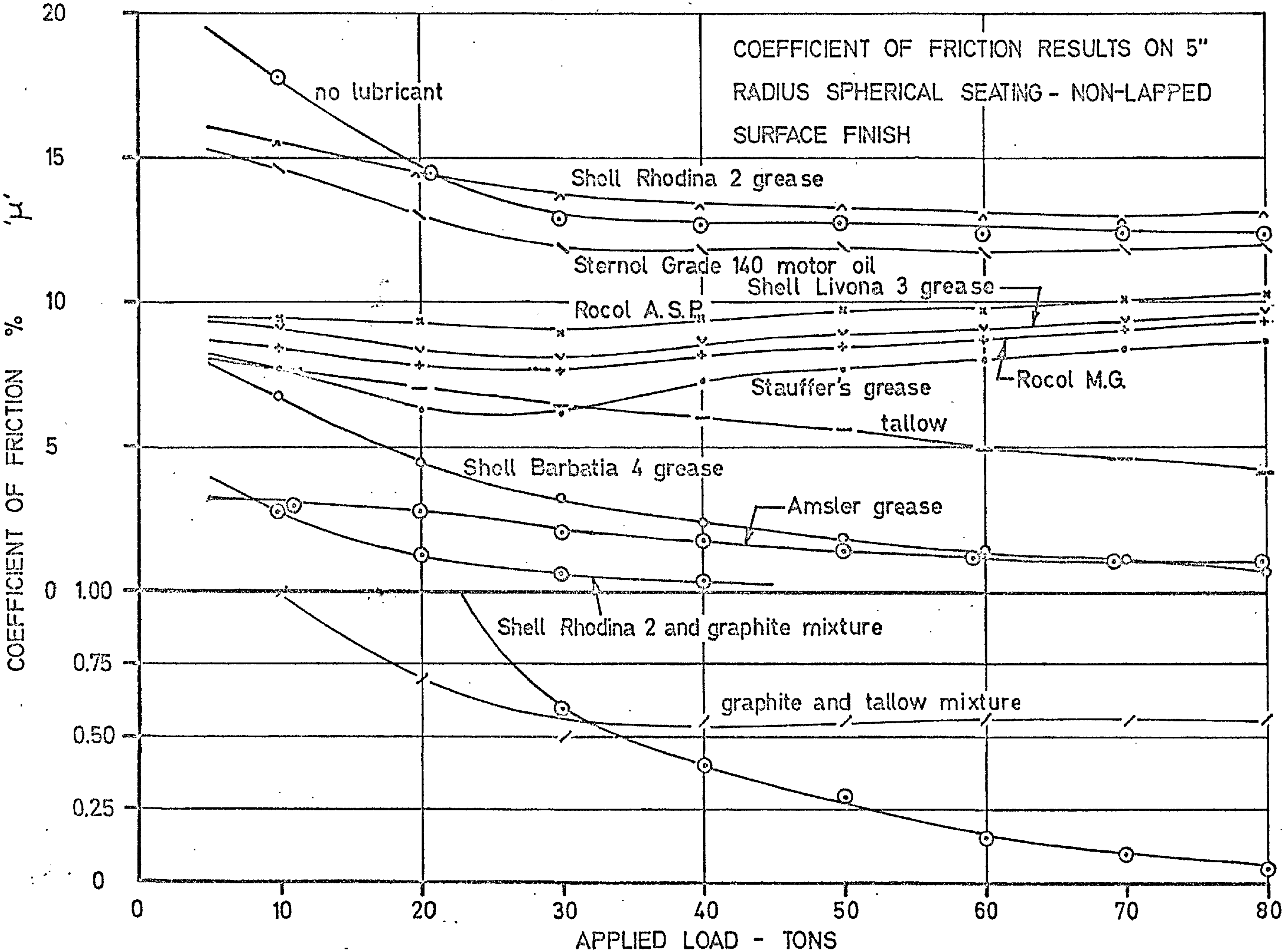
COEFFICIENT OF FRICTION RESULTS ON 5" RADIUS SPHERICAL SEATING - NON-LAPPED SURFACE FINISH
no lubricant
Shell Rhodina 2 grease
Sternol Grade 140 motor oil
Shell Livona 3 grease
Rocol A.S.P.
Rocol M.G.
Stauffer's grease
tallow
Shell Barbatia 4 grease
Amsler grease
Shell Rhodina 2 and graphite mixture
graphite and tallow mixture
COEFFICIENT OF FRICTION % 'μ'
APPLIED LOAD - TONS
20
15
10
5
0
1.00
0.75
0.50
0.25
0
0
10
20
30
40
50
60
70
80

FIG. 8.9

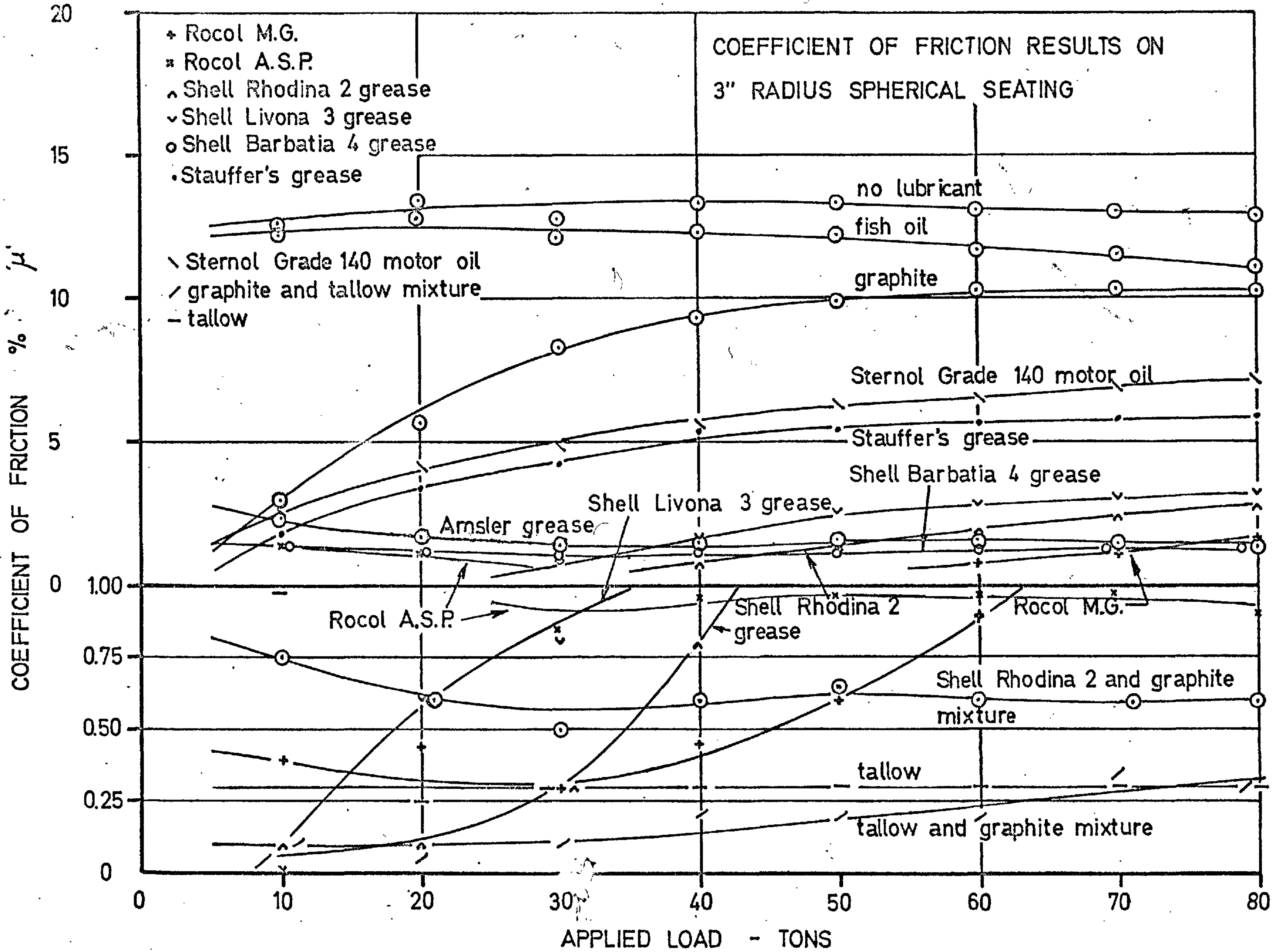

COEFFICIENT OF FRICTION RESULTS ON
3" RADIUS SPHERICAL SEATING
+ Rocol M.G.
x Rocol A.S.P.
^ Shell Rhodina 2 grease
v Shell Livona 3 grease
o Shell Barbatia 4 grease
• Stauffer's grease
\ Sternol Grade 140 motor oil
/ graphite and tallow mixture
– tallow
no lubricant
fish oil
graphite
Sternol Grade 140 motor oil
Stauffer's grease
Shell Barbatia 4 grease
Shell Livona 3 grease
Amsler grease
Rocol A.S.P.
Shell Rhodina 2 grease
Rocol M.G.
Shell Rhodina 2 and graphite mixture
tallow
tallow and graphite mixture
COEFFICIENT OF FRICTION % μ
APPLIED LOAD - TONS

FIG. 8.10

when considering that Tarrant's good lubricants had μ values of 4% and 5.5%. Both an alternative method of mathematical analysis based on an effective moment of inertia method, and a repetition of two tests with only the transfer assembly reversed, provided proof that the results were truly correct.

8.7.1 Pinned End And Fixed End Conditions

As discussed in Section 5.5, spherical seatings should behave in either a pinned or fixed manner. To achieve a pinned condition, the spherical seating must have the resultant force at all times passing through its centre of rotation, that is, the product of the coeficient of friction and seating radius must equal zero. As the latter is always finite positive, the former must equal zero.

Examination of μ results on the 7" radius seating, (see Figure 8.7) shows that with the proper machine finish and contact area, pinned conditions are essentially achieved with 7 different lubricants. The repeatability of these results, their extremely low μ values ($<0.25\%$) and condition of the interfaces after completion of test all provide proof that the steel surfaces were maintained completely apart. The resistance to movement at the interface is therefore provided only by the shear resistance of the lubricant. Figure 8.11, showing the shear resistance of lubricants as a function of shear rate, demonstrates that, at very low velocities as in these tests (approximately 0.5 in. per hr.), the shear resistance for oils,

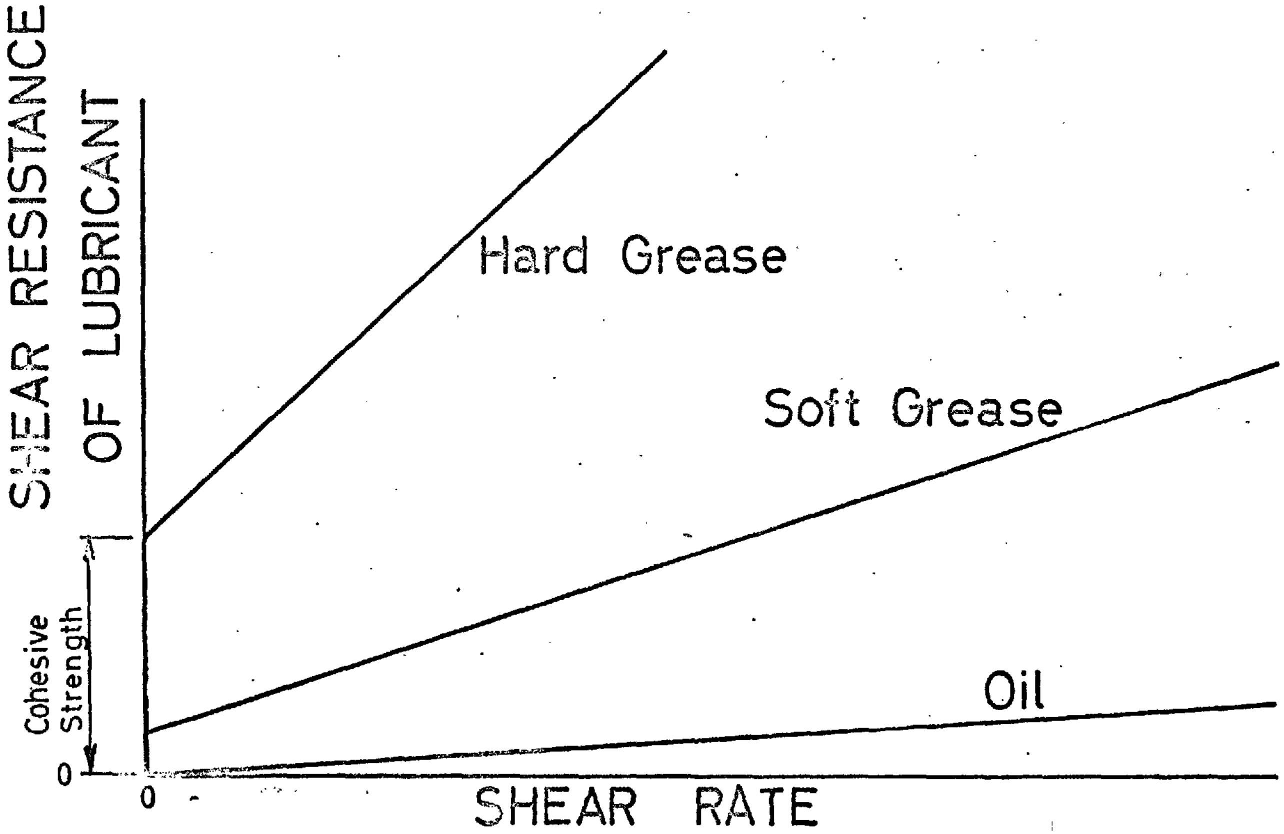

FIG. 8.11 GENERAL RELATIONSHIP BETWEEN THE SHEARING RESISTANCE OF LUBRICANTS AND THE SHEAR RATE

and soft greases will be virtually zero. Consequently, although the sensitivity of the test was inadequate to discriminate between the behaviour of these 7 lubricants, the best lubricant will be the motor oil while the greases rank in order of their cohesive resistance. However, all these 7 greases will have $\mu R'$ values less than 1/64", that is, the centroid of action will be located at less than this distance from the centre of rotation of the seating, and on that basis, may be considered effectively pinned. Examination of Figure 8.8 shows that, with a seating of only 7.0 sq. in. contact area as compared to 78.5 sq. in. in the 7" radius seating thereby increasing the average pressure from 2,300 p.s.i. to 26,000 p.s.i. at 80 tons, most of the lubricants above have insufficient hydrodynamic forces to maintain the surfaces completely separated. In fact, only one of the 7 lubricants discussed above, Rocol A.S.P. was capable of effective lubrication.

For achieving fixed end conditions in routine testing, it is simply necessary to have the product of the interface coefficient of friction and seating radius greater than the distance separating the centre of rotation of the seating and the resultant force of the uniformly deformed specimen. From examination of Figures 8.7 to 8.10, this is most effectively achieved with no lubricant with the above product varying from 0.40" to 1.40" for the seatings tested. To prevent possible corrosion at the interface under long term conditions, a non-lubricant such as a light oil would be required. Except with the high quality 7" radius seating, this is not a difficult problem as fish oil provides little lubrication. However, with the 7"radius seating, this oil developed hydrodynamic forces approaching the magnitude of the applied force due to the large,high-quality contact area of the seating. With such a seating, effective fixity can only be achieved with no lubricant.

8.7.2 Influence of Contact Area and Lubricant on Coefficient of Friction Values

The coefficient of friction values, which were lowest when the steel surfaces were maintained completely apart increased with the degree of steel contact at the interface. Hydrodynamic forces, increasing from zero at the interface boundaries to a maximum at the farthest distance from the boundary, provided, as expected, the best lubrication in the 7" radius seating. Only when using fish oil was there, probably, some contact as demonstrated by its relatively high coefficient of friction, and yet, even here, most of the load was being transmitted across the interface through hydrodynamic action.

With the 5" radius line contact seating, it is apparent that, even at 2300 p.s.i., which is the average pressure of the 7" radius seating at 80 tons, most of the lubricants show a marked increase in μ from that indicated in the 7" radius seating test. Severe boundary conditions here provide insufficient distance for many of the lubricants to develop adequate hydrodynamic resistance. Rocol A.S.P., however, by virtue of its inherently strong bonding nature,[52], is capable of producing extremely high hydrodynamic pressures in a short distance and, therefore, resists the applied force to an average stress of at least 26,000 p.s.i.

Other lubricants which provided good lubrication in the 5" radius line contact seating were three graphite greases and commercial tallow. However, all these greases are relatively hard, as distinguished by the penetration test (A.S.I.M. standard D217-60). As a result, they are capable of keeping the steel faces completely separated, but their relatively large resistance to shearing, roughly proportional to the area of contact, becomes significant when the interface area becomes large. This is demonstrated in Figure 8.7 where the graphite-Rhodina mixture and Amsler grease both have relatively high μ values despite total separation of the two steel faces.

It might at first appear logical that, as long as the steel surfaces were maintained completely separated, the frictional resistance in the lubricant would be proportional to the applied load; that is, μ would be constant. However, the results on the graphite greases, particularly Amsler grease and graphite-Rhodina mixture, indicate that this is not so. For, as the load increases, the resistance to sliding also increases, but at a decreasing rate eventually becoming constant. This results in a decrease in μ with increasing load and an apparently improved behaviour at high load. Although the remainder of the greases behaved linearly over the range tested, it is possible that a similar maximum resistance to sliding will occur at stresses outside the range tested with the harder greases, such as graphite-tallow mixture, becoming constant at higher applied stresses.

The results of the 3" radius seating, with contact area 14.5 sq. in., would be expected to lie intermediate between those of 7" radius and 5" radius, line contact seating with con-contact area of 78.5 and 7.0 sq. in., respectively. These results, however, are generally high, and have been partially influenced by a shortcoming in the load transfer assembly. (see Section 8.3.2) The combined flexibility of the 3" radius male portion and transfer assembly, which produces a severe distribution of stresses across the seating interface, results in some steel contact at points of extreme pressure with a resulting increase in μ. The 5" and 7" radii seatings, on the other hand, due to the very large stiffness of the male section, apply a much more uniform pressure at the interface.

A comparison of the lubricating property of graphite and tallow individually with that of the graphite-tallow mixture (Figure 8.10) indicates that the mixture can behave at least as well as either of its constituents. As it seems logical that th tallow, being obviously the better of the individual lubricants would be the lubricating constituent in the mixture, the μ value of the mixture and individual tallow would be expected to be of the same order. This is shown to be so in both Figures 8.8 and 8.10. For the unlapped seating, the mixture, due to being somewhat harder than the tallow maintains the surfaces completely separate, thereby resulting in the apparently improved lubrication. The behaviour of the graphite-Rhodina mixture as compared to the Rhodina grease(see Figure 8.7) shows that an increase in viscosity has an important effect when considering large area seatings.

8.6.3 Influence of Surface Finish and Lubricant on Coefficient of Friction Values

Comparison of Figure 8.9 with Figures 8.7 and 8.8 shows, conclusively, the great importance of the quality of surface finish on the lubrication behaviour. For, in every case, the μ value is greater with the unlapped 5" radius seating despite its contact area being 40.0 sq. in,. and roughly half-way between that of the 7" radius and 5" radius line contact seatings. Only with the graphite-tallow mixture, Amsler grease and graphite Rhodina mixture were the unlapped steel surfaces kept separated. Yet, due to the hardness of these lubricants, the coefficient of friction is still significant.

With the other lubricants on this seating, it was obvious upon examining the interfaces after test, that steel to steel contact had occurred. As the hardness or viscosity of the lubricant decreased, the lubricating capacity likewise decreased, thereby resulting in an increased proportion of the load being transmitted directly at points of steel contact. This is shown in Figure 8.9 where the hardest greases have the lowest μ values while the oils provide virtually no lubrication.

In his work, Tarrant defines good lubricants as having μ values of the order of 5%. Yet, with this μ value, a displacement of more than 1/4" in a 5" radius seating would be necessary before tilting would occur. Yet, it is highly unlikely that his tests, conducted on 4" cubes, presumably located accurately, would have a displacement of the specimen's resultant of this magnitude. For his tested greases to have behaved in the pinned manner demonstrated, it seems reasonable to suggest that his μ values should have been much lower.

As a result of Tarrant's work, Shell Livona and Rhodina greases are now, 11 years later, used universally on spherical seatings. This is despite the fact that there are now several far superior lubricants for providing the necessary lubrication under extreme pressures.

Although effectively pinned end conditions can be achieved with Rocol A.S.P. grease on either small or large contact area seatings with a 4 to 8 microinch finish, an inferior surface finish should be adequate. Rocol A.S.P. is a suspension of molybdenum disulphide in petroleum jelly; equal proportions by weight. The average size of molybdenum disulphide particles is 1.8 microns(about 70 microinches) with the maximum size being 8.0 microns. It is therefore reasonable to suggest that as long as the surface finish of the steel is significantly less than the average particle size, the grease will still be capable of keeping the steel surfaces apart. On this basis, with each surface lapped to a 16 microinch finish, Rocol A.S.P. would still provide complete lubrication.

8.8 CONCLUSIONS

An investigation on spherical seating behaviour has been conducted. The area and type of lubricant, machine finish of the interfaces, type of lubricant and applied load all have a highly significant effect on the resistance to sliding at the interface. The radius, acting as a moment arm is influential only in deciding the limit of fixity.

The following detailed conclusions have been obtained:

1. To achieve an effectively pinned condition with a spherical seating, the two steel surfaces must be maintained completely separated by either an oil or soft grease. When using an oil, which should be highly viscous, the surface area must be of a high quality (4 to 8 microinch), the contact area large (average pressures within about 2,500 p.s.i.) and boundary effects kept to a minimum. A soft grease with strong adhering properties such as Rocol A.S.P. is also satisfactory even with average pressures up to at least 26,000 p.s.i., and a high quality surface finish, although the finish may be slightly inferior to that described above.

2. Effectively fixed conditions obtained with a spherical seating are best achieved with no lubricant. In corrosive surroundings, however, a light oil will be necessary on the seating interface. Although effective fixity can still be achieved with some seatings that have a light, anti-corrosive oil, other seatings with better machine faces and larger contact areas must have all lubricant removed before effective fixity is obtained.

3. As complete lubrication will only be achieved with total separation of the interfaces, the best lubricant for any seating becomes more viscous or hard as the surface finish reduces in quality. Consequently, as an increase in the lubricant viscosity or hardness produces an increased resistance to shearing, the ability of the seating to behave in a pinned manner simultaneously, reduces.

4. Although it is reasonable to suggest that <u>all</u> greases at some stage acquire a constant resistance to shearing, only the graphite greases displayed this property.

5. With hard greases, there is a significant increase in resistance to sliding at the interface as the contact area increases.

6. The lubrication capacity of a mixture may be as good as either of its constituents when the steel surfaces are kept separated. With poorer quality seatings, the mixture can have better lubrication than either of its constituents as a result of an increase in hardness over that of its softer constituent.

CHAPTER 9

THE INFLUENCE OF TESTING MACHINE CHARACTERISTICS ON THE STRENGTH AND MODE OF FAILURE OF COMPRESSION SPECIMENS

9.1 TESTING MACHINE PROBLEMS REQUIRING EXAMINATION

The two purposes of testing concrete specimens in uniaxial compression are to determine the strength and its variation in strength of concrete in an actual structure. To do this, the test result must either be independent of machine effects as shown by Newman and Lachange (21) or be related empirically to the true uniaxial compressive strength and affected uniformly by different testing machines. Variable cube strengths as influenced by testing machines, (18, 22-26, 29, 30) are caused by variations in such machine characteristics as spherical seating effect, lateral stiffness, machine restraint and specimen alignment, (see Section 5.4). A thorough experimental investigation of these factors comprises the main investigation of this chapter.

In any material, two failure modes only, on the phenomenological level, are usually recognized. Whether the uniaxial compression mode of failure is shear or tensile cleavage has been a popular study of investigation. (6, 14, 56-8) A true uniaxial test to investigate this can only be conducted with effectively pinned ends; that is, the resultant force at all load stages is coincident with the specimen axis. The mode of failure in such a test, therefore, represents the intrinsic weakness of the material in uniaxial compression. The second investigation of this chapter is to determine conclusively this mode, as an aid to standardizing the uniaxial compression test.

9.2 OUTLINE OF TEST SERIES

To investigate the influence of the testing machine characteristics stated above on the mode of failure and strength of concrete, nine separate test series were performed. The object of each test series with a brief description is 'as follows'. A detailed description of the testing procedure is presented in Section 9.4

Test Series 1: Object (1) To show the difference in strength, if any, between using a well-lubricated and an unlubricated seating.

(2) To show the effect of contact area. (Stauffer's grease on 3" and 7" radii seatings) on the cube strength.

(3) To determine the influece of the surface finish of the seating interface on cube strength.

Description of Test:

Twelve 4" segregated cube specimens were tested under each of nine combinations of spherical seating and lubricant. The 3" 5" and 7" radii seatings, all full contact, were used while the lubricants included Rocol M.G., Stauffer's grease and no lubricant.

Test Series 2: Object:

To determine the effect of the type of seating contact (full or strip) on the cube strength.

Description of Test:

Twelve 4" segregated cubes were tested under each of four combinations of seating and lubricant; 3" radius with no lubricant, 3" and 7" radii with Shell Rhodina 2 and 5" radius line contact with Shell Rhodina 2.

Test Series 3: Object:

To investigate the influence of specimen misalignment on specimen strength and its coefficient of variation with both an effectively pinned and a fixed seating.

Description of Test:

Twelve 4" segregated cubes were tested under each of 6 combinations of misalignment and lubrication of the 5" radius unlapped spherical seating. The lateral displacements of the seating were $\frac{1}{4}$" towards and away from the cast face from the centre of the specimen as well as coincident with the centre of the specimen. The best lubricant, graphite-tallow mixture (see Figure 8.9) and no lubricant were the two lubricating conditions.

Test Series 4: Object:

To investigat if concrete cubes can produce the same strength when loaded with a well lubricated seating as when loaded under fixed conditions.

Description of Test

A number of 4" cubes, usually 6, were tested under each of six combinations of misalignment and lubricant with both the 3" and 5" radii full contact seatings . The well lubricated conditions were obtained with Rocol M.G. grease and Rhodina-graphite mixture, respectively, while fixity was achieved with no lubricant. Misalignment of the seating, carried out on the well-lubricated seatings only, were $\frac{3}{8}$" towards and 1/16", $\frac{1}{8}$", $\frac{1}{4}$" and $\frac{1}{2}$" away from the cast face with reference to the specimen centreline. Testing under perfect alignment with both the well-lubricated and unlubricated seatings was also performed.

Test Series 5: Object:

(1) To observe the ratio in failing strengths under each of the basic philosophies of loading. (see Section 5.3) for the standard compression control specimens; 4" and 6" cubes and 6"Ø x 12" cylinders.

(2) To determine the ratio of failing strength between cylinders and cubes as a function of the method of loading.

(3) To establish the basic failing mode of concrete in uniaxial compression.

(4) To investigate the importance of the testing machine lateral stiffness on the ultimate strength of cubes and cylinders.

Description of Test:

Twelve segregated concrete specimens of each of the three standard sizes above were tested under each of the three basic methods of loading. Both ends pinned was achieved with Rocol M.G. grease on the 7" radius seating located at the bottom and Rocol A.S.P. grease on the 3" radius seating at the top. (see Plate 9.1) For one end pinned or both ends fixed, the 3" radius seating lubricated as above or unlubricated respectively were used at the top while the bottom was in both cases the bearing block of the testing machine, as shown in Plate 8.4.

Test Series 6: Object:

To determine whether the relationships and influences as obtained with the segreggted specimens in Test Series 5 are the same for uniform concretes.

Description of Test:

The test is identical to that used in Test Series 5 except for the casting of specimens with a non-segregating concrete.

Test Series 7: Object:

To determine whether the longitudinal stiffness of the testing machine influences the strength of concrete specimens.

Description of Test:

Five 4" cubes were tested under effectively fixed loading conditions in each of two Grade A compression testing machines. The machines used were a 500 ton and a 50 ton with longitudinal stiffnesses, 2×10^7 lbs/in. and 10×10^5 lbs/in., respectively.

Test Series 8: Object:

To determine if the degree of vibration of conrete cubes has any effect on the ratio of strengths obtained from the well lubricated and non-lubricated spherical seatings.

Description of Test:

Twelve naturally segregating 4" cubes were tested under four combinations of method of test and degree of segregation. The two methods of test, as shown above, were both ends effectively fixed and one end pinned, one end fixed while the two degrees of vibration were obtained with the same Kango hammer by vibrating each specimen for a total time of either 10 seconds or 90 seconds. (see Section 9.3.4).

Test Series 9: Object:

To determine the influence of restraint of the loading platens on the ultimate strength of concrete specimens.

Description of Test:

Six 6" cubes were tested under each of six combinations of spherical seating and concrete strength. The cube strengths were approximately 5,000 p.s.i. and 6,500 p.s.i. while the seatings were the 3", 5" and 7" radii seatings (all full contact). A supplementary set of tests were conducted on eleven 6" high strength cubes, about 8,000 p.s.i. with each of the 5" and 7" radii seatings. In every case, fixity was ensured with no lubricant on the seating interface.

9.3 MANUFACTURE OF SPECIMENS

9.3.1. Materials Used

Ordinary Portland Cement supplied by Tunnel Cement Co., from their Pitstone Works was used for all mixes with all the cement coming from the same batch. The cement was brought in steel drums from the cement storage area to the batching area as required.

Potable water used for the mixes was drawn from the standard temperature tank in the mixing laboratory, maintained at 64° F.

All aggregate used was Thames Valley River Gravel supplied by Ham River. Co. from the Chertsey pits. It had been dried to an air dry condition [59] and sieved into each of the British Standard sizes [60] in the aggregate processing plant before being transferred to the batching area, where it was kept in steel bins. At time of batching, the aggregate was at 68°; the temperature of the batching area. The grading was in accordance with Grading Curve 2 or 4 (see Table 9.1) in Road Note 4 [61] with $\frac{3}{4}$" aggregate being the maximum size used.

TABLE 9.1 DETAILS OF CONCRETE MIXES FOR TEST SERIES 1 to 9

TEST SERIES NO.	NO. OF CASTINGS	NO. AND TYPE OF SPECIMEN IN EACH CASTING	W/C RATIO (BY WEIGHT)	A/C RATIO (BY WEIGHT)	GRADING CURVE, SEE FIG. 2 ROAD NOTE 4
1	6	18-4" cubes	0.60	4.5	4
2	2	24-4" cubes	0.60	4.5	4
3	4	18-4" cubes	0.60	4.5	4
4	4	19-4" cubes	0.60	4.5	4
5	3	12-4" cubes 12-6" cubes 12-6" Ø x 12" cylinders	0.60	4.5	4
6	3	12-4" cubes 12-6" cubes 12-6" Ø x 12" cylinders	0.55	7.5	2
7	1	10-4" cubes	0.60	4.5	4
8	2	24-4" cubes	0.60	4.5	4
9	2	18-6" cubes	0.50	6.0	2
	1	24-6" cubes	0.35	2.8	2

9.3.2 Composition of Specimens

The composition of the mixes for all 9 test series is given in Table 9.1. For each of Test Series 1 to 5 and 8, a naturally segregating concrete was required. It was considered that this would indicate the importance of each variable being investigated most significantly. Before selecting these mix proportions, several trial test cubes with varying mix proportions were cast to investigate the one most vulnerable to segregation.

Test Series 6, a relatively stiff mix was, in comparison with Test Series 5, relatively immune to segregation effects. With Test Series 9, high strength mixes were selected as these would be most sensitive to machine restraint.

9.3.3 Batching and Casting Procedure

Each aggregate size and cement were weighed to the nearest gram by the author and placed in steel drums, before being transported to the temperature controlled casting area, maintained at 64^{o}F. The required water was weighed to the nearest gram immediately prior to casting to avoid possible evaporation.

For Test Series 1 to 4, 7 and 8, the constituents were mixed in a "Liner Pan" Cum Flow mixer of 1 cubic foot capacity while the concretes for Test Series 5, 6 and 9 were mixed in a Gustav Eirich EA21 Pan Mixer of 100 litre capacity. In every case, the aggregate and cement was mixed for 2 minutes and then, after addition of water, was mixed for a further 3 minutes.

For the smaller mixes in the "Liner Pan" mixer, the concrete was transferred directly from the mixer into the moulds, care being taken to stir the remaining mix frequently with a shovel. With the larger mixes from the Gustav Eirich Pan Mixer, the contents, after mixing, were dumped into a wheel-barrow, which had been prewetted to avoid loss of moisture. Prior to placing in the moulds, the mix was thoroughly reworked with a shovel. This process was repeated several times to avoid segregation in the wheel-barrow.

In cases where 2 mixes were required on any one day as in each of the castings for Test Series 5 and 6 (see Table 9.1), all attempts to produce an identical mix were employed. To prevent loss of moisture, the mixer and water measuring container were prewetted for the first mix in an attempt to duplicate their moisture retaining properties in the second mix. The first mix was placed in half the moulds which were then vibrated completely before beginning the second mix, thereby ensuring an equal state of plasticity for all specimens during vibration.

All moulds were manufactured in compliance with British Standard specifications (9).

9.3.4 Vibration of Specimens

As repeatability of results was required for successive castings in any test series, a repeatable vibration procedure as well as a consistent batching and casting process was considered important. The general requirements in most test series was a well compacted concrete with a minimum of air voids. In addition, a high degree of segregation in the naturally segregating concrete, Test Series 1 to 5 was achieved. An exception to this was half of Test Series 8 where only a small vibration was conducted to specifically investigate this variable. All specimens in Test Series 1 to 8 were vibrated with a "Kango" hammer while those in Test Series 9 were vibrated on a vibrating table. Details of the vibration procedure for every test series are presented in Table 9.2.

It is regretted that the same vibration procedure could not be used for all the 3 separate castings in each of Test Series 5 and 6. This was due to the "Kango" hammers

TABLE 9.2 VIBRATION DETAILS FOR CONCRETE MIXES IN TEST SERIES 1 TO 9

TEST SERIES NO.	DESCRIPTION OF SPECIMENS	NO. OF LAYERS FOR VIBRATION	LENGTH OF VIBRATION IN EACH LAYER	VIBRATION EQUIPMENT USED
1,3,4	4" cubes	2	45 secs.	Kango, 315 watt, Type C
2	4" cubes	2	12 secs.	Kango, 430 watt, Type F
5	4" cubes	2	12 secs.	Kango, 315 watt, Type C for 1st and 3rd mix
	6" cubes	3	12 secs.	Kango, 430 watt, Type F for 2nd mix.
	6" Øx12" cylinders	4	15 secs. in bottom 3 layers, 20 secs in top layer	
6	4" cubes	2	75 secs. for 1st mix 60 secs. for 2nd, 3rd mixes	Kango 430 watt, Type F for 1st mix. Kango 630 watt, Type K for 2nd and 3rd mixes
	6" cubes	3	75 secs. for 1st mix 60 secs. for 2nd, 3rd mixes	
	6" Øx12" cylinders		75 secs. in bottom 3 layers, and 90secs. in top for 1st mix, 60 secs. in bottom 3 layers and 90 secs. in top for 2nd and 3rd mixes.	
7	4" cubes	2	30 secs.	Kango, 315 watt, Type C
8	4" cubes	2	45 secs for half 5 secs for half	Kango, 430 watt, Type F
9	6" cubes	3	30 secs for bottom 2 layers, 45 secs. in top	Vibrating Table
	6" cubes	3	60 secs.	

being in continual use elsewhere and the desired one not being readily available at time of casting. However, as care was taken to ensure that each specimen size received identical vibration in each casting, a significant relationship is obtained between the results as shown in Sections 9.7 and 9.8.

For all specimens in Test Series 1 to 8, care was taken to ensure that the moulds were completely filled except for the 6" Ø x12" cylinders where space for the capping material was provided. In test series 9 only , the specimens were trowelled after vibration. At approximately two hours after casting, the specimens were covered with polythene sheeting to prevent loss of moisture from the specimens.

9.3.5 Curing

On the morning after casting, all specimens were stripped, marked with a black crayon and placed in curing tanks maintained at 64 °F, in accordance with British Standard 1881: 1952 (9). The cylinders were removed from the curing tanks within 4 days of casting for capping. Following capping, performed with a high strength mix of sand, water and either high alumina cement or amalgamated dental plaster, the cylinders were replaced in the storage tanks until time of testing.

9.4 TESTING PROCEDURE

The specimens tested at an age of 28 days were removed, as required, from the curing tanks and placed in a water filled tank near the 500 ton Avery compression testing machine used for these tests (see Plate 8.4). Prior to placing in the testing machine, the specimens were wiped clean, of surplus moisture and grit and measured to the nearest 0.01" This was performed by taking an average of 3 readings for the cube height and 6 readings for the cylinder diameter. To ensure uniform bearing, both ends of the specimen were scraped with the edge of a platen followed by a thorough wiping of both the platen and specimen ends with a clean towel.

For locating in the testing machine, the bottom platen was accurately positioned axially on the lower machine bearing block. The specimen, upper platen and spherical seating, dowelled to the upper platen (except for Test Series 3 and 4) were then in turn positioned accurately. A small load was applied and immediately removed to ensure parallelness between the upper cross head and the bearing face of the female portion of the spherical seating. Prior to loading to failure, the entire assembly was again carefully checked for alignment. Cubes were always positioned with their cast face to the right (see Plate 3.4) while all cylinders were positioned with their capped end uppermost.

The loading rates to failure were 10, 25 and 20 tons/min. respectively, for the 4" and 6" cubes and cylinder specimens i.e., approximately 1500 p.s.i. per minute in each case.

In Test Series 7, due to the inability of the 50 ton compression machine to load at a uniform stress rate, the loading rates were altered to a constant strain rate with the stress rate in the first 50% of loading being 20 tons/minute.

When using well lubricated seatings, the spherical seating interfaces were prepared as discussed in Section 8.6.2 with 3 pre-compressions to 100 tons in the 200 ton compression machine.

As small differences were being investigated, each test series had an equal number of specimens tested under each condition on each day. For example, in Test Series 1, 2 cubes were tested under each of the 9 conditions on each day. In addition, to allow for any slight increase in strength or variations in operator technique during any one day, the sequence of testing specimens was reversed on successive days.

The same platen, $\frac{7}{8}$" thick, and 4" square for 4" cube and 6" square for 6" cubes and cylinders, were used for any one test series. As they were ground and maintained plane in accordance with British Standard 1881, platen effect was eliminated. In addition, the centre of rotation of the seating was located at the centre of the specimen bearing face. (see Section 5.4.4).

For misalignment tests (Series 3 and 4), the platens and specimen were located axially in the testing machine in every test while the spherical seating was displaced laterally the necessary off-centre distance. This procedure eliminated variations in ram behaviour.

For testing with 2 well lubricated seatings, (Series 5 and 6) the male bearing face of the lower seating was carefully checked for level in both directions in every test, to ensure repeatability of loading (see Plate 9.1).

9.5 THE INFLUENCE OF SPHERICAL SEATING PROPERTIES AND TYPE OF LUBRICANT ON THE CUBE STRENGTH (TEST SERIES 1 AND 2)

The cube results as shown in Table 9.3, fall into two strength groups of approximately 4550 and 4800 p.s.i. The higher strength group failed in accordance with the philosophy of having both ends effectively fixed as revealed by equal failure on all four faces (see Plate 5.2). The lower strength specimens, on the other hand, showed excessive failure on one face thereby giving proof that the seating rotated under load, thus approaching a pinned behaviour. These behaviours agree with the predictions formulated from the results of Chapter 8 (see Figures 8.7, 8.9 and 8.10).

In Section 9.6 it is shown that the centroid of resistance of the cube specimen, when deformed uniformly is about $\frac{1}{8}$" towards the bottom of the specimen, as cast, from its centre line. Therefore, with the seating accurately centred, a 'μR' value (the product of the coefficient of friction at the seating interface and the radius of the sphere) in excess of this value would produce a fixed end

PLATE 9.1 Test assembly for loading concrete specimens under both ends pinned condition

condition. With the unlubricated seatings as well as all the lubricants on the 5" radius seating, (see Table 9.3) the 'μR' value is greater than $\frac{1}{8}$", thereby producing consistent strength results and failure patterns. The 3" radius seating with Stauffer's grease is a marginal condition as its 'μR' equals about $\frac{1}{8}$", as can be observed from Figure 8.10. As 11 of these cubes failed uniformly while the twelfth showed some tilting, these results should, as was seen to be the case, agree with those loaded under effectively fixed conditions.

TABLE 9.3 EFFECT OF SPHERICAL SEATING AND TYPE OF LUBRICANT ON COMPRESSIVE STRENGTH OF 4" CUBES - TEST SERIES 1 (for individual strengths see Appendix A)

RADIUS OF SEATING		NO. LUBRICANT	STAUFFER'S GREASE	ROCOL M.G.
3"	Average Strength	4796	4857	4857
	Standard Deviation	211	134	190
	Coefficient of variation	4.4%	2.8%	4.1%
5"	Average Strength	4876	4760	4809
	Standard Deviation	183	200	210
	Coeff. of Variation	3.8%	4.2%	4.4%
7"	Average Strength	4872	4595	4508
	Stan. Deviation	173	199	175
	Coeff. of Var.	3.5%	4.4%	3.9%

TABLE 9.4 EFFECT OF SPHERICAL SEATING TYPE OF CONTACT ON COMPRESSIVE STRENGTH OF 4" CUBES - TEST SERIES 2

	3" RADIUS w/SHELL RHODINA 2	3" RADIUS SEATING NO LUBRICANT	5" RADIUS w/SHELL RHODINA 2 (LINE CONTACT)	7" RADIUS w/SHELL RHODINA 2
Average Strength	4652	4883	4907	4672
Standard Deviation	188	105	180	256
Coeff. of Variation	4.0%	2.2%	3.7%	5.5%

For the other 3 combinations of spherical seating and lubricant, the 'μR' values are essentially zero (see Figures 8.7 and 8,10). Again, consistent strengths and failure patterns are obtained, as tilting of the sphere in its seating produced excessive failures on the cast face (similar to that shown in Plate 5.1) These results are 5.5% lower than when the seating remains locked.

The general method of test has little effect on the coefficient of variation and standard deviation values as these are observed to be of the same order (see Table 9.3). However, this only applies when great care is taken in ensuring a repeatable loading pattern. As discussed in Section 9.6, inconsistency in the degree of misalignment will have a very serious effect in machines with well lubricated seatings with both lower average strength and increased standard deviation of strength values occurring.

While the analysis of the results of Test Series 1 indicates that the ultimate strength and mode of failure of cubes are influenced by such spherical seating properties as radius, area of contact, surface finish and type of lubricant, Test Series 2 reveals the importance of the type of seating contact. From Table 9.4, it is seen that the results obtained with the 3" radius seating lubricated with Shell Rhodina 2 are reasonably identical to those obtained with the 7" radius seating due to the 'μR' value, in both cases, being essentially zero. Although Fig. 8.10 shows a 'μ' value of 0.8% at 40 tons, this value would probably be nearer zero due to a uniform stressing on the interface as opposed to the non-uniform stress condition occurring in the 'μ' test, as discussed in Section 8.7.2. On the other hand, the 5" radius line contact seating showed a completely fixed behaviour as prdicted from Figure 8.8. Although some difference would be expected between the 3" and 5" radii seatings lubricated with Shell Rhodina 2 grease due to differences in contact area (14.4 and 7.0 sq. ins. respectively), such a complete difference in behaviour cannot be accounted for by difference in contact area alone. This is verified by the fact, that at any average interface pressure, the 'μ' value for the 5" radius seating is greater than that on the 3" radius seating with the above lubricant.

TABLE 9.5 SIGNIFICANCE OF DIFFERENCES IN TEST SERIES 1 - SEE TABLE 9.3

CONSTANT	VARIABLES		ULTIMATE STRENGTH DIFFERENCE	SIGNIFICANCE LEVEL
STAUFFER'S GREASE	3" RADIUS	7" RADIUS	5.4%	0.1%
ROCOL M.G. GREASE	3" RADIUS	5" RADIUS	4.6%	0.25%
ROCOL M.G. GREASE	7" RADIUS	5" RADIUS	6.2%	0.1%
3" RADIUS	NO LUBRICANT	ROCOL M.G.	4.4%	1.75%
7" RADIUS	NO LUBRICANT	ROCOL M.G.	7.5%	0.1%

To establish conclusively the difference in strength observed with different seatings or lubricants, a series of significance calculations were performed in accordance with the method of interpolating data at the Road Research Laboratories,(19) the results of which are presented in Table 9.5. As stated by Wright(19), a 5% significance level implies strong evidence of a real difference while a 1% level indicates reasonable certainty that a real difference exists. The significance levels, as presented in Table 9.5, prove that the differences obtained are conclusive. Combining this analysis with the influence of the spherical seating on the cube behaviour, it is concluded that all factors which affect the behaviour of the spherical seating (see Section 8.1.3) will influence the ultimate strength and mode of failure of cube specimens.

9.6 THE INFLUENCE OF SPECIMEN MISALIGNMENT ON ITS ULIMATE STRENGTH (TEST SERIES 3 and 4)

In commercial testing , small misalignments of the specimen will be general and random, particularly when the lower platen is not accurately dowelled to the lower machine bearing block. Test Series 3, (Section 9.2) performed to investigate the effect of misalignment on cube strength, showed that results are extremely sensitive to misalignment effects with a well lubricated seating. A displacement of the specimen axis with reference to the seating axis of only $\frac{1}{4}$" produced a reduction of strength of 17% in one direction and 4% in the other (see Table 9.6 and Figure 9.1)

TABLE 9.6 EFFECT OF SPECIMEN MISALIGNMENT ON ITS STRENGTH AND DEVIATION - TEST SERIES 3 - (for individual strengths see Appendix A)

DISPLACEMENT OF SEATING AXIS WITH REFERENCE TO SPECIMEN AXIS - 5" RADIUS FULL CONTACT SEATING			
	$\frac{1}{4}$" TOWARD CAST FACE	0	$\frac{1}{4}$" TOWARD BOTTOM FACE
NO LUBRICANT ON SEATING INTERFACE			
Average Strength	4702	4757	4727
Standard Deviation	168	335	219
GRAPHITE - TALLOW MIXTURE ON INTERFACE			
Average Strength	3620	4366	4198
Standard Deviation	264	183	238

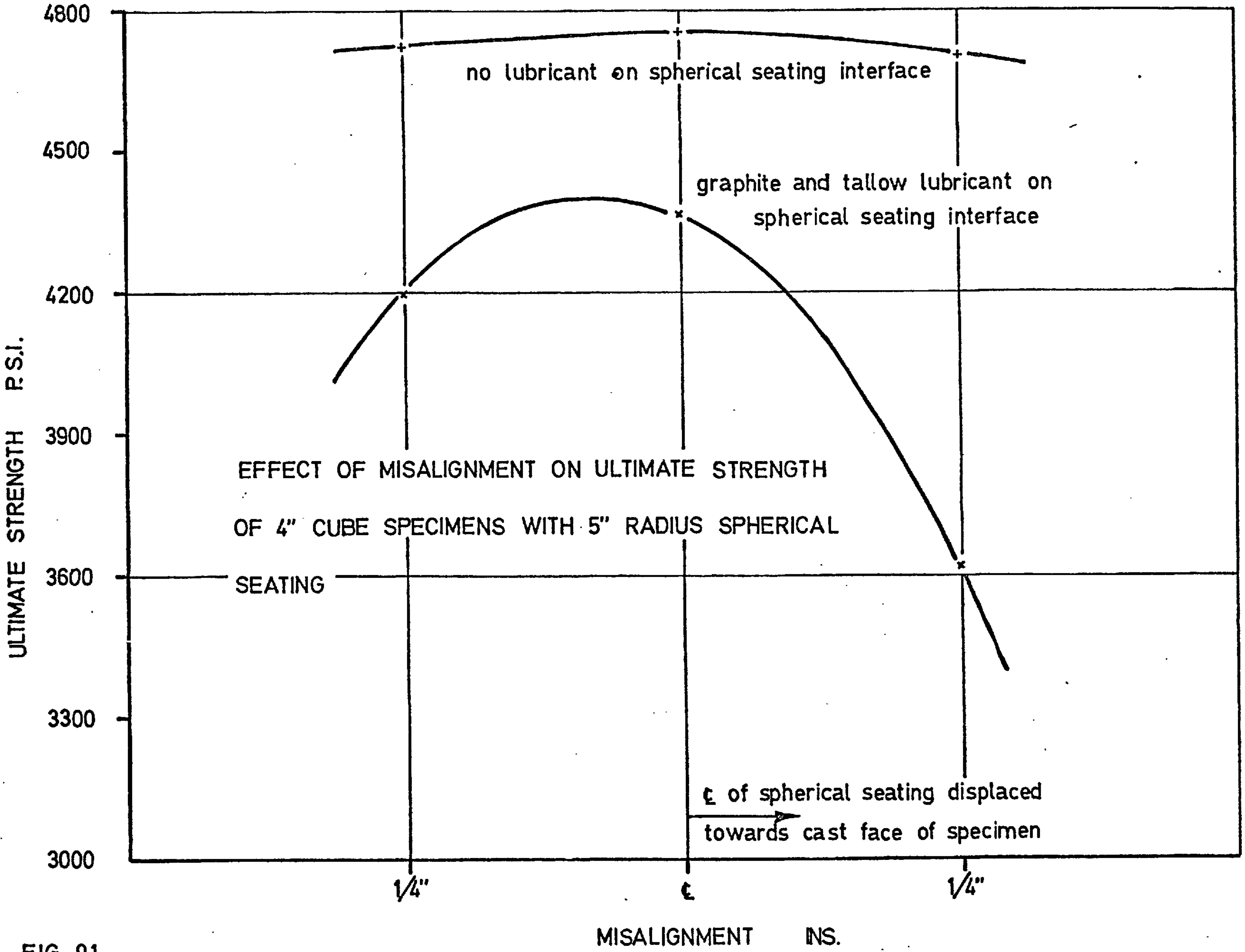
4800
4500
4200
3900
3600
3300
3000
ULTIMATE STRENGTH P.S.I.
no lubricant on spherical seating interface
graphite and tallow lubricant on spherical seating interface
EFFECT OF MISALIGNMENT ON ULTIMATE STRENGTH OF 4" CUBE SPECIMENS WITH 5" RADIUS SPHERICAL SEATING
℄ of spherical seating displaced towards cast face of specimen
1/4"
℄
1/4"
MISALIGNMENT INS.

FIG. 9.1

With unlubricated seatings however, misalignment produced strength results and failure patterns essentially identical for all specimens. (see Fig 9.1). This is due to a uniform deforming of the specimens in every case since the 'μR' vslue is greater than the displacement of the effective resultant of the cube.

Although these deliberate misalignments are rather more than would generally be expected in practise, an exercise to demonstrate the difference in specified strength on the basis of these results reveals the importance of using a machine immune to small misalignment effects. The average strength and its standard deviation for the 36 specimens tested in the fixed condition are 4728 and 204 p.s.i., while for the well lubricated seating, they are 4061 and 394 p.s.i. On the basis of a statistical analysis to determine the strengths above which 99% of the results would be expected to fall, the values are 4250 and 3140 p.s.i. for the unlubricated and well lubricated seatings, respectively, a difference of 26%!

In standard testing machines where random lateral displacement of the specimen occurs, the strengths may be affected by ram behaviour as well as seating behaviour. The former has been eliminated in Test Series 3 and 4 by moving the seating laterally rather than the specimen. Therefore, although it is concluded that ultimate strengths of misaligned specimens tested with effectively locked spherical seatings are independent of the spherical seating, some influence from ram behaviour may result. It is however apparent, from the investigation of Chapter 4, that with long, large diameter and well machined rams, such influences will be only a fraction of that obtained with well lubricated seatings and negligible for the misalignments being considered above. (see Section 5.4.8)

With the well lubricated seating, the failure patterns, excessive on one side in every case was dependent upon the location of the neutral axis of the specimen with reference to the seating axis. As observed in Figure 9.2 the maximum strengths with the lubricated seatings were obtained when the axis of the seating was positioned about $\frac{1}{8}$" towards the bottom of the specimen, as cast. With this particular misalignment, there tended to be excessive failure on a random face. This indicated that the specimens were being loaded at or very near their neutral axis (see Sections 6.3.1 and 6.3.3). However, when the centreline of the seating was moved from the neutral axis of the specimen, excessive failure occurred on the specimen face towards which the seating was displaced.

In Section 6.3.1 and Table 6.1, it was shown that, theoretically, no tilting of the seating would occur if the seating axis were positioned coincident with the neutral

TABLE 9.7 EFFECT OF SPECIMEN MISALIGNMENT ON ITS STRENGTH - TEST SERIES 4 (for individual strengths, see Appendix A)

DISPLACEMENT OF SPHERICAL SEATING AXIS WITH REFERENCE TO SPECIMEN AXIS						
	TOWARDS CAST FACE				TOWARDS BOTTOM FACE	
	$\frac{3}{8}$"	0	1/16"	$\frac{1}{8}$"	$\frac{1}{4}$"	$\frac{1}{2}$"
SERIES 4A: 5" RADIUS SEATING (FULL CONTACT)						
NO LUBRICANT ON SEATING INTERFACE						
Average Strength		4820				
GRAPHITE TALLOW MIXTURE ON SEATING INTERFACE						
Average Strength	3570	4630	-	4600	4255	3475
SERIES 4B: 3" RADIUS SEATING						
NO LUBRICANT ON SEATING INTERFACE						
Average Strength		4720				
ROCOL M.G. ON SEATING INTERFACE						
Average Strength	3510	4320	4530	4490	-	3340

axis of the specimen and that, as a result, the stress patterns and resulting strengths obtained under the three basic methods of loading would be identical. Results of Test Series 4 show, however, that the strengths obtained with the well lubricated seating are always less than those obtained with the non-lubricated seating. (see Table 9.7 and Figure 9.2). Furthermore, as the seating tilted in every case, even when positioned virtually at the neutral axis of the specimen, it is suggested that the neutral

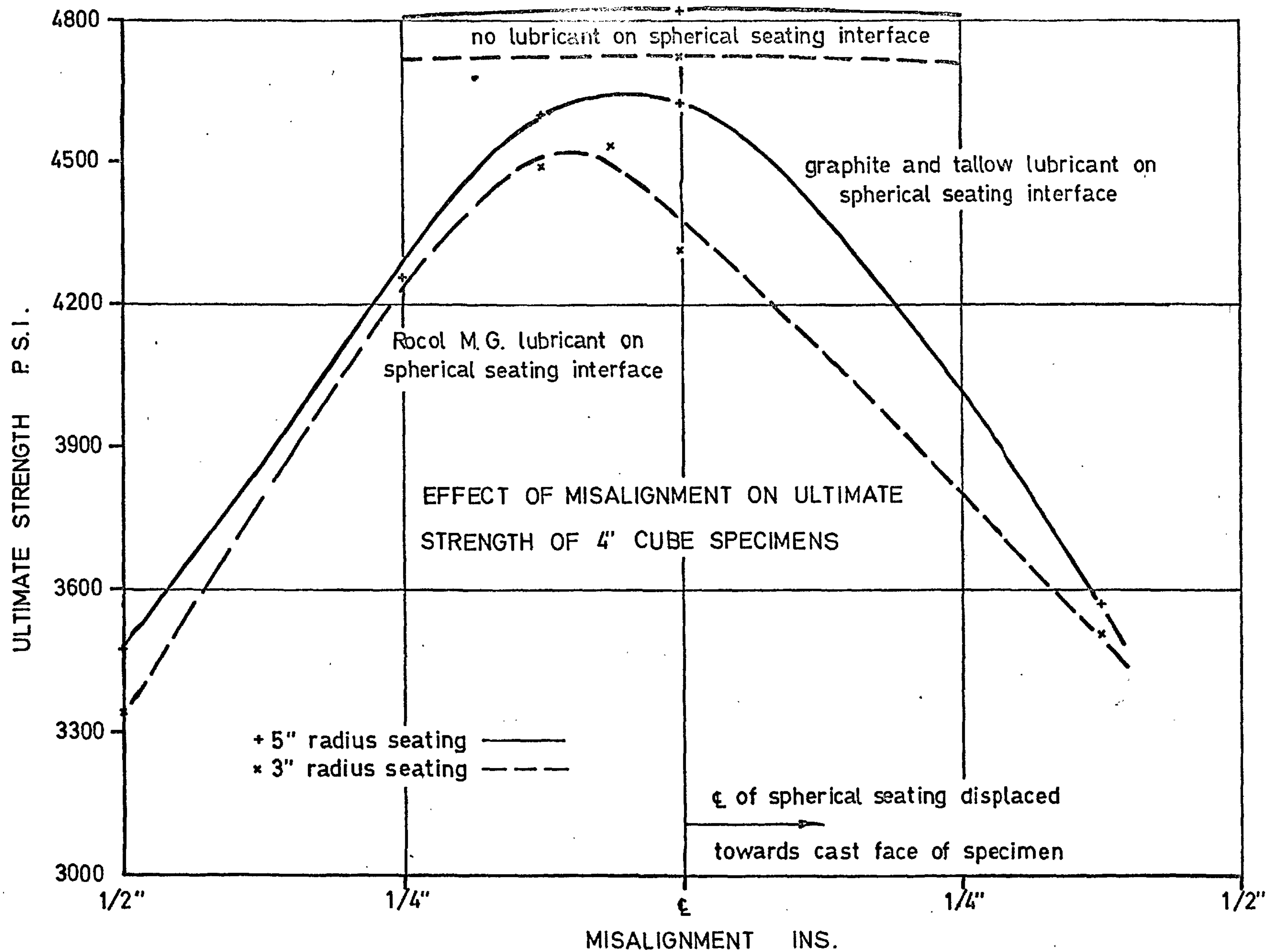
4800
4500
4200
3900
3600
3300
3000
ULTIMATE STRENGTH P.S.I.
no lubricant on spherical seating interface
graphite and tallow lubricant on spherical seating interface
Rocol M.G. lubricant on spherical seating interface
EFFECT OF MISALIGNMENT ON ULTIMATE STRENGTH OF 4" CUBE SPECIMENS
+ 5" radius seating
× 3" radius seating
℄ of spherical seating displaced towards cast face of specimen
1/2"
1/4"
℄
1/4"
1/2"
MISALIGNMENT INS.

FIG. 9.2

axis did not remain constant, but rather altered its position slightly at different load stages. In the theory of Chapter 6, it was assumed that the neutral axis remained constant.

It is concluded that the cube strength obtained with an unlubricated spherical seating is greater than that obtained with a well lubricated spherical seating.

9.7 THE INFLUENCE OF METHOD OF LOADING AND SPECIMEN COMPOSITION ON THE CUBE STRENGTH: CYLINDER STRENGTH RATIO (TEST SERIES 5 & 6)

As shown in Table 9.8 and 9.9, the ratio between 4" and 6" cube strengths is reasonably consistent and independent of the method of loading although the actual cube strengths are very much influenced by the loading system; differences between pinned and fixed end conditions are about 7%. Alternatively, cylinder strengths, due to their direction of testing in relation to casting are only slightly influenced by the method of test, the maximum difference between two methods of loading being 3%. Consequently, the cube: cylinder strength ratio is very much a function of the method of loading.

This ratio, in addition to being dependent upon the method of test, is also influenced by the mix proportions. Williamson[62] in a series of tests to determine the strengths of different sections of concrete cylinders, concluded that, generally, they decreased from the bottom to the top, as cast, due to segregation effects. This

TABLE 9.8 SPTRENGTHS AND THEIR RATIOS AS A FUNCTION OF SPECIMEN SIZE AND METHOD OF LOADING. - TEST SERIES 5 ON SEGREGATED CONCRETE. (for individual strengths, see Appendix A)

END CONDITION		AVERAGE STRENGTH(p.s.i.) AND RATIOS 4" CUBES		6" CUBES		6"Øx12" CYLINDER	
Both Ends Fixed	1st Mix	4695	1.000	4230	0.902	3232	0.690
	2nd Mix	4983	1.000	4789	0.960	3748	0.752
	3rd Mix	4490	1.000	3748	0.836	3151	0.703
	Average	4723	1.000	4258	0.904	3377	0.715
1 End Pinned 1 End Fixed	1st Mix	4562	0.974	3964	0.845	3196	0.681
	2nd Mix	4920	0.988	4626	0.928	3642	0.731
	3rd Mix	4100	0.914	3629	0.810	3028	0.675
	Average	4527	0.959	4073	0.863	3289	0.697
Both Ends Pinned	1st Mix	4438	0.945	4085	0.870	3299	0.703
	2nd Mix	4968	0.997	4464	0.896	3764	0.755
	3rd Mix	3952	0.881	3675	0.820	3166	0.707
	Average	4453	0.945	4075	0.863	3410	0.723

Note: For each specimen size and mix the value given above is the average of 4 specimens.

CONSTANT	RATIO OF VARIABLE
Both Ends Fixed	4" Cube: 6" Cube: Cylinder = 1.000:0.904:0.715
1 End Pinned 1 End Fixed	4" Cube: 6" Cube: Cylinder = 1.000:0.900:0.726
Both Ends Pinned	4" Cube: 6" Cube: Cylinder = 1.000:0.915:0.765
4" Cube	Both Ends Fixed: 1 Pinned, 1 Fixed, Both Ends Pinned =1.000:0.959:0.945
6" Cube	" " " " =1.000:0.957:0.957
Cylinder	" " " " =1.000:0.975:1.010

TABLE 9.9 STRENGTHS AND THEIR RATIOS AS A FUNCTION OF SPECIMEN SIZE AND METHOD OF LOADING - TEST SERIES 6 ON UNIFORM CONCRETE

(for individual strengths, see Appendix A)

END CONDITION		AVERAGE STRENGTH (p.s.i.) AND RATIOS					
		4" CUBES		6" CUBES		6"Øx12" CYLINDERS	
BOTH ENDS FIXED	1st Mix	5321	1.000	4274	0.803	4009	0.754
	2nd Mix	6074	1.000	5578	0.919	4558	0.751
	3rd Mix	5921	1.000	5541	0.935	4614	0.779
	Average	5772	1.000	5131	0.888	4397	0.762
1 END PINNED 1 END FIXED	1st Mix	4811	0.905	4011	0.754	3956	0.744
	2nd Mix	5916	0.974	5431	0.894	4370	0.720
	3rd Mix	5516	0.932	5342	0.902	4572	0.772
	Average	5414	0.938	4928	0.853	4300	0.745
BOTH ENDS PINNED	1st Mix	4886	0.918	3925	0.737	4195	0.788
	2nd Mix	5544	0.913	5432	0.894	4599	0.757
	3rd Mix	5391	0.909	5098	0.860	4439	0.744
	Average	5274	0.914	4818	0.835	4411	0.764

Note: For each specimen size and mix, the value given above is the average of 4 specimens.

CONSTANT	RATIO OF VARIABLE
Both Ends Fixed	4" Cube: 6" Cube: Cylinder = 1.000:0.888:0.761
1 End Pinned 1 End Fixed	" " " = 1.000:0.910:0.799
Both Ends Pinned	" " " = 1.000:0.918:0.837
4" Cube	Both Ends Fixed: 1 Pinned: 1 Fixed: Both Ends Pinned = 1.000:0.938:0.914
6" Cube	" " " = 1.000:0.961:0.940
Cylinder	" " " = 1.000:0.979:1.005

variation, more severe with a naturally segregating concrete, accounts for the higher cylinder:cube strength ratio in the relatively uniform concretes in Test Series 6. This was amplified by observation of the failed cylinder specimens in both Test Series 5 and 6; the former failed more consistently near the top, as cast.

The 6" cube strength, only about 90% of the 4" cube strength is seen to be considerably lower than that generally obtained; 96% as suggested by Newman[40]. This, as will be proven in Section 9.11, is due to machine restraint effect.

9.8 THE INFLUENCE OF METHOD OF LOADING AND MACHINE LATERAL STIFFNESS ON SPECIMEN STRENGTH AND MODE OF FAILURE (TEST SERIES 5 AND 6)

To determine if differences observed in Test Series 5 and 6 are significant, calculations in accordance with the method suggested by Wright[19] were used.

As stated above, the lowest cube strengths are obtained with pinned ends while fixed conditions produce the highest strength. Although the third method of loading produces intermediate results, the significance of differences from that obtained with pinned ends is not conclusive for either the 4" or 6" cubes. However, the probability of both sets of cubes being different for the two methods of loading is 98%, which is significantly conclusive. As the one end

TABLE 9.10 SIGNIFICANCE OF DIFFERENCES IN TEST SERIES 5 AND 6 - SEE TABLE 9.8 AND 9.9 AND APPENDIX A

CONSTANT	VARIABLES		AVERAGE DIFFERENCE (p.s.i.)	% DIFFERENCE	SIGNIFICANCE LEVEL OF DIFFERENCE
4" Cubes	Both Ends Fixed	1 end pinned, 1 end fixed	276	5.3%	0.2%
4" Cubes	Both Ends Pinned	"	114	2.3%	11%
6" Cubes	Both Ends Fixed	"	195	4.2%	0.1%
6" Cubes	Both Ends Pinned	"	54	1.2%	20%
Cylinders	Both Ends Fixed	"	93	2.4%	6%
Cylinders	Both Ends Pinned	"	116	3.0%	4%

pinned, one end fixed loading method is the only one to induce lateral forces (see Sections 5.3 and 6.2), it is concluded that the lateral stiffness of this testing machine, 3.0×10^6 lbs./inch, has a significant effect on the cube strength.

In Plate 5.1, which shows a cube failed under effectively pinned conditions, excessive failure can be seen on the weaker half of the specimen and, not only is there no visible compression failure on the opposite face but in this case, a horizontal tension crack has occurred.

Near failure , the failing face deformed so excessively that an internal hinge developed. The resulting rotation caused the compressive stresses on the strong face to reduce, eventually becoming tensile. Alternatively, with a cube failed under fixed end conditions, as shown in Plate 5.2, failure of the specimen occurs when all the elements on the weakest cross-section have exceeded their load carrying capacity, as demonstrated by an equal amount of failure on all faces of the specimen. The induced lateral force, with the third system of loading whereby one is pinned and the other fixed, produced inclined cracks which followed the lines of principal compressive stress. The resulting failure, although somewhat similar to that shown in Plate 5.1, indicated obvious signs of a shearing mechanism.

Cylinder specimens, in contrast to the cubes, showed comparatively little variation in strength as a function of the method of loading although the one end pinned, one end fixed method produced results about 2½% lower than with the other systems. Such relatively small variations would be expected as a result of the force system being coincident with the resultant of the uniformly deformed specimen; the specimens were carefully centred in every case. Yet, the failure patterns as shown in Plates 9.2, 9.3 and 9.4 differ markedly for the 3 systems of loading. Where one or both

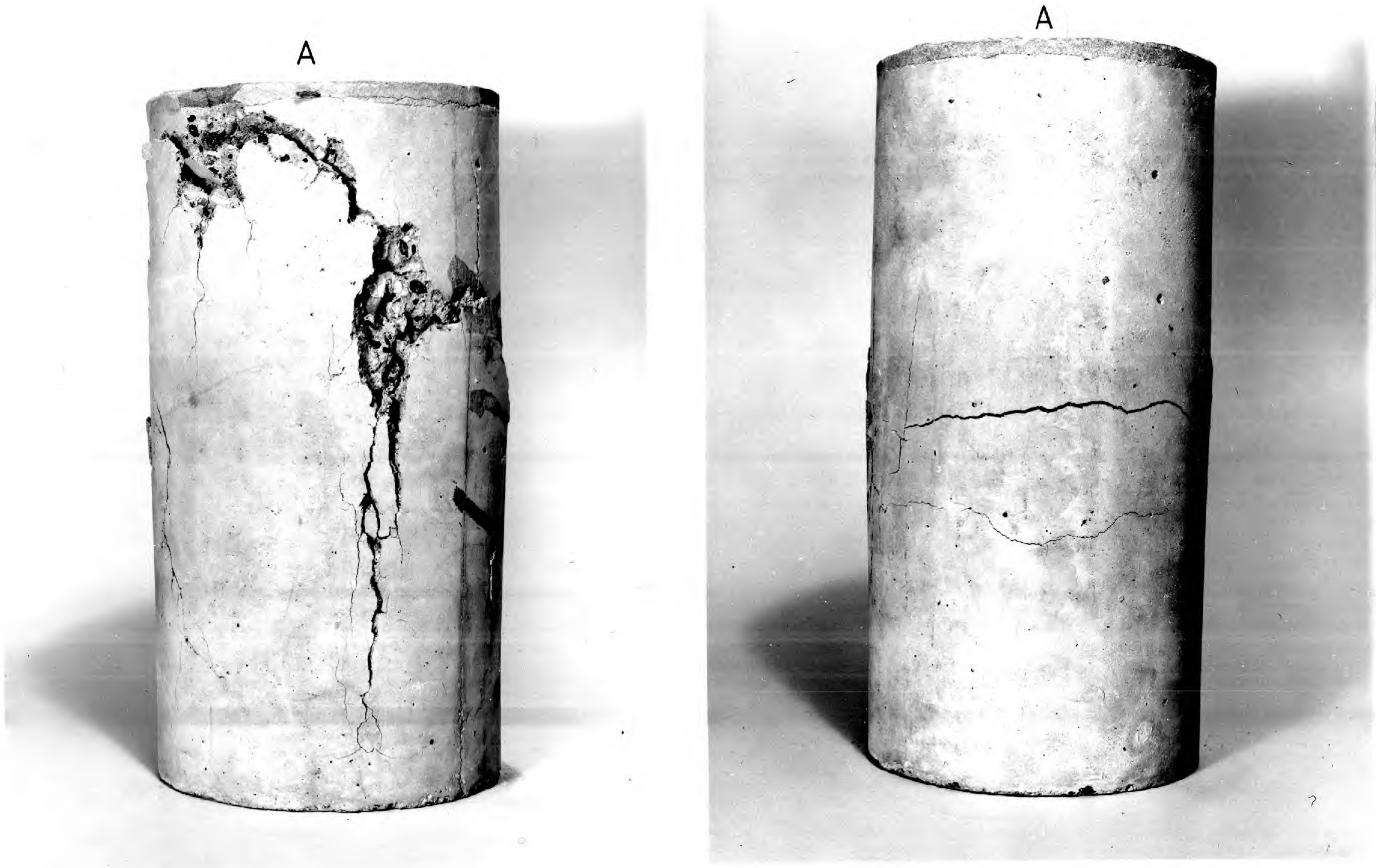

PLATE 9.2 Concrete cylinder loaded to failure with both ends effectively pinned

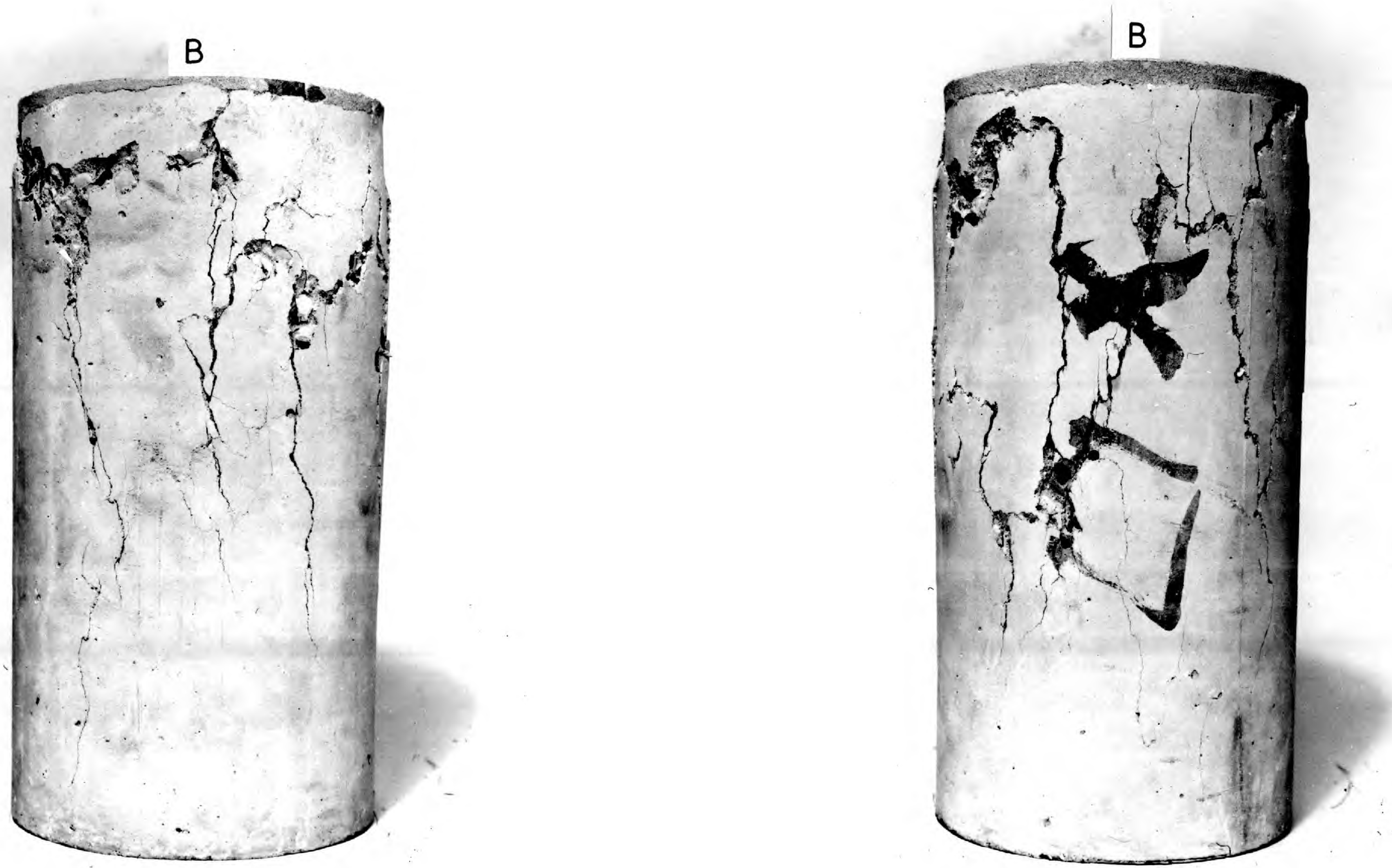

PLATE 9.3 Concrete cylinder loaded to failure with both ends effectively fixed

PLATE 9.4 Concrete cylinder loaded to failure
with one end pinned, one end fixed

ends are loaded with a well lubricated seating, obvious tilting occurred in every case in a random direction, thus producing further verification of the very low 'μ' values obtained in Chapter 8. With specimens loaded under effectively pinned or effectively fixed end conditions, similar failing modes to that obtained with the cubes occurred. Under a both ends effectively pinned condition, a tensile crack was again obtained on one side as shown in Plate 9.3. The shearing mechanism resulting from the induced lateral force in the third loading system was more pronounced with cylinders than with cubes as shown in Plate 9.4. This force, tending to displace the resultant at the fixed end, would account for the slightly lower strengths. (see bottom line in Table 9.9)

Some investigators have, in explaining the mode of uniaxial compression failure, suggested the existence of a shear mechanism on the phenomenological level while others have supported the vertical splitting theory.[6, 14,56-58] In standardizing a suitable compression test, a complete understanding of specimen movements is necessary. The former mechanism infers a lateral deformation in the specimen as well as a longitudinal deformation whereas the latter mechanism infers only a longitudinal deformation. Thus, a compression test for a material intrinsically weak in shear can only be conducted satisfactorily on a machine with both ends effectively pinned whereas a test on a material prone to splitting tensile failures can be conducted with both ends either pinned or fixed. The method whereby one end is pinned and the other is fixed is unsuitable in every case due to induced lateral forces, and the resulting complex distribution of stress (see Section 6.3).

For concrete specimens where lateral forces do not arise from the bending of the specimen i.e.; both ends pinned or fixed, it is readily observed in Plates 5.1, 5.2, 9.2 and 9.3 that the failures obtained are of a splitting tensile mechanism, thereby allowing the loading system of both ends pinned or fixed to be acceptable. However, due to such factors as specimen alignment, stability, spherical seatings, operator technique and ease of altering existing machines, it is concluded that, for control testing of concrete specimens, a system of loading whereby both ends are fixed is the most suitable. (see also Section 6.3.2)

9.9 THE INFLUENCE OF MACHINE LONGITUDINAL STIFFNESS ON SPECIMEN STRENGTH (TEST SERIES 7)

In Section 5.4.1, the influence of testing machine longitudinal stiffness was shown to have no effect on the ultimate strength of concrete specimens, except for a possible psychological effect on the operator with the softer machines. However, Glucklich,(63) in a theoretical and experimental investigation distinguished between the mechanism of failing in soft and hard testing machines. He described these two mechanisms as a "first crack mechanism" and a "mechanism of cracking", which produced brittle and ductile failures, respectively. In his experiments he showed that the strengths obtained in the soft machines were only about 30% of those obtained in the hard machines. However, his results are suspect due to a poor testing technique (see Section 5.1). His method of placing a railway carriage type spiral spring did not only reduce the longitudinal stiffness, but also altered the machine restraint, planeness of platen during loading, lateral stiffness, alignment of the specimen in relation to the resultant force and the spherical seating effect. His low strengths which showed a single vertical crack in the soft machine were probably caused by a punching action of the top platen similar to the splitting tensile test, rather than what he termed "an unlimited store of elastic energy".

To establish conclusively the theory of Section 5.4.1 a series of 4" cubes were tested in both hard and soft Grade A testing machines with longitudinal stiffness, 2×10^7 and 10×10^5 lbs/ins., respectively. To eliminate effects of all other machine charcteristics, the same platens and spherical seating were used, while lateral stiffness effects were eliminated by using an effectively locked seating.

The results, presented in Table 9.11 show a slightly higher strength with the soft machine which is opposite to Glucklich's results. Higher strengths of the magnitude obtained in this Test Series would be expected with the soft machine due to load application considerations. As explained in Section 9.4, the strain rate had to be constant in the specimen's elastic range due to the inability of the soft machine to apply a constant stress rate. The stress rate, although identical for the two machines in the initial stages of loading, becomes more rapid in the soft machine near failure as explained in Section 5.4.7.2.

Wright[22] also conducted a series of tests to examine the influence of longitudinal stiffness. Thirty-six 4" cubes were tested with a 120 ton proving ring placed between the cube and the lower platen and a further thirty six cubes with the ring replaced by a solid steel cylinder 6 ins. in diameter and the same height as the proving ring. The results obtained with the proving ring and steel cylinder agreed to within 1%.

It is concluded, on the basis of the experimental results obtained by Wright and the author as well as the theory of Section 5.4.1 that concrete strengths are independent of machine longitudinal stiffness.

Specimen failures in the soft machine, always highly explosive, caused obvious excessive wear of the platens while very little wear occurred in the stiffer machine. This emphasizes the importance of having stiff machines which

TABLE 9.11 INFLUENCE OF TESTING MACHINE LONGITUDINAL STIFFNESS ON ULTIMATE STRENGTH OF 4" CONCRETE CUBES - TEST SERIES 7

(for individual strengths see Appendix A)

	TESTING MACHINE AND LONGITUDINAL STIFFNESS	
	50 TON COMPRESSION $P/\Delta = 10 \times 10^5$ lbs/in.	500 TON COMPRESSION $P/\Delta = 2 \times 10^7$
Average Strength (p.s.i.)	4660	4605
Standard Deviation (p.s.i.)	218	187

largely eliminate the wear on components due to impact loadings arising from the instability occurring in the falling off portion of the load deformation curve (see Section 5.4.1)

9.10 THE INFLUENCE OF SEGREGATION AND METHOD OF LOADING ON CUBE STRENGTH (TEST SERIES 8)

With only a small amount of vibration, relatively unsegregated, uniform specimens, immune to the method of loading, might be expected. However, the results of Test Series 8, presented in Table 9.12, show that inadequate vibration can cause specimens to be even more sensitive to the method of loading than when adequately compacted. From observation of the failed cubes, the segregation was roughly the same. However, in the specimens receiving only 10 seconds vibration, the entrapped air had not been adequately removed, particularly from the upper half of the specimen.

TABLE 9.12 INFLUENCE OF DEGREE OF VIBRATION AND METHOD OF LOADING ON ULTIMATE STRENGTH OF 4" CUBES - TEST SERIES 8

(for individual strengths, see Appendix A)

LOADING SYSTEM / TOTAL VIBRATION	BOTH ENDS FIXED	1 END PINNED 1 END FIXED
10 secs	4714	4310
90 secs	5052	4808

The resulting increase in strength difference between the two halves of these cubes accounts for the greater difference in strength under the two methods of loading, 8.6% as compared to 4.8% with the well compacted specimens.

From the above it is concluded that the method of loading whereby both ends are fixed is less sensitive to vibration effects of the specimen than when one or both ends are pinned. However, these results emphasize, not only the importance of a proper testing technique, but also the importance of proper preparation of specimens, variations in strength in this test from both factors combined resulted in a maximum difference of 15%.

Inadequate care in preparing specimens has also been shown by Wagner[(64)] to result in low strengths.

9.11 THE INFLUENCE OF RESTRAINT OF THE LOADING PLATEN ON CUBE STRENGTH (TEST SERIES 9)

It was shown, in Section 5.4.5, that an increase in restraint of the loading platens would increase the cube strength by virtue of the increase in lateral applied forces. The results of Test Series 9, presented in Table 9.13 confirms this, although no significant difference in strength is detected between the 5" and 7" radii seatings.

With the 3" radius seating, the cube is larger in cross-section than the seating; 6" square as opposed to 4" diameter . The resulting upwards bending of the sides of the male section of the seating under load will result in a non-uniform deforming of the specimen as well as some sliding at the specimen-platen interface due to a reduction in applied frictional forces. With the 5" and 7" radii seatings, only slight flexural action of the corners with the former while none with the latter are possible due to the larger cross-section dimensions of the seating. Although a small difference would be predicted theoretically on the basis of the amount of expansion at the above interface, this is seen to have a negligible effect on the ultimate strength.

Although the above investigation has been limited to only one end of the specimen, the spherical seating end, the same influence would be obtained at the other end of the specimen, usually the ram end. It is concluded therefore,

TABLE 9.13 INFLUENCE OF THE RESTRAINT OF THE LOADING PLATENS ON ULTIMATE STRENGTH OF 6" CUBES - TEST SERIES 9 (for individual strengths, see Appendix A)

	SPHERICAL SEATING USED					
	3" RADIUS		5" RADIUS FULL CONTACT		7" RADIUS	
	Average Strength	Standard Deviation	Average Strength	Standard Deviation	Average Strength	Standard Deviation
1st Mix	4774	153	5299	275	5259	286
2nd Mix	6408	169	6721	177	6759	161
3rd Mix	-	-	8092	187	7940	209

that, for cube testing, adequate machine restraint is obtained only if the entire spherical seating and ram cross-section dimensions are at least as large as the cube cross-section dimensions. Variations in machine cross-section dimensions above this limit have no significant effect on the cube strength.

9.12 CONCLUSIONS

On the basis of the investigation as presented in this chapter, the following conclusions can be made.

1. All the factors which influence the spherical seating behaviour (area and type of contact, surface finish of interface, radius of seating, type of lubricant and load) can have a highly significant influence on the method of loading and failure strengths of specimens.

2. Concrete strengths are highly sensitive to misalignment of the specimen when tested with well lubricated spherical seatings, but on the other hand, are immune when the seating is fixed.

3. While the standard deviation is unchanged by the method of test as long as great care is employed in placing the specimen accurately, it is highly sensitive to inconsistency in misalignment with a well lubricated seating.

4. The maximum strength of a cube tested with a well lubricated spherical seating is less than that when tested with a locked seating.

5. The cube strength : cylinder strength ratio is very dependent on the method of test and type of concrete, varying generally from 70% to 84%.

6. The reduction in cube strength from effectively fixed to pinned loading conditions is about 8%.

7. Cylinder strengths are essentially identical under effectively pinned or fixed loading conditions provided that the specimens are in every case accurately centred.

8. The lateral stiffness can, in some testing machines, have a significant effect on the cube and cylinder strength as well as the failure mode of the specimen.

9. The intrinsic failure mechanism of concrete in uniaxial compression is a splitting tensile mode. Apparent

shear mechanisms which occur on specimens in some machines are due to induced lateral forces under a system of loading whereby one end rotates whilst the other is fixed.

10. For control testing of concrete specimens in uniaxial compression, the most suitable method of test is one where both ends of the specimen are effectively fixed.

11. The machine longitudinal stiffness has no effect on the ultimate strength of concrete specimens.

12. Longitudinally soft machines produce greater wear of components than stiff machines due to impact loadings in the falling off portion of the load deformation curve.

13. The method of loading where both ends of the specimen are effectively fixed is less sensitive than the other two methods to insufficient compaction of cubes.

14. For cube testing, adequate restraint of the loading platens is obrained only if the entire spherical seating and ram cross-section dimesnions are, at least, as large as the cube cross-section dimensions. Variations in machine cross-section dimensions above this limit have no significant effect on the cube strength.

CHAPTER 10

CONCLUSIONS, RECOMMENDATIONS, SPECIFICATIONS AND FUTURE RESEARCH FROM THE INVESTIGATION OF PARTS I AND II

10.1 CONCLUSIONS

Although conclusions have been given at the ends of previous chapters, it is useful to correlate the more important conclusions with an aim of producing definite recommendations and specifications for testing machines.

Longitudinal stiffness:

The longitudinal stiffness of testing machines has been shown both theoretically (Section 5.4.1) and experimentally (Section 9.9) to have no direct influence on the ultimate strength of concrete specimens. However, due to the greater possibility of explosive failures with the softer machines which would result in excessive wear of machine components and a psychological effect on the operator, the stiffer machines are more suitable, particularly for control testing.

Stability:

When both ends of short specimens such as cubes are effectively pinned, buckling of the machine may be a problem, particularly with long, laterally flexible machines. With tension machines, not only is buckling out of the plane of the frame possible with specimens effectively longer than the machine, but, in addition, both torsional buckling and column buckling are possible with any length of specimen, (Section 5.4.2).

Lateral stiffness:

The lateral stiffness of testing machines may have a significant effect on the ultimate strength and mode of failure of specimens tested with a loading system whereby one end if fixed whilst the other is pinned (Section 9.8)

Spherical Seating Behaviour:

Factors which influence the behaviour of a spherical seating under load are its radius, the area and type of contact at the seating interface, the machine finish of the interface, the type of lubricant and the applied load. Seatings can be effectively locked under load due to a large 'μR' value (product of the coefficient of friction at the interface and the seating radius) or behave in a pinned manner due to a virtually zero 'μR' value or exhibit behaviours between these extremes (Chapter 8).

All the factors which influence the behaviour of spherical seatings can have a significant effect on the ultimate strength and mode of failure of concrete specimens. (Section 9.5).

Platen Restraint Effect:

The platen restraint effect has a significant influence on the cube strength if the cross-section dimensions of any portion of the spherical seating or ram are less than those of the cube. Above this limit, machine restraint has no significant influence. (Section 9.11)

Intermediary Platens:

The thickness of intermediary platens positioned between the cube specimen and machine bearing blocks has no apparent influence on its ultimate strength (Section 7.5).

Section Misalignment:

The stress distribution induced in specimen and its ultimate strength has been proven theoretically (Section 6.3.1) and experimentally (Section 9.6) to be very sensitive to small misalignment in the machine if either one or both ends of the specimen are effectively pinned.

Concrete strength:

The strengths of cubes when either one or both ends are pinned will be less than if both ends are fixed; the difference between both ends pinned and both ends fixed with accurate aligning being about 7% (Section 9.7).

The strengths of cylinders with proper centring are essentially identical when tested with both ends either pinned or fixed. (Section 9.7)

Mode of failure:

The mode of failure of concrete in uniaxial compression is caused by a tensile splitting mechanism at right angles to the direction of loading; apparent shear mechanisms observed in some specimens are the result of an induced lateral force. (Section 9.8).

Ram Effect:

Due to an increase in frictional forces at the ram-cylinder interface, off-centre loadings can produce apparent increased strengths. (Section 4.3)

Machine components:

Testing machines which are sloppy or loose fitting may produce unreliable strength results as a result of non-repeatability of load application and inconsistent machine influence (Section 7.3.4).

End loading conditions:

A testing machine having an unlubricated spherical seating is more suitable for control testing of concrete than one having a well-lubricated seating, i.e.; where specimens are loaded with both ends being effectively fixed. (Section 9.8)

Intrinsic Failure Mode:

In order to determine the basic failure mode of material specimens and their strengths under uniaxial testing, the only satisfactory method of test is one whereby both ends of the specimen are effectively pinned as both ends of the specimen must be able to rotate for a shearing mechanism to occur (Section 9.8).

10.2 RECOMMENDATIONS FOR TESTING MACHINES

Longitudinal stiffness:

The longitudinal stiffness of compression testing machines should be large enough to make explosive failures unlikely. As the falling portion of the load deformation curve for concrete in uniaxial compression has been shown by Turner and Barnard[34,35] to be about one quarter as steep as the initial rising portion, a longitudinal stiffness of about 10×10^6 lbs/in. would be required for 6" cubes. This was obtained from the relationship $\frac{P}{\delta} = \frac{AE}{L}$ where $\frac{P}{\delta}$ denotes the longitudinal stiffness, A and L represent the cross-sectional area and length of the specimen, respectively and E, the modulus of elasticity, is assumed to be equal to 6×10^6 p.s.i. for the initial rising portion of the stress-strain curve for concrete. The above value is of the right order as only slight instability occurred (see Section 5.4.1) on a machine having a longitudinal stiffness of 2×10^7 lbs/in. (see Section 9.9).

Lateral stiffness:

Machines used for control testing of concrete specimens are theoretically immune to the lateral stiffness characteristic if both ends of the specimen are fixed. However, machines which have loose fitting components are prone to random results arising from non-repeatable machine behaviour. Therefore, it is recommended that machines be manufactured with close tolerances, and have a lateral stiffness of at least 5×10^4 to 10×10^4 lbs/in.

End loading Conditions:

To obtain a fixed end condition in the spherical seating, the most suitable method is to remove the lubricant from the spherical seating interface. However, due to possible corrosion effects, a very light oil applied to the interface is advisable. However, if tilting still occurs which is possible with a large, high quality finish seating, then effective fixity can be obtained only with no lubricant.

Size of spherical seating:

Flexural action of the male section of the spherical seating which is particularly critical for cube strengths, can be eliminated by maintaining its cross-section dimensions at least as large as those of the specimen. That is, for the testing of 6" cubes, the entire body of the seating should be at least 6" square or 8.5" in diameter. This suggests a minimum radius of 5".

Intermediary platen:

Although the current British Standard 1881[9] specifies that the centre of the sphere of the seating be at the centre of the specimen bearing face, the insertion of a platen between the bearing face and the specimen has little or no influence on the cube strength. As it is advantageous in cube testing to employ such platens (Section 7.5), their use is recommended, with the bottom one being accurately dowelled to the lower machine bearing block. Also, they should be square, of the same cross-section dimensions as the specimen being tested, ½" to 1" thick and both sides finished plane in accordance with the requirements of British Standard 1881. For the testing of cylinders, the length of one side of the platen should be equal to the diameter of the cylinder.

Rate of loading:

For the loading of specimens, a fine control valve capable of producing a uniform loading rate should be used. The capacity of the loading apparatus should be sufficient to apply a minimum deforming rate of 0.5 in./min. to the specimen. The use of a pacing device on a large well-marked and accurate load indicating panel is recommended for elimination of operator technique.

Ram effect:

The research on ram effect, limited here to investigating variations in indicated load with misalignment of the effective resultant, (Section 4.3) has shown that only slight errors would be expected with the better rams. However, as strength results should always be relatively immune to small lateral movements of the specimen in the machine, a series of tests is recommended as follows for every compression machine to investigate variations arising from ram behaviour, spherical seating behaviour and machine restraint. Thirty-six medium strength 6" cubes cast under well controlled laboratory conditions, (6000 ± 1000 p.s.i. at 28 day age), should be tested to failure at the rate of 2000 p.s.i./min.,(9) at 28 day age with 3 groups of 12 being tested at each of 3 conditions of displacement. The first group would be loaded axially (zero displacement) while the other two groups of 12 would be loaded by displacing them $\frac{3}{8}$" laterally in two mutually opposite directions. If the average strength of any of the 3 groups of 12 deviates by more than 2% from the average strength of the 36 cubes, the machine shall be considered unacceptable for cube testing.

A summary of all these conclusions and recommendations suggests that the ideal cube-crushing machine is a short stiff machine with at least 3 columns which are encastré with the cross-heads at both ends, manufactured with close tolerances, containing a large spherical seating which does not tilt under load during testing and which has a long, large diameter, well-machined ram. In addition, the platens and machine bearing faces should be plane in accordance with British Standard 1881 with the lower intermediary specimen platen accurately dowelled axially to the lower machine bearing block. The loading system should be well designed and manufactured to ensure good load control while the load dial should be highly accurate, preferably within ± 1.0%[8].

Testing machines used in research for analysing the intrinsic failure mode of a specimen and its corresponding strength are conducted satisfactorily only when both ends of the specimen are effectively pinned. This principle applies not only to uniaxial, but also to biaxial and triaxial loading systems. For, it must be appreciated that material specimens which fail in accordance with a 'splitting tensile' or 'cleavage' mechanism in uniaxial compression when an effectively fixed loading system is satisfactory, may alter their failure mode to a shearing mechanism in biaxial or triaxial stress states when an effectively fixed system is no longer satisfactory.

10.3 SPECIFICATIONS

The research in Parts I and II, part of which was generously supported by the Department of Scientific and Industrial Research, has been conducted to improve existing specifications on the requirements of a suitable testing machine and its calibration for uniaxial compression testing of concrete specimens. The following alterations are suggested to the requirements of testing machines in Section 58, British Standard 1881 : 1952.

"The testing machine shall conform to the following requirements.

(1) The testing machine shall be in good alignment, free from loose fitting components and stiff longitudinally and laterally. The machine columns shall be encastré with both the upper and lower cross-heads.

(2) The male section of the spherical seating, usually at the upper end of the specimen, shall at all times be maintained in full contact in its seating. It shall be tilted freely through small angles in any direction during the initial setting up procedure, but shall be effectively prevented from any further tilting during the loading of the specimen.

(3) The centre of rotation of the male section of the spherical seating shall be located at the centre of its bearing face. Allowable tolerances are $\pm \frac{1}{8}$" in each of the horizontal and vertical directions.

(4) For hydraulic machines, the ram shall have a minimum diameter of 8.5 ins. for the testing of 6" cubes and 6" for the testing of 4" cubes and 6" Ø x 12" long cylinders. During loading, the distance between the bottom of the specimen and the top of the ram-cylinder interface shall not be less than 2".

(5) Square platens, having the same cross-sectional dimensions as the specimen being tested and having a thickness of $\frac{1}{2}$" to 1" shall be positioned between the specimen and the testing machine bearing faces. Both bearing surfaces of each platen, when new, shall not depart from a plane by more than 0.0005 in. at any point and they shall be maintained within a permissible variation limit of 0.002 in. The testing machine bearing faces, likewise, shall be manufactured and maintained within the above limits. The lower platen shall be accurately dowelled axially to the lower machine bearing block.

(6) The loading system, capable of applying load uniformly and smoothly, shall be able to deform the specimen at a rate of not less than 0.5 in/min. at all load stages.

(7) As regards accuracy, the machine shall comply with the requirements of Grade A of British Standard 1610 Methods for the Load

Verification of Testing Machines'. In addition, it shall conform to the following requirement, conducted once every four years. On the basis of 36-6" cubes tested at 2000 p.s.i. /min. at 28 day age (average 28 day strength to be 6000 ± 1000 p.s.i.), the average strength of any group of 12, tested either axially or $\frac{3}{8}$" off-centre in one of two directions mutually opposite, shall not deviate from the average of the 36 specimens by more than 2%."

In addition alterations in specifications to Section 59(c) are suggested as follows.

Delete the sentence "The maximum load applied to the cube shall then be recorded and the appearance of the concrete and any unusual features in the type of failure shall be noted" and replace with "The maximum load applied to the cube shall then be recorded and the appearance of the concrete shall be noted. If the failure on any exposed face is more pronounced than on any other exposed face, the result shall be considered suspect. If specimens fail consistently on one side, the machine shall be considered suspect and shall be checked to ensure that it is complying with the requirements of testing machines under Section 58".

10.4 FUTURE RESEARCH

In light of the investigation as presented in Parts I and II, the following areas of useful research are suggested.

(1) Load calibration devices are influenced by small off-centre loadings and shearing actions. Much research, aimed at rendering them immune to such loading effects, is necessary. This can be conducted most effectively under the pinned end conditions of loading.

(2) The ram behaviour in testing machines has received very little attention. As more specialized machines are being continually required for research investigations, an examination aimed at establishing suitable dimensional limits as well as clearances and machining tolerances would provide useful information.

(3) In order to differentiate between good lubricants on a spherical seating (see Figure 8.7) it is necessary to employ a technique more sensitive to small changes in applied moment than that used in Chapter 8. A double spherical seating such as that shown in Figure 10.1 is suggested.

The load, P, would be applied by a standard testing machine while the force, Q, would be applied by a subsidiary machine very sensitive and accurate to low loads, measured by dead weights or a proving ring.

By taking moments about the point, O, thereby eliminating the moment arm of the applied force, P, and assuming that the frictional forces at the two spherical seating interfaces are equal, then

$$QL = 2FR \quad \ldots\ 10.1$$

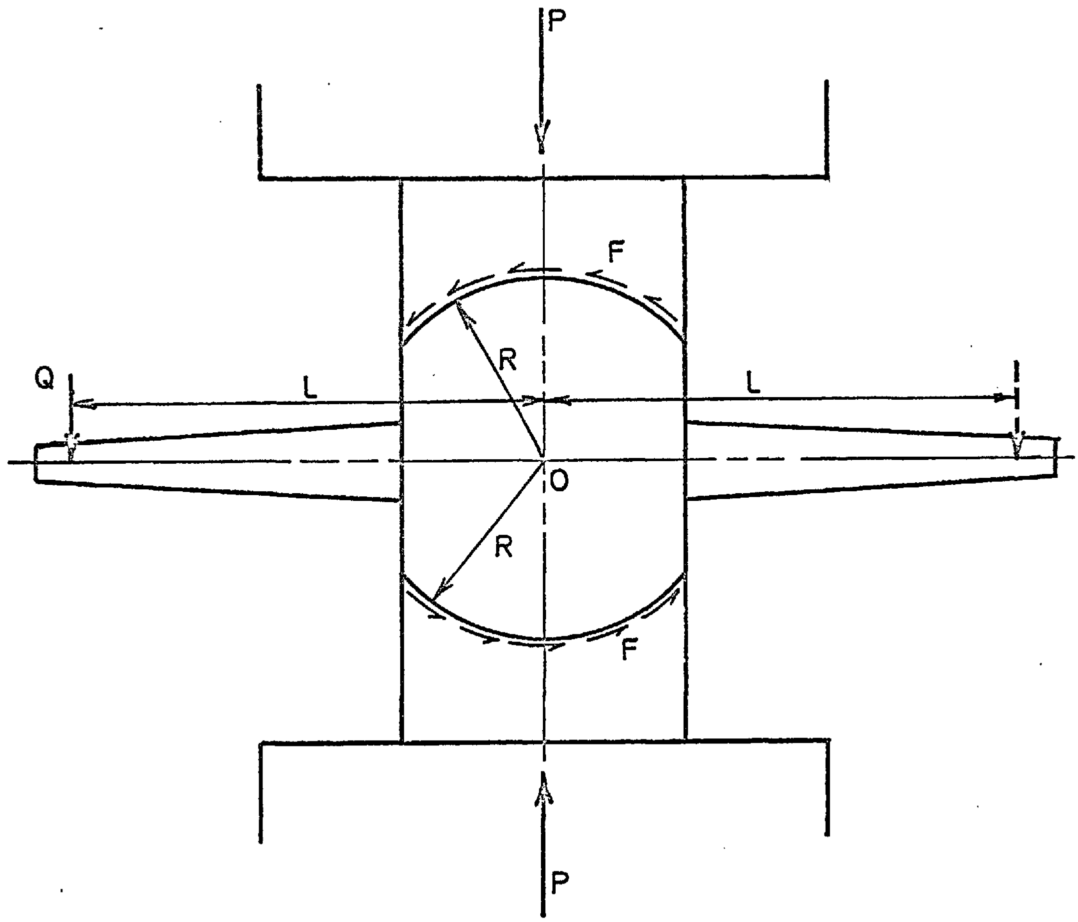

FIG. 10.1 SUGGESTED LOADING METHOD FOR COEFFICIENT OF FRICTION TESTS FOR DIFFERENTIATING BETWEEN GOOD LUBRICANTS

But $\mu = \frac{F}{P}$ ... 10.2

$\therefore \mu = \frac{QL}{2PR}$ ... 10.3

It will be appreciated that, as each of the values on the right hand side of equation 10.3 can be accurately measured, the value of μ will also be very accurate. By conducting the test twice, that is, by loading the rigid arms at the points A and B, the true coefficient of friction would be obtained as an average of that obtained from loading at the individual points, A and B.

PART III

THE BEHAVIOUR OF CONCRETE IN BIAXIAL TENSION AND TENSION-COMPRESSION

CHAPTER 11

REVIEW OF PAST RESEARCH

11.1 INTRODUCTION

Although a large proportion of concrete research has been directed at establishing properties of concrete in uniaxial compression, only a very limited number of investigations have been performed in biaxial states of stress. Yet, such structures as bridge decks, floor and roof slabs, shells, and prestressed beams are all subjected to biaxial stress systems.

A complete understanding of the deformation and strength properties of concrete, as well as its mechanism of fracture and failure, requires a thorough examination of concrete subjected to various combinations of stress based on reliable testing techniques. Such an investigation has been launched at Imperial College with this thesis forming a logical sequence to the results of previous investigators. Lachance[1] and Ward[2] developed uniaxial compression and tension tests, respectively, while Robinson[6] and Vile[7] have each subsequently worked on biaxial compression. The investigation as presented herein will be the result of an examination into the other two biaxial stress systems; biaxial tension and tension-compression.

This chapter describes the investigations conducted by previous researchers along with a critical appraisal of their individual testing techniques. After determining what characteristic concrete properties require examination, a selection of the most suitable test method is made with due consideration of all known methods of achieving both biaxial tension and tension-compression stress states.

11.2 HISTORY OF BIAXIAL TENSION AND TENSION COMPRESSION TESTING

Biaxial stress systems with at least one stress tension have been created with the following test methods.

(1) Plate tests

(2) Hollow cylinders: hoop tension and axial compression.

(3) Hollow cylinders: torsion and axial compression

(4) Direct tension and compression

(5) Flexural tension and compression

(6) Indirect tension test.

It will be apparent from the following discussion that, of the above methods, only the first can induce both biaxial tension and tension-compression. The last five concern biaxial tension-compression stress states only. A brief discussion of the research conducted on concrete specimens by each of the above methods is now presented.

11.2.1 Plate Tests

In obtaining a state of biaxial tension-compression, Blakey and Beresford[65,66] used square slabs loaded on two diagonally opposite corners while being supported on the other two. Under this loading system, principal compression and tension stresses of equal magnitude are obtained in any plane parallel to the surface of the slab. (see Timoshenko and Woinowsky-Krieger[67]). Due to a state of flexure, the stresses vary from a zero value at the neutral axis to a maximum at the outside fibres.

Although the theory requires that slabs be loaded at the corners, this was considered for practical reasons to be impossible. The loading and support points were consequently displaced a few inches in from the corners, but the theory for corner loading was still assumed as being valid. (see Figure 11.1)

For biaxial tension stress states, circular discs were loaded with a central annulus while being supported by a ring around the edge. The resulting loading produces a state of pure moment in the area within the central annulus with biaxial tension of equal magnitude on the bottom face and likewise biaxial compression on the top[67] (see Figure 11.2)

In the support of the disc, the investigators used firstly a laminated wooden ring. After considering this undesirable, a bicycle racing tyre held in position by a wooden disc was selected. Unfortunately, no detailed description of their central loading ring is presented.

The test methods used by Blakey and Beresford were adopted by Imperial College in a series of tests to determine the influence of mix proportions on biaxial strengths[68].

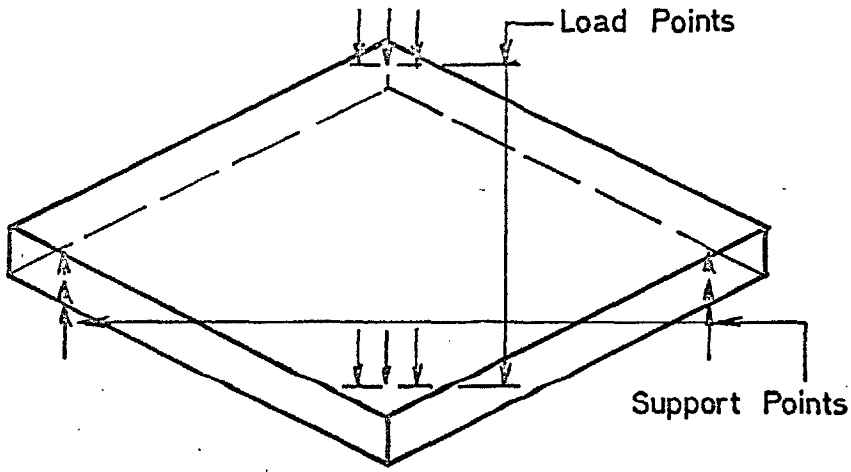

FIG. 11.1 SLAB TEST AS PERFORMED BY BLAKEY AND BERESFORD

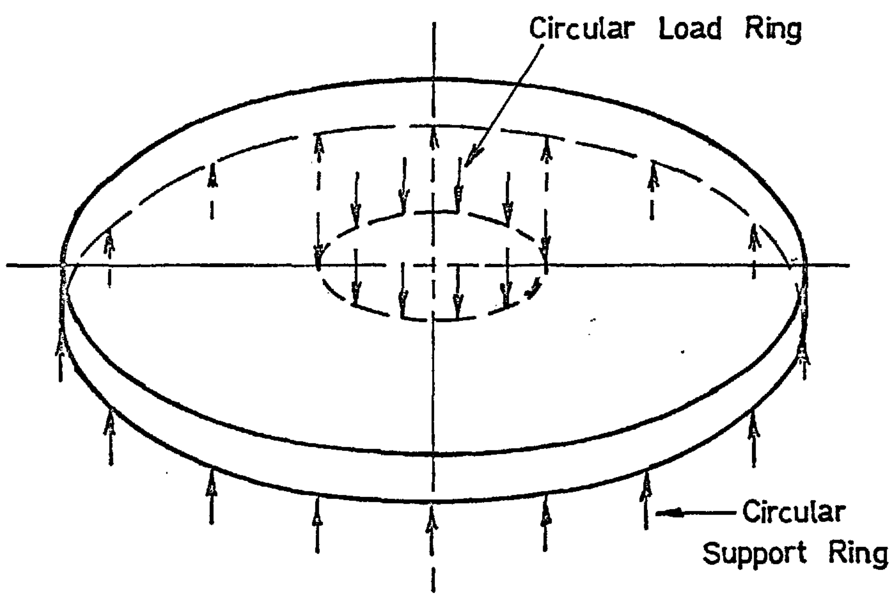

FIG. 11.2 DISC TEST AS PERFORMED BY BLAKEY AND BERESFORD

The same testing techniques were adopted in principle. 21" square slabs were loaded and supported by rollers at approximately 3" in from the corners. (see **Figure** 11.1). With testing of circular discs, a bicycle racing tyre with a support contact diameter of $25\frac{1}{4}$" was used to support a 30" diameter disc. The inner loading annulus was a $6\frac{1}{8}$" diameter knife edge ring. (see **Figure** 11.2). The plates were, in most cases, 4" thick.

<u>11.2.2 Hollow Cylinders; Hoop Tension and Axial Compression</u>

McHenry and Karni,(69) carried out a limited investigation on 24" long hollow cylinders with internal diameter, 10" and external diameter, 14". Loading was applied by an internal fluid pressure, thereby subjecting the cylinder to a hoop tension stress. With the specimen and internal pressure bags positioned in a testing machine, axial compression could be simultaneously applied. (see Figure 11.3)

With the above loading, the concrete was assumed as being in a uniform state of biaxial tension-compression, although recognition was given to the fact that the tensile strain varied linearly across any section, being proportional to the distance from the cylinder axis. The average tensile stress was assumed equal to that at the outer face. In addition, the concrete on the inner face is subjected to compression in the third principal direction, but reduces to zero at the exposed face. This value, always relatively

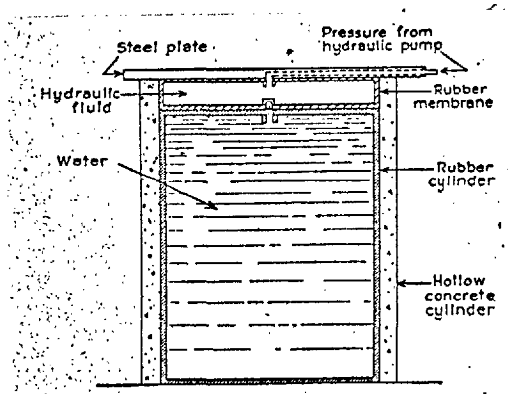

Fig. 1—Method of applying the internal hydrostatic pressure

FIGURE 11.3 Test method used by McHenry and Karni; hoop tension and axial compression.

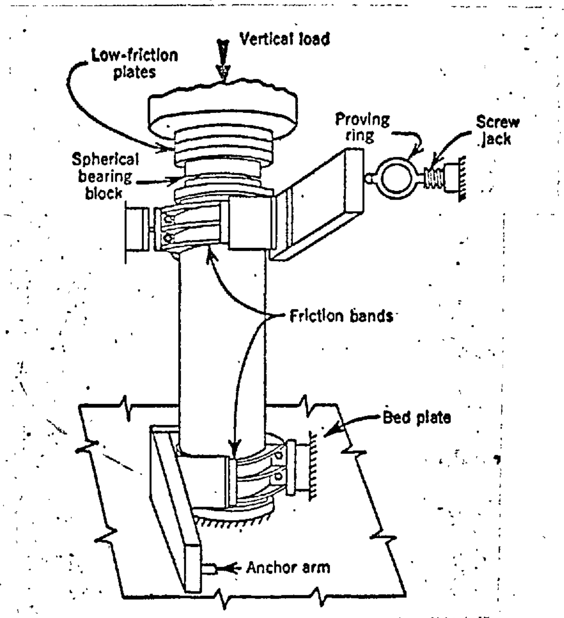

FIGURE 11.4 Test method used by Bresler and Pister; torsion and axial compression

small, was found to have negligible influence when taken into account in the calculations.

11.2.3 Hollow Cylinders: Torsion and Axial Compression

By subjecting hollow cylinders to a combination of torsion and axial compression, firstly, Bresler and Pister[70, 71] and subsequently, Tsuboi and Suenaga[72] were able to obtain failure strengths under numerous combinations of principal tension and compression stress. The 30" long specimens with internal diameter 6" and external diameter, 9" were loaded in direct compression by a standard testing machine while simultaneously, a lateral compression machine applied torsion (see Figure 11.4). As in the case of McHenry and Karni's analyses, these investigators assumed a uniform compression-tension stress state although the twisting strain will be proportional to the distance from the cylinder axis. Again, the average stresses were assumed equal to those on the outer face.

In more recent work at the Indian Institute of Science[73], a pure torsion test on solid cylinders, 16" long and 4" diameter was assumed to induce equal tension and compression principal stresses with the principal planes inclined at 45° to the longitudinal axis. The ultimate stresses obtained with this specimen were combined with ultimate stresses of other tests such as the splitting cylinder test in an attempt to determine the criterion of failure in biaxial tension-compression (see Section 11.2.6).

Failure stresses, propagating from the outer fibres, in the torsion tests above, were assumed to comply with the requirements of elastic theory; that is, no non-linear behaviour occurring prior to failure.

11.2.4 Direct Tension and Compression

Nishizawa[74] used an Amsler compression machine and a horizontal tension machine to subject the central portion of 15 x 15 x 50 cm. prisms to biaxial tension-compression. (see Figure 11.5). The tensile force was achieved by loading 10 bolts embedded in the prism at each end whereas the compression force, distributed over a 15 x 15 cm. area at the mid-section, was applied in the conventional manner.

In his analysis, Nishizawa assumed the central 15 cm. cube to be in a state of uniform biaxial tension-compression with the end portions of the prism being in a state of uniaxial tension.

11.2.5 Flexural Tension and Direct Compression

Smith,[75] in a very brief series of tests, applied compression by a strip loading to the sides of a flexural beam which was simultaneously loaded in flexure by a standard four point loading. (see Figure 11.6)

In the analysis, Smith assumed the tensile strength to be equal to the modulus of rupture while the compressive

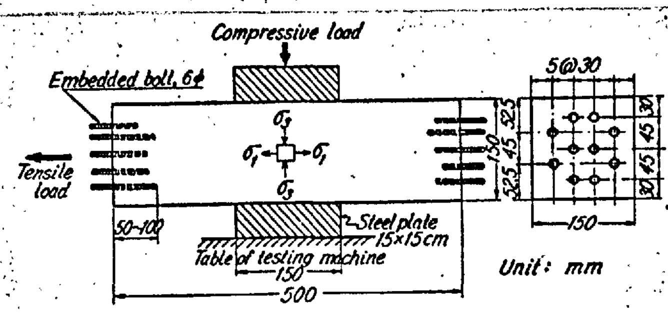

Fig. 1. Concrete specimen.

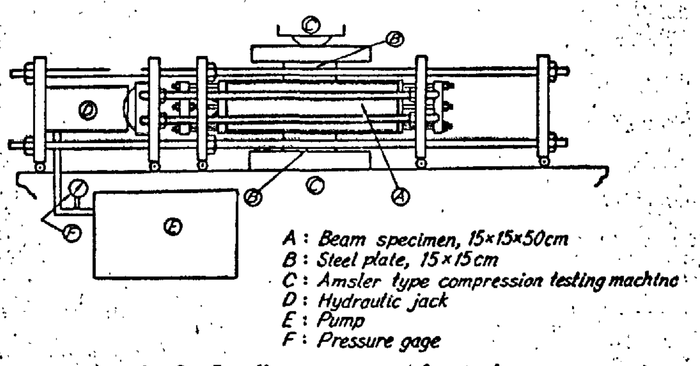

Fig. 2. Loading apparatus, front view.

FIGURE 11.5 Test method used by Nishizawa; direct tension and compression

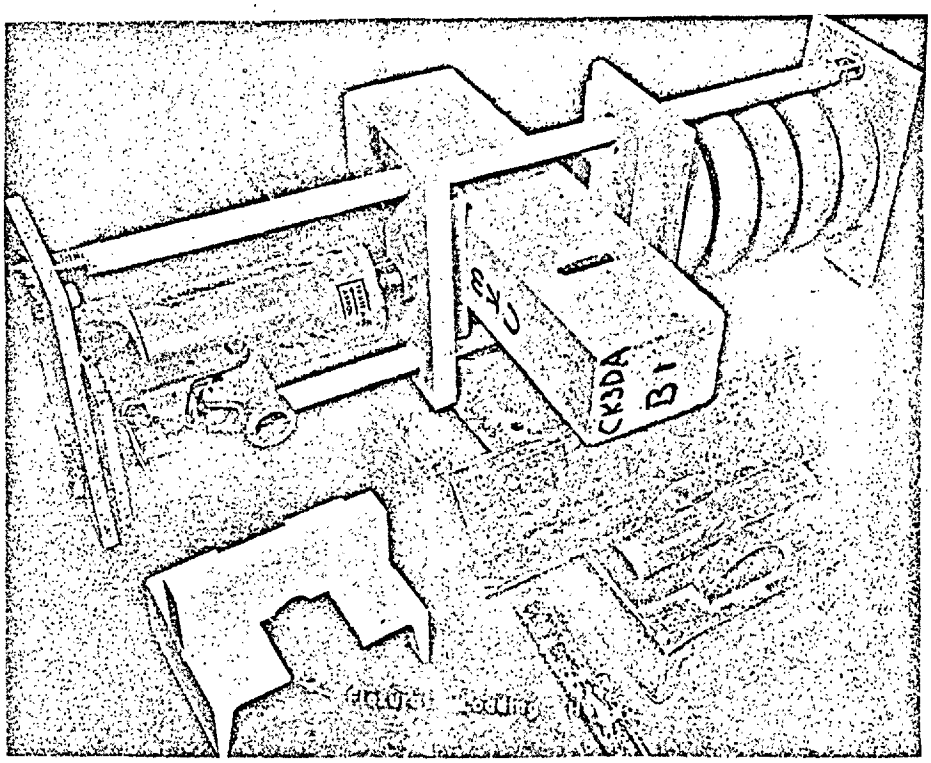

FIGURE 11.6 Test method used by Smith; flexural tension and direct compression.

strength was computed on the basis of the area of the loading strip in contact with the beam. The concrete volume between the compression pads was therefore assumed to be in a uniform state of compression and flexure whereas, outside this bound, the stress sytem was flexure only.

11.2.6 Indirect Tension Test

This test is performed by loading a solid cylinder in compression through line contacts along its full length on opposite ends of a diameter. The resulting splitting of the specimen is brought about by tension stresses perpendicular to the failure plane. Although this test is now extensively used as a measure of the uniaxial tensile strength of concrete,[2, 76-78] the critical section is actually in a state of biaxial compression-tension with the compression stress being three times the tensile stress at the centre. This ratio gradually decreases towards the end of the critical diameter.

Sundara et al[73] combined the results of pure torsion, flexural and compression tests with those of the indirect tension test to obtain a surface of failure, i.e., the theoretical bound in stress space within which any combination of principal stresses will not produce failure, over the biaxial tension-compression range. Wright,[79] Halabi[80] and Mitchell[81] have all conducted extensive investigations with the former two attempting direct correlations with uniaxial tension results. Ward,[2] in a very recent investigation, concluded that, for normal concretes, the uniaxial tension strength is 2% higher than the indirect tensile strength.

Investigations conducted on splitting cubes (2, 73, 82) have shown good correlation with cylinder splitting strengths where the dimensions are similar; i.e. cube side equal to cylinder diameter. A further refinement has been conducted by Durelli et al (83) where the specimen cross-section shape has taken the form of the Greek letter theta, θ. A uniform tensile stress, induced in the central bar from compression at right angles to it suffers in that stresses have to be computed from measured deflections.

11.3 EXAMINATION OF TESTING TECHNIQUES EMPLOYED

Failure results of the above investigations differed widely. Nevertheless, the results of some of the papers aroused extensive interest (84-86) with particular emphasis on correlating data for determining an applicable failure criterion. Although it was appreciated that such factors as mix proportions, specimen size, loading rate, moisture conditions, age of testing and direction of loading accounted for some of the observed discrepancies, an investigation to verify the assumed stress distribution was not performed by any of the authors. Furthermore, as no strain readings were taken by the majority of the investigators, the failure criteria are usually based on the short term ultimate strength of the specimen as determined by a constant stress rate.

11.3.1 Plate Tests

As the square plates tested by Blakey and Beresford[65,66] and Newman[68] had the load and support points located in from the corners and not at the corners as stated in the theoretical derivation, there was reason to suggest that the stress pattern was not uniform. Evidence of this was provided by the generally high results as compared to those of other researchers as well as failures occurring consistently at or near a diagonal. Confirmation of this suspicion is provided in Section 14.2.3 where it is shown that the test methods used were highly erroneous.

Blakey and Beresford indicated that the stress level at which cracks occurred in biaxial tension, as a result of their disc test, was 50% of that in uniaxial tension. Yet, due to a very large scatter in strain readings and no verification that the stress pattern conformed to theoretical requirements, this value must be treated with suspicion.

In the disc tests conducted at Imperial College, the ultimate stress was calculated from formulae based on elastic analysis[67]. Not only is this erroneous due to the non linear stress strain curve for concrete in tension[2], but of more importance, ultimate collapse of the slab occurs somewhat after the failing stress in the most highly stressed portion within the annular loading ring has been reached. Consequently, after this section has begun to fail, an increasing proportion of the load will be distributed to the outer section until collapse of the slab occurs.

The test method was, likewise, in error. Not only did the annular knife edge loading ring provide a restraint effect thereby preventing free contraction of the upper surface of the disc specimen, but also the $6\frac{1}{8}$" diameter to 4" thickness ratio was too small. Consequently, only a minute portion of the slab, if any, would be subjected to the desired biaxial tension stress.

As will be seen in Chapter 15, the above loading methods are highly erroneous and the attainment of a satisfactory testing technique is, in fact, a very difficult task.

11.3.2 Hollow Cylinders: Hoop Tension and Axial Compression

In their analysis, McHenry and Karni[(69)] obtained a rather peculiar S-shaped graphical relationship for their envelopes of failure with sharp curvatures near the states of both uniaxial compression and tension stress. However, a close examination of their testing technique shows that the state of stress in the specimen was considerably different from that assumed due to machine effects.

Their 24" long cylinders with 14" external diameter had a small length: diameter ratio (see Newman[(40)] and Section 5.4.5). Consequently, the effect of machine restraint would have a significant influence on the stress pattern throughout the entire height of the specimen. The sharp increase in tension strength near the uniaxial tension end is accounted for by the omittance of machine restraint under fluid pressure only thereby resulting in uniform hoop tension for the entire height. Similarly, Brice[84] has suggested that the sharp curvature at the uniaxial compression stress state is also due to these parasitic machine restraints.

11.3.3 Hollow Cylinders: Torsion and Compression

The machine restraint influence, arising from using too short specimens, was wisely allowed for in the investigations conducted by Bresler and Pister[70,71] and Tsuboi and Suenega.[72] However, their pure torsion test produced, on the basis of the mean radius, a variation of 40% in shear strain across the thickness of the hollow cylinder.

The resulting induced tension and compression stresses will therefore also vary by 40% in the elastic range. With a uniform axial compressive stress superimposed, the percentage variation of compressive stress across the thickness will reduce as the ratio of axial stress: torsion stress increases. Thus, at different combinations of torsion and compression, the stress variation across the thickness will not only vary, but will vary differently for tension and compression stresses. Also, the method of computing stresses used by the above investigators, whereby the average stress was assumed equal to that at the outer face, produces only very approximate values of the actual stress.

With the tension stress varying by such a large amount, it must be appreciated that a considerable distribution of stress occurs, particularly near failure where the tension stress-strain graph becomes non-linear. Therefore, the values obtained for tension are probably high.

With solid cylinders as used by Sundara et al[73], the torsion test would result in an even greater non-linear distribution of tensile stresses near failure. Consequently, the stresses computed on the basis of elastic theory would be high by a magnitude similar to the increase of modulus of rupture over true uniaxial tensile strength[2]. It is therefore surprising that, in their calculations, Sundara et al[73] reduced their modulus of rupture values by 26.5%, but did not alter their comuted torsion stresses.

1.3.4 Direct Tension and Compression

Achieving a true state of uniaxial tension with the use of embedded bolts or bars has been attempted by numerous investigators.[87-92] Yet, results have, in general, been subjected to large variations arising from eccentric loading even when considerable care was employed. The large scatter of results obtained by Nishizawa (coefficients of variation of 12 to 15%) are therefore not surprising.

To suggest that the central 15 cm. cube section of his prism is in a uniform state of biaxial tension-compression is merely wishful thinking. For, as no attempt has been made to eliminate platen restraint in the compression diredtion, the stress pattern will probably vary, in the zone considered, from uniaxial tension to triaxial compression. Even if a successful attempt had been conducted to eliminate platen restraint, the assumption of a sudden transition from uniaxial tension to uniform biaxial tension-compression implies a discontinuity due to variable lateral deformation. The smooth transfer from one stress state to the other, which should occur, would be expected to require a distance equal to at least the smallest dimension of the specimen on the basis of St. Venant's principle. It is therefore apparent that, before a zone of uniform biaxial tension-compression is assumed, a longer length of uniform contact than used by Nishizawa, free from platen restraint, will be required.

11.3.5 Flexural Tension and ~~Direct~~ Compression

The above criticisms of Nishizawa's work are amplified when considering Smith's investigation (75). For, due to only a strip compression loading, the stress pattern in the critical section will be exceedingly difficult to analyse and will, most certainly not be in a state of biaxial tension-compression as assumed. Furthermore, due to the strip dimensions, the test in many ways resembles an indirect tensile test superimposed on a modulus of rupture test. (see Figure 11.6).

11.3.6 Indirect Tension Test

The splitting cylinder or cube test is, in practice, a very simple test to execute. However, although the failure is caused by a biaxial tension-compression stress state, it is difficult to correlate the ultimate load to a failing stress. For, not only does the tension compression ratio vary across the critical section but the ends of this diametral plane are in a state of triaxial compression. In addition, loading strips cause variable parasitic effects which further detract from the values of the results.

11.4 PROPERTIES TO BE MEASURED IN BIAXIAL TESTING

An investigation into the behaviour of concrete in biaxial tension and tension compression should attempt to establish:

(1) whether concrete behaves in accordance with the laws of elasticity,

(2) the ultimate failing strengths,

(3) the stress and strain at the discontinuity level [6,14].

(4) the governing failure criterion.

11.4.1 Laws of Elasticity

Although the laws of elasticity are known to apply for uniform materials such as steel and aluminium, such a relationship has not been conclusively established as applying to concrete under all stress states. Ward verified that the same modulus of elasticity, E, existed for both tension and compression in the elastic range [2]. It appears reasonable to assume that Poisson's Ratio, ν, would also remain constant for these two stress states, as they involve the same internal distribution of forces and resulting stress pattern. However, in biaxial stress states where a completely different phenomenological stress pattern [93] is induced thereby totally altering the internal distribution of forces, the deformations need not necessarily correspond to the laws of elasticity, particularly in view of the heterogeneous or two phase nature of concrete.

The basic elastic constants for any material are the bulk modulus, K and the shear modulus, G.[94] Although they appear to remain unchanged in uniaxial states of stress due to constant E and ν values, there is some evidence to indicate that they increase with the degree of hydrostatic pressure, particularly in triaxial compression.

Robinson[6] in a recent investigation on concrete in biaxial compression produced insufficient evidence to show that E changed from uniaxial to biaxial compression. However, his ν values decreased initially in biaxial compression and, subsequently, increased. The initial decrease, he considers is due to a stiffening process in the mortar or cement paste phase and the subsequent increase, due to an opening of cracks in the third principal direction.

Other investigators have made no attempt to correlate the elastic properties of concrete under uniaxial and biaxial or triaxial states of stress.

11.4.2. Ultimate Strengths

Most investigations on biaxial stress states have been concerned with obtaining ultimate strengths, based on a constant stress rate to failure, under varying combinations of stress. Of those experiments conducted on biaxial tension and tension-compression, only Blakey and Beresford (65, 66) have attempted to obtain information other than ultimate strength values. This is not surprising as, until recently, the short term ultimate strength has been generally defined as the failure strength of the material.

Graphical representations of the surfaces of failure in biaxial tension-compression have varied widely in shape between the different investigators. (65, 66, 69-75) McHenry and Karni's (69) results showed an S - shaped curve with sharp curvatures near the uniaxial tension and compression stresses. Approximate linear relationships were obtained by Bresler and Pister, (70, 71) Tsuboi and Suenaga, (72) Sundara et al, (73) and Nishizawa. (74) On the other hand, Smith (75) obtained a curve showing proportionally higher biaxial strengths than those of the other investigators.

By plotting the octahedral normal and shearing stresses against each other, a good linear relationship was obtained by all investigators except Smith. As pointed out by Bresler and Pister, (71) the octahedral stresses provide a sound basis of investigation as they represent the mean normal and shear stresses at any point in the material. They have also indicated that the failing strengths depend on the deviatoric strain energy, the volumetric strain energy and a term which is the product of the principal stresses. This has been supported by Blakey and Beresford[66,85] who have calculated their equations on the basis of stresses associated with cracking strains. Their equation constants are, however, vastly different.

11.4.3 Stresses and Strains at the Discontinuity Level

Although it has been shown in recent investigations that cracks in concrete occur prior to commencement of loading, and continue at all load stages,[95,96] the stress-strain curves are reasonably linear to about 60% of the short term ultimate strength in uniaxial compression. Similar results have been obtained in uniaxial tension[2,90] Beyond this stage, however, the marked non-linearity of the stress-strain curve is accompanied by a sharp increase in the rate of internal breakdown of the concrete structure. This has been studied by several investigators with the aid of resonant frequency, pulse velocity and X-ray techniques as well as simply observing sudden transitions in longitudinal and lateral strains and Poisson's Ratio.[6, 56, 57, 65, 66,95, 97-101]

Newman[14] has defined this transition point as the <u>discontinuity</u> level of the concrete. It is at this stage that the material not only becomes discontinuous in a physical sense, but also, mathematical and graphical expressions between load and deformation become markedly discontinuous in a linear sense. Prior to this level, developing cracks will become stable at any load whereas, after the discontinuous stage, cracks will continue to propagate in an unstable manner. Consequently, ultimate strengths as discussed in Section 11.4.2 are random values depending on such variables as loading rate, duration of loading, number of repetitions of load, and size of specimen. It must therefore be appreciated that the discontinuity level represents a much more fundamental property of concrete than does the short term ultimate strength.

In their analysis, Blakey and Beresford (66) related their failure equations to calculated stresses corresponding to strains at the discontinuity level. However, due to their unreliable testing techniques, their equations for failure in biaxial states of stress are unreasonably sophisticated.

11.4.4 Laws of Failure

A conclusive establishing of the governing laws of failure for concrete will ultimately involve examination of stress systems with corresponding strain measurements for almost all stress patterns and certainly, triaxial loading systems. However, the establishing of reliable testing techniques for triaxial testing is an arduous process. Thus, we must be satisfied with tackling the problem, backwards by beginning with a point (uniaxial stress systems), developing to a line (biaxial systems) and finally establishing the surface (triaxial systems) of the failure envelope.

Yet, the results of a well conducted biaxial investigation can provide much useful information on failure theory. On a phenomenological level, only two failures are possible; a cleavage or tensile splitting and a shearing mechanism. When at least one stress is tension, the former will govern (2,66,69-75). In fact, in uniaxial and biaxial compression stress states, a tensile failure still occurs (see Chapter 9 and Robinson (6)). However, under states of triaxial compression where tensile stresses and strains have been prevented, a shearing mechanism or a general pulverizing of the cement paste phase will occur. (85, 102-108)

Although it has been established that concrete will fail by a tensile or cleavage mechanism in biaxial tension and tension-compression, it has not been recognized whether this is due to a limiting stress or strain, limiting volumetric strain, mean stress, maximum energy or some other failure criterion. The results from biaxial analysis should make it apparent as to which of these, if any, is applicable.

11.5 SELECTION OF A SUITABLE TEST METHOD

Fundamentally, there are two states of stress which require examination.

(i) direct or uniform states of stress

(ii) flexural states of stress.

In the former, the entire critical section of the specimen is subjected to the desired stress state whereas in the latter, the principal stresses, created by the action of pure moments, vary from zero values at the neutral axes to maximum values at the extreme fibres.

An ideal test method for the investigation of biaxial tension and tension-compression properties of concrete would require: (1) that specimens for biaxial tension and tension-compression be capable of being loaded in the same machine. (2) a simple testing procedure, (3) that the volume of material being subjected to the desired stress system should remain approximately equal for different states of stress. (4) large specimens so that the results will represent a reliable average behaviour of the material and not be affected by aggregate size. (5) that the critical section of the specimen be subjected to the desired stress state.

The following test methods appeared possible for the necessary investigation.

(1) plate tests

(2) hoop tension and axial tension or compression on hollow cylinders.

(3) torsion and axial tension or compression on hollow cylinders.

(4) direct tension and direct tension or compression.

Of the above methods, only the first produces pure flexural states of stress whereas, only the last results in uniform stress states. Tests on hollow cylinders resulting in uniform states of stress would require massive dimensions.

For example, for a 5% strain variation in a 4" wall thickness, the dimensions of the cylinder would be 12.3 feet in diameter and about 30 feet high. Clearly, tests on such specimens would be impractical.

As far as the first requirement above is concerned, only plates can be loaded in one testing machine whereas, in achieving uniform states of biaxial tension and tension-compression, three different testing machines are necessary. Furthermore, the problem of achieving a uniform state of biaxial tension is very complex in view of difficulties with alignment and methods of applying the tension. (see second requirement of ideal test method above). Thus, the testing of plates, i.e., biaxial flexure testing, was adopted for the examination of concrete characteristics in states of both biaxial tension and tension-compression stress.

CHAPTER 12

THE BIAXIAL FLEXURAL TESTING MACHINE

12.1 REQUIREMENTS

The first requirement of a good testing technique for the testing of plates is a proper testing machine capable of applying the assumed loads without inducing any extraneous influence (see Section 5.1). On the basis of the recommendations set out in Section II, it should satisfy the following requirements:

(1) a longitudinal stiffness equal to or greater than that of the specimen, i.e. it should be a hard[93] testing machine.

(2) high lateral stiffness and no loose fitting components.

(3) stability, if the both ends effectively pinned loading method is used.

(4) effective elimination of restraint effects of load and support points.

(5) facility for positioning specimen accurately.

(6) a loading rate capable of being easily controlled.

(7) a precise well-marked load indicating device.

(8) virtual elimination of ram effects.

It was decided to load all specimens with both ends effectively pinned (see Section 5.3). This was particularly important in the slab tests as the theory is based on equal loading at all corners. If a both ends fixed method had been adopted, the yielding of a localized section near failure would have resulted in unequal loads at the four corners.

12.2 DESIGN AND CONSTRUCTION

The testing machine, which was manufactured by J. and N. Electronics Ltd., London is shown in Plate 12.1 while details of machine components are presented in Figures 12.1 and 12.2

12.2.1 Pinned End Conditions

The method of achieving effectively pinned ends for the loading of discs and slabs is shown in Plates 14.4 and 15.2 respectively. With the testing of both specimens, the upper pin is a $\frac{1}{2}$" diameter ball coated with Rocol A.S.P. (see Section 8.7.1.) With the slabs, the effective lower pin is obtained with rollers at each support point, with two of the rollers being at right angles to the other two. The lower pin in the testing of discs is obtained with a grease pack positioned between the loading ring and the upper surface of the slab.

12.2.2 Longitudinal Stiffness

As seen in Table 12.1, the longitudinal stiffness of the machine with the loading beam is larger than that of the slab specimens. Thus, for the testing of these specimens, the machine is classed as a <u>hard</u> machine. As a result, it is

PLATE 12.1 The biaxial flexural testing machine

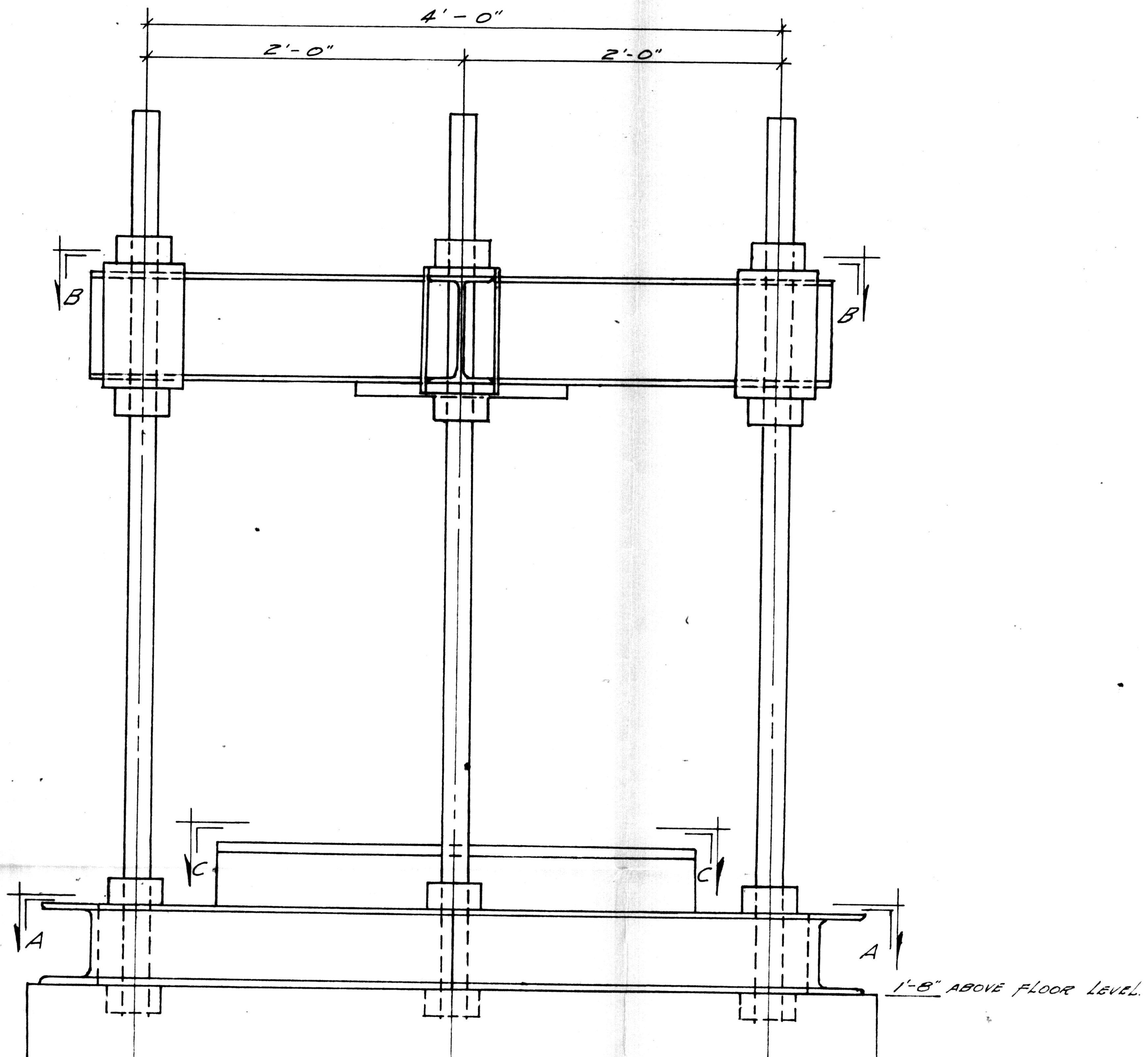

ELEVATION VIEW
ASSEMBLED APPARATUS

SCALE: 1" = 8"

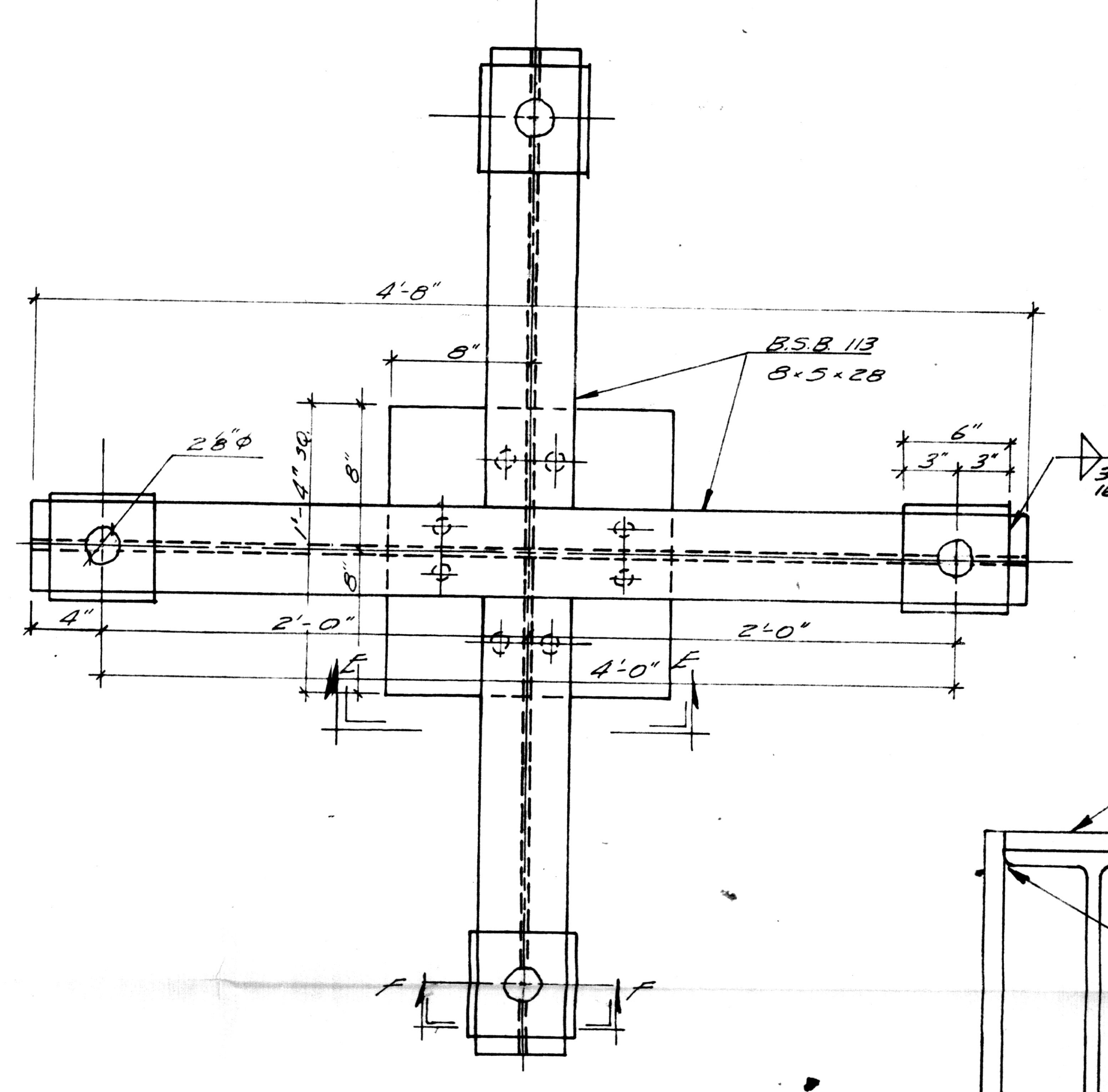

SECTION B-B

SCALE: 1" = 8"

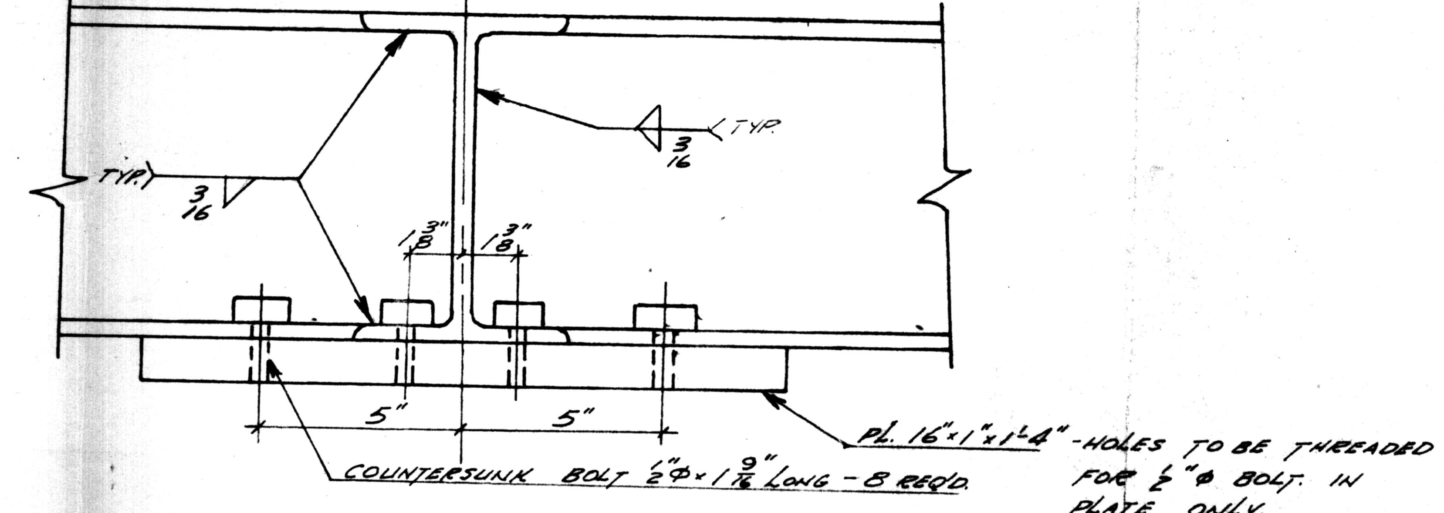

SECTION E-E

SCALE: 1" = 4"

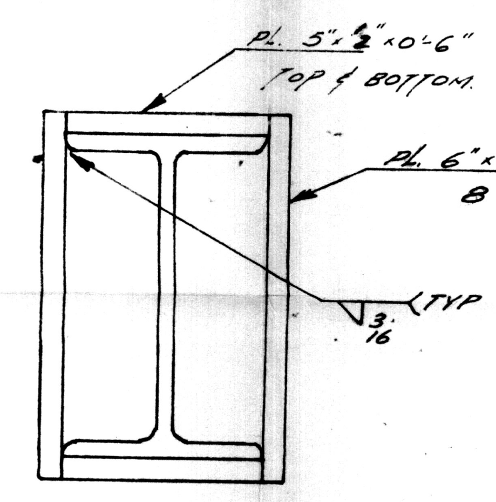

SECTION F-F

SCALE: 1" = 4"

1 SEE DRWG. NO. 2 FOR REVISED DETAIL

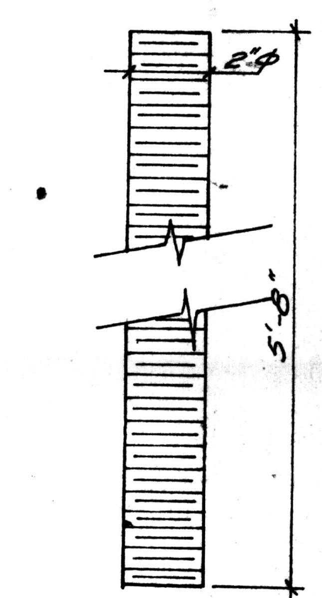

DETAIL OF THREADED COLUMN - 4 REQUIRED

SCALE: 1" = 4"

1. SEE DRWG. NO. 2 FOR REVISED DETAIL.

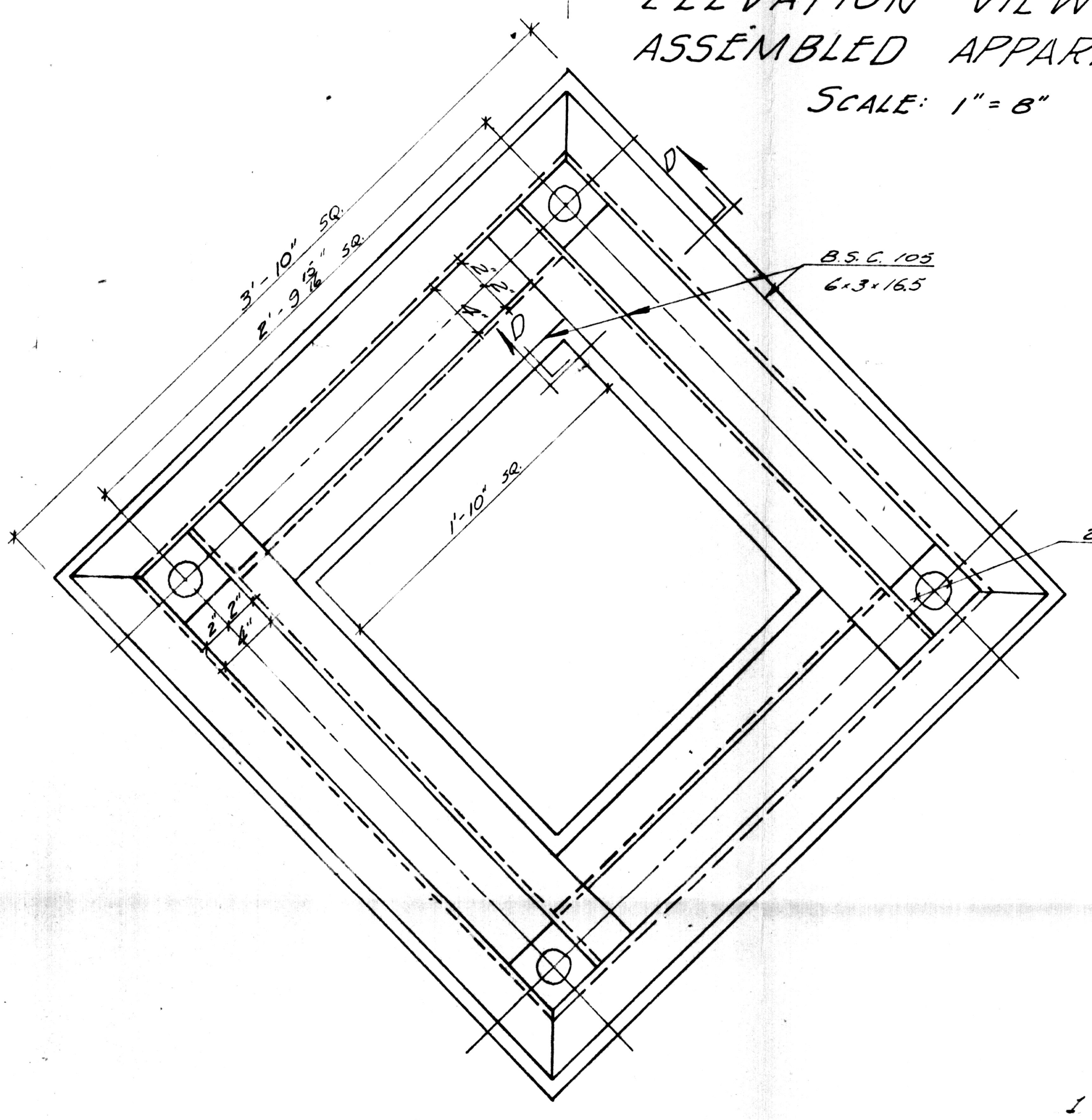

SECTION A-A

SCALE: 1" = 8"

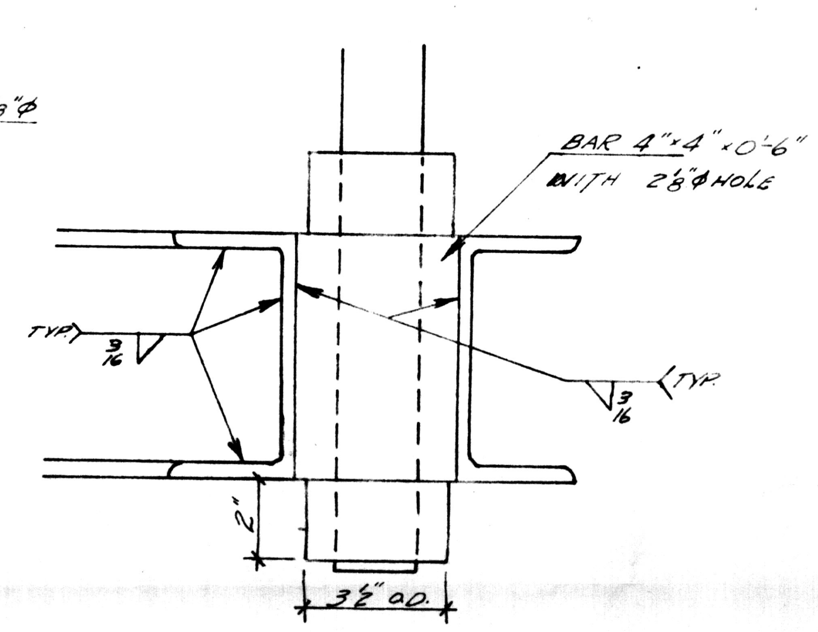

SECTION D-D

SCALE: 1" = 4"

1 SEE DRWG. NO. 2 FOR REVISED DETAIL

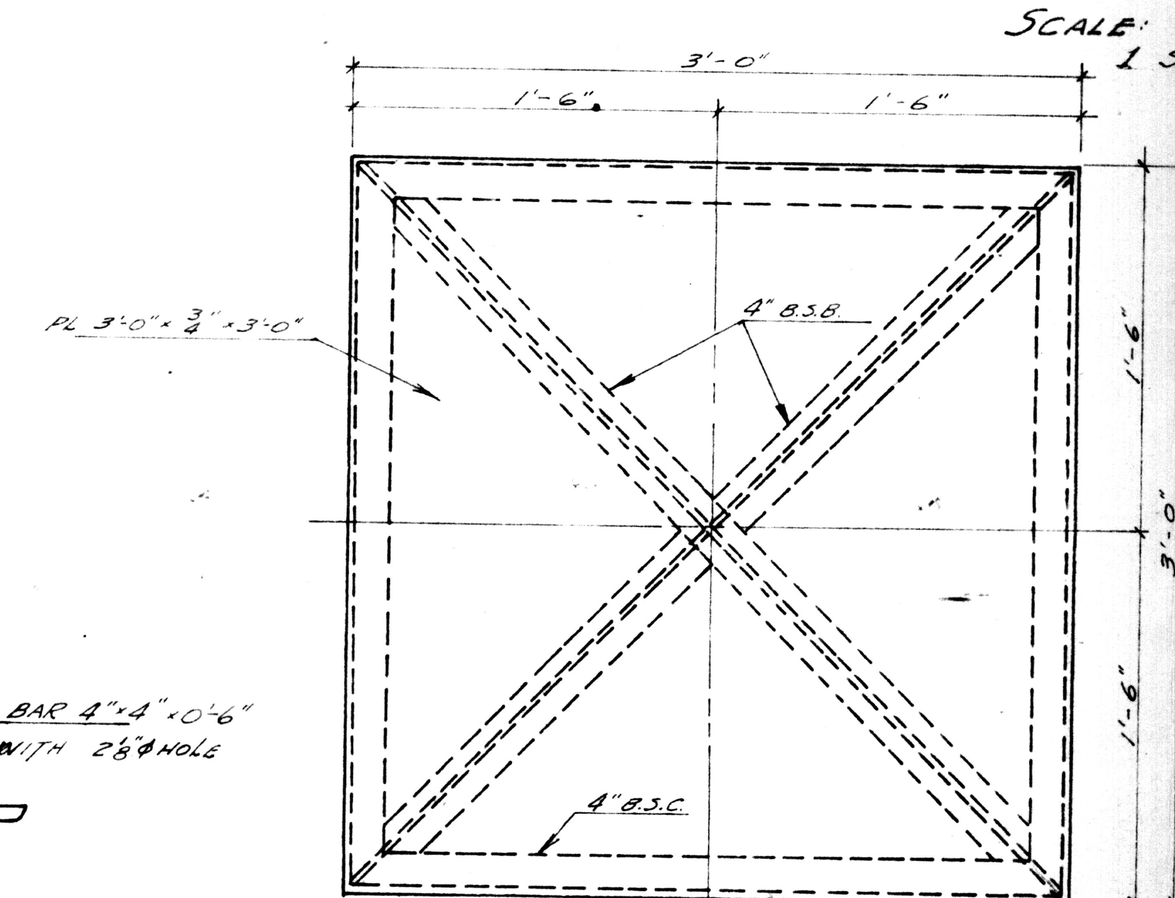

SECTION C-C

SCALE: 1" = 4"

MATERIAL REQUIRED:

1. 1 BSB 113 × 4'-8"
2. 2 BSB 113 × 2'-4"
3. 4 BSC 105 × 3'-8"
4. 2 BSC 105 × 3'-2"
5. 2 BSC 105 × 2'-6"
6. 4 BAR 4"×4"×0'-6"
7. 1 PL. 16"×1"×1'-4"
8. 8 PL. 5"×½"×0'-6"
9. 8 PL. 6"×½"×0'-9"
10. 8 COUNTERSUNK BOLTS ½"Φ × 1 9/16" LONG
11. 4 2"Φ THREADED COLUMNS × 5'-8"
12. 16 NUTS FOR COLUMN ABOVE - SEE SECTION D.D.

NOTES:

1: ALL STEELWORK TO CONFORM TO LATEST BRITISH CODE SPECIFICATIONS.

2: MATERIALS LIST ABOVE EXCLUDES STEEL SHOWN IN SECTION C-C AS THIS IS A COMPLETED ITEM.

REV.	DATE	DESCRIPTION
.1	4-9-63	MINOR STRUCTURAL ALTERATIONS

IMPERIAL COLLEGE - LONDON

CONCRETE LABORATORY

BIAXIAL TEST APPARATUS

ELEVATIONS & DETAILS

DATE: JAN. 10/63	SCALE: AS SHOWN
DRWG. NO: 1	DRAWN BY: Sigvoldason

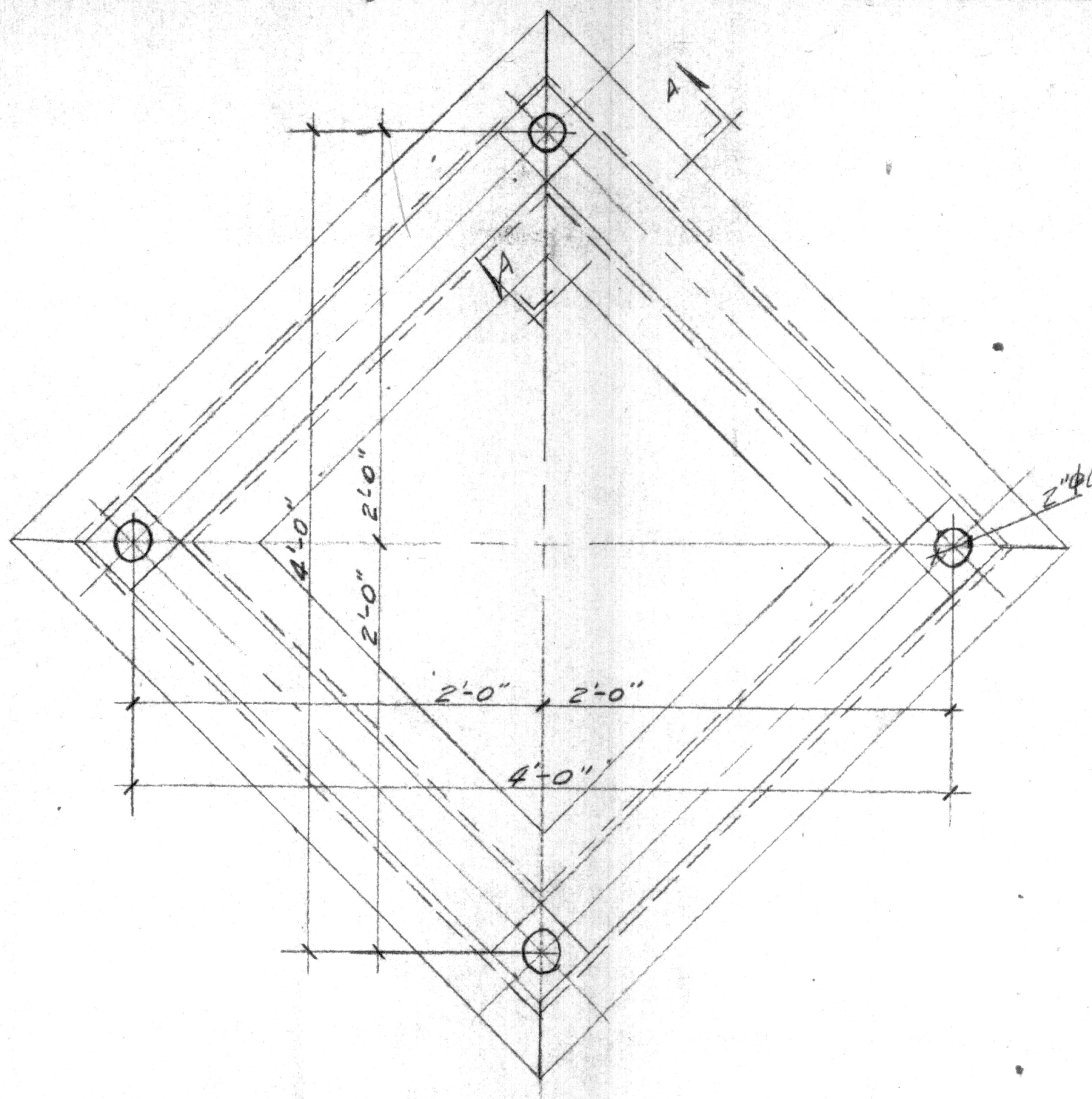

PLAN VIEW
BOTTOM PLATE ASSEMBLY
SCALE: 1"= 0'-8"

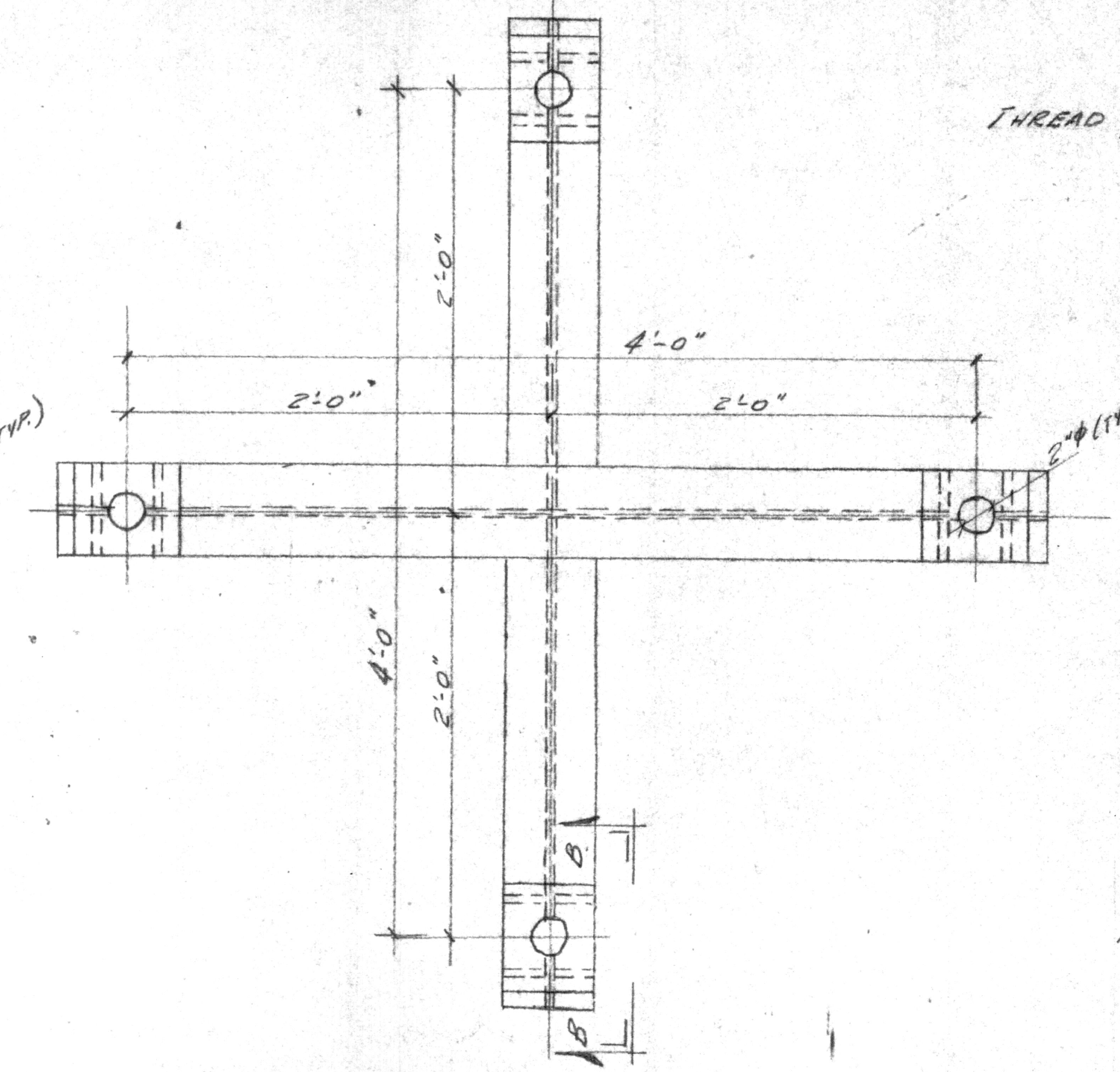

PLAN VIEW
TOP PLATE ASSEMBLY
SCALE: 1"= 0'-8"

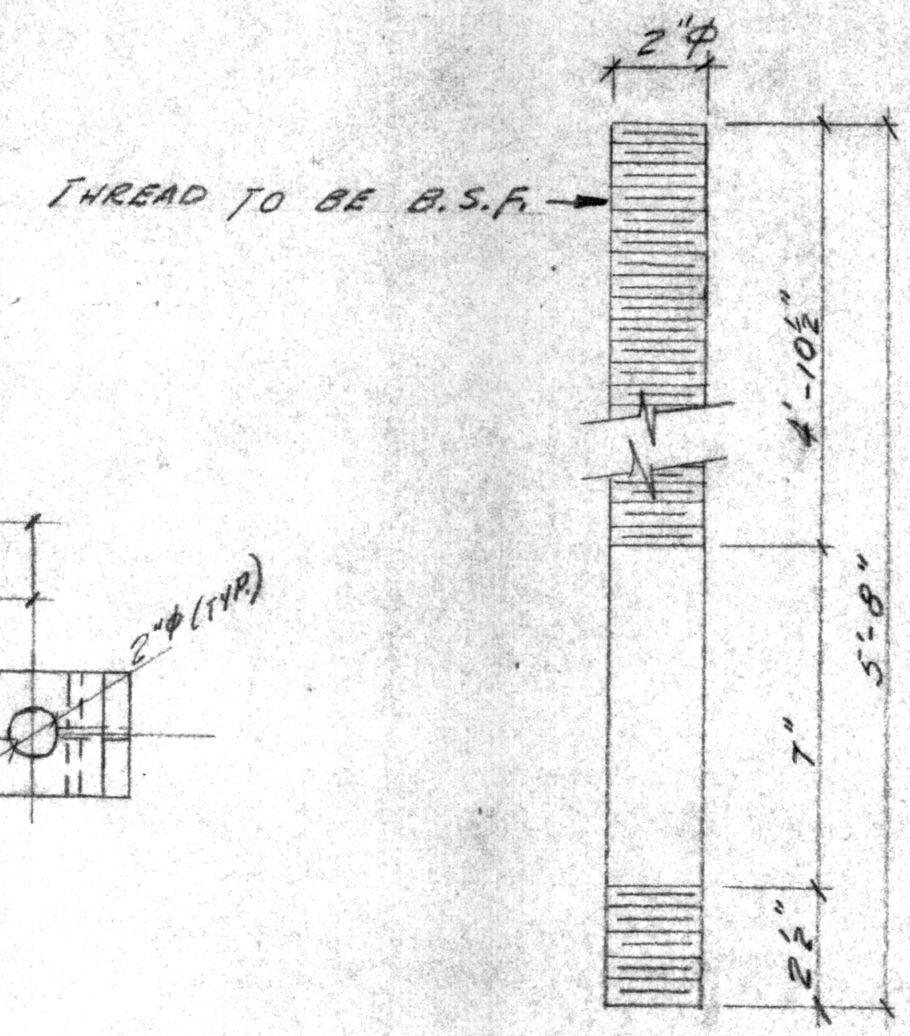

COLUMN DETAIL
N.T.S.
4 REQUIRED.

Notes:

1. Tolerances on dimensions between ℄'s of holes to be ± 0.010 inches.
2. Tolerances between corresponding holes in top plate assembly and bottom plate assembly to be ± 0.002 inches in alignment.
3. The top plate to be machined in order to obtain a sliding fit on the columns.
4. The bottom plate to be machined in order to obtain a push fit on the columns.
5. In case of discrepancy between Drwgs. No. 1 & 2, Drwg 2 supersedes Drwg No. 1.

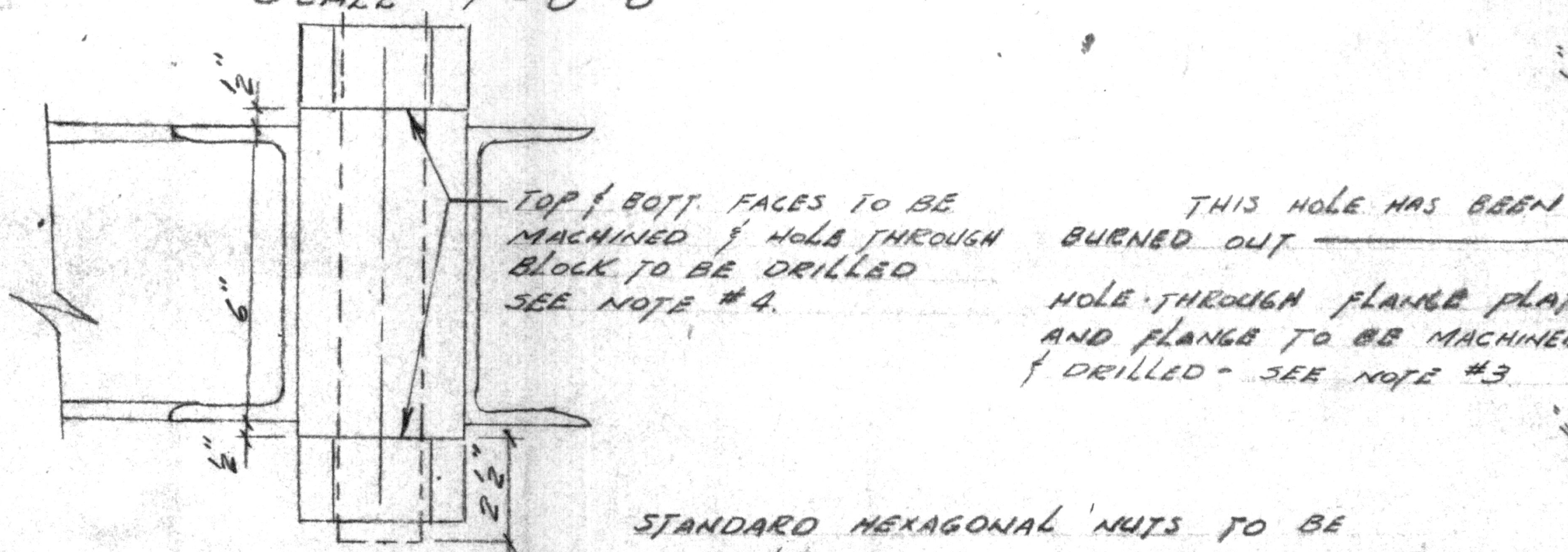

SECTION A-A
N.T.S.

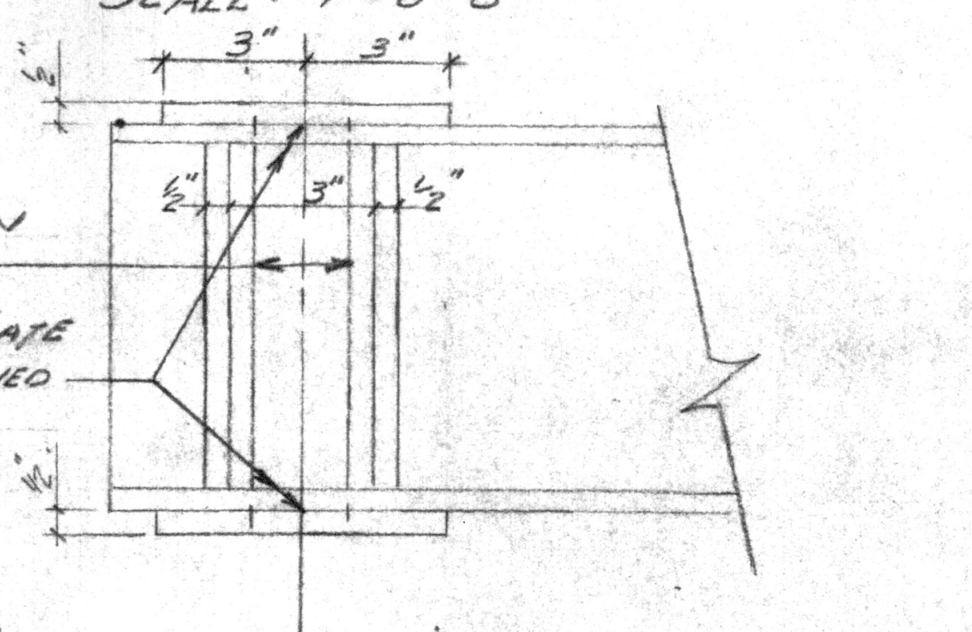

SECTION B-B
N.T.S.

IMPERIAL COLLEGE - LONDON	
CONCRETE LABORATORY	
BIAXIAL TEST APPARATUS	
DETAILS	
Date: Apr 9/63	Scale: As shown
Drwg. No. 2	Drawn by: Sigvaldason

TABLE 12.1 DEFORMATION RELATIONS FOR TESTING MACHINE AND SPECIMEN

Machine Component	Deformation (ins.) (P is in lbs)	Stiffness $K = \frac{P}{\Delta}$ (lbs./inch)
4 columns - 2" ϕ x 30" long	8.0×10^{-8} P	
Upper cross-head	4.29×10^{-7} P	
Loading beam	12.78×10^{-7} P	
Loading jack - 1" column of oil	2.10×10^{-7} P	
Hydraulic fluid in line and 5 ft. of $\frac{1}{4}$" ϕ steel tubing	4.30×10^{-7} P	
hydraulic lines	2.3×10^{-9} P	
Total: Machine with loading beam	2.4×10^{-6} P	4.2×10^{5}
Machine without loading beam	1.15×10^{-6} P	8.7×10^{5}
Specimen: $E = 6 \times 10^{6}$, $\nu = 0.2$, d=3", side length = 30"		
slab with ratio of diagonal lengths, 2:1	15.5×10^{-6} P	6.4×10^{4}
slab with ratio of diagonal length 1:1	10.0×10^{-6} P	10.0×10^{4}
30" diameter disc with 12" diameter loading ring	5.9×10^{-8} P	1.7×10^{7}

Note: Deflections for slabs and discs are computed from Equations 14.21 and 15.14, respectively.

possible to load these specimens at an almost constant deformation rate as well as at a constant loading rate. The high relative stiffness of the machine resulted in strain measurements being obtained in some of the slab tests after the maximum load had been reached as shown, for example, in Figure 17.9.

Alternatively, for the testing of discs, the machine is classified as being soft. The machine stiffness for these tests is further reduced from the value of 8.7 x 10^5lbs/inch given in Table 13.1 because of the soft materials used in the loading and supporting of the specimen. (see Section 15.3.1) Thus, disc specimens can only be loaded at a constant stress rate.

13.2.3 Lateral Stiffness and Stability

To achieve high lateral stiffness and freedom from loose f[illegible]g components, the 2" diameter columns and cross-heads were manufactured so as to have éncastré connections. The lower column - cross-head connections were a tight fit whereas the upper ones were a sliding fit. The latter allowed for adjustment in the elevation of the upper cross-head. Locking nuts were used from both sides on every column-cross head connection.

As a both ends effectively pinned load method was adopted as the explicitly definable method of test, a check on stability was necessary. Assuming a specimen length of 8" and a machine length of 30", the theoretical buckling of this machine would occur at 203 tons (see Equation 5.1). Clearly, with maximum loads of only about 10 tons being applied, stability will not be a problem.

12.2.4 Specimen Alignment and Platen Effects

To obtain precise alignment of the specimen in the machine, the support points were located accurately on the machine base with the aid of dowelling pins. In order to check that proper alignment was being achieved, two tests were performed on an aluminium slab loaded in mutually opposite positions. These results, presented and discussed in Section 14.3.3, show that the machine is in good alignment.

The influence of the load and support points on the stress distribution in the slab and disc specimens, referred to generally as platen effect, was examined in conjunction with the suitable dimensioning of such specimens (see Chapters 14 and 15). For the slab tests, these platen effects have been confined to the extended corners and do not influence the general stress pattern in the slab, as shown in Section 14.3.3. Likewise, for the disc tests, the restraining effects at the load and support rings have been successfully eliminated, as shown in Section 15.3.3

12.2.5 Load Application, Ram Effect and Operator Technique

To achieve a well-controlled and smooth load application system, a very fine control valve, a steady continuous flow of hydraulic fluid and a hydraulic ram which behaves smoothly even at slow rates are the important requirements. The pump unit selected was an Oswald and Ridgeway Beacham Centrifugal Motorized Unit: Type S.700. Flow and load control was obtained with two control valves; an Oswald and Ridgeway 5,000 p.s.i. pressure release valve, Type S.V.1. and a fine control metering spool valve, Type CSW 5971. Hydraulic lines are Ermeto $\frac{1}{4}$" diameter high pressure steel tubing, thus ensuring increased longitudinal stiffness. (see Table 12.1) Details of the hydraulic system are shown in Figure 12.3.

The loading jack selected was a Blackhawk Holl-O-Ram, No. R.C.30 of 30 ton capcity, With 7.2 sq. ins. of ram cross-sectional area, pressures were maintained low (usually to less than 1500 p.s.i.) and control of oil flow through the control valves was therefore easily regulated. (see Section 5.4.9) In addition, the relatively large ram area with the corresponding low pressures resulted in improved longitudinal stiffness of the machine. This was also considered by Barnard in the design of his stiff testing machine.[(35)] The relatively long contact at the ram-cylinder interface, 7", prevented binding action occurring, thus resulting in smooth movement even at slow rates.

To achieve precise and accurate measurements of load, a 3.5 tonf electrical resistance strain gauge load cell, firmly attached axially to the ram, was used (see Plate 12.1).

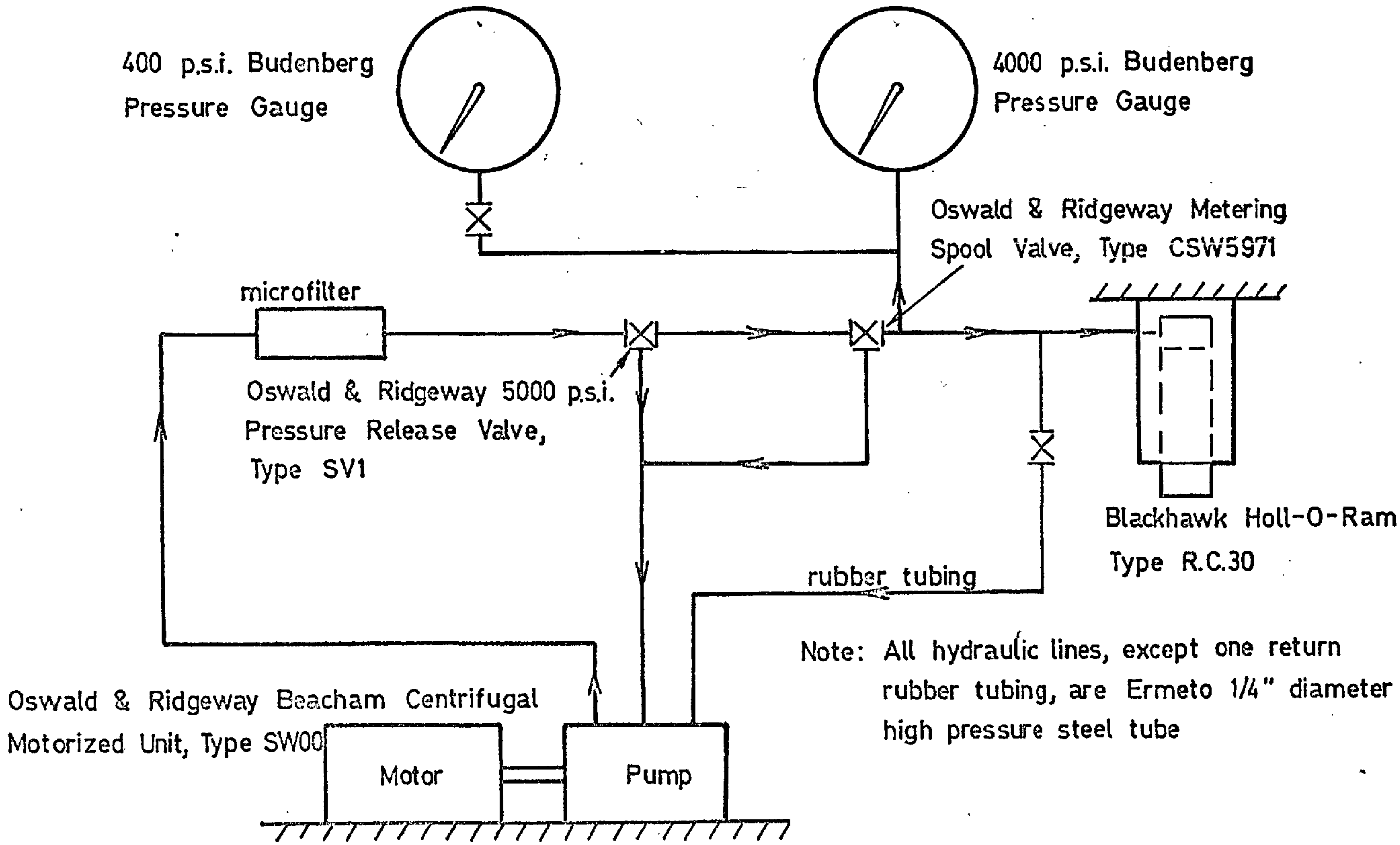

FIG. 12.3 HYDRAULIC LOADING SYSTEM FOR BIAXIAL TESTING MACHINE

Measurement of load was achieved with a Peekel Model 540 DNH strain measuring unit. The high sensitivity is shown by the fact that 1 division represents only about 0.9 lbsf. (see Figure 3.9). The calibration of this device showed excellent repeatability, complying well within the requirements of a Grade A_1 testing machine as discussed in Section 3.3.6 (see Figure 3.9). For loads in excess of 3.5 tonf , a 4,000 p.s.i. pressure gauge connected directly to the hydraulic line was used. This gauge showed good repeatability and satisfied the requirements of a Grade A machine[8] (see Section 3.3.7)

12.3 PERFORMANCE OF MACHINE

With the fine control spool valve, large ram area and centrifugal pump, the control of load was found to be excellent. As the pressure on the ram side of the spool valve was low, the pressure drop across the valve remained essentially constant thereby resulting in a virtually constant deforming rate of the ram with increasing load. This was shown in the loading of most specimens as, over their elastic range, no adjustment of the valve opening was necessary to ensure a constant loading rate.

The good load control and repeatability of machine behaviour produced good repeatability in the modulus of rupture values obtained in testing standard 4" x 4" x 20" flexural beams. (see British Standard 1881[9]). The average coefficient of variation of 2.5% (see Table 16.2) shows a significant improvement over results obtained on the flexural machine (see Section 3.3.5) where, with similar care, Ward obtained an average coefficient of variation of 4.4% (2). It is considered that an average coefficient of variation of only 2.5% represents the true scatter of concrete strengths, independent of machine effects. (31, 109)

The high longitudinal stiffness of the machine was of particular importance in the testing of the reinforced slabs. (see Chapter 18). With these specimens, there was usually a significant drop in load during test, when the concrete on the reinforced face failed in tension. With a soft machine, an impact loading at this stage would have resulted in less reliable results being obtained at later load stages.

CHAPTER 13

MODEL ANALYSIS

13.1 IMPROVEMENT IN TESTING TECHNIQUE WITH MODEL ANALYSIS

In Section 5.1, it was shown that the development of a satisfactory testing technique for examining the deformation and strength properties of materials requires:

(1) a testing machine which loads the material specimens in accordance with theoretical requirements and

(2) a specimen shape and size which produces the desired stress and strain pattern throughout the critical volume being examined.

With a testing machine having been manufactured in accordance with the recommendations of Part II of this thesis (see Section 12.2), the initial development of a satisfactory testing technique has been fulfilled. However, as shown in Chapter 11, the assurance that the specimen is being deformed in accordance with theoretical requirements is as important as the design and manufacture of a good machine.

Before commencing with tests on concrete slabs and discs, it was necessary to investigate the testing technique by subjecting an ideal material specimen to a loading system as specified by the theory. Strain measurements would be recorded at several points on the specimen and compared with the strain pattern obtained theoretically. In the event of good correlation, it was considered that similar results would be obtained with concrete specimens of the same shape. Alternatively, with poor correlation, a complete check on the loading system, specimen shape or validity of the theory would then be necessary. With continued improvements in the testing technique, tests could be repeated until good correlation were obtained between the experimental and theoretical results. With doubt about parasitic effects in the applied force system and the resulting stress and strain pattern in the specimen being conclusively eliminated, full confidence could then be placed in the results of subsequent tests on concrete specimens.

13.2 SELECTION OF A SUIITABLE MATERIAL

An ideal material for the model testing of plates needed to meet the following requirements;

(1) complete elasticity to a relatively high uniaxial strain (about 400×10^{-6})

(2) similar modulus of elasticity to that of a typical concrete.

(3) uniform thickness

(4) simple to cut

(5) negligible creep characteristics

(6) light and easy to handle

(7) low cost

(8) availability

Three materials commonly used as model materials were considered; steel, aluminium and perspex. After considering each of these materials in detail in light of the above requirements, an aluminium plate specimen was selected. The dimensions of the plate as measured by the author were 36" square while the thickness, taken as the average of 16 readings with calipers graduated in 0.0001" divisions, was 0.7620". The variation in thickness, assuming a normal distribution, was a standard deviation of 0.0035", i.e., a coefficient of variation of only 0.46%. This was considered an exceptionally desirable feature as large variations in plate thickness would create severe stress concentrations.

In addition to having good uniformity in plate thickness, aluminium was regarded as being the most suitable material when considering the other requirements above. Although perspex is lighter, it is very susceptible to undesirable creep effects and its plate thickness varies by relatively large amounts. To overcome any possible anelastic or delayed elastic effects in aluminum, the strain readings were recorded at 15 to 30 seconds after each load stage had been reached. Steel, although displaying good elastic behaviour and capable of being manufactured to close tolerances, was rejected because of its weight and high cost.

CHAPTER 14

DEVELOPMENT OF TESTING TECHNIQUE FOR SLAB TESTS

14.1 THEORY OF THE RECTANGULAR SLAB TEST

14.1 General Plate Theory

Timoshenko and Woinowsky-Kreiger (67), in analysing the relationship between bending moment and curvature in the pure bending of plates, derived the formulas.

$$M_x = D\left(\frac{1}{r_x} + \nu\frac{1}{r_y}\right) = -D\left(\frac{\partial^2 w}{\partial x^2} + \frac{\nu\partial^2 w}{\partial y^2}\right) \quad \ldots\ 14.1$$

$$M_y = D\left(\frac{1}{r_y} + \nu\frac{1}{r_x}\right) = -D\left(\frac{\partial^2 w}{\partial y^2} + \frac{\nu\partial^2 w}{\partial x^2}\right) \quad \ldots\ 14.2$$

where M_x and M_y are the bending moments in the x and y principal directions, respectively, r_x and r_y are the radii of curvature in these same two principal directions, respectively and w is the deflection of the middle surface of the plate with respect to the origin: at the origin, the x-y plane is tangential to the middle surface of the plate. D, the flexural stiffness of the slab, is given as

$$D = \frac{Ed^3}{12(1-\nu^2)} \quad \ldots\ 14.3$$

where E is modulus of elasticity, d is the plate thickness, and ν is Poisson's ratio.

Solving Equations 14.1 and 14.2 for $\frac{\partial^2 w}{\partial x^2}$ and $\frac{\partial^2 w}{\partial y^2}$ and integrating twice, we obtain the general formula for deflections of the middle surface of the plate, i.e.;

$$w = -\frac{M_x - \nu M_y}{2D(1-\nu^2)}x^2 - \frac{M_y - \nu M_x}{2D(1-\nu^2)}y^2 \quad \ldots\ 14.4$$

14.1.2 Rectangular Slab Theory

In the slab tests conducted by Blakey and Beresford(65,66) and subsequently, Newman(68), the moments in the x and y - directions were assumed to be of equal magnitude, but of opposite sign, i.e. M_x equal to $-M_y$ (see Section 11.2.1).

Substituting $M_x = -M_y$ into Equation 14.4, then

$$w = \frac{-M_x}{2D(1-\nu)}(x^2 - y^2) \qquad \ldots\ 14.5$$

The surface formed is an anticlastic surface as shown in Figure 14.1 where the curvatures in the two principal directions are equal and opposite as obtained from the substitution of $M_x=-M_y$ into Equations 14.1 and 14.2, i.e.;

$$\frac{1}{r_x} = -\frac{1}{r_y} = -\frac{\partial^2 w}{\partial x^2} = \frac{M_x}{D(1-\nu)} \qquad \ldots\ 14.6$$

Along the lines bisecting the angle between the x and y axis, the deflection 'w' is zero. All lines parallel to these bisecting lines remain straight during bending, rotating only by some angle. A rectangle 'abcd' bounded by such lines will be twisted as shown in Figure 14.1. Along these boundaries, the normal bending moment will be zero as determined from the equation(67)

$$M_n = M_x \cos^2\alpha + M_y \sin^2\alpha \qquad \ldots\ 14.7$$

where the α values, the angles between the 'yz' plane and the planes on which the normal moments, M_n are acting, are $\pm 45^o$.

Along these same sections, the twisting moments, as determined from the equation(67)

$$M_{nt} = \tfrac{1}{2} \sin 2\alpha\,(M_x - M_y) \qquad \ldots\ 14.8$$

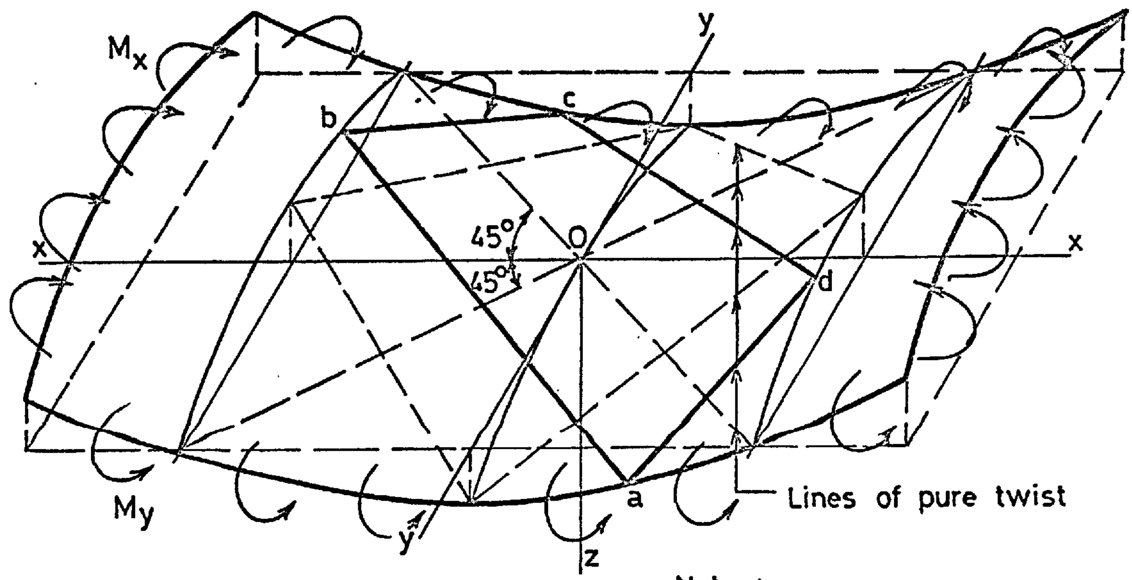

Notes:

1. M_x is equal to M_y
2. Lines of pure twist are also lines of linear deformation

FIG. 14.1 ANTICLASTIC BENDING OF A PLATE BY PURE MOMENTS OF EQUAL MAGNITUDE AND OPPOSITE SIGN

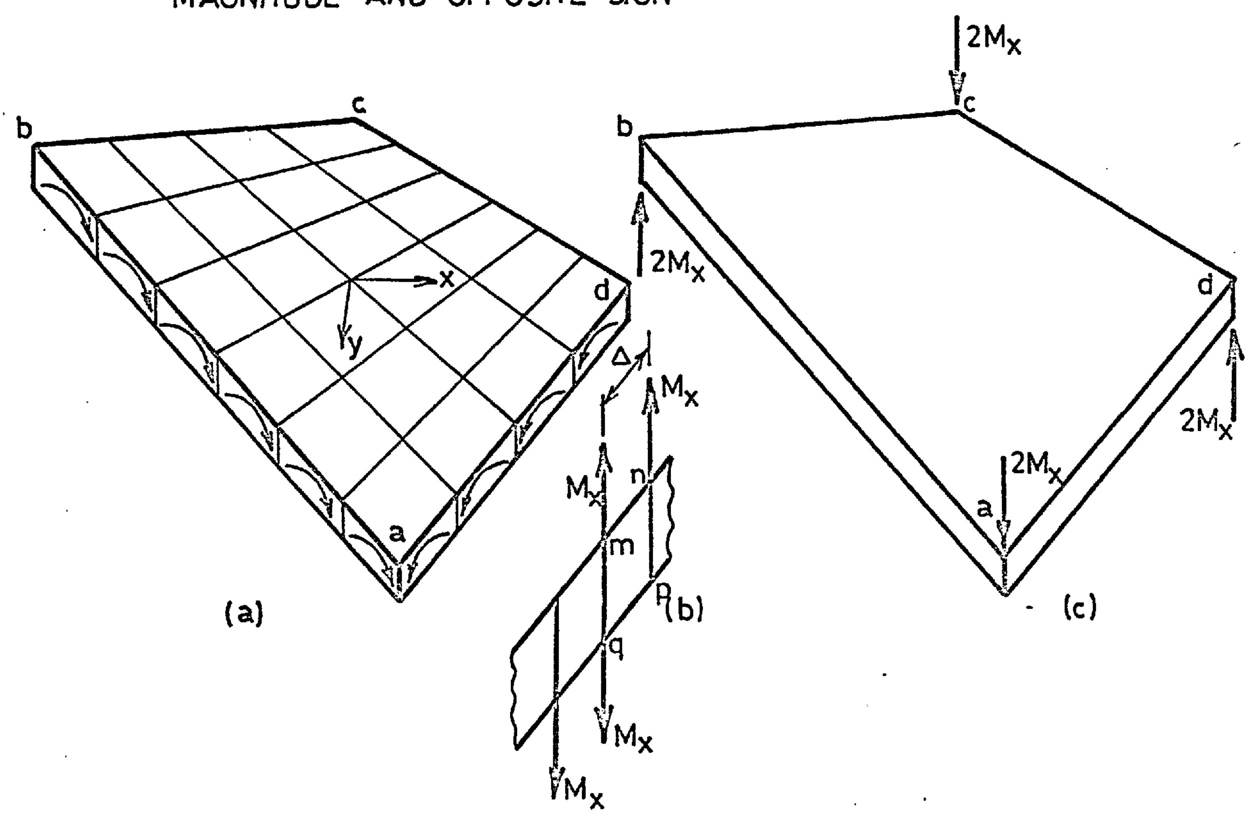

FIG. 14.2 ANTICLASTIC BENDING OF A PLATE RESULTING FROM THE CORNER LOADING OF A RECTANGULAR PLATE

are equal to 'M_x' along the sections 'ad' and 'bc' and '$-M_x$' along 'ab' and 'cd'. Thus, the portion 'abcd' is in a condition of a plate undergoing pure bending produced by twisting moments uniformly distributed along the edge. (see Figure14.2a). To produce this series of moments the edge 'ad' can be divided into a large number of narrow rectangles, such as 'mnpq' in Figure14.2b If Δ is the small width of the rectangle, the corresponding twisting couple is $M_x \Delta$ and can be formed by two vertical forces equal to M_x acting along the vertical sides of the rectangle. This replacement of the distributed horizontal forces by a statically equivalent system of two vertical forces cannot cause any sensible disturbance in the plate, except within a distance comparable to the thickness of the plate, which is assumed to be small. (see discussion of St. Venant's principle in Timoshenko and Goodier[110]). Proceeding in the same manner with all the rectangles, we find that all forces, M_x acting along the vertical sides of the rectangle balance one another and that only two forces, M_x at the corners a and d are left. Making the same transformation along the other edges of the plate, we conclude that bending of the plate to the anticlastic surface shown in Figure 14.2a can be produced by forces concentrated at the corners as shown in Figure 14.2c.

The above theory was first analysed by Lord Kelvin and P. G. Tait in 1883.[111] The verification of the theory was conducted by Nadai[112] in 1915 whereby the deflection of a aquare plate along a diagonal was measured. Discrepancies with the theory occurred only near the edges, but these would be expected in consideration of the transformation of twisting couples along the edges.(110)

14.1.3 Principal Surface Stresses and Strains

With a rectangular slab being loaded at two diagonally opposite corners, the total applied load will be P. But as shown above, the load at each corner equals $2M_x$, i.e.,

$$\frac{P}{2} = 2M_x \qquad \text{... 14.9}$$

At any point, the normal stress, σ at the outer fibre can be obtained from the relationship

$$\sigma = \frac{M}{S} \qquad \text{... 14.10}$$

where S is the section modulus. For a unit width

$$S = \frac{d^2}{6} \qquad \text{... 14.11}$$

where d is the thickness of the slab.

If tensile stresses are assumed to be positive and compression stresses negative, it is observed that for the upper surface of the plate, σ_x is negative and σ_y is positive (see Figure 14.2). For the bottom surface, the opposite will be true. Denoting the upper and lower surfaces by the subscripts 1 and 2 respectively, and proceeding from Equation 14.9, 14.10 and 14.11, then

$$-\sigma_{1x} = \sigma_{2x} = \frac{3P}{2d^2} \qquad \text{... 14.12}$$

Similarly,

$$\sigma_{1y} = -\sigma_{2y} = \frac{3P}{2d^2} \qquad \text{... 14.13}$$

Therefore,
$$\sigma_{1x} = -\sigma_{2x} = -\sigma_{1y} = \sigma_{2y} \qquad \ldots\ 14.14$$

At any point on the surface of the slab, the principal strains, δ_x and δ_y, can be obtained from the relationships (see Timoshenko and Woinowsky-Kreiger[67] p.5)

$$\delta_x E = \sigma_x - \nu\sigma_y \qquad \ldots\ 14.15$$

and
$$\delta_y E = \sigma_y - \nu\sigma_x \qquad \ldots\ 14.16$$

By substituting Equation 14.14 into Equations 14.15 and 14.16 and solving for the principal strains on each surface then it is shown that

$$-\delta_{1x} = \delta_{2x} = \delta_{1y} = \delta_{2y} = \frac{3P}{2d^2}\left(\frac{1+\nu}{E}\right) \qquad \ldots\ 14.17$$

14.2 TESTS ON A SQUARE SLAB

Although the above theory requires that the slab be loaded at the corners, this loading is, in practise, hot simple to achieve. In his tests, Nadai[99] used steel slabs with sides of equal length, i.e.; a square, containing extended corners similar in shape to the mortar slab shown in Plate 14.2.

In the tests on square slabs conducted by Blakey and Beresford[65,66] and later by Newman[68], it was assumed that a negligible effect on the stress and strain pattern occurred if the load and support points were simple moved a few inches towards the centre from the corners. To establish the validity of such assumptions, a comprehensive examination of the strain pattern on the square aluminum slab, described in Section 13.2, was conducted with the load and support points moved toward the centre in a manner similar to that used by the above investigators.

14.2.1 Testing Procedure

In order to obtain a complete representation of the strain pattern on the 36" square aluminum slab, one surface of one quadrant was covered with strain gauges as shown in Figure 14.3. This was considered sufficient as, under any symmetrical loading of the slab, every quadrant of both surfaces are stressed identically. On each surface, the strain pattern is symmetrical with respect to either of the two diagonal axes whilst the strain pattern on either surface is symmetrical to the strain pattern on the opposite surface with respect to those centre line axes which are parallel to the slab sides. The strain gauges were therefore generally placed in pairs in one quadrant symmetrically positioned with reference to one of the latter centre line axes. For example, with the load applied as shown in Figure 14.4, gauge no. 12 (see Figure 14.3) measures not only the tension strain at its location on the top surface, but also the tension strain on the bottom surface at the location of its symmetrically opposed gauge no. 8; the latter strain will be perpendicular to the orientation of gauge no. 8. Furthermore, by repeating each test run on the slab in an inverted position, it is possible to determine the strain pattern on both surfaces of the slab in both of the theoretically principal directions, with the given gauges.

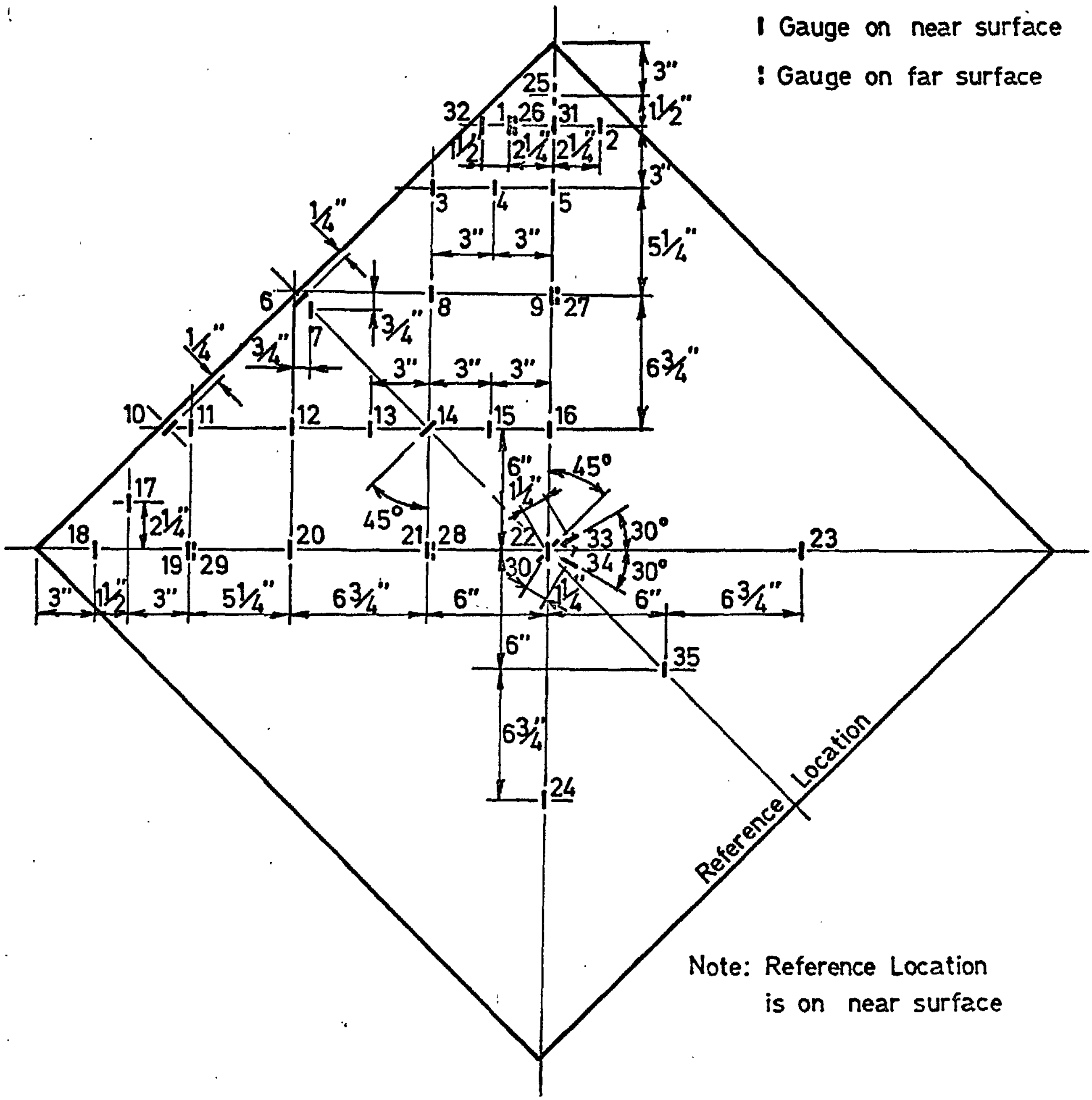

FIG. 14.3 LOCATION AND DESIGNATION OF GAUGES ON ALUMINUM SLAB - TEST SERIES 1

Several additional gauges were added to investigate the strain pattern in other quadrants as well as to check the alignment. For example, readings on gauge nos. 2, 23 and 24 should be identical to the readings obtained on gauge nos. 1, 20 and 9 respectively.

The strain gauges used were Technograph electrical resistance strain gauges of 1" length. Prior to applying each gauge, both the gauge and the aluminum surface were thoroughly cleaned with a cloth and Acetone. Araldite adhesive was used to fasten the gauge to the surface and, after setting, a thin layer of the adhesive was again used to cover each gauge. This not only protected gauges against possible damage, but also, insulated them against small fluctuations in room temperature.

To record the gauge readings, a Solartron data-logger, sensitive to 2 microstrain, was used.

For this first Test Series No. 1, the testing was performed in an auxiliary loading frame, as the biaxial testing machine described in Chapter 12 had not then been constructed. However, the base slab, $1\frac{1}{2}$" diameter x 6" long steel rollers, roller supports and loading beam which eventually formed part of the biaxial testing machine, had been manufactured and were therefore used in this test series. A picture of the general loading assembly is given in Plate 14.1.

The rollers had two supports at one end and one at the other for each of the loading and reaction points. This

PLATE 14.1 Test method used for loading aluminum slab in test series 1.

providdd a stable loading system while ensuring simultaneously that, with proper centring, the effective centroid of load application at each roller coincided with its centre. Each of the roller supports had a spherical cap with the centre of this sphere coinciding with the longitudinal axis of the roller. With the radius of this cap being slightly smaller than the inner spherical surface of contact of the roller, rolling was achieved with a negligible component of vertical movement for the small magnitudes of rolling obtained.

For every test, the slab was positioned on the loading frame with the loading beam placed on top, care being taken in both cases to obtain axial alignment. Both the slab and loading beam were levelled in both directions with the aid of adjusting screws on the roller supports. The load was applied by means of a hydraulic, hand-operated jack with measurement of load being performed with a calibrated proving ring. (see Plate 14.1)

Test Series 1 consisted of four independent sets of tests. For the first three, the load was applied directly by rollers with all rollers being located 3", 2" and 1" from the corners of the slab, respectively. For the fourth test, conducted with the rollers 2" from the corners, the loads were applied through 2" x 2" x $\frac{1}{4}$" steel plates interposed between the rollers and the slab surface. The sides of these plates were parallel to the sides of the aluminum slab. In addition, one thickness of building paper, 2" square was interposed between each of the plates and slab surface.

Each test, consisting of two load stages, was performed three times with three complete sets of readings at each load stage. This procedure was subsequently repeated on the slab in the inverted position. The total applied loads at each of the two load stages were 326 and 787 lbs., producing approximately 105 and 250 microstrain respectively, at the centre of the slab.

14.2.2 Discussion of Results

The averages of the nine strain readings for each gauge at each load stage for each of the various tests in Test Series 1 are presented in Tables 14.1 to 14.4.

In each of the tables, T denotes tensile strain and C denotes compression strain. As the principal strain values over the entire slab surface should be of constant magnitude (see Equation 14.17), the average strains have also been represented as coefficients in relation to the average strain at the centre point of the slab (gauge no. 22). The distribution of the coefficients of longitudinal and lateral strains, assumed as principal strains from theoretical analysis, for one representativ quadrant have been presented for the second load stage in Figures 14.4 to 14.7.

The theory of Section 14.1 is based on small deflections of the slab. Consequently, the coefficients of the first load stage are presented for one test, where the maximum

TABLE 14.1 STRAIN DISTRIBUTION ON ALUMINUM SLAB LOADED WITH STEEL ROLLERS 3" FROM CORNERS

GAUGE No.	SLAB IN UPRIGHT POSITION				SLAB IN INVERTED POSITION			
	1st LOAD STAGE		2nd LOAD STAGE		1st LOAD STAGE		2nd LOAD STAGE	
	STRAIN ($x10^{-6}$)	COEFF	STRAIN ($x10^{-6}$)	COEFF	STRAIN ($x10^{-6}$)	COEFF	STRAIN ($x10^{-6}$)	COEFF
1	53 T	0.530	127 T	0.535	60 C	0.600	137 C	0.578
2	52 T	0.520	127 T	0.535	57.5 C	0.575	138.5 C	0.585
3	82 T	0.818	198 T	0.835	84.5 C	0.842	199.5 C	0.840
4	75 T	0.750	179 T	0.755	80.5 C	0.802	192.5 C	0.810
5	71 T	0.710	170 T	0.715	76 C	0.758	186 C	0.785
6	6 T	-	24 T	-	5.5 T	-	26.5 T	-
7	93 T	0.928	229 T	0.965	91.5 C	0.912	217.5 C	0.915
8	90 T	0.898	214 T	0.902	92 C	0.918	233 C	0.940
9	87 T	0.868	205 T	0.865	91 C	0.908	224 C	0.945
10	13 T	-	49 T	-	12.5 C	-	22.5 C	-
11	95 T	0.948	232 T	0,978	91.5 C	0.912	217.5 C	0.918
12	96 T	0.958	234 T	0.985	98 C	0.978	230 C	0.970
13	96 T	0.958	231 T	0.972	98.5 C	0.982	234.5 C	0.990
14	2 C	-	7 C	-	0.5 C	-	1.5 C	-
15	94 T	0.938	225 T	0.948	99.5 C	0.992	239.5 C	1.008
16	94 T	0.938	222 T	0.935	99 C	0.988	238 C	1.010
17	85 T	0.848	211 T	0.890	83 C	0.828	200 C	0.842
18	67 T	0.670	157 T	0.660	-	-	-	-
19	93 T	0.928	230 T	0.970	91.5 C	0.912	213.5 C	0.898
20	99 T	0.988	241 T	1.015	99 C	0.988	233 C	0.980
21	96 T	0.958	233 T	0.982	100 C	0.998	240 C	1.010
22	99.7 T	0.995	232.3 T	0.980	101.0 C	1.008	242.7 C	1.020
23	99 T	0.988	242 T	1.020	98.5 C	0.982	230.5 C	0.970
24	92 T	0.918	211 T	0.890	93.5 C	0.932	227.5 C	0.958
25	21 C	0.210	54 C	0.228	-	-	-	-
26	56 C	0.560	134 C	0.565	55.5 T	0.555	131.5 T	0.555
27	89 C	0.888	223 C	0.940	90 T	0.898	211 T	0.890
28	99 C	0.988	242 C	1.020	99 T	0.988	236 T	0.995
29	91 C	0.908	217 C	0.915	97 T	0.968	235 T	0.998
30	3 C	-	9 C	-	0.5 T	-	2.5 C	-
31	49 T	0.490	109 T	0.460	49.5 C	0.495	118.5 C	0.500
32	57 T	0.570	138 T	0.580	58.5 C	0.585	140.5 C	0.590
33	50 C	-	126 C	-	47.5 T	-	112.5 T	-
34	51 C	-	126 C	-	49.5 T	-	114.5 T	-
35	99 T	0.988	233 T	0.980	99 C	0.988	238 C	1.002

Note: Average Principal Surface Strain at centre is $100.3x10^{-6}$ at 1st load stage - Total Applied Load of 326 lbs.: $237.5x10^{-6}$ at 2nd load stage - Total Applied Load of 787 lbs.

The coefficient values of the 2nd load stage above are presented diagrammatically in Figure 14.4

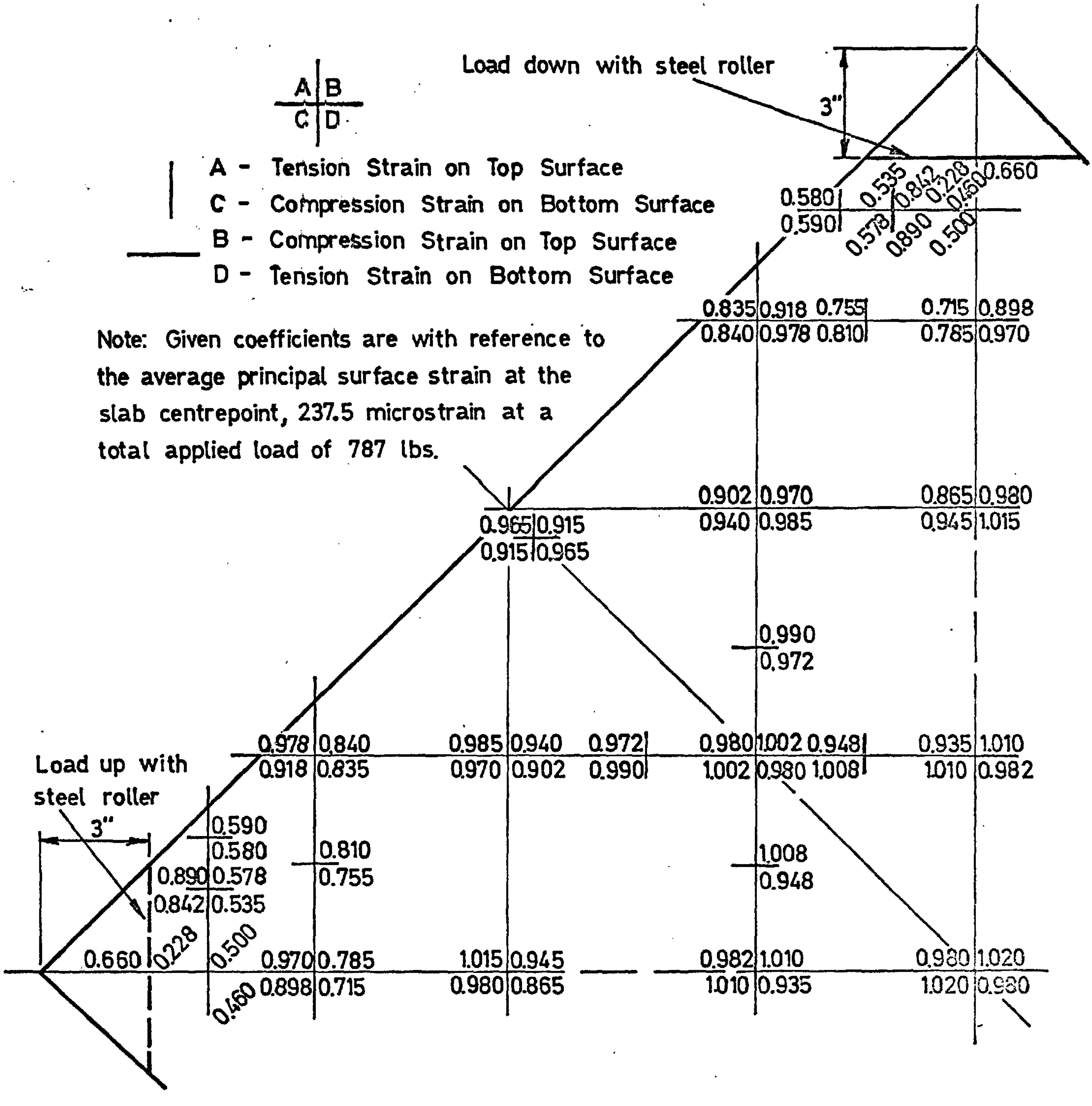

FIG. 14.4 STRAIN DISTRIBUTION ON ALUMINUM SLAB LOADED AND SUPPORTED BY STEEL ROLLERS AT 3" FROM CORNERS

TABLE 14.2 STRAIN DISTRIBUTION ON ALUMINUM SLAB LOADED WITH STEEL ROLLERS 2" FROM CORNERS

GAUGE No.	SLAB IN UPRIGHT POSITION				SLAB IN INVERTED POSITION			
	1st LOAD STAGE		2nd LOAD STAGE		1st LOAD STAGE		2nd LOAD STAGE	
	STRAIN ($x10^{-6}$)	COEFF	STRAIN ($x10^{-6}$)	COEFF	STRAIN ($x10^{-6}$)	COEFF	STRAIN ($x10^{-6}$)	COEFF
1	74.5 T	0.708	178.5 T	0.715	80 C	0.760	191 C	0.765
2	75 T	0.712	178 T	0.712	79 C	0.750	190 C	0.760
3	91 T	0.865	219 T	0.878	94 C	0.892	225 C	0.900
4	88 T	0.835	207 T	0.830	93 C	0.882	227 C	0.908
5	84 T	0.798	200 T	0.800	91.5 C	0.870	222.5 C	0.890
6	4 T	-	26 T	-	7 T	-	32 T	-
7	101 T	0.960	243 T	0.972	99 C	0.940	232 C	0.928
8	96 T	0.912	229 T	0.918	102.5 C	0.972	245.5 C	0.980
9	92 T	0.872	220 T	0.880	102 C	0.968	248 C	0.992
10	13.5 T	-	37.5 T	-	1 C	-	2 T	-
11	100 T	0.950	242 T	0.968	95 C	0.902	229 C	0.918
12	102 T	0.970	245 T	0.980	102.5 C	0.972	242.5 C	0.970
13	101.5 T	0.965	243.5 T	0.975	105 C	0.998	250 C	1.000
14	1.5 C	-	2.5 C	-	2 T	-	1 T	-
15	98.5 T	0.935	234.5 T	0.940	105.5 C	1.002	255.5 C	1.022
16	99.5 T	0.945	233.5 T	0.935	107 C	1.018	256 C	1.025
17	98 T	0.930	234 T	0.938	90.5 C	0.860	219.5 C	0.878
18	87 T	0.825	207 T	0.830	87.5 C	0.830	198.5 C	0.795
19	102.5 T	0.975	250.5 T	1.002	103 C	0.980	239 C	0.955
20	104 T	0.988	252 T	1.008	105 C	0.998	247 C	0.990
21	103 T	0.980	241 T	0.965	105.5 C	1.002	254.5 C	1.020
22	102.3 T	0.972	239.2 T	0.958	108.2 C	1.030	260.8 C	1.042
23	105.5 T	1.002	252.2 T	1.010	105.5 C	1.002	246.5 C	0.985
24	99 T	0.940	229 T	0.918	107 C	1.018	255 C	1.020
25	50 C	0.475	115 C	0.460	48 T	0.455	116 T	0.465
26	78 C	0.740	183 C	0.732	76.5 T	0.725	182.5 T	0.730
27	99 C	0.940	239 C	0.958	97 T	0.920	228 T	0.912
28	105 C	0.998	247 C	0.988	104.5 T	0.992	250.5 T	1.002
29	100 C	0.950	231 C	0.925	105 T	0.998	257 T	1.028
30	7 C	-	14 C	-	1.5 C	-	5.5 C	-
31	69 T	0.655	162 T	0.648	74 C	0.702	180 C	0.720
32	71 T	0.675	173 T	0.692	76 C	0.720	179 C	0.715
33	50.5 C	-	124.5 C	-	52.5 T	-	118.5 T	-
34	56.5 C	-	134.5 C	-	49 T	-	118 T	-
35	104 T	0.988	246 T	0.985	108 C	1.025	256 C	1.022

Note: Average Principal Surface Strain at Centre is : $105.2x10^{-6}$ at 1st Load Stage - Total applied load of 326 lbs.
: $250.0x10^{-6}$ at 2nd Load Stage - Total applied load of 787 lbs.

The coefficient values of the 2nd Load Stage are presented in Figure 14.5

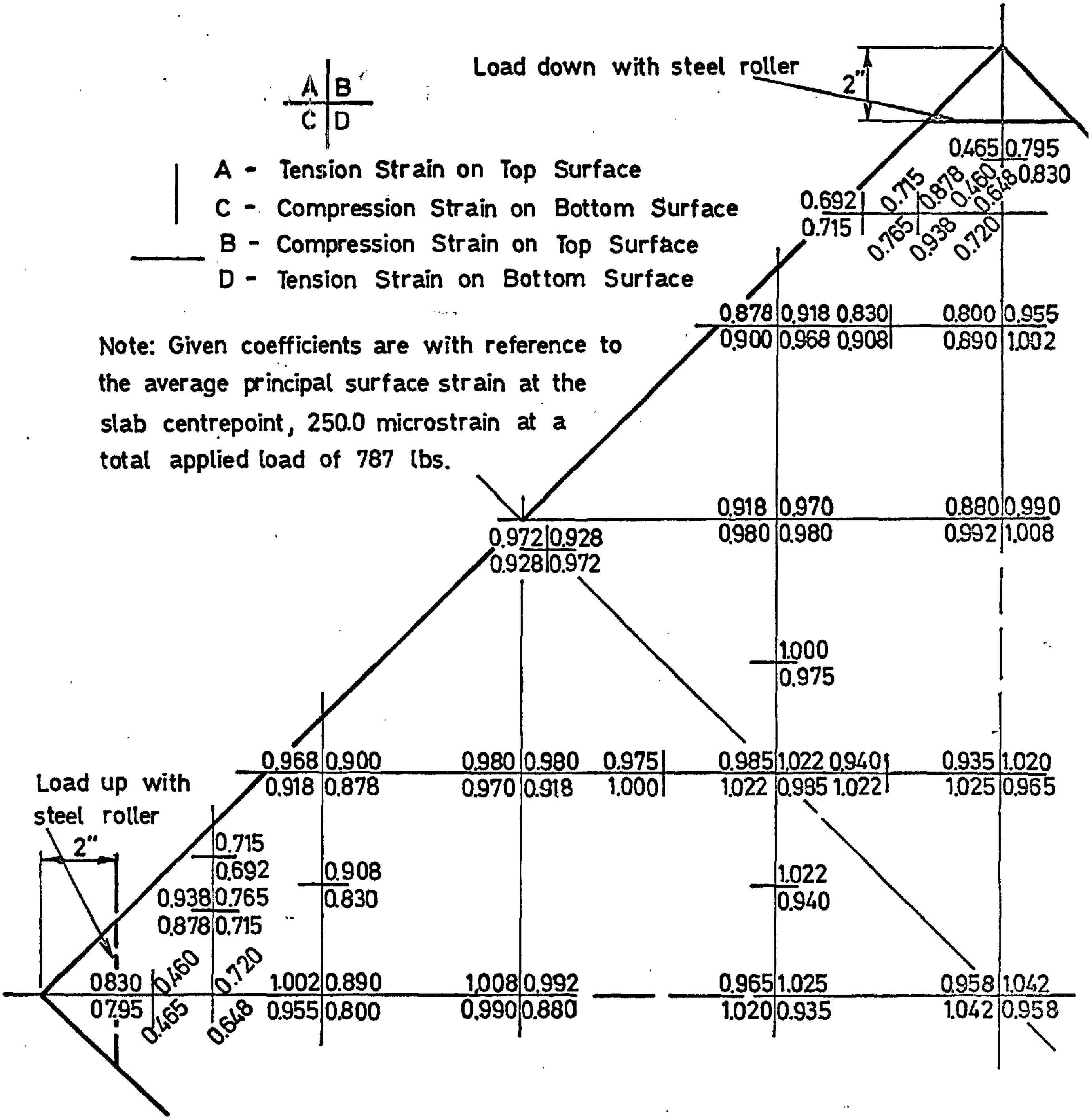

FIG.14.5 STRAIN DISTRIBUTION ON ALUMINUM SLAB LOADED AND SUPPORTED BY STEEL ROLLERS AT 2" FROM CORNERS

14.3 STRAIN DISTRIBUTION ON ALUMINUM SLAB LOADED WITH STEEL ROLLERS AND 2" SQUARE STEEL PLATES 2" FROM CORNERS

GAUGE NO.	SLAB IN UPRIGHT POSITION				SLAB IN INVERTED POSITION			
	1st LOAD STAGE		2nd LOAD STAGE		1st LOAD STAGE		2nd LOAD STAGE	
	STRAIN ($x10^{-6}$)	COEFF	STRAIN ($x10^{-6}$)	COEFF	STRAIN ($x10^{-6}$)	COEFF	STRAIN ($x10^{-6}$)	COEFF
1	74.5 T	0.712	175.5T	0.700	80 C	0.765	191 C	0.762
2	76 T	0.728	178. T	0.710	78 C	0.748	189 C	0.755
3	93.5 T	0.895	223.5T	0.892	92.5C	0.885	223.5 C	0.892
4	88.5 T	0.848	208.5T	0.832	93 C	0.890	225 C	0.898
5	87 T	0.832	203 T	0.810	92.5C	0.885	225.5 C	0.900
6	3.5 T	-	24.5T	-	8.5T	-	33.5 T	-
7	102.5T	0.982	247.5T	0.988	99 C	0.948	232 C	0.925
8	98.5 T	0.942	232.5T	0.930	101 C	0.968	244 C	0.972
9	97 T	0.930	224 T	0.895	101 C	0.968	247 C	0.985
10	12 T	-	35 T	-	2.5C	-	2.5 T	-
11	101 T	0.968	246 T	0.982	95 C	0.910	227 C	0.908
12	104 T	0.995	251 T	1.002	101.5C	0.972	241.5 C	0.965
13	105 T	1.005	248 T	0.990	104 C	0.998	248 C	0.990
14	1 C	-	4 C	-	2. T	-	2 T	-
15	103 T	0.988	240 T	0.958	105 C	1.008	256 C	1.022
16	101 T	0.968	237 T	0.945	105 C	1.008	255 C	1.018
17	98.5 T	0.942	236.5T	0.945	91 C	0.872	219 C	0.875
18	94 T	0.900	228 T	0.910	-	-	-	-
19	105 T	1.005	256 T	1.022	103.5C	0.992	239.5 C	0.955
20	106.5T	1.020	255.5T	1.020	105 C	1.008	247 C	0.985
21	104 T	0.995	244 T	0.975	105.5C	1.010	253.5 C	1.010
22	103 T	0.988	243 T	0.970	105.7C	1.012	257.7 C	1.030
23	107 T	1.025	258 T	1.030	103 C	0.988	244 C	0.975
24	99 T	0.948	231 T	0.922	101 C	0.968	251 C	1.000
25	46.5 C	0.445	110.5C	0.440	-	-	-	-
26	76.5 C	0.732	180.5C	0.720	76 T	0.728	181 T	0.722
27	99 C	0.948	244 C	0.975	97 T	0.930	229 T	0.915
28	106 C	1.015	252 C	1.005	103.5T	0.992	248.5 T	0.992
29	101 C	0.968	236 C	0.942	1065T	1.020	258.5 T	1.030
30	0.5T	-	7.5C.	-	1.5C	-	5.5 C	-
31	73 T	0.700	167 T	0.668	77.5C	0.742	183.5 C	0.732
32	75 T	0.720	176 T	0.702	73.5C	0.705	176.5 C	0.705
33	51 C	-	128 C	-	50.5T	-	117.5 T	-
34	53 C	-	132 C	-	48.5T	-	118.5 T	-
35	106.5T	1.020	249.5T	0.995	103 C	0.988	253 C	1.010

Note: Principal surface strain at centre is : 104.3 $x10^{-6}$ at
1st load stage - Total applied load of 326 lbs.
: 250.3 $x10^{-6}$ at
2nd load stage - Total applied load of 787 lbs.

The coefficient values of the 2nd load stage are presented diagrammatically in Figure 14.6.

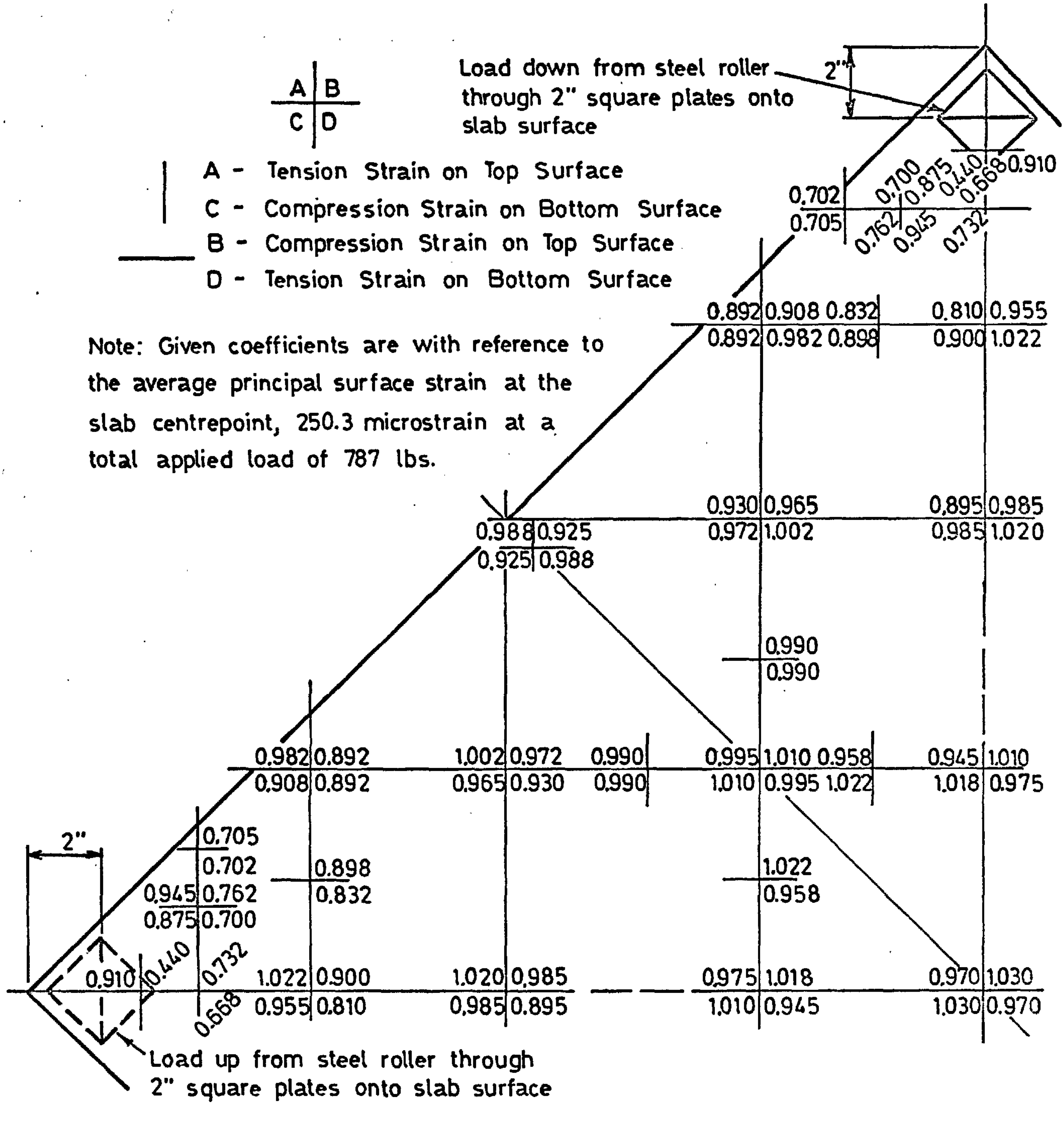

FIG. 14.6 STRAIN DISTRIBUTION ON ALUMINUM SLAB LOADED AND SUPPORTED BY STEEL ROLLERS AND 2" SQUARE PLATES AT 2" FROM CORNERS

TABLE 14.4 STRAIN DISTRIBUTION ON ALUMINUM SLAB LOADED WITH STEEL ROLLERS 1" FROM CORNERS

GAUGE NO.	SLAB IN UPRIGHT POSITION				SLAB IN INVERTED POSITION			
	1st LOAD STAGE		2nd LOAD STAGE		1st LOAD STAGE		2nd LOAD STAGE	
	STRAIN ($x10^{-6}$)	COEFF	STRAIN ($x10^{-6}$)	COEFF	STRAIN ($x10^{-6}$)	COEFF	STRAIN ($x10^{-6}$)	COEFF
1	93.5 T	0.840	229.5 T	0.868	97 C	0.872	236 C	0.892
2	99.5 T	0.895	236.5 T	0.895	98.5 C	0.886	238.5 C	0.902
3	107.5 T	0.970	255.5 T	0.965	103 C	0.9[illegible]	245 C	0.925
4	103.5 T	0.932	246.5 T	0.932	104 C	0.938	254 C	0.960
5	102.5 T	0.922	239.5 T	0.905	104 C	0.938	254 C	0.960
6	4 T	-	27 T	-	11.5 T	-	37.5 T	-
7	109 T	0.980	268 T	1.012	103.5 C	0.932	244.5 C	0.925
8	107.5 T	0.968	253.5 T	0.958	107 C	0.965	261 C	0.985
9	104.5 T	0.940	246.5 T	0.932	108.5 C	0.978	266.5 C	1.008
10	5.5 T	-	22.5 T	-	6.5 T	-	21.5 T	-
11	111 T	1.000	268 T	1.012	104.5 C	0.942	244.5 C	0.925
12	112 T	1.010	269 T	1.018	108.5 C	0.978	253.3 C	0.958
13	110.5 T	0.995	263.5 T	0.995	109 C	0.980	262 C	0.990
14	2 C	-	7 C	-	3.5 T	-	2.5 T	-
15	110 T	0.990	257 T	0.970	109.5 C	0.985	269.5 C	1.020
16	109.5 T	0.988	253.5 T	0.958	111 C	1.000	270 C	1.020
17	108.5 T	0.978	264.5 T	1.000	101 C	0.910	240 C	0.908
18	105.5 T	0.950	255.5 T	0.965	103 C	0.928	243 C	0.918
19	110.5 T	0.995	272.5 T	1.030	108.5 C	0.978	251.5 C	0.950
20	114 T	1.025	272 T	1.028	110.5 C	0.995	258.5 C	0.978
21	108.5 T	0.978	259.5 T	0.980	111 C	1.000	265 C	1.002
22	110.8 T	0.998	258.2 T	0.975	111.3 C	1.002	270.7 C	1.025
23	113 T	1.018	273 T	1.030	108.5 C	0.978	253.5 C	0.958
24	108 T	0.972	249 T	0.940	112 C	1.010	273 C	1.030
25	89.5 C	0.805	215.5 C	0.815	89 T	0.800	205 T	0.775
26	99.5 C	0.895	242.5 C	0.918	99 T	0.890	232 T	0.876
27	109.5 C	0.988	272.5 C	1.030	107.5 T	0.968	248.5 T	0.940
28	112 C	1.010	270 C	1.020	113 T	1.020	262 T	0.990
29	107.5 C	0.968	255.5 C	0.965	115 T	1.035	276 T	1.042
30	1 C	-	9 C	-	0.5 T	-	3.5 C	-
31	93 T	0.882	230 T	0.870	96.5 C	0.868	235.5 C	0.890
32	89.5 T	0.805	216.5 T	0.820	89 C	0.800	213 C	0.805
33	56 C	-	141 C	-	54 T	-	125 T	-
34	58.5 C	-	143.5 C	-	54 T	-	125 T	-
35	112 T	1.010	263 T	0.995	112.5 C	1.012	267.5 C	1.010

Note: Principal surface strain at centre is: 111.0 $x10^{-6}$ at 1st load stage - Total applied load of 326 lbs.
: 264.5 $x10^{-6}$ at 2nd load stage - Total applied load of 787 lbs.

The coefficient values of the 2nd and 1st load stages are presented, diagrammatically in Figures 14.7 and 14.8 respectively.

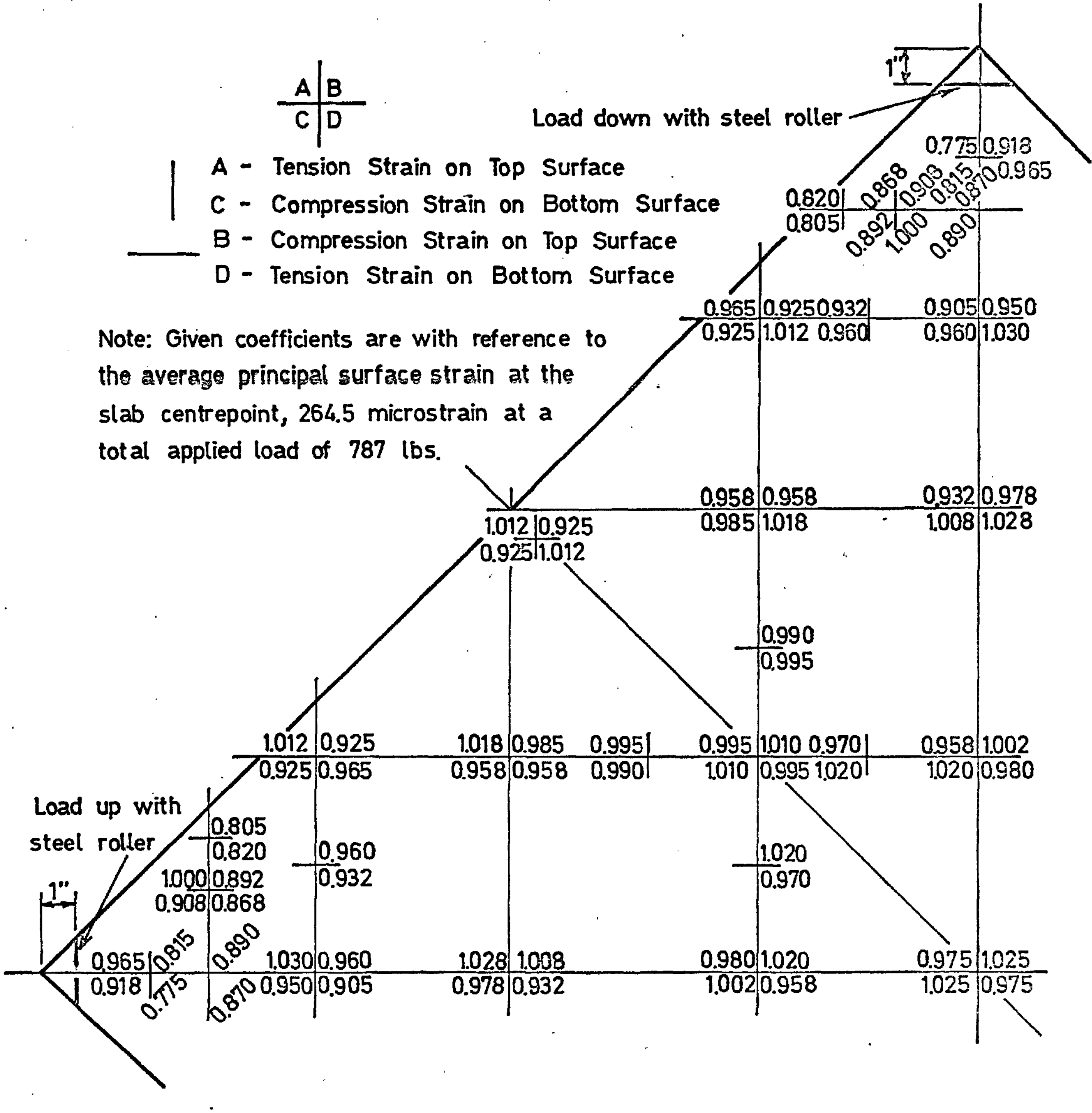

FIG. 14.7 STRAIN DISTRIBUTION ON ALUMINUM SLAB LOADED AND SUPPORTED BY STEEL ROLLERS AT 1" FROM CORNERS

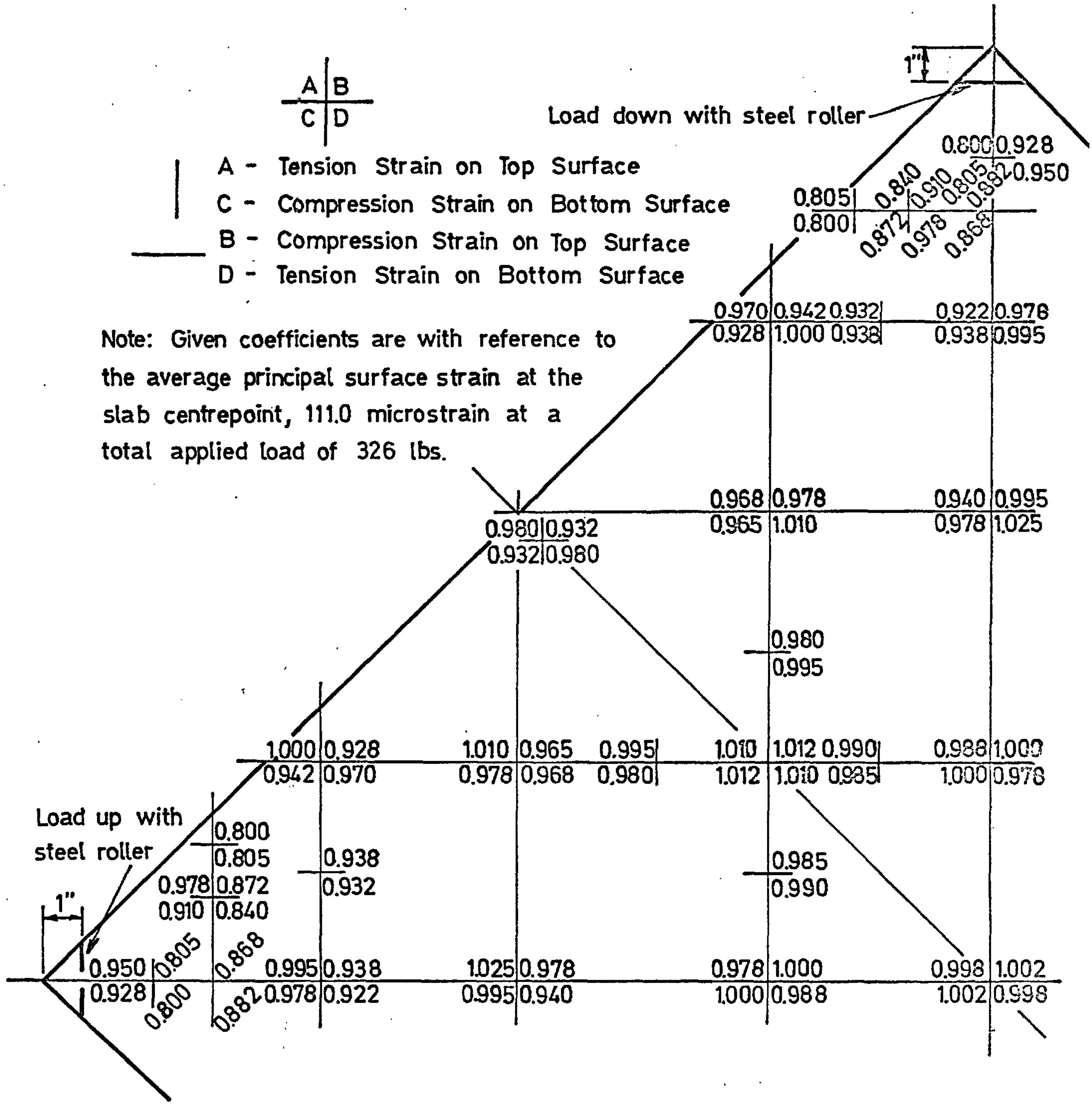

FIG. 14.8 STRAIN DISTRIBUTION ON ALUMINUM SLAB LOADED AND SUPPORTED BY STEEL ROLLERS AT 1" FROM CORNERS

deflection, with respect to the slab centre point is only 0.10" as opposed to 0.24" for the second load stage, (see Figures 14.7 and 14.8).

From Figures 14.4 to 14.8, the folowing conclusions are drawn:

1. With a loading system whereby the load is not applied directly at the corners, the strain distribution will vary markedly as opposed to the constant distribution assumed.

2. This non-uniformity of strain distribution decreases as the loading points move nearer their respective corners.

3. The average strain and corresponding stress at the centre increases as the load points move nearer the corners. For example, the average strain increased from 237.5 to 264.5 microstrain, at 787 lbs. load when all load points were moved from 3" to 1" from their respective corners. This is an increase of 11.4%.

4. The general strain pattern remains independent of the method of applying the load except in the immediate vicinity of load application. Although there appears to be some difference in the coefficients in Figures 14.5 and 14.6, this difference, is consistent (about 1%) and is due to small errors in the measured strain at the slab centre-point. (gauge 22) As all the coefficients in Table 14.1 to 14.4 are related to the average measured strain at the slab centre (see Tables 14.1 to 14.4), a small error in the reading of the gauge at the centre, no. 22, will produce similar

percentage errors in the coefficients of the other gauges. When the above test was repeated in Test Series 2 (see Section 14.3.3), the average strains at the centrepoint of the slab were virtually identical for the two tests and, as a result, the strain patterns over the surface of the specimen for the two tests were remarkably similar, except in the immediate vicinity of the load and support points.

5. The strain pattern is more consistent with small deflections of the slab. This is shown by comparing Figures 14.7 and 14.8 where, at the 1st load stage, corresponding to a deflection of only 0.10" (Figure 14.8), the strain at each gauge point is closer to being identical for the two separate tests and also, the strains across a section parallel to a diagonal are more consitent, than at the second load stage. (Figure 14.7) At the latter load stage, a significant maximum deflection of 0.24" with reference to the slab centrepoint occurred.

It is apparent from the foregoing that the non-uniform stress and strain pattern arising from loading even a small distance in from the corners will have a very significant effect on the discontinuity level stresses as well as the ultimate strengths. Likewise, a significant influence on modulus of elasticity values will occur.

For example, using the average strain values obtained at the slab centrepoint with a total load of 787 lbs. and a ν value of 0.343 (see Section 14.6), then, from Equation 14.17, the calculated E values are 11.5 x10 ^{6}, 10.9x10 ^{6} and

10.3×10^6 p.s.i. with the load points 3", 3" and 1" from the corners, respectively. Extrpolating to a theoretical distance of 0", the E value obtained would be about 9.7×10^6 p.s.i. This compares very favourably with the average value of 9.85×10^6 p.s.i. obtained from the tests on the aluminum slabs with extended corners (see Section 14.6).

It should be appreciated that the centrepoint strains selected above produce the most realistic values of E. At any other point, the calculated E value will be even more grossly in error due to measured principal strains having smaller values.

As the calculated E values at the slab centrepoint increase by about 19%, when the applied loads are moved from 0" to 3" in from the corners, the calculated stress values simultaneously decrease by 19% at any value of applied load. As the slab centrepoint is the most highly stressed point on the slab when the load points are not at the corners, it is apparent that, near failure, an increasing proportion of the load will be transferred to less highly stressed portions before ultimate collapse of the slab occurs. As such a redistribution of stresses would not occur with slabs loaded at the corners where all points of the slab are equally stressed, the difference in ultimate strengths would be expected to be even greater than 19%, probably 25 to 30%.

14.2.3 Assessment of Previous Testing Techniques

From the above discussion, it is obvious that the test methods as used by Blakey and Beresford (65,66) and subsequently by Newman[68] were highly unsatisfactory. The slabs tested by Newman,[68] 21" square with the load points 3" in from the corners, would exhibit even greater variations in strain than any of the tests on the 36" square aluminum slab, discussed above. Consequently, be extending the above analysis, the modulus of elasticity, discontinuity level stresses and ultimate strengths would all by high, probably by as much as 40%.

The largest average tensile strains across a section occur at or near a diagonal and reduce towards the load points. This verifies the type of failures obtained by both Blakey and Beresford and Newman where it was observed that almost all failures occurred at or very near a diagonal.

From the foregoing, it is obvious that, with a testing technique in which the loads are not applied at the corners as specified in the theoretical requirements, the increase in modulus of elasticity, ultimate strength and other related properties are enormous. It can be concluded that a reliable technique is possible only if the loads are applied at the corners.

14.3 TESTS ON SQUARE SLABS WITH EXTENDED CORNERS

As it is impossible in practise to load a square slab at its corners, it was necessary to produce extensions at the corners through which the loads could be applied. Then, the centroids of the loads could be made to coincide with the intersection of the protection of the slab sides.

The following discussion is concerned with the development of suitable corners for performing such a test satisfactorily, followed by an investigation of the resulting strain pattern on the slab.

14.3.1. Results of Tests on Pilot Mortar Slabs

The first two slabs tested, 30" square x 2" thick, one of which is shown in Plate 14.2, had 4" square corners with the centre of each corner coinciding with the intersection of the projection of the two adjacent slab sides. The method of loading the slab was essentially identical to that shown in Plate 14.1 except that 4" square x 5/16" thick steel plates were positioned between the rollers and slab surface. Several electrical resistance strain gauges were attached to the slab surface to investigate the strain pattern.

On loading to failure, the principal strains remained reasonably constant except near the edges. However, as failure of the first slab occurred at the intersection of the slab side and corner projection, it was concluded that the loading method caused high stress concentrations in this localized area.

Following this initial failure, the broken section was glued together with a very strong adhesive, Certite, and the slab was subsequently reloaded to failure twice. Plate 14.2 shows the slab after it has been loaded to failure three times. For the first slab, failure in every case occurred at the location of the re-entrant corner whereas,

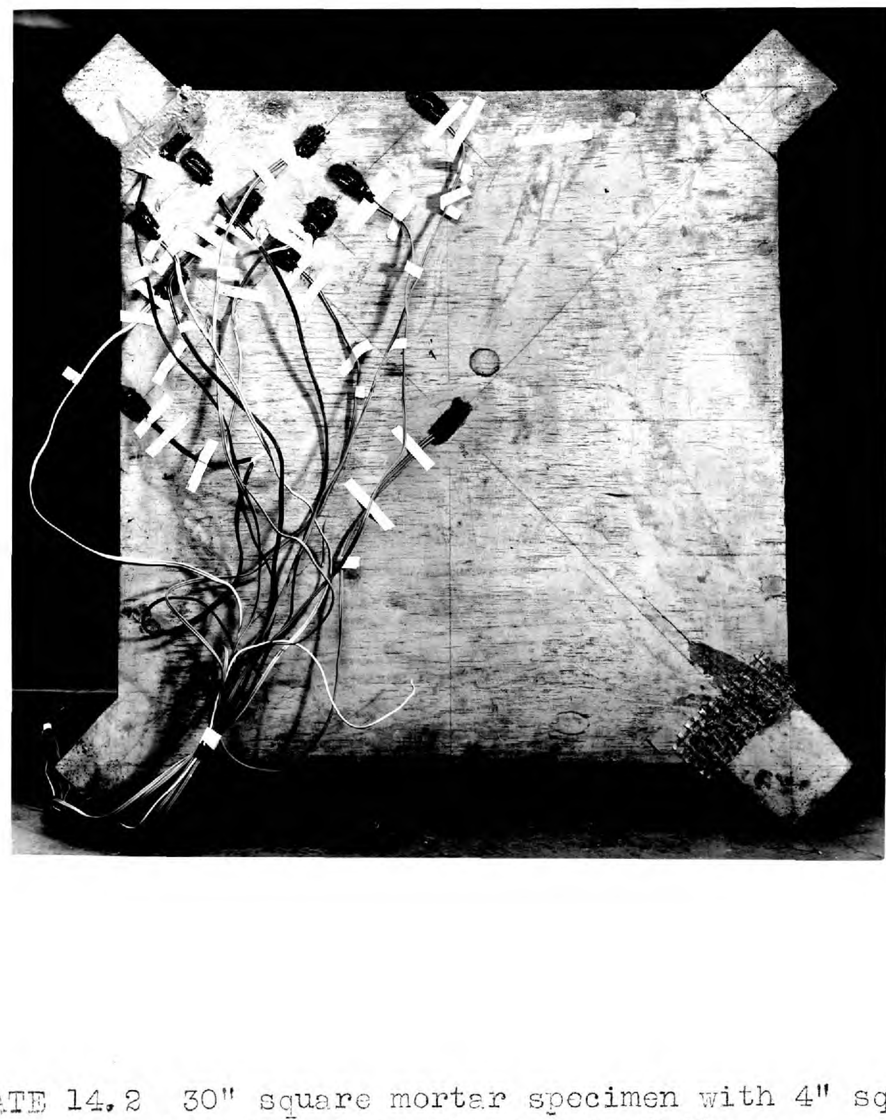

PLATE 14.2 30" square mortar specimen with 4" square corners after being loaded to failure three times

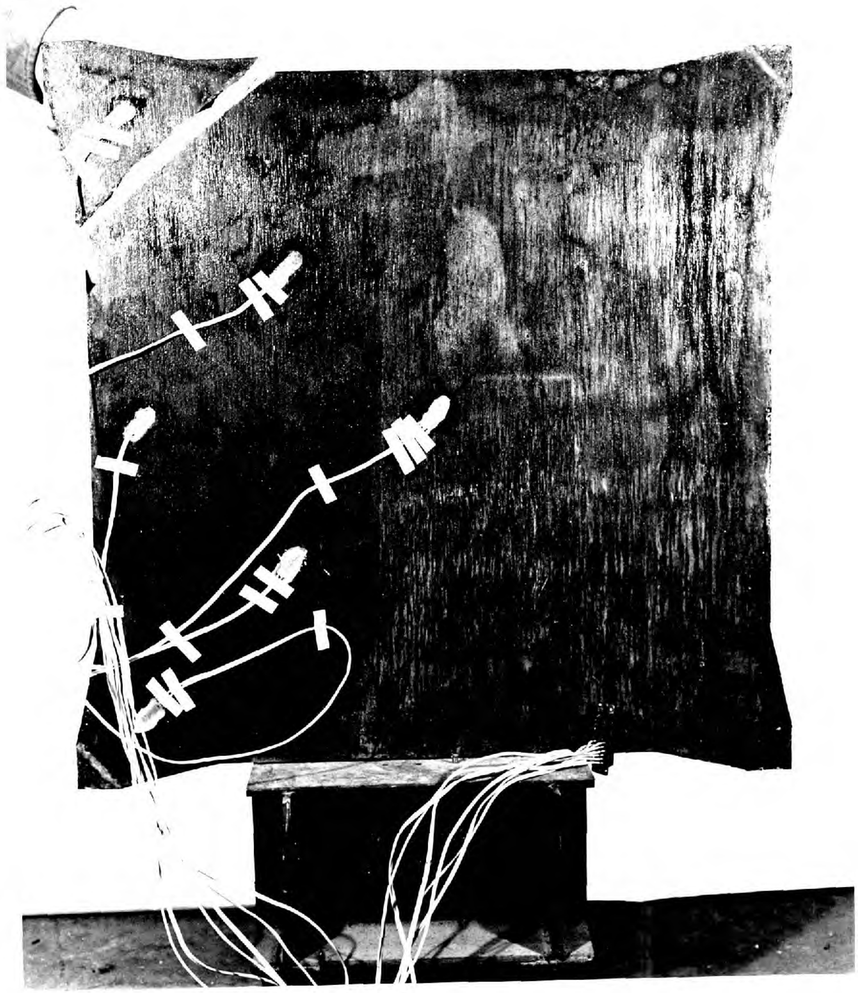

PLATE 14.3 30" square mortar specimen with 2" square corners at failure

for the second slab which was identical in shape to the first, failure occurred away from the corners. From the results of the above tests, a redesign of the corners was considered necessary. This was not only to avoid failure occurring at the re-entrant corners, but also, because it was considered that the excessive volume of material in the corners, could influence the stress distribution in the slab.

A second pair of slabs, 30" x 30" x 2" were cast, the first of which is shown in Plate 14.3. The corners of this slab have been reduced to 2" square with a smooth transition from the corners to the slab sides. When loaded to failure with simultaneous recordings of strain, sensibly constant values of principal strain over the surface were obtained. Failure occurred at a section located several inches from the corner, where any possible stress concentration effects from corner loading were eliminated. As a result, this slab shape was considered satisfactory.

The last slab tested was rather similar in shape to the one shown in Plate 14.3 but had the size of the corners further reduced to 1" square. Again there was a smooth transition from the corners to the slab sides. However, when testing it, great care had to be employed to prevent instability of the test set-up as the load points were very small. In addition, as the failure occurred at about 2" from a corner, it was considered that stress concentrations arising from the load points at the corners influenced the failure. It was concluded therefore that 1" square corners were too small.

From the foregoing investigation, a 30" square slab with 2" square corners having a smooth transition curve from the corners to the slab sides was accepted as being the most suitably shaped specimen for achieving the desired uniform stress pattern.

14.3.2 Tests on Aluminum Slab

A comprehensive investigation was made of the strain pattern on an aluminum specimen similar in shape to the mortar specimen specified above. The 36" square aluminum slab used in Test Series 1 had a 1" width removed from each side except at the corners, thus leaving a 34" square aluminum slab with 2" square corners and a smooth transition curve from the corners to the slab sides (see Figure 14.9).

As a few of the gauges used in Test Series 1 had been removed in the cutting operation, new ones were attached, particularly to measure strains near the edge of the slab. The majority of the gauges used in Test Series 1 were, however, reused in this test series, hereafter referred to as Test Series 2. The Solartron data-logger was again used to record the strain readings.

As the biaxial testing machine described in Chapter 12 had, at this stage, been manufactured and assembled, all tests were performed in this machine (see Plate 14.4

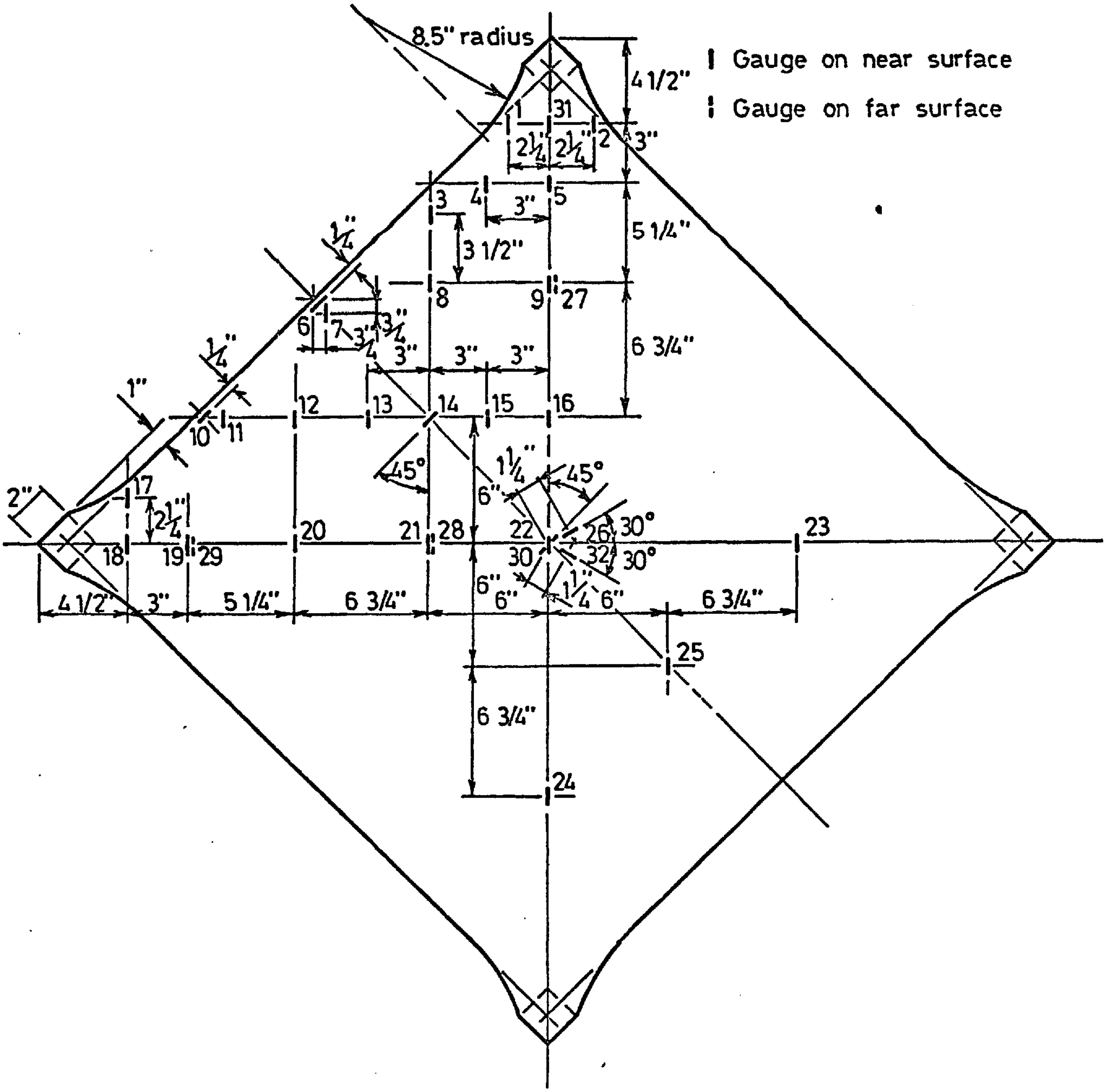

FIG. 149 LOCATION AND DESIGNATION OF GAUGES ON ALUMINUM SLAB (SQUARE) WITH EXTENDED CORNERS - TEST SERIES 2

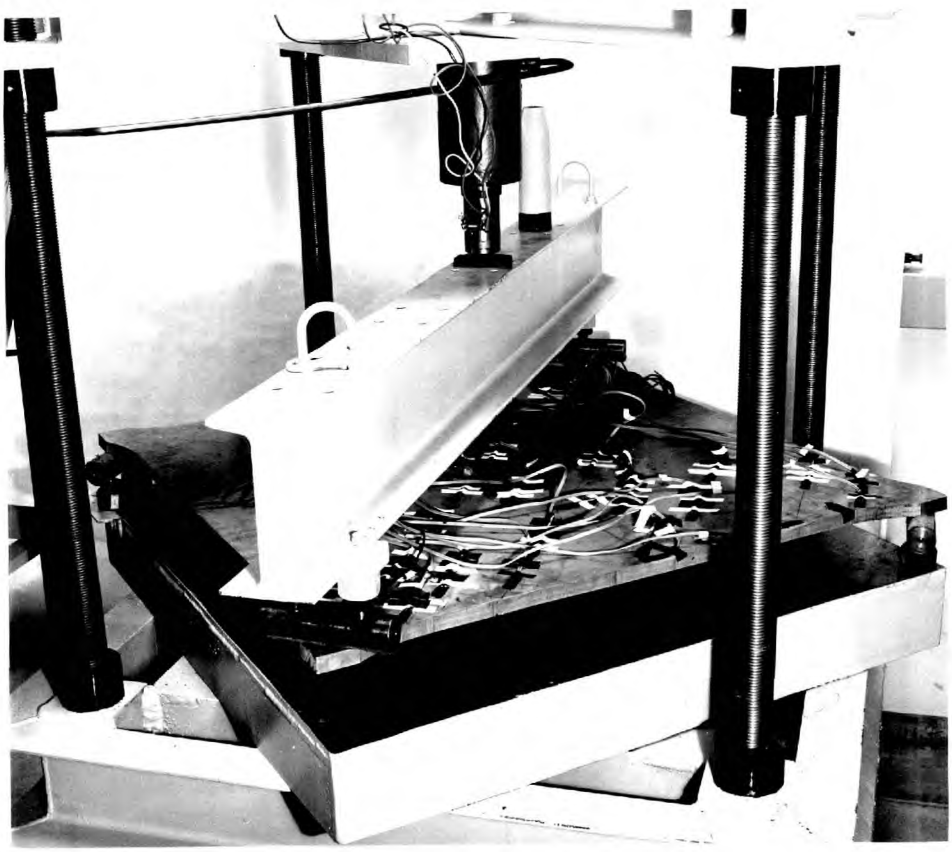

PLATE 14.4 Testing method for loading and supporting square plates at corners

for the test set-up). Before each test, the slab and beam were carefully positioned axially and levelled.

Test Series 2 consisted of three independent sets of tests with the centroid of each corner load coinciding, in every case, with the intersection of the adjacent projected slab sides. In the first test, the load was applied to the slab surface directly from the rollers, as observed in Plate 14.4. In the second test, 2" x 2" x $\frac{1}{4}$" steel plates were positioned between the rollers and slab surface with two sides of these plates being flush with the specimen corners. In addition, one thickness of building paper 2" square was positioned between each of the plates and the slab surface. The third test, to check the alignment of the biaxial machine, was performed by rotating the slab 180° about a vertical axis from a position as shown in Plate 14.4.

As in the case of Test Series 1, the slab was loaded three times with three readings at each load with a subsequent repetition on the slab in the inverted position. In every case, there was one load stage only of 705 lbs., total applied load.

14.3.3 Discussion of Results

The average of nine strain readings for each gauge for each test in this test series is presented in Tables 14.5 to 14.7 in which T is tensile strain and C is compression strain. The corresponding distributions of strain in one slab quadrant, based on the average recorded principal surface strains at the slab centrepoint, have been presented in Figures 14.10 to 14.12.

From examination of Figure 14.10, it is apparent that the principal surface strains are very nearly constant, seldom differing by more than 5% from the average principal strains at the slab centrepoint, except in the immediate vicinity of the corners. The variations which do exist are, in large part, accounted for by the excessive deflections of the slab, as explained in Sections 14.2.2 and 14.5.2.

At the slab corners and immediate vicinity, there is a reduction in strain from that obtained generally on the slab surface. This is particularly desirable as failure will then occur at a uniformly and more highly stressed section, sufficiently removed from the immediate vicinity of the corner.

Comparison between Figures 14.10 and 14.11 shows that loading the slab with steel plates positioned between the rollers and slab surface, produces the same general distribution of strain, as that obtained by loading directly with the rollers. In fact, only in the immediate vicinity of the corners are any differences detected and these would not be sufficient to cause any alterations in ultimate strength or other measured properties. Consequently, for all subsequent tests on mortar and concrete specimens, the load was simply applied

TABLE 14.5 STRAIN DISTRIBUTION ON SQUARE ALUMINUM SLAB WITH EXTENDED CORNERS LOADED WITH STEEL ROLLERS ONLY

GAUGE NO.	SLAB IN UPRIGHT POSITION			SLAB IN INVERTED POSITION		
	STRAIN(x10-6)		COEFF	STRAIN($\times 10^{-6}$)		COEFF
1	252.7	T	1.022	250.7	C	1.013
2	259.0	T	1.048	251.0	C	1.016
3	256.0	T	1.037	246.0	C	0.996
4	253.7	T	1.027	257.0	C	1.040
5	244.3	T	0.988	256.0	C	1.036
6	34.7	T	-	23.0	T	-
7	257.7	T	1.042	233.7	C	0.945
8	249.7	T	1.010	249.0	C	1.008
9	240.0	T	0.971	255.7	C	1.033
10	19.7	T	-	23.3	T	-
11	261.7	T	1.060	236.0	C	0.955
12	259.3	T	1.049	237.0	C	0.959
13	254.3	T	1.029	242.7	C	0.982
14	5.0	C	-	2.3	T	-
15	244.0	T	0.987	252.7	C	1.022
16	240.7	T	0.974	252.0	C	1.020
17	238.7	T	0.964	219.7	C	0.889
18	227.7	T	0.922	210.7	C	0.854
19	257.7	T	1.042	228.7	C	0.926
20	259.7	T	1.051	234.0	C	0.947
21	246.3	T	0.996	245.3	C	0.993
22	243.0	T	0.983	251.7	C	1.018
23	259.0	T	1.048	234.7	C	0.950
24	241.7	T	0.978	256.7	C	1.040
25	250.7	T	1.015	250.7	C	1.014
26	133.3	C	-	116.7	T	-
27	269.3	C	1.090	239.0	T	0.968
28	257.0	C	1.040	242.3	T	0.980
29	238.0	C	0.963	252.0	T	1.020
30	10.3	C	-	7.0	C	-
31	238.7	T	0.966	237.0	C	0.959
32	136.0	C	-	113.7	T	-

Note: Average principal surface strain at centre is 247.3×10^{-6} at a total applied load of 705 lbs.

Coefficient values above are presented diagrammatically in Figure 14.10.

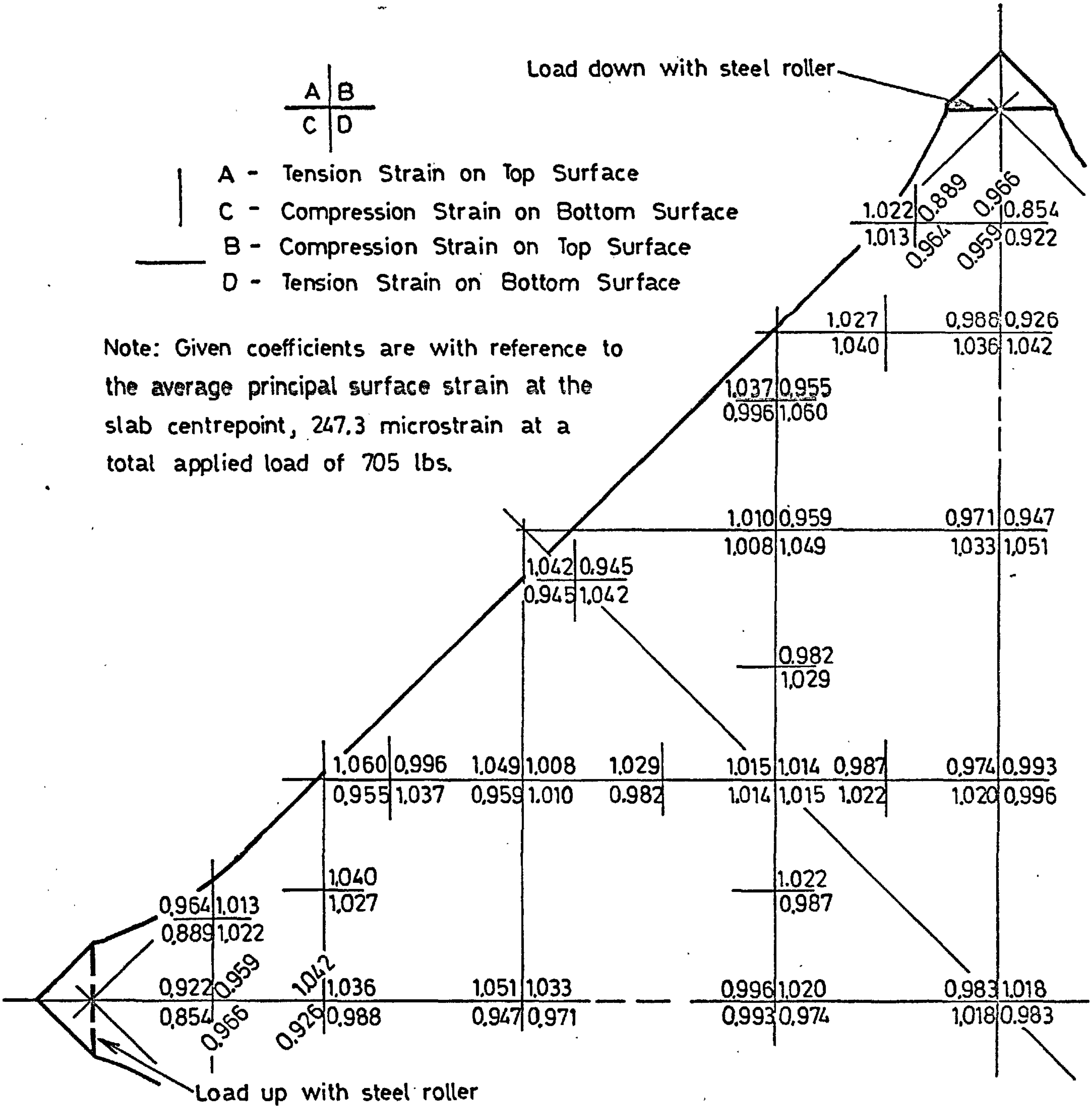

FIG. 14.10 STRAIN DISTRIBUTION ON SQUARE ALUMINUM SLAB WITH EXTENDED CORNERS LOADED AND SUPPORTED BY STEEL ROLLERS AT CORNERS

TABLE 14.6 STRAIN DISTRIBUTION ON SQUARE ALUMINUM SLAB WITH EXTENDED CORNERS LOADED WITH STEEL ROLLERS AND 2" SQUARE PLATES

GAUGE NO.	SLAB IN UPRIGHT POSITION STRAIN($x10^{-6}$)		COEFF	SLAB IN INVERTED POSITION STRAIN($x10^{-6}$)		COEFF
1	260	T	1.050	245.0	C	0.990
2	259.3	T	1.047	250.0	C	1.008
3	260.0	T	1.050	244.0	C	0.985
4	259.0	T	1.045	253.3	C	1.022
5	249.0	T	1.005	254.0	C	1.025
6	36.7	T	-	27.7	T	-
7	261.3	T	1.053	232.3	C	0.938
8	251.7	T	1.017	246.0	C	0.993
9	243.0	T	0.980	256.0	C	1.032
10	23.0	T	-	21.3	T	-
11	264.3	T	1.067	233.0	C	0.940
12	262.7	T	1.060	235.7	C	0.950
13	256.0	T	1.032	243.3	C	0.982
14	6.0	C	-	0		-
15	247.7	T	0.999	252.0	C	1.018
16	241.7	T	0.975	252.7	C	1.020
17	240.3	T	0.971	216.3	C	0.833
18	232.3	T	0.939	211.3	C	0.853
19	259.7	T	1.048	228.3	C	0.923
20	260.7	T	1.052	236.0	C	0.952
21	248.7	T	1.003	244.0	C	0.985
22	244.3	T	0.987	251.7	C	1.015
23	261.3	T	1.054	235.7	C	0.952
24	242.3	T	0.978	258.7	C	1.036
25	251.7	T	1.016	252.3	C	1.018
26	135.3	C	-	114.0	T	0.459
27	271.0	C	1.093	237.7	T	0.955
28	257.7	C	1.040	243.3	T	0.981
29	238.7	C	0.964	252.0	T	1.017
30	10.0	C	-	5.7	C	-
31	243.3	T	0.983	237.7	C	0.960
32	134.3	C	-	115.7	T	-

Note: Average principal surface strain at centre is $248.0 x10^{-6}$ at a total applied load of 705 lbs.

Coefficient values above are presented diagrammatically in Figure 14.11.

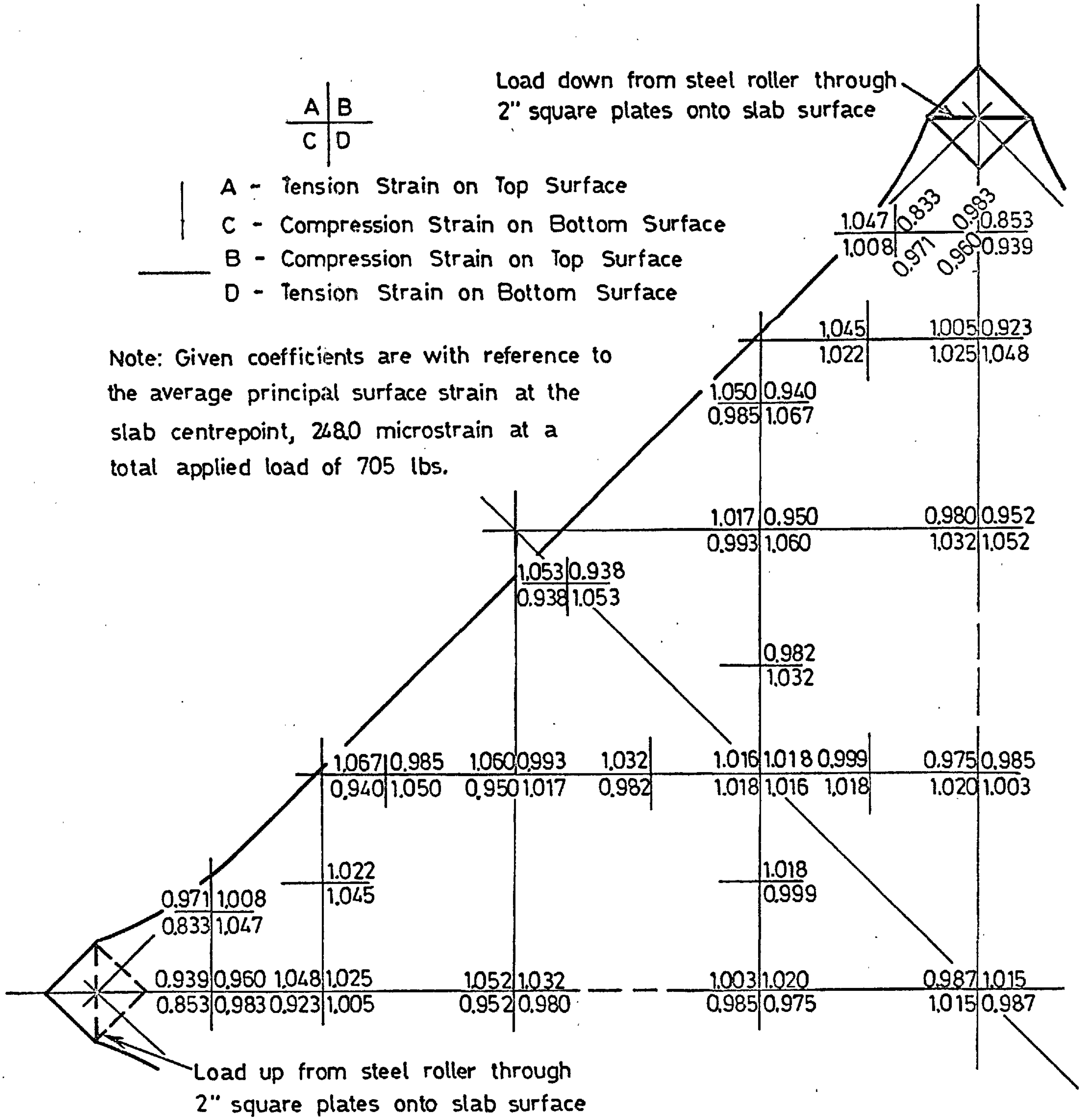

FIG. 14.11 STRAIN DISTRIBUTION ON SQUARE ALUMINUM SLAB WITH EXTENDED CORNERS LOADED AND SUPPORTED BY STEEL ROLLERS AND 2" SQUARE PLATES AT CORNERS

TABLE 14.7 STRAIN DISTRIBUTION ON SQUARE ALUMINUM SLAB WITH EXTENDED CORNERS LOADED WITH STEEL ROLLERS ONLY

GAUGE NO.	SLAB IN INVERTED POSITION		
	STRAIN(x10-6)		COEFF
1	246.7	C	1.008
2	248.0	C	1.013
3	241.3	C	0.987
4	251.3	C	1.027
5	253.0	C	1.034
6	28.3	T	-
7	230.7	C	0.943
8	246.3	C	1.007
9	253.7	C	1.037
10	22.3	T	-
11	230.3	C	0.941
12	234.7	C	0.960
13	241.7	C	0.988
14	1.3	T	-
15	250.3	C	1.023
16	250.3	C	1.023
17	211.7	C	0.865
18	207.7	C	0.849
19	227.0	C	0.928
20	234.7	C	0.959
21	243.3	C	0.994
22	248.7	C	1.018
23	234.7	C	0.960
24	256.3	C	1.048
25	250.0	C	1.022
26	116.7	T	-
27	237.0	T	0.969
28	242.0	T	0.989
29	249.7	T	1.021
30	7.0	C	-
31	238.7	C	0.976
32	115.3	T	-

Note: Coefficient values are based on coefficient value at gauge 22, 1.018, as obtained from Table 14.5.

Coefficient values are presented diagrammatically in Figure 14.12.

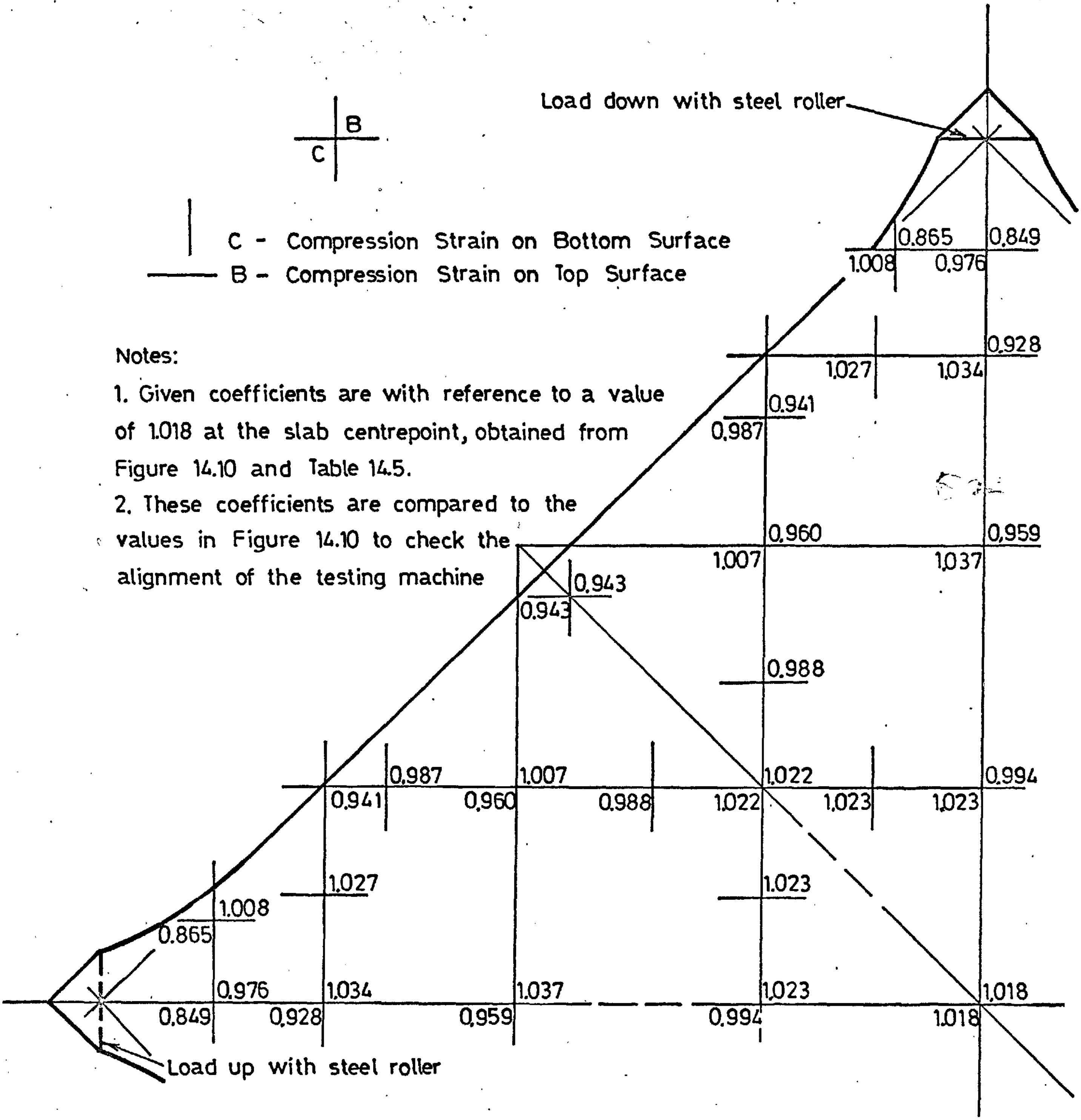

Notes:

1. Given coefficients are with reference to a value of 1.018 at the slab centrepoint, obtained from Figure 14.10 and Table 14.5.
2. These coefficients are compared to the values in Figure 14.10 to check the alignment of the testing machine

FIG. 14.12 STRAIN DISTRIBUTION ON SQUARE ALUMINUM SLAB WITH EXTENDED CORNERS LOADED AND SUPPORTED BY STEEL ROLLERS AT CORNERS at the corners from the rollers to the slab surface.

It is obvious from comparison of Figures 14.10 and 14.12 that the strain pattern is independent of the orientation of the slab in the testing machine. Any minute differences which do exist are well within the bounds of experimental error. It is consequently concluded that the biaxial testing machine is in good alignment and thereby capable of producing a repeatable loading system. (see Section 12.2.4)

14.4 THEORY OF THE PARALLELOGRAM SLAB TEST

In the foregoing investigation, a suitable technique for inducing principal tension and compression stresses of equal magnitude in slab specimens has been developed. However, in any comprehensive study of a material under biaxial states of stress, a detailed examination of its behaviour under each of several different ratios of principal stress is necessary.

To produce these different ratios of tension to compression stress while simultaneously performing the test on slabs; (i.e. flexural states of stress), the author has developed the following theory as a natural extension to the theory presented by Timoshenko and Woinowsky-Kreiger(67).

14.4.1 Parallelogram Slab Theory

In the general case of pure bending to an anticlastic surface,

$$M_x = -mM_y \qquad \ldots\ 14.18$$

where m is any positive value (see Figure 14.13).

Substituting Equation 14.18 into Equation 14.7, then,

$$M_n = M_x \cos^2\alpha - \frac{M_x}{m} \sin^2\alpha \qquad \ldots\ 14.19$$

By setting M_n equal to zero and solving Equation 14.19 for α, then

$$\pm\ \alpha = \tan^{-1} \sqrt{m} \qquad \ldots\ 14.20$$

That is, there are two sets of parallel lines where only twisting moments exist. These lines can be selected to produce a parallelogram as shown in Figure 14.13.

By substituting Equation 14.20 into Equation 14.8, the twisting moments along the sections 'ad' and 'bc' are equal to $\frac{1}{\sqrt{m}} M_x$ whilst the moments along 'ab' and 'cd' are equal to $-\frac{1}{\sqrt{m}} M_x$. Thus, the portion of the plate 'abcd' is the condition of a plate undergoing pure bending produced by twisting moments uniformly distributed along the edges.

By employing the same analysis as used in Section 14.1 and shown in Figure 14.2, it is concluded that the twisting of any one side can be produced by forces concentrated at the corners. Each of these are equal to $\frac{2}{\sqrt{m}} M_x$ acting <u>down</u> at the points 'a' and 'c' and <u>up</u> at the points 'b' and 'd'.

Substituting Equation 14.18 into Equation 14.4, then the deflection of any point of the middle surface of the slab is given by

$$w = \frac{M_y}{2D(1-\nu^2)} \left[(m+\nu)x^2 - (1+\nu m)\, y^2 \right] \qquad \ldots\ 14.21$$

It should be appreciated that the above theory produces general formulae for anticlastic bending of which the formulae for a rectangle, as presented in Section 14.1 are a special

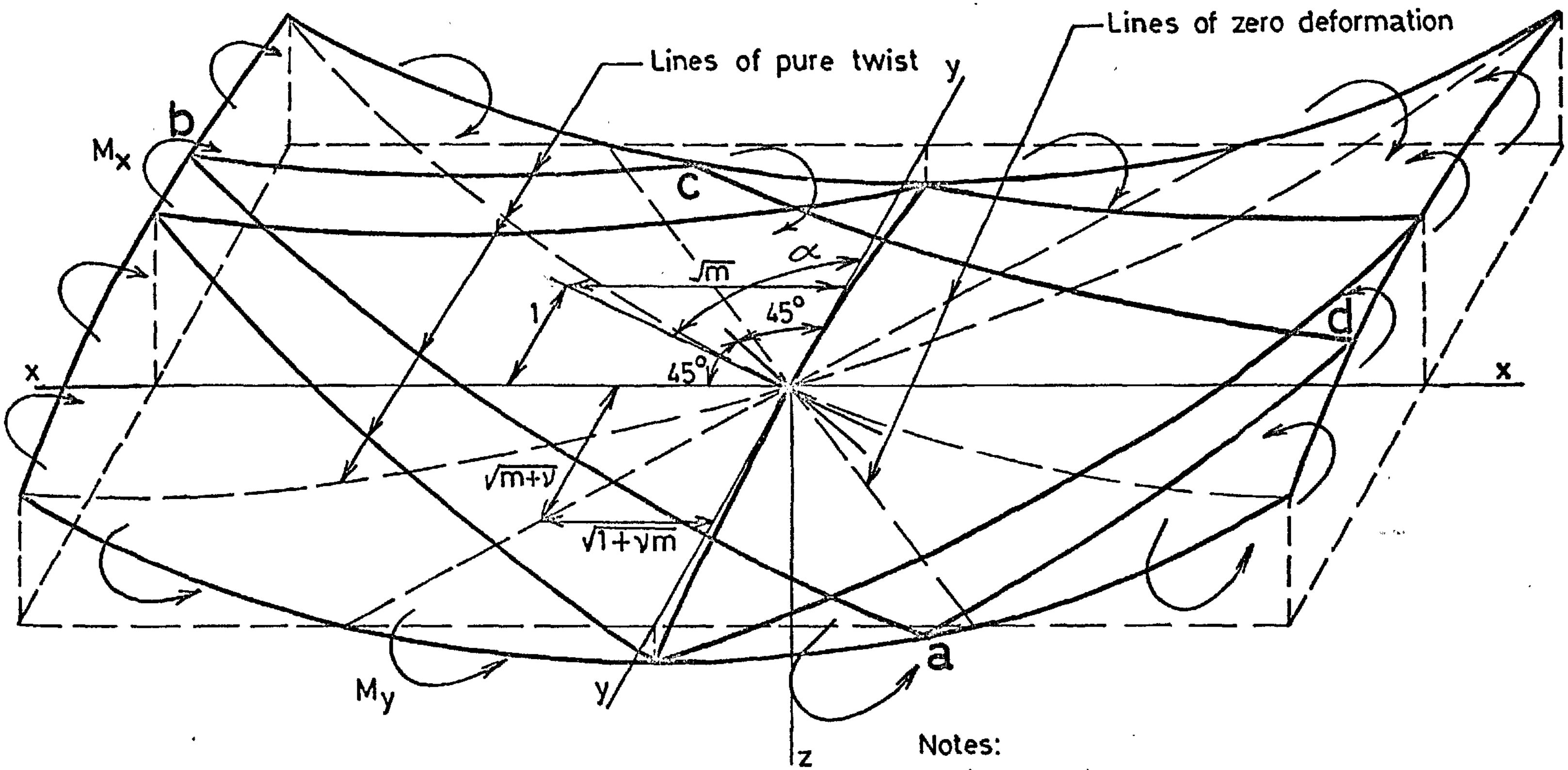

Notes:

1. $M_x = -m M_y$ where m is any positive value
2. ν denotes Poisson's ratio
3. Lines of linear deformation are parallel to lines of zero deformation

FIG. 14.13 ANTICLASTIC BENDING OF A PLATE BY PURE MOMENTS OF OPPOSITE SIGN case. For example, as $M_x = -M_y$ in Section 14.1 then 'm' in Equation 14.18 must be equal to 1. As a result, α values in Equation 14.20, $\pm 45^{\circ}$, define a rectangle and concentrated loads at corners become $2M_x$, whilst the general equation for deflection of the slab, Equation 14.21, reduces to the form shown in Equation 14.5.

Although the sides of the rectangle shown in Figure 14.1 and all sides parallel to it were concluded to be straight, this is not true for the general case of the parallelogram. This may be somewhat difficult to visualize at first, particularly as there are no bending moments along the edges to produce such curvatures. However, after examining the orientation and magnitudes of principal curvatures in relation to the sections considered, the above statements are seen to be logical. To clarify this, the following analysis is conducted.

When Equation 14.21 is factorized, then the deflection is shown to be.

$$w \doteq \frac{M_y}{2D(1-\nu^2)}\left[\sqrt{m+\nu}\; x - \sqrt{1+\nu m}\; y\right]\left[\sqrt{m+\nu}\; x + \sqrt{1+\nu m}\; y\right] \qquad \ldots\ 14.22$$

For the deflection 'w' to be linear with a linear change in either 'x' or 'y', then either of the above factors contained within brackets must be a constant; if both factors vary, w is parabolic. That is,

$$x = \pm\sqrt{\frac{1+\nu m}{m+\nu}}\; y + k \qquad \ldots\ 14.23$$

where k is any constant, defines the equations of all lines where 'w' is linear.

But, from Equation 14.20 and Figure 14.13 the equation of the lines of pure twist are

$$\tan x = \pm \sqrt{my} + k \qquad \ldots\ 14.24$$

where again, k is any constant.

It is obvious, from comparison of Equations 14.23 and 14.24 that the lines of linear deformation and lines of pure twist will only coincide when m = 1; the particular case of a rectangle discussed in Section 14.1. Furthermore, in any quadrant, the above lines will always exist on opposite sides of the 45° line; i.e. the line bisecting that particular quadrant (see Figure 14.13).

From Equation 14.20

$$\tan \alpha = \pm \sqrt{m} \qquad \ldots\ 14.25$$

But $\tan\alpha$ represents the ratio of diagonal lengths in the case where the above parallelogram is a rhombus. Therefore, it follows that, for rhombi, the ratio of the magnitude of pure bending moments is proportional to the square of the ratio of the diagonal lengths.

14.4.2 Surface Stressss and Strains

With a parallelogram loaded at diagonally opposite corners, the total applied load will be P. But as shown above, the applied load at each corner (Figure 14.13) is $\frac{2}{\sqrt{m}} M_x$, i.e.;

$$\frac{P}{2} = \frac{2}{\sqrt{m}} M_x \qquad \ldots\ 14.26$$

Proceeding as in Section 14.1.3 and from Equations 14.10, 14.11 and 14.26, we obtain the principal surface stresses in the x-direction, i.e.;

$$-\sigma_{1x} = \sigma_{2x} = \frac{3\sqrt{m}\,P}{2d^2} \qquad \ldots\ 14.27$$

Similarly, from Equations 14.10, 14.11 14.18 and 14.26, the principal surface stresses in the x-direction are

$$\sigma_{1y} = -\sigma_{2y} = \frac{3P}{2\sqrt{m}\,d^2} \qquad \ldots\ 14.28$$

To obtain the principal surface strains, Equations 14.27 and 14.28 are substituted into Equations 14.15 and 14.16. Thus,

$$-\epsilon_{1x} = \epsilon_{2x} = \frac{3P}{2d^2E\sqrt{m}}(m + \nu) \qquad \ldots\ 14.29$$

and

$$\epsilon_{1y} = -\epsilon_{2y} = \frac{3P}{2d^2E\sqrt{m}}(1 + \nu m) \qquad \ldots\ 14.30$$

In the investigation to follow, the loads P and principal surface stresses and strain will be measured experimentally. With this information, the E and ν values may be obtained by the simultaneous solution of Equations 14.29 and 14.30. The calculation is, however, performed more conveniently by substituting directly into equations for E and ν. Therefore, by solving Equations 14.29 and 14.30 algebraically for these values, we obtain

$$E = \frac{3P(1 - m^2)}{2d^2\sqrt{m}(\epsilon_{1y} + m\epsilon_{1x})} \qquad \ldots\ 14.31$$

$$\nu = \frac{-\epsilon_{1x} + m\epsilon_{1y}}{\epsilon_{1y} + m\epsilon_{1x}} \qquad \ldots\ 14.32$$

Although the above formulas for E and ν have been given in terms of the strains on the upper surface only, very similar relationships are obtained from strains on the lower surface. This is due to the principal strains on the two surfaces being theoretically identical in magnitude, but of opposite algebraic sign. (see Equations 14.29 and 14.30) As a result, in the investigation conducted (see Section 14.5), the values of strain in each of the principal directions, for substitution into Equations 14.31 and 14.32, were the average of the measured strains on both the upper and lower surfaces.

In the particular case of a parallelogram where m equals unity, i.e.; a rectangle, it is observed that both Equations 14.31 and 14.32 are indeterminate. This is due to ϵ_{1y} being equal to $-\epsilon_{1x}$ (see Equation 14.17) and, as a result, the denominators of both Equations 14.31 and 14.32 are equal to zero. Thus, only one equation can be obtained for the value of the two elastic constants, E and ν in terms of the applied load and measured strains (see Equation 14.17).

14.5 TESTS ON A RHOMBUS SLAB

14.5.1 Method of Test

To verify the above theory, it was necessary to load a flat slab with a general parallelogram shape at the corners. Such a specimen was obtained by cutting the aluminum specimen used in Test Series 1 and 2 to the shape shown in Figure 14.14 where the internal angles are 80° and 100°. The

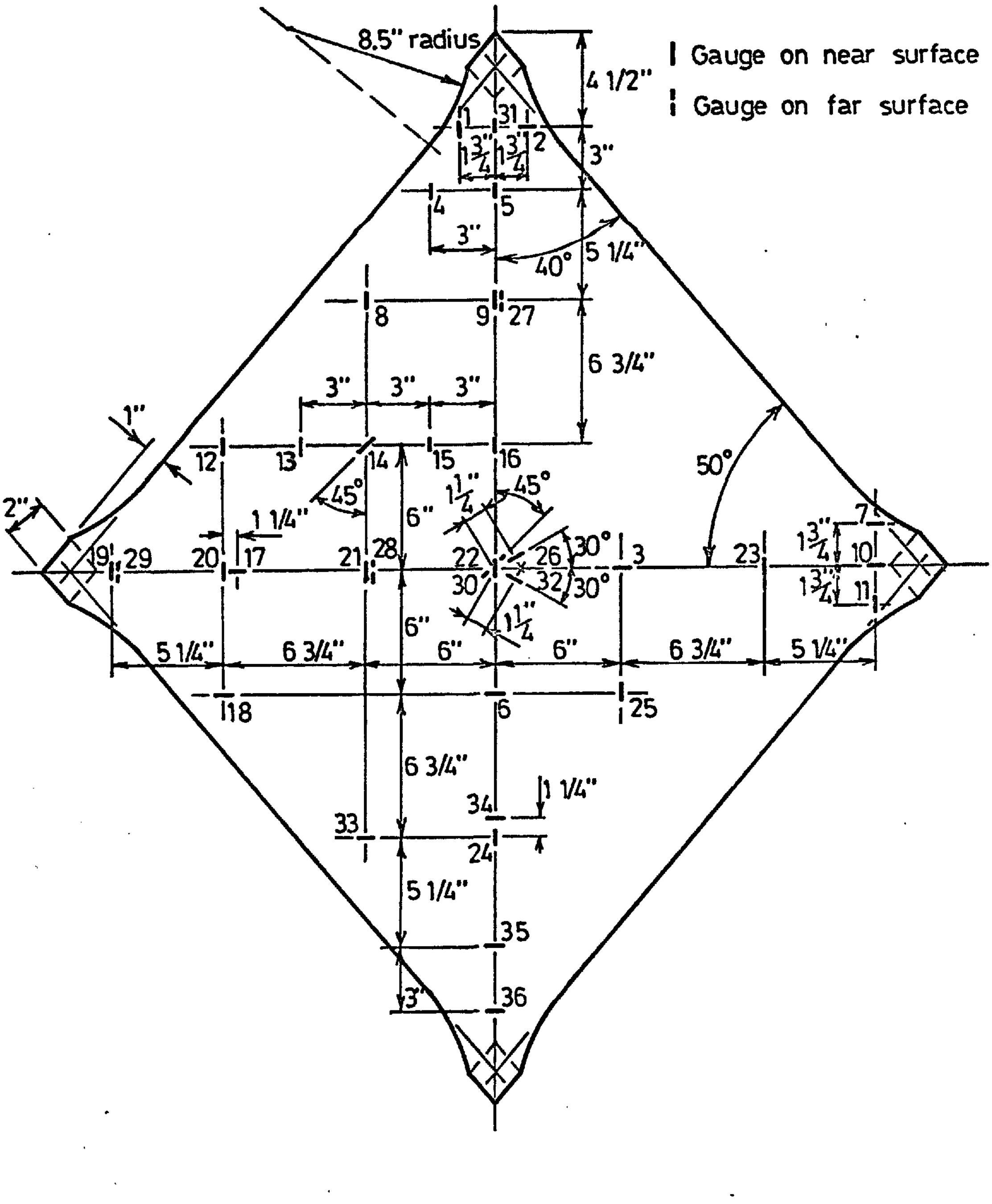

FIG. 14.14 LOCATION AND DESIGNATION OF GAUGES ON RHOMBUS ALUMINUM SLAB WITH EXTENDED CORNERS - TEST SERIES 3

recommendation of Section 14.3.3 stating that extended corners be used was again employed here, with the corners being very similar in shape to those on the square slabs in Test Series 2. Care was exercised in ensuring that the centroid of the load at each corner coincided with the intersection of the adjacent projected sides.

When cutting the aluminum slab, care was taken to cut it so that the majority of the gauges used in Test Series 1 and 2 would again be measuring principal strains in this test series, hereafter referred to as Test Series 3. However, although with the square slab, the measurement of one principal strain on one surface was theoretically identical with the principal strain on the opposite surface in a perpendicular direction at a corresponding point (see Section 14.2.1), this will not be so for the rhombus test. Consequently, several additional gauges were added in this test series so that a complete representation of the strain pattern in both principal directions in one guadrant could be obtained. (see Figure 14.14) Again, as in the previous test series, the test was repeated on the slab in the inverted position in order to obtain the strain distribution on both faces.

Test Series 3 was carried out in virtually an identical manner to Test Series 2 (see Section 14.3.2). One test only was performed, consiting of three runs on the slab in each of the upright and inverted positions. Each run consisted of two load stages, 270 and 630 lbs. total applied loads with three complete sets of readings at each load stage. The loads were applied directly to the slab corners through steel rollers (see Section 14.3.3)

14.5.2 Discussion of Results

The average of nine strain readings for each gauge for each test in this test series is presented in Table 14.8. The corresponding distributions of strain in one representative slab quadrant in relation to the average principal strain in the more highly stressed principal direction are presented in Figures 14.15 and 14.16. The principal strain in the lateral direction at the slab centrepoint have been computed from the readings of the four gauges at the slab centre by using Mohr's circle of strain method. (see Timoshenko and Goodier[110].

It is apparent from either of the above mentioned figures that the strain pattern in either of the two principal directions is virtually constant, seldom differing by more than 2% from that at the slab centre, except in the immediate vicinity of the corners. Again, as discussed in Section 14.3.3, the stress at the corners is less than elsewhere on the slab, so that failure would occur across a uniformly stressed section away from any of the corners.

By comparing Figure 14.15 to 14.16, it is seen that the larger slab deflections produce greater variations in strain from one face to the other at any point as well as greater variations in strain at any one section. This

TABLE 14.8 STRAIN DISTRIBUTION ON RHOMBUS ALUMINUM SLAB WITH EXTENDED CORNERS LOADED WITH STEEL ROLLERS

GAUGE NO.	SLAB IN UPRIGHT POSITION				SLAB IN INVERTED POSITION			
	1st LOAD STAGE		2nd LOAD STAGE		1st LOAD STAGE		2nd LOAD STAGE	
	STRAIN ($x10^{-6}$)	COEFF	STRAIN ($x10^{-6}$)	COEFF	STRAIN ($x10^{-6}$)	COEFF	STRAIN ($x10^{-6}$)	COEFF
1	103.0 T	0.976	240.5 T	0.984	99.7 C	0.944	235.7 C	0.965
2	73.0 C	0.691	169.5 C	0.694	75.5 T	0.715	174.5 T	0.714
3	90.5 C	0.857	215.0 C	0.880	89.0 T	0.834	201.3 T	0.823
4	107.3 T	1.016	251.3 T	1.028	105.5 C	1.008	250.7 C	1.027
5	107.0 T	1.014	245.7 T	1.005	106.0 C	1.010	252.0 C	1.031
6	88.3 C	0.837	208.7 C	0.854	90.0 T	0.844	207.0 T	0.848
7	83.0 C	0.787	196.5 C	0.804	78.5 T	0.755	185.0 T	0.758
8	107.0 T	1.014	247.0 T	1.011	102.5 C	0.986	244.0 C	0.997
9	104.5 T	0.991	240.3 T	0.983	104.5 C	1.000	252.3 C	1.032
10	72.5 C	0.687	172.3 C	0.705	70.5 T	0.661	160.5 T	0.657
11	86.7 T	0.821	202.5 T	0.829	86.5 C	0.812	196.0 C	0.802
12	109.7 T	1.039	255.0 T	1.048	104.5 C	0.986	240.3 C	0.984
13	107.3 T	1.018	250.0 T	1.024	105.0 C	1.002	244.0 C	0.998
14	8.0 T	0.076	16.0 T	0.065	7.0 C	0.060	17.7 C	0.072
15	106.0 T	1.004	243.0 T	0.985	105.5 C	1.004	252.0 C	1.031
16	104.5 T	0.991	238.5 T	0.978	105.5 C	1.004	251.0 C	1.027
17	91.0 C	0.862	214.7 C	0.879	89.0 T	0.841	201.0 T	0.823
18	90.0 C	0.853	208.0 C	0.851	92.0 T	0.873	211.7 T	0.867
19	85.5 T	0.810	200.0 T	0.819	81.0 C	0.770	189.7 C	0.777
20	107.0 T	1.014	249.5 T	1.020	101.0 C	0.967	234.0 C	0.957
21	105.0 T	0.995	243.0 T	0.994	104.5 C	0.993	244.3 C	0.999
22	105.0 T	0.995	239.7 T	0.981	106.0 C	1.004	249.3 C	1.021
23	107.0 T	1.014	250.0 T	1.023	100.0 C	0.958	234.3 C	0.960
24	104.0 T	0.986	240.0 T	0.983	107.0 C	1.014	254.0 C	1.040
25	107.0 T	1.014	248.0 T	1.014	107.0 C	1.014	250.3 C	1.025
26	43.5 C	0.412	100.0 C	0.409	39.5 T	0.379	88.3 T	0.361
27	109.0 C	1.033	259.0 C	1.060	105.0 T	0.995	241.0 T	0.988
28	106.3 C	1.008	248.5 C	1.018	107.0 T	1.002	244.3 T	1.000
29	82.0 C	0.777	190.5 C	0.780	86.5 T	0.815	201.0 T	0.822
30	10.0 C	0.095	24.3 C	0.099	7.0 T	0.071	16.5 T	0.067
31	100.5 T	0.952	232.5 T	0.951	98.5 C	0.929	231.0 C	0.945
32	41.0 C	0.389	98.5 C	0.403	40.5 T	0.384	91.3 T	0.373
33	88.0 C	0.834	204.0 C	0.834	91.5 T	0.869	216.0 T	0.884
34	87.0 C	0.824	204.7 C	0.839	91.5 T	0.871	214.0 T	0.876
35	87.0 C	0.824	200.0 C	0.819	91.0 T	0.858	213.0 T	0.872
36	78.3 C	0.741	181.3 C	0.742	80.0 T	0.758	186.3 T	0.762

Note: Average principal surface strains at centre are; 105.5 and 89.0 microstrain at a total applied load of 270 lbs.
; 244.5 and 206.0 microstrain at a total applied load of 630 lbs.

Coefficient values above are presented diagrammatically in Figures 14.15 and 14.16.

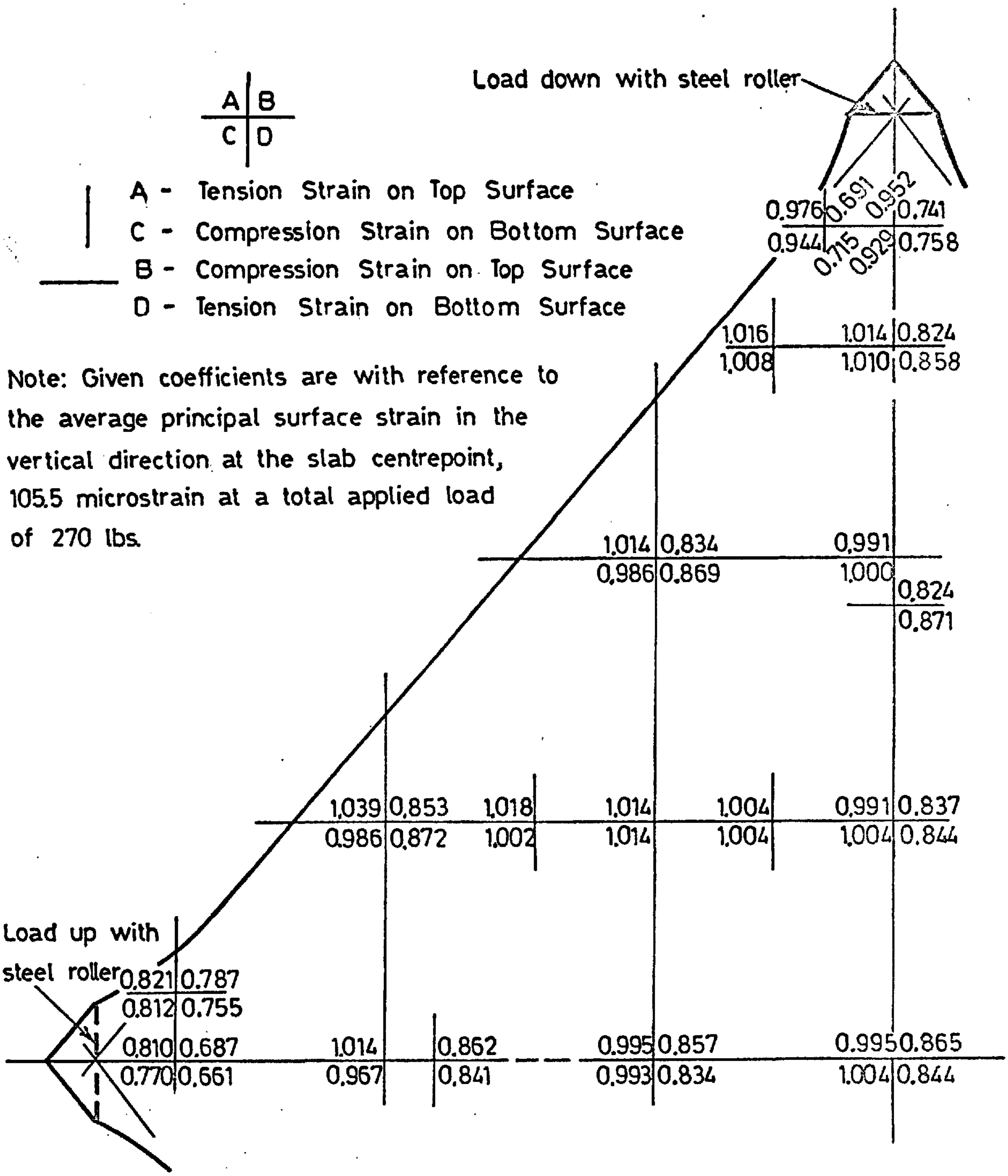

FIG. 14.15 STRAIN DISTRIBUTION ON RHOMBUS ALUMINUM SLAB LOADED AND SUPPORTED BY STEEL ROLLERS AT CORNERS (1st LOAD STAGE)

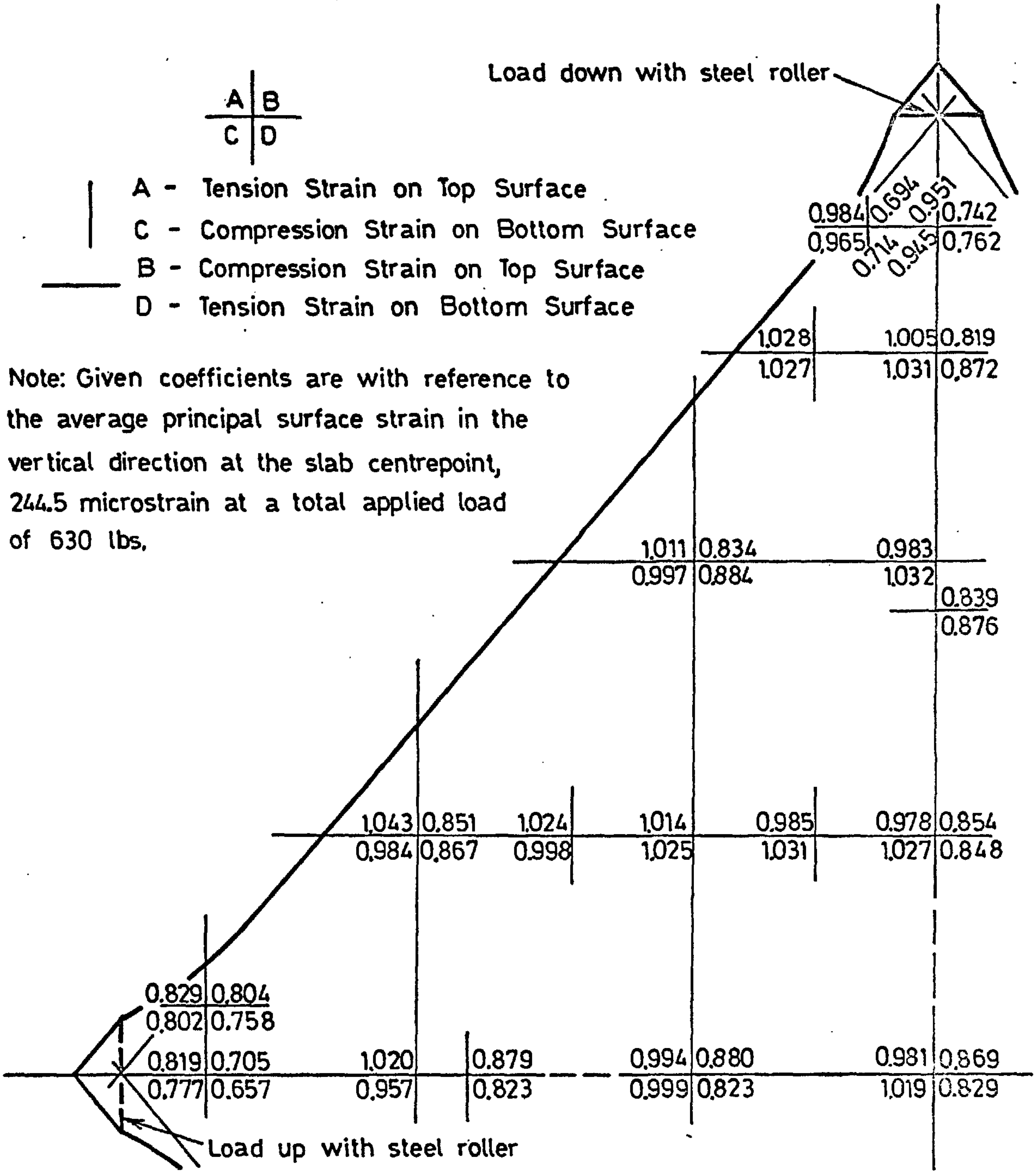

FIG. 14.16 STRAIN DISTRIBUTION ON RHOMBUS ALUMINUM SLAB LOADED AND SUPPORTED BY STEEL ROLLERS AT CORNERS (2nd LOAD STAGE)

substantiates the findings of Test Series 1 where similar trends were observed. (see Section 14.2.2) From this, it is recommended that the maximum deflection of the slab centrepoint should be small; preferably to less than 10% of the slab thickness.

14.6 PRECISION OF SUGGESTED TEST METHOD

From the results of Test Series 2 and 3, it is apparent that a uniform strain pattern with a correspondingly uniform stress pattern can be achieved with the proper technique of loading at the corners. As a result, this test method was adopted for the testing of concrete slabs to obtain information on their behaviour under different combinations of biaxial tension-compression stress. However as strains at the centre could be used to provide elasticity properties of the material, it was considered useful to analyse the results of Test Series 1, 2 and 3 to assess the precision of the above test methods for providing such information.

From Figure 14.15 and Table 14.8, the average principal surface strains in the two principal directions at the rhombus slab centrepoint are 105.5 and 89.0 microstrain at the first load stage. From Equations 14.31 and 14.32, the corresponding values for Poisson's Ratio, ν , and modulus of elasticity, E, are 0.343 and 9.81 $\times 10^6$ p.s.i., respectively. For the second load stage, where the strains are 244.5 and 206.0 microstrain, the above elasticity values are 0.340 and 9.88 $x10^6$ p.s.i. These values show not only excellent agreement with each other, but are also, representative values for aluminum. Fairman and Cutshall[113] give values of 0.33 and $10x10^6$ p.s.i. for the above elasticity properties.

As shown in Section 14.5.2, Equations 14.31 and 14.32 become indeterminate for rectangular slabs. As a result, only one equation with the two unknowns, ν and E, is obtained (see Equation 14.17) Consequently, for the square slabs discussed in Section 14.3.3, ν has been assumed as being 0.340 (from above) and E has been calculated as being 9,84 $x10^6$ p.s.i. (from Equation 14.17).

This shows good agreement with the above results. Furthermore, from the analysis of Section 14.2.2, it has been shown, from extrapolation, that with a perfectly square slab with loading right at the corners, the modulus of elasticity value obtained would be about 9.7 $x10^6$ p.s.i.

From the consistency of these results as well as the close agreement in strain pattern obtained experimentally with that predicted theoretically, it is recognized that the small variations observed are in large part accounted for by possible imperfections in the material itself. As shown in Chapter 13, the variations in slab thickness was only minute, but variations in measured strain of the order of 0.5 to 1% would be expected because of this. Similarly, it is reasonable to suggest that other small variations will arise from lack of planeness in the slab surface and even, non-homogenity in the material itself.

From the above analysis, it is concluded that the loading method as adopted in Test Series 2 and 3 induced not only uniform stress and strain over the general slab area, but also, these values were in excellent agreement with theoretical predictions. Furthermore, the measurement of elasticity properties can be made with confidence anywhere on the slab except in the immediate vicinity of the corners or slab edges.

14.7 SUMMARY

A comprehensive investigation of the induced strain pattern and resulting elasticity values has been conducted on both the general parallelogram slab and the rectangular slab using an aluminum specimen.

The results of the first test series, which investigates the testing technique of previous researchers,[65,66,68] have suggested that excessively high values arise for ultimate strengths and elasticity properties when the slabs are not loaded at the corners. Thus, the importance of a testing technique whereby the slabs are loaded at the corners was emphasized.

Subsequent investigation on slabs with extended corners has shown that it is possible to achieve a uniform stress and strain distribution when care is taken to load the slab directly at the corners. These corners can be made small enough to have a negligible influence on the general stress and strain pattern while simultaneously, reducing the values in the immediate vicinity of the corner so that failure is induced at a section where the above values are constant. Elimination of re-entrant corners by having gradual transition curves from the corners to the slab sides is also important.

The author has presented a theoretical analysis of the pure bending of plates to an anticlastic surface as a result of the corner loading of a parallelogram. The theory has been experimentally verified by the corner loading of a rhombus having internal angles of 80° and 100°. The experimental and theoretical results are found to be in good agreement with a uniform strain and corresponding stress distribution being obtained. The calculation for the elasticity values show good agreement not only with those of the previous tests, i.e. the square slab, where a different combination of biaxial tension-compression stress was induced, but also with general values obtained for aluminum by other investigators.

CHAPTER 15

DEVELOPMENT OF TESTING TECHNIQUE FOR DISC TESTS

15.1 THEORY OF THE DISC TEST

The slab tests described in the last chapter produced anticlastic bending with uniform bending moments of opposite sign thereby resulting in biaxial tension-compression stresses, To achieve a state of biaxial tension in plates, a test, hereafter referred to as the disc test, is used. The disc, circular in shape, is supported along its periphery while being concentrically loaded. (see Figure 11.2) This creates a uniform state of biaxial moment within the loading ring resulting in uniform biaxial tension on one face and biaxial compression on the opposite face. In principle, this test method is analogous to the four point loading of beams in two dimensions.

15.1.1 Deflection and Slope at Mid-Plane of Disc

In the analysis of the symmetrical bending of circular plates, Timoshenko and Woinowsky-Kreiger[67] developed the formulas,

$$M_r = -D\left(\frac{d^2w}{dr^2} + \frac{\nu}{r}\frac{dw}{dr}\right) \qquad \text{... 15.1}$$

$$M_t = -D\left(\frac{1}{r}\frac{dw}{dr} + \nu\frac{d^2w}{dr^2}\right) \qquad \text{... 15.2}$$

where M_r and M_t are the radial and tangential bending moments per unit width on any element in the plate, D is the flexural stiffness, (see Equation 14.3), w is the deflection of the middle surface of the plate, r is the distance from the centre of the plate to the element being considered and ν is Poisson's Ratio.

By analysing the distribution of moments and shear forces at any element in the disc, Timoshenko and Woinowsky-Kreiger (67) obtained the differential equation.

$$\frac{d}{dr}\left[\frac{1}{r}\frac{d}{dr}\left(\frac{r\,dw}{dr}\right)\right] = \frac{Q}{D} \qquad \ldots\ 15.3$$

where Q is the total shearing force at the radius, r. From this basic equation, the radial curvature, $\frac{d^2w}{dr^2}$, the tangential curvature, $\frac{1}{r}\frac{dw}{dr}$, the slope, $\frac{dw}{dr}$ and deflection, w at any point in the plate surface can be computed.

For the particular case of loading where the load is applied through a concentric ring and supported along the periphery, the above authors have analysed the loadings independently as shown in Figure 15.1.

From Figure 15.1 (a) where only bending moments, uniformly distributed along the edge of a circular concentric hole are considered, the successive integrations of equation 15.3 yields.

$$\frac{dw}{dr} = \frac{a^2b^2M_1}{D(1-\nu)(a^2-b^2)}\left(\frac{1}{r} + \frac{1-\nu}{1+\nu}\frac{r}{a^2}\right) \qquad \ldots\ 15.4$$

where a and b represent the radii of the outer support and inner circular hole, respectively.

Integrating again, we obtain

$$W = -\frac{b^2 M_1(a^2-r^2)}{2(1+\nu)D(a^2-b^2)} + \frac{a^2 b^2 M_1 \log\frac{r}{a}}{(1-\nu)D(a^2-b^2)} \qquad \ldots\ 15.5$$

where w = 0 at the location, r = a

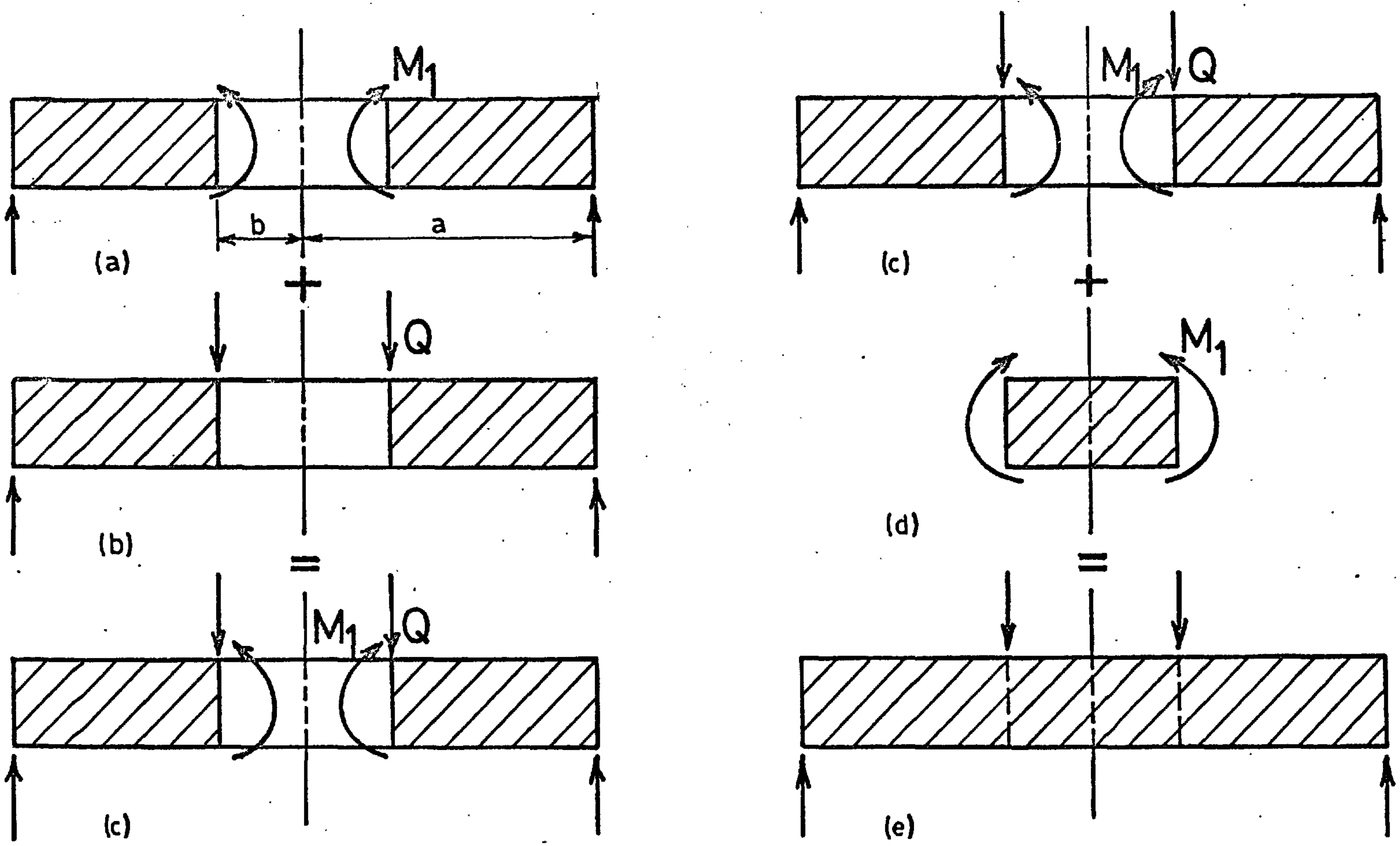

FIG. 15.1 INDIVIDUAL CASES ANALYSED FOR DETERMINING MOMENTS, CURVATURES, SLOPES AND DEFLECTIONS IN A CONCENTRICALLY LOADED DISC

Similarly, for the condition of loading shown in Figure 15.2(b), where only shear forces are considered,

$$\frac{dw}{dr} = \frac{\bar{P}r}{4\pi D}\left[\log\frac{r}{a} - \frac{1}{1+\nu} + \frac{b^2}{a^2-b^2}\log\frac{b}{a}\left(1+\frac{a^2}{r^2}\left(\frac{1+\nu}{1-\nu}\right)\right)\right] \quad \ldots\ 15.6$$

$$w = \frac{Pr^2}{8\pi D}\left[\log\frac{r}{a} - \frac{1}{2}\left(\frac{3+\nu}{1+\nu}\right) + \frac{b^2}{(a^2-b^2)}\log\frac{b}{a}\left[1+\frac{a^2}{r^2}\left(\frac{2(1+\nu)}{1-\nu}\log\frac{r}{a}-1\right)\right] + \frac{a^2}{2r^2}\left(\frac{3+\nu}{1+\nu}\right)\right] \quad \ldots\ 15.7$$

The addition of Equations 15.4 and 15.6 gives the slope at any point on the middle surface of the plate under the combined loading shown in Figure 15.1(c). Similarly, the addition of Equations 15.5 and 15.7 gives the value of the accompanying deflection.

For that portion located within the loading ring (Figure 15.1(d), the plate is in a condition of pure bending, as a result of the uniformly distributed moment, M_1. The magnitude of this moment is found from the condition of continuity along the circle, $r = b$, from which it follows that both portions of the plate have, at that circle, the same slope.

For the inner portion of the plate, (see Figure 15.1(d)). the curvature can be found from Equations 14.1 and 14.2 whereby

$$\frac{1}{r_x} = \frac{1}{r_y} = \frac{M_1}{D(1+\nu)} = -\frac{d^2w}{dr^2} \quad \ldots\ 15.8$$

By integrating Equation 15.8 with respect to r, then,

$$\frac{dw}{dr} = -\frac{M_1 r}{D(1+\nu)} \quad \ldots\ 15.9$$

where $\frac{dw}{dr} = 0$ at $r = 0$.

By equating Equation 15.9 to the sum of Equations 15.4

and 15.6 at the value, $r = b$, and solving for M_1, we obtain

$$M_1 = \frac{(1-\nu)P(a^2-b^2)}{8\pi a^2} - \left(\frac{1+\nu)P\log b/a}{4\pi}\right. \qquad \ldots\ 15.10$$

Substitution of this value of M_1 into Equation 15.5 yields the deflection, w, of any point on the portion of the disc, outside the load ring, due to the moment M_1. Adding this deflection to that obtained in Equation 15.7, for shearing forces only, then the actual deflection for the outer part of the disc is

$$w = \frac{P}{8\pi D}\left[(a^2-r^2)\left(1+\frac{1}{2}\left(\frac{1-\nu}{1+\nu}\right)\left(\frac{a^2-b^2}{a^2}\right)\right) + (b^2+r^2)\log\frac{r}{a}\right] \qquad \ldots\ 15.11$$

At the particular case, $r = b$, we obtain,

$$w = \frac{P}{8\pi D}\left[(a^2-b^2)\left(1+\frac{1}{2}\left(\frac{1-\nu}{1+\nu}\right)\left(\frac{a^2-b^2}{a^2}\right)\right) + 2b^2\log\frac{b}{a}\right] \qquad \ldots\ 15.12$$

To find the deflection of the inner portion of the plate, the deflection obtained from the pure bending of this inner portion is added to the value given by Equation 15.12. Therefore, by integrating Equation 15.9 and setting $w=0$ at $r=b$, then,

$$w = \frac{M_1}{2D(1+\nu)}(b^2-r^2) \qquad \ldots\ 15.13$$

By substituting Equation 15.10 into Equation 15.13 and adding to Equation 15.12, the deflection for the inner part of the plate is

$$w = \frac{P}{8\pi D}\left[(b^2+r^2)\log\frac{b}{a} + (a^2-b^2)\frac{(3+\nu)a^2-(1-\nu)r^2}{2a^2(1+\nu)}\right] \qquad \ldots\ 15.14$$

15.1.2 Surface Stresses and Strains

In order to evaluate the bending moments in the plate, M_r and M_t, it is necessary to determine the first and second differentials of the deflection, w. (see Equations 15.1 and 15.2). For the outer portion of the disc, the slope and curvature of the middle surface are obtained from Equation 15.11. Thus,

$$\frac{dw}{dr} = \frac{P}{8\pi D}\left[-2r\left(1+\frac{1}{2}\left(\frac{1-\nu}{1+\nu}\right)\left(\frac{a^2-b^2}{a^2}\right)\right) + \frac{1}{r}(b^2+r^2) + 2r\log\frac{r}{a}\right] \quad \ldots \; 15.15$$

$$\frac{d^2w}{dr^2} = \frac{P}{8\pi D}\left[1 - \left(\frac{1-\nu}{1+\nu}\right)\left(\frac{a^2-b^2}{a^2}\right) - \frac{b^2}{r^2} + 2\log\frac{r}{a}\right] \quad \ldots \; 15.16$$

Substituting Equations 15.15 and 15.16 into Equation 15.1, then the radial moment, M_r, is

$$M_r = \frac{P}{8\pi}\left[\left(\frac{(1-\nu)\, b^2(a^2-r^2)}{a^2r^2}\right) - 2(1+\nu)\log\frac{r}{a}\right] \quad \ldots \; 15.17$$

Likewise, by substituting Equations 15.15 and 15.16 into Equation 15.2, the tangential moment, M_t, is

$$M_t = \frac{P}{8\pi}\left[\left(\frac{(1-\nu)(2a^2-b^2)}{a^2}\right) - \left(\frac{(1-\nu)b^2}{r^2}\right) - 2(1+\nu)\log\frac{r}{a}\right] \quad \ldots \; 15.18$$

For the inner portion of the plate, by proceeding as above from Equation 15.14, then

$$\frac{dw}{dr} = \frac{Pr}{8\pi D}\left[2\log\frac{b}{a} - \left(\frac{a^2-b^2}{a^2}\right)\left(\frac{1-\nu}{1+\nu}\right)\right] \quad \ldots \; 15.19$$

$$\frac{d^2w}{dr^2} = \frac{P}{8\pi D}\left[2\log\frac{b}{a} - \left(\frac{a^2-b^2}{a^2}\right)\left(\frac{1-\nu}{1+\nu}\right)\right] \quad \ldots \; 15.20$$

Substitution of Equation 15.19 and 15.20 into Equation 15.1 yields

$$M_r = \frac{P}{8\pi}\left[\left(\frac{a^2-b^2}{a^2}\right)(1-\nu) - 2(1+\nu)\log\frac{b}{a}\right] \quad \ldots \; 15.21$$

$$= M_t$$

It is observed that, at r=b, Equations 15.17, 15.18 and 15.21 are all identical.

At any point, the normal stress at the outer fibre, f is calculated from the expression (see Section 14.1.3)

$$\sigma = \frac{M}{S} \quad \dots 15.22$$

where M is the bending moment and. S is the section modulus given by

$$S = \frac{d^2}{6} \quad \dots 15.23$$

where d is the plate thickness, Therefore

$$\sigma = \frac{6M}{d^2} \quad \dots 15.24$$

For the outer portion of the disc, the radial stress is computed from Equation 15.17 and 15.24. That is,

$$\sigma_r = \frac{3P}{4\pi d^2}\left[\frac{(1-\nu)\, b^2(a^2-r^2)}{a^2r^2} - 2(1+\nu)\log\frac{r}{a}\right] \quad \dots 15.25$$

Likewise, the transverse stress, computed from Equations 15.18 and 15.24, is

$$\sigma_t = \frac{3P}{4\pi d^2}\left[\frac{(1-\nu)(2a^2-b^2)}{a^2} - \frac{(1-\nu)b^2}{r^2} - 2(1+\nu)\log\frac{r}{a}\right] \quad \dots 15.26$$

Similarly, for the inner portion of the disc, the radial and transverse stresses, as computed from Equations 15.21 and 15.24 are,

$$\sigma_r = \sigma_t = \frac{3P}{4\pi d^2}\left[\left(\frac{a^2-b^2}{a^2}\right)(1-\nu) - 2(1+\nu)\log\frac{b}{a}\right] \quad \dots 15.27$$

At any point on the disc surface, (see Timoshenko and Woinowsky-Kreiger(67), p. 5), the radial and transverse strains are, respectively

$$\delta_r = \frac{\sigma_r}{E} - \frac{\nu\sigma_t}{E} \quad \dots 15.28$$

and

$$\delta_t = \frac{\sigma_t}{E} - \frac{\nu\sigma_r}{E} \quad \dots 15.29$$

By substituting Equations 15.25 and 15.26 into Equation 15.28, then the radial strain for the outer portion of the disc is

$$\delta_r = \frac{3P}{4\pi d^2 E}(1-\nu)\left[\frac{b^2}{r^2}(1+\nu) - \frac{b^2}{a^2}(1-\nu) - 2\nu - 2(1+\nu)\log\frac{r}{a}\right] \quad \dots 15.30$$

Similarly, by substituting Equations 15.25 and 15.26 into Equation 15.29, then the transverse strain for the outer portion is

$$\delta_t = \frac{3P(1-\nu)}{4\pi d^2 E}\left[2 - \frac{b^2}{a^2}(1-\nu) - \frac{b^2}{r^2}(1+\nu) - 2(1+\nu)\log\frac{r}{a}\right] \qquad \ldots\ 15.31$$

The radial and transverse strains on the inner portion of the disc are similarly obtained by substituting Equation 15.27 into Equations 15.28 and 15.29. That is,

$$\delta_r = \delta_t = \frac{3P(1-\nu)}{4\pi d^2 E}\left[\left(\frac{a^2-b^2}{a^2}\right)(1-\nu) - 2(1+\nu)\log\frac{b}{a}\right] \qquad \ldots\ 15.32$$

Again, at r=b, equations 15.30, 15.31 and 15.32 are identical, as expected.

15.2 INITIAL TESTS PERFORMED ON ALUMINIUM DISC

The experimental verification of the above theory, to the best of the author's knowledge, has not been previously performed. Consequently, the aluminium plate used in the tests on the square and rhombus slabs in Chapter 14 was again used not only to verify the above theory, but also, to assist in the development of a suitable technique for achieving the desired state of stress and strain. The plate was cut into the shape of a circular disc of 30" diameter. Although several of the strain gauges which were used in the previous tests had been retained, a few new ones were added to provide a more comprehensive indication of the radial and transverse strains (see Figure 15.2).

15.2.1 Method of Test

In the first series of tests on the aluminium disc, hereafter referred to as Test Series 4, the load was applied through a circular load ring of 12 " diameter (see Plate 15.1). The load was transmitted to the ring at four points by means of a cruciform welded to the load ring. The steel ring is 1½" square cross-section with an integral ¼" radius loading strip. This allows the load to be maintained on a 12" diameter circle, despite small changes in the slope of the plate immediately beneath the ring.

As the top surface of the aluminium disc is in a state of biaxial compression, a contraction of this surface will occur. Alternatively, the loading ring due to being in a state of vertical compression will exhibit an increase in circumference

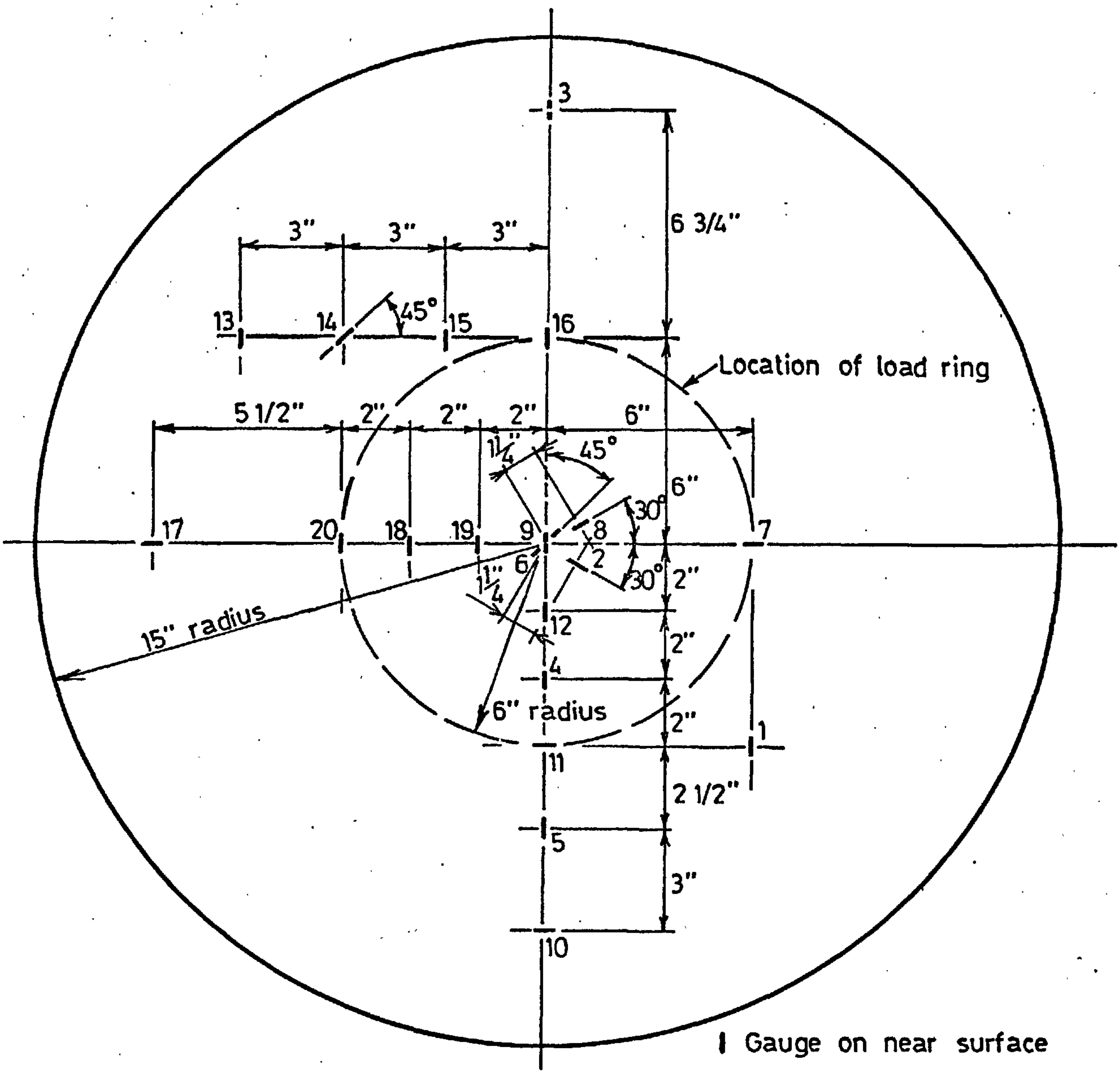

| Gauge on near surface

¦ Gauge on far surface

FIG. 15.2 LOCATION AND DESIGNATION OF GAUGES ON CIRCULAR ALUMINUM DISC

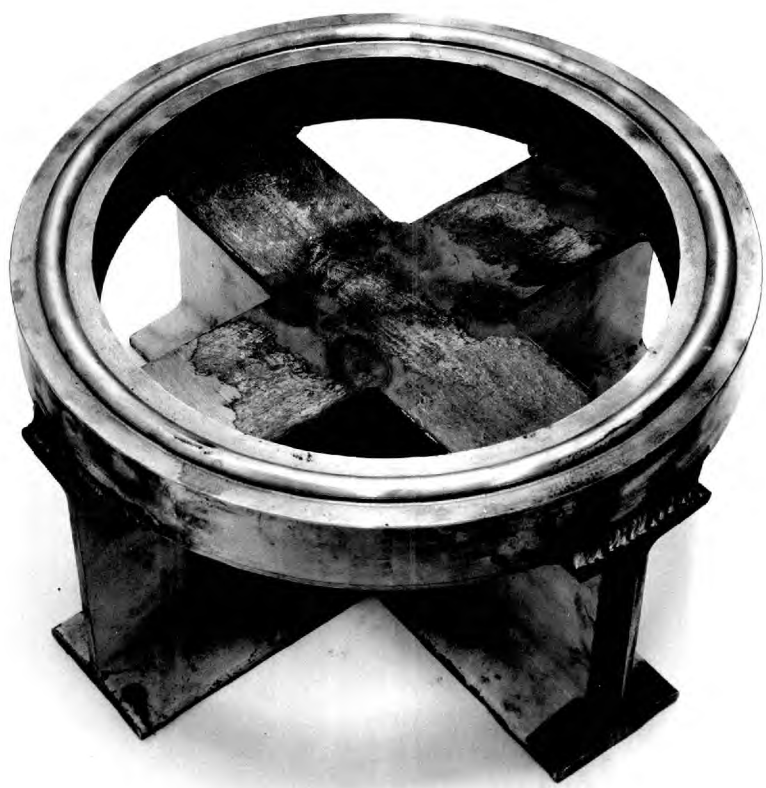

PLATE 15.1 Circular ring and cruciform used for loading aluminum disc in test series 4

due to the Poisson's ratio effect. Consequently, provision was made for sliding with negligible restraint effect at this interface. This was performed with grease packs interposed between the disc surface and loading ring. Each of the three sheets of the selected grease pack was a cellulose sheet, Acetate, of 0.003" thickness. Between the lower two sheets, Stauffer's grease, a relatively soft grease (see Chapter 8) was applied whereas a mixture of yellow commercial tallow and black lead, equal proportions by weight, was applied between the upper two acetate sheets. This ensured friction-free sliding between the lower two layers while the highly viscous graphite-tallow mixture produced a more uniform distribution of load.

To ensure that the grease packs functioned during loading, it was necessary to apply uniform pressure to them while, simultaneously, maintaining the load on a narrow strip. Thus, a $\frac{1}{2}$" wide strip of a Paxolein hardboard with a mean diameter of 12" was interposed between the grease packs and the loading ring.

For supporting the aluminium disc, a bicycle racing tyre with a mean contact diameter of $25\frac{1}{4}$" was used. This was, in principle, identical to the supports used by Blakey and Beresford (65,66) and, subsequently, by Newman (68). To maintain the tyre at a constant and known diameter as well as locating it during test, a circular wooden disc which functioned as the rim of a bicycle wheel, was used.

The entire assembly was carefully positioned axially on the biaxial machine base with the aid of a scale graduated in $\frac{1}{32}$" divisions.

The disc was positioned with the majority of the gauges on the bottom surface.

Test Series 4 consisted of three independent sets of tests. In the first test, the principal axes of the cruciform were located so as to bisect each of the quadrants of the aluminium disc in Figure 15.2. The second test was identical to the first except that the loading ring was rotated 45^{o}; i.e., the principal axes of the cruciform were aligned with the principal axes of the aluminium disc. The third test differed from the second in that the Paxolein hardboard strip had been rotated 45^{o}.

One load stage only of 4,098 lbs. was applied three times for each test with three complete sets of strain readings at zero load and the applied load. All strain readings were recorded by a Solartron data logger, sensitive to two microstrain.

15.2.2 Discussion of Results

The results of the test series are presented in Table 15.1. Along with the actual recorded strains are a series of coefficients based on a value of 1.00 for the average strain at the disc centre, calculated from the average recording of gauge numbers 2, 6, 8, and 9 (see Figure 15.2)

From Equation 15.32, it was observed that the strain distribution within the loading ring should be constant at any load stage. However, from the coefficients given in Table 15.1, it is shown that there is a very large scatter in results, ranging from 75% to 158% of the average strain at the disc centre. These large discrepancies are primarily due to the bending of the load ring and the shortcomings of the

TABLE 15.1 STRAIN DISTRIBUTION ON ALUMINIUM DISC FOR TEST SERIES 4 (see Figure 15.2 for location of strain gauges)

GAUGE NO.	TEST A STRAIN ($\times10^{-6}$)	TEST A COEFF	TEST B STRAIN ($\times10^{-6}$)	TEST B COEFF	TEST C STRAIN ($\times10^{-6}$)	TEST C COEFF
1	113 T	0.574	104.0 T	0,527	100 T	0.506
2	182 T	0.924	185.5 T	0.940	189 T	0.959
3	48 T	0.244	52.5 T	0.266	51 T	0.258
4	213 T	1.082	198 T	1.003	194.5 T	0.987
5	74 T	0.376	71.5 T	0.362	70.5 T	0.357
6	190 C	0.966	183.5 C	0.930	189 C	0.958
7	168 T	0.854	207 T	1.048	210 T	1.064
8	225 T	1.143	227.5 T	1.152	220 T	1.116
9	190 T	0.966	193 T	0.979	191 T	0.969
10	113 T	0.574	121.5 T	0.616	127 T	0.645
11	223 T	1.132	292.5 T	1.482	311 T	1.578
12	189 T	0.960	186 T	0.943	183 T	0.929
13	65 T	0.330	52.5 T	0.266	59.5 T	0.301
14	179 T	0.910	130.5 T	0.660	155.5 T	0.78[illegible]
15	140 T	0.711	141 T	0.714	165 T	0.83[illegible]
16	147 T	0.747	195 T	0.988	176 T	0.89[illegible]
17	34 C	0.173	40 C	0.202	41 C	0.20[illegible]
18	191 T	0.971	233.5 T	1.182	214 T	1.085
19	194 T	0.987	210.5 T	1.066	198 T	1.003
20	189 T	0.960	246.0 T	1.246	230 T	1.166

Note; average strain ($\times10^{-6}$) for gauge no.'s 2,6,8 and 9 corresponding to a coefficient of 1.00 is for test A, 196.8

test B, 197.4

test C, 197.2

Perspex strip. Slight irregularities in the thickness of the aluminium disc could also account for small variations. These will each be discussed briefly.

(1) The load ring Although the load ring shown in Plate 15.1 is relatively bulky and therefore, stiff, it did bend up

between the cruciform ends, thereby causing zones of stress concentration at the four ends of the cruciform. This is shown in the results of both tests A and B (Table 15.1). In test B, where the load was applied to the load ring from the cruciform directly above gauge nos, 7, 11, 16 and 20, the recorded strains for these gauges are 19.1% higher than the strains obtained at the centre. Alternatively, in test A, where the above gauges are equidistant from the cruciform ends, the recorded strains are 7.7% lower than at the slab centre. From the above observation as well as a similar trend on gauge nos. 1 and 14, it was concluded that the load ring was insufficiently stiff.

(2) Paxolein strip. Paxolein is a very hard material. With irregularities in its own thickness as well as those arising from the aluminium slab surface, the material was unable to deform sufficiently to produce a uniform intensity of loading. Instead, with only isolated points of contact, uneven load concentrations resulted. This is borne out in comparing the results of tests B and C, Table 15.1 where the readings of several of the gauges changed markedly, particularly those which are located under or near the load strip. For example, compare coefficients of gauge nos. 7, 11, 15, 16, 18 and 20.

(3) Aluminium surface The aluminium disc, which had not been machined perfectly plane, would have slight irregularities in its surface. This is shown in Table 15.1 where certain gauges in all tests recorded consistently high or low values of strain. For example, gauge no. 11 was always higher whereas

gauge no. 16 tended to be lower than the average strain at the centre of the disc. This indicated that the aluminum surface was slightly high at the former and low at the latter, thereby being prone to such localized intensities of load.

In addition to the strains being non-uniform due to the above causes, the method of support was incorrect. For the particular loading being considered, where the support radius, a, in Equations 15.30, 15.31 and 15.32, is $12\frac{5}{8}$", it was assumed that the portion of the disc outside the support ring had no influence on the overall stress pattern. Although the radial stresses theoretically reduce to zero at the support ring, (Equation 15.25). The transverse stresses are still large. This is shown by solving Equations 15.26 and 15.27 ($a = 12.62"$, $b=6"$, $\nu = 0.342$) where, theoretically, the transverse surface stresses at the outer support ring are calculated as being 41% of the surface stresses in the central section. As a result, the transverse stresses existing outside the support ring would be expected to influence the overall results. This is borne out in the calculation of the modulus of elasticity, E. With a Poisson's ratio, ν, equal to 0.342 (as obtained from Chapter 14) and an average strain at the centre of 197×10^{-6} (see Table 15.1) at the applied load of 4098 lbs., E is calculated as 14.1×10^{6} p.s.i. from Equation 15.32. This result, when compared to values obtained in Chapter 14, is high by 43%!

15.3 FINAL TESTS PERFORMED ON ALUMINIUM DISC

15.3.1 Testing Technique Alterations

The results of Section 15.2 showed that definite improvements were required before a suitable testing technique could be established. In particular, it was important that the loading ring should be capable of applying a uniform load and that the support ring should be located at the periphery of the slab as theoretically specified.

Following from the previous investigation, it was apparent that the most satisfactory technique for achieving uniform load and uniform support was with a soft packing material. The resulting deflections in this medium would then dampen out the influence of small irregularities on the disc surface or from variations in the thickness of the packing material. Consequently, for the support ring, rubber of Shore hardness 60 was used. The support was 2.5" high and 1" thick at the bottom being reduced to o.5" at the top by chamfering both the inside and outside edges. For the loading ring, the Paxolein strip used in the previous tests, was replaced with two circular 0.5" wide strips of Sundeela soft grade building board of 12" mean diameter, each strip being approximately $\frac{1}{2}$" thick.

To prevent differential deflections of the load ring, the cruciform used for Test Series 4 (Plate 15.1) was replaced with a solid circular steel plate of $2\frac{1}{4}$" thickness. (see Plate 15.2). Two small holes only were drilled to allow electrical leads to pass through to strain gauges positioned on the upper surface within the loading ring.

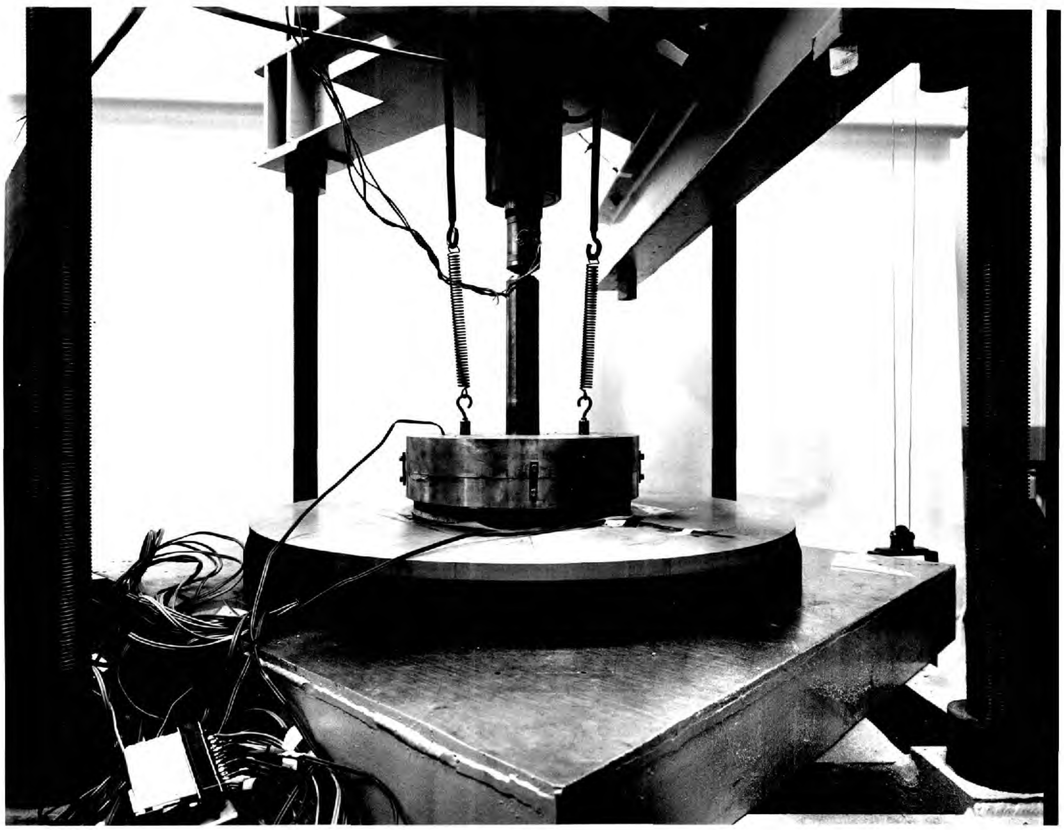

PLATE 15.2 Test method used for loading circular discs

15.3.2 Description of Test

Five separate tests, hereafter referred to as Test Series 5, were performed on the aluminium disc with the altered equipment described above. In the first three tests, the majority of the gauges were on the bottom surface, i.e., in tension. (see Figure 15.2) Test B differed from Test A only in that the disc was rotated 90°. Test C which was performed to investigate possible restraint between the support ring and disc, differed from Test B only in that a greased packing was interposed between the support ring and disc surface. This greased packing was identical to the one used between the loading strips and the upper disc surface. (for description, see Section 15.2.1) Test D and E, performed on the disc in the inverted position, i.e.; with most of the gauges on the top surface in compression, were mutually similar except for the disc being rotated 90° between the two tests.

For each test, the slab was loaded three times with two complete sets of readings at zero load and the applied load of 2621lbs. All readings were taken with a different Solartron data-logger, sensitive and repeatable to 1 microstrain. For test E, three load stages of 1342, 2621, and 3989 lbs. were performed to investigate the influence on strain pattern of deflection of the slab.

15.3.3 Discussion of Results

With the gauges as positioned in Figure 15.2 and values of a = 14.75", b = 6.00" and ν = 0.342, the <u>theoretical</u> values of stress and strain at the gauge points have been calculated from Equations 15.25, 15.26, 15.27, 15.30, 15.31 and 15.32. (see Table 15.2) These values of radial and transverse stresses and strains across a typical radius have been plotted graphically in Figure 15.3 and the strain values have been presented diagrammatically in Figure 15.4(a). As a sharp decrease in radial strain occurs at r = 6" (see Figure 15.3), the theoretical strains on the radial gauges nos. 7 and 16 were determined by integrating the strains over the distance r = 5.5" to r = 6.5", thereby obtaining the coefficient, 0.965. For all other gauges the strain was obtained from the 'r' value at the gauge

TABLE 15.2 THEORETICAL DISTRIBUTION OF STRESS AND STRAIN OVER SURFACE OF ALUMINIUM DISC
(a = 14.75", b = 6,00", ν = 0.342)

RADIUS r (ins.)	GAUGE Nos.	RADIAL STRESS σ_r (xP)	TRANSVERSE STRESS σ_t (xP)	RADIAL STRAIN ϵ_r ($x\frac{P}{E}$)	COEFF OF STRAIN	TRANSVERSE STRAIN ϵ_t ($x\frac{P}{E}$)	COEFF OF STRAIN
0-6	2,4,6 8,9,11 12,18, 19,20.	1.220		0.804	1.000	0.804	1.000
6	7,16	1.188		0.776	0.965		
6.71"	15	1.044	1.152	0.650	0.810	0.795	0.990
8.484	5	0.702		0.370	0.461		
	14		0.972			0.732	0.912
10.81	13	0.381	0.757	0.122	0.152	0.627	0.782
11.50	17	0.304		0.065	0.081		
	10		0.699			0.595	0.741
12.75	3	0.176		-0.028	-0.035		
			0.598			0.538	0.670
14.75		0	0.454	-0.153	-0.190	0.454	0.564

Note: Theoretical coefficients of strain at gauge nos. 15 and 13, computed from Mohr's respresentation of strain, are 0.846 and 0.588 respectively.

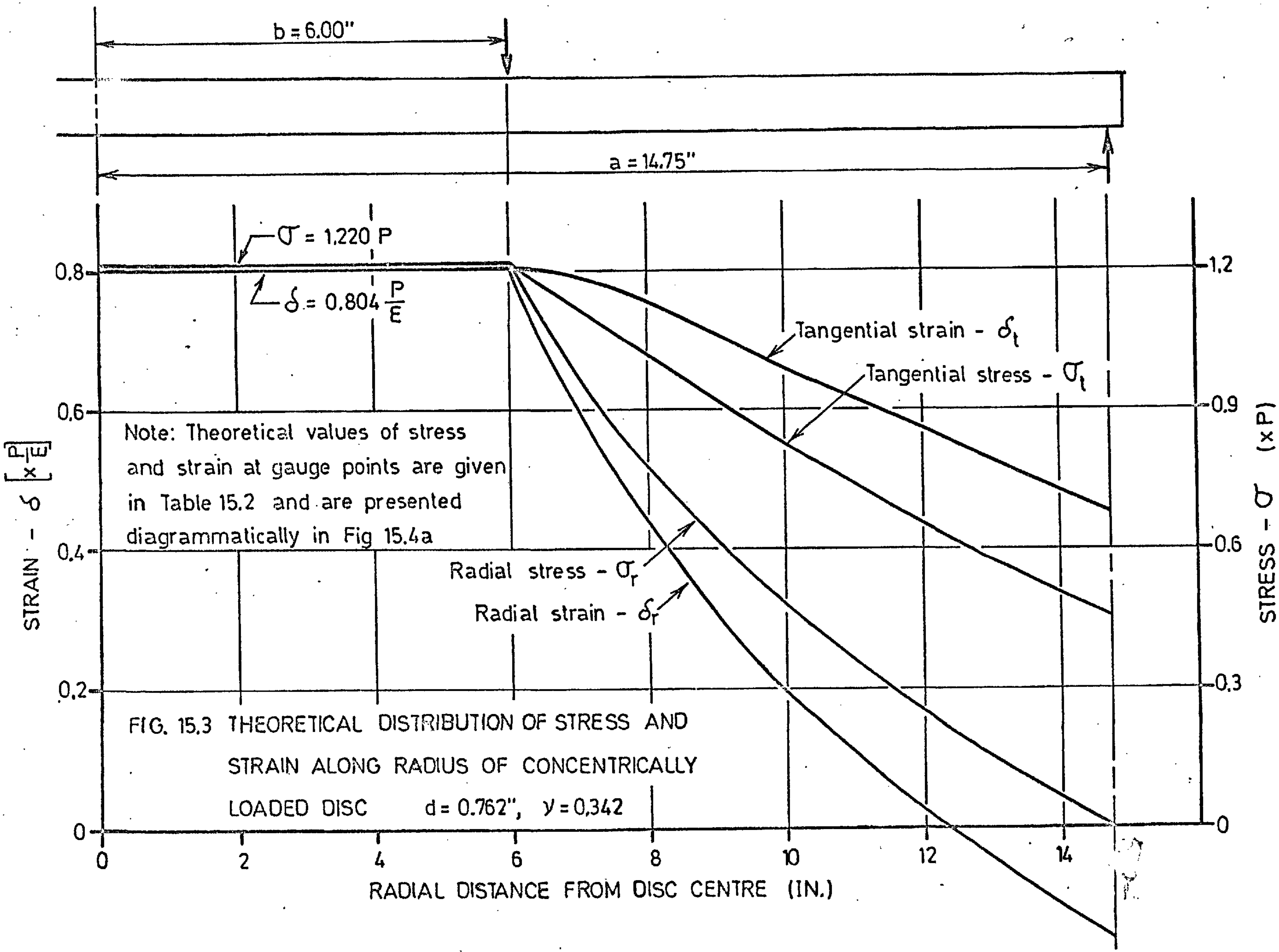

FIG. 15.3 THEORETICAL DISTRIBUTION OF STRESS AND STRAIN ALONG RADIUS OF CONCENTRICALLY LOADED DISC $d = 0.762''$, $\nu = 0.342$

centre. For gauge nos. 13 and 15, i.e. those which are neither radial nor transverse, the theoretical strain was computed from Mohr's circular representation of strain.(110)

TABLE 15.3 STRAIN DISTRIBUTION ON ALUMINUM DISC FOR TEST SERIES 5
(Most strain gauges on bottom surface in tension)

GAUGE No.	TEST A STRAIN ($x10^{-6}$)	TEST A COEFF	TEST B STRAIN ($x10^{-6}$)	TEST B COEFF	TEST C STRAIN ($x10^{-6}$)	TEST C COEFF
1	149.3T	0.709	141.0T	0.682	144.0T	0.700
2	214.0T	1.015	216.0T	1.044	207.2T	1.007
3	7.9T	-0.037	10,8T	-0.052	8.4T	-0.041
4	217.8T	1.032	208.0T	1.006	213.7T	1.039
5	105.6T	0.500	97.5T	0.471	102.0T	0.497
6	207.8C	0.984	204.2C	0.987	199.8C	0.972
7	204.2T	0.969	215.7T	1.042	200.5T	0.977
8	210.0T	0.996	219.3T	1.062	215.7T	1.049
9	214.8T	1.018	207.7T	1.003	210.2T	1.024
10	148.0T	0.702	159.0T	0.769	155.3T	0.755
11	207.0T	0.982	216.0T	1.044	211.7T	1.030
12	216.4T	1.023	207.8T	1.003	211.7T	1.030
13	129.2T	0.612	121.8T	0.589	123.3T	0.600
14	192.4T	0.912	190.3T	0.920	189.3T	0.921
15	189.3T	0.898	181.8T	0.879	181.0T	0.880
16	213.6T	1.013	208,0T	1.006	204.5T	0.996
17	18.0T	0.086	22.7T	0.110	25.1T	0.122
18	213.8T	1.013	205.6T	0.994	209.8T	1.020
19	214.5T	1.018	206.0T	0.997	209.8T	1.020
20	210.5T	0.999	202.0T	0.978	207.6T	1.011

		Test A	Test B	Test C
Average of gauge nos 2,4,8,9,12,18,19	=	214.2	210.0	211.0
6	=	207.8	204.2	199.8
Average strain (coeff. = 1.000)	=	211.0	207.1	205.6

Coefficients for Tests A to C are presented diagrammatically in Figure 15.4 (b) to 15.4 (d).

TABLE 15.4 STRAIN DISTRIBUTION ON ALUMINUM DISC FOR TEST SERIES 5 (most Strain Gauges on Top Surface in Compression)

GAUGE NO.	TEST D		TEST E					
	STRAIN ($x10^{-6}$)	COEFF	1st LOAD STAGE		2nd LOAD STAGE		3rd LOAD STAGE	
			STRAIN ($x10^{-6}$)	COEFF	STRAIN ($x10^{-6}$)	COEFF	STRAIN ($x10^{-6}$)	COEFF
1	143 C	0.682	74.9C	0.700	149.2C	0.703	223.2C	0.703
2	209 C	0.997	110.3C	1.031	214.6C	1.012	318.6C	1.005
3	7.5C	-0.036	3.0C	-0.028	5.4C	-0.025	6.9C	-0.022
4	205.5C	0.980	104.9C	0.981	208.2C	0.981	310.8C	0.980
5	96 C	0.458	51.3C	0.479	100.5C	0.474	148.8C	0.469
6	212 T	1.012	110.3T	1.031	218.6T	1.030	328.0T	1.033
7	-	-	-	-	-	-	-	-
8	205 C	0.979	102.0C	0.953	204.4C	0.964	306.3C	0.966
9	207 C	0.988	102.0C	0.953	203.4C	0.959	301.0C	0.949
10	156 C	0.745	80.8C	0.755	162.1C	0.764	246.0C	0.775
11	-	-	-	-	-	-	-	-
12	206.5C	0.986	102.5C	0.958	203.4C	0.959	303.6C	0.957
13	126.5C	0.604	64.0C	0.598	127.7C	0.601	191.3C	0.604
14	191.5C	0.914	100.0C	0.934	199.0C	0.938	298.3C	0.941
15	-	-	-	-	-	-	-	-
16	-	-	-	-	-	-	-	-
17	18 C	0.084	9.9C	0.092	17.2C	0.081	24.2C	0.076
18	208.5C	0.995	102.5C	0.958	204.0C	0.961	306 C	0.965
19	207.5C	0.990	102.5C	0.958	203.4C	0.959	304.7C	0.961
20	-	-	-	-	-	-	-	-

	Test D	Test E 1st	Test E 2nd	Test E 3rd
		(load stages)		
Average strain of gauge no. 2,4,8,9,12,18,19 =	207.0	103.8	205.9	307.3
6 =	212.0	110.3	218.6	328.0
Average of top and bottom (coeff = 1.00)	209.5	107.0	212.2	317.6

Coefficients for Tests D and 2nd load stage of Test E are presented diagrammatically in Figure 15.4(e) to (f).

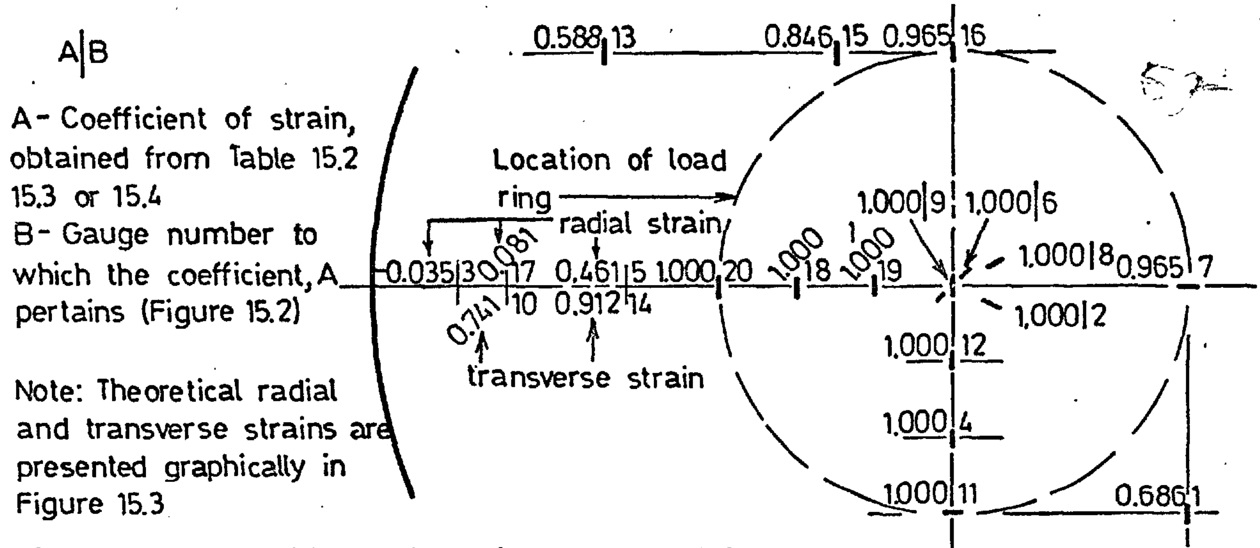

(a) Theoretical Coefficients of Strain at Gauge Points

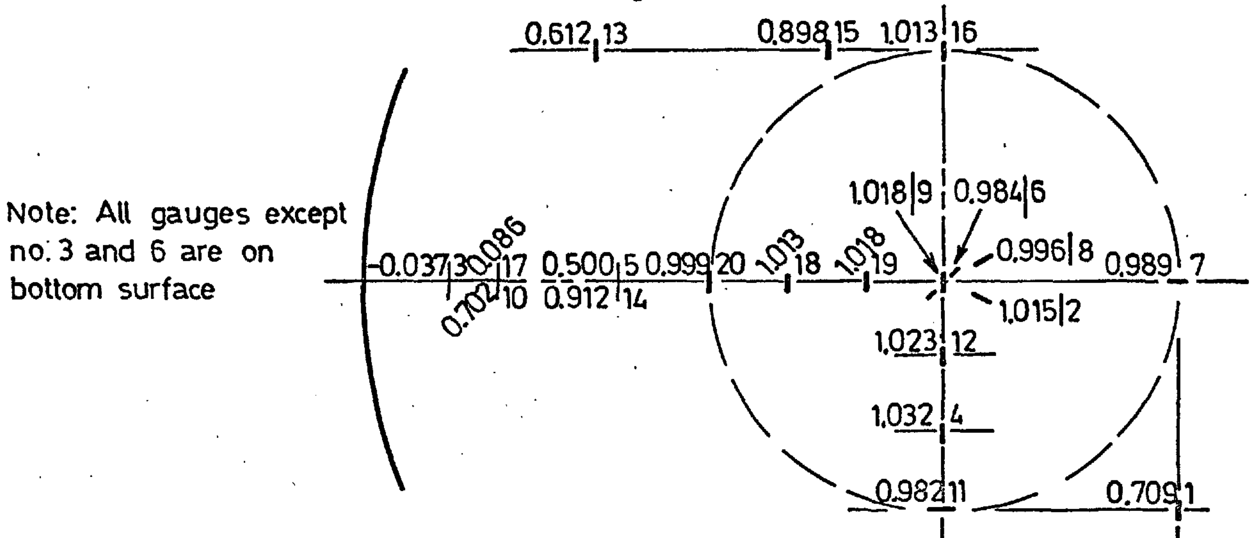

(b) Coefficients of Strain from Test A

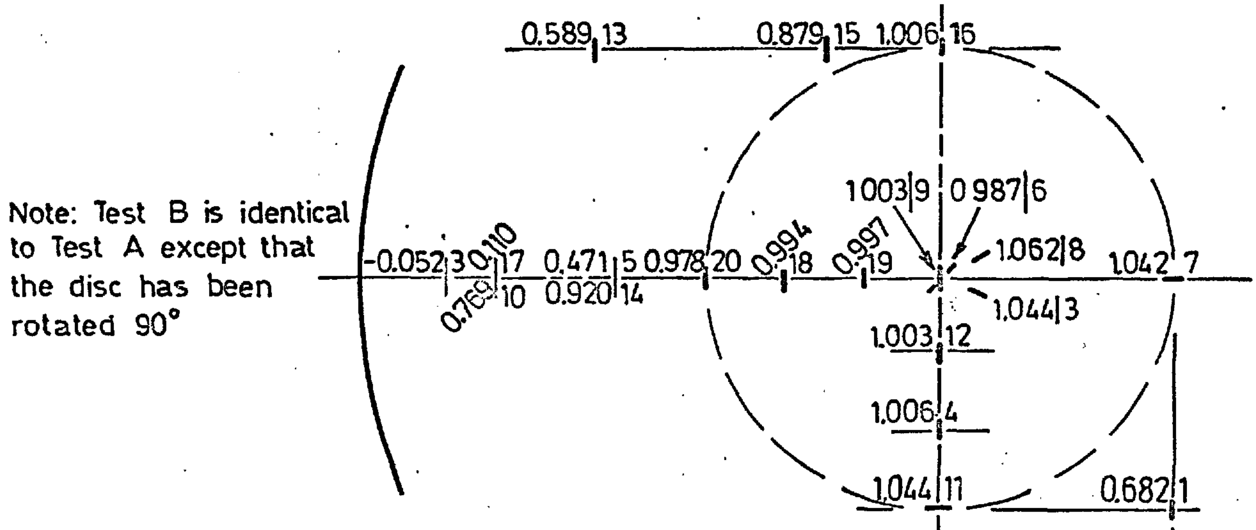

(c) Coefficients of Strain from Test B

FIG. 15.4 STRAIN DISTRIBUTION ON ALUMINUM DISC CONCENTRICALLY LOADED AND SUPPORTED AT PERIPHERY - TEST SERIES 5 (cont.)

Note: Test C is identical to Test B except that a grease pack has been positioned between the support ring and disc surface

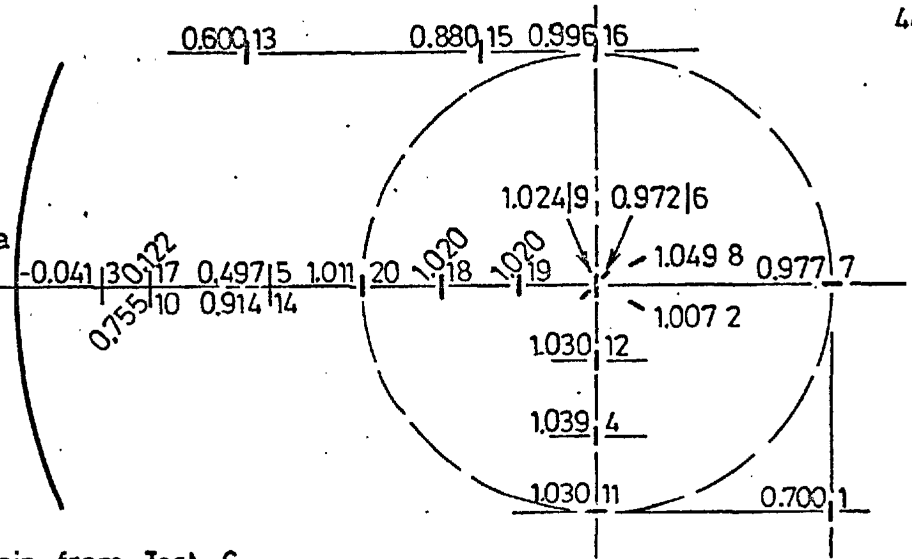

(d) Coefficients of Strain from Test C

Note: Test D is similar to Test A except that the disc has been inverted

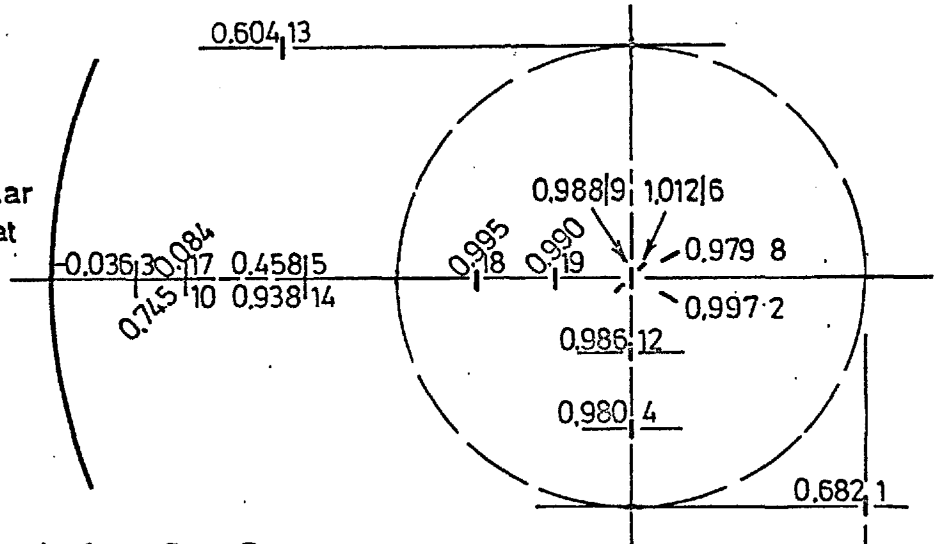

(e) Coefficients of Strain from Test D

Note: Test E is identical to Test D except that the disc has been rotated 90°

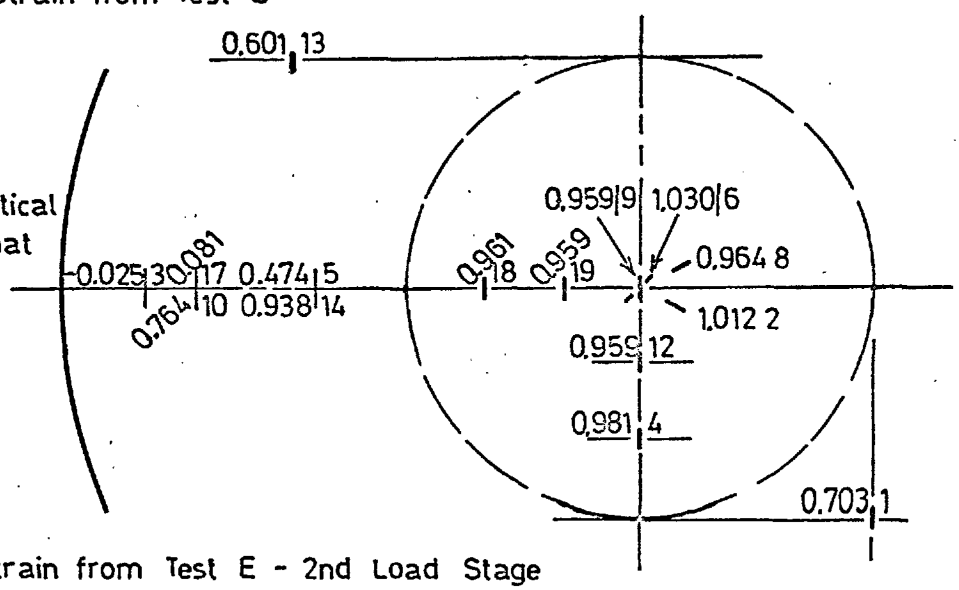

(f) Coefficient of Strain from Test E - 2nd Load Stage

FIG. 15.4 STRAIN DISTRIBUTION ON ALUMINUM DISC CONCENTRICALLY LOADED AND SUPPORTED AT PERIPHERY - TEST SERIES 5

The strain values and corresponding coefficients related to a value of 1.000 for the central section for Test Series 5 are given in Tables 15.3 and 15.4. The coefficient values at the applied load of 2621 lbs. are presented diagrammatically in Figures 15.4 (b) to (f).

From comparison of Figure 15.4(a) with Figures 15.4 (b) to (f), it is seen that the strain pattern obtained experimentally agrees very closely with the strains derived theoretically. For example, in the central section, the strains are very consistent, seldom differing by more than 4% from the average. Similarly, outside the load ring, there is good agreement in the values of the coefficients.

Any possible restraint effect between the support ring and slab surface is negligible. This is borne out in comparing the results of Tests B and C in Table 15.3 or Figure 15.4 (c) and (d), where it is observed that the strain pattern remains sensibly unchanged. Particularly, with those gauges such as nos. 3, 10 and 17 near the support ring, which would be most susceptible, the small differences observed are insignificant. It is therefore concluded that the restrainteffect of the rubber support ring is negligible.

Taking the average of the average strains in the central section for Tests A to E, a value of 209.1×10^{-6} in/in. has been obtained at the applied load of 2621 lbs. Using ν equal to 0.342, the value of the modulus of elasticity, E, as computed from Equation 15.32 is 10.04×10^{6} p.s.i. As the above calculation is based on an outer radius, a, of 14.75", there would be some error expected as there are actually 15.00" of radius resisting the applied moment, i.e.; the actual stresses would be slightly lower than obtained theoretically. To correct for this, the summation of the transverse stresses across any radius was obtained by integrating equations 15.26 and 15.27 over the distance, r = 0 to r = 14.75" and subsequently, over the distance, r = 0 to r = 15.00". From the ratio of these values, equal to 0.995, it was apparent that the calculated stresses were 0.5% high. By applying this correction to the above E value, the corrected modulus of elasticity is 9.99×10^6 p.s.i.

This value of E is only about 1.5% larger than the values obtained from the results of the slab tests described in Chapter 14. In view of the completely different method of testing to obtain these E values as well as the different equipment used to measure strain, i.e.; different data loggers, it is apparent that the above close relationship falls within the bounds of experimental error.

As is seen in Table 15.4, the different load stages for Test E produce no significant alterations in strain pattern. This would be predicted theoretically as the deflections of the centre of the disc, 0.016", 0.032" and 0.048" for the three respective load stages, are small in relation to the slab thickness of 0.762". As concrete and mortar discs are both thicker and fail at lower strain values, (see Chapter 17) it is concluded that the influence of deflection is negligible.

15.4 SUMMARY

From the basic equations for the deflection and curvature of circular plates or discs supported uniformly at the periphery and loaded uniformly by a concentric load ring, formulae for surface stresses and strains have been derived.

In order to achieve a satisfactory testing technique for applying a uniform intensity of load and support, it is necessary that a soft packing medium be used. The resulting deflections in this packing medium will then dampen out small irregularities on the disc surface or thickness of the medium. In the tests performed by the author, a rubber support ring of 2.5" height with Shore hardness 60 and a loading strip of 1" thick soft building board were used. For transferring the load from the load cell to the load strip, a rigid steel ring, firmly attached to a $2\frac{1}{4}$" thick plate, was used.

The distribution of strain agreed very closely with the theoretical distribution, seldom differing by more than 4%. Furthermore, the value for the modulus of elasticity, 9.99×10^6 p.s.i. based on the average of the strain readings in the centre, agrees within 1.5% of the average result obtained in the slab tests of Chapter 14. It is therefore concluded that the above testing technique does produce stresses and strains, which are in very close agreement with theoretical predictions.

CHAPTER 16

EXPERIMENTAL PROCEDURE ON CONCRETE AND MORTAR SPECIMENS

16.1 OUTLINE OF EXPERIMENTAL WORK

The main test series consisted of loading slabs, discs, beams and uniaxial tension and compression specimens to failure while simultaneously obtaining reliable values for the modulus of elasticity, Poisson's ratio, ultimate strengths and discontinuity level stresses and strains. One mortar with an effective W/C ratio of 0.425 and A/C ratio, 1.8 was tested while the concrete investigated had the same W/C ratio, 0.425, an A/C ratio of 4.05 and a fine aggregate/coarse aggregate ratio of 40/60. The tests were generally performed at an age of 28 days.

The technique used for the manufacture of the specimens and for the preparation and testing is described in this chapter. The results of the individual slab, disc and beam specimens are presented and discussed in Chapters 17 and 18.

Since nine different shaped specimens were required to achieve a satisfactory range of biaxial stress combinations, four separate castings of both the concrete and mortar were necessary. This was due to only two different shaped specimens being tested satisfactorily at any one time. In order to maintain a check that the mix proportions and concrete properties were consistent, control specimens were used.

These consisted of three 4" x 4" x 12" prisms for assessing the compressive strength, 4" x 4" x 20" waisted specimes for the uniaxial tensile strength (see Ward[2]) and 4" x 4" x 20" flexural beams for modulus of rupture values. The results of these tests are discussed in Section 16.6.

Although the above concrete specimens were initially designed with an A/C ratio of 4.5, an error in the design of one of the initial mixes was not discovered until after the specimens had been cast. Rather than repeat this mix, it was decided to accept the ratio of 4.05 for the main test series.

Mix Designation	W/C Ratio	A/C Ratio	Age at Testing (days)	Description of Specimens Cast
M1	0.40	2.0	7	2:1 slab
M2	0.40	2.0	28	2:1 slab
M3	0.425	1.8	28	2:1 slab, 1:1 slab
M4	"	"	"	1.58:1 slab, 2:1 reinforced slab
M5	"	"	"	2:1 reinforced slab, 2.5:1 reinforced slab
M6	"	"	"	1.58:1 reinforced slab, beam, disc.
C1	0.425	4.5	28	1:1 slab
C2	0.425	4.05	28	2.5:1 reinforced slab
C3	"	"	"	2:1 slab, 1.58:1 slab
C4	"	"	"	1:1 slab, 1.58:1 reinforced slab
C5	"	"	"	2.5:1 reinforced slab, 2:1 reinforced slab, disc, beam.

TABLE 16.1

SUMMARY OF MIXES

Note: 1 Mix designation letter M denotes mortar, C denotes concrete.

2. All concretes have a fine aggregate/coarse aggregate ratio of 40/60.

3. All slabs are defined by the ratio of their diagonal lengths.

However, as a test on a square concrete slab with an A/C ratio of 4.5 had already been performed, this result is included. (mix designation C1 in Table 16.1).

Likewise the results of an initial investigation on two mortar slabs, W/C ratio, 0.40 and A/C ratio, 2.0, with diagonal lengths ratio of 2:1 are included. These slabs, 2" thick, as opposed to all other slabs with 3" thickness, were tested at 7 day and 28 day age, respectively. (mix designation nos. M1 and M2 in Table 16.1)

16.2 PRECAUTIONS TAKEN FOR ACHIEVING A SIGNIFICANT CORRELATION IN THE RESULTS OF DIFFERENT SHAPED SPECIMENS

In the first instance, it was accepted that no concrete or mortar can be manufactured uniformly because of segregation during casting, whereby the coarser material settles to the bottom of the mould. To minimize such an effect, it was necessary to have a relatively stiff mix which could then be excessively vibrated to eliminate air voids. Consequently, the mixes selected in the main test series, particularly, the concretes, are classed as dry mixes of low workability.

The upper slab surface will have a lower modulus of ēlasticity and will be slightly weaker than the opposite surface due to the segregation effect. It was thus decided to test all slab, disc and beam specimens so that failure would propagate from the cast face as this would in fact be the failing face with the square shaped slabs. This also proved to be more suitable with the reinforced slabs where, as shown in Chapter 18, it was easier to achieve accurate positioning of the reinforcement in the bottom of the slab.

As the slab, disc and beam specimens are all subjected to flexural states of stress, the depth of the section would be influential on the results. This has been shown by Wright[(48)] in tests conducted on flexural beams, where the modulus of rupture values were reduced by 30% when the depth of the test specimen increased from 3" to 8" while maintaining a constant span: depth ratio. It was thus considered imperative that the thickness of all the flexural specimens should be constant.

The determination of the best slab thickness involved a compromise. Although it had to be sufficiently thin to be considered as a slab, it required adequate thickness to make the maximum aggregate size small in raltion to the slab thickness. In the case of the reinforced slabs, a significant distance was also required between the neutral axis and the steel both before and after cracking. With these considerations in mind, a thickness of 3" was selected as the most suitable size.

For the purpose of the beam test, i.e.; the uniaxial flexural test, a special beam was designed and manufactured with the above thickness of 3". To avoid any possibility of an arching action as that which occurs in the standard modulus of rupture test[9], it was necessary to increase the distance between the load and support points. The specimen selected, 3" x 4" x 40", was loaded and supported symmetrically with the load points 18" apart and the support points 36" apart. The central section was thereby subjected to a state of uniform, uniaxial moment.

16.3 MANUFACTURE OF SPECIMENS

The manufacture of the specimens followed principles adopted by previous researchers of the Imperial College Concrete Materials Research Group. These have been presented in detail by Ward[2]. However, a brief description of the techniques employed in the preparation of the materials and the mixing, casting and curing processes will be presented here.

16.3.1 Description of Materials

The cement used was ordinary Portland Cement supplied in one batch from the Kent Works of the Cement Marketing Company. It was blended and stored in air tight steel drums until used.

The water for the mixes was drawn from the Imperial College mains. As there was a 24 hour pre-soaking period, the water was at laboratory temperature at time of mixing.

All aggregate used was Thames Valley River Gravel, supplied by the Stone Court and Ballast Co., from their Rickmansworth pit. The fine aggregate (passing 3/16")[60] was stored in two sizes;

(i) retained on sieve 25

(ii) passing sieve 25.

As the fine aggegate, when supplied, was 72% and 28% respectively in the above two sizes, these proportions were maintained for the complete test series.

As the slabs being tested were only 3" thick, a maximum size aggregate of $\frac{3}{4}$" was considered to be excessively large. Likewise, with some of the reinforced slabs where the space between the bars was only $\frac{3}{8}$", the large aggegate would tend to settle on the reinforcing bars thereby creating a surplus of mortar between and beneath the bars. To overcome the above size and space limitations, the size of the coarse aggregate in all the concrete tests was that retained on the 3/16" sieve, but passing $\frac{3}{8}$".[60]

16.3.2 Preparation of Aggregate

In the new aggregate processing plant at Imperial College, the aggregate is washed in an L.A. Mitchell horizontal rotary washer and subsequently, dried to a 'bone dry' condition[59] in an L.A. Mitchell 90 kilowatt rotary drier. Following sieving, it is stored in air tight steel bins until used.

For the tests considered, the required amount of aggregate was removed from the steel bins and weighed 24 hours prior to casting. By then adding sufficient water to immerse the weighed-out aggregate in each drum, complete saturation of the aggregate was ensured. To provide an effective water-cement ratio, additional water was allowed for the absorption of the aggregate. This amounted to 1.8% for the coarse aggregate and 1.0% for the fine aggregate as shown by Ward's[(2)] tests conducted in accordance with principles established by Newman[(59)].

A few minutes before mixing, the excess water in the individual aggregate drums was poured off, thereby leaving the exact amount required for the effective water cement ratio and aggregate absorption.

16.3.3 Mixing and Casting

The aggregate and water were placed in a 1.5 cubic feet Eirich Pan Mixer, Type SWG11, and then were mixed thoroughly for three minutes. The preweighed cement was subsequently added and the contents mixed for a further three minutes. Following this, the mix was taken directly from the pan and placed in the moulds. As several batches were required on every casting day, each successive batch was mixed independently after each emptying of the pan.

The vibration was performed on an Allam 776 vibrating table by holding the moulds firmly on to the vibrating table until full compaction was obtained, as indicated by removal of the majority of entrapped air. After removing the moulds from the vibrating table to a level surface, the top of each moubd was levelled and floated with a steel trowel.

16.3.4 Moulds

All control specimens were manufactured in standard 4" x 4" x 20" flexural specimen moulds conforming to the requirements of British Standard 1881 (9). For the diredt tension and compression specimens, small modifications to these moulds have been made, as described by Ward (2).

The moulds used for the slab, disc and beam specimens were manufactured in the Civil Engineering Department workshop. They consisted of a $\frac{7}{8}$" plywood base, firmly screwed to 2" x 2" slats, which prevented warping of the base. The sides, 3" high, were screwed into the base and into each other, thereby ensuring a tight fit. To prevent moisture seeping out of the edges, a grease layer was applied to all mating components of the mould, thus providing an effective seal.

The above specimens were of dimilar dimensions to those used in the basic investigation on the aluminum slabs and discs discussed in Chapters 14 and 15, respectively. This was achieved with slabs, whose side lengths were 30" and discs, whose diameters were also 30". The exception was the 2.5.1 slabs whose side lengths were 29". The beam specimens were 3" x 4" x 40".

16.3.5 Curing

After the specimens had achieved an initial set, i.e.; at about three hours after casting, the specimens were covered with saturated hessian and polythene sheeting to prevent drying. The control specimens were removed from the moulds 20 hours after casting and placed directly into curing tanks. With the larger slab, disc or beam speciments, it was considered unsuitable to handle them at such an early age and they were, therefore, left in their moulds for a further day. These latter specimens, after being demoulded were usually placed on their edge, i.e.; with their principal faces in a vertical plane, in the curing tank to prevent surface stresses occurring.

The curing tanks, being thermostatically controlled, maintained the water at 70^{o}F. However, on several occasions faults occurred resulting in the temperature deviating significantly from the above temperature. However, as the temperature was in all cases restored to normal within a few hours, this was considered not to have any effect on the results.

16.4 PREPARATION OF SPECIMENS FOR TESTING

16.4.1 Application of Strain Gauges

As the entire investigation was limited to saturated specimens, a technique had to be developed for applying electrical resistance strain gauges to the surfaces of such specimens, while simultaneously preventing any influential drying action taking place. The following procedure was adopted.

(1) The specimen, after being removed from the tank on the day prior to testing, was wiped thoroughly with a clean hand towel and then marked out for gauge locations.

(2) A membrane curing compound, Super Febcure, was then immediately applied over the entire surface area, except in the vicinity of the gauge points.

(3) These points were then scraped with a knife edge, thereby removing surface laitance and simultaneously providing a firm base for the bonding of the gauges. For the cast face of the specimen, some smoothing was usually performed with a an emery cloth.

(4) After the gauge point areas had become dry, they were wiped clean and washed with Acetone. This operation occurred at about one hour after removal of the specimen from the tank.

(5) The strain gauges, also washed in Acetone, were then fastened to the surface at about ten to thirty minutes after the above operation It was necessary that a quick setting adhesive such as PS Adhesive, manufactured by Tokyo Sokki Kenkyujo be used for this operation. Care was taken to remove all air bubbles beneath the gauge.

(6) After the adhesive had hardened, (10 to 15 minutes) the immediate area around the bounds of the adhesive was coated with Super Febcure, thereby preventing further

evaporation. The entire slab area was also simultaneously recoated with the above curing compound.

(7) The electrical leads were soldered to the gauges several hours after application of the gauges. It is important that sufficient time be allowed to elapse as soldering too soon will destroy the bond between the strain gauges and adhesive.

(8) Prior to testing, the gauges were coated with yellow tallow or a grease thereby insulating them against small fluctuations in room temperature.

(9) The curing compound is not totally impermeable. Consequently, while the slab was waiting to be tested, it was covered with polythene sheeting to prevent evaporation of moisture.

With the above method whereby the entire specimen is effectively sealed, internal moisture movement resulted in the zone of concrete immediately beneath the gauge becoming saturated soon after application of the gauge. It was observed when a strain gauge had to be removed or replaced, that this resaturation occurred within an hour of placing the original gauge.

Any drying action greater than necessary can cause marked alterations in the values of the results obtained, particularly with cement paste specimens and, to a lesser extent, with mortars. Several cement paste specimens were cast and tested, but the drying action associated with the application of the strain gauges resulted in failure occurring through the gauges at abnormally low values. Similar difficulties have also been encountered by Alexander[114] in tests on the cement paste-aggregate bond strength. These difficulties resulted in the abandoning of the test series on cement paste specimens. Likewise, in tests on a few mortar specimens where sufficient care had not been taken in preventing excessive drying at the gauge points, the results were doubtful and therefore have been discarded.

The strain gauges used were Technograph 1" etched foil electrical resistance strain gauges except for the last mix, C5, when Saunders Roe 1" etched foil electrical resistance strain gauges were used.

16.4.2 Positioning of Specimen

All tests on slabs, discs and beams were performed in the biaxial flexural machine. (see Chapter 12) The methods of positioning the slabs and discs were identical to those used on the model aluminum specimens discussed in Sections 14.3.2 and 15.3.2, respectively. The beam specimens, described in Section 16.2 were accurately positioned with the aid of dowelling holes.

For the slabs and beams, the load was applied by means of a counterbalanced beam so that the true applied load is that which is actually recorded. In the case of the disc specimens, it was not easy to counter-balance the loading ring. Consequently, in the calculations, its weight is added to the indicated load at each load stage for determining the true applied load.

The uniaxial compression and tension specimens were positioned in a Denison compression and Ward tension machine,[2] respectively. In both cases, care was taken for achieving accurate alignment; dowelled platens being used in the former case whereas in the latter, a technique developed by Ward[2] was followed.

The 4" x 4" x 20" flexural specimens were tested in the biaxial flexural machine. The bottom supports were accurately located with dowelling holes whereas the flexural specimen and upper loading assembly were positioned with a steel scale and levelled, care being taken in every case to obtain good alignment. The method of test conformed to the requirements of British Standard 1881 except that the beam was loaded at right angles to the direction of casting and, the loading rate was altered, so that the outer fibre was being stressed at the rate of 150 p.s.i./minute (see Section 16.5.2).

16.5 METHOD OF TEST

16.5.1 Slab, Disc and Beam Specimens

The ultimate loads varied from approximately 900 lbs. with the 4" x 3" x 40" concrete beam to almost 14,000 lbs. with the mortar disc. As a result, some variations in the method of test had to be accepted due to the limitations of the equipment and the scope of the investigation. In particular, with specimens whose ultimate strength was in excess of 3.5 tonf, i.e.; the capacity of the load cell, the loading was conducted twice. The first loading was performed slowly with the load cell in place, strain readings being taken at each of several load stages up to a level significantly below the discontinuity level. (assumed as 80 microinches strain for concrete and 150 microinches for mortar). This provided accurate information on the load-deformational behaviour of the material in the 'so-called' elastic range. The second loading, performed directly by the hydraulic ram with loads being measured with the 4000 p.s.i. Budenberg pressure gauge, (see Figure 3.9) was conducted at a constant loading rate to failure. Again, the readings of all the gauges were obtained at several load stages.

With specimens whose ultimate strengths were less than 3.5 tonf., the specimens were usually loaded directly to failure with numerous train readings being taken. However, with the 4" x 3" x 40" beams, where accurage comparisons of Poisson's ratio and modulus of elasticity between tension and compression were required, a more comprehensive investigation was conducted. In the first test, the beam, positioned with the cast face uppermost i.e.; in compression, was loaded several times in the 'so-called' elastic range with strain readings taken at each of several load stages. In the second test the beam was simply reversed so that the cast face would be in tension, and the above testing procedure was then repeated. However, in the last run, the beam was loaded continuously to failure at a constant loading rate.

Although considerable information on some specimens was obtained in the elastic range by repeated loadings, this was not expected to have a significant effect on the ultimate strength.[44] However, after the discontinuity level has been reached, the loading rate would be influential on the shape of the stress-strain curve and the ultimate strength[14,40,43,44] Therefore, the last loading of each specimen was performed at a continuous rate with failure occurring in about ten minutes. Thus, the results obtained are compatible with and representative of the short term behaviour of the material.

With each specimen shape having a different ratio of biaxial stresses, it was necessary to load each specimen at a different rate so as to induce failure in approximately the same time. It was assumed that all the specimens for the mortar or concrete would fail at a similar principal tensile strain. On this basis, the loading rate was calculated as

$$\text{Loading rate} = 150(1 - m\nu) \text{ p.s.i.} \qquad \ldots 16.1$$

where m is the ratio of principal bending moments ($-M_x/M_y$) (see Equation 14.18) and ν is Poisson's ratio. Therefore, in uniaxial tension the stressing rate was 150 p.s.i. per minute[2] while in biaxial compression-tension, the loading produced a slower increase in the rate of the larger principal tensile stress.

The strain values for any test were recorded on either of two Solartron data loggers. For the first few mixes, M1 to M3, C1 and C2, the data logger used, operating on a pulse excitation system, was sensitive to two microstrain and recorded the results at the rate of ten per second. As a result, at any load stage, no significant difference in load occurred during the reading of the gauges, despite a continuous application of load. The second data logger used, operating on a continuous pulse system, was sensitive to one microstrain and repeatable to one microstrain for up to 72 hours. However, its slower output of strain readings (two per second) resulted in a small increase in load during the reading of the gauges. To allow for this increase, small adjustments in the load corresponding to the strain for each gauge were required.

16.5.2 Control Specimens

The direct compression and tension control specimens were loaded to failure at the rate of 1500 and 150 p.s.i. per minute, respectively[2]. The 4" x 4" x 20" flexural specimens were loaded so that the rate of increase in the modulus of rupture value was also 150 p.s.i. per minute, compatible with the direct tension specimens above. For those direct tension and compression specimens which had strain gauges, the above loading rates were maintained with strain readings obtained at each of several load stages.

All control specimens were tested in the saturated state.

16.6 RESULTS OF CONTROL TESTS

In order to ensure that constant mix proportions were being used, control specimens for mixes M3 to M6 and C1 to C5 were cast and tested, the results of which are shown in Table 16.2. In most cases, three specimens of each type were tested. Where fewer specimens were tested, these are shown with the number, 1 or 2, beside the average result representing the number of specimens.

Although differences in strength are observed between mixes with identical mix proportions, these are not consistent with all specimens and in no case is there conclusive evidence that a mix is too strong or weak. Differences which do exist are probably due to variations in the degree of vibration. (see Section 9.10) As each slab, disc and beam was vibrated independently, no correction to any of the results was therefore justified.

TABLE 16.2 RESULTS OF CONTROL TESTS

MIX DESIG.	UNIAXIAL COMPRESSION			UNIAXIAL TENSION			MODULUS OF RUPTURE		
	STRENGTH	STAND DEV.	COEFF. OF VAR	STRENGTH	STAND DEV.	COEFF. OF VAR.	STRENGTH	STAND DEV.	COEFF. OF VAR
M3	7615	329	4.3%	530	4.6	0.9%			
M4	7880(2)	78	1.0%	622	33.7	5.4%	989	36.5	3.7%
M5	7450	134	1.8%	717	19.9	2.8%	1020	28.5	2.8%
M6	8480	110	1.3%	651(1)			1026	51.3	5.0%
C1	5490	341	6.2%	387	18.9	4.9%			
C2	7160	19	2.4%	482	11.7	2.4%	720(2)	4.0	0.5%
C3	8220	98	1.2%	516	23.7	4.6%	815	8.1	1.0%
C4	7260(1)								
C5	7470	195	2.5%	451	25.2	5.6%	788	16.5	2.1%

CHAPTER 17

THE BEHAVIOUR OF CONCRETE AND MORTAR UNDER UNIXIAL AND BIAXIAL TENSION AND TENSION-COMPRESSION STATES OF STRESS

17.1 INTRODUCTION

In any experimental investigation of the properties of concrete under different states of stress, the following points must be examined (see Section 11.4)

(1) the applicability of the laws of elasticity

(2) the ultimate failing strengths

(3) stresses and strains at the discontinuity level

(4) the governing failure criterion

In this chapter, the test results of one mortar and one concrete are presented and discussed with particular emphasis on the first three points above. Although some comments are made on possible failure criteria, this is covered in greater detail in Chapter 19 where the results of both this and Chapter 18 are considered together.

17.2 UNIAXIAL TENSION AND COMPRESSION

An investigation to determine the fundamental values of Poisson's ratio, ν and modulus of elasticity, E in uniaxial states of stress was conducted on three differently shaped specimens; 4" x 4" x 12" prisms for direct compression, 4" x 4" x 20" waisted specimens for direct tension and 3" x 4" x 40" specimens for flexure. The stress-strain graphs for these specimens are presented graphically in Figures 17.1 to 17.6, the mortar in Figures 17.1 to 17.3 and the concrete in Figures 17.4 to 17.6. All data is given in Appendix B whilst the details of the mix proportions are presented in Table 16.1.

Figure 17.1, showing the longitudinal and lateral strains on both the tension and compression faces of the mortar beam in two separate tests (see Section 16.5.1), indicates conclusively that both the ν and E values are unchanged in tension and compression. This is particularly significant as, for each load stage in the second test, the material at every gauge point is subjected to the same magnitude of stress, but of opposite sign, as in the first test.

Although data obtained by Ward[(2)], Todd[(115)] and Blakey and Beresford[(66)] indicate that the moduli of elasticity in tension and compression are the same, it has not previously been shown that Poisson's ratio is the the same in tension and compression.

Unfortunately, for the same flexural test performed on a concrete, the data logger behaved somewhat erratically (see Figure 17.4). As a result, any differences observed in E and ν, particularly the latter, cannot be considered significant in view of the scatter in relation to the maximum value of the strains being recorded. For example, the strains in the lateral direction at the discontinuity level were only of the order of 10 microstrain. However, despite the scatter in

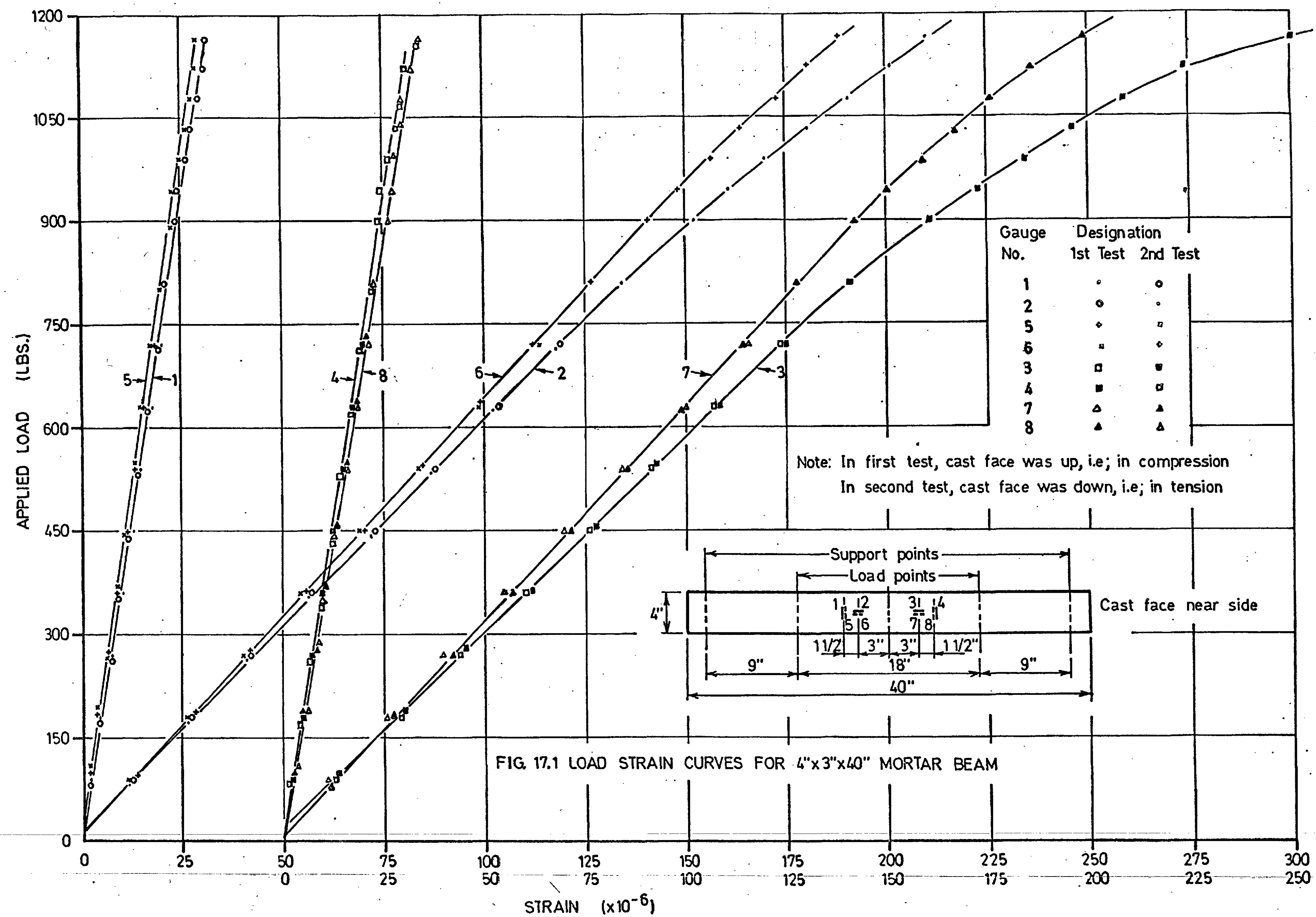

FIG. 17.1 LOAD STRAIN CURVES FOR 4"x3"x40" MORTAR BEAM

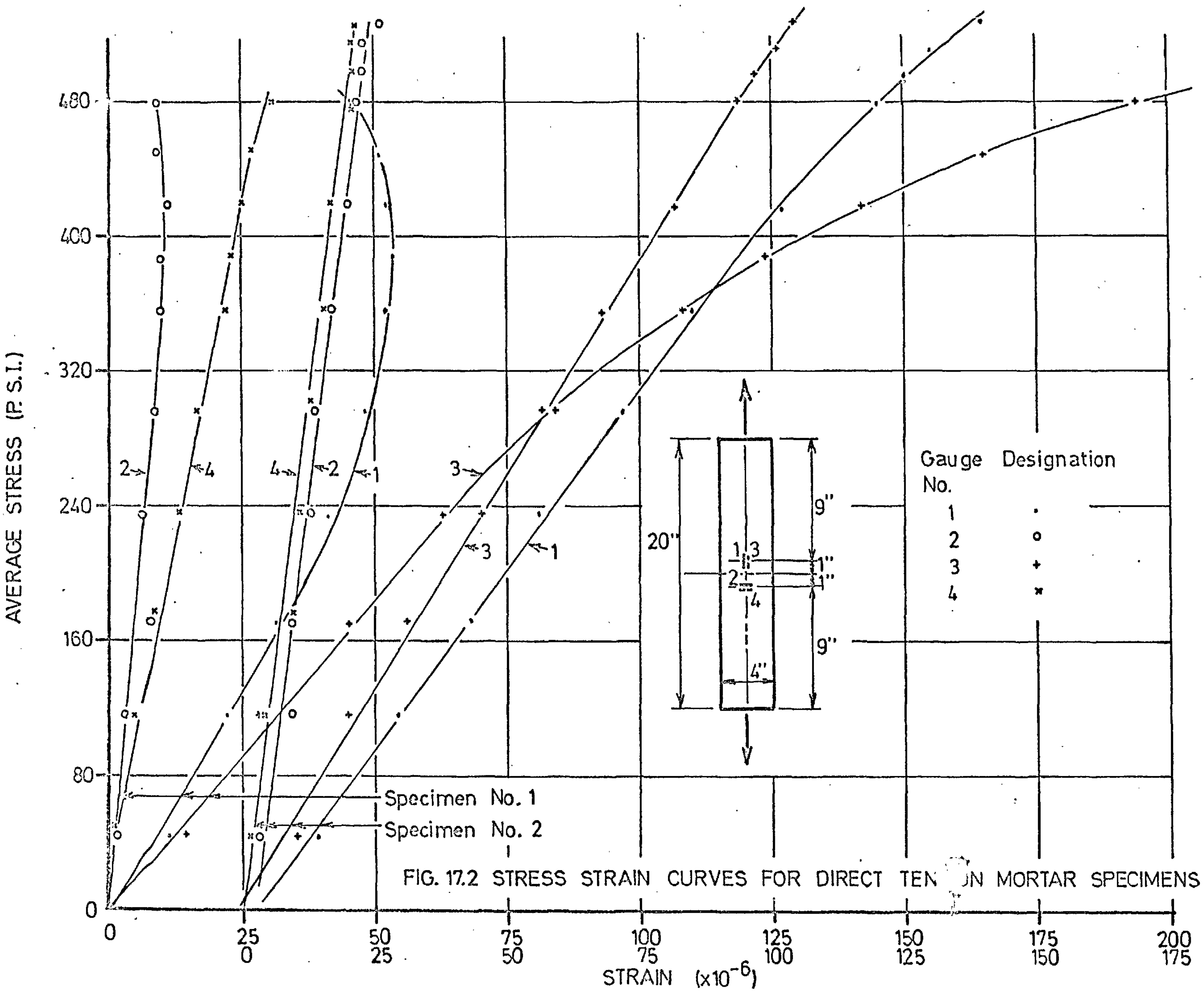

FIG. 17.2 STRESS STRAIN CURVES FOR DIRECT TENSION MORTAR SPECIMENS

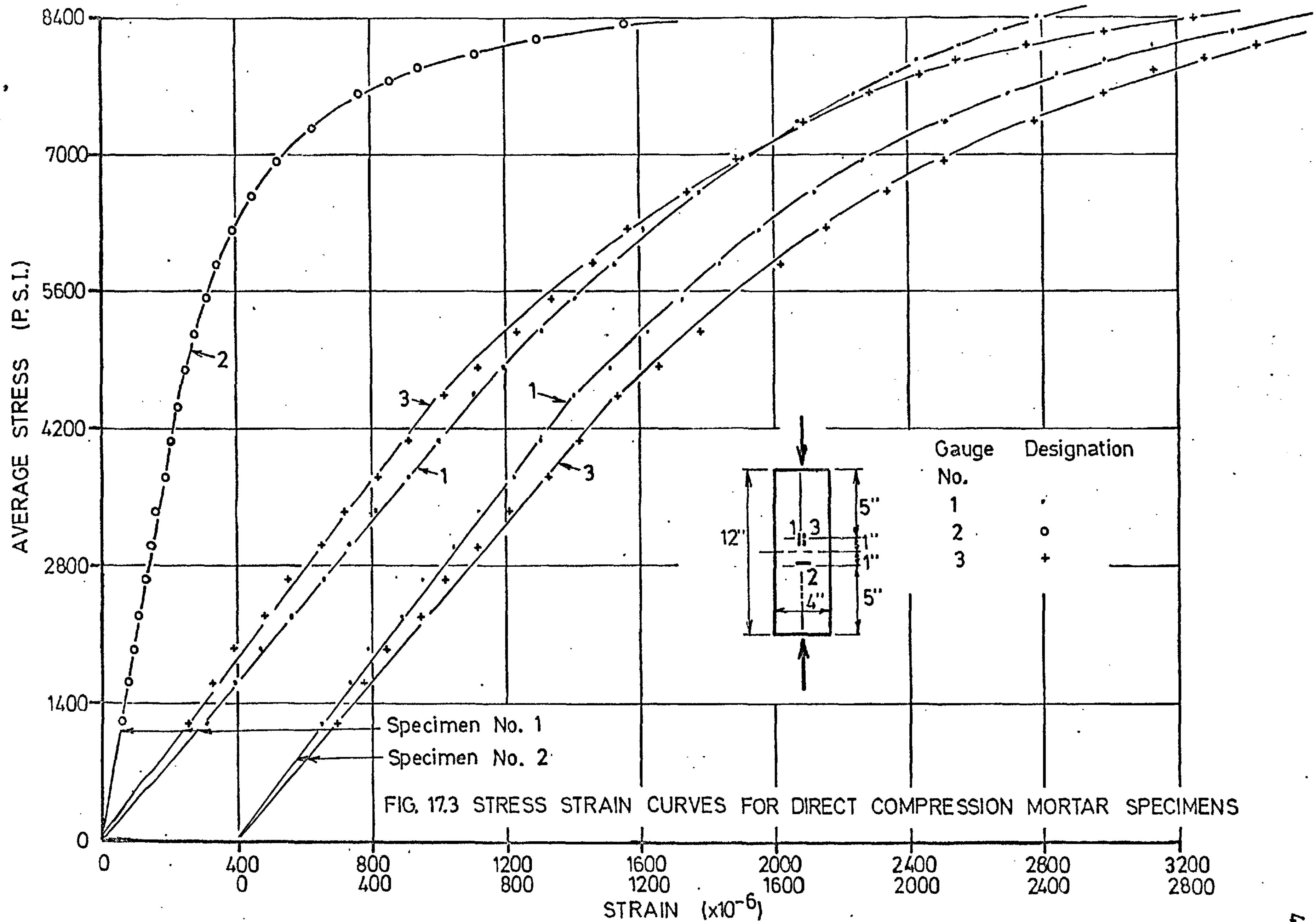

FIG. 17.3 STRESS STRAIN CURVES FOR DIRECT COMPRESSION MORTAR SPECIMENS

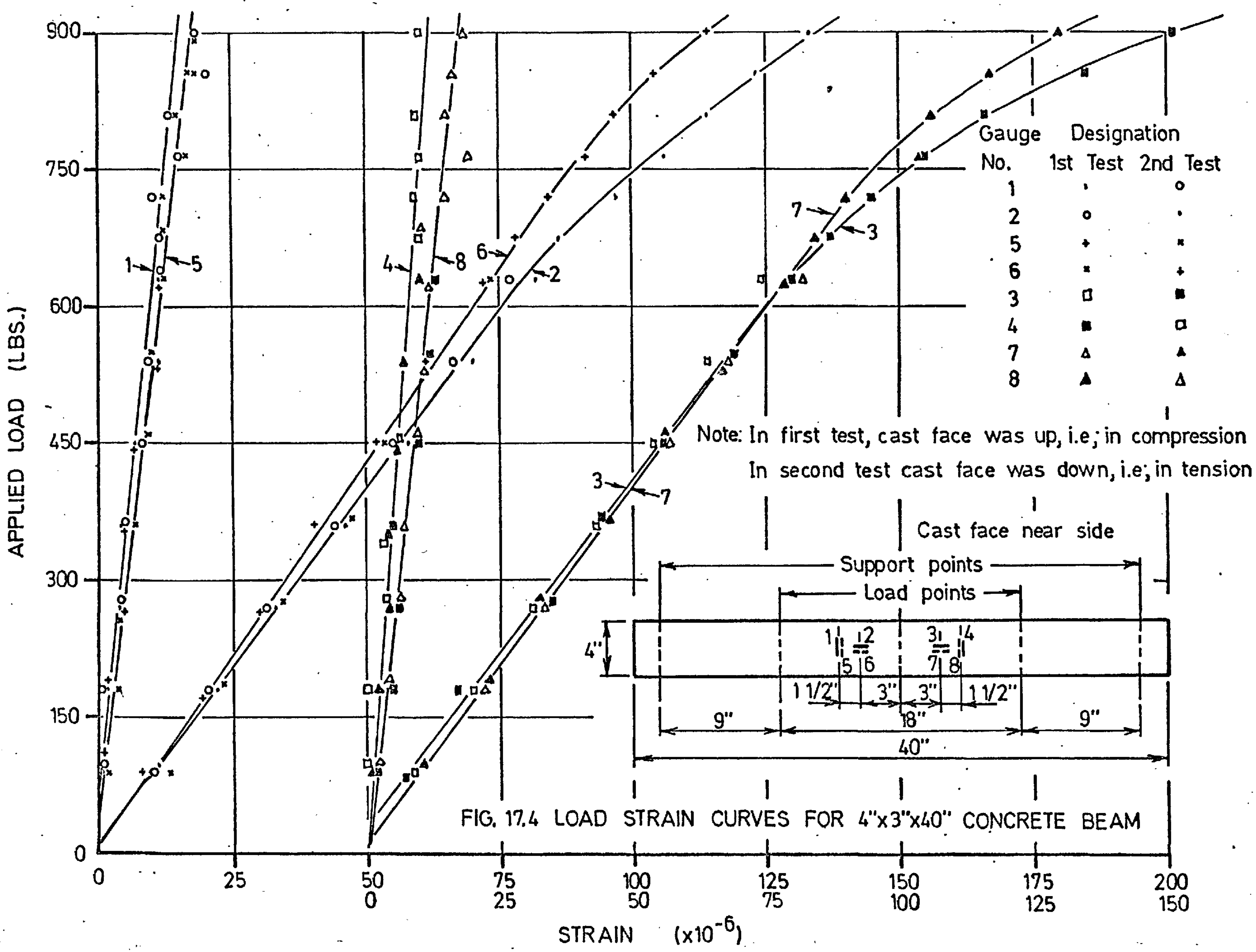

FIG. 17.4 LOAD STRAIN CURVES FOR 4"x3"x40" CONCRETE BEAM

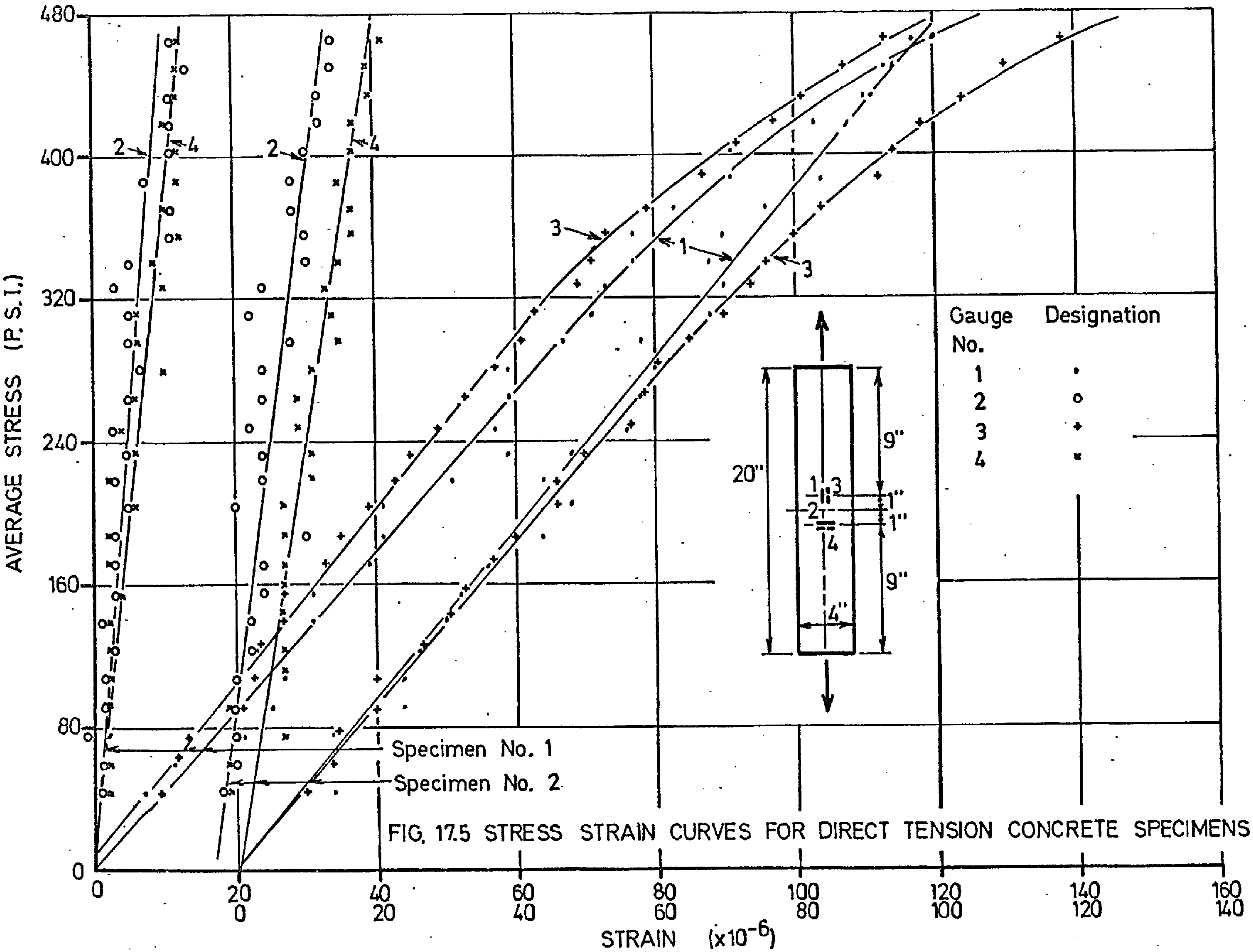

FIG. 17.5 STRESS STRAIN CURVES FOR DIRECT TENSION CONCRETE SPECIMENS

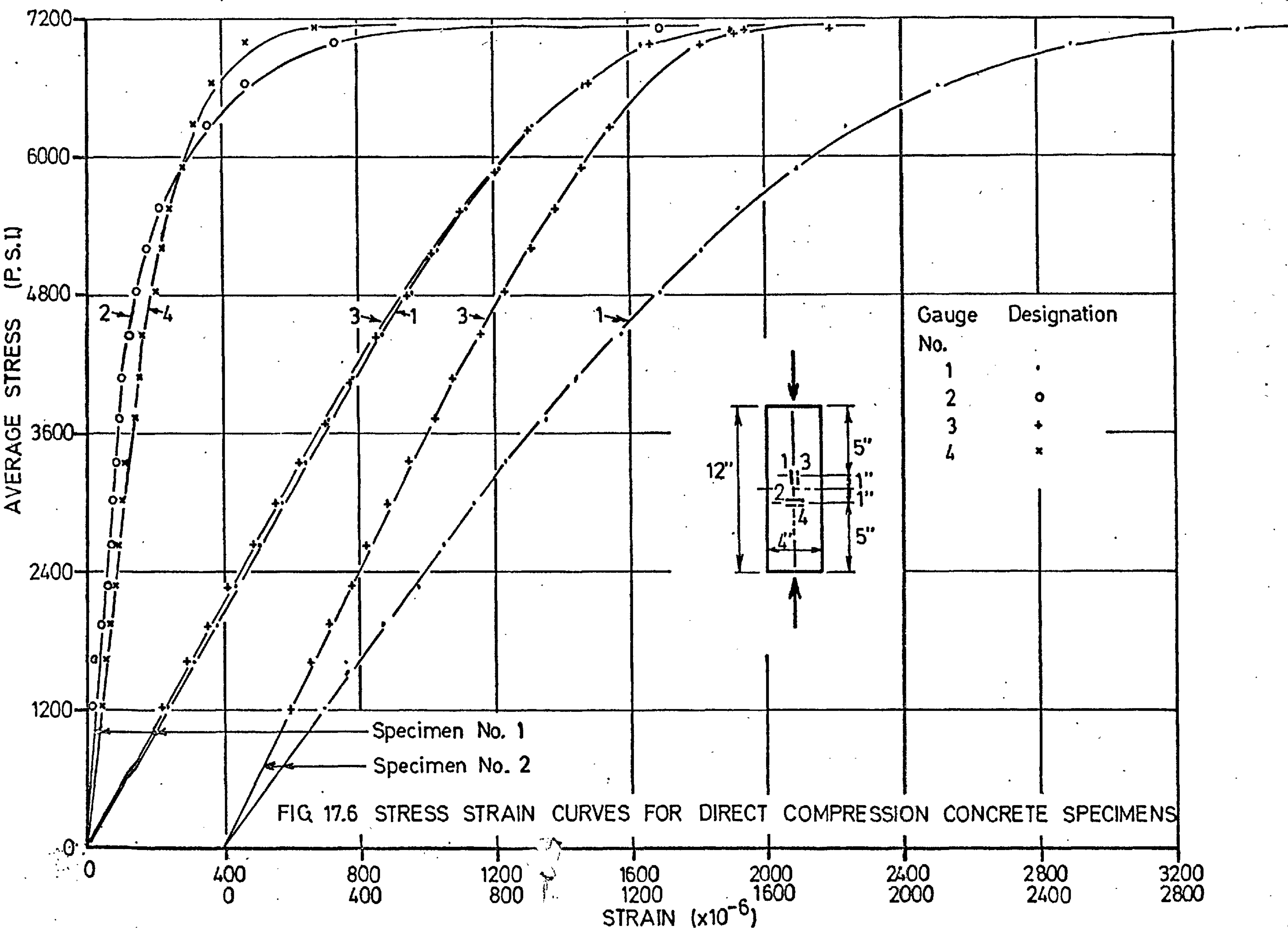

FIG. 17.6 STRESS STRAIN CURVES FOR DIRECT COMPRESSION CONCRETE SPECIMENS

results, both the lateral and longitudinal gauges showed strains of very similar magnitude and opposite sign at each load stage in the two separate tests. In uniaxial tension and compression, it seems logical to expect, from a phenomenological approach, that both the E and ν values should remain the same.

Figures 17.2 and 17.5 show the longitudinal and lateral strains on direct tensile specimens for the mortar and concrete respectively. The non-uniform strains which arose on opposite faces were not due to non-axiality in setting-up, but instead, were caused by slipping at the grips. As the specimens were coated in Super Febcure (see Section 16.4.1) which, at time of testing, was a hard packing material with low frictional restraint (21, 116), the surfaces in contact with the grips tended to slide along the interface. Even after scraping the Febcure off the surface with a knife edge, slipping still occurred occasionally as the curing compound, on initial application, permeated into the surface of the specimen.

Nevertheless, as the lateral and longitudinal gauges on either side of the specimen are located very near each other, it is reasonably accurate to accept the measurements as being the longitudinal and lateral strains at the same point. With this qualification, the ν values for each specimen are computed by averaging the ν values obtained from opposite sides of the specimen. The E values are similarly computed on the basis of the average longitudinal strains on the opposite faces of each specimen. With the concrete specimens, the relatively large

TABLE 17.1 ELASTICITY PROPERTIES OF UNIAXIAL SPECIMENS

		MODULUS OF ELASTICITY E (p.s.i.)		POISSON'S RATIO (ν)	
			AVERAGE		AVER.
MORTAR SPECIMENS					
Beam Test:	cast face	4.11×10^6	4.46×10^6	0.162	0.168
	bottom face	4.81×10^6		0.171	
Direct Tension:	Specimen 1	4.45×10^6	4.59×10^6	0.167	0.176
	Specimen 2	4.74×10^6		0.185	
Direct Compression:	Specimen 1	4.46×10^6	4.49×10^6	0.196	0.196
	Specimen 2	4.52×10^6		-	
CONCRETE SPECIMENS					
Beam Test:	cast face	6.27×10^6	6.31×10^6	0.129	0.135
	bottom face	6.36×10^6		0.140	
Direct Tension:	Specimen 1	4.76×10^6	4.73×10^6	0.114	0.141
	Specimen 2	4.70×10^6		0.169	
Direct Compression:	Specimen 1	5.27×10^6	5.14×10^6	0.158	0.158
	Specimen 2	5.00×10^6		-	

scatter in strain measurement was due to these measurements being recorded with the first data-logger, sensitive to 2 microstrain only.

The results of the direct compression specimens are shown in Figures 17.3 and 17.6.

The ν and E values, recorded in Table 17.1, show good agreement with the different mortar specimens. The observed differences in E between the two faces of the beamwas due to a segregation effect. That is, the stiffness increased towards the bottom of the specimen, as cast, because of the increased concentration of stiffer aggregate particles. (see Section 6.2) However, the average E in this test agrees very closely with the values obtained in the direct states of stress.

With the concrete specimens, on the other hand, there was larger scatter, particularly in the E values obtained. In comparison to the values obtained in the slab tests, where good agreement is obtained for E values under different states of stress, (see Table 17.2) it is apparent that the beam test (Table 17.1) resulted in excessively high values for E while the E value obtained for the direct tension test was low. It is difficult to account for such apparently large errors in E when considering the care employed in the preparation of the specimens and the method of test. However, as the data-logger was behaving somewhat erratically on the particular day which the beam was tested, this is the probable source of error. That this is so is further substantiated by the apparently large E value also obtained for the disc test which was tested on the same day (see Section 17.4). Similarly, the low E value for the direct tension test may possibly be due to some odd behaviour in the first data-logger used.

17.3 BIAXIAL TENSION-COMPRESSION (RHOMBUS SLAB TESTS)

17.3.1 Presentation of Results

For the biaxial tension-compression tests, six unreinforced and six reinforced rhombus slabs were tested. The results of the six unreinforced slabs are discussed in this section whereas the reinforced slabs will be discussed in the next chapter. The six slabs discussed here (Figures 17.7 to 17.12) consisted of three each of mortar and concrete with the ratio of diagonal lengths being 1:1, 1.58:1 and 2:1. As shown in Section 14.41 each of these ratios is equal to $\sqrt{m}$ where (-m) is the ratio of the principal bending moments.

The first slabs tested were the mortar specimens with ratios of diagonal lengths, 1:1 and 2:1 (see Figures 17.7 and 17.9). As the slab specimens were considerably thicker than the aluminum specimen (3" as compared to 0.75") used in the pilot investigation, it was necessary to obtain a complete indication of the strain pattern over the surface of the specimen in order to detect possible parasitic effects arising from the increase in thickness. It is observed in Figure 17.7 and 17.9 that the strains in either of the two principal directions on either surface are very consistent, even to within 1" of the edge. Thus, it is concluded that, for the specimen dimensions used in this investigation, the influence of thickness has a negligible effect on the stress pattern.

As with the mortar beam discussed in Section 17.2, segregation was seen to occur with the mortar slabs. For example, in Figure 17.9, the strain values indicate that the modulus of elasticity is larger at the bottom of the specimen, as cast, than at the top. With the concrete specimens, the segregation effect is only very slight.

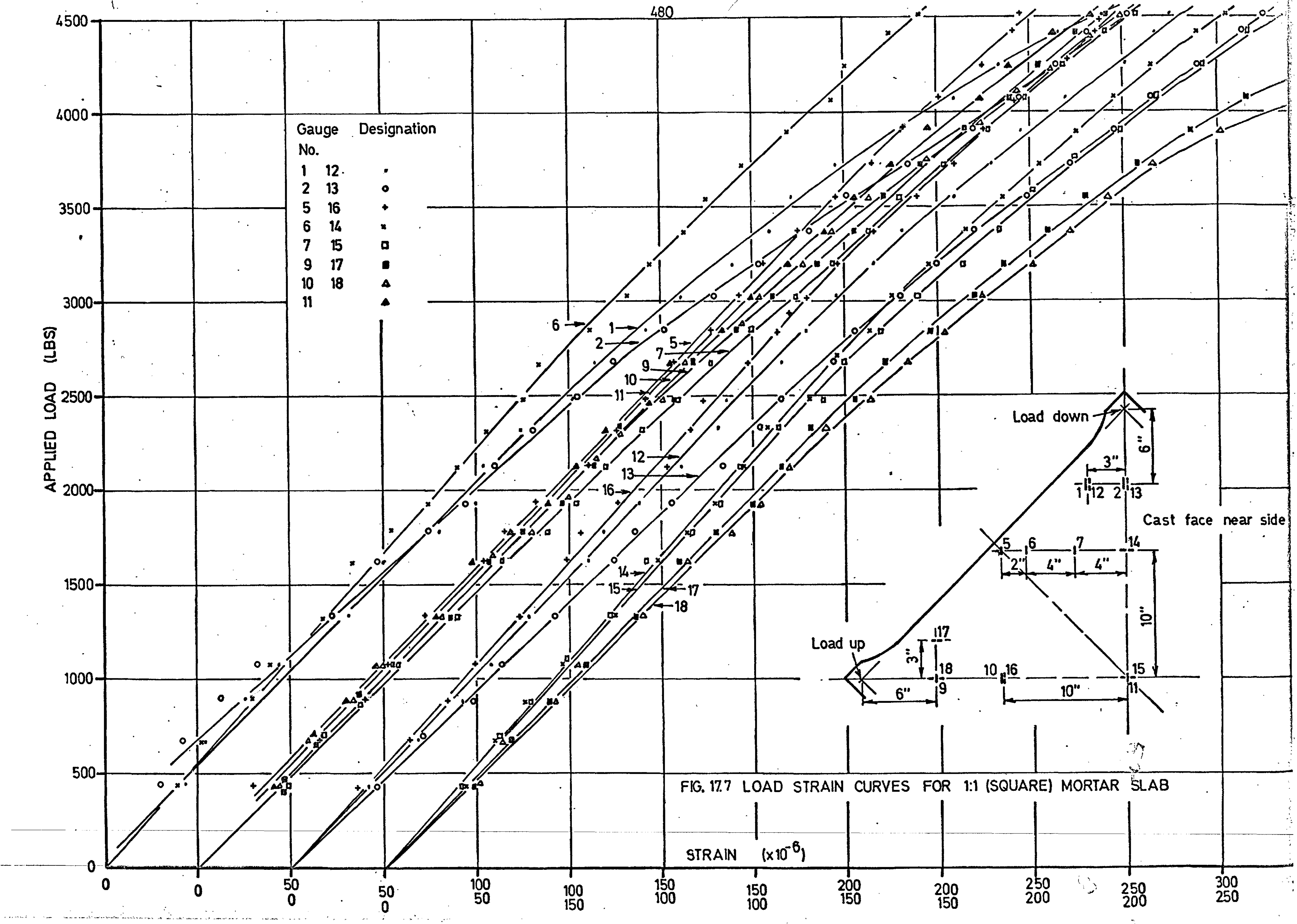

FIG. 17.7 LOAD STRAIN CURVES FOR 1:1 (SQUARE) MORTAR SLAB

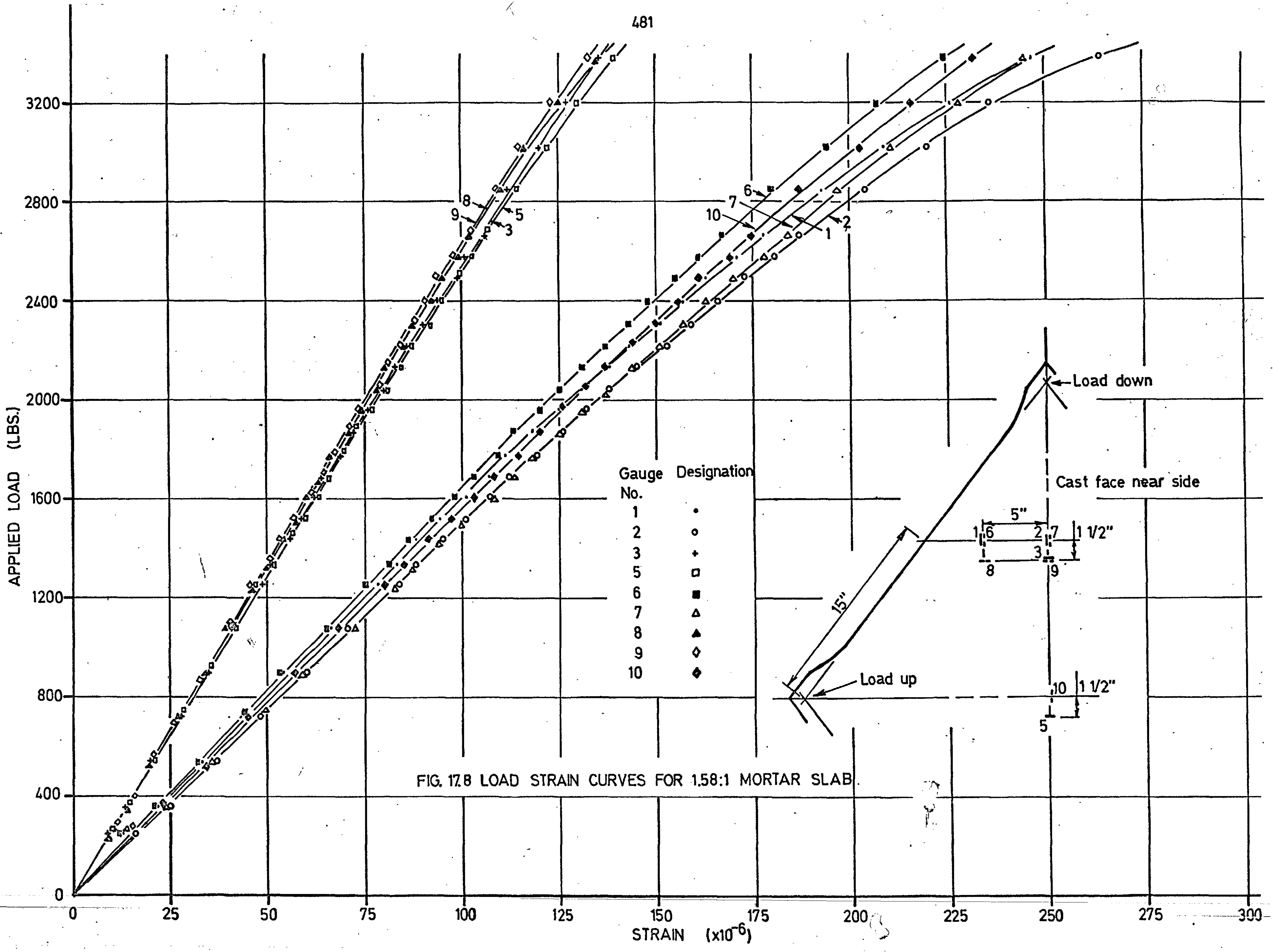

FIG. 17.8 LOAD STRAIN CURVES FOR 1.58:1 MORTAR SLAB.

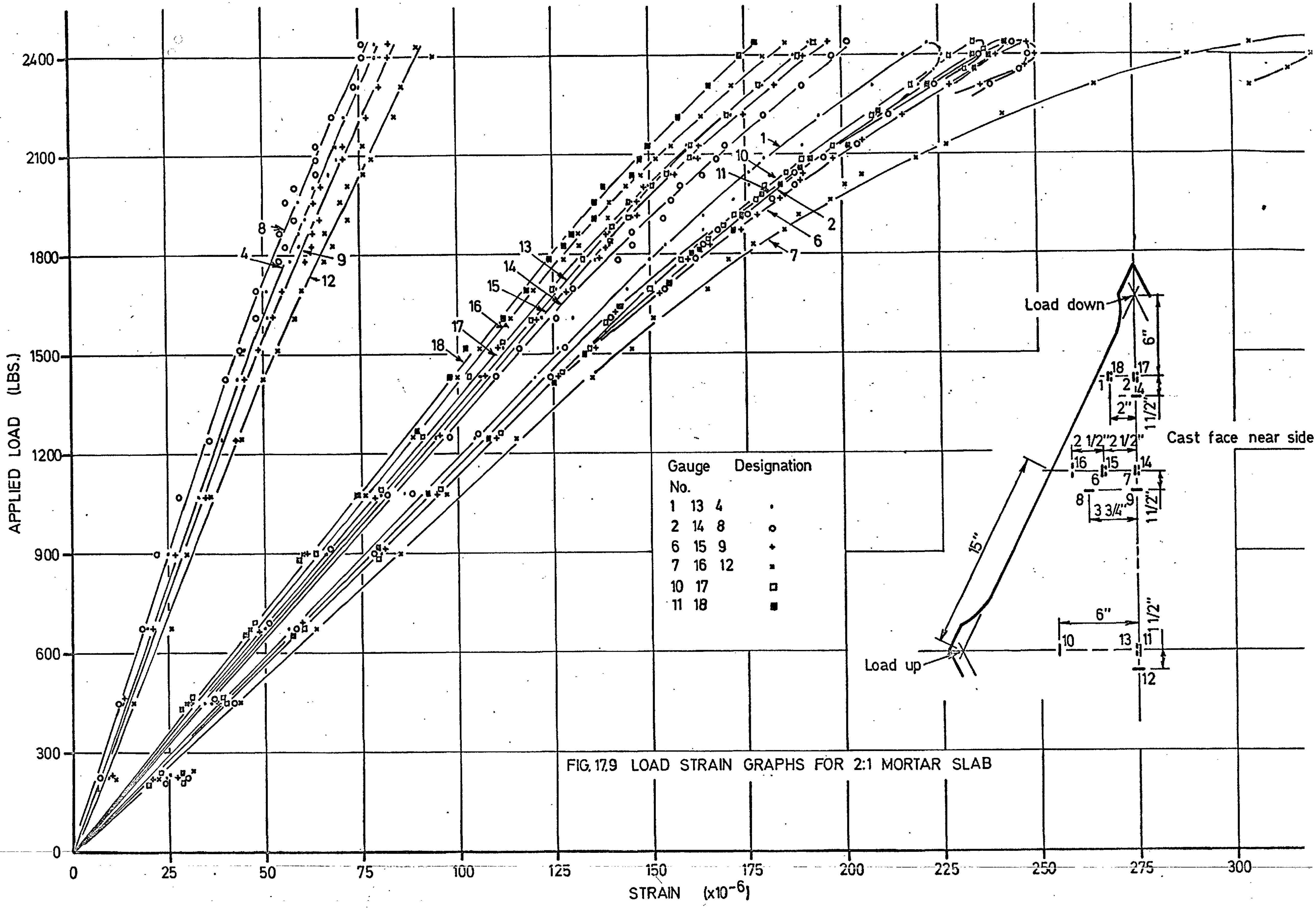

FIG. 17.9 LOAD STRAIN GRAPHS FOR 2:1 MORTAR SLAB

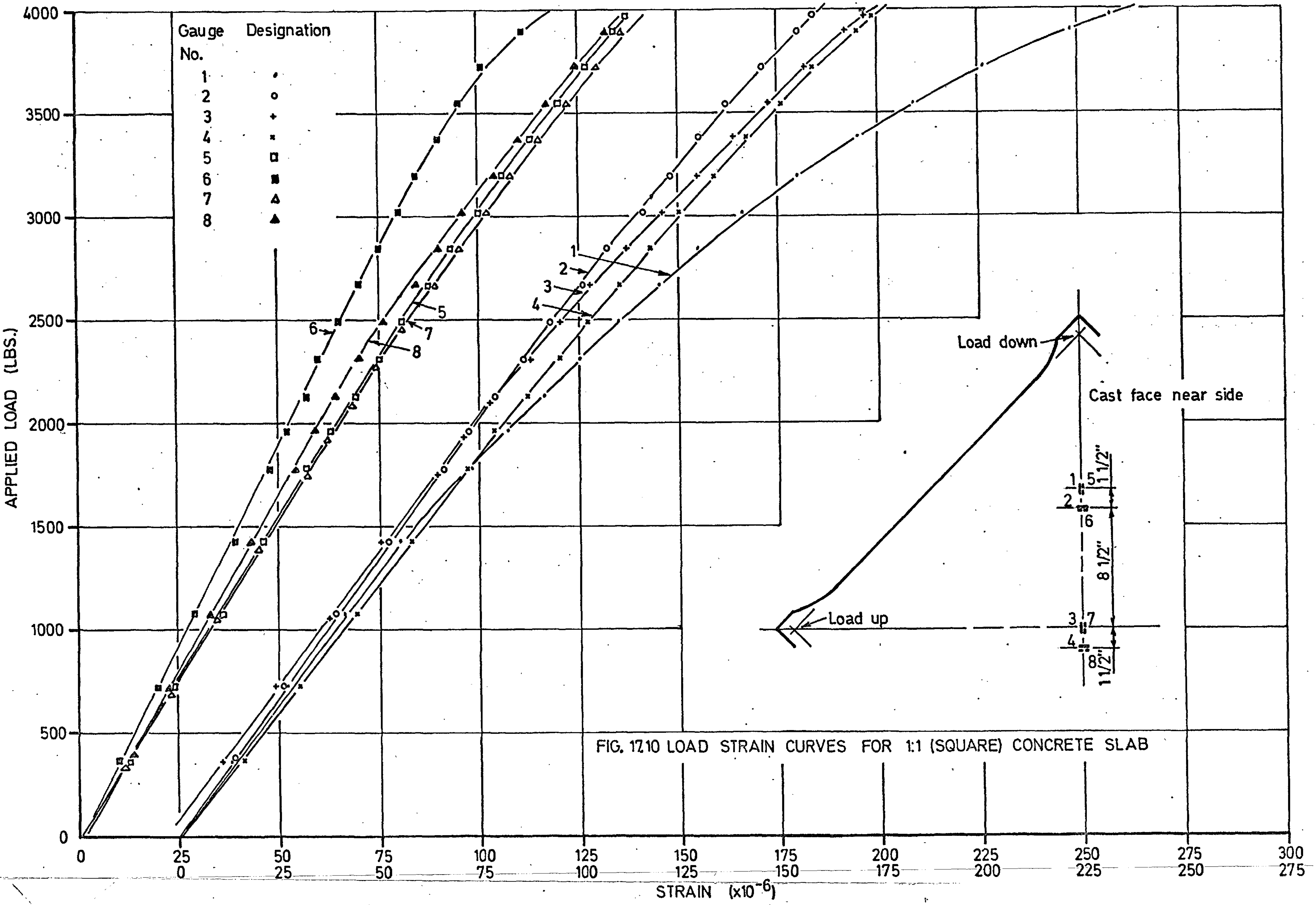

FIG. 17.10 LOAD STRAIN CURVES FOR 1:1 (SQUARE) CONCRETE SLAB

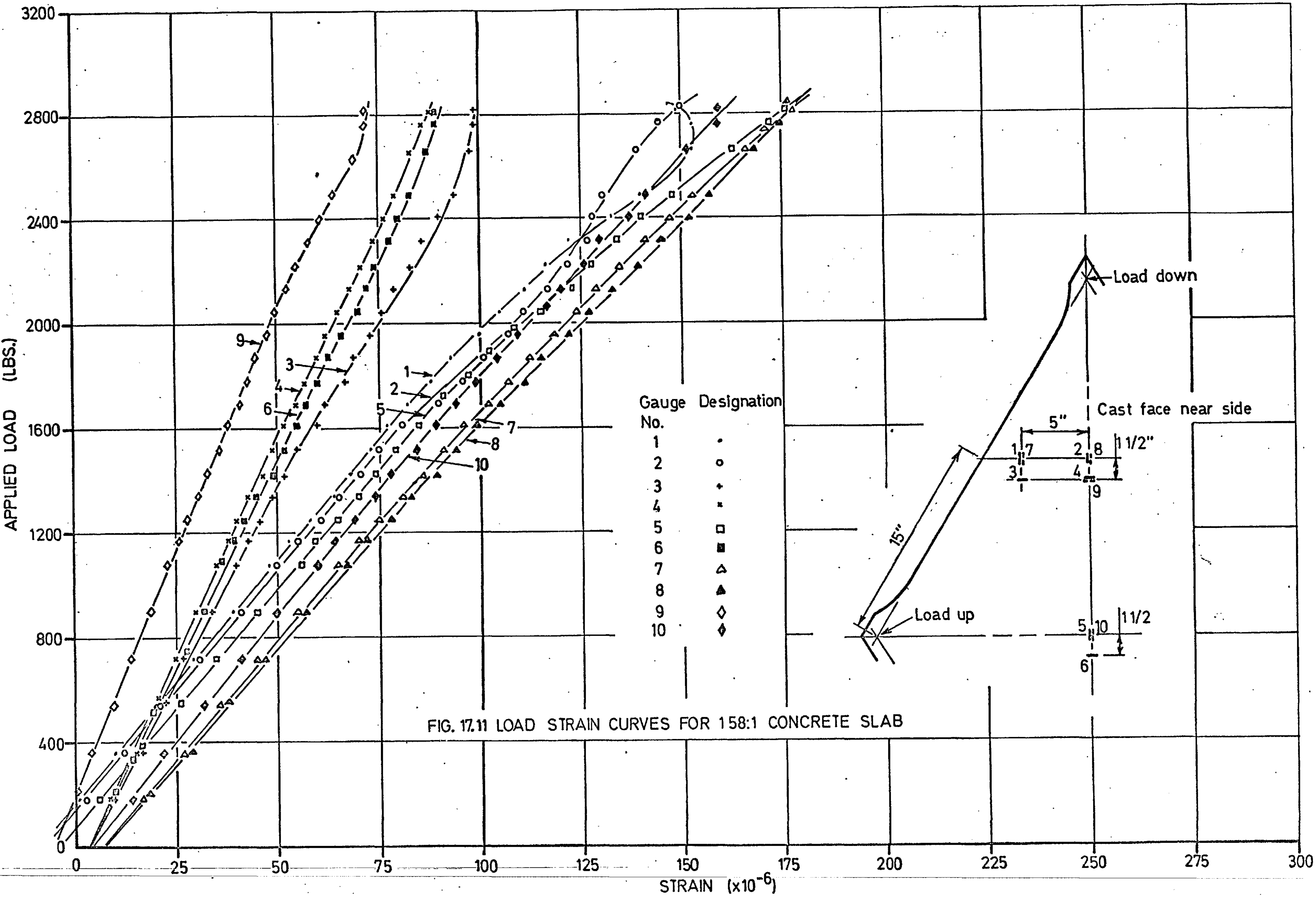

FIG. 17.11 LOAD STRAIN CURVES FOR 158:1 CONCRETE SLAB

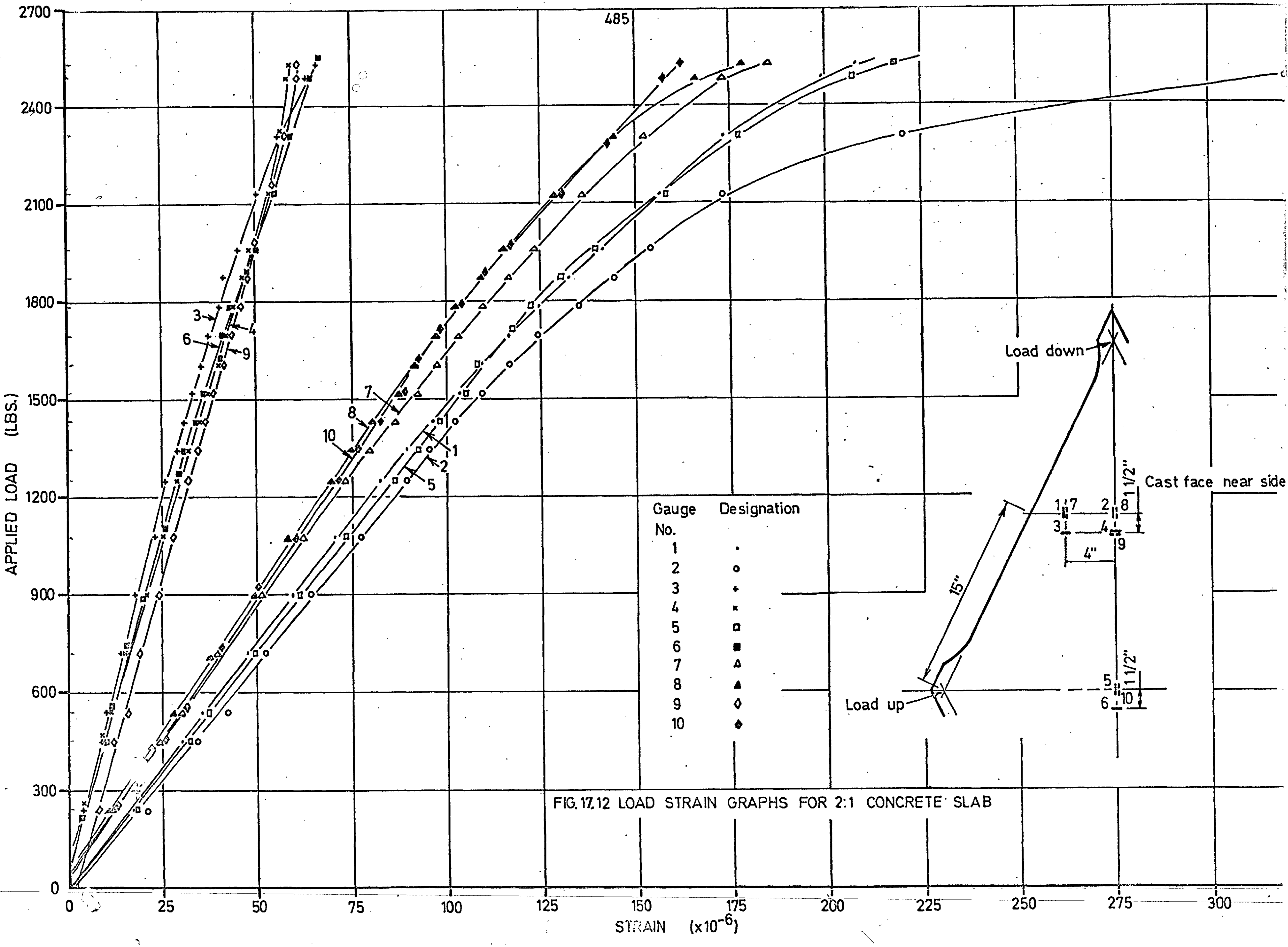

FIG. 17.12 LOAD STRAIN GRAPHS FOR 2:1 CONCRETE SLAB

The relative stiffness of the testing machine (see Section 12.2.2) led to a considerable portion of the descending part of the load deformation curve being examined on some occasions, before collapse of the slab occurred. For example, with testing the 2:1 mortar slab, a hinge or yield line which was developing resulted in strains away from this critical crack reducing with reduction in load (see Figure 17.9). However, the strain gauges measuring the large principal tensile stresses returned in a loop with the observed difference in strain at each load stage being caused by the combined creep and dilatation of the material.

Typical failed specimens are shown in Plate 17.1. It is observed that failures occurred perpendicularly to the longer diagonal, i.e., at the location of the larger principal moment with the failure being caused by the corresponding principal tensile stress. The failures, which occurred at a random section removed from the extended corners, were caused by a uniform moment, calculated directly from Equations 14.18 and 14.26.

17.3.2 Elasticity Properties

It has been shown in Section 14.4.2 that the elastic constants, E and ν for the slab tests are computed from the equations (see Equations 14.31 and 14.32)

$$E = \frac{3P \ (1 - m^2)}{2d^2 \sqrt{m} \ (\epsilon_{1y} + \epsilon_{1x})} \qquad \ldots \ 17.1$$

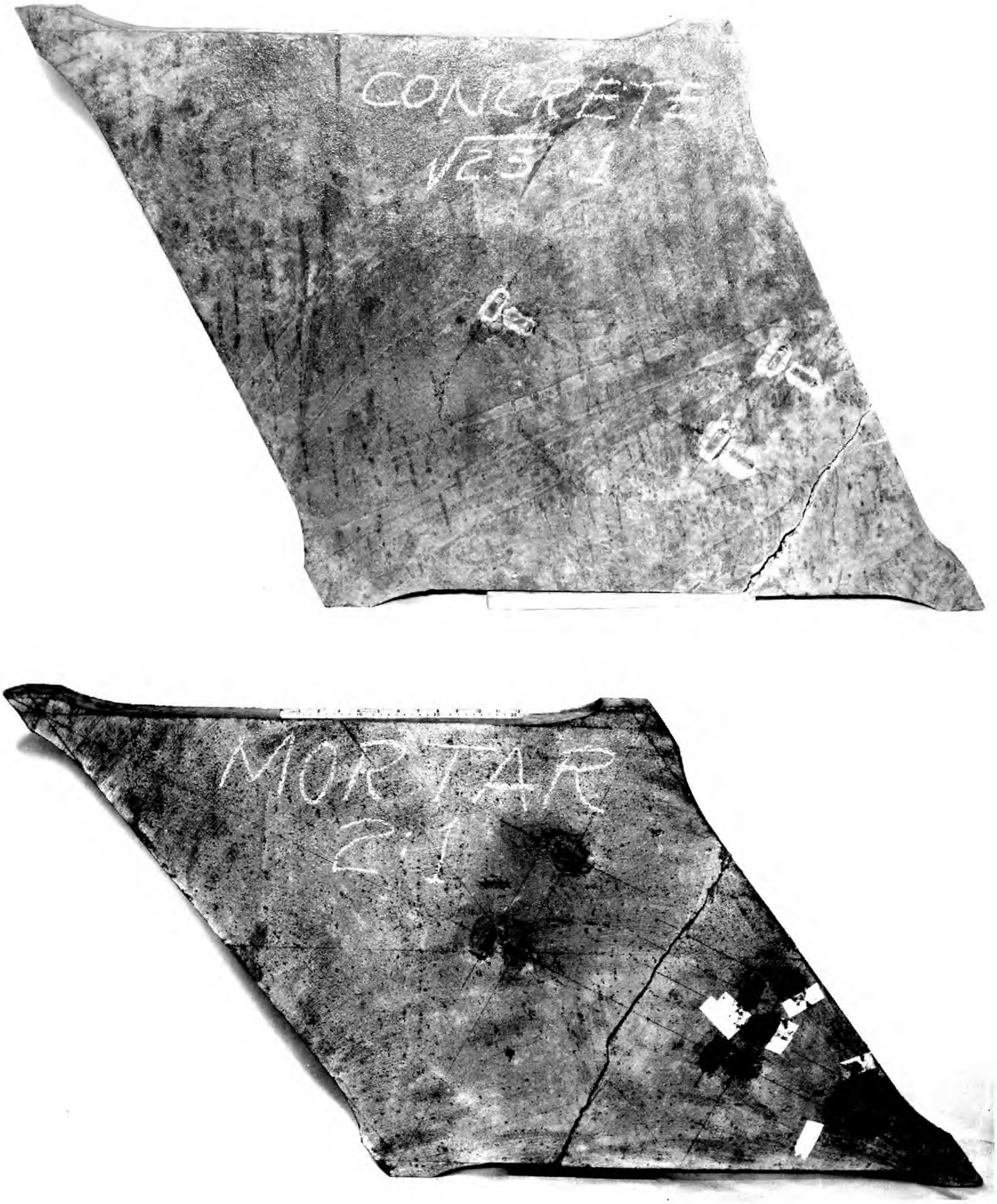

PLATE 17.1 Typical unreinforced slab specimens at failure

and $$\nu = \frac{-(\epsilon_{1x} + m\epsilon_{1y})}{(\epsilon_{1y} + m\epsilon_{1x})} \qquad \ldots\ 17.2$$

The values of E and ν have been computed from the average measured principal strains obtained from the top and bottom surface in the quasi-elastic range. (see discussion of Equations 14.31 and 14.32 in Section 14.4.2). These are presented in Table 17.2. With the square slabs, i.e.; $\epsilon_{1y} = -\epsilon_{1x}$ and m = 1, Equations 17.1 and 17.2 are both indeterminate. E is therefore calculated directly from Equation 14.17, i.e.;

$$E = \frac{3P}{2d^2\epsilon}(1 + \nu) \qquad \ldots\ 17.3$$

The value of ν used in Equation 17.3 is obtained from the average value in the uniaxial tests, Table 17.1.

From Table 17.2, it is observed that, whereas the E values remain reasonably constant, relatively large differences occur in the values of ν. These differences in ν are partially accounted for by the susceptibility of these values to small errors in measured strains. This is shown by the fact that the numerator in Equation 17.2 is generally a small difference of two large numbers. However, the large differences observed in the values of ν cannot be completely accounted for by this susceptibility. It is observed that the ν values increase as the applied compression increases. For example it is seen that for both the mortar and concrete, the ν values for the

TABLE 17.2 ELASTICITY VALUES FOR SLAB TESTS

SPECIMEN SHAPE	E (p.s.i.)	ν	
Mortar			
2:1	4.64×10^6	0.161	
1.58:1	4.55×10^6	0.263	
1:1	4.00×10^6	0.180	(assumed)
Concrete			
2:1	5.43×10^6	0.157	
1.58:1	5.30×10^6	0.217	
1:1	5.59×10^6	0.145	(assumed)

1.58:1 specimen is larger than for the 2:1 specimens. In the former case, the compression stress is 40% of the tension stress whereas in the latter case, this ratio is only 25%. The increased ν values obtained for these unreinforced slabs are also observed on the reinforced slabs (see Section 18.6).

The modulus of elasticity values in Table 17.2 show generally good agreement with the values in Table 17.1, except for the square mortar slab where the E value is somewhat low. It is thus concluded that the modulus of elasticity values for biaxial tension-compression states of stress over the range examined are in reasonable agreement with the values obtained in uniaxial tension and compression.

17.4 BIAXIAL TENSION - DISC TESTS

The results of the two disc tests are presented in Figures 17.13 and 17.14 with all data being given in Appendix B.

With the concrete specimen, Figure 17.14, it is interesting to observe the extensive cracking which occurred in the central section prior to collapse of the slab. At about 70% of ultimate load, the gauges on the tensile face behaved in random manner, depending on the location of the cracks. For example, gauge 2, adjacent to a crack showed a definite reduction in stress after about 85% of ultimate load due to the local stress relieving.

The extensive cracking in the central section is also observed in Plate 17.2. On the bottom face in the central section, the cracks developed in random directions under the influence of biaxial tension. With further loading, the cracks propagated radially as a result of the high transverse stresses (see Figure 15.3) until these cracks reached the periphery at which time, the specimen collapsed.

The mortar disc, (Figure 17.13) being considerably stronger than the concrete disc could not be loaded to failure due to the limitation of the rubber support ring. At roughly 14,000 lbs., the ring collapsed in a buckling mode. However, due to the deviation from the theory of Section 15.1, loads and strains beyond the discontinuity level are only of secondary interest. (see Section 11.3.1)

As with the square slab specimens, it is not possible in the analysis of the disc tests to obtain two equations for determining simultaneous values for E and ν. As a result, E was calculated by substituting average values of ν obtained

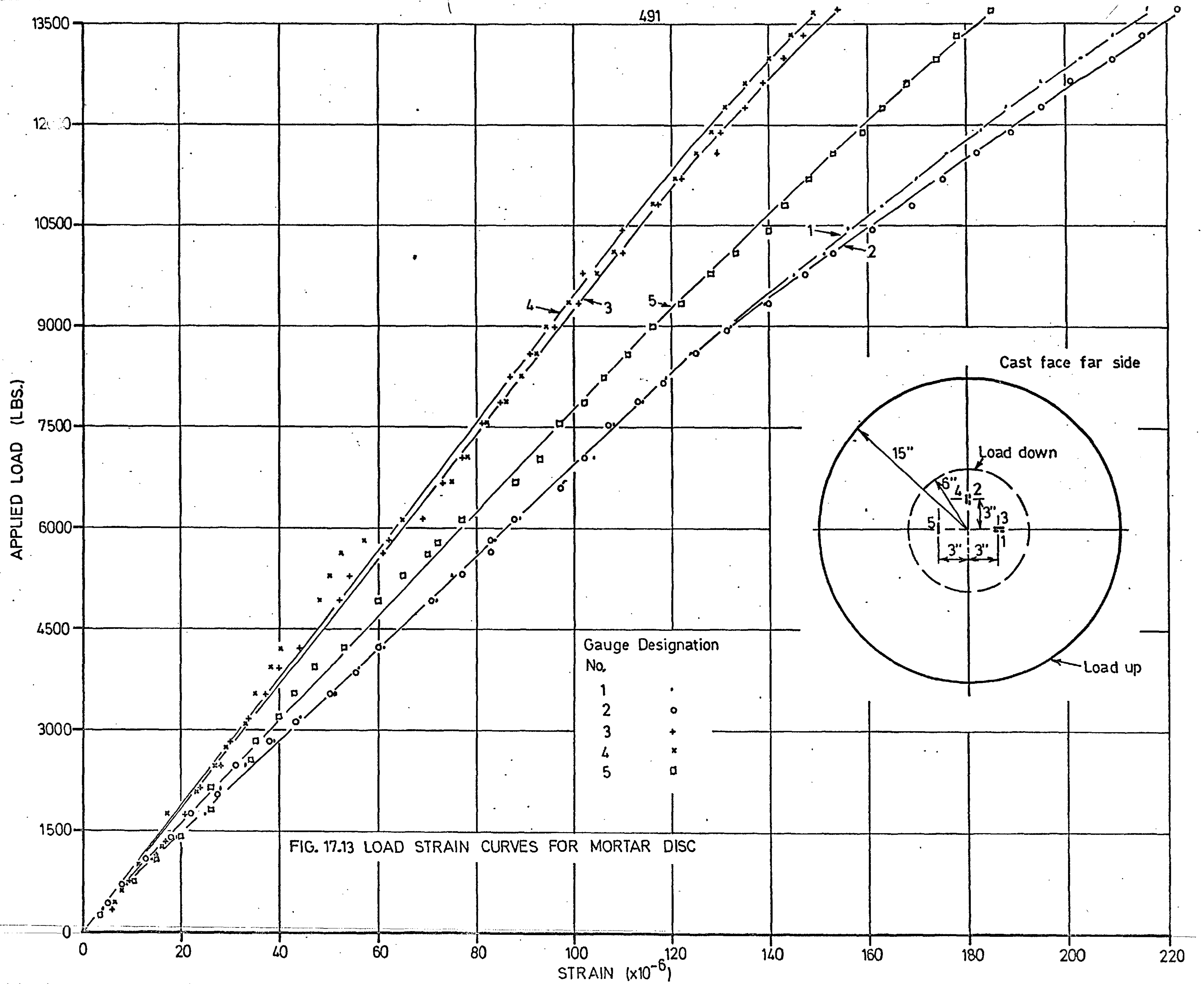

FIG. 17.13 LOAD STRAIN CURVES FOR MORTAR DISC

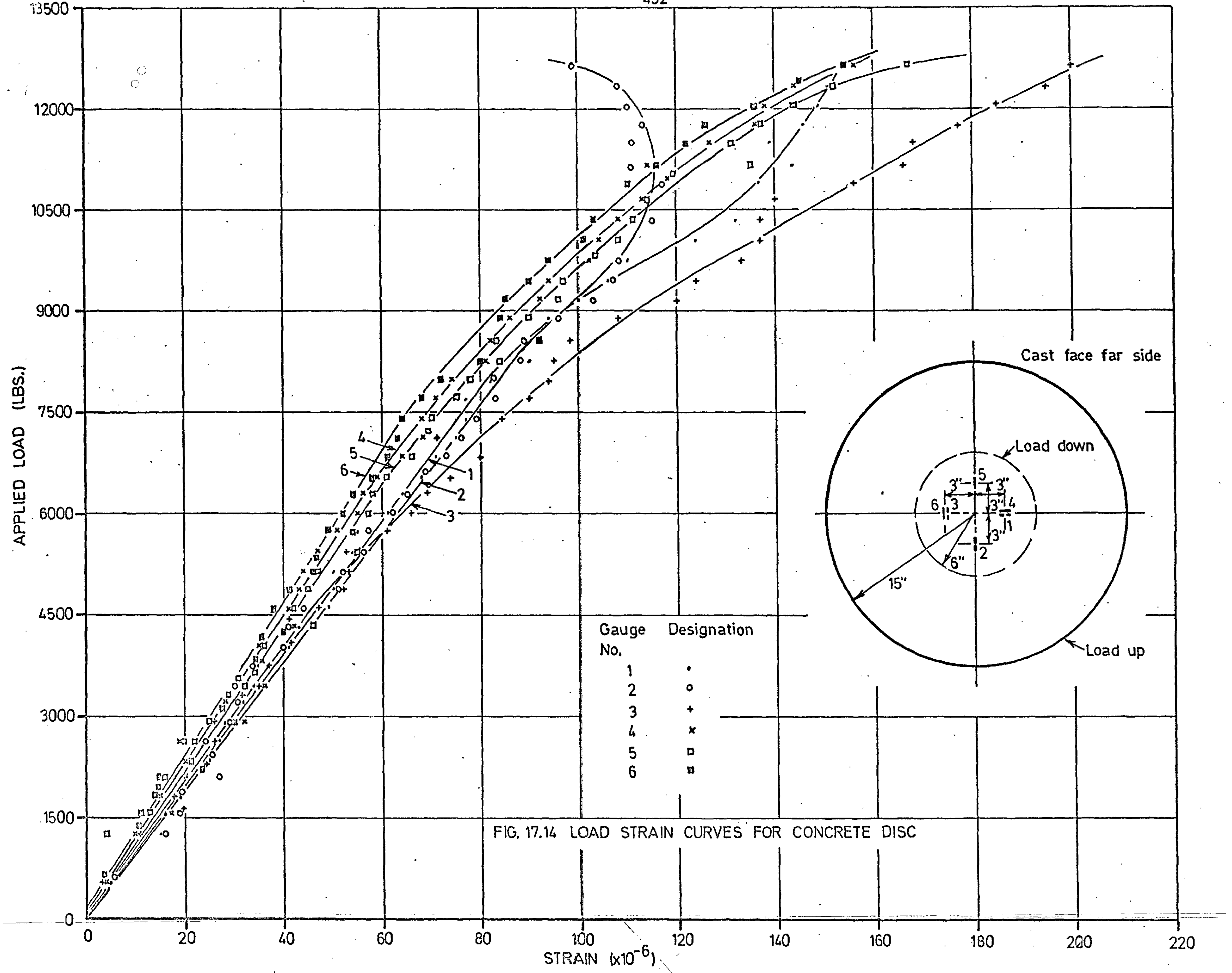

FIG. 17.14 LOAD STRAIN CURVES FOR CONCRETE DISC

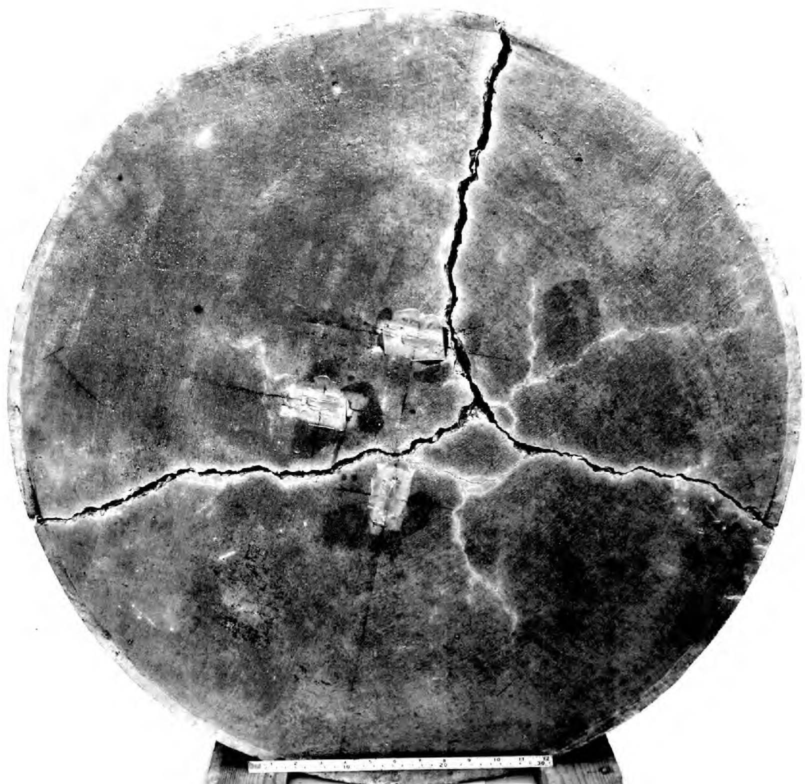

PLATE 17.2 Concrete disc at failure

from Table 17.1 into Equation 15.32. An average strain value obtained from the measured strains on both faces of the specimen prior to the discontinuity level and the corresponding load were also substituted into Equation 15.32. Although the E value for the mortar, 4.61×10^6 p.s.i. is in good agreement with the results given in Tables 17.1 and 17.2, the E value for the concrete 6.07×10^6 p.s.i. is high. However, as explained in Section 17.2, the large value for the concrete is believed to be due to the faulty behaviour of the data-logger.

17.5 DISCONTINUITY LEVEL STRESSES AND STRAINS AND ULTIMATE STRENGTHS

17.5.1 Flexural and Direct States of Stress

As has been shown in Section 11.5, there are two fundamental states of stress;

(1) direct states of stress

(2) flexural states of stress

In the former, the stress or strain will be constant throughout the critical volume whereas in the latter, the strain will vary linearly from a zero value at the neutral axis to maximum values at the extreme fibres. In the quasi-elastic range, formulas for stress in terms of strain, based on elastic analysis will be exact from a phenomenological view-point, although it is recognized that stress concentrations exist because of the general heterogeneous nature of concrete.

Therefore, with concrete or mortar subjected to either direct tensile stress or flexural stress, the discontinuity level would be expected to occur at the same stress and strain level

With specimens loaded above the discontinuity limit however, the material will exhibit non-linear stress-strain behaviour. Under direct states of stress, the formulas for average stress obtained by dividing the applied load by the cross-sectional area will still be correct whereas, for the flexural test, the stress at the outer fibre calculated from elastic analysis will be increasingly erroneous with continued application of load. As a result, the calculated failing stress in flexure, known as the modulus of rupture, is higher than the true tensile stress at the outer fibre. Ward[(2)] showed that the average uniaxial tensile strength was 74% and 81% of the average modulus of rupture for concrete and mortar, respectively.

In the slab tests, (flexural states of stress in two dimensions) the calculated failing stresses when based on elastic analysis would be expected to be higher than failing stresses obtained from tests under direct states of stress by a similar magnitude to those observed by Ward in his uniaxial tests. As the beam test can be considered to be a particular case of a biaxial flexural test, the failing strengths from the slab tests will be based on elastic analysis and the tensile strengths will be classified as the modulus of rupture values in biaxial tension-compression.

17.5.2 Discontinuity Level Stresses and Strains

From Figures 17.1 to 17.14, the strains at the discontinuity level have been obtained by observing the onset of definite non-linearity on those load-strain curves representing the larger principal tensile strains. The average of these strains for each specimen and the corresponding stress using the modulus of elasticity values from Table 17.1 or 17.2 are presented in Table 17.3.

It is observed that the principal tensile strain at the discontinuity level is virtually constant for the mortar, over the range examined whereas, for the concrete, this strain decreases from a state of biaxial tension-compression to the biaxial tension state (see Table 17.3). On examining the corresponding stresses, it is seen that for the concrete, the principal tensile stresses at discontinuity are reasonably constant whereas, for the mortar, the stresses tend to increase from the biaxial tension-compression stress state to the biaxial tension state.

The discontinuity levels for the direct tension and compression specimens have also been included, except for the mortar tension specimens where the problem with slipping at the grips was encountered (see Section 17.2.). It is observed that the discontinuity level for concrete and mortar in direct compression occurs at a considerably larger principal extensional strain than in Tension. Although the internal distribution of forces would be expected to remain the same in

TABLE 17.3 DISCONTINUITY LEVEL STRESSES AND STRAINS AND MODULUS OF RUPTURE VALUES

SPECIMEN SHAPE	THICKNESS d (in.)	DISCONTINUITY LEVEL Principal Tension Strain ($x10^{-6}$)	Stress (p.s.i.) Tension	Stress (p.s.i.) Comp.	FAILING STRESSES Failing Load (lbs.) (including specimen weight)	Stress (p.s.i.) Ten.	Stress (p.s.i.) Com
Mortar							
SLAB (1:1)	3.07"	122	414	414	4560	728	728
SLAB (1.58:1)	3.00"	126	519	208	3467	915	366
SLAB (2:1)	3.07"	130	578	145	2447	792	198
BEAM (4"x3"x40")	3.02"	123	576	0	1178	897	0
DISC	3.02"	119	670	-670	-	-	-
DIRECT TENSION	-	-	-	-	-	623	0
DIRECT COMPRESSION	-	205	0	4700	-	0	7840
Concrete							
SLAB (1:1)	3.01"	-	-	-	3993	662	662
SLAB (1.58:1)	3.01"	85	415	166	2810	738	294
SLAB (2:1)	3.04"	82	366	92	2504	836	209
BEAM (4"x3"x40")	2.98"	75	499	0	911	729	0
DISC	3.10"	70	497	-497	12,680	-	-
DIRECT TENSION	-	66	312	0	-	483	0
DIRECT COMPRESSION	-	125	0	4060	-	0	7610

the compression and tension states of stress, the mechanism of fracture for concrete will probably be different. This will be examined in Chapter 19, by considering the results of Chapter 18 in conjunction with the results of this section.

17.5.3 Failure Strengths

The modulus of rupture values for the flexural tests and the failing stresses for the direct tension and compression tests are given in Table 17.3.

The general trends observed for the stresses of the discontinuity level are repeated with the moduli of rupture values with the former being about 63% and 56% of the latter for the mortar and concrete, respectively.

Although the concrete and mortar have very similar compressive strengths, the direct tensile strength of the mortar is 28% greater than that of the concrete. This agrees generally with results obtained by Jones and Kaplan[117] and Ward[2].

It is of particular interest to observe that both the discontinuity level stresses and the failing strengths showed no sudden drop from uniaxial tension to biaxial tension-compression. This supports the criticisms of McHenry and Karni's testing technique,[69] discussed previously in Section 11.3.2. The restraint effects in their biaxial tension-compression tests produced different states of stress to that assumed, as opposed to their uniaxial tensile test, where these restraint effects were eliminated.

17.6 INFLUECE OF MIX PROPORTIONS AND AGE OF TEST ON ULTIMATE STRENGTH

In comparing the uniaxial tensile and compressive strengths, Ward[2] concluded that all factors which cause the compressive strength to increase will also produce an increase in the tensile strength. As both compression and tension failures are usually caused by the limiting strdngth of the cement paste phase or the bond at the cement paste aggregate interface, it is reasonable to consider the strength of concrete in terms of the factors which affect these strengths.

It has been shown by Brunaour and Copeland (118) that the strength of the cement paste is determined by the extent and nature of the tobermorite gel. For example, an increase in W/C ratio produces less gel per unit volume with a corresponding decrease in the average strength of the gel. Also, the chemical reaction between the cement clinker and free water continues for many years, thereby producing more gel per unit volume with a corresponding increase in strength with age. Furthermore, it has been shown by Alexander (114,119) and Hsu et al (95,120) that the aggregate-cement paste bond strength increases as the strength of the cement paste increases.

It was observed from examination of the failed specimens that, in general, concrete and mortars in biaxial tension and tension-compression fail along the cement paste-aggregate interface and through the cement paste phase. As these failures are of the same general type as those which occur in uniaxial tension and compression, it would be expected that those factors which increase the strength in uniaxial states of stress would also increase the failing strengths in biaxial states of stress.

To experimentally verify the influence of age, two mortar slabs with ratio of diagonal lengths, 2:1 were tested to failure, the first at 7 days age and the second at 28 day age. (see mixes M1 and M2 in Table 16.1). For the two specimens, the moduli of rupture values were, respectively, 661 and 807 p.s.i., i.e.; the former being 82% of the latter. This agrees generally with ratios obtained by Ward (2) in uniaxial tension tests on mortars at the same ages.

For examining the influence of mix proportions, the failing strengths of mix C1 (Table 16.1) can be compared with those of mix C4. It was observed that mix C1 with the higher A/C ratio resulted in lower uniaxial tensile and compressive strengths than Mix C4 (see Table 16.2). The modulus of rupture values for the square slab similarly reduced from 661 to 610 p.s.i.

It is concluded from the above investigation that all factors which lead to an increase in uniaxial tensile or compressive strength will likewise result in an increase in biaxial tension and tension-compression strengths.

17.7 SUMMARY

The results of the disc and slab tests have been analysed in order to assess fundamental elasticity and strength properties for mortar and concrete subjected to biaxial tension and tension-compression. These have been compared with results obtained in uniaxial states of stress.

In uniaxial tension and compression, it has been shown that both the modulus of elasticity and Poisson's ratio are reasonably unaltered in the different states of stress. In particular, it has been verified that, for mortar, these values are identical for tension and compression in the quasi-elastic range. For biaxial states of stress, there is reasonable agreement in the values of the elastic constant, E whereas ν tends to be larger than in uniaxial states of stress.

The stresses and strains at the discontinuity level for the biaxial flexural tests, i.e.; the slabs, discs and beams, showed fairly constant values for the different states of stress, although the discontinuity level stresses were more constant than the strains. The failing strengths, referred to as biaxial modulus of rupture values showed nearly constant values for the different states of stress.

It was shown that the discontinuity level in uniaxial compression occurs at a significantly higher principal tensile strain than in uniaxial tension.

From comparing the influence of age of test and A/C ratio on the ultimate strength of slabs, it is concluded, in light of the results of other investigators, that all factors which influence the short term ultimate strengths in uniaxial states of stress will have a similar influence on the ultimate strengths in biaxial tension and tension-compression states of stress.

CHAPTER 18

REINFORCED RHOMBUS SLAB TESTS

18.1 INTRODUCTION

The loading of a parallelogram slab specimen at the corners will generally produce different ratios of principal tension to compression stress on opposite faces (see Section 14.4.2) with the ratio of these stresses on one face being the inverse of that on the other. However, as shown in Table 17.3, failure of such specimens made from concrete or mortar will propagate from the face having the larger tension stress, with the corresponding compression-tension ratio being equal to or less than unity.

As the compressive strength of concrete is of the order of ten times its tensile strength, only about 10% of the possible biaxial tension-compression strength combinations can be obtained with the unreinforced slabs. To produce failures with a compression to tension ratio greater than unity while simultaneously ensuring that the stress state is flexural (see Section 17.5.1), the author has developed what is hereafter referred to as the reinforced rhombus test.

Basically, the slab is reinforced in one direction on one face to resist the large principal tensile force arising from the larger principal moment, M_X. On the opposite face, the concrete will be in a state of biaxial compression-tension stress with the ratio of these stresses being greater than unity. By varying the amount of reinforcement and the specimen shape, it is possible to test specimens with different ratios of compression to tension stress while also ensuring that failure propagates from the unreinforced face.

18.2 THEORY OF THE REINFORCED RHOMBUS TEST

In Section 14.4.1, it was shown theoretically that the corner loading of a parallelogram slab induced pure bending moments, M_x and M_y, which were constant throughout the entire volume of the slab.

The experimental verification of the parallelogram plate theory was confined to a specimen composed of isotropic, homogeneous material. However, it is reasonable to suggest that, on specimens which are not necessarily homogeneous, but which have a uniform thickness and flexural stiffness in each principal direction, the transformation of forces along the sides of the slab will result in a pure twisting moment along all lines parallel to the slab sides. It follows from this that the principal bending moments will be (see Section 14.4.1)

$$M_x = \frac{P\sqrt{m}}{4} \qquad \ldots \; 18.1$$

$$M_y = \frac{-P}{4\sqrt{m}} \qquad \ldots \; 18.2$$

where P is the total applied force and the value m is equal to $-M_x/M_y$. For the case of a rhombus shaped specimen, it has been shown that the ratio of the diagonal lengths is equal to $\sqrt{m}$ (see Section 14.4.1).

By using an alternative analysis, the same theoretical results are obtained. As shown in Figure 18.1, the moment at any section perpendicular to the x - axis at a distance 'C' from the corner, will be equal to $\frac{P}{2} . C$. But it will be observed that $\frac{C}{x}$ is equal to the ratio of the diagonal lengths of the rhombus specimen, i.e.;

$$\frac{C}{x} = \sqrt{m} \qquad \ldots \; 18.3$$

The total moment on the cross-section is consequently equal to $\frac{P}{2}\sqrt{m}x$. As this moment is resisted by a width of 2x, then the average moment per unit width, M_x is

$$M_x = \frac{\frac{P}{2}\sqrt{m}x.}{2x} = \frac{P\sqrt{m}}{x} \qquad \ldots \; 18.4$$

It is observed that Equation 18.4 is identical to Equation 18.1 Similarly, by taking a section perpendicular to the y axis, M_y is shown to be equal to the value obtained in Equation 18.2.

In Section 18.5, it is shown that the moments, M_x and M_y, are essentially constant throughout the entire slab since the measured surface strains in either principal direction are constant.

It is recognised that for the general case, the concrete on the reinforced face will fail in tension due to the larger principal moment, M_x, before the concrete on the opposite face begins to fail. However, it is appreciated that in cases

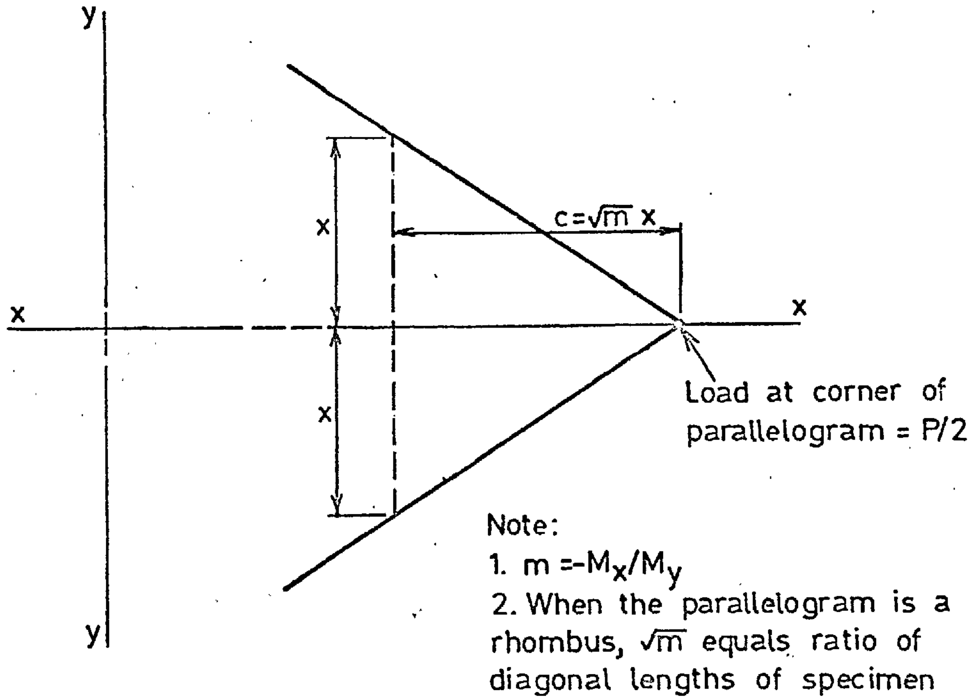

FIG. 18,1 CORNER OF PARALLELOGRAM SHAPED SPECIMEN

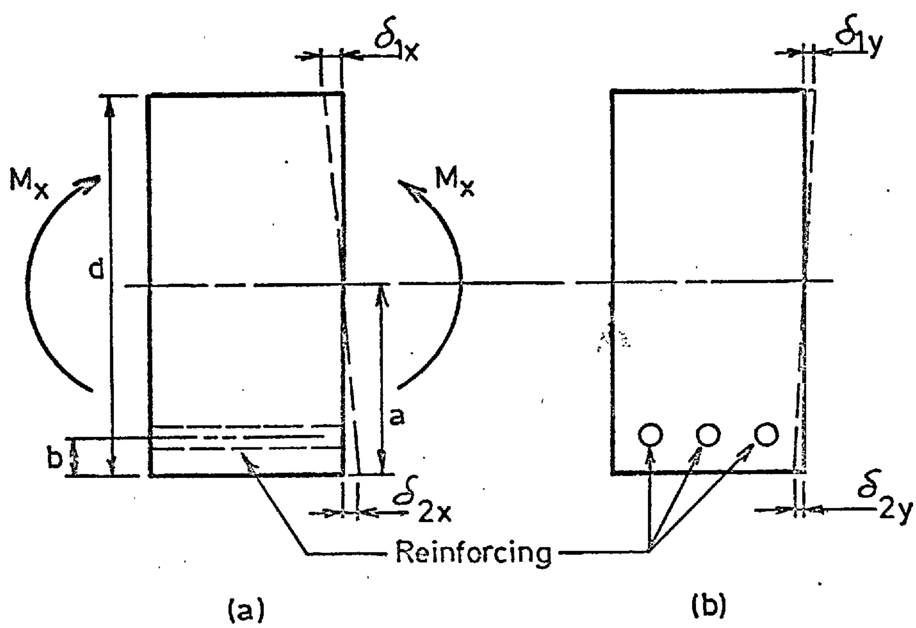

FIG. 18.2 INDUCED STRAINS IN THE PRINCIPAL DIRECTIONS DUE TO THE PRINCIPAL MOMENT, M_x

where the principal moments are very nearly of the same magnitude or where a large amount of reinforcing steel is used, then the concrete on the unreinforced face may be stressed past the discontinuity limit at an earlier load stage than the concrete on the reinforced face. Although it would be most desirable to allow the concrete on the unreinforced face to reach its discontinuity limit first, i.e.; where the compression to tension ratio is greater than unity, severe practical problems occur with regard to placing the reinforcement and allowing sufficient space between the bars for the largest aggregate particles to pass freely. Consequently, two load stages are assumed.

(i) Prior to the tensile failure of the concrete on the reinforced face, the tension force due to the larger principal moment, M_x is resisted by both the concrete and the steel.

(ii) After the concrete on the reinforced face has effectively failed in tension, then the tension force due to the moment, M_x, will be resisted by the tension steel only. These two cases will by analysed independently.

For the surface stresses and strains due to the combined influence of M_x and M_y, the method of super-position is used, i.e.; the stresses and strains are determined for each moment independently and subsequently added arithmetically when considering the moments M_x and M_y acting together.

18.2.1 Surface Stresses and Strains for Uncracked Concrete

In the analysis, the stresses and strains at the exposed faces will have the subscripts 1x, 2x, 1y and 2y where x and y denote the principle x and y directions and 1 and 2 refer to the upper and lower faces, respectively. The reinforcement will be in the x direction on the lower face.

18.2.1.1 Stresses and strains due to M_x

It is assumed that, under the action of pure moment, the strain is linear across the section. Also, within the Quasi-elastic range of the material, the stress will be proportional to the strain.

In order to determine the location of the neutral axis, it is necessary to determine the forces on either side of the neutral axis in terms of the neutral axis distance. By then equating these forces, the position of the neutral axis is obtained.

In Figure 18.2, the induced strains due to the moment per unit width, M_x, are shown on a prismatic section of depth d and unit width and breadth. With ε denoting strain, E representing modulus of elasticity and a being the distance from the bottom of the slab to the neutral axis, then;

Total force above neutral axis = $\varepsilon_{1x} E \frac{(d-a)}{2}$ ... 18.5

Below the neutral axis, the force taken by the concrete is equal to $\left[\varepsilon_{2x} E \frac{a}{2} - \varepsilon_{2x} \frac{(a-b)}{a} EA\right]$ where A is the cross-sectional area of the steel per unit width of section. Similarly, the force taken by the steel equals $\sigma_{2x}\left(\frac{a-b}{a}\right) E_{st} A$ where E_{st} represents the modulus of elasticity of the steel. By addition, it is seen that;

Total force below neutral axis

$$= \sigma_{1x} E \frac{a}{2} + \sigma_{2x}\left(\frac{a-b}{a}\right) A\,(E_{st} - E) \qquad \ldots\ 18.6$$

But, from Figure 18.2 (a),

$$\sigma_{1x} = -\left(\frac{d-a}{a}\right)\sigma_{2x} \qquad \ldots\ 18.7$$

By substituting Equation 18.7 into Equation 18.5, multiplying by -1 and then equating to Equation 18.6, the location of the neutral axis is obtained, i.e.;

$$a = \frac{\frac{d^2}{2} + (n-1)Ab}{d + (n-1)A} \qquad \ldots\ 18.8$$

$$\text{where } n = E_{st}/E \qquad \ldots\ 18.9$$

The moment, M_x, is then obtained by integrating over the depth, d, the product of the force on each elemental strip and its distance from the neutral axis. Therefore,

$$M_x = \sigma_{2x}\left[d\left(\frac{d^2}{3a} - d + a\right) + A\frac{(a-b)^2}{a}(n-1)\right] \qquad \ldots\ 18.10$$

Solving for σ_{2x}, then

$$\sigma_{2x} = M_x\left[\frac{a}{\frac{d}{3}(d^2 - 3ad + 3a^2) + A(a-b)^2(n-1)}\right] \qquad \ldots\ 18.11$$

and the corresponding strain is

$$\epsilon_{2x} = \frac{M_x}{E}\left[\frac{a}{\frac{d}{3}(d^2 - 3ad + 3a^2) + A(a-b)^2(n-1)}\right] \qquad \ldots\ 18.12$$

From Equations 18.7 and 18.12, the principal strain, δ_{1x}, on the upper face is

$$\delta_{1x} = -\frac{M_x}{E}\left[\frac{d-a}{\frac{d}{3}(d^2 - 3ad + 3a^2) + A(a-b)^2(n-1)}\right] \qquad \ldots\ 18.13$$

and the corresponding stress is

$$\sigma_{1x} = -M_x\left[\frac{d-a}{\frac{d}{3}(d^2 - 3ad + 3a^2) + A(a-b)^2(n-1)}\right] \qquad \ldots\ 18.14$$

Due to the Poisson's ratio effect (see Figure 18.2(b))

$$\delta_{1y} = -\nu\delta_{1x} \qquad \ldots\ 18.15$$

Therefore, from Equations 18.13 and 18.15

$$\delta_{1y} = +\frac{M_x}{E}\nu\left[\frac{d-a}{\frac{d}{3}(d^2 - 3da + 3a^2) + A(a-b)^2(n-1)}\right] \qquad \ldots\ 18.16$$

Similarly,

$$\delta_{2y} = -\frac{M_x}{E}\nu\left[\frac{a}{\frac{d}{3}(d^2 - 3ad + 3a^2) + A(a-b)^2(n-1)}\right] \qquad \ldots\ 18.17$$

18.2.1.2 Stresses and strains due to M_y

Due to the moment, M_y, the surface stress is computed directly from the moment-surface stress relationship shown in Equations 14.10 and 14.11, i.e.;

$$\sigma_{1y} = -\frac{6M_y}{d^2} \qquad \ldots\ 18.18$$

and

$$\sigma_{2y} = \frac{6M_y}{d^2} \qquad \ldots\ 18.19$$

The corresponding strains are

$$\delta_{1y} = -\frac{6M_y}{d^2 E} \qquad \ldots\ 18.20$$

and $$\delta_{2y} = \frac{6M_y}{d^2 E} \qquad \ldots\ 18.21$$

The steel is expected to have a negligible effect on the general stress pattern across the section due to the moment, M_y. However, the natural expansion of the steel in the x-direction due to the Poisson's ratio effect would be only a fraction of that of the concrete as the steel is a stiffer material. For example, the natural expansion of the concrete, represented by the strains δ^1_{1x} and δ^1_{2x} (see Figures 18.3 and 18.4) would be (from Equations 18.20 and 18.21)

$$\delta^1_{1x} = \frac{6\nu M_y}{d^2 E} \qquad \ldots\ 18.22$$

and $$\delta^1_{2x} = \frac{-6\nu M_y}{d^2 E} \qquad \ldots\ 18.23$$

At the level of the steel, the natural expansion of the concrete would be

$$\delta = \delta^1_{2x} \left(\frac{\frac{d}{2} - b}{d/2}\right) \qquad \ldots\ 18.24$$

If the steel had the same ν/E value as the concrete, then the natural expansion of the steel would be equal to that given in Equation 18.24. However, as the steel is stiffer, i.e.; higher E value, than the concrete, then the amount of natural expansion in the steel will be less than that given by Equation

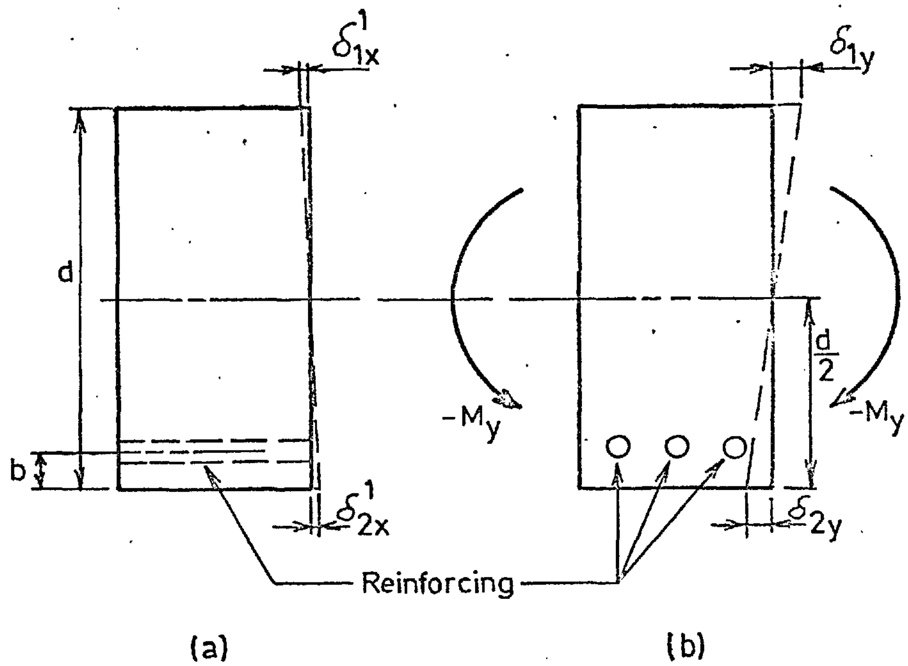

Note: See Fig. 18.4 for the actual strains in the x-direction

FIG 18.3 NATURAL STRAINS IN THE PRINCIPAL DIRECTIONS DUE TO THE MOMENT, $-M_y$

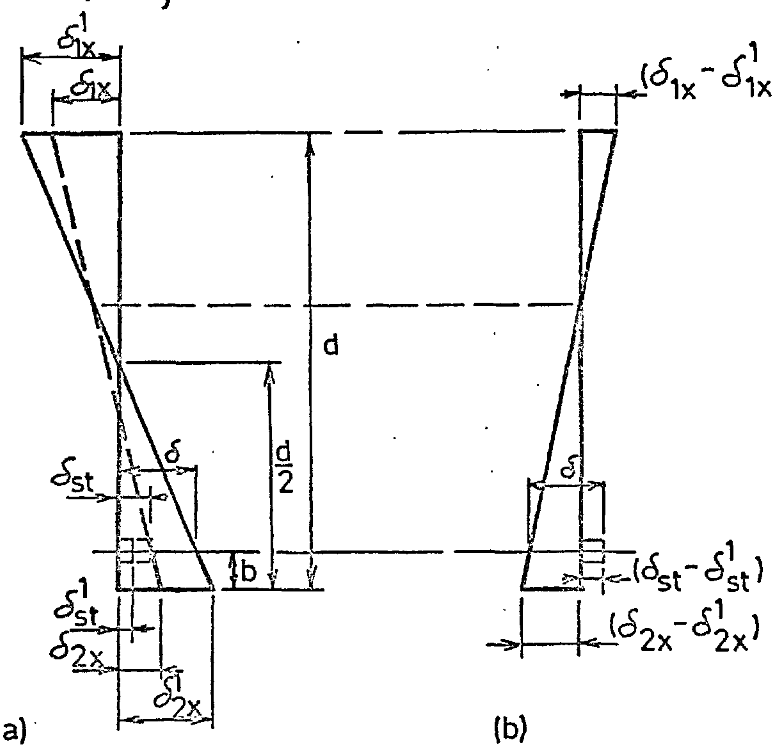

FIG. 18.4 ACTUAL STRAINS IN THE X - DIRECTION DUE TO THE MOMENT, $-M_y$

18.24. As the ν values for steel and concrete are of a similar order, then the ratio of the actual natural expansion of the steel to that given in Equation 18.24 is approximately equal to 1/n (see Equation 18.9), i.e. (Figure 18.4),

$$\delta_{st}^{1} = \delta_{2x}^{1} \frac{(\frac{d}{2} - b)}{d/2} \frac{1}{n} \qquad \dots\ 18.25$$

However from Equations 18.25 and Figure 18.4 it is seen that an incompatibility occurs between the natural expansion of the concrete (represented by the straight line between δ_{1x}^{1} and δ_{2x}^{1}) and the steel, δ_{st}^{1}. As the sections remain plane, stresses are created in the x-direction with a tensile force in the steel and an equal and opposite compression force in the concrete being produced. This is represented in Figure 18.4(a) by a dotted line where it is seen that the steel is stretched to produce a total extensional strain, δ_{st}, compatible with the strains in the concrete represented by δ_{1x} and δ_{2x}.

From Figure 18.4 (b);

$$\text{Force in steel} = (\delta_{st} - \delta_{st}^{1})\, A\, E_{st} \qquad \dots\ 18.26$$

and

$$\text{Force in concrete} = \frac{(\delta_{1x} - \delta_{1x}^{1}) + (\delta_{2x} - \delta_{2x}^{1})}{2} E\, d \qquad \dots\ 18.27$$

However, as the tension force in the steel is equal to the compressive force in the concrete, then by multiplying Equation 18.26 by (-1) and equating to Equation 18.27, we obtain

$$(\delta_{st} - \delta_{st}^{1})AE_{st} = -\frac{(\delta_{1x} - \delta_{1x}^{1}) + (\delta_{2x} - \delta_{2x}^{1})Ed}{2} \qquad \ldots\ 18.28$$

At the level of the steel the sum of the extension of the steel and the contraction of the concrete must be equal to theincompatibility in strain, $(\delta - \delta_{st}^{1})$, shown in Figure 18.4(a). Therefore, by subtracting Equation 18.25 from Equation 18.24, then

$$\delta - \delta_{st}^{1} = \frac{\delta_{2x}^{1}(d - 2b)}{d} \left(\frac{n-1}{n}\right) \qquad \ldots\ 18.29$$

The amount of contraction of the concrete at the level of the steel (see Figure 18.4(a)) is

$$\delta - \delta_{st} = \left[(\delta_{2x}^{1} - \delta_{2x}) - (\delta_{1x}^{1} - \delta_{1x})\right] \frac{b}{d} \qquad \ldots\ 18.30$$

Therefore, from Equations 18.29 and 18.30 and Figure 18.4, we obtain,

$$\delta_{2x}^{1}\left(\frac{d-2b}{d}\right)\left(\frac{n-1}{n}\right) = (\delta_{st} - \delta_{st}^{1}) + \left[(\delta_{2x}^{1} - \delta_{2x}) - (\delta_{1x}^{1} - \delta_{1x})\right]\frac{b}{d} \qquad \ldots\ 18.31$$

As the tensile and compressive forces of the steel and concrete, respectively, must not only be equal and opposite, but also, the effective resultants must be coincident, it is possible to take moments of the forces about any point and equate them. By taking moments about the bottom surface, then,

$$-A_{st}(\delta_{st} - \delta_{st}^{1})b = (\delta_{1x} - \delta_{1x}^{1})Ed\,\frac{d}{2} + \left[(\delta_{2x} - \delta_{2x}^{1}) - (\delta_{1x} - \delta_{1x}^{1})\right]\frac{Ed}{2}\cdot\frac{d}{3} \qquad \ldots\ 18.32$$

It is seen that Equations 18.22, 18.23, 18.25, 18.28, 18.31 and 18.32 produce six equations for the six terms, δ_{st}, δ_{st}^{1}, δ_{1x}, δ_{1x}^{1}, δ_{2x}, and δ_{2x}^{1}. By suitable substitution, it is thus possible to solve for the actual strain values, ϵ_{1x} and ϵ_{2x} corresponding to the applied moment, M_y.

By solving Equation 18.28 for $(\epsilon_{st} - \epsilon^{1}_{st})$ and substituting into Equation 18.32, then

$$(\epsilon_{2x} - \epsilon^{1}_{2x}) = (\epsilon_{1x} - \epsilon^{1}_{1x}) \left[\frac{3b-2d}{d-3b}\right] \qquad \ldots\ 18.33$$

By substituting Equations 18.22, 18.23, 18.25 and 18.33 into Equation 18.31, then

$$(\epsilon_{1x} - \epsilon^{1}_{1x}) = - \frac{12\nu M_y (d-2b)(d-3b)A(n-1)}{d^2 E \left[d^3 + 4nA(d^2 - 3bd + 3b^2)\right]} \qquad \ldots\ 18.34$$

By substituting Equation 18.33 into Equation 18.34

$$(\epsilon_{2x} - \epsilon^{1}_{2x}) = \frac{12\nu M_y (d-2b)(2d-3b)A(n-1)}{d^2 E \left[d^3 + 4nA(d^2 - 3bd + 3b^2)\right]} \qquad \ldots\ 18.35$$

The corresponding stresses, σ_{1x} and σ_{2x} are

$$\sigma_{1x} = - \frac{12\nu M_y (d-2b)(d-3b)A(n-1)}{d^2 \left[d^3 + 4nA(d^2 - 3bd + 3b^2)\right]} \qquad \ldots\ 18.36$$

$$\sigma_{2x} = \frac{12\nu M_y (d-2b)(2d-3b) A(n-1)}{d^2 E \left[d^3 + 4nA(d^2 - 3bd + 3b^2)\right]} \qquad \ldots\ 18.37$$

Due to the strains in the x-direction as shown by Equations 18.33 and 18.34, there will also be strains induced in the y-direction by the Poisson's ratio effect. Although these strains will tend to reduce the values given in Equations 18.20 and 18.21, the reductions are only of the order of 0.5% of the values given in Equations 18.20 and 18.21 and can therefore be neglected.

18.2.1.3 Surface strains due to M_x and M_y

As discussed in Section 18.1, the method of super-position, which is employed in plate theory, is used here to determine the surface strains due to the combined action of the principal moments, M_x and M_y. Thus, for determining the strain, ϵ_{1x}, the values given by Equations 18.13, 18.22 and 18.34 are simply added. By substituting Equations 18.1 and 18.2 so as to obtain the strain in terms of the applied load, P, then,

$$\epsilon_{1x} = -\frac{\sqrt{m}P}{4E}\left\{\frac{(d-a)}{\frac{d}{3}(d^2-3ad+3a^2)+(a-b)^2(n-1)A} + \frac{6\nu}{md^2} - \frac{12\nu}{md^2}\,\frac{(d-2b)(d-3b)A(n-1)}{\left[d^3 + 4nA(d^2-3bd+3b^2)\right]}\right\} \qquad \ldots\ 18.38$$

Similarly, from Equations 18.1, 18.2, 18.12, 18.23 and 18.35,

$$\epsilon_{2x} = \frac{\sqrt{m}P}{4E}\left\{\frac{a}{\frac{d}{3}(d^2-3ad+3a^2)+A(a-b)^2(n-1)} + \frac{6\nu}{md^2} - \frac{12\nu}{md^2}\,\frac{(d-2b)(2d-3b)A(n-1)}{\left[d^3+4nA(d^2-3bd+3b^2)\right]}\right\} \qquad \ldots\ 18.39$$

In the y-direction, the strains are (from Equations 18.1, 18.2, 18.16 and 18.20)

$$\epsilon_{1y} = \frac{\sqrt{m}P}{4E}\left\{\frac{\nu(d-a)}{\frac{d}{3}(d^2-3ad+3a^2)+A(a-b)^2(n-1)} + \frac{6}{md^2}\right\} \qquad \ldots\ 18.40$$

and from Equations 18.1, 18.2, 18.17 and 18.21

$$\epsilon_{2y} = -\frac{\sqrt{m}P}{4E}\left\{\frac{\nu a}{\frac{d}{3}(d^2-3ad+3a^2)+A(a-b)^2(n-1)} + \frac{6}{md^2}\right\} \qquad \ldots\ 18.41$$

<u>18.2.1.4 Modulus of elasticity and Poisson's ratio</u>

In the experiments conducted, the surface strains and the applied load were measured. (see Section 18.6) In order to determine the basic elasticity constants in terms of these measured results, it is necessary to solve Equations 18.38 to 18.41 for E and ν. As the strains on the top surface would be expected to be slightly different from those on the bottom surface due to the segregation effect of the concrete, it is necessary to solve for E and ν on the basis of the recorded strains on each surface. Thus, two values for both E and ν will be obtained with the subsripts 1 and 2 denoting top and bottom surface, respectively.

For ease of calculation, let

$$X = \frac{d-a}{\frac{d}{3}(d^2-3ad+3a^2)+(a-b)^2(n-1)A} \quad \ldots \; 18.42$$

and

$$Y = \frac{2(d-2b)(d-3b)A(n-1)}{\left[d^3+4nA(d^2-3bd+3b^2)\right]} \quad \ldots \; 18.43$$

Thus, Equations 18.38 and 18.40 become

$$\sigma_{1x} = -\frac{\sqrt{m}P}{4E}\left[X+\frac{6\nu}{md^2}(1-Y)\right] \quad \ldots \; 18.44$$

$$\sigma_{1y} = \frac{\sqrt{m}P}{4E}\left[\nu X+\frac{6}{md^2}\right] \quad \ldots \; 18.45$$

By solving Equations 18.44 and 18.45 for E_1 and ν_1, then

$$E_1 = \frac{P\sqrt{m}}{4}\,\frac{\left[\frac{36}{md^2}(1-Y)-X^2md^2\right]}{\left[6\sigma_{1y}(1-Y)+X\sigma_{1x}md^2\right]} \quad \ldots \; 18.46$$

$$\nu_1 = -\frac{\left[\delta_{1x}\frac{6}{md^2} + \delta_{1y}X\right]}{\left[\delta_{1y}\frac{6}{md^2}(1-Y) + \delta_{1x}X\right]} \qquad \ldots\ 18.47$$

Similarly, from Equations 18.39 and 18.41 we obtain the elasticity values on the bottom surface, i.e.,

$$E_2 = \frac{P\sqrt{m}}{4}\frac{\left[md^2 X^2\left(\frac{a}{d-a}\right)^2 - \frac{36}{md^2}\left(1-\frac{(2d-3b)}{(d-3b)}Y\right)\right]}{\left[\delta_{2x} md^2 X\frac{a}{d-a} + 6\delta_{2y}\left(1-\frac{(2d-3b)}{(d-3b)}Y\right)\right]} \qquad \ldots\ 18.48$$

$$\nu_2 = -\frac{\left[\delta_{2y}X\frac{a}{d-a} + \delta_{2x}\frac{6}{md^2}\right]}{\left[\delta_{2x}X\frac{a}{d-a} + \delta_{2y}\frac{6}{md^2}\left(1-\frac{(2d-3b)}{(d-3b)}Y\right)\right]} \qquad \ldots\ 18.49$$

It is observed that all the values of E and ν are dependent on the location of the neutral axis represented by the distance, a (see Equations 18.8, 18.42 and 18.43). However, as the distance, a, is dependent on the modulus of elasticity of the concrete (Equations 18.8 and 18.9), then the values of E and ν calculated from Equations 18.46 to 18.49, are based on an assumed E value for the concrete. Therefore, the true value of E and ν must be computed by a trial and error process. In the calculation for E and ν (see Section 18.6), the assumed value for E was an average value obtained from the results of the unreinforced slabs discussed in Chapter 17. Although small differences were obtained between the assumed E value and the computed E values obtained from Equations 18.46 and 18.48, further calculation by substituting the computed

E value into Equations 18.8 and 18.9 resulted in negligible changes in the calculated values of a. Consequently, one calculation only was required for the individual value of E and ν in Equations 18.46 to 18.49 for each specimen.

18.2.2 Surface Stresses and Strains After Tension Failure of Reinforced Face

After the concrete on the reinforcing face has begun to crack and fail, there is a general transition in the slopes of the load-strain curves for the individual strain gauges (see Figures 18.6 to 18.11). When the concrete on the reinforcing face has failed completely with all the tension force due to the moment, M_x, being resisted by the steel, the curves will again become linear as long as the steel, and the concrete on the unreinforced face are still in the elastic or quasi-elastic range.

It is recognised that the concrete on the reinforced face will not fail completely in tension as some of the material, particularly near the neutral axis, will be subjected only to a very small strain. However, as this material also has a very small moment arm, its contribution to the moment of resistance is assumed to be negligible.

A detailed theoretical analysis of the relationship between the principal surface strains and the applied load was conducted on the assumption that all the concrete on the tensile side of the neutral axis had failed. Although this is reasonable when considering the relationship between the applied moment and surface stresses, large errors can occur in the computed values of the strains due to Poisson's ratio effect. For example, as shown in Figure 18.5, there will be a natural contraction of the concrete on the upper surface, ϵ_{1x}, due to the moment, M_x, and a corresponding natural expansion in the y-direction, ϵ_{1y}. On the lower surface, however, the measured strain, ϵ_{2x} consists of series of fine cracks without any appreciable expansion in the material itself. As a result it might be assumed that there is no Poisson's ratio effect in the y-direction (see Figures 18.5 (b) and (c)). However, as this would imply a discontinuity at the neutral axis, stresses would be created in the y-direction so as to obtain a plane section. The effect of these stresses is to reduce the amount of expansion on the upper surface and to produce a compression on the lower surface. By conducting a theoretical analysis analogous to that used in Section 18.2.1.2, it can be shown that ϵ_{1y}^{1} equals $0.5\epsilon_{1y}$ when $a_1 = d/2$ and that ϵ_{1y}^{1} decreases as a_1 increases.

Alternatively, if it is assumed that the concrete shortens naturally in the y-direction as shown in Figure 18.5(d), the theoretical analysis shows that the actual strain ϵ_{1y}^{1} is of the order of $0.9\epsilon_{1y}$. As either of the above assumptions may be considered reasonable, it is obvious that large variations in the theoretical values of strain and the corresponding values of stress will occur. Consequently, a

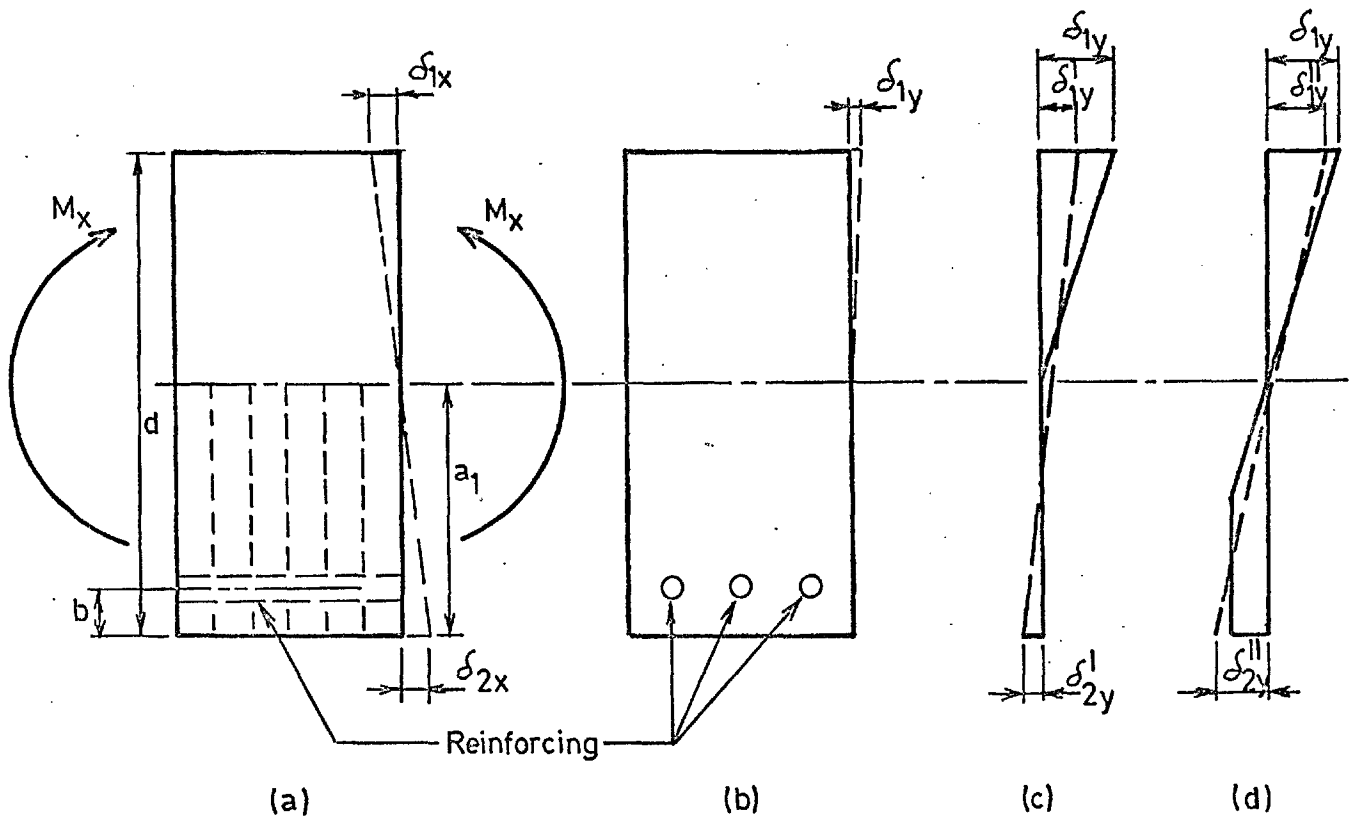

FIG. 18.5 INDUCED STRAINS IN THE PRINCIPAL DIRECTIONS DUE TO THE MOMENT, M_x AFTER TENSILE FAILURE OF THE CONCRETE ON THE REINFORCED FACE

detailed analysis analogous to that used in Section 18.2.1 is not justified.

For computing the principal stresses on the upper surface, two methods are employed. In the first method, described in the next section, approximate values are obtained from a brief elastic analysis. The second method, described in Section 18.2.2.2, is based on determining the stresses from the measured strains.

18.2.2.1 Elastic analysis

For determining the stress, σ_{1x}, it is necessary to obtain the location of the neutral axis represented by the distance, a_1 in Figure 18.5 (a). As the tension force in the steel and the compression force in the concrete are of equal magnitude and opposite sign, it is possible to obtain the values for these forces in terms of the distance, a_1. By then equating these forces, the value of a_1 can be obtained, i.e.;

$$\text{Compressive force in concrete} = \sigma_{1x} E(d-a_1) \tfrac{1}{2} \qquad \ldots\ 18.50$$

and

$$\text{Tensile force in steel} = -\sigma_{1x} \left(\frac{a_1-b}{d-a_1}\right) A\, E_{st} \qquad \ldots\ 18.51$$

By solving for a_1, we obtain

$$a_1 = (d+An) - An\sqrt{1 + \frac{2(d-b)}{An}} \qquad \ldots\ 18.52$$

As the moment, M_x, is equal to the product of the force in the concrete (or the steel) and the moment arem, then

$$M_x = (-\sigma_{1x}(d-a_1)\tfrac{1}{2})\left[(a_1-b)+\tfrac{2}{3}(d-a_1)\right] \quad \ldots\ 18.53$$

By solving Equation 18.53 for σ_{1x}, we obtain

$$\sigma_{1x} = -\frac{6M_x}{(d-a_1)(2d+a_1-3b)} \quad \ldots\ 18.54$$

The corresponding strain δ_{1x} will be

$$\delta_{1x} = -\frac{6M_x}{E(d-a_1)(2d+a_1-3b)} \quad \ldots\ 18.55$$

The corresponding strain in the y-direction, δ_{1y}, would be expected to be equal to $-\nu\delta_{1x}$. However, as shown in Figure 18.5, the actual strain in the y-direction will be somewhat less because of the incompatability of strain across the section. (Figure 18.5 (c) and (d)) with the actual strain being generally between $0.5\,\delta_{1y}$ and $0.9\,\delta_{1y}$. An approximation is made by assuming that the actual strain is $0.75\,\delta_{1y}$.

As δ_{1y} is the natural expansion of the material and $0.75\,\delta_{1y}$ is the actual assumed expansion, it is apparent that a compression stress, σ_{1y}, will be induced at the upper surface with the magnitude of this stress corresponding to the difference in the above strains, i.e;

$$\sigma_{1y} = (0.75\delta_{1y} - \delta_{1y})E \quad \ldots\ 18.56$$

As δ_{1y} is approximately equal to $-0.2\,\delta_{1x}$ ($\delta_{1y} = \nu\delta_{1x}$)

then from Equations 18.54, 18.55 and 18.56,

$$\sigma_{1y} = 0.05\ \sigma_{1x} \quad \ldots\ 18.57$$

Due to the moment, M_y, the stress σ_{1y} can be computed from Equation 18.18. Although there will be stresses induced in the x-direction due to the incompatibility of the natural lateral strains of the concrete and steel, these will be relatively small and are therefore neglected.

Thus, from Equations 18.1, 18.2, 18.18, 18.54 and 18.57

$$\sigma_{1x} = -\frac{3}{2}\,\frac{P\sqrt{m}}{(d-a_1)(2d+a_1-3b)} \quad \ldots\ 18.58$$

and
$$\sigma_{1y} = \frac{3}{2}\,P\sqrt{m}\left(\frac{1}{md^2} - \frac{0.05}{(d-a_1)(2d+a_1-3b)}\right) \quad \ldots\ 18.59$$

<u>18.2.2.2 Stresses from observed strain values</u>

It has been shown that, for any element subjected to biaxial stress conditions that (see Timoshenko and Woinowsky Kreiger(67) p. 5),

$$\delta_{1x}E = \sigma_{1x} - \nu\sigma_{1y} \quad \ldots\ 18.60$$

$$\delta_{1y}E = \sigma_{1y} - \nu\sigma_{1x} \quad \ldots\ 18.61$$

As the strains, δ_{1x} and δ_{1y} are measured and the E and ν values can be obtained from the computed elasticity values prior to cracking (Equations 18.46 to 18.49), it is seen that Equations 18.60 and 18.61 provide two equations for the two unknowns, σ_{1x} and σ_{1y}. By solving them simultaneously, we obtain,

$$\sigma_{1x} = \frac{E(\delta_{1x} + \delta_{1y})}{(1-\nu^2)} \quad \ldots\ 18.62$$

$$\sigma_{1y} = \frac{E(\delta_{1y} + \delta_{1x})}{(1-\nu^2)} \quad \ldots\ 18.63$$

For the unreinforced rhombus slabs, the ratio of the principal moments as well as the principal stresses was shown to be equal to the square of the ratio of the diagonal lengths (see Sections 14.4.1 and 14.4.2). For the reinforced rhombus slabs, this relationship will still apply for the ratio of the principal moments although this will not generally be the case for the principal stresses. This is due to the neutral axes in the two principal directions being at different locations for the latter case. This will be true both beofore and after the tensile failure of the concrete on the reinforced face.

18.3 REINFORCEMENT

18.3.1 Design of Reinforcement

In the design of suitable reinforcement in the slabs it was necessary that the reinforcement should satisfy certain requirements. These were; (1) There must be sufficient steel to allow the upper surface of the concrete to fail in biaxial tension-compression before the steel reaches its yield strength. (2) The distance between the individual bars should be small in relation to the distance to the neutral axis. (3) The space between the bars must be adequate to allow the largest aggregate particles to pass freely, i.e. there must be no tendency for the aggregate particles to settle on top of the reinforcement during casting.

For practical reasons, it was also necessary that the mortar and concrete specimens be reinforced in an identical manner (see Section 18.3.2).

To satisfy all these requirements, a compromise was required. After investigating several possibilities, the final selection was as shown in Table 18.1.

TABLE 18.1 REINFORCING DETAILS OF SLAB SPECIMENS

Diagonal Length Ratio	Reinforcing Details
2.5:1	$\frac{3}{8}$" Ø bars @ $\frac{7}{8}$" centres
2.0:1	$\frac{1}{4}$" Ø bars @ $\frac{5}{8}$" centres
1.58:1	$\frac{1}{4}$" Ø bars @ $\frac{7}{8}$" centres

18.3.2 Positioning of Reinforcement

It was imperative that the reinforcement be positioned accurately, not only with regard to conforming to the 'between centres' distance given in Table 18.1, but also with reference to the distance from the surface of the specimen. To satisfy these requirements, the following procedure was adopted for placing the reinforcement.

Prior to attaching the sides of the mould (see Plate 18.1), the base of the mould was marked with parallel lines, the distance between the lines being the 'between centres' distance of the reinforcing bars. These lines were also parallel to the longer diagonal of the rhombus specimen. After cutting the reinforcing bars to the correct length (see Plate 18.1), they were firmly secured in place by means of wires (see Plates 18.1, 18.3 and 18.5. Each wire passed over the top of the bar and along opposite sides of a spacer (a $\frac{1}{4}$" Ø reinforcing bar cut to a length of about $\frac{3}{4}$"). Each end of the wire was then passed through a small hole drilled in the base of the slab and over a second spacer bar on the bottom side of the base of the mould. By then twisting the two ends of the wire around each other, it was possible to anchor the reinforcing bar securely while simultaneously maintaining it at an accurate distance from the base of the mould. At least two supports were selected for each reinforcing bar. With bars more than about 24" in length, three and, in some cases, four supports were used.

As it was important that the steel bars should be a uniform distance above the base of the mould, straight bars only were selected.

On the basis of ten readings, with calipers graduated in 0.0001" divisions it was observed that the bar diameter was generally within 0.002" of the diameter given in Table 18.1. With such small variations in bar diameter, it was considered sufficiently accurate to perform all calculations on the basis of the diameters given in Table 18.1.

To prevent movement of the bars or damage to the anchor wires during casting, the concrete or mortar was placed in small quantities with short vibrations until the bars were completely immersed. By employing such care, no difficulty was experienced with any of the reinforcement becoming loose.

To remove a specimen from its mould, the specimen was overturned and all the wires were cut. The mould then was lifted off the specimen with the wires passing through the holes. Following this operation, the wires were again cut so that the ends would be flush with the surface of the concrete or mortar specimen.

18.4 EXPERIMENTAL DEVELOPMENT

It was found in the initial tests that the testing technique was unsuitable, the resulting failure being due to such factors as bond breakdown and diagonal tension. In this section, the problems which were encountered and the successive steps taken to prevent a repetition of these problems are discussed.

18.4.1 Initial Specimen

The initial specimen tested, a 2.5:1 slab (Mix designation C2, Table 16.1) had straight bars (see Plate 18.1). The specimen failed at one of the acute-angled load points with failure being initiated by a breakdown in the bond between the reinforcing bars and the concrete as shown in Plate 18.2. After the bond failure had propogated past the load point, a diagonal tension failure occurred.

Close examination of the failed specimen showed that cracks occurred at the end of each reinforcing bar. From this, it was concluded that a breakdown of the bond between the concrete and the steel had occurred at the end of each reinforcing bar.

18.4.2 Second Specimen

To overcome the breakdown in bond at the ends of the individual bars, some form of anchoring was necessary. This was obtained by bending up every bar at both ends as shown in Plate 18.3. For the three bars at the acute angled load points,

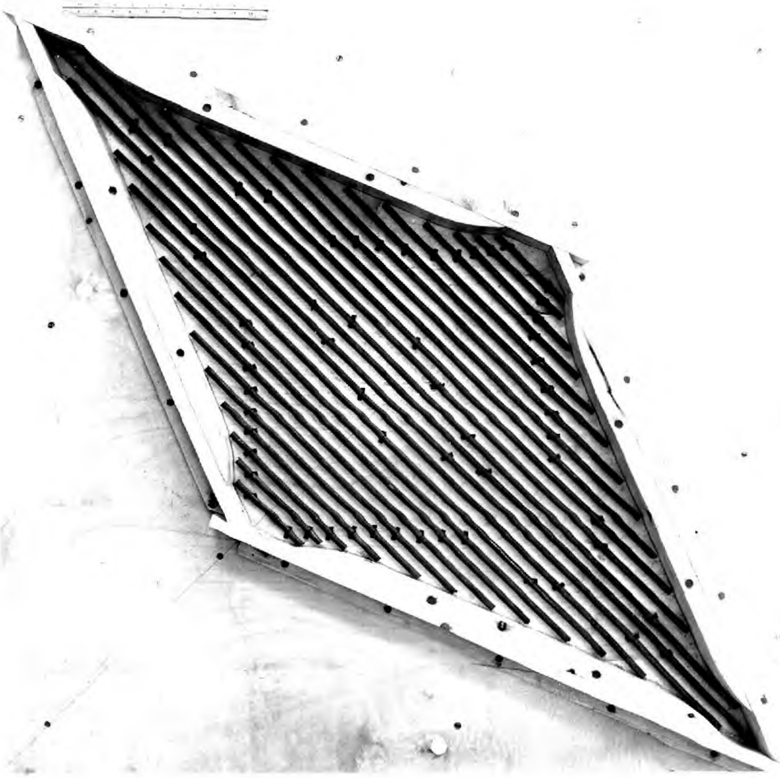

PLATE 18.1 Reinforcing in initial slab specimen

PLATE 18.2 Initial slab specimen at failure

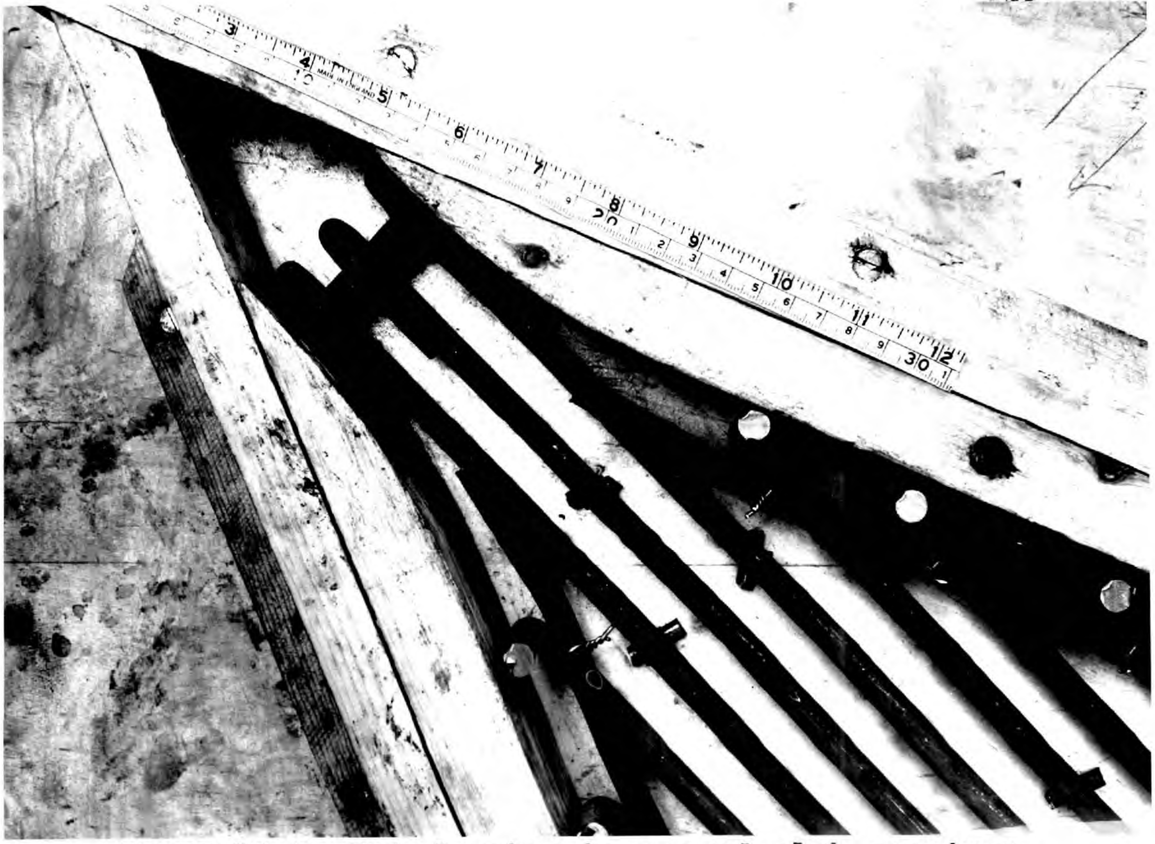

PLATE 18.3 Reinforcing in second slab specimen

PLATE 18.4 Second slab specimen at failure

the bars were turned and a $\frac{1}{2}$" Ø bar was placed crosswise to provide a more suitable anchor in the mortar in this zone of high stress concentration. For additional anchoring of the ends of the bars, a $\frac{3}{8}$" Ø bar was placed parallel to the sides of the mould, and was secured to each bar by means of a wire (see Plate 18.3).

Although it may be thought initially that this bar would influence the stress distribution in the specimen, closer examination shows that this effect is negligible. From Section 18.1, it was shown that the sides of the specimen and all lines parallel to it are in a state of pure twist. Consequently, as the bar is parallel to the side of the specimen, it will not generally be subjected to any longitudinal stress.

The specimen tested was a mortar (Mix designation M4, Table 16.1) with a ratio of diagonal lengths of 2:1. Unfortunately, failure occurred again at an acute angled corner with the failure probably being initiated by a combination of bond breakdown and a splitting mechanism at the ends of the three bars extending into the corner. (see Plate 18.4). This developed into a diagonal tension failure with breakdown of the bond between the mortar and steel occurring at the turned up ends of the bars nearest the acute angled corners as seen in Plate 18.4.

18.4.3 Final Reinforcing Procedure

To eliminate failure of the concrete in the acute angled corners of the specimen, two steps were taken. So that failure would not be initiated at the load points, the three corner bars were extended as far as possible past the load point before being bent up. These bars were then bent back along the opposite surface of the spedimen as shown in Plate 18.5 In order that failure did not occur as a result of diagonal tension in the concrete or bond breakdown on the vertical section of the bent up bars, the bars nearest the corners were bent up and then back on the opposite face. Stirrups were included so that the tension force induced by the corner loading would be effectively resisted by the steel.

A corner of a 2.5:1 slab is shown in Plate 18.5. As the extra reinforcing is confined to the two acute-angled corners of the specimen, it is considered that this reinforcement would have no significant influence on the general distribution of stress in the specimen. All specimens were tested satisfactorily with this general arrangement of reinforcement although the 2:1 and 1.58:1 slab specimens had less corner reinforcing due to lower applied loads at failure.

18.5 PRECISION OF TEST METHOD

Six reinforced slab specimens, three mortar and three concrete were tested for elasticity and strength properties. The mix proportions for these specimens are given in Table 16.1 while the method of test is discussed in Sections 16.4 and 16.5. Load-strain graphs for the individual specimens are

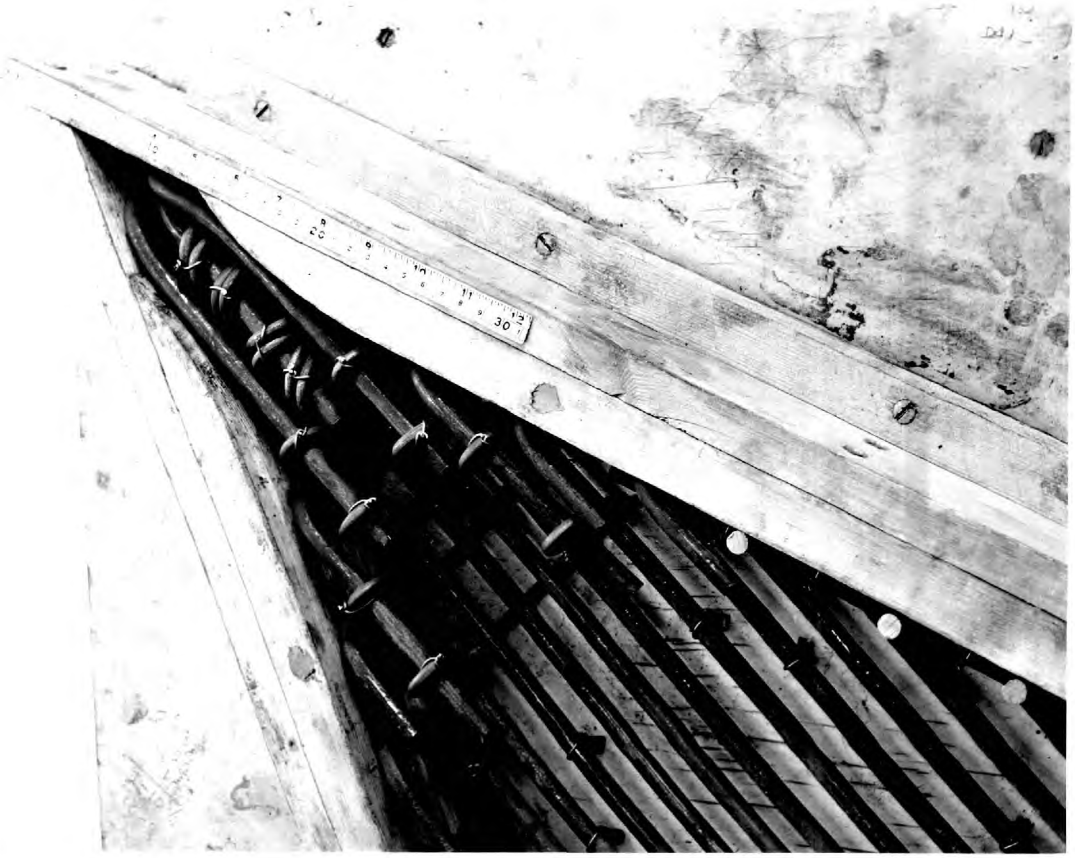

PLATE 18.5 Final reinforcing procedure in acute angled corner of slab specimen

given in Figures 18.6 to 18.11.

In Section 18.2, it was shown that the average moment on any principal section must be equal to the values given in Equations 18.1 and 18.2. If the principal moments at all points are constant, then the values for the moment at every point must conform to the values given by these equations. Under this condition, it also follows that the principal surface stresses and strains must be constant at all points.

In Figures 18.6 to 18.11, the principal strains on each surface have been recorded with two sets of electrical resistance strain gauges. Half of the gauges have been positioned at or near the centrepoint of the slab while the other half have been placed roughly halfway between the centre and a corner of the specimen. The principal strains in each direction on each surface are observed to be remarkably coincident in almost every case. The small differences detected can be accounted for by small variations in the property of the material or thickness of the slab specimen.

In view of the theoretical presentation of Section 18.2 and the experimental confirmation as discussed above, it is concluded that the induced principal moments are constant throughout the slab and therefore can be computed accurately from Equations 18.1 and 18.2. It is, however, recognized that a small error will occur near the sides of the specimen due to the transformation of twisting moments as discussed in Section 14.1.2.

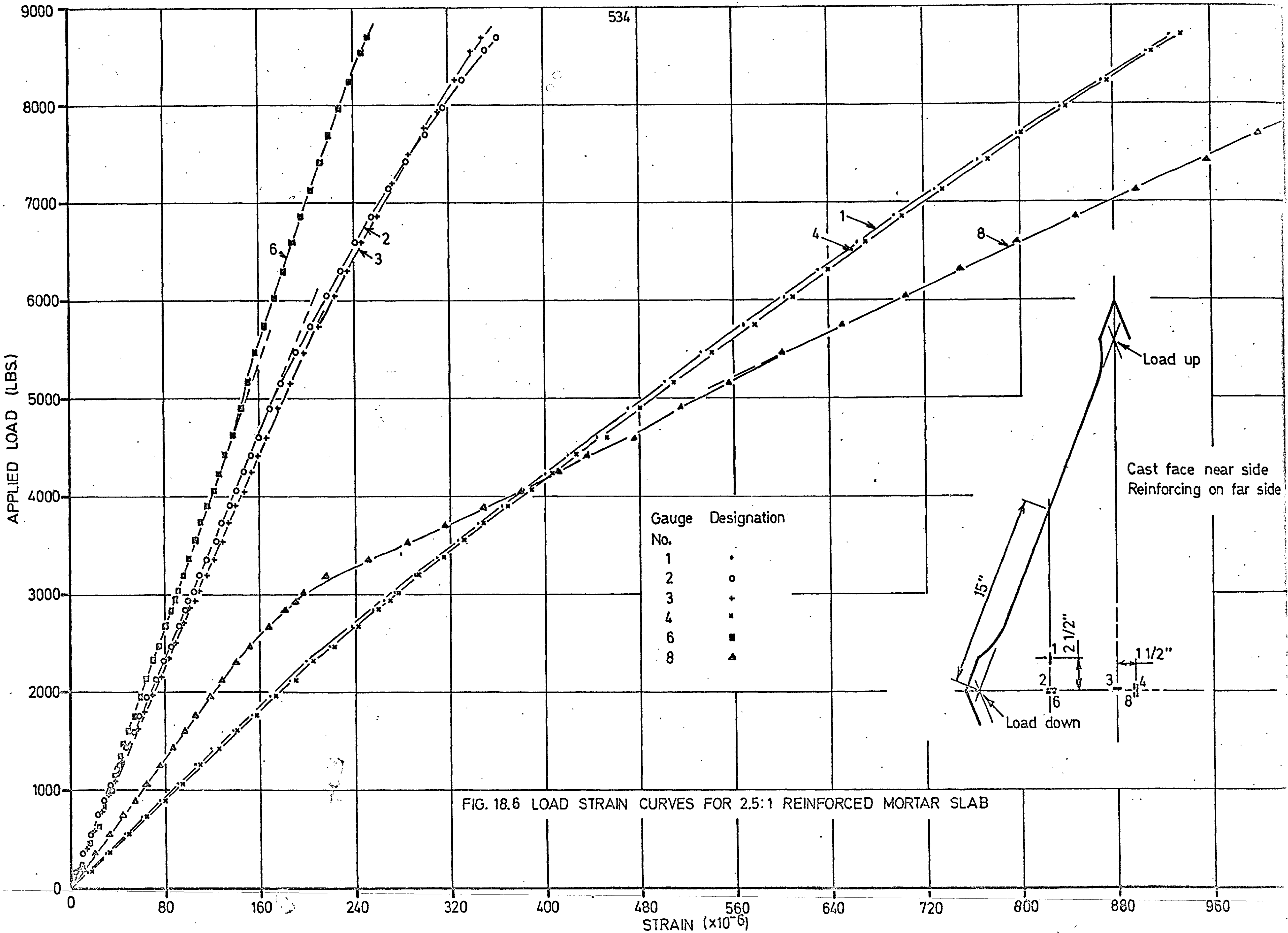

FIG. 18.6 LOAD STRAIN CURVES FOR 2.5:1 REINFORCED MORTAR SLAB

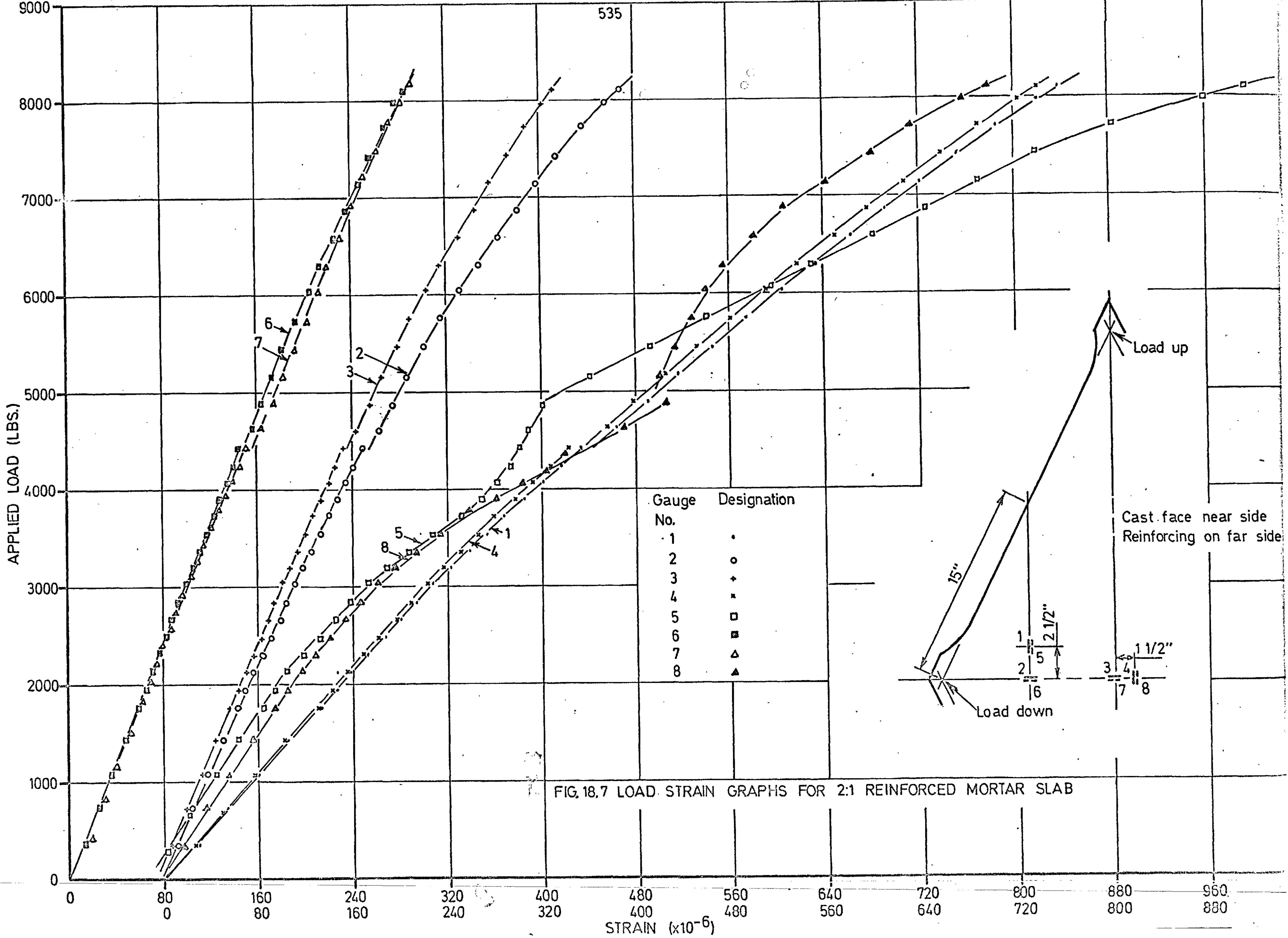

FIG. 18.7 LOAD STRAIN GRAPHS FOR 2:1 REINFORCED MORTAR SLAB

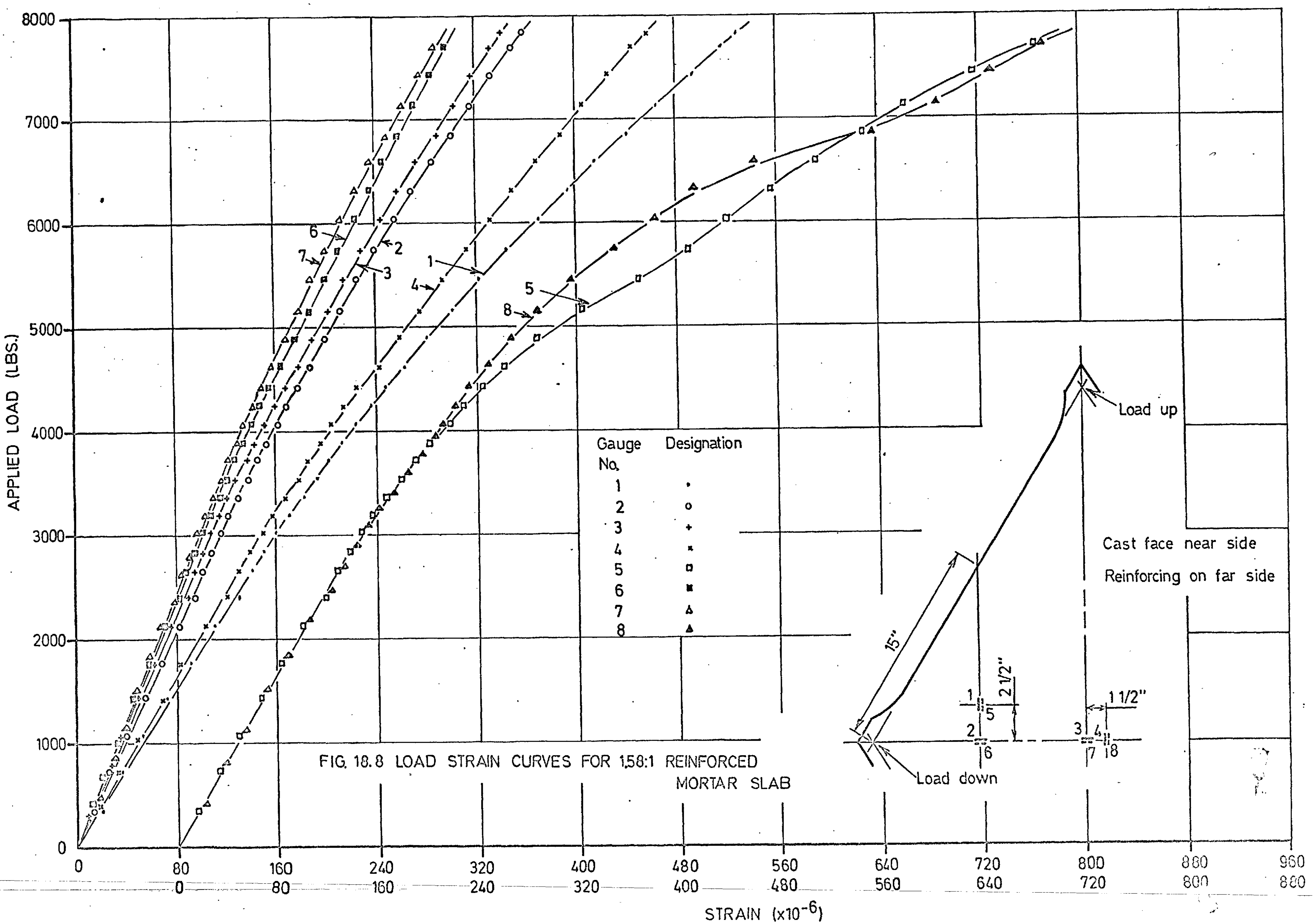

FIG. 18.8 LOAD STRAIN CURVES FOR 1.58:1 REINFORCED MORTAR SLAB

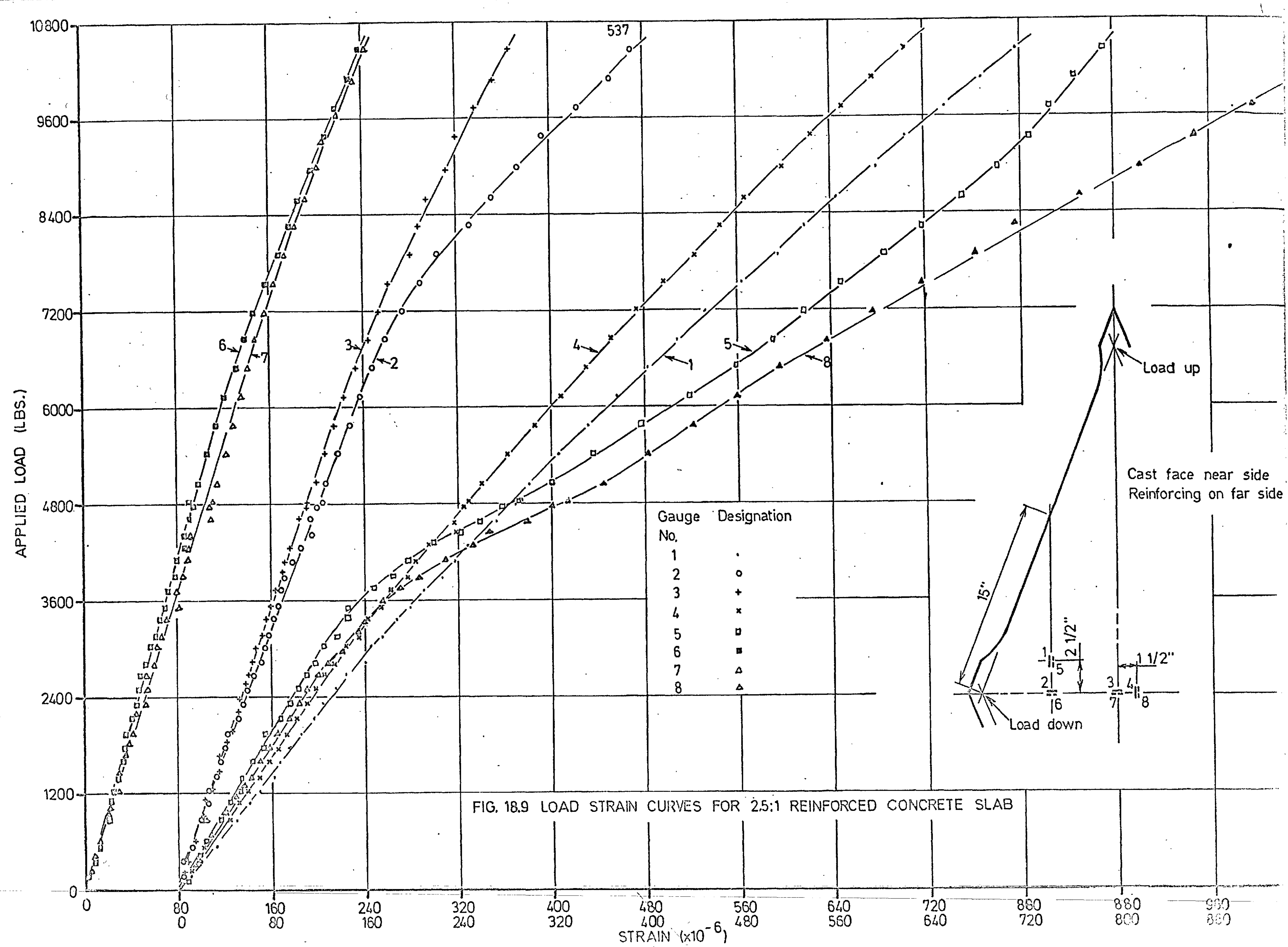

FIG. 18.9 LOAD STRAIN CURVES FOR 2.5:1 REINFORCED CONCRETE SLAB

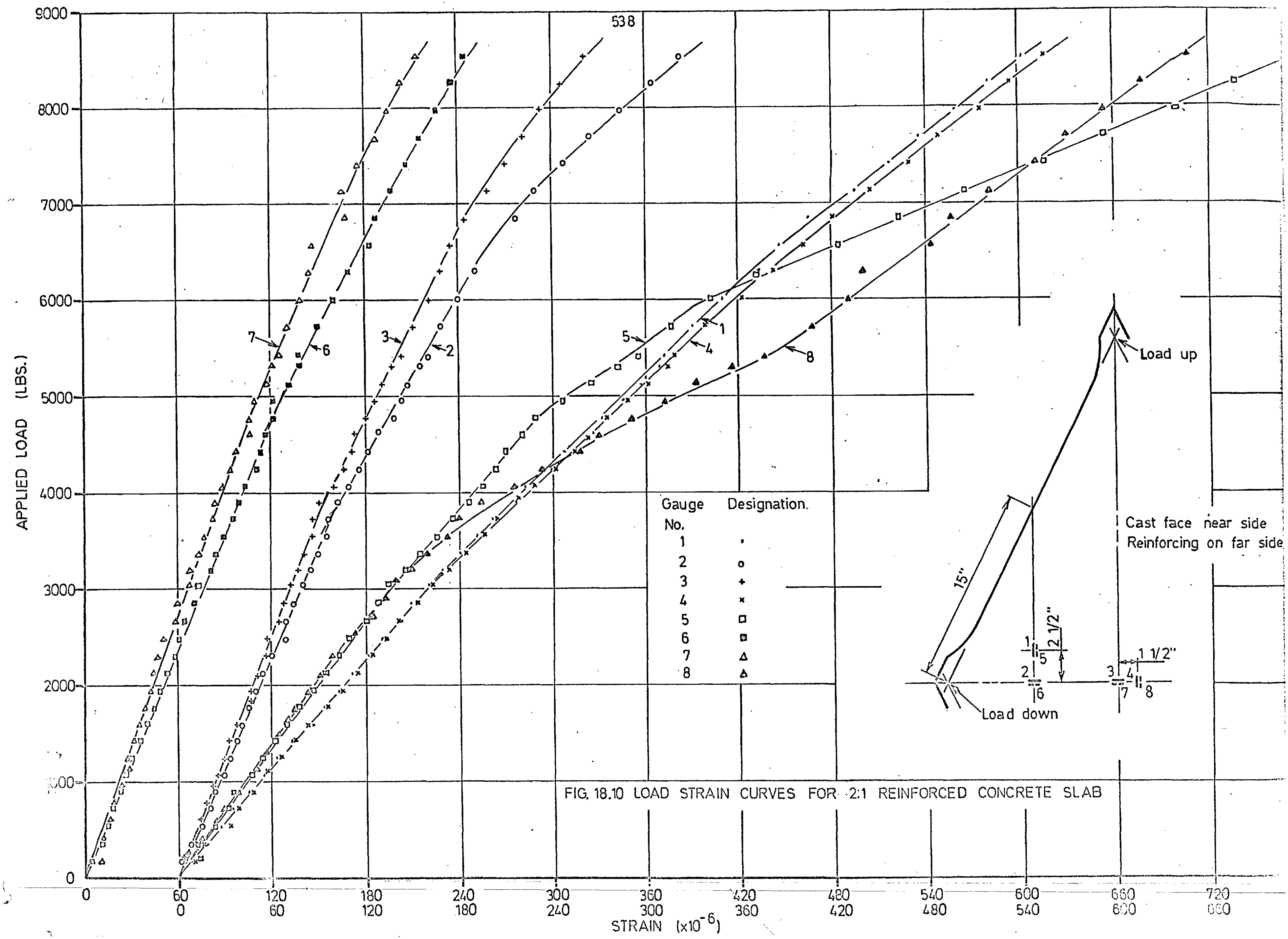

FIG. 18.10 LOAD STRAIN CURVES FOR 2:1 REINFORCED CONCRETE SLAB

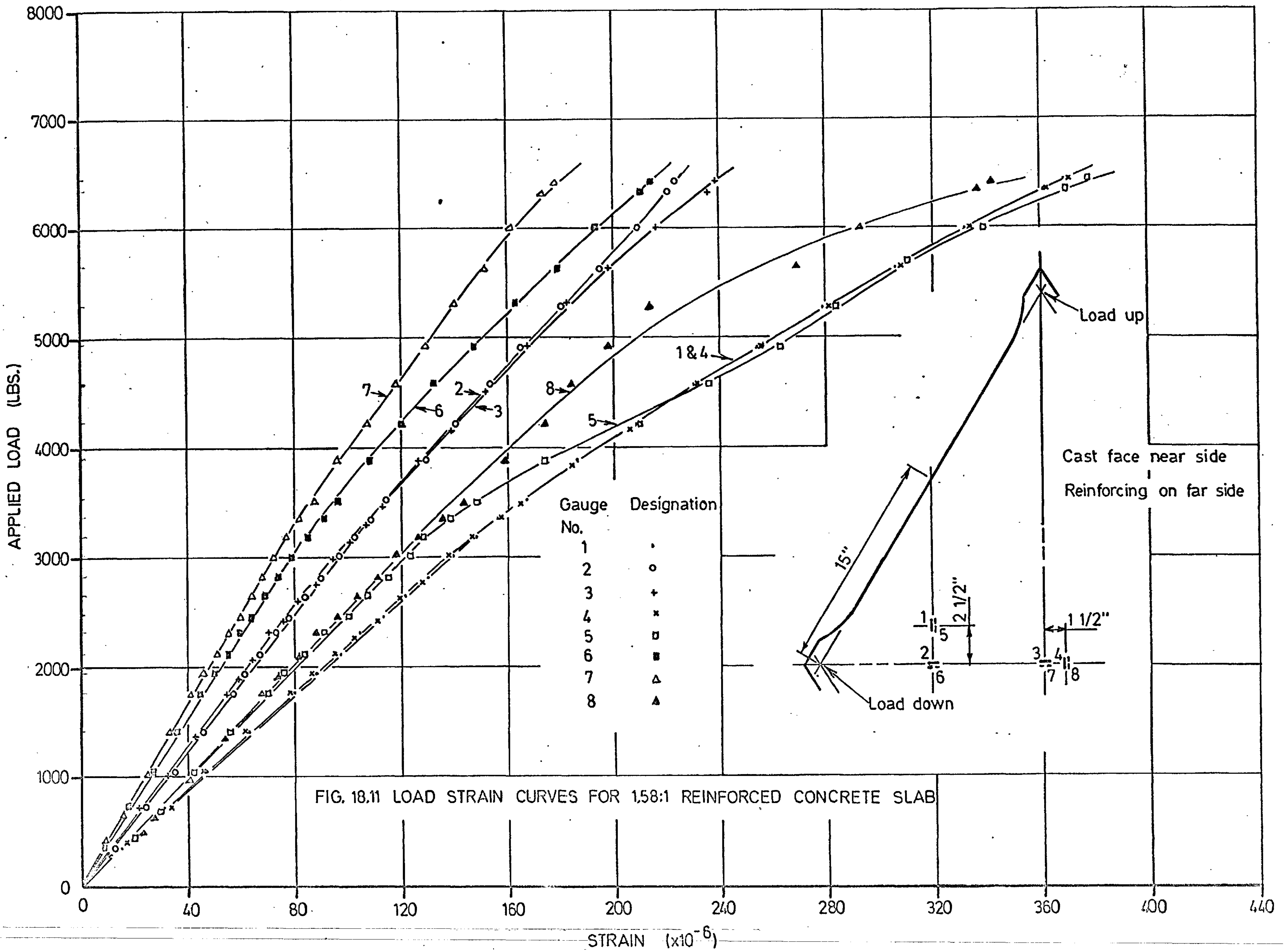

FIG. 18.11 LOAD STRAIN CURVES FOR 1.58:1 REINFORCED CONCRETE SLAB

As observed in Figures 18.6 to 18.11, there is a transition in the slopes of all the curves following the tensile failure of the concrete or mortar on the reinforced face (see Section 18.2). As the curves again become linear with the 2:1 and 2.5:1 slabs, it is possible to determine the moduli of rupture values by two alternate methods, as discussed in Section 18.2.2. Unfortunately, with both the 1.58:1 slab specimens, the material on the unreinforced face had exceeded its discontinuity level before the tensile failure on the reinforced face had effectively ceased (see Section 18.2). For these specimens, the modulus of rupture values are obtained only by the approximate method developed in Section 18.2.2.1

18.6 ELASTICITY PROPERTIES

By using Equations 18.46 to 18.49, the elasticity values, E and ν have been computed for the upper and lower surface of the specimen on the basis of observed strains prior to the tension failure of the concrete on the reinforced face. (see Table 18.2)

As discussed in Section 17.3.2, the mortar specimens tended to be stiffer at the bottom than at the top due to segregation whereas, for the concrete specimens, this effect was only slight. This effect is again observed with the 2.5:1 and 2:1 reinforced slab specimens although the 1.58:1 specimens showed an opposite trend. The reason for the apparently high value for E, for these last specimens, particularly the mortar, were probably due to somewhat large values for recorded strain on the upper surface. This is further substantiated by the odd Poisson's ratio value obtained for these same specimens.

TABLE 18.2 ELASTICITY VALUES FOR REINFORCED SLAB TESTS

SPECIMEN SHAPE	$E_1 (x10^6)$ p.s.i.	ν_1	$E_2 (x10^6)$ p.s.i.	ν_2
Mortar				
2.5:1	4.30	0.231	4.97	0.291
2.0:1	4.11	0.245	4.68	0.334
1.58:1	5.30	0.394	4.67	0.266
Concrete				
2.5:1	6.50	0.303	6.50	0.277
2.0:1	5.80	0.233	6.16	0.238
1.58:1	6.49	0.430	6.25	0.239

Although the modulus of elasticity values for the reinforced mortar specimens showed generally good agreement with the values obtained for the unreinforced mortar specimens (see Tables 17.1 and 17.2), the reinforced concrete specimens tended to yield slightly higher values of E than for the unreinforced specimens. Furthermore, it is observed that the value of E for the concrete tends to increase as the ratio of compression to tension stress increases.

With regard to Poisson ratio values, it is observed that the relatively high values obtained for the unreinforced slab specimens (Table 17.2) are again observed with the reinforced slab specimens (Table 18.2). Although no consistent trend for ν in relation to the induced stresses was observed with the mortar specimens, the ν values for the concrete specimens generally increased as the ratio of compression to tension stress increased (see Tables 17.2 and 18.2).

It is difficult to account for differences in elasticity values as a function of the induced loading system. Robinson[6] has obtained smaller ν values for concrete in biaxial compression while Vile[7] has observed, also from biaxial compression tests, that the values of E may increase by as much as 40% from that obtained in uniaxial compression. These changes have been described as being due to a general reduction in the internal voids or a general stiffening of the cement paste or mortar phase. It is logical to suggest that the increase in E resulting from the increased ratio of compression to tension would be caused by an alteration in the internal distribution of stresses which tends to cause an increasing proportion of the load to be transmitted through the stiffer aggregate particles. Similarly, an alteration in measured values of ν can be accounted for by considering the internal distribution of stresses as a function of the variable restraint effect by the aggregate particles on the cement paste phase as well as the general multi-phase nature of the material.

18.7 DISCONTINUITY LEVEL STRESSES AND STRAINS AND ULTIMATE STRENGTHS

18.7.1 Discontinuity Level Stresses and Strains

The discontinuity level strains have been obtained from Figures 18.6, 18.7, 18.9 and 18.10 by observing the average strain at which the gauges in the principal tensile direction on the unreinforced face (gauge nos. 2 and 3 in every case) deviate from non-linearity. These values are recorded in Tables 18.3. Although the graphs become non-linear at an earlier load stage, this is caused by the redistribution of stresses corresponding to the tensile failure of the reinforced face. (see Sections 18.2 and 18.5).

It is apparent, from the values given in Table 17.3 and 18.3, that the discontinuity level strains for both mortar and concrete generally increase as the ratio of compression to tension increases. For example, when the ratio of principal compression to tension stress is zero (uniaxial tension), the discontinuity level for the concrete occurred at a principal tensile strain of $75x10^{-6}$. When the above ratio of principal stresses was increased to about six (20:1 specimen, Table 18.3), the strain increased to $183x10^{-6}$, an increase of 145%. Although large increased in tensile strain were also observed with the mortar specimens, the percentage increase was generally smaller, than that obtained for the concrete specimens.

TABLE 18.3 DISCONTINUITY LEVEL STRESSES AND STRAINS AND MODULUS OF RUPTURE VALUES

SPECIMEN SHAPE	Thickness d (ins.)	Discontinuity Level			Failing Stresses		
		Principal Tension Strain ($x10^{-6}$)	Stress (p.s.i.) Tension	Comp	Failing Load (lbs)	Stress (p.s.i.) Tens.	Com.
Mortar							
2.5:1	3.01	192	250 (266)	2310 (2420)	8850	400 (430)	3725 (3910)
2.0:1	3.07	215	312 (435)	1750 (1840)	8255	513 (715)	2880 (3020)
1.58:1	3.05	-	-	-	7915	676	2640
Concrete							
2.5:1	3.25	160	230 (235)	2530 (2680)	10660	390 (400)	4310 (4570)
2.0:1	3.06	183	327 (570	2080 (2100)	8626	524 (915)	3340 (3370)
1.58:1	3.07	-	-	-	6480	538	2280

Note: Values of stress enclosed in brackets were obtained from Equations 18.62 and 18.63 whilst the other stress values were obtained from Equations 18.58 and 18.59.

The fact that mortars and concretes can withstand larger extensional strains as the ratio of compression to tension stress increases is shown also by examining the principal tensile strains near failure. (see Figures 18.6 to 18.11). For example, with concrete, the largest average recorded tensile strains are 120, 160 and 290 microstrain for compression to tension ratios of 0 (flexural beam test), 0.4 (1.58 unreinforced slab) and 6 (2:1 reinforced slab), respectively.

18.7.2 Modulus of Rupture

To calculate the modulus of rupture values, (see Section 17.5.1), Equations 18.58, 18.59, 18.62 and 18.63 were again used with the failure strengths being computed on the basis of elastic analysis.

Two typical specimens at failure are shown in Plate 18.6. Although the unreinforced specimens discussed in Section 17.3.1 tended to fail at a random section, the reinforced specimens failed consistently near an obtuse angled corner. Unfortnately, as the stress pattern near the edge of the spedimen would be affected by the edge conditions, it is reasonable to suggest that the modulus of rupture values obtained are slightly low (of the order of 5%). This is borne out by the fact that, for those gauges which measured the principal tensile strain on the unreinforced face, the graphs did not become as horizontal as in the case of some of the load strain graphs for the unreinforced slab specimens (Figures 17.7 to 17.12) This suggests that some reserve of strength was still available over the general slab volume when the concrete or mortar near the corner failed. Furthermore, stresses at the discontinuity level for the reinforced slabs were about 65 to 70% of the modulus of rupture values as compared to about 60% for the unreinforced specimens.

It is interesting to observe that failure always occurred at a section, which was subjected to principal tension stress (Plate 18.6). This is in general agreement with the types of failures observed with the unreinforced specimens as discussed

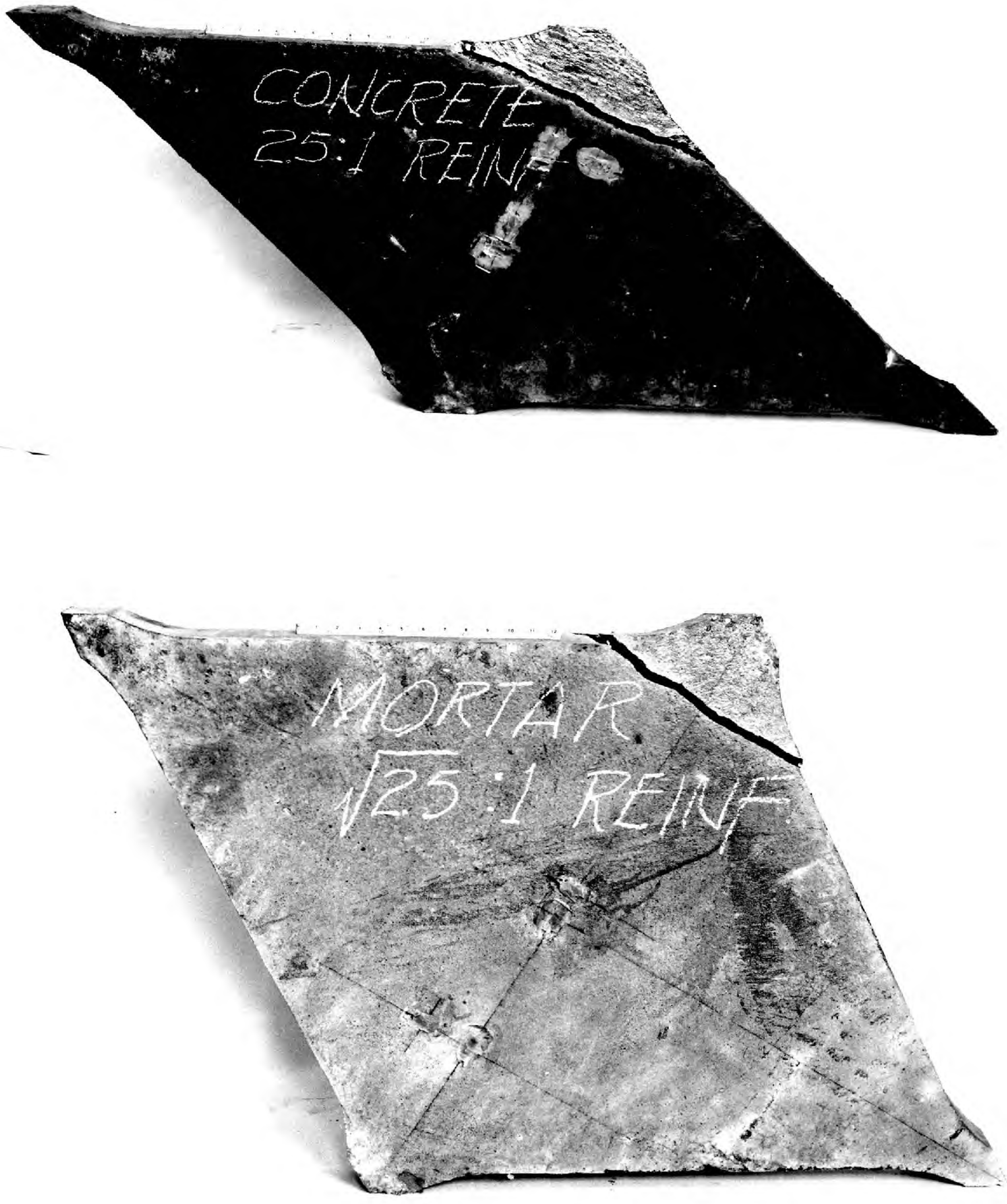

PLATE 18.6 Typical reinforced slab specimens at failure

in the last chapter.

18.8 APPRAISAL OF TEST METHOD

As discussed in Section 18.5, it was shown conclusively that the induced moments, M_x and M_y, obtained from the theory of Section 18.2 were accurate and that, as a result, the slab was subjected to a known and constant state of biaxial moment. Although the surface stresses and strains could not be similarly verified with the theory, it is considered that the theoretical values for stress and strain (Section 18.2.1) are in close agreement with the actual values obtained. On this basis, it is also reasonable to assume that the calculated values for E and are accurate if the recorded strains are reliable. As shown in Section 18.5, the recorded strains were usually found to be uniform, thereby conforming to theoretical predictions. However, when some strain readings were suspect as occurred with the upper surface of the 1.58:1 slab specimens, the values of E and ν were also found to be suspect.

After cracking of the concrete on the reinforced face, the principal moments will still be in good agreement with the theoretical values obtained in Section 18.2 (Equations 18.1 and 18.2). However, as shown in Section 18.2.2, the calculations for surface stresses and strains are only approximate, being not only susceptible to theoretical assumptions (Section 18.2.2.1), but also to strain measurements (Section 18.2.2.2) This was shown in Table 18.3 where, for the two methods of calculating the principal stresses, large differences occurred in some cases. (for example, see the 2:1 mortar slab Table 18.3).

The greatest criticism of the reinforced slab test is the fact that it is an impractical specimen to use, as the reinforcing procedure is an extremely time-consuming operation. It is estimated that about 30 to 40 hours was required in preparing each specimen for test with the reinforcing requiring about 80% of the total time. Thus, in order to perform an examination of the behaviour of one concrete under different biaxial tension-compression states of stress, a two to three months programme is necessary. Clearly, for any extensive investigation on the inter-relation of several parameters such as water/cement ratio and aggregate/cement ratio, this test method is unsuitable.

18.9 SUMMARY

In order to examine the behaviour of concrete under biaxial tension-compression states of stress where the compression to tension ratio is greater than unity while simultaneously ensuring flexural states of stress, the reinforced rhombus test has been developed. A detailed theoretical analysis has been conducted to determine the surface strains, moduli of elasticity and Poisson's ratio values in terms of the applied load, P, prior to the onset of failure on the reinforced face. For establishing the surface stresses on the unreinforced face after the tensile failure of the material on the reinforced face, two separate analyses have been conducted.

It has been shown from strain measurements at different points on the specimen surface that, as the principal strains in either direction on either surface were constant, the slab was being subjected to a known and uniform state of biaxial moment.

From the calculated modulus of elasticity values, it was shown that with mortar, good agreement with the values for the unreinforced slabs and uniaxial specimens was generally obtained. However, for concrete, there tended to be a small increase in the E value as the ratio of compression to tension stress increased. With regard to Poisson ratio values, there was a general increase from that obtained under uniaxial states of stress. This was shown to be in general agreement with the trends obtained for the unreinforced slab specimens. However, no significant trend in relation to the induced combination of principal stresses was observed.

The principal tensile strains at the discontinuity level increased for both mortar and concrete as the ratio of compression to tension stress increased. Under certain ratios of principal compression to tension stress, it was observed that the strain at the discontinuity level was more than twice as large as that obtained in uniaxial tension.

Similar increases were also observed with the strains at failure. This increase tended to be more marked with the concrete than with the mortar.

CHAPTER 19

THE STRENGTH OF CONCRETE AND MORTAR UNDER BIAXIAL TENSION AND TENSION-COMPRESSION STATES OF STRESS

19.1 INTRODUCTION

Although the results of the unreinforced specimens and reinforced specimens have been analyzed independently in Chapters 17 and 18 respectively, it is necessary to consider these together when investigating the mechanism of fracture and failure of concrete and mortar in the full range of biaxial tension and tension-compression states of stress. In this chapter, the principal stress plot for the strength of concrete under biaxial tension and tension-compression is examined in terms of the discontinuity level stresses as well as the ultimate strengths. An examination is also conducted on the principal strains obtained at the discontinuity level. The results of these analyses are combined with the results obtained by other investigators to demonstrate the probable criterion of fracture and failure for concrete under biaxial tension and tension-compression states of stress.

From an initial examination of concrete under different states of biaxial tension and tension-compression states of stress at Imperial College, suspicious discrepancies occurred in the principal stress plot. Such a curve is compared with the results of Chapters 17 and 18 where, with the necessary developments in testing techniques, the results can be treated with greater confidence.

Finally, a brief description of the probable mechanism of fracture and failure for concrete under different combinations of principal stress is presented.

19.2 FAILURE OF CONCRETE IN BIAXIAL TENSION AND TENSION-COMPRESSION

Most theories proposed for establishing a reasonable failure criterion for concrete under biaxial states of stress have been based on the assumption that concrete is a homogeneous, isotropic material. With this assumption, McHenry and Karni[69] were able to show that an almost linear relationship existed between the octahedral shear and normal stresses. These parameters also have been used more recently by Bresler and Pister,[70,71] Nishizawa[74], Tsuboi and Suenega[72] and Sundara et al[73,121]. Bresler and Pister extended their examination on the phenomenological level by representing the equation for the surface of failure in terms of the octahedral stresses and the principal stress invariants.

Robinson[6] showed that, as the octahedral shear stress is very insensitive to relatively large changes in the tensile strength, an apparently good linear relationship may be obtained even when the tensile strength results are highly erroneous. Furthermore, as the value of the octahedral shear stress varies for different combinations of principal stress, i.e. is not a constant as specified in the theory,[122] it is difficult to attach a physical meaning to such a plot.

It has been shown by Alexander[114,119] and Hsu et al[95,120] that the fracture of concrete is initiated by a breakdown of the bond at the cement paste-aggregate interface. Yet, no failure theory presented for concrete has explained or even suggested the connection between the breakdown of the bond and the observed strength under the various combinations of stress.

In the following analysis, the discontinuity level stresses and failure strengths of concrete will be analyzed in terms of the probable mechanism of bond breakdown at the cement paste-aggregate interface. For the mortar, on the other hand, failure is analyzed in terms of ph nomenological values as the strength appears to be basically a function of the intrinsic strength of the cement paste phase.

19.2.2 Discontinuity Level Stresses and Failure Strengths

In Figure 19.1, the discontinuity level stresses and the failing strengths for the concrete and mortar have been plotted on a biaxial stress graph. For all cases except the uniaxial compressive strength, the values have been obtained for flexural states of stress where the specimen thickness has been kept constant (see Section 16.2). As discussed in Section 17.5.1, the discontinuity level stresses would be expected to be approximately equal for direct and flexural states of stress, whereas the calculated ultimate strengths, when based on elastic analysis, would be larger with the flexural states of stress than with the direct

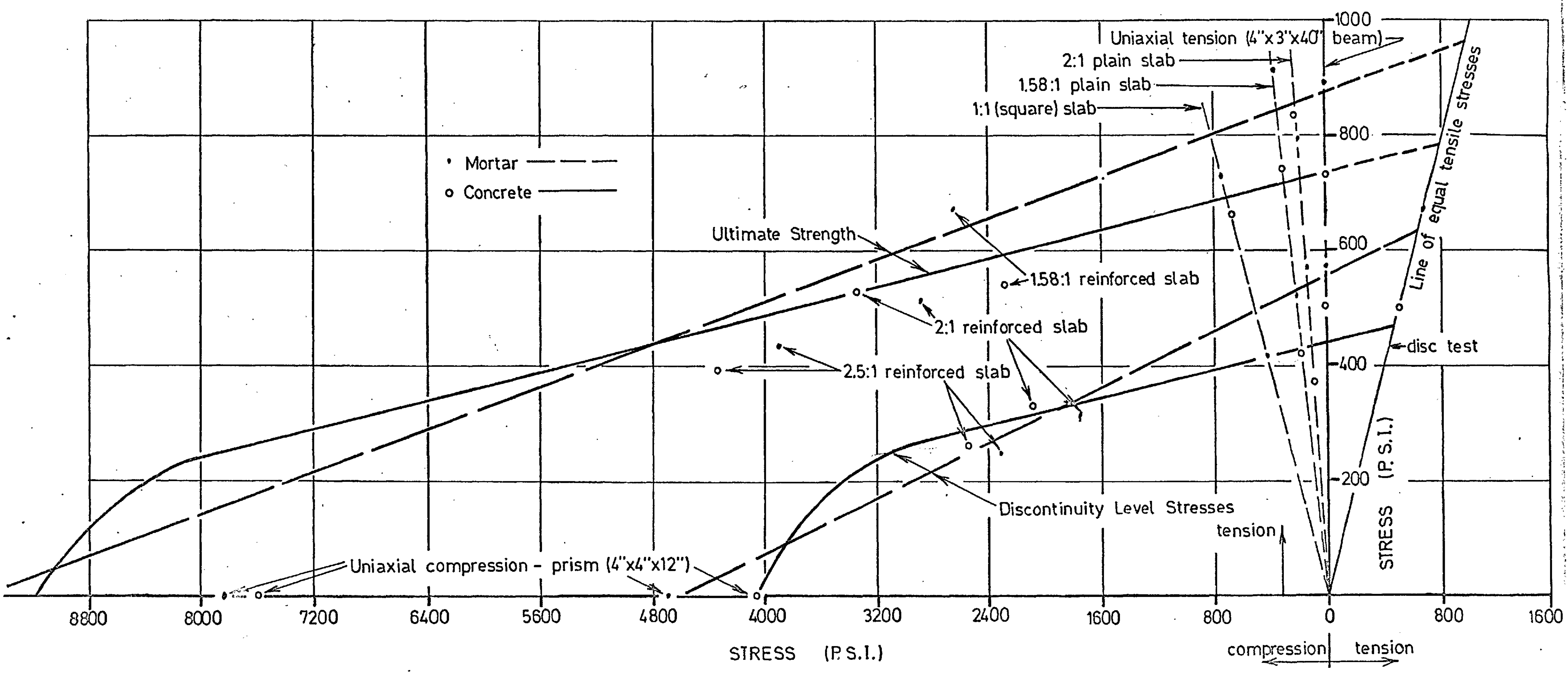

FIG. 19.1 PRINCIPAL STRESS PLOTS FOR CONCRETE AND MORTAR

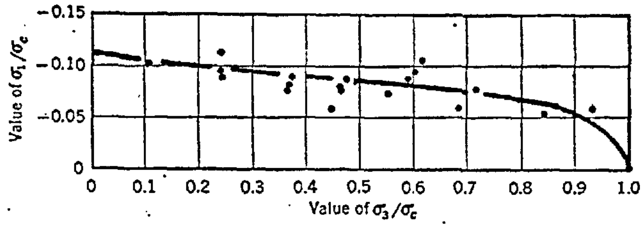

FIGURE 19.2 Principal stress plot obtained by Bresler and Pister from combined torsion and axial compression.

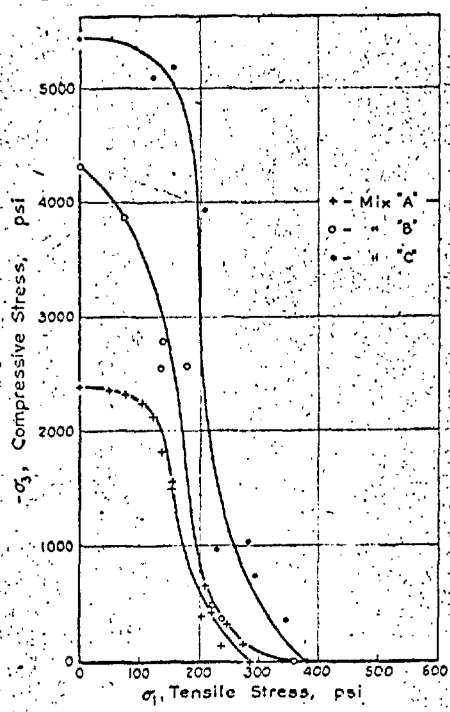

Fig. 2—Relationships between combined stresses at failure

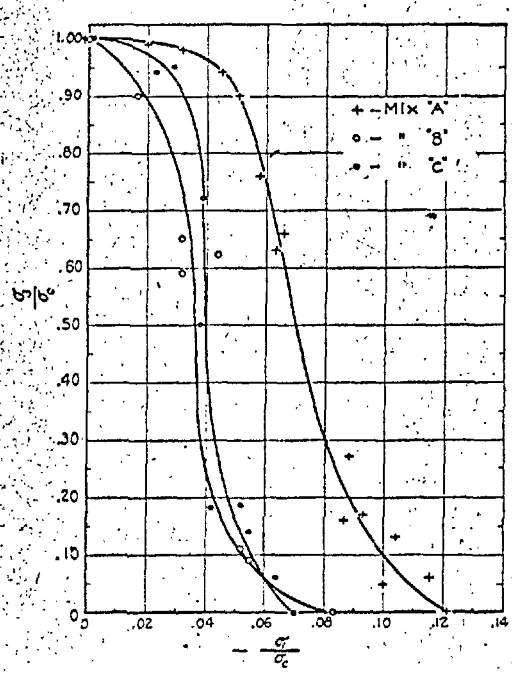

Fig. 3—Relationships between combined stresses at failure when expressed as dimensionless ratios

FIGURE 19.3 Principal stress plots obtained by McHenry and Karni from hoop tension and axial compression.

states of stress. To account for these higher ultimate strengths obtained with flexual tests as well as taking into consideration the slight reserve of strength available in the reinforced slab specimens at collapse (Section 18.7.2), the ultimate strength graphs have been moved slightly up and extended at the uniaxial compression end (Figure 19.1).

(1) Concrete

From Figure 19.1, it is seen that the surface of failure for concrete cannot be strictly expressed in terms of either a constant stress or a constant strain criterion. Furthermore, due to the sharp curvature near the uniaxial compression end of the principal stress plot, it is unlikely that any of the other classical failure criteria[6] will satisfy the given data.

The principal biaxial tension-compression stress plots obtained by Bresler and Pister[70] and McHenry and Karni[69] have been presented in Figures 19.2 and 19.3, respectively. As discussed in Sections 11.3.2 and 11.3.3, the sharp curvatures near the uniaxial tension end of the principal stress plot for McHenry and Karni's results can be accounted for by the variable platen restraint effect while Bresler and Pister's method of analysis was shown to be slightly faulty. Nevertheless, these graphs are included as they are sufficiently accurate for showing the general shape of the principal stress plot for biaxial tension-compression states of stress. Furthermore, as the ratio of the discontinuity level stresses to the ultimate strengths are very nearly a constant for the different states of biaxial tension-compression stress (see Figure 19.1), it is possible to interpret results where only ultimate strengths are available in terms of discontinuity level stresses.

From Figures 19.1, 19.2 and 19.3, it is seen that the general shape of the principal stress plot is remarkably similar for the three separate investigations. In every case, a slight and almost linear reduction in tensile stress is obtained with increasing compressive stress prior to the sharp curvature at the uniaxial compression end of the curve. These sharp curvatures, observed in Figures 19.1 to 19.3, would suggest that there is a transition from one mechanism of failure to another. This is also supported by the fact that uniaxial compression failures appear to be different in some respects from uniaxial tension failures. Although both these failures are represented by crack patterns perpendicular to the principal extensional direction, the uniaxial compression failure results in a greater degree of breakdown throughout the entire structure than occurs in the uniaxial tensile specimen at failure.

From Figure 19.4(a), it is shown that, in uniaxial tension, the initial bond breakdown will occur at points of tensile stress concentration between large pieces of aggregate in planes perpendicular to the direction of the applied load. This has also been considered by Ward[2] from examination of failed specimens. It

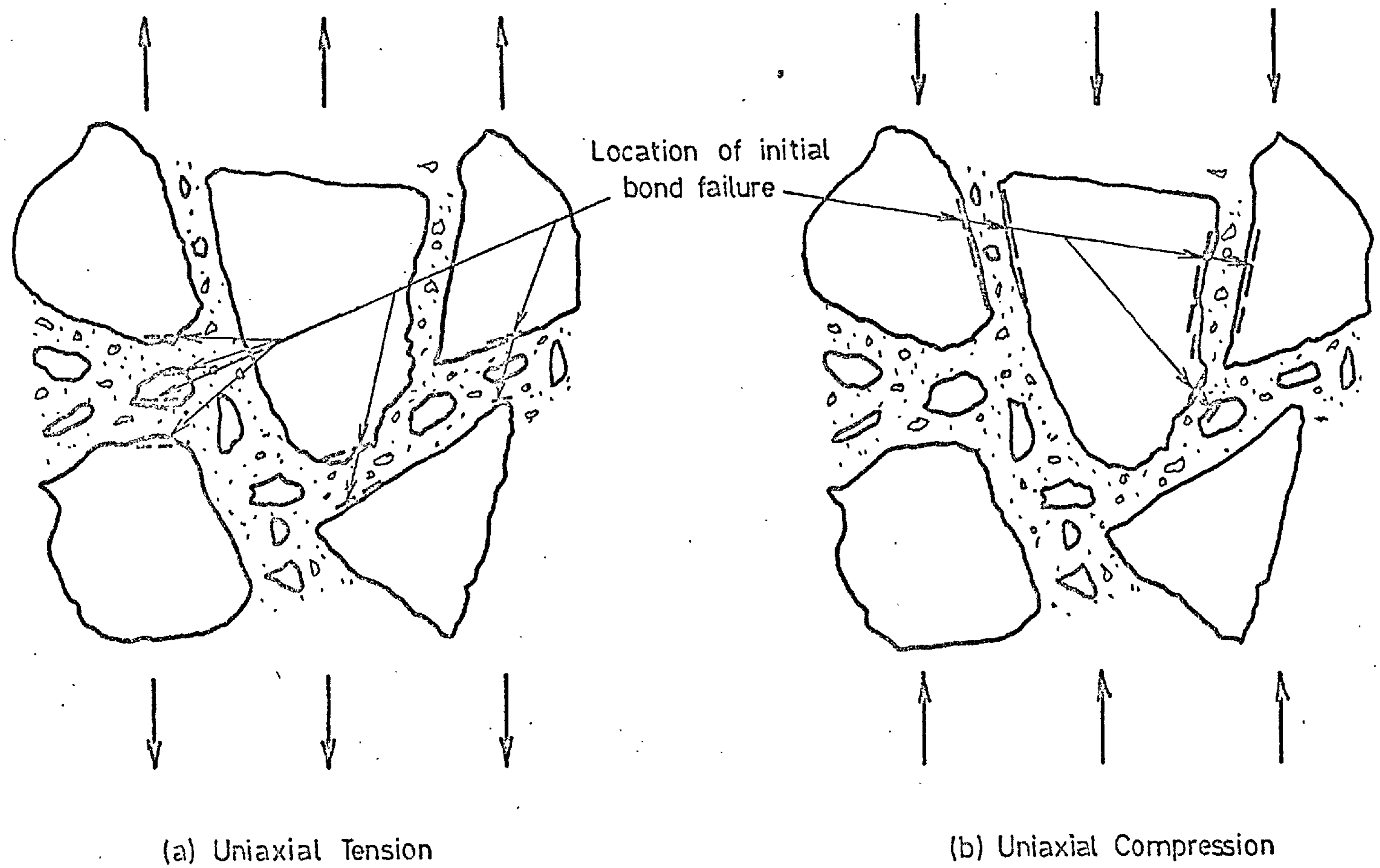

FIG. 19.4 LOCATIONS OF INITIAL FAILURE FOR A TYPICAL CONCRETE

has also been suggested that, for uniaxial compression, failure is similarly caused by tensile stresses in the lateral direction (5,6).

However, closer examination of the probable internal distribution of forces suggests that the bond breakdown in uniaxial compression is initiated by a shearing failure on the cement paste-aggregate interface rather than a direct tensile failure. From recent work conducted at Leeds University,(123) it has been shown that the Poisson's ratio for different aggregates varies generally from about 0.26 to 0.30. This value is in close agreement with the value of 0.25 obtained for cement paste by Anson(3). As the longitudinal shortening of the cement paste and aggregate will be of a similar order, then the lateral expansions in these two phases will also be similar. It is thus reasonable to suggest that the development of direct tensile bond stresses in the lateral direction will be only minute and therefore will not be the reason for the initiation of bond breakdown in uniaxial compression.

In Figure 19.4(b), the probable locations of initial bond breakdown for a uniaxial compression test are shown as occurring on inclined planes where the bond stresses are a high shear and a low normal stress. Following these initial breakdowns, the failure will propagate along the surface of the aggregate particles which are orientated approximately in the direction of the applied load as well as through the cement paste phase, thereby connecting with similar failures on adjacent aggregate particles. That such a failure mode is possible is shown by examination of compression specimens after failure. Numerous aggregate particles tend to have two cones of mortar or cement paste at opposite ends with the axes of these cones roughly aligned with the direction of the applied loading.

It has been shown that most failures in biaxial tension and tension-compression are of very similar appearance to those which occur in uniaxial tension with the failure plane being at right angles to the direction of the principal tensile stress. (see Plates 17.1, 17.2 and 18.6) It is also observed in Figures 19.1 to 19.3 that the failure strength is basically dependent upon the principal tensile stress.

In extending the above hypothesis, for biaxial tension-compression states of stress, it seems reasonable to suggest that, where the compression to tension ratio is low, (less than that which produces the sharp curvature in the principal stress plot) the initial bond failures will still generally occur at the same locations as under the action of uniaxial tension and the direct tension bond stresses at these critical points will be basically dependent on the principal tensile stress only. Thus, it is more reasonable to think of the mechanism of failure for concrete in biaxial tension-compression, in terms of a maximum principal tensile <u>stress</u> rather than the tensile <u>strain</u>. That is, as the effect of Poisson's ratio from the applied compression will cause a lateral expansion without significantly increasing the critical bond stress, the extensional strain at the discontinuity level increases as the ratio of compression to tension increases (see Section 19.2.3).

For high ratios of compression to tension stress (on the uniaxial compressive side of the sharp curvature in the principal stress plot -see Figures 19.1 to 19.3), it is suggested that failure is caused by a similar shearing bond failure at the cement paste-aggregate interface as has been suggested for uniaxial compression.

The above hypothesis, which suggests that initiation of failure in uniaxial tension and most biaxial tension-compression states of stress is caused by the limiting direct tensile bond strength of the cement paste-aggregate interface, can also be applied to biaxial tension states of stress. However, the number of locations of potential bond breakdown is substantially increased as failure can occur in any direction in the plane of the applied stresses as opposed to only one direction in the other stress states considered. Thus, from a statistical consideration, a small reduction in the stress at the discontinuity level would be expected. However, from Figure 19.1, such an effect appears to be insignificant.

(2) Mortar

For the mortar specimens, it is apparent that a different failure criterion exists than for the concrete as demonstrated by a virtually straight line relationship on the principal stress plot.

Guest[(124)] in 1900 extended Coulomb's original internal

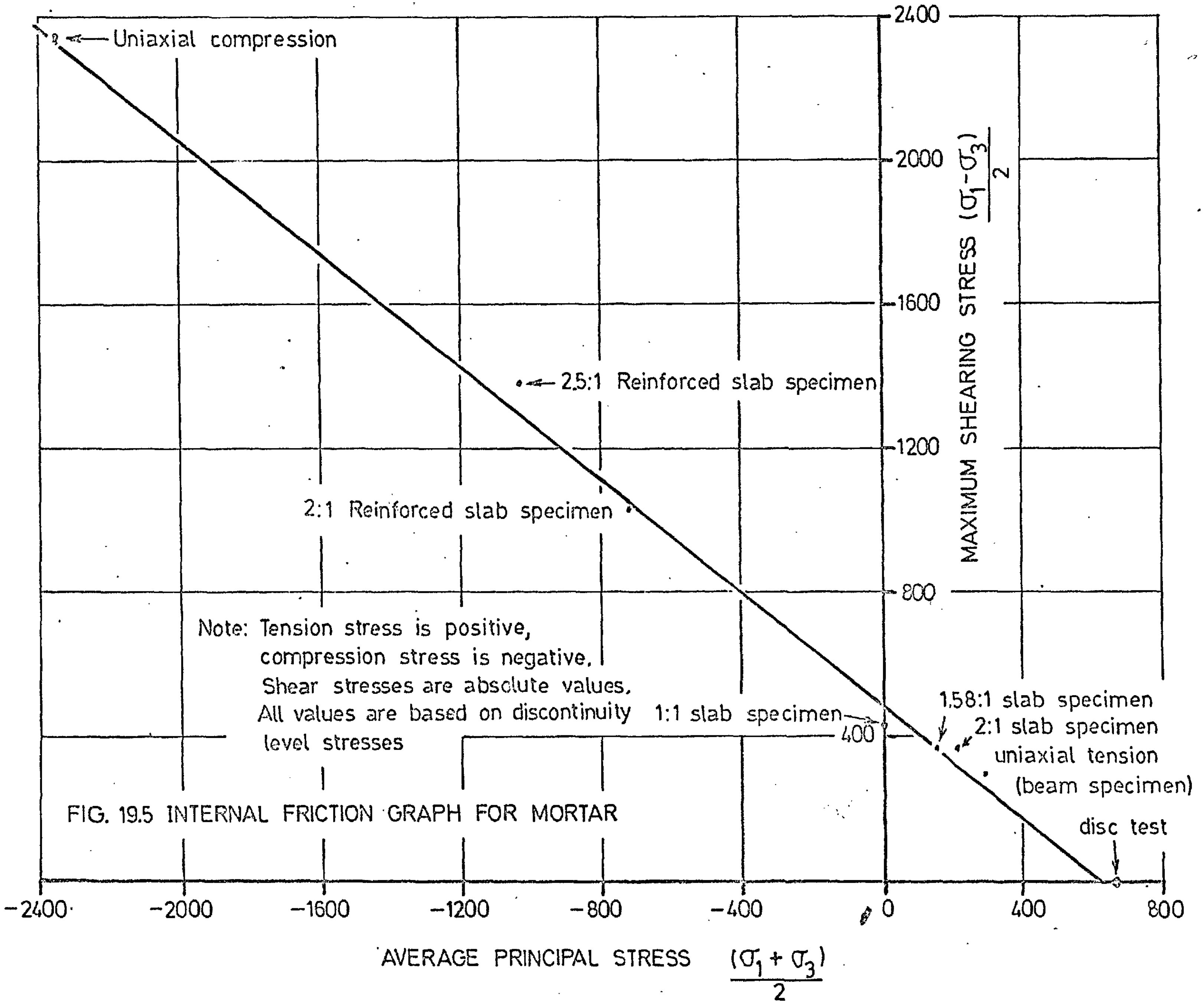

FIG. 19.5 INTERNAL FRICTION GRAPH FOR MORTAR

friction theory represented by the equation

$$\sigma_1-\sigma_3=2c_1 + c_2 \; (\sigma_1 + \sigma_3) \qquad \ldots 19.1$$

for showing when ductile materials begin to yield. In Equation 19.1, the left hand side represents the maximum shearing stress while the value, $\sigma_1+\sigma_3$, represents the volumetric stress. The constant c_1 is the intrinsic shear strength while c_2 is a material constant which shows the importance of the volumetric stress on the yield strength. As pointed out by Guest, brittle and ductile materials will have values of unity and zero, respectively, for c_2.

In Figure 19.5, the values of $\frac{(\sigma_1-\sigma_3)}{2}$ have been plotted against the values of $\frac{(\sigma_1+\sigma_3)}{2}$ for the mortar in order to investigate the applicability of an internal friction theory to mortar. It is observed that the values obtained satisfy the straight line relationship extremely well. By substituting in suitable values of σ_1 and σ_3 from Figure 19.4 into Equation 19.1 then Equation 19.1 becomes, for the mortar;

$$\frac{\sigma_1-\sigma_3}{2} = 480 + 0.8 \; \frac{(\sigma_1+\sigma_3)}{2} \qquad \ldots 19.2$$

This shows that the intrinsic discontinuity level shear strength of the mortar is 480 p.s.i. Also, with the value of $c_2 = 0.8$ being so large, it is apparent that over the range of stresses investigated, mortar tends to be a brittle material. From the above, it is concluded that the failure criterion for mortar for the complete range of biaxial tension and tension-compression states of stress can be expressed in terms of Coulomb's internal friction theory.

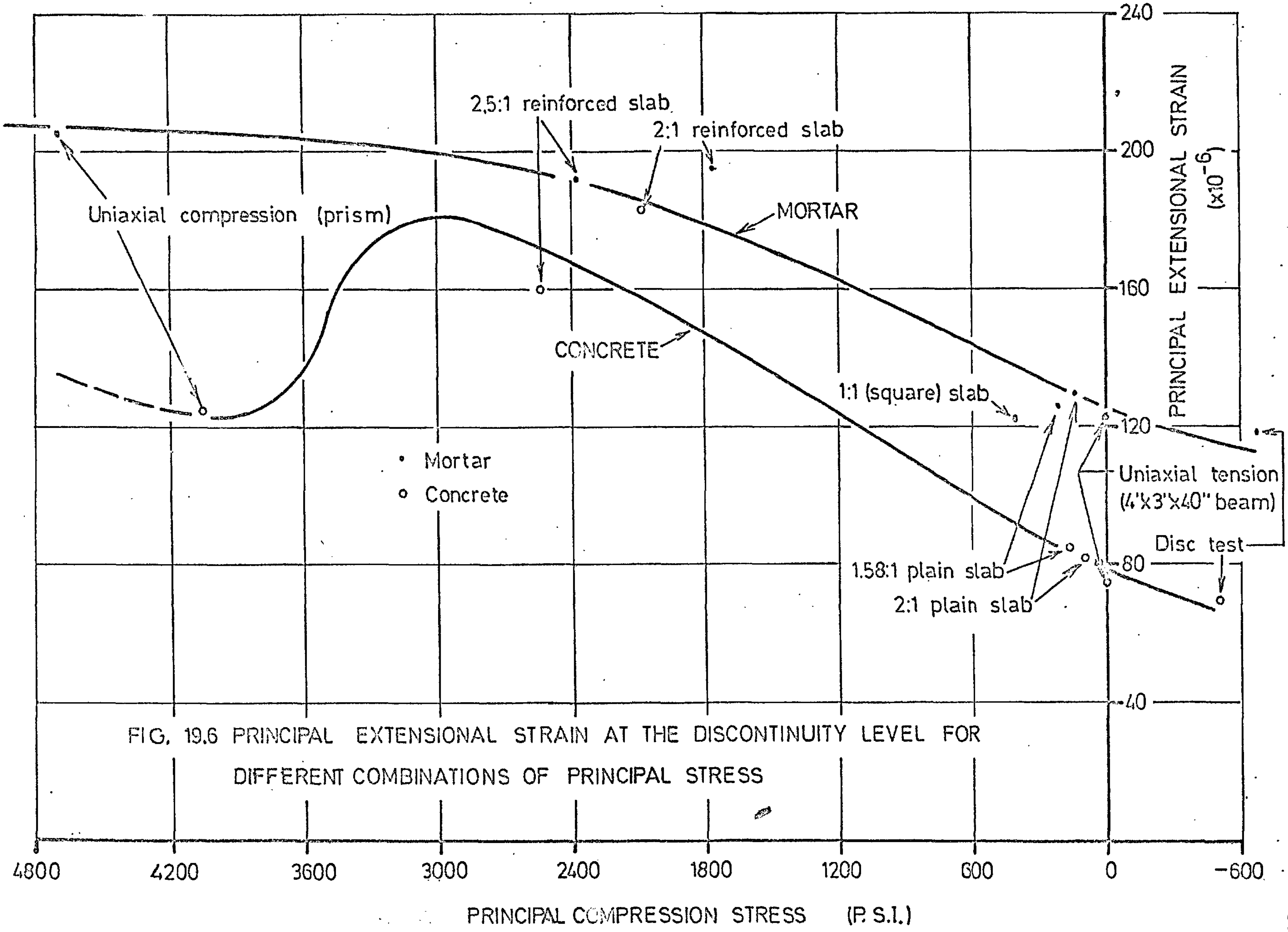

FIG. 19.6 PRINCIPAL EXTENSIONAL STRAIN AT THE DISCONTINUITY LEVEL FOR DIFFERENT COMBINATIONS OF PRINCIPAL STRESS

It is of interest to note the work of Karman and Böker (see Nadai[94] pp 238-244) in tests on marble and sandstone under complex states of stress. In their analyses, they showed that these materials exhibited brittle behaviour under uniaxial states of stress, but under high triaxial compression, these materials became extremely ductile. As mortar is composed chiefly of calcium silicates and silica, thereby having a somewhat similar chemical composition to the materials above, it is reasonable to suggest that it would also exhibit a more ductile behaviour at higher values of volumetric compression thereby resulting in a simultaneous reduction of the value of c_2 in Equation 19.1.

19.2.3 Strains at the Discontinuity Level

Previous investigators have suggested that the failure criterion for concrete in uniaxial tension and compression and other states of stress may be caused by a limiting tensile strain[2,6]. However, as shown in Figure 19.6, the principal tensile strain at the discontinuity level for concrete increases initially as the compression to tension ratio increases and is observed, under certain combinations of tension-compression stress to be very significantly larger than the principal extensional strain for either uniaxial tension or compression. It is thus concluded that, for concrete in biaxial tension and tension-compression, the criterion of failure cannot be expressed in terms of the maximum principal extensional strain.

It is seen that the sharp transition which occurs in the plot of the principal strains (Figure 19.6) corresponds to the transition in the principal stress plot (Figure 19.1). That such a sudden transition must occur in the graph for principal strains will also be evident when considering Bresler and Pister and McHenry and Karni's curves (Figures 19.2 and 19.3) in terms of principal extensional strains. For, if we assume that ν is constant, the extensional strains corresponding to high values of compression to tension ratio will be very much larger than in uniaxial compression with a sudden transition occurring at the location of the sharp curvature in their principal stress plots. The fact that ν actually increases in biaxial tension-compression from that in uniaxial states of stress simply exaggerates this transition (see Section 18.6).

Although in biaxial compression, it is shown that the extensional strain capacity of concrete increases as the mean normal stress, $\left(\frac{\sigma_1 + \sigma_2 + \sigma_3}{3}\right)^{(7)}$, increases, this is not true in biaxial tension-compression states of stress as demonstrated by the large strain capacity seen in Figure 19.6.

For mortar, the extensional strain capacity is observed to generally increase as the mean normal stress or applied compressive stress increases. The general curvature observed is accounted for by the higher values of Poisson's ratio observed in biaxial tension-compression states of stress. Again, it is apparent that a failure criterion for mortar in terms of a limiting extensional strain cannot be used successfully.

19.3 TESTING TECHNIQUES

At this stage, it is of interest to consider the results

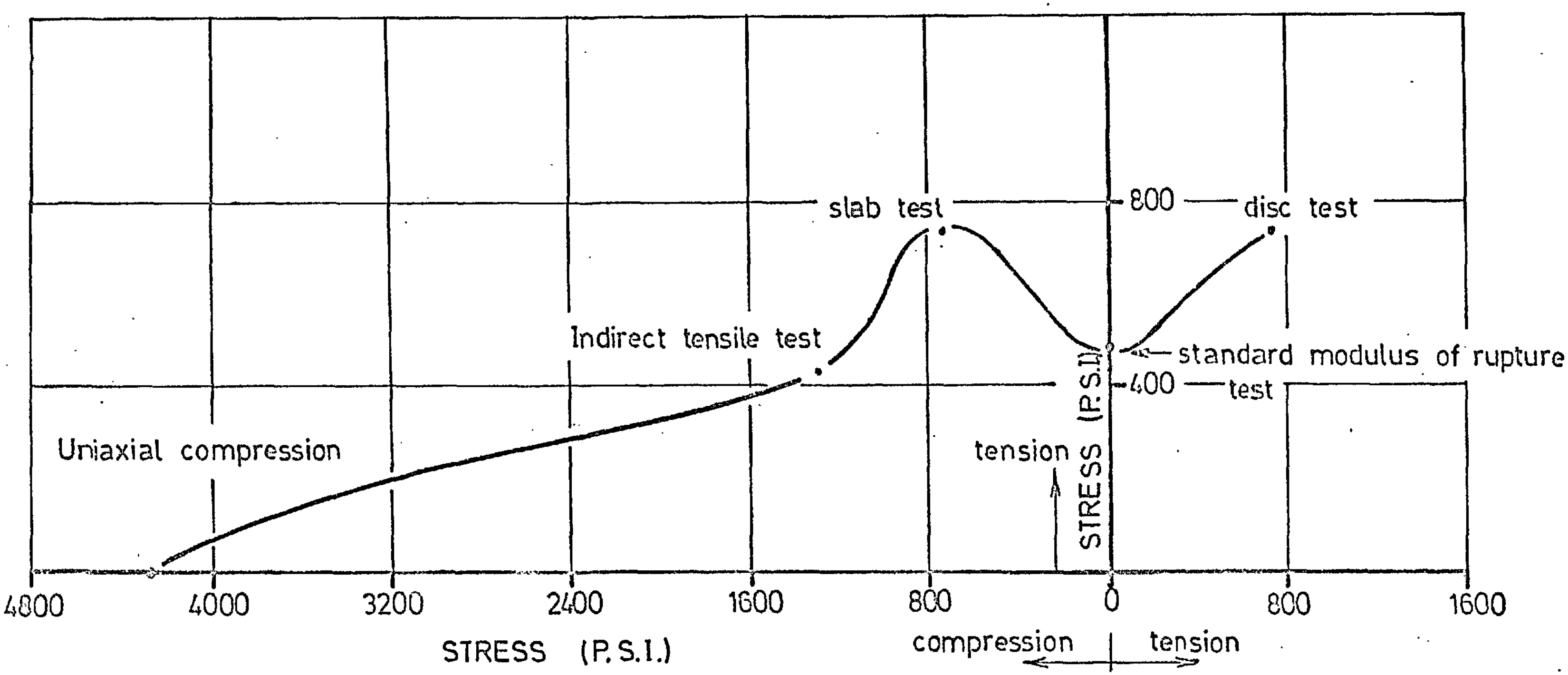

FIG. 19.7 PRINCIPAL STRESS PLOT FROM INITIAL TESTS AT IMPERIAL COLLEGE

obtained in terms of the care employed in achieving a precise and accurate testing technique. In Section 2.1, it was mentioned how, in initial tests at Imperial College, on concrete subjected to various states of stress, unrealistic discrepancies occurred in the surface of failure. A typical example is shown in Figure 19.7. As has been shown in previous sections of this thesis, these discrepancies are accounted for by shortcomings in the original testing techniques. For example, the biaxial tensile strength was too high as the ultimate stress was computed on the basis of the maximum recorded load whereas, in fact, the critical section had exceeded its maximum load carrying capacity at an earlier load stage (see Sections 11.3.1 and 17.4). Similarly, the results of the square slab test (biaxial tension-compression with the tensile stress equal to the compressive stress) are observed to be too large (see Sections 11.3.1 and 14.2.3). For the compression to tension ratio of 3, the ultimate strength was obtained by means of the splitting tensile test. Yet, this test can neither be classified as a flexural nor direct state of stress and, as a result, it is not logical to correlate it directly to the plotted values of the slab, disc and flexural beam tests (see Section 17.5.1).

In Figure 19.1, it is observed that, where the errors in testing technique have been eliminated, the discontinuity level stresses and ultimate failing strengths show a linear relationship with all suspicious discrepancies removed.

19.4 MECHANISM OF FAILURE FOR CONCRETE UNDER DIFFERENT STATES OF STRESS

Whereas the failure criteria for mortar can logically be analyzed from a phenomenological consideration, this is not the case for concrete (see Section 19.2). That different analyses must be considered for mortar and concrete has also been observed by Vile[(7)] from work in biaxial compression. In the following discussion, different failure criteria are suggested for concrete subjected to different states of stress. It is recognized that these criteria do not necessarily apply for mortar.

Although it has been suggested in Section 19.2.2 that the mechanism of fracture and failure for concrete is different in uniaxial tension and compression with the transition stage occurring in the biaxial tension-compression range, it is of interest to consider the different types of failure which are likely to occur under all the different combinations of principal stress. In order to do this, a definition of failure is necessary.

The surface of failure has been defined as the theoretical bound in stress space within which any combination of principal stresses is admissible[(69)]. However, this is not entirely satisfactory as it does not state whether a certain combination of stresses can be applied to a certain volume of concrete and then be removed before loading the same volume of concrete under a different combination of principal stresses. Clearly, if a volume of concrete were loaded in triaxial compression to a load stage where all the internal matrix were pulverized, the effective tensile strength would be reduced to virtually zero. Consequently, for the author's purpose, the surface of failure has been redefined as the theoretical bound in stress space within which the concrete can be loaded and still withstand all combinations of principal stress within the bound. It is considered that the discontinuity level under any combination of principal stresses will defect this load stage.

With the above definition for failure, it is considered that failure of concrete can occur under all possible combinations of principal stress. For concretes where the aggregate is stronger than the cement paste, three different types of failure will probably occur.

(1) tensile bond failure at cement paste-aggregate interface

(2) shear bond failure at cement paste-aggregate interface

(3) internal failure of the cement paste phase

In uniaxial, biaxial, and triaxial tension and over most of the biaxial tension-compression and triaxial tension-tension-compression and tension-compression -compression states of stress, the fracture will be basically initiated by the direct tensile failure of the cement paste-aggregate bond(as discussed in Section 19.2.2). It is appreciated, however, that with certain angular and coarse textured aggregates that failure will occur through sections of the aggregate particles and cement paste phase due to the high bonding strengths(as discussed by Alexander (114)). Nevertheless, these failures will be basically dependant on the maximum principal tensile stress as long as the Poisson's ratio values for the cement paste and aggregate are reasonably the same.

In uniaxial and biaxial compression and biaxial and triaxial tension-compression states of stress where the compression to tension ratio is large, failure is more likely to be initiated by a shearing bond failure at the cement paste-aggregate interface. (see Section 19.2.2) Again, with angular and coarse textured aggregates where the shearing bond strength is improved, increased strengths will be obtained. However, the same mechanism of fracture is still expected to occur with the shearing taking place through the cement paste matrix as well as the aggregate particles. That such a mechanism does exist in uniaxial compression has been demonstrated by examination of different aggregate particles at failure where, cones of mortar or cement paste have been observed at opposite ends of aggregate particles (as discussed in Section 19.2.2). Similar failures have been observed by Vile[7] in biaxial compression tests where these cones tend to become ridges around the aggregate with the plane containing this continuous ridge being coincident with the plane of the applied forces.

Although the above concept of a shearing bond failure would also be expected in triaxial compression where one or two stresses are large in relation to the third, this would not occur under more nearly equal values for the three compressive stresses. For this latter condition, the bond stresses developed will be almost entirely of a compressive nature. As bond failures are possible only when tension or shear stresses are induced at the cement paste-aggregate interface, it will be seen that failure cannot be initiated at such interfaces. As the aggregate is stronger than the cement paste phase, the only possible mechanism of failure will occur by a breakdown of the cement paste structure. Brunauer and Copeland (118) have shown that the tobermorite gel, which is the principal constituent of the cement paste phase, is a highly indeterminate structure composed of an extremely large number of interconnected fibres with minute voids between the fibres. With this structural concept, it is reasonable to suggest that, under very high compressive loads, the individual fibres will fail either by buckling or shearing. The successive failures with the continual redistribution of loads will produce, on the phenomenological level, a ductile behaviour with a relatively large flow of the material. However, to be in accord with the definition for the surface of failure presented above, it is suggested that the beginning of the flow will be classified as the surface of failure for high triaxial compression states of stress.

CHAPTER 20

CONCLUSIONS TO PART III OF THESIS AND SUGGESTIONS FOR FUTURE RESEARCH

20.1 SUMMARY AND CONCLUSIONS

The main conclusions for Part I and II of this thesis have been summarized in Chapter 10. In the present chapter, the main conclusions from Part III of this thesis will be put forward.

Testing techniques

From a review of previous investigations on the strength of concrete under biaxial tension and tension-compression states of stress, it has been shown that there has never been any verification to ensure that the method of test produced the desired state of stress. As observed differences between the results of different investigators are caused by errors in this assumption, it is concluded that for any method of test, a verification of the testing technique is necessary. A model specimen composed of homogeneous, isotropic material with good elasticity properties should be used to verify the testing technique. Aluminium is suggested as beingthe most suitable material.

Testing machine

A testing machine used for the investigation of concrete properties in biaxial tension and tension-compression states of stress was designed in accordance with the recommendations of Part II of this thesis. The method of loading was with both ends effectively pinned, and complete stability was ensured at all loads. The machine was <u>hard</u> for the slab tests (biaxial tension compression states of stress) while being <u>soft</u> for the disc tests (investigation into biaxial tension). It was laterally stiff, free from loose-fitting components and was shown to have good alignment. With a highly sensitive and repeatable load cell firmly attached to the specimen side of the ram, loads were measured precisely and accurately while ram effects were simultaneously eliminated. The load control was also shown to be very good.

Testing technique for plain slab tests

(i) When square or rectangular plates are loaded at diagonally opposite corners while simultaneously being supported at the other two corners, principal biaxial moments of equal magnitude but opposite sign are induced. These produce biaxial tension compression stresses and strains throughout the slab, which are also of equal magnitude.

(ii) When the load and supports points are moved in from the corners, even a small distance, erroneous values are obtained which reflect in high results for the ultimate strength, stress at the discontinuity level and modulus of elasticity.

(iii) With small extended corners whereby the centroid of the load and support points coincide with the intersections of the projected sides of the slab specimen, the strain pattern obtained experimentally agrees very will with theoretical predictions. The small reductions in strain near the corners are a desirable feature as failure of concretes and mortars will then occur away from the corners where the state of stress is known and constant. It is important that the transition curve from the corners to the slab sides be smooth.

(iv) With the loading of diagonally opposite corners of a parallelogram while simultaneously supporting it on the other two corners, principal biaxial moments of different magnitude and opposite sign will be induced which will be constant throughout the slab. This will produce biaxial tension-compression states of stress with the ratio of these stresses being dependent only on the angles of the parallelogram.

(v) From experimental results on slabs with small extended corners, the above theory has been experimentally verified. Again, with the strain being lower in the corners than in the general slab volume, failure of concrete and mortar specimens will occur across a section removed from the corners where the state of stress is known and constant.

Testing technique for disc tests

(i) By the uniform concentric loading of a circular plate while simultaneously supporting it uniformly along the periphery, the central section (that portion which is contained within the circular loading ring) will be subjected to a pure state of biaxial moment which produces biaxial tension on one face and biaxial compression on the opposite face.

(ii) When the concentric support is not positioned at the periphery, but some distance in from the periphery, the theory is no longer valid and the results obtained yield high values for the ultimate strength, stress at the discontinuity level and the modulus of elasticity.

(iii) By using soft packing mediums for both the support and load rings while simultaneously ensuring that the support ring is positioned at the periphery of the circular plate, it is possible to achieve uniform load and support. Under this system of loading, uniform strains are obtained in the central section in accordance with the theory. With the calculated modulus of elasticity being within 1.5% of that obtained for the slab tests, the testing technique is satisfactory as the experimental values of stress and strain are precise and accurate.

Reinforced slab specimens

By reinforcing a parallelogram shaped specimen to resist the tension force from the larger principal moment and by loading and supporting it at the corners as for the plain slab tests discussed above, principal biaxial moments of opposite sign and different magnitude are induced. The principal stresses and strains both before and after cracking are obtained from elastic analysis.

Modulus of elasticity

(i) The modulus of elasticity for concrete and mortar is apparently the same in uniaxial tension and uniaxial compression.

(ii) In biaxial tension-compression, the modulus of elasticity for mortar is the same as in uniaxial states of stress. Although the modulus of elasticity values for concrete in biaxial tension-compression tended to be larger than in uniaxial states of stress, this is not conclusive.

Poisson's ratio

(i) For mortar, Poisson's ratio is the same in uniaxial tension and uniaxial compression.

(ii) In biaxial tension-compression, Poisson's ratio for both mortar and concrete increases to values of the order of twice as large as in uniaxial states of stress.

Mix proportions and age

All factors which influence the short term ultimate strengths in uniaxial states of stress should have a similar influence on the short term ultimate strengths in biaxial tension and tension-compression states of stress.

Failure of concrete

(i) The mechanism of failure of concrete is considered to be different in uniaxial tension from that in uniaxial compression. In uniaxial tension, the failure is probably initiated for concretes with smooth aggregate, by a direct tensile bond failure at the cement paste-aggregate interface. In uniaxial compression, however, the initiation of failure is more likely to be caused by a shearing bond failure at the interface.

(ii) In biaxial tension and most tension-compression states of stress, the failure of concrete is basically dependent on the principal tensile stress.

(iii) In biaxial tension-compression states of stress where the compression to tension ratio is very large, there is an apparent transition in the mechanism of internal breakdown resulting in a sharp curvature in the principal stress plot. This transition is suggested as being due to the bond failures at the cement paste-aggregate interface changing from a direct tensile failure as in uniaxial tension to a shearing type failure as in uniaxial compression.

(iv) The criterion of failure for concrete in biaxial tension and tension-compression states of stress is not due to a constant limiting extensional strain.

Failure of mortar

(i) For biaxial tension and tension-compression states of stress, the principal stress plot produces a straight line for the surface of failure.

(ii) For the above states of stress, the Coulomb internal friction theory satisfies the discontinuity level stresses. For the particular mortar investigated, the intrinsic shear strength at the discontinuity level is 480 p.s.i. and the mortar is basically a brittle material by virtue of its dependence on the volumetric stress.

Discontinuity level stresses and failure strengths

The ratio between the discontinuity level and ultimate failing strengths for both mortar and concrete is very nearly constant for the full range of biaxial tension-compression states of stress, being about 65% for mortar and 55% for concrete.

20.2 SUGGESTIONS FOR FUTURE RESEARCH

Further research into the properties of concrete and mortar in biaxial and triaxial states of stress is necessary for the following reasons:

(i) As the basic elasticity values, the modulus of elasticity and Poisson's ratio, vary under different combinations of principal stress, it is necessary to determine these values so that the design engineer may be better equipped to predict the behaviour of different structures subjected to compex loading conditions.

(ii) Also, a more fundamental investigation into establishing the reasons why the modulus of elasticity and Poisson's ratio are affected by the loading system is required in order that the deformational behaviour for concretes, for which these values have not been measured, can be logically predicted.

(iii) The investigation of the complete failure envelope will provide useful information for establishing the laws which govern the mechanism of failure under different states of stress.

As has been suggested in previous sections of this thesis, the onset of failure for concrete is usually governed by the manner in which the bond between the cement paste and aggregate begins to fracture. A research project directed at establishing the strength of this bond under the various combinations of shear and normal stress is thus considered necessary. Although research in this direction has been conducted by Taylor and Broms (125) at Cornell University, whereby an aggregate slice was placed between two relatively large volumes of mortar with the orientation of the slice being at any one of several angles to the direction of loading, it is difficult to correlate the results of their tests with the actual internal stresses in the concrete. It is more logical when considering the macroscopic structure of concrete to think in terms of layers of cement paste between aggregate particles than in terms of layers of aggregate between volumes of cement paste. By employing the same general test method as that used at Cornell, but using layers of cement paste between large aggregate particles, it should be possible to obtain not only ultimate strengths, but also with the use of surface strain gauges, shear and normal strains in both the aggregate and cement paste phase. With this information, it should then be possible to estimate with reasonable accuracy, the magnitude and type of internal stresses in the aggregates and the cement paste phase as well as at the interfaces and from this, establish conclusively, the manner in which failures in concrete initiate and propagate under the different combinations of principal stresses.

REFERENCES

1. LACHANCE, L. The effect of end restraint, shape and size on the elastic properties and failure characteristics of concrete specimens under compression. M.Sc. Thesis, University of London, 1962.

2. WARD, M.A. The testing of concrete materials by precisely controlled uni-axial tension. Ph.D. Thesis, University of London, 1964.

3. ANSON, M. An investigation into a hypothetical deformation and failure mechanism of concrete. Ph.D. Thesis, University of London, 1962.

4. ANSON, M. An investigation into a hypothetical deformation and failure mechanism for concrete. Magazine of Concrete Research, Cement and Concrete Association, Vol 16, no. 47, June, 1964 pp. 73-82.

5. BAKER, A.L.L. An analysis of deformation and failure characteristics of concrete. Magazine of Concrete Research, Cement and Concrete Association, Vol. 11, No. 33, Nov. 1959, pp. 119-128.

6. ROBINSON, G. S. The failure mechanism of concrete with particular reference to the biaxial compressive strength. Ph.D. Thesis, University of London, 1964

7. VILE, G.W.D. Thesis to be presented to the University of London for the degree of Ph.D.

8. BRITISH STANDARDS INSTITUTION B.S. 1610:1964 Methods for the load verification of testing machines, London pp. 21.

9. BRITISH STANDARDS INSTITUTION B.S. 1881:1952 Methods of testing concrete, London pp. 61.

10. SIGVALDASON, O.T. The influence of the testing machine on the compressive strength of concrete. Symposium on Concrete Quality, November, 1964. Cement and Concrete Association 1965.

11. NEWMAN, K. and SIGVALDASON, O.T. Testing machine and specimen characteristics and their effect on the mode of deformation, failure and strength of materials. To be presented at a convention on Developments in Materials Testing Machine Design, Institution of Mechanical Engineers, Manchester, September 1965.

12. SIGVALDASON, O. T. Spherical seating behaviour in testing machines. The Engineer (to be submitted for publication).

13. SIGVALDASON, O. T. The influence of testing machine characteristics on the cube and cylinder strength of concrete. The Engineer (to be submitted for publication).

14. NEWMAN, K. The structure and engineering properties of concrete. International Symposium on the Theory of Arch Dams. Southampton, April, 1964.

15. SWINDELLS, B. and Evans, J.C. – Measurement of load by elastic devices. Notes on Applied Science No. 21, National Physical Laboratory.

16. SWINDELLS, B., GOYMOUR, E.P. Measuring compressive forces accurately. Engineering., 4 October, 1963 pp. 418-419.

17. SWINDELLS, B., GOYMOUR, E.P., NPL's improved force measuring device. Engineering, 7 August, 1964 p. 185

18. COLE, D.G. - The relationship between the apparent variation in compressive strength of concrete cubes and the inaccuracies found in the calibration of compression testing machines. Symposium on Concrete Quality. Nov., 1964, Cement and Concrete Association 1965.

19. WRIGHT, P.J.F. Statistical methods in concrete research Magazine of Concrete Research, 1954 Vol. 5., No. 15 pp. 139-149.

20. DAVIES, O.L. Statistical methods in research and production 2nd Edition London, Oliver and Boyd. 1949.

21. NEWMAN, K. and LACHANCE, L. The testing of brittle materials under uniform uniaxial compressive stress Prodeedings. American Society for Testing and Materials, Vol 65, 1965.

22. WRIGHT, P.J.F. Compression testing machines for concrete. The Engineer, Vol. 203, April, 1957.

23. BARCLAY, M. Which cube crusher? Ove Arup and Parthers News-letter No. 20, 1964 pp. 39-40.

24. GRAHAM, G and MARTIN, F.R. HEATHROW: The construetion of high grade quality concrete paving for modern transport aircraft. Journal of the Institution of Civil Engineers, Vol. 26, No. 6, April 1946 pp. 117-190.

25. KILIAN, M.G. Le contrôle de la qualité des bétons utilisés sur les chantiers des grands barrages. Annales de l'Institut technique du bâtiment et des Travaux Publics, Vol 7, No. 74 February 1954 pp. 159-192.

26. AMERICAN SOCIETY FOR TESTING AND MATERIALS. Report on investigation of mortars by seven laboratories. Proceedings of the American Society for Testing and Materials. Vol. 40 1940 pp. 222-223.

27. AMERICAN SOCIETY FOR TESTING AND MATERIALS. Method of test for compressive strength of moulded concrete cylinders. A. S. T. M. C39-64.

28. TARRANT, A.G. Measurement of friction at very low speeds. The Engineer Vol. 198 No. 5142 pp. 262-3.

29. TARRANT, A.G. Frictional difficulty in concrete testing. The Engineer Vol. 198 No. 5159. pp 801-802.

30 DWYER, J.R. Effect of departure from plane-ness of varying surfaces on compressive strength of 2 in. mortar cubes. Proceedings of the American Society for Testing and Materials Vol. 36 Part 2 1936 pp. 351-356.

31. [illegible]NI[illegible]ONT, G. Precision and accuracy of test methods. A.S.T.M. Special Technical Publication No. 103 - 194[illegible] pp. 13-35.

32. HOFF, N.J. Buckling and stability. Journal of the Royal Aeronautical Society, Vol. 58, 1954 pp. 1-52.

33. BERNHARD, R. K. Influence of the elastic constant of tension testing machines. American Society for Testing and Materials, Bulletin No. 88, October 1937, pp. 14-15.

34. BARNARD P.R. Researches into the complete stress-strain curve for concrete. Magazine of Concrete Research, Cement and Concrete Association. Vol 16, No. 49, December 1964, pp. 203-210.

35. TURNER, P.W. and BARNARD P.R. Stiff constant strain rate testing machine. The Engineer, Vol. 214, No. 5557, 27th July, 1962, pp. 146-148.

36. BROCK, G. Concrete: complete stress: strain curves, Engineering 4 May, 1962, Vol. 193 pp. 606-608.

37. HINDE, P.B. Testing machine stiffness problem. The Engineer 26th June, 1964, Vol. 217, pp. 1124-1127.

38. CHILVER, A.H. The instability of testing machines. Proceedings of the Institution of Mechanical Engineers Vol. 169, No. 25 1955 pp. 407-18.

39. FLINT, A.R. Reply to paper "The instability of testing machines" by A. H. Chilver. Proceedings of the Institution of Mechanical Engineers. Vol. 169, No. 25 1955 pp. 414-415.

40. NEWMAN, K. Concrete control tests as a measure of the properties of concrete. Symposium on Concrete Quality, Nov. 1964. Cement and Concrete Association, 1965.

41. DAVIS, H.E., TROXELL, G.E. and WISKOCIL, C.T. - The testing and inspection of engineering materials. McGraw-Hill, New York, 1941.

42. L'HERMITE, R. Present day ideas of concrete technology R.I.L.E.M. Bulletin No. 18, June, 1954.

43. McHENRY, D. and SHIDELER, J. J. Review of data on effect of speed on mechanical testing of concrete. American Society for Testing and Materials, 1956. Special Technical Publication No. 185 pp. 72-82.

44. RUSCH, H. Physical problems in the testing of concrete. Cement-Kalk-Gips. Vol. 12, No. 1 1959. pp. 1-9 London, Cement and Concrete Association, 1960. Library Translation No. 86, p. 21.

45. EVANS, R. H. Extensibility and modulus of rupture of concrete. The Structural Engineer Vol. 24 Dec. 1946 pp. 636-659.

46. TIMOSHENKO, S. Strength of materials. Vol I 3rd Edition, March 1955. New Jersey, D. Van Nostrand Company, Inc.

47. STEEL CONSTRUCTION. Manual of the American institute of steel construction. Fifth Edition p. 373.

48. WRIGHT, P.J.F. The effect of the method of test on the flexural strength of concrete, Magazine of Concrete Research No. 11 October 1952 pp. 67-76.

49. SCHUYLER, M. Spherical seatings. Proceedings A.S.T.M. Vol. 13, 1913 pp. 1004-1018.

50. TEMPLIN, R.L. Hydraulically supported spherically seated compression testing machine platens. Proceedings A.S.T.M. Vol. 42, 1942 pp. 968-76.

51. HUBER, A.W. Fixtures for testing pin-end columns A.S.T.M. Bulletin 234, December, 1958. pp. 41-45.

52. VINEALL, G.J. Molybdum disulphide, Institution petroleum. Rev. V.17 N.195 Mar. 1963 pp. 80-86.

53. WOOD, K. B. Molybdenum disulphide as a lubricant, Metal progress V.81, May 1962, pp. 140.

54. STOCK, Arthur J. Graphite, molybdenum disulphide and P.T.F.E.- a comparison. Journal of the American Society of Lubrication Engineers V.19 N.8 Aug. 1963 pp. 333-8.

55. BRAITHWAITE, E.R. "Graphite and molybdenum disulphide". Nuclear Engineering, March 1957.

56. JONES, R. The development of microcracks in concrete. Rilem Bulletin No. 9 Dec. 1960 pp. 110-114.

57. BLAKEY, F.A. Some considerations of the cracking or fracture of concrete. Civil Engineering and Public Works Review, Vol. 52, No. 615, September 1957, pp. 1000-3.

58. NEVILLE, A.M. Some aspects of the strength of concrete. Civil Engineering and Public Works Review, Vol. 54, October 1959, pp. 1153; November 1959 pp. 1309; December 1959, pp. 1435.

59. NEWMAN, K. The effect of water absorption by aggregates on the water/cement ratio of concretes. Magazine of Concrete Research No. 33, Nov. 1959 pp. 135-142.

60. BRITISH STANDARDS INSTITUTION. British standard 882: 1954, Concrete aggregate from natural sources. London 1954.

61. ROAD RESEARCH LABORATORIES. Road note No. 4, Design of concrete mixes. 2nd Edition 1960.

62. WILLIAMSON, G.R. An investigation of standard concrete cylinders. Journal of American Concrete Institute Feb. 1964 V.61 pp. 151-153.

63. GLUCKLICH, J. The influence of sustained loads on the strength of concrete. Rilem Bulletin No. 5 December, 1959 pp. 14-17.

64. WAGNER, W.K. Effect of sampling and job curing procedures on compressive strength of concrete. A.S.T.M. Journal August 1963 pp. 629-34.

65. BLAKEY, F.A. and BERESFORD, F.D. Tensile strains in concrete, Part I, C.S.I.R.O. Report C2.2-1, Melbourne, 1953.

66. BLAKEY, F. A. and BERESFORD, F.D. Tensile straind in concrete Part II, C.S.I.R.O. Report C2.2-2 Melbourne, 1955.

67. TIMOSHENKO and WOINOWSKY-KRIEGER. Theory of plates and shells. 2nd Edition McGraw Hill Book Company.

68. NEWMAN, K. The influence of mix proportions and loading characteristics on the mode of failure of concrete. Thesis to be submitted to the University of London for the degree of Ph.D.

69. McHENRY, DOUGLAS and KARNI, JOSEPH. Strength of concrete under combined tensile and compressive stress. A.C.I. Journal April, 1958 V. 54 pp. 829-40.

70. BRESLER, B., and PISTER, K.S. Failure of plain concrete under combined stresses. Transactions A.S.C.E. V.122 1957 p. 1049-59.

71. BRESLER, B., and PISTER, K.S. Strength of concrete under combined stresses, A.C.I. Journal Sept. 1958. Vol. 55 Proceedings pp. 321-45.

72. TSUBOI, Y. SUENAGA, Y. Experimental study on failure of plain concrete under combined stresses. Part 3, University of Tokyo, February, 1960.

73. SUNDARA RAJA IYENGAR, K.T. CHANDRASHEKHARA, K. and KRISHNASWAMY, K.T. On the determination of true tensile strength of concrete, Rilem Bulletin 21, December 1963 pp. 39-45.

74. NISHIZAWA, NORIAKI. Strength of concrete under combined tensile and compressive loads. Japan Cement Engineering Association, Review of the Fifteenth General Meeting held in Tokyo, May, 1961, pp. 126-131.

75. SMITH, G. M. Failure of concrete under combined tensile and compressive stresses, A.C.I. Journal, October 1953. Vol. 50 Proceedings pp. 137-140.

76. CARNEIRO, F.L.L.B., BARCELLOS, A. Concrete tensile strength, R.I.L.E.M. No. 13 March 1953.

77. AKAZAWA, T. Tension test method for concrete. R.I.L.E.M. No. 16 November 1953.

78. A. S. T. M. Tentative standard C-T 1962 splitting tensile strength of moulded concrete cylinders.

79. WRIGHT, P. J. F. Comments on the indirect tensile test on concrete cylinders. Magazine of concrete research, Vol. 7, No. 20 July, 1955 pp. 87-96.

80. HALABI, A., Recherches expérimentales systématiques sur la résistance à la traction des bétons. Revue des Matériaux. No. 561 June 1962 pp. 168-180.

81. MITCHELL, N. B. The indirect tension test for concrete. A. S. T. M. Materials Research and Standards, Vol. 1 Oct. 1961 pp. 780-788.

82. NILSSON, A. The tensile strength of concrete determined by splitting tests on cubes. R. I. L. E. M. Bulletin No. 11 1961.

83. DURELLI, A. J., MORSE, S., PARKS, V. The theta specimen for determining tensile strengths of brittle materials. Materials Research and Standards. Vol. 2 February, 1962 pp. 114-117.

84. Discussion of Paper by DOUGLAS McHENRY and JOSEPH KARNI. Strength of concrete under combined tensile and compressive stress by Louis P. Brice, A Coüard, K. W. Johansen, Gonzalo de Navacerrada Y Farias and Authors. A. C. I. Proceedings, Vol. 54 pp. 1301-08.

85. Discussion of Paper by B. BRESLER and K. PISTER. Failure of plain concrete under combined stresses. by F. A. Blakey and F. D. Beresford, Paul Rice, Henry J. Cowan, and Authors. Transactions A. S. C. E. V. 122, 1957 pp. 1060-68.

86. Discussion of Paper by B. BRESLER and K. PISTER. Strength of concrete under combined stresses. by C. J. Bernhardt, Michael Chi, A. Coüard, K. W. Johansen and Authors. A. C. I. Proceedings, Vol 55 pp. 1035-46.

87. MILLS, A. P. Materials of construction. London, Blackie and Son, Ltd., 1915.

88. DAVIS, R. E. Discussion to Paper Compression flexure and tension tests of plain concrete by H. F. Gonnerman and E. C. Schuman. Proc., A. S. T. M., Vol. 28, Part II, 1928, p. 527.

89. SCHUMAN, L., and TUCKER, J. Tensile and other properties of concretes made with various types of cement. U. S. National Bureau of Standards Research Paper, R. P. 1552, Vol. 31, 1943 pp. 107-124.

90. KAPLAN, M.F. Strains and stresses of concrete at initiation of cracking and near failure. Journal A.C.I. Vol. 60.

91. ROBERTSON, R.G. and ROBERTSON, D.C. Some investigations into the elastic properties of concrete. Trans. South African Inst. of Civil Engineers, Vol. 6 September, 1956.

92. HUMPHRIES, R. Direct tensile strength of concrete. Civil Engineering and Public Works Review. Vol. 52. No. 614, August 1957. pp. 882 - 883.

93. FREUDENTHAL, A. "The inelastic behaviour of engineering materials and structures". 1st Edition - John Wiley & Sons, Inc.

94. NADAI, A. Theory of flow and fracture of solids, Vol. 1 McGraw - Hill Book Company, Inc.

95. HSU, Thomas T. C., SLATE, FLOYD, O., STURMAN, GERALD, M., and WINTER, GEORGE., Microcracking of plain concrete and the shape of the stress strain curve. A. C. I. Journal, Proceedings V.60, No. 2, February, 1963 pp. 209-224.

96. HSU, Thomas T. C. Mathematical Analysis of Shrinkage Stresses in a model of hardened concrete. A.C.I. Journal, Proceedings V.60 No. 3 Mar, 1963 pp. 371-390.

97. SLATE, F. O., and OLSEFSKI, S. X-Rays for study of internal structure and microcracking of concrete, A.C.I. Journal, Proceedings, V.60 No. 5 May, 1963.

98. BERG, O. Y. The problem of strength and plasticity of concrete. Translation as Road Research Library Communication No. 165, Department of Scientific and Industrial Research of the U.K. London, 1951.

99. JONES, R. "A method of studying the formation of cracks in a material subjected to stress". British Journal Applied Physics Vol. 3., July, 1952 pp. 229-32.

100. BLAKEY, F. A., Mechanism of fracture of concrete, Nature. Vol. 170, December, 1952 pp. 1120.

101. RUSCH, H. Physical problems in the testing of concrete. Cement and Concrete Association Library Translation No. Cj. 86 from Zement-Kalk-Gips. (Weisbaden) Vol. 12, No. 1 Jan. 1959 pp. 1-9.

102. RICHART, F. E. BRANDTZAEG, A., and BROWN, R.L., "A study of the failure of concrete under combined compressive stresses". Bulletin No. 185, University of Illinois, Engineering Experimental Station, Nov. 1928.

103. BALMER, C. G. Shearing strength of concrete under high triaxial stress. Laboratory Report No. SP-23, U.S. Department of the Interior, Bureau of Reclamation, October 1949.

104. BELLAMY, C. J. Strength of concrete under combined stress, Journal of the American Concrete Institute. October 1961. Proceedings V.58 pp. 367-380.

105. CAMPBELL-ALLAN D. Strength of concrete under combined stresses. Constructional Review. (Sydney) V.35 No. 4, April, 1962.

106. AKROYD, T. N. W. "Failure mechanism of saturated concrete. Engineering, Vol. 191, No. 4960. May 12, 1961, pp. 658-659.

107. AKROYD, T. N. W. Concrete under triaxial stress. Magazine of Concrete Research, Vol. 13, No. 39, November, 1961.

108. COWAN, H. J. The strength of plain, reinforced and prestressed concrete under the action of combined stresses. Mag. Concr. Res. Vol. 5 1953 pp. 75-86.

109. FULTON, F. S. Concrete technology. A South African Handbook. The Portland Cement Institute. Johannesburg, 1961.

110. TIMOSHENKO, S., and GOODIER, J. N. Theory of elasticity. 2nd Edition, McGraw-Hill Book Co., Inc.

111. THOMSON and TAIT. Treatise on natural philosophy, Vol. 1 part 2, 1883, p. 203.

112. NADAI, A. Elastische platten. Berlin, 1925, p. 42.

113. FAIRMAN, S. and CUTSHALL, C. S. Mechanics of materials. John Wiley & Sons, Inc. New York.

114. ALEXANDER, K. M. Strength of the cement-aggregate bond. Proceedings of the American Concrete Institute. V. 56 no. 5 Nov. 1959. pp. 377-390.

115. TODD, J. D. The determination of tensile stress-strain curves for concrete. Proceedings, Inst. of Civil Engineers. Vol 4, No. 2, March 1955, pp. 202-211.

116. VILE, G. W. D. and SIGVALDASON, O. T. Reply to paper "Strength of concrete under biaxial compression" by K. T. Sundara, Raja Iyengar, K. Chandrashekhara and K. T. Krishnaswamy. A. C. I. Journal, September, 1965.

117. JONES, R. and KAPLAN, M. F. Effect of coarse aggregate on the mode of failure of concrete in compression and flexure, Magazine of Concrete Research (London) V. 9. No. 26, August 1957, pp. 89-94.

118. BRUNAUER, S. and COPELAND, L. E. The chemistry of concrete American Scientist, April 1964, pp. 80-91.

119. ALEXANDER, K. M. A study of concrete strength and mode of fracture in terms of matrix, bond and aggregate strengths. Tewksbury Symposium on Fracture, University of Melbourne, August 1963, 27 pp.

120. HSU, T. C., and SLATE, F. O. Tensile bond strength between coarse aggregate and cement paste or mortar. A.C.I. Journal, Proceedings V.60, No. 4, April 1963, pp. 465-486.

121. SUNDARA RAJA IYENGAR, K. T., CHANRASHEKHARA, K. and KRISHNASWAMY, K. T. Strength of concrete under biaxial compression. Proceedings Journal of the American Concrete Institute, February, 1965.

122. TIMOSHENKO, S. Strength of materials. Vol. II 1956, New Jersey, D. Van Nostrand Company, Inc.

123. BENNETT, E.W., and KHILJI, Z. M. The effect of some properties of the coarse aggregate in hardened concrete. Journal, British Granite and Whinstone Federation Vol. No. 2 Autumn 1963 and Vol. 4 No. 1, Spring 1964.

124. GUEST, J. J., "On the strength of ductile materials under combined stress". Philosophical Magazine, Vol. 50, July, 1900, pp. 69-132.

125. TAYLOR, Michael A. and BROMS, BENGT B. Shear bond strength between coarse aggregate and cement paste or mortar. A.C.I. Journal, Proceedings V. 61, No. 8, August, 1964 pp. 939-957.

APPENDIX A

STRENGTH RESULTS (p.s.i.) OF TEST SERIES' FOR DETERMINING THE INFLUENCE OF THE TESTING MACHINE CHARACTERISTICS ON THE STRENGTH AND MODE OF FAILURE OF

COMPRESSION SPECIMENS

(see Chapter 9)

TEST SERIES 1

(FULL CONTACT)

NO LUBRICANT

	3" RADIUS	5" RADIUS	7" RADIUS
	4560	4910	4810
	4560	4790	4700
	4440	4940	4700
	4550	4480	4820
	4910	4930	5050
	4990	4770	4940
	5100	4900	4740
	4850	5200	5280
	4930	4710	4740
	4880	4840	4800
	4850	4950	4880
	4930	5090	5010
AVERAGE	4796	4876	4872

STAUFFER'S GREASE

	3" RADIUS	5" RADIUS	7" RADIUS
	4770	4710	4200
	4640	4655	4960
	4930	4760	4620
	4770	4625	4710
	4920	4715	4610
	4800	4770	4470
	4850	5130	4840
	5150	4925	4690
	4970	4340	4420
	4790	4670	4470
	4750	4825	4590
	4940	4990	4560
AVERAGE	4857	4760	4593

ROCOL M.G.

	3" RADIUS	5" RADIUS	7" RADIUS
	4640	4690	4400
	4560	4990	4600
	4430	4520	4090
	4600	4630	4490
	4520	5000	4510
	4610	4780	4600
	4590	4850	4400
	4910	5210	4720
	4660	4700	4630
	4340	4510	4390
	4280	4900	4720
	4900	4930	4550
AVERAGE	4587	4809	4508

TEST SERIES 2

	3" RADIUS SEATING WITH RHODINA 2 GREASE	3" RADIUS SEATING NO LUBRICANT	5" RADIUS LINE CONTACT RHODINA 2 GREASE	7" RADIUS SEATING RHODINA 2 GREASE
	4305	4760	4880	4800
	4450	4855	5080	4670
	4870	4960	4840	4720
	4665	4880	5165	4545
	4735	4755	4720	4020
	4400	4735	4665	4575
	4730	4935	4910	4725
	4575	4950	5170	4570
	4650	4820	5105	4895
	4900	4865	4830	4830
	4830	5030	4710	4750
	4710	5050	4815	5070
AVERAGE	4652	4883	4907	4672

TEST SERIES 3

DISPLACEMENT OF SEATING AXIS WITH REFERENCE TO SPECIMEN AXIS
5" RADIUS FULL CONTACT SPHERICAL SEATING

NO LUBRICANT ON SEATING INTERFACE

	$\frac{1}{4}$" TOWARDS CAST FACE	0	$\frac{1}{4}$" TOWARDS BOTTOM FACE
	4900	5000	4660
	4680	4650	4570
	4490	4480	4660
	4900	4660	4790
	4850	4900	4940
	4550	4580	4780
	4620	4930	5290
	4800	4980	5000
	4880	5170	5070
	4400	4690	4490
	4700	4650	4750
	4650	4390	4720
AVERAGE	4702	4757	4727

TEST SERIES 3 (CONT$_{D}$)

GRAPHITE - TALLOW MIXTURE ON INTERFACE

	3270	4220	4120
	3400	3960	4540
	3540	4250	4450
	3750	4580	4110
	3430	4480	4160
	3740	4660	4350
	3800	4470	4110
	3320	4390	4150
	4230	4330	4420
	3530	4340	4240
	3680	4420	4110
	3750	4290	3620
AVERAGE STRENGTH	3620	4366	4198

TEST SERIES 4

	DISPLACEMENT OF SPHERICAL SEATING AXIS WITH REFERENCE TO SPECIMEN AXIS					
	TOWARDS CAST FACE		TOWARDS BOTTOM FACE			
	$\frac{3}{8}$"	0	1/16"	$\frac{1}{8}$"	$\frac{1}{4}$"	$\frac{1}{2}$"
SERIES 4A:5" RADIUS FULL CONTACT SEATING						
No Lubricant on Seating Interface						
		4490				
		4610				
		4700				
		4710				
		5040				
		5010				
		5190				
		4790				
AVERAGE STRENGTH		4820				
GRAPHITE TALLOW MIXTURE ON SEATING INTERFACE						
	3080	4400		4500	3970	3450
	3475	4730		4640	4210	3400
	3480	4480		4440	4500	3390
	3700	4490		4460	4190	3640
	3900	4800		4700	4490	3080
	3800	4860		4840	4160	3890
AVERAGE STRENGTH	3570	4630		4600	4255	3475

TEST SERIES 4 (CONTD)

SERIES 4B 3" RADIUS SEATING
No lubricant on Seating Surface

	3/8"	0	1/16"	1/8"	1/4"	1/2"
		4590				
		4810				
		4860				
		4490				
		4940				
		4760				
		4610				
		4690				
AVERAGE STRENGTH		4719				
ROCOL M.G. ON SEATING INTERFACE						
	3550	4290	4510	4280		3370
	3620	4110	4750	4810		2910
	3420	4240	4460	4100		3100
	3590	4620	4400	4270		3610
	3390	4540	4510	4780		3710
	3480	4110	4570	4720		
AVERAGE STRENGTH	3508	4318	4533	4493		3340

TEST SERIES 5

	4" CUBES	6" CUBES	6" Ø x 12" LONG CYLINDERS
BOTH ENDS EFFECTIVELY FIXED			
1st MIX	4840	4320	3330
	4860	4270	2905
	4670	4130	3270
	4410	4200	3425
2nd MIX	4990	4940	3730
	4610	4695	3615
	5350	5045	3775
		4475	3870
3rd MIX	4410	3660	3210
	4530	3770	3145
	4520	3770	3060
	4500	3790	3190
AVERAGE STRENGTH	4723	4258	3377
1 END PINNED, 1 END FIXED			
1st MIX	4610	3695	3090
	4700	4130	3195

TEST SERIES 5 (CONTD)

	4" CUBES	6" CUBES	6" Ø x 12" LONG CYLINDERS
1st MIX	4360	4000	3300
	4580	4030	3200
2nd MIX	5120	4640	3620
	4720	4635	3580
	4920	4610	3570
		4620	3800
3rd MIX	3890	3660	3150
	4130	3675	3085
	4250	3660	2880
	4130	3520	2995
AVERAGE STRENGTH	4527	4073	3289

BOTH ENDS EFFECTIVELY PINNED

	4" CUBES	6" CUBES	6" Ø x 12" LONG CYLINDERS
1st MIX	4380	3760	3200
	4560	4400	3400
	4250	4105	3195
	4560	4075	3400
2nd MIX	5010	4570	3920
	5150	4440	3390
	4760	4465	3815
	4950	4380	3930
3rd MIX	3950	3700	2970
	3850	3520	3285
	3980	3830	3170
	4030	3650	3240
AVERAGE STRENGTH	4453	4075	3410

TEST SERIES 6

BOTH ENDS EFFECTIVELY FIXED

	4" CUBES	6" CUBES	6" Ø x 12" LONG CYLINDERS
1st MIX	5085	4090	3960
	4640	4390	4225
	6150	4525	4000
	5410	4090	3850
2nd MIX	6195	5745	4925
	6145	5195	4420
	5775	5720	4235
	6180	5650	4650
3rd MIX	5950	5545	4500
	5560	5530	4660
	6090	5350	4560
	6085	5740	4735
AVERAGE STRENGTH	5772	5131	4397

TEST SERIES 6 (CONTD)	4" CUBES	6" CUBES	6" Ø x 12" CYLINDERS
BOTH ENDS EFFECTIVELY FIXED			
1st MIX	5085	4090	3960
	4640	4390	4225
	6150	4525	4000
	5410	4090	3850
2nd MIX	6195	5745	4925
	6145	5195	4420
	5775	5720	4235
	6180	5650	4650
3rd MIX	5950	5545	4500
	5560	5530	4660
	6090	5350	4560
	6085	5740	4735
AVERAGE STRENGTH	5772	5131	4397
1 END PINNED, 1 END FIXED			
1st MIX	4960	3855	4075
	4590	4095	4060
	4900	3935	3675
	4795	4160	4015
2nd MIX	5110	5110	4150
	5895	5545	4600
	6400	5770	4400
	6260	5300	4330
3rd MIX	5390	5140	4600
	5500	5170	4420
	5510	5485	4460
	5665	5573	4810
	5414	4928	4300
BOTH ENDS EFFECTIVELY PINNED			
1st MIX	5010	3715	4055
	4990	4040	4365
	4810	3795	4260
	4735	4150	4100
2nd MIX	5585	5420	4820
	5560	5490	4510
	5520	5400	4560
	5510	5420	4505
3rd MIX	4990	5235	4690
	5645	4875	4575
	5205	5080	4230
	5725	5200	4260
AVERAGE STRENGTH	5274	4818	4411

TEST SERIES 7

	50 TON AVERY COMPRESSION MACHINE	500 TON AVERY COMPRESSION MACHINE
	4510	4440
	4950	4750
	4760	4590
	4390	4835
	4690	4410
AVERAGE STRENGTH	4660	4605

TEST SERIES 8

	TOTAL VIBRATION OF 90 SECONDS	TOTAL VIBRATION OF 10 SECONDS
NO LUBRICATION ON SEATING INTERFACE		
	5000	4705
	5090	4555
	5115	4810
	5040	4900
	5270	4465
	5030	4825
	4990	4620
	5005	4755
	4970	4530
	4880	4785
	5080	4960
	5150	4660
AVERAGE STRENGTH	5052	4714
AMSLER GREASE ON SEATING INTERFACE		
	5100	4375
	4720	4185
	4780	4470
	4605	4380
	4840	4410
	4760	4300
	5000	4260
	4860	4355
	4820	4295
	4540	4000
	4890	4295
	4775	4400
AVERAGE STRENGTH	4808	4310

TEST SERIES 9

1st MIX	3" RADIUS SEATING	5" RADIUS SEATING (FULL CONTACT)	7" RADIUS SEATING
	4750	4990	5725
	4615	5465	4950

TEST SERIES 9 (CONTD)

	3" RADIUS SEATING	5" RADIUS SEATING (FULL CONTACT)	7" RADIUS SEATING
1st MIX	4640	5310	5355
	4770	5085	5385
	4830	5745	5070
	5040	5200	5070
AVERAGE STRENGTH	4774	5299	5259
2nd MIX	6580	6500	6660
	6470	6900	6605
	6510	6690	6900
	6220	6535	6880
	6255	6910	6930
	6310	6790	6580
AVERAGE STRENGTH	6408	6721	6759
3rd MIX		7820	7770
		8370	8290
		8050	8100
		7880	7760
		7910	7890
		8170	7670
		8030	8100
		8300	7680
		8100	7910
		8340	7990
		8040	8180
		8092	7940

APPENDIX B

LOAD AND STRAIN DATA FOR SLAB, DISC BEAM AND DIRECT TENSION AND COMPRESSION SPECIMENS.

MORTAR BEAM (4" x 3" x 40")

APPLIED LOAD (LBS.)	STRAIN $(x10^{-6})$							
	GAUGE NUMBERS							
	1	2	3	4	5	6	7	8
Initial Position								
0	0	0	0	0	0	0	0	0
90	2.0	12.6	12.9	2.4	2.0	11.8	11.3	2.4
180	4.8	27.4	29.2	5.0	3.9	25.9	25.5	4.8
270	7.6	42.0	43.7	7.2	6.7	40.0	39.8	7.8
360	10.3	57.3	60.1	10.0	8.7	54.5	54.9	10.3
450	12.9	72.8	75.8	12.6	11.8	68.8	69.7	13.1
540	15.0	87.6	91.5	15.0	13.3	83.5	84.1	15.5
630	17.9	103.5	107.4	17.4	15.7	98.7	100.2	18.1
720	20.2	118.5	123.9	20.0	18.5	113.4	115.8	20.7
Final Position								
0	0	0	0	0	0	0	0	0
90	2.0	12.8	12.5	2.0	1.7	12.8	12.8	2.7
180	4.6	27.8	28.5	4.9	3.6	27.5	27.2	5.6
270	7.6	42.6	44.0	7.2	6.6	41.0	42.3	7.6
360	9.1	57.6	61.0	10.1	8.8	56.0	56.7	10.8
450	11.8	72.7	76.6	12.8	10.8	70.1	71.1	13.1
540	14.5	87.6	92.3	14.8	12.8	84.2	85.5	16.0
630	17.0	103.1	108.4	17.4	14.7	97.9	99.5	18.4
720	19.9	118.6	125.2	19.4	17.4	112.3	114.3	21.3
810	20.6	134.7	141.3	22.6	20.6	126.8	127.8	22.4
899	23.6	152.5	161.0	23.6	22.6	140.3	142.4	26.5
944	24.6	161.1	173.0	24.6	22.6	148.2	150.2	27.5
988	26.5	170.0	184.7	26.5	24.6	157.1	159.2	27.5
1033	27.5	180.9	196.4	28.5	26.5	164.0	167.0	29.5
1077	29.5	190.8	209.2	29.4	27.5	172.8	176.0	30.5
1121	30.4	201.3	224.0	30.4	28.5	180.7	185.8	32.4
1165	31.4	210.2	250.5	34.3	28.5	188.7	199.5	33.4

Note: All strains corresponding to 720 lbs. or less are the average of three readings. Above 720 lbs. the strains are obtained from one reading.

UNIXIAL TENSION SPECIMENS (MORTAR)

AVERAGE STRESS (p.s.i.)	STRAIN (x10^{-6})							
	SPECIMEN No. 1				Specimen No.2			
	GAUGE NUMBER							
	1	2	3	4	1	2	3	4
0	0	0	0	0	0	0	0	0
45	11	2	14	1	14	3	10	2
117	22	3	28	5	29	9	20	4
171	31	8	45	8	43	9	31	9
233	41	6	63	13	56	13	45	11
296	48	8	84	16	72	14	57	13
356	52	9	108	22	85	17	68	16
387	53	9	124	23				
418	52	11	142	25	102	20	82	17
449	51	9	165	27				
480	46	9	194	31	120	22	94	21
495					125	2[illegible]	97	21
510					130	23	101	21
526					140	26	104	22

UNIAXIAL COMPRESSION SPECIMENS (MORTAR)

AVERAGE STRESS (p.s.i.)	Spec. No. 1, Gauge 1	Spec. No. 1, Gauge 2	Spec. No. 1, Gauge 3	Spec. No. 1, Gauge 4	Spec. No. 2, Gauge 1	Spec. No. 2, Gauge 2	Spec. No. 2, Gauge 3	Spec. No. 2, Gauge 4
0	0	0	0		0		0	
1230	306	60	252		245		288	
1600	386	80	322		331		376	
1960	468	90	392		391		442	
2290	560	106	480		485		544	
2650	630	126	550		551		618	
3010	732	142	650		643		718	
3360	806	156	720		717		808	
3725	908	182	820		823		928	
4090	1000	204	914		903		1018	
4455	1100	226	1018		1005		1136	
4820	1194	244	1116		1111		1256	
5190	1310	276	1236		1223		1384	
5550	1402	308	1338		1325			
5910	1522	338	1460		1439		1628	
6275	1612	384	1564		1557		1758	
6630	1780	450	1744		1721		1946	
6985	1904	520	1888		1863		2104	
7350	2074	626	2090		2113		2376	
7600	2240	762	2290		2301		2582	
7840	2352	856	2436		2445		2730	
7980	2432	942	2546		2587		2882	
8120	2558	1114	2758		2727		3036	
8250	2670	1292	2986		2963		3296	
8390	2788	1548	3248					

CONCRETE BEAM (4" x 3" x 40")

APPLIED LOAD (LBS)	STRAIN (x10^{-6}) GAUGE NUMBER 1	2	3	4	5	6	7	8
Initial Position								
0	0	0	0	0	0	0	0	0
90	1	10	9	2	1	13	-	1
180	2	20	20	5	2	22	22	2
270	4	31	31	6	5	33	33	4
360	4	44	43	5	5	46	-	4
450	7	54	54	10	7	53	57	6
540	11	66	64	12	11	-	68	7
630	11	77	74	13	11	73	82	10
Final Position								
0	0	0	0	0	0	0	0	0
90	1	10	8	0	2	8	9	2
180	1	22	17	0	4	20	21	4
270	4	33	34	3	4	30	31	6
360	5	46	43	3	7	40	44	7
450	8	58	56	6	9	52	55	9
540	9	70	68	-	10	61	68	11
630	11	82	80	-	12	72	79	12
675	11	86	87	10	12	78	84	10
720	10	97	95	9	12	84	90	15
765	15	106	105	10	16	91	104	19
810	13	114	116	9	14	96	106	15
865	20	123	135	-	17	104	117	16
900	18	133	151	10	18	114	130	18

Note: All strains corresponding to 630 lbs. or less are the average of five readings. Above 630 lbs., the strains are obtained from one reading.

UNIXIAL TENSION SPECIMENS (Concrete)

AVERAGE STRESS p.s.i.	STRAIN $(x10^{-6})$							
	SPECIMEN NO. 1				SPECIMEN NO. 2			
	GAUGE NUMBER							
	1	2	3	4	1	2	3	4
0	0	0	0	0	0	0	0	0
45	7	1	9	2	14	-2	10	-1
60	11	1	11	2	20	0	14	-1
76	21	-1	13	2	14	0	14	7
91	25	1	21	2	24	0	20	-1
107	27	1	23	2	24	0	20	7
123	23	3	23	2	26	2	26	7
139	31	1	27	2	30	2	30	7
155	31	3	27	4	32	4	32	7
171	39	3	33	2	36	4	36	7
187	41	3	35	2	44	10	40	7
202	41	5	39	6	48	0	46	7
218	51	3	43	2	44	4	46	11
233	59	5	45	6	48	4	50	11
247	57	3	49	4	56	2	56	9
265	59	5	53	6	58	4	58	9
280	59	7	57	10	60	4	60	11
296	67	5	61	6	58	8	65	15
311	71	5	63	6	68	2	70	14
326	73	3	69	10	70	4	74	13
341	77	5	71	8	68	10	76	15
356	77	11	73	12	70	10	80	17
371	83	11	79	10	76	8	84	17
387	91	7	87	12	84	8	92	15
402	91	11	91	12	80	10	94	17
418	103	11	97	10	88	12	98	17
433	111	11	101	12	90	12	104	19
449	113	13	107	12	94	14	110	19
464	117	11	113	12	100	14	118	21

UNIAXIAL COMPRESSION SPECIMENS (Concrete)

AVERAGE STRESS p.s.i.	STRAIN ($x10^{-6}$)					
	SPECIMEN NO. 1				SPECIMEN NO. 2	
	GAUGE NUMBERS					
	1	2	3	4	1	3
0	0	0	0	0	0	0
1230	232	12	214	40	291	197
1600	308	22	286	50	379	251
1960	372	42	352	66	469	309
2290	432	62	416	80	569	371
2650	500	72	484	90	647	421
3010	570	78	554	106	739	481
3360	640	82	626	116	831	549
3725	710	92	706	136	949	621
4090	780	102	776	150	1041	679
4455	872	122	864	170	1167	759
4820	958	142	946	200	1289	831
5190	1030	172	1024	220	1407	909
5550	1118	210	1112	240	1521	977
5910	1212	-	1216	280	1689	1061
6275	1310	352	1316	318	1839	1141
6630	1460	472	1474	366	2107	-
6985	1632	732	1664	450	2501	1409
7140	1898	1688	1946	676	2991	1501
7140					3331	1791

MORTAR SLAB (1 x 1)

APPLIED LOAD (LBS.)	STRAIN ($x10^{-6}$)							
	GAUGE NUMBER							
	1	2	5	6	7	9	10	11
0	0	0	0	0	0	0	0	0
450	22	15	40	19	24	22	22	21
675	27	21	58	27	34	32	30	30
899	38	31	70	39	44	42	42	40
1077	47	41	76	45	54	52	50	48
1342	66	61	86	59	70	68	66	64
1600	75	73	102	67	82	78	78	74
1784	90	87	108	77	94	88	90	84
1938	100	97	116	87	102	98	98	94
2135	102	105	130	95	110	106	106	102
2314	112	115	138	103	120	116	114	110
2493	126	127	146	113	130	128	126	122
2671	132	137	154	117	138	134	132	128

(CONT)

	1	2	5	6	7	9	10	11
2847	146	151	164	131	150	146	146	142
3023	156	165	172	141	162	156	152	150
3199	170	177	178	147	172	168	164	160
3376	180	191	188	157	182	178	172	170
3553	186	201	198	163	190	186	182	178
3729	198	217	208	173	202	196	196	188
3902	216	235	216	185	214	208	210	198
4075	230	247	226	196	224	220	220	212
4248	242	257	238	201	234	228	232	220
4425	258	271	246	213	246	238	242	232
4514	270	277	248	221	254	246	250	242

GAUGE NUMBERS

	12	13	14	15	16	17	18
0	0	0	0	0	0	0	0
450	21	23	22	21	18	24	25
675	34	35	30	29	32	34	32
899	46	49	38	39	42	44	46
1077	54	57	48	47	50	54	52
1342	64	71	62	61	62	68	70
1608	80	87	74	71	74	80	82
1784	84	93	82	83	78	90	94
1938	94	103	90	91	88	100	102
2135	106	117	98	97	102	108	110
2314	116	127	104	107	108	116	120
2493	118	133	116	119	112	128	132
2671	134	147	122	125	124	136	142
2847	140	153	132	135	132	148	152
3023	148	165	138	145	140	160	162
3199	158	175	148	157	148	168	176
3376	166	185	158	167	158	180	186
3553	180	199	168	175	170	190	196
3729	190	211	178	187	180	204	208
3902	198	223	188	199	188	218	226
4075	210	233	198	211	196	234	248
4248	226	245	208	221	210	276	278
4425	234	257	220	233	218	378	356
4514	238	263	228	245	220	500	528

MORTAR SLAB (1.58:1)

APPLIED LOAD (LBS.)	STRAIN ($x10^{-6}$) GAUGE NUMBER				
	1	2	3	4	5
0	0	0	0	0	0
225	13	16	9	24	10
360	22	25	14	34	14
540	33	37	20	49	21
720	43	48	28	65	28
899	54	60	35	80	35
1077	66	70	41	97	42
1253	78	84	49	115	48
1342	83	88	51	124	52
1430	88	95	56	132	56
1519	94	101	59	140	60
1608	101	107	62	147	63
1696	107	112	64	155	66
1784	111	119	69	162	69
1872	118	126	72	170	72
1961	125	132	76	179	77
2048	131	138	80	185	81
2135	138	145	83	195	84
2224	143	153	86	204	87
2313	151	159	90	212	92
2402	157	166	94	223	95
2492	163	173	99	233	99
2582	171	181	101	244	103
2671	178	187	106	253	106
2846	193	204	112	273	114
3023	209	220	120	297	122
3199	226	236	127	320	130
3378	247	264	136	350	139

APPLIED LOAD (LBS.)	6	7	8	9	10
0	0	0	0	0	0
225	12	13	10	10	14
360	21	24	14	14	23
540	32	36	20	20	35
720	43	48	27	27	45
899	53	59	34	33	57
1077	65	72	39	40	68
1253	75	83	47	46	80
1342	81	88	50	50	85
1430	86	95	54	53	91
1519	92	101	58	57	97
1608	98	108	60	61	103
1696	103	113	63	63	108
1784	109	119	66	67	114
1872	113	125	71	70	120

(CONT)	6	7	8	9	10
1961	120	132	74	73	125
2048	125	138	78	78	131
2135	131	144	80	80	137
2224	137	151	85	84	143
2313	143	157	87	87	150
2402	148	163	92	91	156
2492	155	170	95	94	161
2582	161	178	99	98	169
2671	167	184	102	102	175
2846	180	197	110	109	187
3023	194	211	116	115	203
3199	207	228	125	123	216
3378	224	245	135	133	232

MORTAR SLAB (2:1)

APPLIED LOAD (LBS.)	STRAIN ($x10^{-6}$) GAUGE NUMBER							
	1	2	4	6	7	8	9	10
0	0	0	0	0	0	0	0	0
225	24	30	9	27	30	7	10	30
450	36	42	13	38	43	12	13	40
675	56	58	19	58	63	18	21	60
899	80	78	25	80	85	22	27	80
1077	86	88	33	94	97	28	35	94
1253	104	104	39	110	115	36	43	110
1430	120	124	43	126	135	40	45	126
1519	126	128	45	136	145	44	49	134
1608	130	140	51	140	151	48	53	140
1696	144	154	51	154	165	48	55	150
1784	150	162	57	160	171	54	61	158
1828	154	164	59	166	177	56	63	164
1872	164	168	59	174	185	54	63	168
1916	164	176	61	178	189	58	65	172
1961	172	182	59	184	197	56	63	178
2005	176	188	63	188	201	58	65	180
2048	176	188	67	190	205	64	-	186
2092	180	196	69	198	219	64	71	190
2135	190	204	69	204	227	64	71	198
2224	194	212	71	216	241	68	77	208
2313	208	224	75	228	265	74	81	218
2402	216	236	79	240	289	76	83	228
2447	222	244	79	248	305	76	83	234
2402	226	248	75	250	321	74	79	236
2358	224	246	73	246	315	70	75	232
2313	220	238	73	236	305			

(CONT) GAUGE NUMBER

	11	12	13	14	15	16	17	18
0	0	0	0	0	0	0	0	0
225	28	11	24	25	21	22	21	21
450	38	16	34	36	31	30	31	30
675	58	26	50	50	49	46	47	46
899	78	30	66	66	61	60	63	60
1077	92	36	80	82	79	76	79	74
1253	108	44	94	98	95	88	91	88
1430	126	50	106	110	107	100	103	98
1519	134	54	112	116	111	106	111	102
1608	140	58	122	126	121	114	119	112
1696	154	60	126	130	129	120	125	118
1784	160	66	136	142	137	128	133	124
1828	164	68	140	146	139	132	139	128
1872	172	66	140	146	139	132	139	130
1916	174	72	146	154	147	140	145	136
1961	178	70	146	156	147	140	145	136
2005	184	72	150	158	149	144	151	138
2048	188	76	156	164	157	148	155	146
2092	192	78	162	168	163	152	161	148
2135	202	76	160	170	163	156	161	150
2224	208	84	172	180	175	164	171	158
2313	222	86	180	190	183	172	179	166
2402	234	94	188	198	191	180	189	174
2447	242	90	192	202	197	186	193	178
2402	238	88	188	198	189	182	189	172
2358	234	86	186	196	189	178	185	168

CONCRETE SLAB (1.58:1)

APPLIED LOAD (LBS)	STRAIN ($x10^{-6}$) GAUGE NUMBER				
	1	2	3	4	5
0	0	0	0	0	0
180	1	3	10	9	6
360	10	12	17	15	16
540	20	21	22	20	26
720	29	31	27	25	35
899	39	41	34	30	45
1077	48	50	40	35	56
1165	53	55	43	38	59
1253	58	61	46	40	65
1342	64	65	49	43	70
1430	68	71	52	47	74
1519	73	75	55	49	79
1608	77	81	60	52	85
1696	82	90	62	55	90

(CONT)

	1	2	3	4	5
1784	88	96	67	57	96
1872	93	101	69	60	101
1961	100	107	73	62	107
2048	105	111	76	65	115
2135	111	117	79	68	123
2224	116	122	83	71	128
2313	122	127	86	74	134
2402	133	128	90	77	140
2492	140	131	94	79	148
2671	153	139	98	83	163
2758	153	145	99	86	172
2810	149	149	99	88	176

GAUGE NUMBER

	6	7	8	9	10
0	0	0	0	0	0
180	9	17	17	0	14
360	15	27	28	4	22
540	20	36	37	10	32
720	27	45	47	14	41
899	32	55	57	19	50
1077	36	65	67	23	60
1165	39	70	72	26	64
1253	42	75	78	28	69
1342	45	81	83	31	74
1430	49	86	89	33	78
1519	52	91	94	36	84
1608	55	96	99	38	89
1696	57	102	105	41	94
1784	60	107	111	43	99
1872	63	112	115	45	104
1961	66	118	122	48	109
2048	70	124	127	50	115
2135	72	129	133	53	120
2224	74	135	139	55	126
2313	78	141	145	58	130
2402	80	147	152	61	137
2492	83	153	157	64	141
2671	87	166	168	69	152
2758	89	173	175	72	159
2810	88	178	176	72	159

CONCRETE SLAB (2:1)

APPLIED LOAD (LBS)	STRAIN ($x10^{-6}$) GAUGE NUMBER 1	2	3	4	5	6	7	8	9	10
0	0	0	0	0	0	0	0	0	0	0
243	17	21	4	4	18	4	12	11	8	12
450	30	34	9	9	32	10	24	23	12	25
540	35	42	10	11	37	11	30	28	16	30
720	47	52	14	15	49	15	39	38	19	39
899	59	64	18	21	61	20	51	49	24	49
1077	70	77	23	25	73	25	62	58	28	60
1253	82	89	26	29	86	29	73	69	32	71
1342	89	95	29	32	92	31	79	74	34	76
1430	96	102	31	35	98	34	86	80	36	82
1519	103	109	33	37	105	36	92	87	38	88
1608	109	116	35	40	108	40	97	91	41	91
1696	116	124	37	42	116	41	103	97	43	97
1784	124	135	40	44	122	43	109	102	46	103
1872	132	144	41	46	130	47	116	109	47	109
1961	141	154	45	48	139	50	123	115	49	116
2135	156	173	50	53	158	55	136	128	54	129
2313	173	220	56	56	177	59	152	144	58	142
2492	199	320	63	58	207	64	173	166	61	157
2537	208	366	66	59	218	66	185	178	61	162

CONCRETE SLAB (1:1)

APPLIED LOAD (LBS.)	STRAIN ($x10^{-6}$) GAUGE NUMBER							
	1	2	3	4	5	6	7	8
0	0	0	0	0	0	0	0	0
360	13	13	11	16	13	10	12	12
720	27	26	24	30	24	20	24	23
1077	41	39	38	44	36	29	35	33
1430	55	52	50	58	46	39	46	43
1784	73	66	65	72	57	48	58	54
1961	82	72	72	79	63	52	63	59
2135	91	79	79	87	69	57	69	64
2313	100	86	88	95	75	60	75	70
2492	110	93	95	102	81	65	82	76
2671	120	101	103	110	87	70	89	84
2846	130	107	112	118	93	75	95	90
3023	141	116	121	125	100	80	102	96
3199	155	123	130	134	106	84	108	104
3378	170	130	139	142	113	90	115	110
3551	184	137	148	151	120	95	122	117
3729	201	146	157	159	127	101	130	124
3902	223	155	167	170	134	111	136	132
3989	233	159	172	174	137			

MORTAR DISC

APPLIED LOAD (LBS)	STRAIN ($x10^{-6}$) GAUGE NUMBER				
	1	2	3	4	5
0	0	0	0	0	0
360	4	4	5	5	5
720	9	8	9	9	12
1077	14	13	14	12	15
1430	19	18	17	17	20
1784	25	22	21	17	25
2135	28	28	24	24	26
2492	33	31	28	27	33
2846	39	38	30	30	35
3199	44	44	34	34	40
3551	51	50	37	35	43
3902	56	56	40	38	47
4248	61	60	44	40	53
4951	72	71	52	48	60
5312	75	77	54	50	65
5666	80	83	61	52	70
5842	84	83	62	57	72
6150	89	88	69	67	77
6858	98	98	73	75	88
7204	104	102	77	78	93
7550	108	107	81	82	97
7900	114	113	85	86	102
8251	119	119	87	89	106
8626	124	125	91	92	111
9002	132	132	96	94	116
9377	139	140	101	99	122
9753	145	147	102	105	128
10103	151	153	110	108	133
10471	156	161	110	-	140
10838	163	169	117	116	143
11200	170	175	122	121	148
11561	176	182	129	125	153
11922	183	189	130	128	159
12290	188	195	135	131	163
12644	195	201	139	135	168
12998	203	209	143	140	174
13352	209	215	147	144	178
13706	216	222	154	149	185

Note: For all readings above 5842 lbs., the following load should be added to the given load to obtain the actual load corresponding to each recorded strain.

GAUGE NUMBER	CORRECTION TO APPLIED LOAD (LBS)
1	90
2	110
3	130
4	150
5	170

CONCRETE DISC

APPLIED LOAD (LBS)	STRAIN ($x10^{-6}$) GAUGE NUMBER 1	2	3	4	5	6
0	0	0	0	0	0	0
578	5	5	3	4	3	-
1270	15	16	11	10	4	10
1542	16	19	19	17	13	11
1824	19	19	18	15	14	14
2101	18	27	-	20	16	15
2378	25	25	25	20	21	25
2654	27	24	26	19	22	20
2931	28	29	26	32	25	30
3208	32	31	31	28	28	28
3485	34	30	35	36	30	32
3762	35	34	37	35	35	34
4038	41	40	41	35	36	35
4319	43	41	41	42	46	41
4600	49	44	47	41	42	38
4881	50	51	52	43	45	41
5162	50	52	53	44	47	46
5442	54	56	53	47	55	47
5725	55	57	61	51	54	49
6008	61	62	66	55	57	52
6291	64	65	69	56	58	54
6574	68	68	74	59	61	58
6858	71	73	80	64	66	61
7137	75	76	71	68	68	63
7415	77	79	84	68	70	64
7694	77	83	90	71	75	68
7972	82	82	94	74	78	72
8251	90	88	95	81	84	80
8551	-	89	98	82	83	92
8852	94	96	108	86	90	84
9152	100	103	120	92	96	85
9453	106	107	124	94	97	90
9753	110	108	133	102	102	94
10,042	124	-	137	104	108	101
10,332	132	115	137	108	111	103
10,621	-	-	140	113	114	-
10,911	137	117	156	117	118	110
11,200	144	111	166	114	135	116
11,490	139	111	168	127	131	122
11,778	146	113	177	136	137	126
12,067	149	110	185	138	144	136
12,356	151	108	195	144	152	144
12,644	-	99	200	156	167	154

Note: For all readings above 578 lbs., the following load should be added to the given load to obtain the actual load corresponding to each recorded strain.

GAUGE NO.	CORRECTION TO APPLIED LOAD (LBS)
1	10
2	20
3	30
4	50
5	60
6	70

REINFORCED SLABS

MORTAR (1.58:1) (REINFORCED)

APPLIED LOAD (LBS)	STRAIN ($x10^{-6}$)							
	GAUGE NUMBER							
	1	2	3	4	5	6	7	8
0	0	0	0	0	0	0	0	0
360	20	14	13	17	17	12	12	19
720	37	26	26	35	34	23	23	35
1077	53	40	37	53	50	34	33	51
1430	72	54	50	70	67	46	44	69
1784	91	68	63	84	84	58	56	85
2135	111	82	76	104	101	71	67	103
2413	130	95	89	121	119	83	80	121
2671	141	101	95	131	128	89	85	130
2846	150	109	102	141	138	96	92	140
3023	160	117	109	150	147	102	97	148
3199	170	123	115	158	157	109	104	158
3378	182	131	122	168	168	116	111	169
3551	192	138	129	177	180	122	117	179
3729	201	146	138	185	191	128	122	191
3902	211	153	144	195	202	135	130	201
4076	223	162	152	203	218	142	135	211
4248	235	169	160	214	229	148	143	223
4425	247	177	168	224	244	155	149	233
4618	262	187	178	243	262	165	158	249
4900	280	199	190	259	286	176	169	267
5184	300	211	202	274	325	187	178	288
5470	321	225	214	294	369	199	188	315
5755	344	239	229	312	410	210	200	350
6040	369	255	244	332	440	224	212	382
6320	393	269	257	349	475	235	224	414
6595	415	284	272	367	511	246	236	462
6870	440	300	288	387	549	258	250	556
7150	464	315	303	406	582	270	262	608
7430	493	333	317	426	637	284	275	650
7705	516	349	332	445	686	295	287	692
7845	529	358	341	457				

Note: Corrections to be applied to all loads above 4425 lbs. - See end of this appendix.

MORTAR (2:1) (REINFORCED)

APPLIED LOAD (LBS)	STRAIN (x10^{-6}) GAUGE NUMBER							
	1	2	3	4	5	6	7	8
0	0	0	0	0	0	0	0	0
360	30	11	7	27	5	14	16	17
720	54	24	21	53	24	26	26	35
1077	80	36	33	78	44	36	36	55
1430	105	50	45	103	63	48	49	75
1784	133	63	56	130	85	59	61	94
1961	146	70	64	142	94	66	66	105
2135	158	77	70	155	105	71	73	117
2313	172	85	77	168	118	76	78	129
2492	187	92	83	182	132	83	83	141
2671	200	99	89	196	146	88	89	154
2846	213	105	94	208	158	93	95	166
3023	227	112	101	222	173	99	101	181
3199	242	119	107	236	188	106	106	195
3378	258	126	115	250	207	112	113	213
3551	273	133	121	265	228	118	120	234
3729	288	141	127	279	251	124	126	257
3902	305	147	134	296	269	129	132	281
4076	321	154	140	311	282	135	139	304
4248	336	161	146	327	294	140	146	326
4425	353	169	153	342	301	145	150	341
4614	384	183	164	376	309	157	165	390
4899	410	195	176	398	329	164	175	426
5185	436	207	186	425	361	173	183	421
5470	465	222	199	453	412	182	193	433
5755	495	236	209	480	460	194	203	448
6040	525	253	223	511	510	206	213	460
6310	552	268	234	538	550	214	219	474
6595	583	284	250	569	601	226	230	500
6870	611	301	264	597	646	236	239	526
7150	641	317	277	627	690	247	248	561
7430	672	335	292	658	738	256	261	600
7705	705	355	307	689	802	267	271	631
7985	740	375	322	723	878	277	282	676
8120	757	387	331	740	912	283	287	697

Note: Corrections to be applied to all loads above 4425 lbs. - see end of Appendix.

MORTAR SLAB (2.5:1) (REINFORCED)

APPLIED LOAD (LBS)	STRAIN (x10^{-6}) GAUGE NUMBER 1	2	3	4	6	8
0	0	0	0	0	0	0
180	15	4	6	18	8	11
360	30	10	13	31	12	21
540	46	17	20	49	18	33
720	60	23	26	65	24	44
899	76	29	31	80	29	55
1077	91	34	38	95	33	65
1253	106	41	44	110	39	76
1430	122	48	50	126	43	87
1608	137	54	57	142	48	97
1784	153	59	63	157	54	106
1961	169	66	70	174	59	118
2135	185	73	76	191	64	128
2313	203	80	84	207	70	140
2492	218	86	90	223	75	152
2671	235	92	97	242	81	168
2846	254	98	102	259	86	182
2934	263	100	107	268	89	189
2934	266	102	107	272	90	192
3023	272	105	110	277	91	197
3199	289	110	116	294	96	216
3378	308	116	123	315	101	251
3551	326	123	129	333	106	284
3729	343	128	135	349	110	316
3902	363	135	141	369	116	348
4076	382	142	148	390	122	380
4248	400	148	154	407	126	407
4425	419	154	160	427	129	435
4614	443	160	167	454	139	476
4900	470	170	177	481	145	515
5185	501	181	188	511	151	556
5470	532	192	199	543	157	601
5755	568	205	211	578	165	652
6040	602	217	224	611	174	706
6310	631	228	235	641	181	752
6595	664	241	247	673	189	800
6890	695	255	259	705	196	849
7150	729	269	272	738	205	900
7430	766	284	285	775	212	957
7705	798	300	298	804	219	1000
7985	834	315	312	841	228	1052
8255	869	333	326	875	237	1099
8550	907	351	339	912	247	1151
8710	927	362	348	936	252	1182

Note: Corrections to be applied to all loads above 4425 lbs. - see end of Appendix.

CONCRETE SLAB 1.58:1 (REINFORCED)

APPLIED LOAD (LBS.)	STRAIN ($x10^{-6}$) GAUGE NUMBER							
	1	2	3	4	5	6	7	8
0	0	0	0	0	0	0	0	0
360	15	13	12	15	15	9	8	16
720	31	24	22	31	30	18	17	30
1077	47	35	33	46	42	27	25	42
1430	63	46	44	61	56	36	33	55
1784	80	57	55	78	70	45	41	68
1961	88	61	60	87	76	50	46	75
2135	97	67	66	95	84	55	51	82
2313	104	73	71	104	91	60	55	88
2492	113	78	78	113	100	64	60	96
2671	121	84	83	120	107	69	64	103
2846	130	90	90	129	115	74	68	111
3023	139	96	95	137	123	79	72	118
3199	148	102	102	147	128	85	77	127
3378	156	108	10[illegible]	157	138	91	82	135
3551	167	114	114	167	148	96	87	143
3900	186	129	126	187	174	108	96	159
4246	208	140	140	208	209	120	107	174
4600	230	153	154	231	236	132	118	184
4954	254	165	167	255	263	147	129	198
5305	279	180	181	281	284	163	140	213
5660	306	195	198	308	308	179	151	269
6010	332	209	216	333	339	193	161	313
6365	361	220	236	362	370	210	173	337
6455	369	223	239	371	378	214	178	342

CONCRETE SLAB (2:1) (REINFORCED)

APPLIED LOAD (LBS)	STRAIN (x10^{-6}) GAUGE NUMBER 1	2	3	4	5	6	7	8
0	0	0	0	0	0	0	0	0
180	8	1	2	10	12	4	11	3
360	18	8	-	17	12	11	11	14
540	27	15	13	33	23	15	14	22
720	35	20	17	38	32	18	17	29
899	45	23	22	48	35	23	23	38
1077	55	29	25	55	47	26	27	43
1253	63	33	30	65	54	31	28	54
1430	73	37	33	75	62	36	31	62
1608	86	41	38	83	69	40	35	68
1784	93	45	46	94	77	45	39	75
1961	102	50	47	104	86	49	43	83
2135	111	54	52	114	94	53	44	91
2313	121	60	55	124	103	58	47	99
2492	130	69	57	133	109	62	51	111
2671	143	69	65	142	120	64	59	122
2846	149	74	68	153	128	71	60	130
3023	160	80	72	162	134	74	68	136
3199	169	85	77	173	146	81	68	149
3378	180	89	81	184	154	85	74	159
3551	191	95	86	196	165	90	77	172
3729	201	96	86	204	176	96	82	179
3902	216	102	91	216	186	100	84	194
4076	222	109	100	228	195	104	89	215
4248	239	116	106	241	203	111	94	233
4425	248	122	111	254	209	114	98	258
4603	266	128	112	265	220	117	107	270
4780	272	138	120	275	229	122	106	291
4957	285	143	126	288	247	122	110	313
5135	297	147	131	303	265	132	118	332
5312	309	154	137	315	282	139	121	356
5442	312	160	143	318	295	138	126	376
5725	331	168	151	339	316	150	131	407
6008	350	179	161	363	343	160	139	430
6291	373	190	168	382	373	170	145	440
6574	387	216	175	402	424	183	147	483
6858	405	-	184	421	463	187	168	496
7136	435	229	199	445	506	197	166	521
7415	457	248	210	470	556	207	175	550
7693	476	264	221	488	594	215	187	570
7972	499	284	233	514	639	226	195	594
8251	520	304	246	534	676	236	203	618
8529	542	323	261	556	712	244	213	646

Note: Corrections to be applied to all loads above 5312 lbs. - see end of Appendix

CONCRETE SLAB (2.5:1) (REINFORCED)

APPLIED LOAD (LBS)	STRAIN (x10^{-6}) GAUGE NUMBER							
	1	2	3	4	5	6	7	8
0	0	0	0	0	0	0	0	0
90	4	-1	2	5	4	1	2	4
180	10	4	4	8	9	3	4	7
360	19	3	10	16	15	8	6	16
540	33	12	12	20	21	11	11	22
899	50	19	19	44	35	19	18	37
1077	61	22	23	51	43	22	22	45
1254	69	25	28	59	53	24	28	53
1430	82	32	33	68	54	27	27	61
1607	87	35	33	77	63	33	32	69
1784	95	41	40	85	72	34	36	76
1961	104	42	45	91	74	35	42	83
2135	116	51	49	100	87	40	45	94
2313	124	56	53	109	95	44	52	103
2492	134	59	57	117	102	46	53	109
2671	143	65	59	124	109	47	52	119
2846	161	72	63	133	116	52	59	127
3023	164	74	66	143	123	57	62	143
3199	175	77	72	154	135	61	61	152
3378	187	82	75	162	144	65	70	159
3551	198	86	79	171	145	69	82	173
3729	210	90	84	181	167	71	79	188
3902	225	92	89	195	183	78	84	205
4076	237	99	92	201	195	79	89	227
4248	246	105	97	213	211	85	89	251
4336	252	110	101	219	225	90	95	257
4336	255	109	-	217	236	85	96	268
4425	-	116	-	238	241	86	91	266
4600	273	114	104	235	258	90	109	298
4777	288	120	111	244	276	94	108	320
4865	294	123	111	248	291	90	110	332
5091	300	127	118	258	318	98	114	363
5442	326	137	126	281	354	106	122	402
5796	351	147	134	305	396	114	128	441
6150	376	156	142	326	438	121	135	478
6504	402	166	152	348	477	130	141	515
6858	428	178	163	370	509	138	147	556
7204	453	193	173	392	536	146	155	594
7550	483	208	180	416	567	156	163	637
7900	514	222	199	443	604	167	172	682
8251	537	250	206	464	637	177	181	716
8626	564	268	213	485	671	184	191	771
9002	598	291	231	518	701	196	201	823
9377	623	313	239	543	729	207	209	867
9753	657	342	256	569	746	215	219	918
10,114	688	370	271	595	767	226	229	972
10,476	717	389	284	623	791	135	242	1018

(CONT)

Note: Correction to be applied to all loads above 4865 lbs. - see following table.

CORRECTIONS TO BE ADDED TO GIVEN LOAD FOR REINFORCED SLABS TO OBTAIN THE ACTUAL LOAD CORRESPONDING TO EACH RECORDED STRAIN

GAUGE NO.	CORRECTION (LBS.) DIAGONAL RATIO OF REINF. SLAB	
	MORTAR 1.58:1, 2.5:1	CONCRETE 2:1, 2.5:1
1	40	0
2	50	10
3	60	20
4	70	30
5	80	40
6	90	50
7	100	60
8	110	70